SUBMARINE GROUNDWATER DISCHARGE: IMPACTS ON COASTAL ECOSYSTEM BY HIDDEN WATER AND DISSOLVED MATERIALS

EDITED BY: Makoto Taniguchi, Isaac R. Santos, Henrietta Dulai, Ryo Sugimoto, Abhijit Mukherjee and Jun Shoji

PUBLISHED IN: Frontiers in Environmental Science and Frontiers in Marine Science

frontiers Research Topics

frontiers

ISSN 1664-8714
ISBN 978-2-88966-535-8
DOI 10.3389/978-2-88966-535-8

About Frontiers

Frontiers is more than just an open-access publisher of scholarly articles: it is a pioneering approach to the world of academia, radically improving the way scholarly research is managed. The grand vision of Frontiers is a world where all people have an equal opportunity to seek, share and generate knowledge. Frontiers provides immediate and permanent online open access to all its publications, but this alone is not enough to realize our grand goals.

Frontiers Journal Series

The Frontiers Journal Series is a multi-tier and interdisciplinary set of open-access, online journals, promising a paradigm shift from the current review, selection and dissemination processes in academic publishing. All Frontiers journals are driven by researchers for researchers; therefore, they constitute a service to the scholarly community. At the same time, the Frontiers Journal Series operates on a revolutionary invention, the tiered publishing system, initially addressing specific communities of scholars, and gradually climbing up to broader public understanding, thus serving the interests of the lay society, too.

Dedication to Quality

Each Frontiers article is a landmark of the highest quality, thanks to genuinely collaborative interactions between authors and review editors, who include some of the world's best academicians. Research must be certified by peers before entering a stream of knowledge that may eventually reach the public - and shape society; therefore, Frontiers only applies the most rigorous and unbiased reviews.
Frontiers revolutionizes research publishing by freely delivering the most outstanding research, evaluated with no bias from both the academic and social point of view. By applying the most advanced information technologies, Frontiers is catapulting scholarly publishing into a new generation.

What are Frontiers Research Topics?

Frontiers Research Topics are very popular trademarks of the Frontiers Journals Series: they are collections of at least ten articles, all centered on a particular subject. With their unique mix of varied contributions from Original Research to Review Articles, Frontiers Research Topics unify the most influential researchers, the latest key findings and historical advances in a hot research area! Find out more on how to host your own Frontiers Research Topic or contribute to one as an author by contacting the Frontiers Editorial Office: frontiersin.org/about/contact

SUBMARINE GROUNDWATER DISCHARGE: IMPACTS ON COASTAL ECOSYSTEM BY HIDDEN WATER AND DISSOLVED MATERIALS

Topic Editors:
Makoto Taniguchi, Research Institute for Humanity and Nature, Japan
Isaac R. Santos, University of Gothenburg, Sweden
Henrietta Dulai, University of Hawaii at Manoa, United States
Ryo Sugimoto, Fukui Prefectural University, Japan
Abhijit Mukherjee, Indian Institute of Technology Kharagpur, India
Jun Shoji, The University of Tokyo, Japan

Citation: Taniguchi, M., Santos, I. R., Dulai, H., Sugimoto, R., Mukherjee, A., Shoji, J., eds. (2021). Submarine Groundwater Discharge: Impacts on Coastal Ecosystem by Hidden Water and Dissolved Materials. Lausanne: Frontiers Media SA.
doi: 10.3389/978-2-88966-535-8

Table of Contents

frontiers in Environmental Science

EDITORIAL
published: 20 January 2021
doi: 10.3389/fenvs.2020.629509

Editorial: Submarine Groundwater Discharge: Impacts on Coastal Ecosystem by Hidden Water and Dissolved Materials

Henrietta Dulai[1], Isaac R. Santos[2,3], Makoto Taniguchi[4], Ryo Sugimoto[5], Jun Shoji[6] and Abhijit Mukherjee[7]*

[1]Department of Earth Sciences, School of Ocean Earth Science and Technology, University of Hawai'i at Manoa, Honolulu, HI, United States, [2]Department of Marine Sciences, University of Gothenburg, Gothenburg, Sweden, [3]National Marine Science Centre, School of Environment, Science and Engineering, Southern Cross University, Coffs Harbour, NSW, Australia, [4]Research Institute for Humanity and Nature, Kyoto, Japan, [5]Research Center for Marine Bioresources, Fukui Prefectural University, Obama, Japan, [6]Atmosphere and Ocean Research Institute, The University of Tokyo, Bunkyo, Japan, [7]Indian Institute of Technology Kharagpur, Kharagpur, India

Keywords: Submarine groundwater discharge, coastal hydrology, geochemistry, trophic food webs, coastal contamination, radium, nitrogen, silicon

Editorial on the Research Topic

Submarine Groundwater Discharge: Impacts on Coastal Ecosystem by Hidden Water and Dissolved Materials

OPEN ACCESS

Edited and reviewed by:
Björn Vinnerås, Swedish University of Agricultural Sciences, Sweden

****Correspondence:***
Henrietta Dulai
hdulaiov@hawaii.edu

Specialty section:
This article was submitted to Water and Wastewater Management, a section of the journal Frontiers in Environmental Science

Received: *15 November 2020*
Accepted: *08 December 2020*
Published: *20 January 2021*

Citation:
Dulai H, Santos IR, Taniguchi M, Sugimoto R, Shoji J and Mukherjee A (2021) Editorial: Submarine Groundwater Discharge: Impacts on Coastal Ecosystem by Hidden Water and Dissolved Materials. Front. Environ. Sci. 8:629509. doi: 10.3389/fenvs.2020.629509

This Research Topic advances our understanding of submarine groundwater discharge (SGD), a hydrological process involving the discharge of terrestrial freshwater combined with the exchange of seawater along coastal margins (Burnett et al., 2003). SGD occurs worldwide and has a range of impacts including its role in shifting ecosystems' ecological states on local scales (Lecher and Mackey, 2018) or contributing greenhouse gases with global implications (Lecher et al., 2015; Sadat-Noori et al., 2016). In spite of remaining unknowns, this Research Topic takes us a step closer, through methodological improvements in SGD quantification, to understanding the contribution of SGD to coastal nutrient and chemical balances, and the effects these chemical subsidies have on coastal trophic food webs. Finally, a review paper synthesizes progress in SGD research over the last decade, including a focus on its economical and cultural values.

METHODOLOGICAL IMPROVEMENTS AND NUTRIENT FLUX CHARACTERIZATION

Four papers are devoted to refining methods of quantification of SGD. A common indirect approach of quantifying SGD rates is to apply a mass balance of a chemical with concentration in groundwater exceeding those in seawater. Lamontagne and Webster caution that inadequate sampling focusing on surface water only when vertical mixing is slow may lead to biased SGD estimates. Short-lived radium (Ra) isotope distributions revealed that slow vertical mixing creates vertical gradients that need to be accounted for when building mass balance models.

Tamborski et al. apply naturally occurring Ra isotopes in a semi-enclosed basin to estimate SGD and associated nutrient fluxes. Because the four Ra isotopes have different ingrowth rates, they are sensitive to different time-scale processes. Specifically, short-lived Ra isotopes trace short-scale SGD

processes such as wave or tidal pumping, and their mass balance is also sensitive to contributions from sediments in addition to SGD. In contrast, long-lived Ra isotope mass balances are highly sensitive to fluxes at the boundaries of the study domain and less sensitive to short- and small-scale SGD.

Oehler et al. revisit the use of dissolved silicon (DSi) as SGD tracer. DSi becomes enriched in groundwater due to biogenic silica dissolution and water-rock interactions. Depending on the hydrogeologic settings, DSi can trace terrestrial and brackish SGD or can be used as a tracer for marine SGD. They emphasize that DSi is a nutrient and may exhibit non-conservative behavior in the coastal ocean. A large improvement in DSi application is a recent progress in its chemical analysis that allows measurements from 1-ml sample volumes. This helps with the recurring problem of end-member characterization, especially from low-volume pore water samples.

Characterization of SGD and nutrient fluxes from coastal karst aquifers was the focus of Bejannin et al. SGD estimates in karstic coastlines are difficult due to the combined presence of different water sources that include springs, pore water exchange, and rivers. Horizontal eddy diffusivity from offshore ^{224}Ra transects and nutrient gradients were used to derive SGD nutrient fluxes. With this approach, the authors bypass the need for an exact characterization of the SGD endmember, minimizing uncertainties. However, this method is only applicable when the SGD tracers and nutrients behave conservatively within the timeframe of coastal mixing and have no significant external sources.

ANTHROPOGENIC CHEMICAL SIGNATURES IN SUBMARINE GROUNDWATER DISCHARGE

It has long been recognized that SGD is a significant source of nutrients to the coastal ocean. Over the last decades progress has also been made on characterizing the origin of nutrients in SGD, mainly implicating anthropogenic sources. However, in many settings single tracing techniques alone cannot discriminate between sources. Tamborski et al. used boron (B) and boron isotopes ($\delta^{11}B$) in combination with $\delta^{15}N$ and $\delta^{18}O$ to trace sources of NO_3^- to two subterranean estuaries and constrain end-member isotopic signatures. They concluded that $\delta^{15}N$ and $\delta^{18}O$ in NO_3^- alone could not differentiate nitrogen sourced from septic waste, fertilizer and precipitation. However, $\delta^{11}B$ revealed that the STE was affected by agricultural fertilizer inputs and N was predominantly sourced from nitrification of ammonium.

Nutrients are not the only anthropogenically sourced chemicals in SGD. Welch et al. studied legacy and currently-used pesticides in groundwater, stream baseflow, and SGD in an oceanic island. SGD and baseflow carried as much as 1 g of glyphosate and 9 g of DDT per day into Faga'alu Bay. While glyphosate is currently widely applied and its presence in groundwater is not surprising, the persistence of DDT in groundwater is noteworthy since it has been phased out in the 1970s. The sustained flux of glyphosate and DDT via SGD could have chronic effects on reef health and should be investigated in more detail. These observations shed light into the role of SGD as an overlooked source of contaminants of emerging concerns to the coastal ocean.

SUBMARINE GROUNDWATER DISCHARGE SUPPORTS BIOLOGICAL PRODUCTIVITY

SGD-derived nutrients sustain primary production, which in turn increases food availability to higher trophic levels. Andrisoa et al. showed that mussel growth rates and condition is greater at groundwater exposed sites. High growth rates were the consequence of both the higher winter temperatures moderated by groundwater discharging at constant temperatures, and groundwater-derived nutrient supply that increased food availability. This study provides direct evidence for the "downstream" ecological impacts of groundwater discharge on higher trophic levels and that SGD can have a local economic effect.

The propagating effect of SGD along trophic linkages was also explored by Fujita et al. who investigated how SGD enhances the productivity and biomass of producers, primary consumers, and secondary consumers. Carbon stable isotopes revealed that nutrients from terrestrial SGD were utilized by juvenile marbled sole. Fish biomass across three sites in the western North Pacific were also related to high SGD locations.

Starke et al. argue that apart from nutrient inputs, temperature should also be considered to drive fish distribution around fresh SGD sites in the tropics, perhaps due to the higher oxygen content of colder water. They demonstrated that fish are attracted to SGD sites using a biofouling experiment. The enhanced settlement of filamentous sessile algae near SGD sites became the food source attracting fish. The results presented showed that submarine springs attract fish in tropical settings and represent some of the first manipulative experiments in the SGD context.

REVIEW OF THE STATUS QUO

The recent advances in the field are highlighted in a review by Taniguchi et al. The field has now entered a "mature stage" with a large number of research groups exploring the multiple hydrological, geochemical, biological, and oceanographic facets of SGD. The review includes updates on technological advances of SGD measurement, description of geophysical drivers, magnitudes, and biological effects of SGD and porewater exchange. It is recognized that terrestrial freshwater discharge, processes driven by wave setup and tidal pumping, as well as pore water exchange are not necessarily synergistic or additive. It has also become clear that global fresh SGD only accounts for a minor fraction of river discharge (Luijendijk et al., 2020) while the total (saline + fresh) SGD is often much greater than river inputs (Cho et al., 2018).

The economic and cultural implications of SGD are now finally being evaluated. SGD's role in supporting coastal

ecosystems and food resources had also had significance in various cultures historically, these cultural values and roles of SGD are being described in the scientific literature.

CONCLUSION

This collection of studies from multiple parts of the globe including France, Australia, Japan, Pacific Islands, and the USA further illustrates the overall widespread significance of SGD for water, nutrient, and contaminant delivery to the coastal ocean. These papers show improved ways of quantifying the different components of SGD and pore water exchange. Through multiple examples presented here now we also have clearer evidence for the importance of SGD in driving food webs, fish stocks, and therefore indirectly also economies. Multiple challenges however remain, for example, in upscaling SGD to regional and global scales and in better understanding its temporal variation. For example, with climate change SGD drivers such as precipitation patterns and sea level are changing and we are yet to see how SGD and related water, nutrient, and other chemical fluxes will be affected. But there is progress made in producing more and more representative SGD measurements that provide the baseline on which future studies can build on.

AUTHOR CONTRIBUTIONS

All authors listed have made a substantial, direct and intellectual contribution to the work, and approved it for publication.

ACKNOWLEDGMENTS

We thank all authors for their contribution to this Research Topic.

REFERENCES

Burnett, W. C., Bokuniewicz, H., Huettel, M., Moore, W. S., and Taniguchi, M. (2003). Groundwater and pore water inputs to the coastal zone. *Biogeochemistry* 66 (1–2), 3–33. doi:10.1023/b:biog.0000006066.21240.53

Cho, H. M., Kim, G., Kwon, E. Y., Moosdorf, N., Garcia-Orellana, J., and Santos, I. R. (2018). Radium tracing nutrient inputs through submarine groundwater discharge in the global ocean. *Sci. Rep.* 8, 2439. doi:10.1038/s41598-018-20806-2

Lecher, A. L., Kessler, J. D., Sparrow, K. J., Kodovska, F. G-T., Dimova, N., Murry, J., et al. (2015). Methane transport through submarine groundwater discharge to the North Pacific and Arctic Ocean at two Alaskan sites. *Limnol. Oceanogr.* doi:10.1002/lno.10118

Lecher, A., and Mackey, K. (2018). Synthesizing the effects of submarine groundwater discharge on Marine Biota. *Hydrology* 5 (4), 60. doi:10.3390/hydrology5040060

Luijendijk, E., Gleeson, T., and Moosdorf, N. (2020). Fresh groundwater discharge insignificant for the world's oceans but important for coastal ecosystems. *Nat. Commun.* 11, 1260. doi:10.1038/s41467-020-15064-8

Sadat-Noori, M., Maher, D. T., and Santos, I. R. (2016). Groundwater discharge as a source of dissolved carbon and greenhouse gases in a subtropical estuary. *Estuar. Coast.* 39 (3), 639–656. doi:10.1007/s12237-015-0042-4

Conflict of Interest: The authors declare that the research was conducted in the absence of any commercial or financial relationships that could be construed as a potential conflict of interest.

frontiers in Environmental Science

ORIGINAL RESEARCH
published: 18 June 2019
doi: 10.3389/fenvs.2019.00082

Increase in Fish Production Through Bottom-Up Trophic Linkage in Coastal Waters Induced by Nutrients Supplied *via* Submarine Groundwater

Koji Fujita[1], *Jun Shoji*[1,2*], *Ryo Sugimoto*[3], *Toshimi Nakajima*[3], *Hisami Honda*[4], *Masaru Takeuchi*[3], *Osamu Tominaga*[3] *and Makoto Taniguchi*[4]

[1] Graduate School of Biosphere Science, Hiroshima University, Higashi-Hiroshima, Japan, [2] Atmosphere and Ocean Research Institute, The University of Tokyo, Kashiwa, Japan, [3] Department of Marine Bioscience, Fukui Prefectural University, Obama, Japan, [4] Research Institute for Humanity and Nature, Kyoto, Japan

Submarine groundwater is richer in nutrients compared to surface (river) water and therefore has been considered to be an essential component of biological production in marine coastal ecosystems. However, there has been no information on the effects of submarine groundwater on animals at high-order trophic levels such as fishes. Here, we show the first direct evidence that fish feeding and growth are elevated by submarine groundwater discharge (SGD) by on-site experiments and quantitative sampling. An experiment using cages moored on the sea bottom confirmed that juvenile marbled sole *Pseudopleuronectes yokohamae* obtained elevated levels of nutrition in the vicinity of SGD. Quantitative sampling at three sites with different hydrodynamic properties in coastal waters of the western North Pacific showed correspondence of high SGD with high biological production or biomass from producer to secondary consumers. These findings demonstrate that nutrients of terrestrial origin provided via submarine groundwater in coastal areas promote marine fish production.

Keywords: groundwater discharge, cage experiment, feeding, flounder, growth, radon, terrestrial origin, trophic flow

OPEN ACCESS

Edited by:
Efthalia Chatzisymeon, University of Edinburgh, United Kingdom

Reviewed by:
Wui Seng Ang, Public Utilities Board, Singapore
Alanna L. Lecher, Lynn University, United States

***Correspondence:**
Jun Shoji
jshoji@aori.u-tokyo.ac.jp

Specialty section:
This article was submitted to Water and Wastewater Management, a section of the journal Frontiers in Environmental Science

Received: *01 March 2019*
Accepted: *21 May 2019*
Published: *18 June 2019*

Citation:
Fujita K, Shoji J, Sugimoto R, Nakajima T, Honda H, Takeuchi M, Tominaga O and Taniguchi M (2019) Increase in Fish Production Through Bottom-Up Trophic Linkage in Coastal Waters Induced by Nutrients Supplied via Submarine Groundwater. Front. Environ. Sci. 7:82. doi: 10.3389/fenvs.2019.00082

INTRODUCTION

Water flowing from the land to the marine coastal area is an essential component supporting the high biological production by supplying nutrients of terrestrial origin (Field et al., 1998). Freshwater provided from terrestrial areas to coastal areas can be divided into surface water (river water) and groundwater. More studies have been undertaken on how variability in river waters affects biological production in marine ecosystems compared to groundwater supply influences (Moosdorf and Oehler, 2017). Groundwater discharge was estimated to approximate or exceed 50% of the freshwater input to bays (Valiela et al., 1990; Slomp and van Cappellen, 2004). In a temperate bay, a high contribution of nutrients (e.g., 65% of total dissolved inorganic phosphorus (DIP) provided through all freshwater) has been estimated to be supplied *via* submarine groundwater, which is richer in nutrients, especially phosphorus (Sugimoto et al., 2016). Therefore, submarine groundwater is considered to have high potential for promotion of trophic flow in coastal ecosystems.

High levels of submarine groundwater discharge (or seepage: SGD) have been shown to correspond with elevated primary production in coastal waters worldwide (Rodellas et al., 2015; Sugimoto et al., 2017; **Figures 1A,B**). Recent studies have indicated elevated abundance of primary

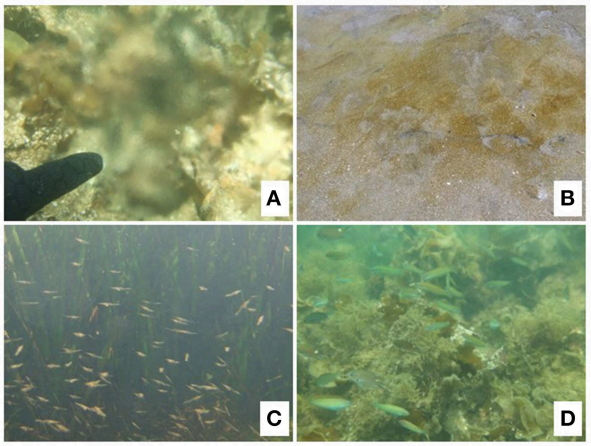

FIGURE 1 | Underwater view of spring-type submarine groundwater discharge (SGD) at a volcanic coast in Beppu Bay, southwestern Japan **(A)**, benthic microalgae flourishing around SGD at a sandy beach in Yamagata Prefecture **(B)**, misids gathering around SGD at a seagrass bed in Hokkaido Prefecture **(C)**, and aggregation of labrid and pomacentrid fishes around SGD in Beppu Bay, Japan **(D)**. All image credits: JS.

and secondary consumers (invertebrate macro-benthos and fishes) in nearby areas containing SGD (Waska and Kim, 2010; Hata et al., 2016; Utsunomiya et al., 2017; **Figures 1C,D**). Herbivore grazing is influenced by ecological stoichiometry of macrophytes that depend on nitrogen-rich SGD (Tomas et al., 2011; Peterson et al., 2012). To date, however, there is still limited information on the influence of SGD on the production of animal communities at high-order trophic levels, such as secondary consumers including fishes (Sanders et al., 2011; Moosdorf and Oehler, 2017). A missing trophic linkage in the coastal boundary area can be demonstrated if the utilization of nutrients of terrestrial origin provided through SGD by marine animals at the high-order trophic levels is elucidated.

In the present study, to test the hypothesis that nutrients provided *via* SGD drive marine food web and promote production of animals of high-order trophic levels, productivity and biomass at three trophic levels (producer, primary consumer, and secondary consumer) are compared between areas with high and low SGD in three coastal marine areas with different hydrological features in coastal waters of Japan, the western North Pacific. A continuous mooring time series observation was conducted to evaluate the contribution of SGD to animals at high-order trophic levels by comparing feeding and growth of juvenile fish together with nutrients of terrestrial origin [dissolved inorganic nitrogen (DIN) and DIP], primary productions (phytoplankton and benthic microalgae), and abundance of primary consumers as fish prey.

MATERIALS AND METHODS

Study Sites

Three survey sites (**Figure 2**) were selected to cover the different levels of maximum daily tidal amplitude (DTA) during the spring tide period in the western North Pacific (I: Sea of Japan coast with a low DTA of 0.4 m, II: Pacific coast of Japan with an intermediate DTA of 1.5 m; III: coastal area of the Seto Inland Sea with a high DTA of 4.0 m). Field experiments and quantitative sampling were conducted at the three sites to test if production and biomass of organisms at three trophic levels (producer, primary, and secondary consumers) in the benthic ecosystem are elevated in and around the area with high SGD.

Radon-222 (^{222}Rn) is a naturally occurring radioactive gas and a powerful tracer of groundwater inputs to oceans. The ^{222}Rn concentration is typically two to three orders of magnitude higher in groundwater than in surface waters (Church, 1996; Kim et al., 2005). The ^{222}Rn concentration has been applied as one of the indices for the detection of SGD in shallow waters worldwide since the half-life of ^{222}Rn is ∼3.8 days (Taniguchi et al., 2002; Swarzenski et al., 2007; Charette et al., 2008; Dimova et al., 2009; Santos et al., 2010). Salinity is also an indicator of fresh SGD input because SGD is composed of fresh SGD and recirculated SGD (Stieglitz et al., 2013). In the present study, two sampling stations within each site were selected according to the results of previous ^{222}Rn and salinity measurements (site I: Hosono et al., 2012; Kobayashi et al., 2019; site II: Honda et al., 2015; Shoji et al., 2017; site III: Hata et al., 2016). At each of the three sites, production of benthic microalgae, abundances of gammarid crustaceans (as dominant primary consumer and also as major prey organisms for fish), and carnivorous fishes were compared between the two stations with different levels of ^{222}Rn concentration and salinity in water as an indicator for SGD (sts. a, c, and e for high SGD; sts. b, d, and f for low SGD).

Primary Production and Primary and Secondary Consumers' Biomass

Surveys for primary production by benthic microalgae and biomass of primary consumers (epibenthic crustaceans) and secondary consumers (carnivorous demersal fishes) were conducted on 5 June at site I, on 2 August at site II, and on 12 June at site III in 2016. Production of benthic microalgae was estimated by an onsite experiment. Four polyethylene plates (30 × 25 cm, 1.5 mm thick) were set at 0.3 m above the sea bottom at each station for 2–5 days. Benthic microalgae on the plate was scraped and filtered onto Whatman GF/C glass-fiber filters. Samples were preserved frozen at −40°C until measurement of dry carbon weight with a mass spectrometer at the Research Institute for Humanity and Nature (RIHN), Kyoto, Japan. Primary production of the benthic microalgae was expressed as increase in carbon weight (mg C day^{-1} m^{-2}). Subsamples were preserved in 10% seawater formalin and were identified under a binocular microscope to the lowest possible taxon.

Epibenthic invertebrates were collected by towing a sledge-net (0.4 m width, 0.3 m height, and 0.3 mm mesh) for 20 m at a velocity of 1.0 m s^{-1}. Fish sampling was conducted by a round seine net (2 m high, 30 m long, and 4 mm mesh aperture) using the previously described method (Kamimura and Shoji, 2013). Each fish collection covered an area of 100 m^2. The invertebrate and fish samplings were conducted at four separate locations randomly selected within each station ($n = 4$ for each

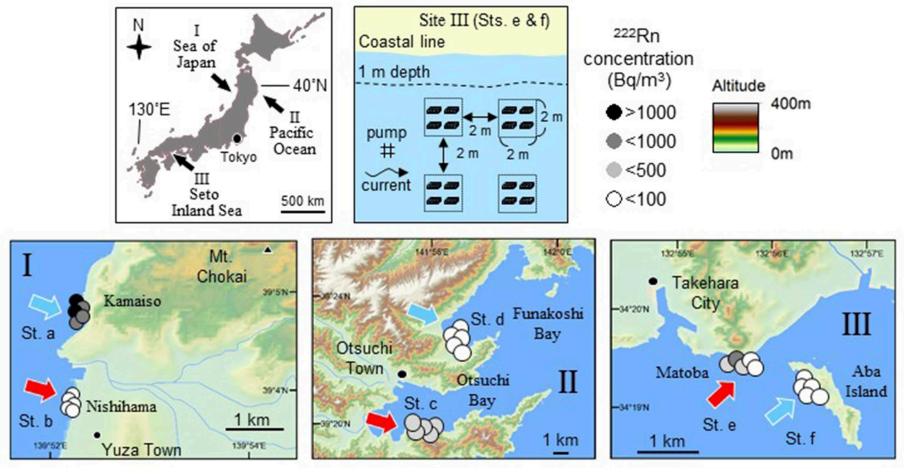

FIGURE 2 | Maps showing three survey sites where influence of SGD on trophic flow and fish feeding and growth was investigated (**top left**). The three sites (**bottom** panels) were selected to cover different levels of maximum daily tidal amplitude (DTA) during spring tide period in the northwest Pacific (I: Sea of Japan with a low DTA of 0.4 m, II: Pacific Ocean with an intermediate DTA of 1.5 m; III: Seto Inland Sea with a high DTA of 4.0 m). Production of benthic microalgae and abundances of gammarid crustacean (as dominant primary consumers and also as major prey organisms for fish) and fish were compared between two stations with different levels of ^{222}Rn concentration and salinity in water as an indicator for SGD (sts. a, c, and e for high SGD; sts. b, d, and f for low SGD) within each site (data for sites I, II, and III from Hata et al., 2016; Kobayashi et al., 2017; Nakajima et al., 2018, respectively). In order to evaluate the effect of SGD on fish feeding and growth, a cage experiment for 2 weeks was conducted using juvenile marbled sole *Pseudopleuronectes yokohamae* at site III. Physical and biological environmental conditions and stomach contents and growth rate of the juveniles were compared between the two stations (e and f). Arrangement of the experimental cages, pump, and current direction are shown (**top right**). Four experimental groups composed of four cages each are surrounded by a dotted line and depth contour of 1 m at low tide is indicated by a broken line.

station). Tidal levels ranged from 50 to 130 cm during these samplings. Samples were preserved on ice and were identified in the laboratory. Abundance of gammarids, which are the major prey items for demersal fishes in the survey sites (Hata et al., 2016; Shoji et al., 2017; Utsunomiya et al., 2017), was expressed as number of individuals m^{-2}. Fish biomass was calculated in wet weight (g 100 m^{-2}). Subsamples of gammarids and marbled sole were collected at site III and preserved frozen at −30°C until further processing for carbon and nitrogen stable isotope ratios.

Cage Experiment for Fish Feeding and Growth

To evaluate the effect of SGD on fish feeding and growth, a cage experiment for 2 weeks was conducted using juvenile marbled sole *Pseudopleuronectes yokohamae* at site III. The marbled sole is widely distributed in coastal waters in the western North Pacific and use low salinity coastal waters as nursery habitats during the juvenile stage (Wada et al., 2007). Juvenile marbled sole are abundant around areas with high SGD on a tidal flat in the Seto Inland Sea, southwestern Japan, and fed mainly on macrobenthos such as polychaetes and gammarids (Hata et al., 2016). Physical and biological environmental conditions and juvenile stomach contents and growth rate were compared between two stations (e and f) with different levels of SGD.

St. e is located in an area with high ^{222}Rn concentrations along the coast of Honshu Island, main island of Japan, and the other (st. f) is on the western coast of Aba Island, an unpopulated island. The distance between these two stations is ∼1.5 km. There is no river running into adjacent waters at each station. Majority (>A m 85%) of the sea bottom at both stations is composed of mud and sand with diameter <2.0 mm (Hata et al., 2016). Tidal amplitude is ∼4 m during spring tides and 2 m during neap tides.

Mooring time series surveys were conducted for 24 h from 16:00 on 6 June to 16:00 on 7 June 2017 at the two stations. Seawater was pumped at 5 L min^{-1} by a submersible bilge pump (800GPH, Rule) from 30 cm above the seafloor (1.5 m of sea depth at low tide). Data loggers for depth (DEFI2-D5HG, JFE Advantech), temperature, and salinity (A7CT2-USB, JFE Advantech) were mounted with the pump. The ^{222}Rn activity in seawater was measured according to Burnett et al. (2001). Seawater was directly flowed into an air/water exchanger (RAD Aqua, Durridge, Inc). Then, equilibrated air was sent into a radon detector (RAD7, Durridge, Inc.) for analysis of ^{222}Rn after passing through desiccant. The ^{222}Rn activity in seawater was measured every 20 min. Atmospheric ^{222}Rn activity was also measured during the same period. Uncertainties based on the counting errors were <20% for ^{222}Rn. Data obtained by the data loggers and RAD7 were averaged hourly to eliminate short-term variability in the present study. Hourly changes in SGD and compositions of fresh and recirculated SGDs were analyzed in a previous study (Nakajima et al., 2018).

In order to estimate SGD rate, continuous heat-type automated seepage meters (Taniguchi and Iwakawa, 2001) were deployed near the submersible pump at each site. The sensors were calibrated in the laboratory before and after the field survey. Voltage measured by the seepage meter at 5-min intervals was

converted into ml min^{-1} using calibration curves and then converted to cm day^{-1} using the area of the chambers by the same method as Kobayashi et al. (2017). Temperature and salinity were monitored at 5-min intervals by a temperature and salinity logger (MDS Mk-V, Advantech) attached inside the chamber.

Nutrient samples (NO_3^-, NO_2^-, NH_4^+, and PO_4^{3-}) were collected hourly from the pumped water and were immediately filtered through syringe filters (ADVANTEC, cellulose-acetate membrane, 0.8 μm pore size). Concentrations of NO_3^-, NO_2^-, and PO_4^{3-} were measured using an autoanalyzer (TRAACS-800, Bran-Luebbe). NH_4^+ concentration was measured fluorometrically using the orthophthaldialdehyde method (Holmes et al., 1999) with a Trilogy fluorometer with a colored dissolved organic matter (CDOM)/NH_4 module (Model 7200-041, Turner Designs). We defined DIN as the sum of NO_3^-, NO_2^-, and NH_4^+, and DIP as PO_4^{3-}. Chlorophyll-a (Chl-a) concentration in the pumped water was measured using the calibrated chlorophyll sensor (Cyclops-7, Turner Designs). These measurements were conducted every hour.

Feeding and growth of juvenile marbled sole were compared between the two stations (e and f). Juvenile marbled sole cultured at Kudamatsu Sea-farming Center, Yamaguchi Prefecture, Japan, were transported to the Takehara Marine Laboratory, Hiroshima University, and were maintained in a stocking tank for 4 days. On 12 June 2017, each juvenile (mean body length: 49.7 mm, SD: 2.8) was separately put in a cage (0.45 × 0.45 × 0.3 m). The juvenile stocking density for the experiment (4.9 ind. m^{-2}) was maintained at less than half of that (9.9 ind. m^{-2}) found to be suitable for juvenile feeding and growth according to the previous experiment to evaluate appropriate juvenile stocking density for the cage experiment (Fujita et al., 2017). Four cages were set within an experimental square of 2 × 2 m on the sea bottom at the two stations. Four experimental squares were located within a larger 6 m × 6 m square at each station. As a result, a total of 16 (4 × 4) experimental cages composed of four groups (four cages per group) were set at each station.

On 26 June, the juvenile marbled sole were collected from each cage and was preserved on ice. Total length of each juvenile was measured at the start and end of the experiment. Mean absolute growth rate (G, mm day^{-1}) for the experimental period (14 days) was calculated as:

$$G = (L_{14} - L_0)/14$$

where L_{14} is the total length at the end of the experiment (day 14) and L_0 is that at the start of the experiment (day 0).

Stomach contents of the juvenile marbled sole were identified under a dissecting microscope at a maximum of 100× magnification. Each prey item was measured in length and width using an ocular micrometer. Prey mass was calculated from previously reported length–mass relationships of Sirois and Dodson (2000). Stomach content composition (% in weight) was calculated for each juvenile.

Stable carbon isotope ratio analysis was applied for the wild and cultured juvenile marbled sole and their possible prey items in order to obtain verification that nutritional source of the juveniles in the experimental cages shifted from artificial pellets fed in the tank prior to the experiment to wild prey organisms in nature during the field experiment. The half-life period of carbon stable isotopic ratios in marbled sole juvenile muscles has been reported to be about 2 weeks in a diet-switch experiment (Hamaoka et al., 2016). Twenty cultured juveniles (fed only hatchery pellets) were sampled from the stocking tank at the start of the experiment. Fifteen juveniles cultured and kept in the cages for 2 weeks (fed natural prey for 2 weeks) were sampled from sts. e and f, respectively (one fish was lost/dead during the experiment at each station), at the end of the cage experiment.

Muscles of the right side of the body of wild juveniles collected at sts. e ($n = 20$) and f ($n = 6$), hatchery pellet ($n = 4$), and gammarids collected at sts. e and f as major prey organisms for the wild juveniles ($n = 4$ for each station, bulk sample) were processed for stable isotope analysis following the methods of Nagata and Miyajima (2008).

Stable isotope ratios of carbon ($\delta^{13}C$) and nitrogen ($\delta^{15}N$) were measured with an isotope mass spectrometer fitted with an elemental analyzer at RIHN. Isotope ratios are expressed as:

$$\delta X = (R_{\text{sample}}/R_{\text{standard}} - 1) \times 1000$$

where δX is the stable isotope ($\delta^{13}C$ or $\delta^{15}N$) in units of ‰, and $R = {}^{13}C/{}^{12}C$ or ${}^{15}N/{}^{14}N$. Atmospheric nitrogen (N_2) and Pee Dee belemnite were used as the standards for nitrogen and carbon stable isotopes, respectively. In order to verify the accuracy of the analysis, DL-alanine was used as a secondary standard for carbon. Precision for isotopic analysis was within ±0.28‰ for both $\delta^{13}C$ and $\delta^{15}N$.

Statistical Analyses

Production of benthic microalgae; gammarid and fish abundance at sites I, II, and III (four replicates for each); stomach content weight; and growth rate of juvenile marbled sole by experimental group were compared between the two stations (four replicates for each value per station) by Mann–Whitney *U*-test. Hourly SGD, salinity, DIN, DIP, Chl-a, and stomach content weight and growth rate of individual juvenile were compared between the two stations by Student's *t*-test. Stable carbon isotope ratio of the juveniles used for the cage experiment ($n = 15$ for each) and wild ($n = 20$ at st. e and $n = 6$ at st. f) was compared between the two stations by Mann–Whitney *U*-test. All of the statistical analyses were performed in R (3.4.1: R Development Core Team).

RESULTS

Primary Production and Primary and Secondary Consumers' Biomass at the Three Sites

At all sites (I, II, and III), the benthic microalgae production was significantly higher at the stations with a higher SGD signal (sts. a, c, and e) than at the stations with a lower SGD signal (sts. b, d, and f: Mann–Whitney *U*-test, $p < 0.05$ for all, **Figure 3**). The benthic microalgae were mostly composed of *Amphora* spp., *Navicula* spp., and *Synedra* spp. at all sites. The dominant fish species were Japanese sillago (*Sillago japonica*), surfperches (Embiotocidae spp.), and red seabream (*Pagrus major*) at sitessite I, II, and III,

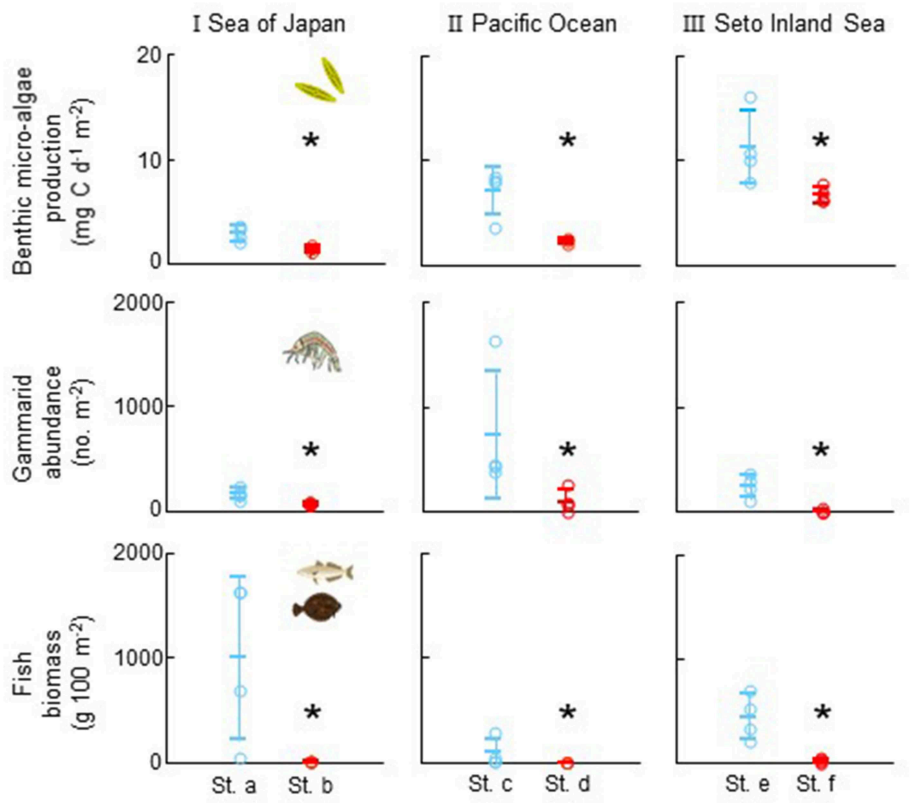

FIGURE 3 | Comparison of benthic microalgae production **(top)**, abundance of gammarids (as dominant primary consumer and also as major prey organisms for fish: **middle)** and fish biomass **(bottom)** between the two stations with different levels of ^{222}Rn concentrations as an indicator of SGD within each site (I: Sea of Japan, II: Pacific Ocean, and III: Seto Inland Sea). Circles indicate each data and bars show mean and standard deviation. Asterisk shows significant difference within each site (Mann–Whitney *U*-test, $p < 0.05$ for all).

respectively. The abundance of both gammarids and fishes was also significantly higher at the stations with higher SGD signal than at the stations with lower SGD signal (Mann–Whitney *U*-test, $p < 0.05$ for all, **Figure 3**).

Submarine Groundwater Discharge, Nutrient Supply, and Chlorophyll-a Concentration During the Mooring Time Series Surveys

During the mooring time series survey conducted at site III for the cage experiment, the mean hourly ^{222}Rn concentrations ranged between 31.6 and 97.9 Bq m^{-3} at st. e and between 23.8 and 70.6 Bq m^{-3} at st. f. There was a significant difference in the average of the mean hourly ^{222}Rn concentrations between the two stations [st. e: 54.3 (±20.1) Bq m^{-3}; st. f: 34.2 (±10.4) Bq m^{-3}, Student's *t*-test, $p = 0.0002$; **Figure 4A**]. The mean hourly SGD varied between 25.3 and 159.3 cm day^{-1} at st. e and between 1.9 and 32.8 cm day^{-1} at st. f. There was a significant difference in the average of the mean hourly SGD between the two stations (st. e: 99.8 cm day^{-1}; st. f: 4.9 cm day^{-1}, Student's *t*-test, $p < 0.0001$; **Figure 4B**). Average (±SD) of the mean hourly water temperature was 18.3°C (±0.25°C) and 18.2°C (±0.23°C) and values for salinity was 32.1 (±0.22) and 33.0 (±0.00) at sts. e and f, respectively. The difference was significant for salinity (Student's *t*-test, $p < 0.0001$; **Figure 4C**) but not for temperature ($p > 0.05$).

The hourly DIN concentration ranged between 0.61 and 1.05 μM at st. e and between 0.45 and 0.63 μM at st. f (**Figure 4D**). The hourly DIP concentration ranged between 0.14 and 0.26 μM at st. e and between 0.09 and 0.20 μM at st. f (**Figure 4E**). The means of both hourly DIN (st. e: 0.76 μM, st. f: 0.52 μM) and DIN (st. e: 0.20 μM, st. f: 0.16 μM) were significantly higher at st. e (Student's *t*-test, $p < 0.0001$ for both DIN and DIP).

The hourly Chl-a concentration ranged between 1.01 and 2.82 μg L^{-1} at st. e and between 1.07 and 1.72 μg L^{-1} at st. f. The average was slightly higher at st. e (1.94 μg L^{-1}) than at st. f (1.72 μg L^{-1}), without significant difference between the two sites (Student's *t*-test, $p = 0.058$; **Figure 4F**).

Feeding and Growth of Juvenile Marbled Sole by Cage Experiment

A total of 92.3% (12 of 13 fishes) and 72.7% (10 of 13 fishes) of juvenile marbled sole analyzed for their stomach contents at sts. e and f, respectively, had prey items in their stomachs. The most dominant prey organisms were gammarids, accounting for 71.2%

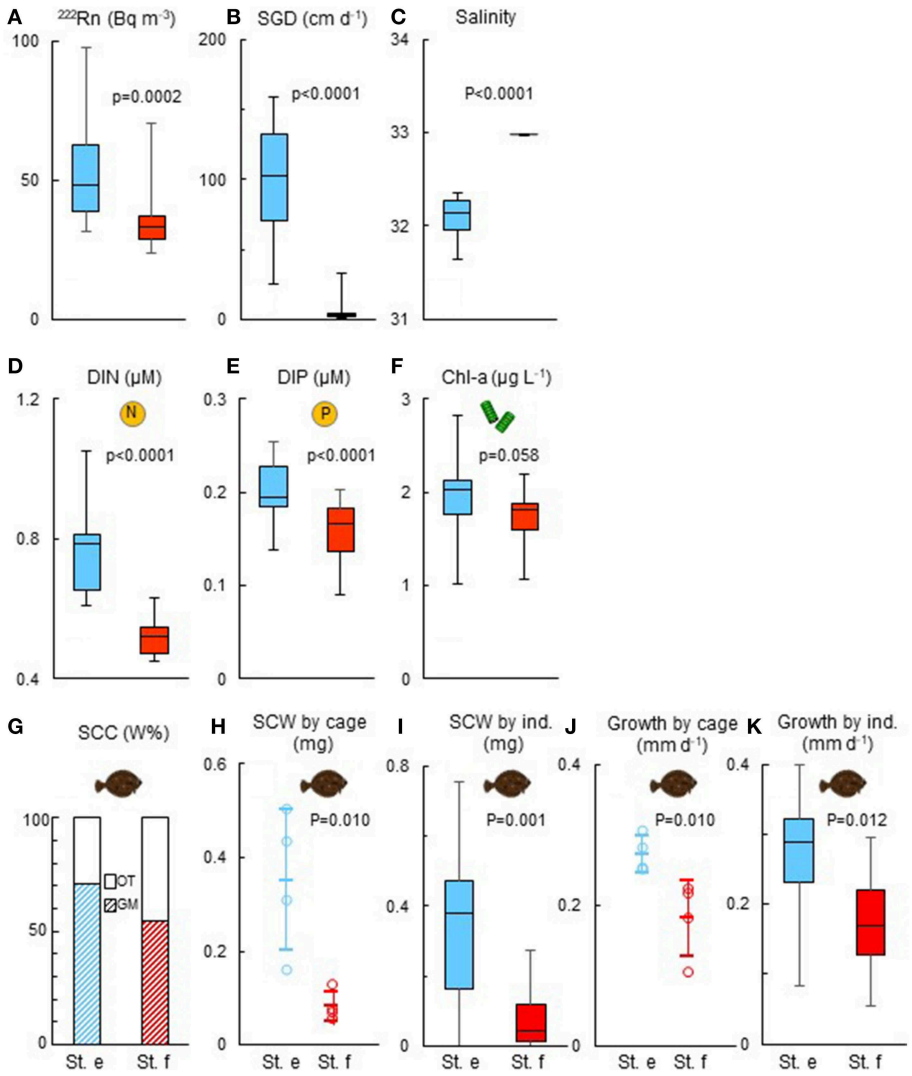

FIGURE 4 | Comparisons of ^{222}Rn **(A)**, submarine groundwater discharge (SGD: **B**), salinity **(C)**, dissolved inorganic nitrogen (DIN) **(D)**, dissolved inorganic phosphorus (DIP) **(E)**, and chlorophyll-a (Chl-a: **F**) concentrations monitored every hour for 24 h at sts. e and f in survey site III. Juvenile stomach content composition (SCC, weight%: **G**), stomach content weight (SCW) by cage **(H)** and individual fish **(I)**, and growth for 2 weeks by cage **(J)** and individual fish **(K)** were compared between the two stations at the end of the cage experiment. Vertical bars and boxes **(A–F,I,K)** indicate every 25% range of the data. Circles **(H,J)** indicate each data and bars show mean and standard deviation. The *p* value of statistical analysis for comparison between the two stations is presented for each panel (Student's *t*-test for **A–F,I,K**; Mann–Whitney *U*-test for **H,J**). Hourly data from Nakajima et al. (2018) were processed for panels **(A–C)** in the present study in order to provide evidence of SGD signal at the survey site.

at st. e and 54.7% at st. f, followed by ostracods (20.8% at st. e; 43.8% at st. f; **Figure 4G**). Other prey organisms accounted for 7.9 and 1.5% at sts. e and f, respectively.

Mean juvenile stomach content weight of each experimental group ranged between 0.16 ± 0.15 and 0.50 ± 0.17 mg at st. e and between 0.06 ± 0.03 and 0.13 ± 0.13 mg at st. f (**Figure 4H**). There was a significant difference between the two stations (Mann–Whitney *U*-test, $p < 0.05$). Mean of stomach content weight of individual juvenile at st. e (0.36 ± 0.09 mg) was also significantly higher than that at st. f (0.09 ± 0.02 mg; **Figure 4I**).

Mean juvenile growth rates by experimental group ranged between 0.25 ± 0.10 and 0.31 ± 0.07 mm day^{-1} at st. e and between 0.11 ± 0.03 and 0.22 ± 0.07 mm day^{-1} at st. f (**Figure 4J**). The difference between the two stations was significant (Mann–Whitney *U*-test, $p < 0.05$). Mean of individual juvenile growth rate at st. e (0.27 ± 0.09 mm day^{-1}) was also significantly higher than that at st. e (0.18 ± 0.07 mm day^{-1}: student's *t*-test, $p = 0.012$; **Figure 4K**).

Mean stable carbon isotope ratio of the juvenile marbled sole sampled at the end of the experiment from the cages at sts. e (−18.26 ± 0.19‰) and f (−18.11 ± 0.17‰) was intermediate between values of the juveniles sampled from the stock tank at the start of the cage experiment (−18.9 ± 0.46‰) and wild marbled sole juveniles collected at sts. e (−16.64 ± 0.32‰) and f (−16.00 ± 0.43‰; **Figure 5**). The stable carbon isotope ratio of the juveniles in the stock tank was slightly higher than the values

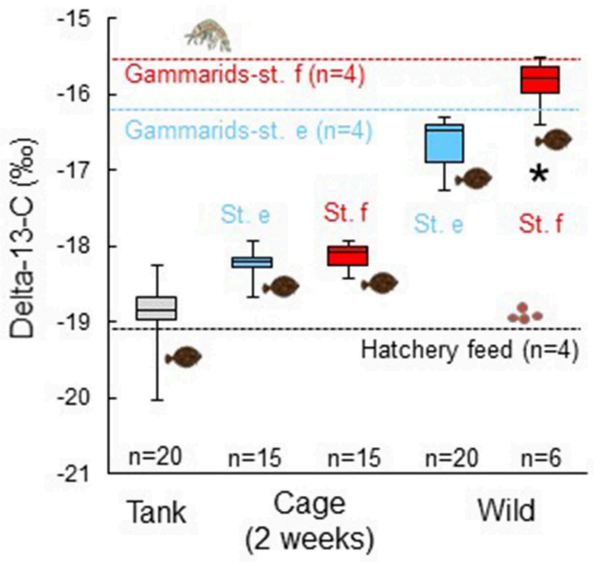

FIGURE 5 | Stable carbon isotope ratio of muscle of juvenile marbled sole sampled from the rearing tank before the experiment (Tank), after the cage experiment for 2 weeks (Cage), and wild marbled sole collected at sts. e and f (Wild). Vertical bars and boxes indicate every 25% range of the data. Mean values for gammarids as major prey organisms for the juvenile marbled sole at sts. e and f and hatchery feed for the juveniles are shown as broken lines. Asterisk shows a significant difference in the isotope ratio of wild fishes between sts. e and f ($p = 0.0006$).

of the hatchery feed (-19.08 ± 0.17‰) and the values of wild juveniles were slightly lower than those of gammarids collected at each station, with the most dominant prey item both in the juvenile stomachs and water (e: -16.16 ± 1.80‰; f: -15.66 ± 1.31‰). The stable carbon isotope ratio of the juvenile marbled flounder sampled from the cages was not significantly different between sts. e and f (Mann–Whitney U-test, $p = 0.504$). The values of both wild juvenile marbled sole and gammarids at st. e were lower than those at st. f. There was a significant difference in the stable carbon isotope ratio of the wild juveniles between the two stations (U-test, $p = 0.0006$).

DISCUSSION

In the present study, first direct evidence that fish feeding and growth were elevated by submarine groundwater was obtained by an on-site experiment and quantitative samplings. The experiment using cages moored on the sea bottom confirmed that the fishes obtained nutrition at a fixed place in nature. The quantitative sampling at three sites with different hydrodynamic properties showed that correspondence of high SGD with high biological production from producer to secondary consumers prevails in coastal marine areas. These findings demonstrate a missing trophic linkage in the coastal boundary area that originates from nutrients of terrestrial origin provided *via* submarine groundwater and promotes marine fish production.

Validity of Cage Experiment

The mean growth rate of juvenile marbled sole at the area with higher SGD (st. e: 0.22 ± 0.09 mm day^{-1} at 18.3 ± 0.25°C) approximates those of juveniles cultured under the same temperatures (0.25 mm day^{-1} at 17.8°C: Mutsutani, 1988; 0.11–0.96 mm day^{-1} at 8–26°C: Kusakabe et al., 2017), although the juvenile growth rate varies, being highly affected by ambient temperatures. It is plausible that the condition for feeding during the experiment at st. e was maintained at a level generally appropriate for their growth. The period of the experiment (2 weeks) is considered long enough to evaluate the effect of difference in environmental conditions for feeding on their growth because of the half-life period of carbon and nitrogen stable isotopic ratios in the juvenile muscles (about 2 weeks: Hamaoka et al., 2016). These results indicate that the difference observed in the feeding and growth of juvenile marbled sole between the experimental stations reflects the environmental properties that were affected by the presence/absence of effects of SGD in surrounding water.

Effects of Submarine Groundwater Discharge on Primary Production and Primary Consumer

Nutrients supplied *via* SGD increase microalgal and macrophyte biomass and production in marine ecosystems of the world (Lecher et al., 2015, 2017; Lecher and Mackey, 2018). In tropical systems, nitrogen-enriched groundwater enhances primary production of benthic ecosystems (Fourqurean et al., 1992; Peterson and Heck, 2001; Fourqurean and Zieman, 2002; Carruthers et al., 2005; Bowen et al., 2007; de Sieyes et al., 2008). In the present study, nutrients supplied *via* submarine groundwateris potentially important for primary production in the coastal sea areas because there are no rivers nearby the three survey sites. The higher primary production rate of benthic microalgae in the areas with high SGD commonly observed at all three sites with different hydrographic features in the present study shows that nutrients provided *via* SGD contributed to primary production in the benthic ecosystems in these sites. In the pelagic ecosystem, on the other hand, the effect of SGD on phytoplankton production has been reported to differ between types of SGD (Sugimoto et al., 2017). An *in situ* experiment to elucidate the response of phytoplankton primary productivity to SGD clarified that the mechanism by which SGD affects phytoplankton production differs from one ecosystem to another because of variable hydro-geographical properties, such as the type of groundwater discharge (i.e., spring type or seepage type: Sugimoto et al., 2017). At a site in Obama Bay, central Japan, which is characterized by seepage-type SGD, a significant positive relationship between *in situ* phytoplankton primary productivity and ^{222}Rn concentration was observed probably due to nutrient-limited water column conditions. On the other hand, at volcanic coastal sites in northern and southern Japan, which are dominated by spring-type SGD, no clear relationships between *in situ* phytoplankton primary productivity and ^{222}Rn concentration were found, suggesting that submarine springs have negative impacts on phytoplankton growth rates around

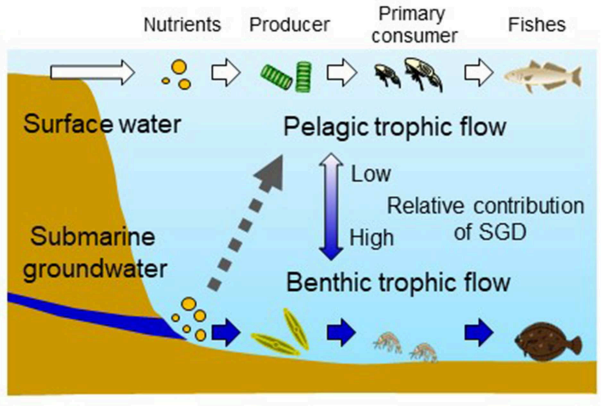

FIGURE 6 | A schematic drawing of contribution of nutrients provided by surface (river) water and SGD to pelagic and benthic trophic flows of coastal waters. Contribution of nutrients of SGD origin to the pelagic trophic flow has been still unknown or underestimated due to mixing of water and nutrients (indicated by an arrow with a broken line). Relative contributions of surface water and submarine groundwater are considered to be higher to the production of high-order ecosystem organisms of pelagic and benthic trophic flow, respectively. The contribution of nutrients of SGD origin to both pelagic and benthic trophic flows is assumed to be higher in an area where the influx of surface water is minimal and water mixing by tide prevails such as in the survey site III (Seto Inland Sea) in the present study.

vent sites, possibly due to gradient in environmental conditions such as temperature and salinity (Sugimoto et al., 2017).

In addition to the SGD type, tidal current would affect pelagic primary production through mixing water. The maximum DTA during spring tide period around site III located in the Seto Inland Sea exceeds 4 m. The chlorophyll-a concentration as an index of phytoplankton production was not significantly different between the two stations (sts. e and f) while difference in the benthic microalgae production was significant. In contrast, the effect of SGD on primary production would be more visible in the near-bottom layer of the water column regardless of physical properties and SGD types in each area. Consequently, the contribution of nutrition provided *via* SGD to the benthic food web is expected to be higher in coastal marine waters with high tidal mixing and less freshwater input through rivers flowing into the surrounding area as site III in the present study (**Figure 6**). Further studies applying the experimental protocols developed in the present study will enable elucidation of how SGD contributes to the pelagic and benthic food web depending on different tidal periods, geographical shapes of coastal area, and SGD type.

Groundwater discharge has been shown to have impacts on benthic microalgae and macrofauna in other coastal areas (Miller and Ullman, 2004; Waska and Kim, 2010). In the present study, the abundance of gammarids, the main prey organisms of juvenile marbled sole, was 2.4 (site I) to 15.2 (site III) times higher in the vicinity of the SGD (**Figure 3**). These gammarids include herbivores that feed on phytoplankton and benthic microalgae (Hata et al., 2016), showing the influence of SGD-originated nutrients on the primary consumer through elevation of the benthic primary production. Further, the gammarids seem to play an important role in connecting benthic primary production with high-order trophic level predators in the vicinity of SGD in the present study sites (**Figure 6**).

Influence on Fish Production

The present study is the first case to evaluate the influence of SGD on fish growth and feeding in marine coastal waters. The SGD has been believed to highly contribute to the coastal fisheries production at many locations of the world (Moosdorf and Oehler, 2017). To date, elevation of fish abundance and biomass has been observed in the vicinity of SGD (Hata et al., 2016; Shoji et al., 2017; Utsunomiya et al., 2017). However, whether the fishes grow utilizing the nutrients originated from SGD remains unknown. In the present study, the carbon stable isotope analysis supports the conclusion that nutrients of terrestrial origin provided *via* SGD were utilized by juvenile marbled sole. The stable carbon isotope ratio at the end of the field experiment was intermediate between juveniles sampled from the stock tank and wild juveniles, indicating that these juveniles in the cages were acclimating to prey organisms in nature during the 2-week experiment, which approximates the time length of half-life of the isotope ratio of this species (Hamaoka et al., 2016). The lower values of stable carbon isotope ratio of gammarids at st. e than at st. f would prove the higher influence of nutrients provided *via* SGD on marbled sole juveniles through benthic food web (Hata et al., 2016) prevailing at st. e than at st. f.

DATA AVAILABILITY

The raw data supporting the conclusions of this manuscript will be made available by the authors, without undue reservation, to any qualified researcher.

ETHICS STATEMENT

All applicable institutional and/or national guidelines for the care and use of animals were followed. The procedures and protocols followed the guidelines of the Committee for Animal Experiment of Hiroshima University (CD001651) and those for the use of fishes in research by the Ichthyological Society of Japan (http://www.fish-isj.jp/english/guidelines.html). No ethic or law violations are included in the present study.

AUTHOR CONTRIBUTIONS

KF, JS, RS, and MakT designed the study. KF, JS, RS, TN, HH, MasT, and OT performed the field survey. KF, JS, RS, TN, and HH analyzed data. JS and RS drafted the manuscript.

FUNDING

This study was partially supported by Grants-in-Aid for Scientific Research (B) (16H04971 and 17H04624 to JS) and by the Ministry of Agriculture, Forestry and Fisheries of Japan.

ACKNOWLEDGMENTS

The authors would like to thank Mr. Sadaharu Iwasaki, Yuji Terada, Shohei Takemoto, Kentaro Note, Kentaro Yoshikawa, and other members of the Takehara Marine Laboratory, Hiroshima University, for their assistance in the field experiment and two reviewers for their valuable comments on the manuscript.

REFERENCES

Bowen, J. L., Kroeger, K. D., Tomasky, G., Pabich, W. J., Cole, M. L., Carmichael, R. H., et al. (2007). A review of land–sea coupling by groundwater discharge of nitrogen to New England estuaries: mechanisms and effects. *Appl. Geochem.* 22, 175–191. doi: 10.1016/j.apgeochem.2006.09.002

Burnett, W. C., Kim, G., and Lane-Smith, D. (2001). A continuous monitor for assessment of 222Rn in the coastal ocean. *J. Radioanal. Nucl. Chem.* 249, 167–172. doi: 10.1023/A:1013217821419

Carruthers, T. J. B., van Tussenbroek, B. I., and Dennison, W. C. (2005). Influence of submarine springs and wastewater on nutrient dynamics of Caribbean seagrass meadows. *Est. Coast. Shelf Sci.* 64, 191–199. doi: 10.1016/j.ecss.2005.01.015

Charette, M. A., Moore, W. S., and Burnett, W. C. (2008). "Uranium- and thorium-series nuclides as tracers of submarine groundwater discharge," in *U–Th Series Nuclides in Aquatic Systems,* eds S. Krishnaswami and J. Kirk-Cochran (Amsterdam: Elsevier), 155–91.

Church, T. M. (1996). An underground route for the water cycle. *Nature* 380, 579–580. doi: 10.1038/380579a0

de Sieyes, N., Yamahara, K., Layton, B., Joyce, E., and Boehm, A. (2008). Submarine discharge of nutrient-enriched fresh groundwater at Stinson Beach, California is enhanced during neap tides. *Limnol. Oceanogr.* 53, 1434–1445. doi: 10.4319/lo.2008.53.4.1434

Dimova, N., Burnett, W. C., and Lane-Smith, D. (2009). Improved automated analysis of radon (222Rn) and thoron (220Rn) in natural waters. *Environ. Sci. Technol.* 43, 8599–8603. doi: 10.1021/es902045c

Field, C. B., Behrenfeld, M. J., Randerson, J. T., and Falkowski, P. (1998). Primary production of the biosphere: integrating terrestrial and oceanic components. *Science* 281, 237–240. doi: 10.1126/science.281.5374.237

Fourqurean, J. W., and Zieman, J. C. (2002). Nutrient content of the seagrass *Thalassia testudinum* reveals regional patterns of relative availability of nitrogen and phosphorus in the Florida Keys USA. *Biogeochemistry* 61, 229–245. doi: 10.1023/A:1020293503405

Fourqurean, J. W., Zieman, J. C., and Powell, G. V. N. (1992). Phosphorus limitation of primary production in Florida Bay: evidence from C:N:P ratios of the dominant seagrass, *Thalassia testudinum*. Limnol. *Oceanogr.* 37, 162–171. doi: 10.4319/lo.1992.37.1.0162

Fujita, K., Tomiyama, T., and Shoji, J. (2017). "Does submarine groundwater discharge affect growth of juvenile flatfish? A cage experiment in the Seto Inland Sea, Japan," in *Abstract retrieved from Abstract book of the International Flatfish Symposium-2017* (Saint-Malo).

Hamaoka, H., Shoji, J., and Hori, M. (2016). Turnover rates of carbon and nitrogen stable isotopes in juvenile marbled flounder *Pleuronectes yokohamae* estimated by diet switch. *Ichthyol. Res.* 63, 201–206. doi: 10.1007/s10228-015-0488-1

Hata, M., Sugimoto, R., Hori, M., Tomiyama, T., and Shoji, J. (2016). Occurrence, distribution and prey items of juvenile marbled sole *Pseudopleuronectes yokohamae* around a submarine groundwater seepage on a tidal flat in southwestern Japan. *J Sea Res.* 111, 47–53. doi: 10.1016/j.seares.2016.01.009

Holmes, R. M., Aminot, A., Kerouel, R., Hooker, B. A., and Peterson, B. J. (1999). A simple and precise method for measuring ammonium in marine and freshwater ecosystems. *Can. J. Fish. Aquat. Sci.* 56, 1801–1808. doi: 10.1139/f99-128

Honda, H., Taniguchi, M., Ono, M., Hosono, T., Umezawa, Y., Sugimoto, R., et al. (2015). "Relationship between radon-222 concentrations in coastal water and environmental conditions in Japan," *Abstract retrieved from Abstract book of the 10th International Conference on the Methods and Applications of Radioanalytical Chemistry MARC X* (Kailua-Kona, HI).

Hosono, T., Ono, M., Burnett, W. C., Tokunaga, T., Taniguchi, M., and Akimichi, T. (2012). Spatial distribution of submarine groundwater discharge and associated nutrients within a local coastal area. *Environ. Sci. Technol.* 46, 5319–5326. doi: 10.1021/es2043867

Kamimura, Y., and Shoji, J. (2013). Does macroalgal vegetation cover influence post-settlement survival and recruitment potential of juvenile black rockfish Sebastes cheni? *Estuar. Coast. Shelf Sci.* 129, 86–93. doi: 10.1016/j.ecss.2013.05.028

Kim, G., Ryu, J. W., Yang, H. S., and Yun, S. T. (2005). Submarine groundwater discharge (SGD) into the Yellow Sea revealed by 228Ra and 226Ra isotopes: implications for global silicate fluxes. *Earth Planet. Sci. Lett.* 237, 156–166. doi: 10.1016/j.epsl.2005.06.011

Kobayashi, S., Ikuta, K., Sugimoto, R., Honda, H., Yamada, M., Tominaga, O., et al. (2019). Estimation of submarine groundwater discharge and its impact on nutrient environment in Kamaiso beach, Yamagata, Japan. *Bull. Jap. Soc. Fish. Sci.* 85, 30–39. doi: 10.2331/suisan.18-00020

Kobayashi, S., Sugimoto, R., Honda, H., Miyata, Y., Tahara, D., Tominaga, O., et al. (2017). High-resolution mapping and time-series measurements of 222Rn concentrations and biogeochemical properties related to submarine groundwater discharge along the coast of Obama Bay, a semi-enclosed sea in Japan. *Prog. Earth Planet. Sci.* 4:6. doi: 10.1186/s40645-017-0124-y

Kusakabe, K., Hata, M., Shoji, J., Hori, M., and Tomiyama, T. (2017). Effects of water temperature on feeding and growth of juvenile marbled flounder *Pseudopleuronectes yokohamae* under laboratory conditions: evaluation by group- and individual-based methods. *Fisheries Sci.* 83, 215–219. doi: 10.1007/s12562-016-1053-1

Lecher, A. L., Mackey, K., Kudela, R., Ryan, J., Fisher, A., Murray, J., et al. (2015). Nutrient loading through submarine groundwater discharge and phytoplankton growth in Monterey bay, CA. *Environ. Sci. Technol.* 49, 6665–6673. doi: 10.1021/acs.est.5b00909

Lecher, A. L., and Mackey, K. R. M. (2018). Synthesizing the effects of submarine groundwater discharge on marine biota. *Hydrology* 5:60. doi: 10.3390/hydrology5040060

Lecher, A. L., Mackey, K. R. M., and Paytan, A. (2017). River and submarine groundwater discharge effects on diatom phytoplankton abundance in the Gulf of Alaska. *Hydrology* 4:61. doi: 10.3390/hydrology4040061

Miller, D. C., and Ullman, W. J. (2004). Ecological consequences of ground water discharge to Delaware Bay, United States. *Ground Water* 42, 959–970. doi: 10.1111/j.1745-6584.2004.tb02635.x

Moosdorf, N., and Oehler, T. (2017). Societal use of fresh submarine groundwater discharge: an overlooked water resource. *Earth Sci. Rev.* 171, 338–348. doi: 10.1016/j.earscirev.2017.06.006

Mutsutani, K. (1988). Growth and metamorphosis of the marbled sole larvae limanda yohohamae (GÜNTER) in culture. *Aquacul. Sci.* 36, 27–32.

Nagata, T., and Miyajima, T. (2008). *Stable Isotopes in Environmental Assessment of Watersheds—Progress Towards an Integrated Approach*. Kyoto: Kyoto University Press.

Nakajima, T., Sugimoto, R., Tominaga, O., Takeuchi, M., Honda, H., Shoji, J., et al. (2018). Fresh and recirculated submarine groundwater discharge evaluated by geochemical tracers and a seepage meter at two sites in the Seto Inland Sea, Japan. *Hydrology* 5:61. doi: 10.3390/hydrology5040061

Peterson, B. J., and Heck, K. L. Jr. (2001). Positive interactions between suspension-feeding bivalves and seagrass: Aa facultative mutualism. *Mar. Ecol. Prog. Ser.* 213, 143–155. doi: 10.3354/meps213143

Peterson, B. J., Stubler, A. D., Wall, C. C., and Gobler, C. J. (2012). Nitrogen-rich groundwater intrusion affects productivity, but not herbivory, of the tropical seagrass *Thalassia testudinum*. *Aquat. Biol.* 15, 1–9. doi: 10.3354/ab00413

Rodellas, V., Garcia-Orellanaa, J., Masquéa, P., Feldmane, M., and Weinsteine, Y. (2015). Submarine groundwater discharge as a major source of nutrients to the Mediterranean Sea. *Proc. Natl. Acad. Sci. U.S.A.* 112, 3926–3930. doi: 10.1073/pnas.1419049112

Sanders, T. G. Jr., Biddanda, B. A., Stricker, C. A., and Nold, S. C. (2011). Benthic macroinvertebrate and fish communities in Lake Huron are linked to submerged groundwater vents. *Aquat. Biol.* 21, 1–11. doi: 10.3354/ab00318

Santos, I. R., Peterson, R. N., Eyre, B. D., and Burnett, W. C. (2010). Significant lateral inputs of fresh groundwater into a stratified tropical estuary: evidence from radon and radium isotopes. *Mar. Chem.* 121, 37–48. doi: 10.1016/j.marchem.2010.03.003

Shoji, J., Sugimoto, R., and Tominaga, O. (2017). *Land–Ocean Interactions Through Groundwater/Submarine Groundwater and Human Society*. Tokyo: Koseisha-koseikaku.

Sirois, P., and Dodson, J. J. (2000). Influence of turbidity, food density and parasites on the ingestion and growth of larval rainbow smelt *Osmerus mordax* in an estuarine turbidity maximum. *Mar. Ecol. Prog. Seri.* 193, 167–179. doi: 10.3354/meps193167

Slomp, C. P., and van Cappellen, P. (2004). Nutrient inputs to the coastal ocean through submarine groundwater discharge: controls and potential impact. *J. Hydrol.* 295, 64–86. doi: 10.1016/j.jhydrol.2004.02.018

Stieglitz, T. C., van Beek, P., Souhaut, M., and Cook, P. G. (2013). Karstic groundwater discharge and seawater recirculation through sediments in shallow coastal Mediterranean lagoons, determined from water, salt and radon budgets. *Mar. Chem.* 156, 73–84. doi: 10.1016/j.marchem.2013.05.005

Sugimoto, R., Honda, H., Kobayashi, S., Takao, Y., Tahara, D., Tominaga, O., et al. (2016). Seasonal changes in submarine groundwater discharge and associated nutrient transport into a tideless semi-enclosed embayment (Obama Bay, Japan). *Estuar. Coast.* 39, 13–26. doi: 10.1007/s12237-015-9986-7

Sugimoto, R., Kitagawa, K., Nishi, S., Honda, H., Yamada, M., Kobayashi, S., et al. (2017). Phytoplankton primary productivity around submarine groundwater discharge in nearshore coasts. *Mar. Ecol. Prog. Seri.* 563, 25–33. doi: 10.3354/meps11980

Swarzenski, P. W., Reich, C., Kroeger, K. D., and Baskaran, M. (2007). Ra and Rn isotopes as natural tracers of submarine groundwater discharge in Tampa Bay, Florida. *Mar. Chem.* 104, 69–84. doi: 10.1016/j.marchem.2006.08.001

Taniguchi, M., Burnett, W. C., Cable, J. E., and Turner, J. V. (2002). Investigation of submarine groundwater discharge. *Hydrol. Process* 16, 2115–2129. doi: 10.1002/hyp.1145

Taniguchi, M., and Iwakawa, H. (2001). Measurements of submarine groundwater discharge rates by a continuous heat-type automated seepage meter in Osaka Bay, Japan. *J. Groundwater Hydrol.* 43, 271–277. doi: 10.5917/jagh1987.43.271

Tomas, F., Abbott, J. M., Steinberg, C., Balk, M., Williams, S. L., and Stachowicz, J. J. (2011). Plant genotype and nitrogen loading influence seagrass productivity, biochemistry, and plant-herbivore interactions. *Ecology* 92, 1807–1817. doi: 10.1890/10-2095.1

Utsunomiya, T., Hata, M., Sugimoto, R., Honda, H., Kobayashi, S., Miyata, Y., et al. (2017). Higher species richness and abundance of fish and benthic invertebrates around submarine groundwater discharge in Obama Bay, Japan. *J. Hydrol.* 11, 139–146. doi: 10.1016/j.ejrh.2015.11.012

Valiela, I., Costa, J., Foreman, K., Teal, J. M., Howes, B., and Aubrey, D. (1990). Transport of groundwater-borne nutrients from watersheds and their effects on coastal waters. *Biogeochemistry* 10, 177–197. doi: 10.1007/BF00003143

Wada, T., Aritaki, M., Yamashita, Y., and Tanaka, M. (2007). Comparison of low-salinity adaptability and morphological development during the early life history of five pleuronectid flatfishes, and implications for migration and recruitment to their nurseries. *J. Sea Res.* 58, 241–254. doi: 10.1016/j.seares.2007.03.004

Waska, H., and Kim, G. (2010). Differences in microphytobenthos and macrofaunal abundances associated with groundwater discharge in the intertidal zone. *Mar. Ecol. Prog. Ser.* 407, 159–172. doi: 10.3354/meps08568

Conflict of Interest Statement: The authors declare that the research was conducted in the absence of any commercial or financial relationships that could be construed as a potential conflict of interest.

frontiers in Marine Science

ORIGINAL RESEARCH
published: 02 July 2019
doi: 10.3389/fmars.2019.00357

Theoretical Assessment of the Effect of Vertical Dispersivity on Coastal Seawater Radium Distribution

Sébastien Lamontagne[1] and Ian T. Webster[2]*

[1] CSIRO Land & Water, Waite Laboratories, Urrbrae, SA, Australia, [2] Retired, Canberra, ACT, Australia

Trends in radium (Ra) activity in coastal seawater are frequently used to infer submarine groundwater discharge. In general, unlike in the deep oceans, Ra samples are only collected from the surface of the mixed layer in coastal areas. The assumption is that the water column is well mixed, as often evidenced by uniform temperature and salinity profiles. However, if the timescale for vertical mixing is similar to or less than the timescale for radioactive decay, the vertical profiles in Ra activity may not be uniform. In the present work, a two-dimensional dispersion model was developed to evaluate the potential effects of slow vertical mixing on Ra distribution in the mixed layer of an inner shelf. The variables considered were the vertical coefficient of solute dispersivity (K_z), the offshore coefficient of solute dispersivity (K_x), the coastal Ra flux (F_o), the benthic Ra flux (F_B), and the slope of the seabed. The shorter-lived Ra isotopes (^{223}Ra and ^{224}Ra; $t_{1/2}$ = 3.66 and 11.4 days, respectively) were sensitive to K_z when its value was low ($<10^{-4}$ m^2 s^{-1}), resulting in complex activity patterns in the water column as a function of the other variables. Ra-228 ($t_{1/2}$ = 5.75 years) was only moderately impacted by low K_z but the long-lived ^{226}Ra ($t_{1/2}$ = 1600 years) was insensitive to K_z. Surface water samples may not always be representative of water column Ra activity when K_z is low, which will need to be taken into account in future field programs for seawater Ra distribution in shelf environments.

Keywords: submarine groundwater discharge, radium, dispersion, vertical mixing, seawater

OPEN ACCESS

Edited by:
Henrietta Dulai, University of Hawai'i at Mānoa, United States

Reviewed by:
Joseph James Tamborski, Woods Hole Oceanographic Institution, United States
Jennifer Joan Verduin, Murdoch University, Australia

****Correspondence:***
Sébastien Lamontagne
sebastien.lamontagne@csiro.au

Specialty section:
This article was submitted to Marine Ecosystem Ecology, a section of the journal Frontiers in Marine Science

Received: *01 March 2019*
Accepted: *07 June 2019*
Published: *02 July 2019*

Citation:
Lamontagne S and Webster IT (2019) Theoretical Assessment of the Effect of Vertical Dispersivity on Coastal Seawater Radium Distribution. Front. Mar. Sci. 6:357. doi: 10.3389/fmars.2019.00357

INTRODUCTION

The radium (Ra) quartet (^{223}Ra, ^{224}Ra, ^{226}Ra, and ^{228}Ra) are among the most commonly used environmental tracers for evaluating submarine groundwater discharge (SGD) (Charette and Scholten, 2008), including its terrestrial groundwater and recirculated seawater components (Burnett et al., 2003). One common experimental design to evaluate SGD with these tracers is to collect water samples along transects perpendicular to the shoreline, and use simple advective-dispersive transport models to quantify the offshore coefficient of solute dispersivity (K_x), the tracer flux from the coastline (F_o), and the tracer flux from the seabed (F_B) (Moore, 2000; Hancock et al., 2006). Several assessments have been made of the validity of this approach. For example, Knee et al. (2011) have shown how activity measurement error can bias the application of the Ra transport models, Moore (2015) highlighted some of the limitations in the use of ^{228}Ra and ^{226}Ra to evaluate mixing and advection rates, Li and Cai (2011) evaluated the effect of neglecting advection on K_x estimates, and Lamontagne and Webster (2019) showed how K_x could be tracer-dependent.

However, unlike in deep oceans and shelf environments, where ^{228}Ra, ^{226}Ra, and ^{222}Rn vertical profiles have been used to estimate vertical mixing (Broecker et al., 1967; Chung and Craig, 1973; Glover and Reeburgh, 1987; Koch-Larrouy et al., 2015), Ra measurement in shallower inner shelf environments are typically only taken from the top of the mixed layer (Moore, 2000; Dulaiova and Burnett, 2006; Lamontagne et al., 2008). The assumption is that vertical mixing is relatively rapid in the mixed layer so Ra activities should be approximately uniform vertically. However, few studies have been conducted to test this assumption (see below). A water column may appear to be well mixed as evidenced by near uniformity in temperature or salinity profiles but may appear to be less well mixed for radioactive tracers if the timescale of mixing is similar to, or longer, than the timescale of radioactive decay.

Where vertical Ra profiles have been measured on the inner shelf, some variations in activity have been reported. For example, Moore et al. (1995) observed noticeable vertical variations in ^{226}Ra, ^{228}Ra, and ^{224}Ra on the Amazon shelf, but these were attributed in part to variations in salinity (i.e., mixing of different sources of water). Levy and Moore (1985) observed increases in ^{224}Ra activity with depth in the mixed layer off the coast of South Carolina and Georgia, which they attributed to input from the seafloor. During an extensive survey of the South Atlantic Bight, occasional sampling near the surface and the bottom of the mixed layer showed that in most cases Ra activities were similar (Moore, 2007). Thus, vertical variations in Ra activity in the mixed layer may occur under some conditions in inner shelf environments.

Here, a theoretical assessment was made to show how variations in the vertical mixing rate could influence water column Ra activities in a shelf environment. As the focus here was on the short-lived Ra isotopes (^{223}Ra and ^{224}Ra), only dispersive transport was considered because advective transport in the offshore direction is usually not important for them (Lamontagne and Webster, 2019). The assessment was made by developing a two-dimensional model that included dispersion in the vertical direction, based on a previous one-dimensional offshore dispersive transport model by Hancock et al. (2006). In a first step, the effect of variations in the vertical coefficient of solute dispersivity (K_z) on Ra distribution in the water column was evaluated. In a second step, the effect of other transport variables (K_x, F_o, and F_B) on Ra distribution in the water column was evaluated.

In the following, the 2D model is described along with the range in parameter values considered. Whether the current experimental design for tracer surveys in coastal areas provides biased estimates of water column Ra activities is discussed.

MATERIALS AND METHODS

In this study, the model domain for Ra transport was considered to be the cross-section of a sloping continental shelf (**Figure 1**). The sources of Ra to the water column were from the coast and the seabed. Tracer transport was assumed to occur via dispersive processes only, which can be described by the diffusion equation in the x (offshore) and z (depth) directions:

$$\frac{\partial A}{\partial t} = \frac{\partial K_x \partial A}{\partial^2 x} + \frac{\partial K_z \partial A}{\partial^2 z} - \lambda A \quad (1)$$

where A is the Ra activity, t is time and λ the decay constant for a given isotope. Considering the steady-state condition and anisotropic cross-section, Eq. (1) simplifies to:

$$K_x \frac{\partial^2 A}{\partial x^2} + K_z \frac{\partial^2 A}{\partial z^2} = \lambda A \quad (2)$$

This equation was solved numerically using the finite difference method. The numerical grid incorporated a single cell at the coastline and 200 vertical cells at the offshore boundary (**Figure 1**). Boundary conditions included a constant flux F_o (Bq m^{-1} s^{-1}) at the coastline and a constant benthic flux F_B (Bq m^{-1} s^{-1}) spread evenly between the cells on the seabed. A no-flux boundary condition (F_e = 0) was assigned to the offshore end. Cell dimensions were 200 m in the x and 2 m in the z directions, ensuring the offshore boundary was far enough away from the coast (40 km) in order to reasonably meet the F_e = 0 boundary condition at this boundary (vertical profiles were investigated for the first 10 km only).

The literature was scanned for a reasonable range in K_x, K_z, F_o, and F_B for a shelf environment – these are summarized in **Tables 1**, **2**. In a first step, Eq. (2) was solved for different K_z values for each Ra isotope using default values for K_x, F_o, and F_B (**Table 2**). This process identified which isotope if any was sensitive to variations in K_z in terms of uneven activity distribution in the water column. For those isotopes sensitive to K_z, the additional effects of variations in K_x, F_o, F_B, and seabed slope (m) on vertical Ra distribution were evaluated for a relatively low K_z value. The MATLAB script used to solve Eq. (2) is provided as **Supplementary Material**.

RESULTS

K_z

The range of K_z values found in the literature – including both coastal and deep ocean areas – spanned 7.5 × 10^{-6} to 10^{-1} m^2 s^{-1}. Thus, K_z values ranging from 10^{-6} to 10^{-2} m^2 s^{-1} were used here. Variations in K_z did result in noticeable changes in the vertical and horizontal distribution of the shorter-lived tracers. For example, when using the default values for F_o and F_B for ^{223}Ra, K_z = 10^{-6} m^2 s^{-1}, and K_x = 10 m^2 s^{-1}, ^{223}Ra distribution was clearly lower at the surface than at depth at a given distance from the shoreline, especially when farther offshore (**Figure 2**).

The simulations showed that vertical patterns in Ra activity as a function of K_z were complex, with the highest activities either at the surface, the seabed, or at intermediate depths depending on the magnitude of K_z, the Ra isotope, and the offshore distance. To emphasize these, vertical variations in Ra activity were demonstrated at x = 2, 5, and 10 km for various K_z values (**Figure 3**). In general, water column Ra activity was nearly constant when K_z > 10^{-4} m^2 s^{-1}, with the exception of the longest – lived ^{226}Ra which was insensitive to K_z under

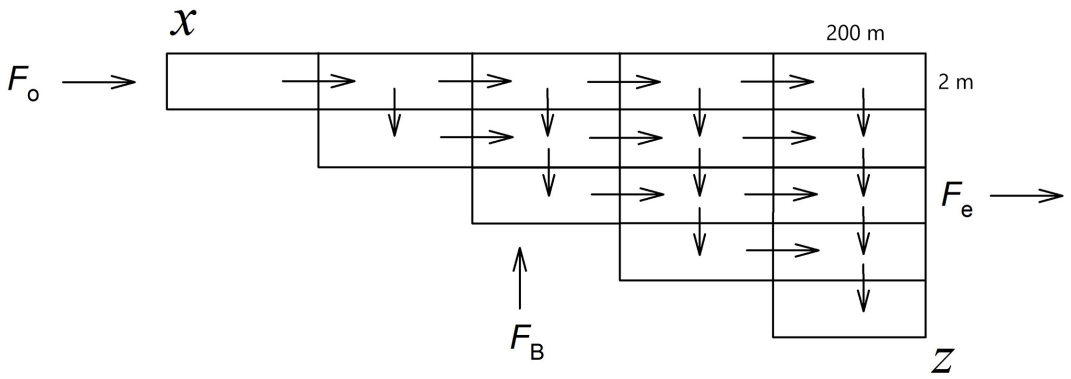

FIGURE 1 | Conceptual representation of the cross-section for a sloping continental shelf with key boundary conditions controlling the Ra flux. F_o, coastal flux; F_B, benthic flux; F_e, offshore boundary flux (set to 0). Solute exchange between cells occurs via dispersive processes.

the conditions tested. For the cases when $K_z < 10^{-4}$ m^2 s^{-1}, ^{223}Ra and ^{224}Ra activities were highest near the seabed at 2 km and in proximity of the surface at 5 and 10 km. The differences in activity through the water column were substantial at low K_z values for ^{223}Ra and ^{224}Ra. For example, ^{224}Ra activities at 2 km were ∼2 mBq L^{-1} near the surface and ∼ 5 mBq L^{-1} near the seabed. The differences in activity through the water column were more subdued for ^{228}Ra and only noticeable at the lowest K_z value. For example, ^{228}Ra at 2 km varied from ∼0.30 to ∼0.35 mBq L^{-1} through the water column (which would probably not be apparent in a field setting due to measurement uncertainty). Overall, only sampling for surface water would tend to bias the estimate of water column activity at low K_z values for ^{223}Ra, ^{224}Ra, and possibly ^{228}Ra but not for ^{226}Ra under the conditions evaluated.

K_x

In addition to slow mixing of the water column, the complex distribution in Ra activity at low K_z also reflects the presence of two sources of Ra (coast and seabed) and how Ra from these sources is being dispersed through the water mass, especially as it becomes deeper offshore. Firstly, the effect of K_x was evaluated for ^{224}Ra, ^{223}Ra, and ^{228}Ra for a relatively low K_z value (10^{-5} m^2 s^{-1}). Ra-226 was not evaluated because it was insensitive to K_z under the conditions tested, as demonstrated in the previous section.

The horizontal and vertical ^{223}Ra and ^{224}Ra distributions were substantially impacted by variations in K_x (**Figure 4**). In general, there was a tendency for the lowest ^{223}Ra and ^{224}Ra activities to be found near the seabed at low K_x values and near the surface at the higher K_x values. For example, for ^{224}Ra at 5 km (**Figure 4B**), activities were ∼0.5 mBq L^{-1} near the surface and ∼0.1 mBq L^{-1} near the seabed for $K_x \leq 1$ m^2 s^{-1} but ∼0.3 mBq L^{-1} near the surface and ∼1.5 mBq L^{-1} near the seabed for $K_x = 100$ m^2 s^{-1}. In other words, with a low K_z and a high K_x, there is a tendency for Ra produced via a benthic source to be exported in the offshore direction rather than to be mixed into the overlying water column (see also **Figure 2**). Whilst the overall magnitude of the activity changed, unlike for ^{223}Ra and ^{224}Ra, variations in K_x did not noticeably change the vertical distribution in ^{228}Ra.

F_o, F_B, and Seabed Slope

For simplicity, this part of the analysis only considered ^{224}Ra (the worst-case scenario due to its shortest half-life). Variations in the magnitude of the coastal and seabed fluxes as well as seabed slope had a noticeable impact on the vertical ^{224}Ra profiles (using $K_z = 10^{-5}$ m^2 s^{-1}). Changing the magnitude of F_o changed vertical ^{224}Ra profiles when getting closer to the shoreline (**Figures 5A,B**) but not offshore (**Figure 5C**). This demonstrated that the coastal flux does not contribute any ^{224}Ra to the water column at 10 km and beyond under the conditions tested (i.e., all the ^{224}Ra originates from the seabed). In contrast, variations in F_B impacted the profiles at 2, 5, and 10 km with a tendency for ^{224}Ra activity to be highest near the surface at higher F_B (**Figures 5D–F**) This may seem counterintuitive at first but can be explained by the sloping seabed. The highest ^{224}Ra activities occur near the shoreline due the combined F_o and F_B fluxes and a smaller dilution potential in the shallower water column there (**Figure 2**). This ^{224}Ra is then primarily dispersed laterally (that is, near the surface) due to $K_x >> K_z$ in the simulations.

The assessment of the effect of seabed slope (m) required a small modification to the finite difference model, where the thickness of the cells on the z-axis was modified (to 1 m for $m = 0.005$ and 4 m for $m = 0.02$). These simulations suggested that a bias associated with slow vertical mixing would tend to become more significant along transects with deeper mixed layers (**Figures 5G–I**), especially farther offshore.

DISCUSSION

Whilst the simulations were based on a simplistic representation of solute transport in coastal environments, especially for vertical mixing (Pacanowski and Philander, 1981; Durski et al., 2004), they clearly indicated that short-lived radiotracers like ^{223}Ra and ^{224}Ra may have a non-uniform vertical activity distribution

in shelf environments when vertical dispersion is low. This is of concern for the design of sampling programs for SGD tracers in coastal environments, where only surface water samples are often collected. Moreover, it is not possible to generalize if there will be a tendency to under- or overestimate whole water column activities by surface water sampling because this will be in part determined by other factors, such as location along the transect, K_x, and the source and magnitude of the tracer flux.

TABLE 1 | Literature estimates for K_z in different marine environments.

K_z (m^2 s^{-1})	Location	References
7.5×10^{-6}	Monterey Bay Shelf, California	Moniz et al., 2014
9×10^{-5}	Swan River Estuary, Australia	Etemad-Shahidi and Imberger, 2001
5×10^{-5} to 1.5×10^{-4}	Southwest Gulf of Maine	Benitez-Nelson et al., 2000
2.7×10^{-4}	North West Shelf, Australia	Webster, 1986
4×10^{-4}	Sea of Japan	Okubo, 1980
2×10^{-3}	Inner Shelf, Bering Sea	Glover and Reeburgh, 1987
10^{-3} to 10^{-2}	Southern Ocean	Charette et al., 2007
10^{-4} to 10^{-3}	Atlantic Ocean	Broecker et al., 1967
10^{-2}	Pacific Ocean	Broecker et al., 1967
10^{-6} to 10^{-1}	Indonesian Archipelago	Koch-Larrouy et al., 2015
10^{-2}	Surf zone	Kumar and Feddersen, 2017

Whilst methodology vary, the lower K_z are typically associated with coastal environments rather than the open ocean.

TABLE 2 | Parameter range for K_z, K_x, F_o, and F_B used in the simulations.

Variable	Range	References
K_z (m^2 s^{-1})	10^{-6}, $\underline{10^{-5}}$, 10^{-4}, 10^{-3}, and 10^{-2}	Refer to **Table 1**
K_x (m^2 s^{-1})	0.01, 0.1, $\underline{1}$, 10, and 100	de Silva Samarasinghe et al., 2003; Colbert and Hammond, 2007; Lamontagne and Webster, 2019
F_o and F_B (Bq m^{-1} s^{-1})		
^{223}Ra and ^{224}Ra	0.01, 0.1, $\underline{1}$, 10, 1, and 00	Lamontagne et al., 2015; Lamontagne and Webster, 2019
^{228}Ra	10^{-5}, 10^{-4}, $\underline{10^{-3}}$, and 10^{-2}	Lamontagne et al., 2015; Lamontagne and Webster, 2019
^{226}Ra	10–^{6}, 10^{-5}, $\underline{10^{-4}}$, and 10^{-3},	Lamontagne et al., 2015; Lamontagne and Webster, 2019
Seabed slope (*m*)	0.002, $\underline{0.01}$, and 0.02	

Underlined values represents the default unless otherwise noted in the text. For simplicity, a similar range in F_o and F_B was used for a given isotope to contrast the effect of the coastal and benthic Ra sources.

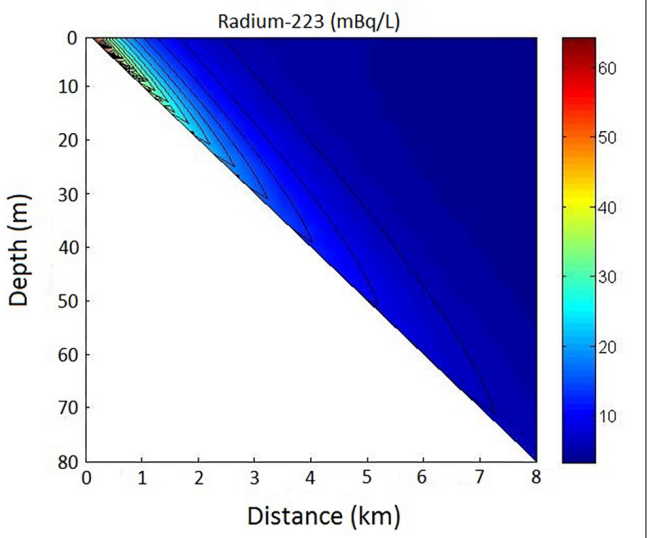

FIGURE 2 | Variations in ^{223}Ra activity in the water column for a relatively low K_z (10^{-6} m^2 s^{-1}) and high K_x (10 m^2 s^{-1}).

Lietzke and Lerman (1975) made similar observations to this study when evaluating the role of anisotropy in diffusivity on the vertical distribution in ^{222}Rn in Santa Barbara Basin. As for ^{223}Ra and ^{224}Ra distribution along a sloping seabed evaluated here, they found that much of the ^{222}Rn in the water column of this basin was from benthic production at shallower depth moving laterally owing to $K_x >> K_z$. The basin also had a noticeable vertical gradient in ^{222}Rn activity. Levy and Moore (1985) occasionally observed vertical ^{224}Ra gradients in the mixed layer off the coast of North Carolina and Georgia, which they attributed to a ^{224}Ra input from the seafloor. Such gradients may be more common than previously recognized for shelf environments.

Comparison With Characteristic Mixing Timescales

The simulation results are consistent with a qualitative assessment of the characteristic timescales of vertical mixing relative to radioactive decay. In general, transport processes tend to be less important in the mass-balance of a tracer when they occur more slowly than radioactive decay. For example, the characteristic timescale for vertical mixing by dispersion will be L^2/K_z, where L (m) is a representative mixed layer thickness. If $L^2/K_z >> 1/\lambda$, then vertical mixing is unlikely to contribute to differences in Ra activity in the water column. For example, assuming L = 20 m and $K_z = 10^{-5}$ m^2 s^{-1}, the characteristic timescale for vertical mixing will be 4×10^7 s, whereas the timescales for radioactive decay (=$1/\lambda$) are 4.6×10^5 s, 1.4×10^6 s, 2.6×10^8 s, and 7.2×10^{10} s for ^{224}Ra, ^{223}Ra, ^{228}Ra, and ^{226}Ra, respectively. This scaling is consistent with the numerical simulations performed here, which showed large vertical variations in activity due to slow mixing for ^{224}Ra and ^{223}Ra, small variations for ^{228}Ra, and no effect for ^{226}Ra.

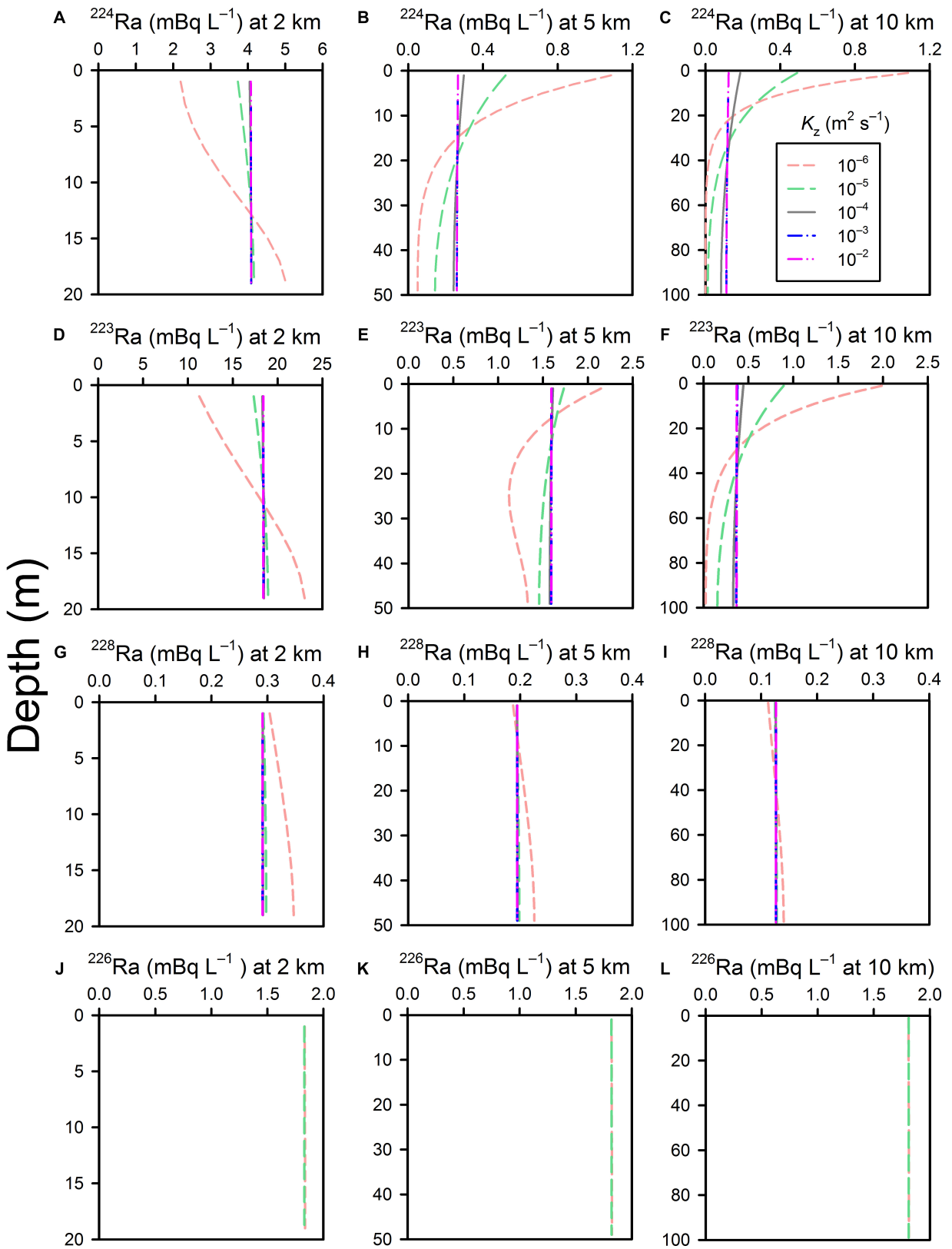

FIGURE 3 | Vertical variations in Ra activity for a range in K_z values for ^{223}Ra **(A–C)**, ^{224}Ra **(D–F)**, ^{228}Ra **(G–I)**, and ^{226}Ra **(J–L)** at 2 km (left column), 5 km (middle column) and 10 km from the coastline (right column).

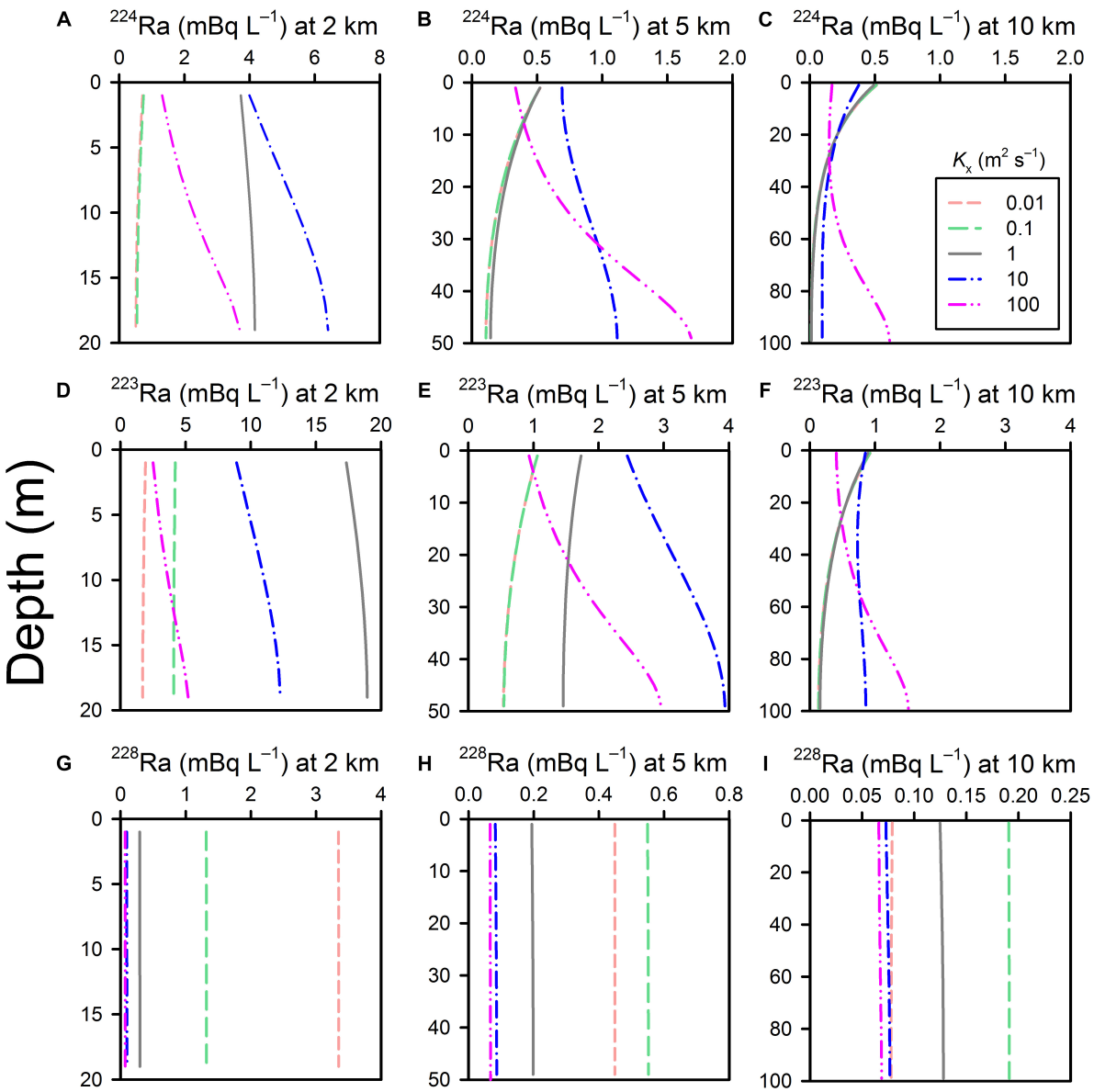

FIGURE 4 | Variations in ^{224}Ra **(A–C)**, ^{223}Ra **(D–F)**, and ^{228}Ra **(G–I)** activity as a function of K_x for a relatively low K_z value (10^{-5} m^2 s^{-1}) at 2 km (left column), 5 km (middle column), and 10 km (right column).

Radon-222 is another common SGD tracer (Stieglitz et al., 2013; Tait et al., 2016) with a half-life (3.82 days) comparable to ^{224}Ra. Thus, surface water sampling for ^{222}Rn may similarly, not be representative of the whole water column activity when the vertical mixing rate is low. Being a dissolved gas, a further complication with ^{222}Rn would be degassing, which has a characteristic timescale L/v (where v is the degassing velocity). The characteristic degassing timescale for ^{222}Rn would typically be slightly slower than its timescale for radioactive decay. For example, for L = 20 m and v = 1 m day^{-1} ($\sim$1.2 $\times$ 10^{-5} m s^{-1}), the characteristic timescale for degassing is $\sim$2 $\times$ 10^6 s (relative to $\sim$5 $\times$ 10^5 s for radioactive decay). This is also similar to the timescale of vertical mixing 4 $\times$ 10^6 s for $\sim K_z$ = 10^{-4} m^2 s^{-1} and L = 20 m. Thus, slow vertical mixing may impact on ^{222}Rn activities in the water column because it can be slower than the timescales of both radioactive decay and degassing.

K_z

A potentially mitigating or complicating factor in our analysis is that a constant K_z was assumed across the model domain, which may be unrealistic in some field settings (Koch-Larrouy et al., 2015). K_z is an empirical parameter summing-up a range of potential dispersive

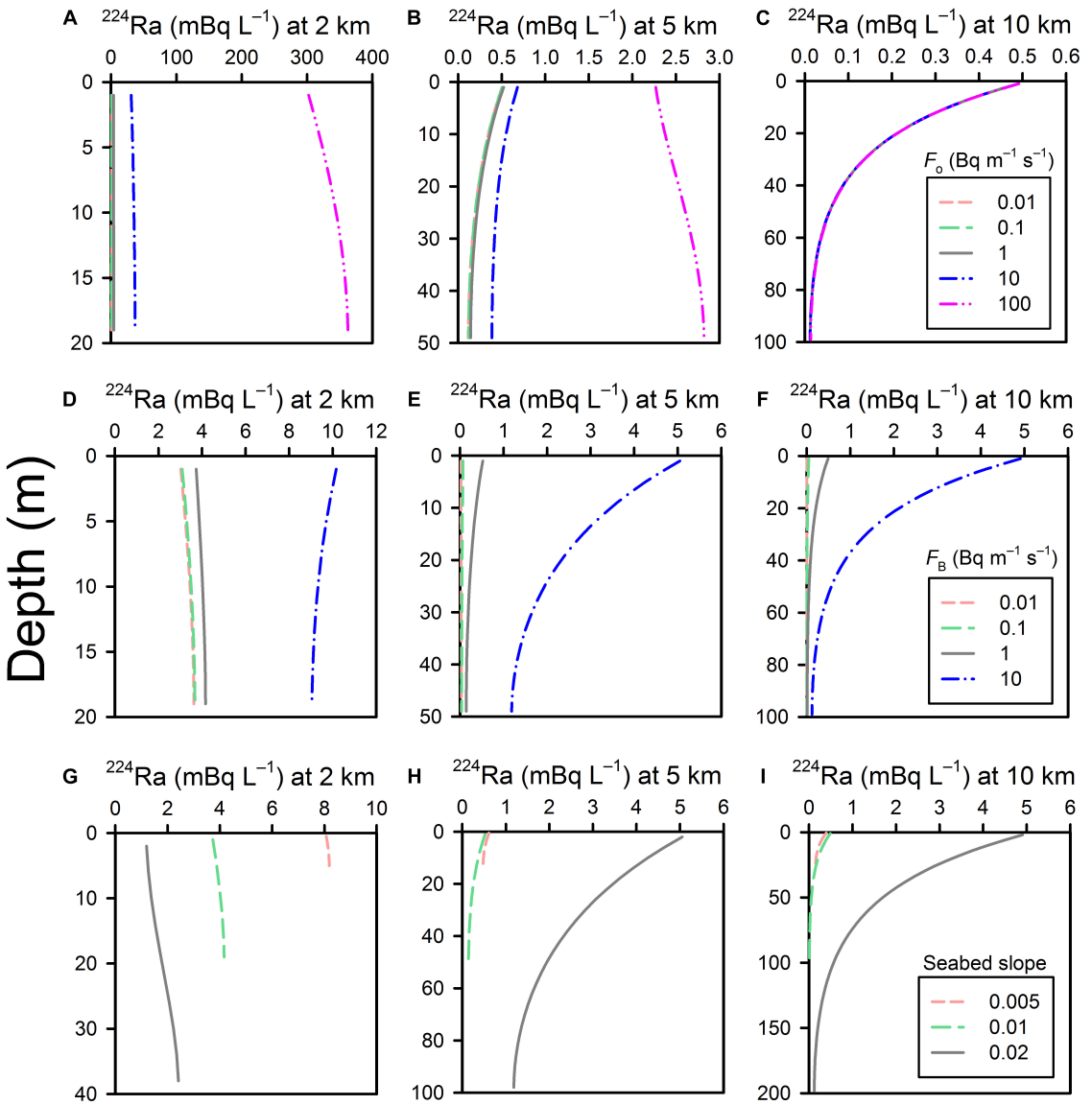

FIGURE 5 | Effects of variations in F_o **(A–C)**, F_B **(D–F)**, and seabed slope **(G–I)** on the vertical distribution of ^{224}Ra for a relatively low K_z value (10^{-5} m^2 s^{-1}).

processes induced by wind, tides, and other driving forces. As per other similar empirical dispersion parameters, K_z should be anticipated to be scale-, and time-dependent. For example, K_z can change significantly between calm and stormy conditions (Manucharyan et al., 2011) or following changes in wind direction (Kirincich and Barth, 2009). Some coastal embayments have periods with no tidal movements (de Silva Samarasinghe, 1998), which should also temporarily reduce K_z. This temporal variations in K_z could either mitigate or accentuate biases arising from surface sampling for tracers. As an example, if atmospheric fronts generating greater K_z have a characteristic timescale less then radioactive decay for a given tracer, the increased mixing of the water column they generate would tend to homogenize water column activities. Considering the paucity of data about vertical variations in Ra activity in inner shelf environments, the simple representation of K_z used here is probably sufficient on a preliminary basis.

Quantifying the Bias

Due to the paucity of information on vertical variability in Ra activity for inner shelves, it is not possible here to test the findings of this theoretical assessment with measurements under different field conditions. The potential magnitude of the bias can be evaluated here by comparing the longitudinal profiles for Ra from surface water relative to the depth-averaged values across the mixed layer generated from the simulations. For simplicity, this evaluation will be restricted to ^{224}Ra (a worse-case scenario due to its short half-life). The evaluation will be made for K_z varying from 10^{-6} to 10^{-4} m^2

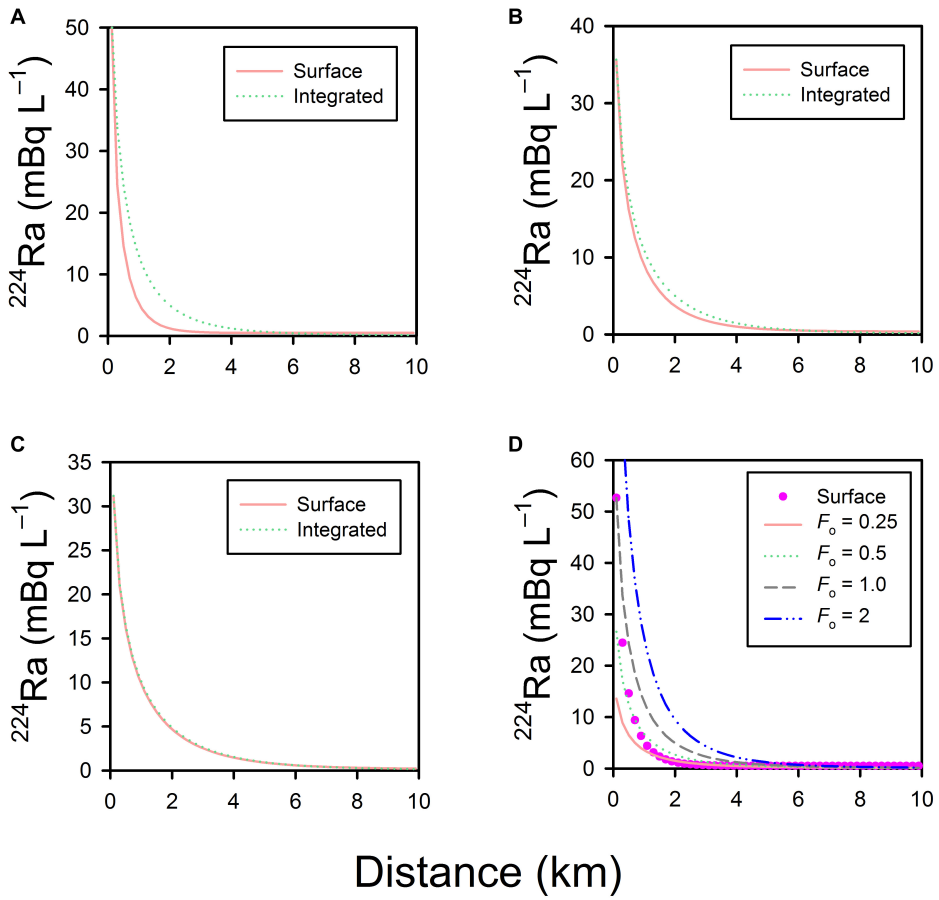

FIGURE 6 | Comparison of longitudinal Ra profile between surface samples and depth-averaged ^{224}Ra activities for **(A)** $K_z = 10^{-6}$ m^2 s^{-1}, **(B)** $K_z = 10^{-5}$ m^2 s^{-1}, and **(C)** $K_z = 10^{-4}$ m^2 s^{-1} (for $K_x = 10$ m^2 s^{-1}, F_o, and $F_B = 1$ Bq m^{-1} s^{-1}). **(D)** Evaluation of the bias in F_o when only using surface relative to depth-average ^{224}Ra activities.

s^{-1} (and for $K_x = 10$ m^2 s^{-1}, $F_o = 1$ Bq m^{-1} s^{-1} and $F_B = 1$ Bq m^{-1} s^{-1}).

Consistent with previous analyses, the bias was greatest for $K_z = 10^{-6}$ m^2 s^{-1} between surface and depth-average ^{224}Ra activities, with a tendency for surface samples to underestimate activities inshore and slightly overestimate activities offshore (**Figure 6A**). The bias was less pronounced for $K_z = 10^{-5}$ m^2 s^{-1} and negligible for $K_z = 10^{-4}$ m^2 s^{-1} (**Figures 6B,C**). For $K_z = 10^{-6}$ m^2 s^{-1}, simulations were then run to better match the "observed" surface ^{224}Ra activities using different F_o values (with K_x and F_B remaining unchanged). The closest match to the surface ^{224}Ra activities was for $F_o \sim 0.25$ to 0.50 Bq m^{-2} s^{-1}, or 50–75% of the correct value (1 Bq m^{-1} s^{-1}) (**Figure 6D**). Whilst only a crude evaluation in the absence of field measurements, this analysis suggests the bias caused by surface water sampling when K_z is low could be important.

CONCLUSION

There is a paucity of vertical Ra profiles over inner continental shelves. We demonstrated here that when vertical mixing is slow, vertical variations in short-lived radionuclides activity in a coastal mixed layer are possible. This is of concern for field programs aiming to measure SGD or other processes using these tracers. When the water column is not well mixed relative to a given tracer, only sampling near the surface (the current practice) will lead to biased estimates of the spatial distribution of the tracer and, consequently, of the inferred SGD estimates. Despite the significant effort required to collect Ra samples from seawater (Henderson et al., 2013), future field programs for SGD tracers over continental shelves should aim to collect at least one vertical profile in the mixed layer for short-lived tracers to evaluate the potential for slow vertical mixing. A potential benefit in measuring the vertical distribution in SGD tracers in the water column could be to help evaluate its recirculated component, which has a large component originating from the seabed.

DATA AVAILABILITY

No new dataset was generated in this study. The MATLAB script used to perform the simulations is available as **Supplementary Material**.

AUTHOR CONTRIBUTIONS

SL scoped the theoretical analysis, did the numerical simulations, and drafted the manuscript. IW contributed to the theoretical development and drafting of the manuscript.

FUNDING

This manuscript was made possible by funding from CSIRO Land & Water to SL.

ACKNOWLEDGMENTS

We acknowledge the insightful comments from reviewers on a previous publication, who recommended that we also explore biases associated with vertical dispersivity.

SUPPLEMENTARY MATERIAL

The Supplementary Material for this article can be found online at: https://www.frontiersin.org/articles/10.3389/fmars.2019.00357/full#supplementary-material

REFERENCES

Benitez-Nelson, C. R., Buesseler, K. O., and Crossin, G. (2000). Upper ocean carbon export, horizontal transport, and vertical eddy diffusivity in the southwestern gulf of Maine. *Cont. Shelf Res.* 20, 707–736. doi: 10.1016/s0278-4343(99)00093-x

Broecker, W. S., Li, Y. H., and Cromwell, J. (1967). Radium-226 and radon-222: concentration in atlantic and pacific oceans. *Science* 158, 1307–1310. doi: 10.1126/science.158.3806.1307

Burnett, W. C., Bokuniewicz, H., Huettel, M., Moore, W. S., and Taniguchi, M. (2003). Groundwater and pore water inputs to the coastal zone. *Biogeochemistry* 66, 3–33. doi: 10.1023/b:biog.0000006066.21240.53

Charette, M. A., Gonneea, M. E., Morris, P. J., Statham, P., Fones, G., Planquette, H., et al. (2007). Radium isotopes as tracers of iron sources fueling a southern ocean phytoplankton bloom. *Deep Sea Res. Part 2 Top. Stud. Oceanogr.* 54, 1989–1998. doi: 10.1016/j.dsr2.2007.06.003

Charette, M. A., and Scholten, J. C. (2008). Marine chemistry special issue: the renaissance of radium isotopic tracers in marine processes studies. *Mar. Chem.* 109, 185–187. doi: 10.1016/j.marchem.2008.04.001

Chung, Y.-C., and Craig, H. (1973). Radium-226 in the eastern equatorial pacific. *Earth Planet. Sci. Lett.* 30, 306–318. doi: 10.1016/0012-821x(73)90195-7

Colbert, S. L., and Hammond, D. E. (2007). Temporal and spatial variability of radium in the coastal ocean and its impact on computation of nearshore cross-shelf mixing rates. *Cont. Shelf Res.* 27, 1477–1500. doi: 10.1016/j.csr.2007.01.003

de Silva Samarasinghe, J. R. (1998). Revisiting upper gulf st vincent in south australia: the salt balnace and its implications. *Estuar. Coast Shelf Sci.* 46, 51–63. doi: 10.1006/ecss.1997.0249

de Silva Samarasinghe, J. R., Bode, L., and Mason, L. B. (2003). Modelled response of gulf st vincent (South Australia) to evaporation, heating and winds. *Cont. Shelf Res.* 23, 1285–1313. doi: 10.1016/s0278-4343(03)00129-8

Dulaiova, H., and Burnett, W. C. (2006). Radon loss across the water-air interface (Gulf of Thailand) estimated experimentally from222Rn-224Ra. *Geophys. Res. Lett.* 33:L05606.

Durski, S. M., Glenn, S. M., and Haidvogel, D. B. (2004). Vertical mixing schemes in the coastal ocean: comparison of the level 2.5 mellor-yamada scheme with an enhanced version of the K profile parameterazation. *J. Geophys. Res.* 109:C01015.

Etemad-Shahidi, A., and Imberger, J. (2001). The estimation of vertical eddy diffusivity in estuaries. *Water Pollut.* 3, 455–463.

Glover, D. M., and Reeburgh, W. S. (1987). Radon-222 and radium-226 in southeastern bering sea shelf waters and sediments. *Cont. Shelf Res.* 7, 433–456. doi: 10.1016/0278-4343(87)90090-2

Hancock, G. J., Webster, I. T., and Stieglitz, T. C. (2006). Horizontal mixing of great barrier reef waters: offshore diffusivity determined from radium isotope distribution. *J. Geophys. Res. Oceans* 111:C12019.

Henderson, P. B., Morris, P. J., Moore, W. S., and Charette, M. A. (2013). Methodological advances for measuring low-level radium isotopes in seawater. *J. Radioanal. Nucl. Chem.* 296, 357–362. doi: 10.1007/s10967-012-2047-9

Kirincich, A. R., and Barth, J. A. (2009). Time-Varying across-shelf ekman transport and vertical eddy viscosity on the inner shelf. *J. Phys. Oceanogr.* 39, 602–620. doi: 10.1175/2008jpo3969.1

Knee, K. L., Garcia-Solsona, E., Garcia-Orellana, J., Boehm, A. B., and Paytan, A. (2011). Using radium isotopes to characterize water ages and coastal mixing rates: a sensitivity analysis. *Limnol. Oceanogr. Methods* 9, 380–395. doi: 10.4319/lom.2011.9.380

Koch-Larrouy, A., Atmadipoera, A., Van Beek, P., Madec, G., Aucan, J., Lyard, F., et al. (2015). Estimates of tidal mixing in the indonesian archipelago from multidisciplinary INDOMIX in-situ data. *Deep Sea Res. Part 1 Oceanogr. Res. Pap.* 106, 136–153. doi: 10.1016/j.dsr.2015.09.007

Kumar, N., and Feddersen, F. (2017). The effect of stokes drift and transient rip currents on the inner shelf. part I: no stratification. *J. Phys. Oceanogr.* 47, 227–241. doi: 10.1175/jpo-d-16-0076.1

Lamontagne, S., La Salle, C. L., Hancock, G. J., Webster, I. T., Simmons, C. T., Love, A. J., et al. (2008). Radium and radon radioisotopes in regional groundwater, intertidal groundwater, and seawater in the adelaide coastal waters study area: implications for the evaluation of submarine groundwater discharge. *Mar. Chem.* 109, 318–336. doi: 10.1016/j.marchem.2007.08.010

Lamontagne, S., Taylor, A. R., Herpich, D., and Hancock, G. J. (2015). Submarine groundwater discharge from the South Australian limestone coast region estimated using radium and salinity. *J. Environ. Radioact.* 140, 30–41. doi: 10.1016/j.jenvrad.2014.10.013

Lamontagne, S., and Webster, I. T. (2019). Cross-Shelf transport of submarine groundwater discharge tracers: a sensitivity analysis. *J. Geophys. Res. Oceans* 124, 453–469. doi: 10.1029/2018jc014473

Levy, D. M., and Moore, W. S. (1985). 224Ra in continental shelf waters. *Earth Planet. Sci. Lett.* 73, 226–230. doi: 10.1016/0012-821x(85)90071-8

Li, C. Y., and Cai, W. J. (2011). On the calculation of eddy diffusivity in the shelf water from radium isotopes: high sensitivity to advection. *J. Mar. Syst.* 86, 28–33. doi: 10.1016/j.jmarsys.2011.01.003

Lietzke, T. A., and Lerman, A. (1975). Effects of bottom relief in two-dimensional oceanic eddy diffusion models. *Earth Planet. Sci. Lett.* 24, 337–344. doi: 10.1016/0012-821x(75)90139-9

Manucharyan, G. E., Brierley, C. M., and Fedorov, A. V. (2011). Climate impacts of intermittent upper ocean mixing induced by tropical cyclones. *J. Geophys. Res. Oceans* 116:C11038.

Moniz, R. J., Fong, D. A., Woodson, C. B., Willis, S. K., Stacey, M. T., and Monismith, S. G. (2014). Scale-dependent dispersion within the stratified interior on the shelf of northern monterey bay. *J. Phys. Oceanogr.* 44, 1049–1064. doi: 10.1175/jpo-d-12-0229.1

Moore, W. S. (2000). Determining coastal mixing rates using radium isotopes. *Cont. Shelf Res.* 20, 1993–2007. doi: 10.1016/s0278-4343(00)00054-6

Moore, W. S. (2007). Seasonal distribution and flux of radium isotopes on the southeastern U.S. continental shelf. *J. Geophys. Res.* 112:C10013. doi: 10.1016/s0278-4343(00)00054-6

Moore, W. S. (2015). Inappropriate attempts to use distributions of 228Ra and 226Ra in coastal waters to model mixing and advection rates. *Cont. Shelf Res.*105, 95–100. doi: 10.1016/j.csr.2015.05.014

Moore, W. S., Astwood, H., and Lindstrom, C. (1995). Radium isotopes in coastal waters on the Amazon shelf. *Geochim. Cosmochim. Acta* 59, 4285–4298. doi: 10.1016/0016-7037(95)00242-r

Okubo, T. (1980). Radium-228. *J. Oceanogr. Soc. Japan* 36, 263–268.

Pacanowski, R. C., and Philander, S. G. H. (1981). Parameterizationof vertical mixing in numerical moels of tropical oceans. *J. Phys. Oceanogr.* 11, 1443–1451. doi: 10.1175/1520-0485(1981)011<1443:povmin>2.0.co;2

Stieglitz, T. C., Clark, J. F., and Hancock, G. J. (2013). The mangrove pump: the tidal flushing of animal burrows in a tropical mangrove forest determined from radionuclide budgets. *Geochim. Cosmochim. Acta* 102, 12–22. doi: 10.1016/j.gca.2012.10.033

Tait, D. R., Maher, D. T., Macklin, P. A., and Santos, I. R. (2016). Mangrove pore water exchange across a latitudinal gradient. *Geophys. Res. Lett.* 43, 3334–3341. doi: 10.1002/2016gl068289

Webster, I. T. (1986). The vertical structure of currents on the north west shelf of australia at subtidal frequencies. *J. Phys. Oceanogr.* 16, 1145–1157. doi: 10.1175/1520-0485(1986)016<1145:tvsoco>2.0.co;2

Conflict of Interest Statement: The authors declare that the research was conducted in the absence of any commercial or financial relationships that could be construed as a potential conflict of interest.

frontiers in Marine Science

ORIGINAL RESEARCH
published: 13 September 2019
doi: 10.3389/fmars.2019.00563

DSi as a Tracer for Submarine Groundwater Discharge

Till Oehler[1], Joseph Tamborski[2], Shaily Rahman[3], Nils Moosdorf[1,4], Janis Ahrens[5], Corinna Mori[5], René Neuholz[5], Bernhard Schnetger[5] and Melanie Beck[5]*

[1] Department Biogeochemistry and Geology, Leibniz Centre for Tropical Marine Research (ZMT), Bremen, Germany, [2] Department of Marine Chemistry and Geochemistry, Woods Hole Oceanographic Institution, Woods Hole, MA, United States, [3] Department of Geological Sciences, University of Florida, Gainesville, FL, United States, [4] Institute of Geosciences, Kiel University (CAU), Kiel, Germany, [5] Institute for Chemistry and Biology of the Marine Environment (ICBM), Carl von Ossietzky University of Oldenburg, Oldenburg, Germany

Submarine groundwater discharge (SGD) is an important source of nutrients and metals to the coastal ocean, affects coastal ecosystems, and is gaining recognition as a relevant water resource. SGD is usually quantified using geochemical tracers such as radon or radium. However, a few studies have also used dissolved silicon (DSi) as a tracer for SGD, as DSi is usually enriched in groundwater when compared to surface waters. In this study, we discuss the potential of DSi as a tracer in SGD studies based on a literature review and two case studies from contrasting environments. In the first case study, DSi is used to calculate SGD fluxes in a tropical volcanic-carbonate karstic region (southern Java, Indonesia), where SGD is dominated by terrestrial groundwater discharge. The second case study discusses DSi as a tracer for marine SGD (i.e., recirculated seawater) in the tidal flat area of Spiekeroog (southern North Sea), where SGD is dominantly driven by tidal pumping through beach sands. Our results indicate that DSi is a useful tracer for SGD in various lithologies (e.g., karstic, volcanic, complex) to quantify terrestrial and marine SGD fluxes. DSi can also be used to trace groundwater transport processes in the sediment and the coastal aquifer. Care has to be taken that all sources and sinks of DSi are known and can be quantified or neglected. One major limitation is that DSi is used by siliceous phytoplankton and therefore limits its applicability to times of the year when primary production of siliceous phytoplankton is low. In general, DSi is a powerful tracer for SGD in many environments. We recommend that DSi should be used to complement other conventionally used tracers, such as radon or radium, to help account for their own shortcomings.

Keywords: submarine groundwater discharge, DSi, silica, tracer, radon, radium

OPEN ACCESS

Edited by:
Ryo Sugimoto,
Fukui Prefectural University, Japan

Reviewed by:
Shiho Kobayashi,
Kyoto University, Japan
Yaser Nikpeyman,
Shahid Beheshti University, Iran

****Correspondence:***
Till Oehler
Till.Oehler@leibniz-zmt.de

Specialty section:
This article was submitted to Marine Ecosystem Ecology, a section of the journal Frontiers in Marine Science

Received: *30 April 2019*
Accepted: *27 August 2019*
Published: *13 September 2019*

Citation:
Oehler T, Tamborski J, Rahman S, Moosdorf N, Ahrens J, Mori C, Neuholz R, Schnetger B and Beck M (2019) DSi as a Tracer for Submarine Groundwater Discharge. Front. Mar. Sci. 6:563. doi: 10.3389/fmars.2019.00563

INTRODUCTION

Submarine groundwater discharge (SGD) is an important source of nutrients and metals for the coastal ocean (Slomp and Van Cappellen, 2004; Moore, 2010), affects coastal ecosystems (Lecher and Mackey, 2018) and is a relevant and important water resource for coastal communities (Moosdorf and Oehler, 2017). SGD represents the discharge of terrestrial (fresh), marine (saline),

or a mixture of both (brackish) groundwater (or pore water) into the ocean (Burnett et al., 2003; Moore, 2010).

Geochemical tracers have widely been applied to calculate SGD fluxes. This requires detailed knowledge of the tracer concentration coupled to potential sources and sinks, its residence time in the coastal water column and its endmember concentration in groundwater. Radium (Ra) and Radon (^{222}Rn) isotopes are commonly used as geochemical tracers for SGD, as both tracers are in general enriched in groundwater by several orders of magnitude compared to surface waters (Swarzenski, 2007; Moore, 2010). The "radium quartet" is advantageous for SGD quantification, as the wide range in half-lives of the four isotopes (^{223}Ra = 11.4 days, ^{224}Ra = 3.66 days, ^{226}Ra = 1,600 years and ^{228}Ra = 5.75 years) can be used to trace flow paths and processes over variable time-scales. However, Ra data should be interpreted cautiously when fluid ionic strength changes, which affects the partitioning of Ra between solid and solution phases (Webster et al., 1995; Beck and Cochran, 2013). Furthermore, Ra analyses typically require large sampling volumes (tens to hundreds of liters) (Moore and Reid, 1973) and rapid measurement after sampling, as the short-lived Ra isotopes decay within days to weeks. Radon (^{222}Rn = 3.83 days) is an inert noble gas that is not partitioned between solid and solution phases like its counterpart Ra. ^{222}Rn measurements are automated (Burnett and Dulaiova, 2003), which facilitates rapid data collection over large spatial areas (Dulaiova et al., 2010) and at stationary time-series. However, ^{222}Rn cannot be accurately applied as a tracer in high energy environments (winds, waves), as it is prone to degassing (Fanning et al., 1982).

Dissolved silicon (DSi) is also used as a geochemical tracer for SGD (Street et al., 2008; Garcia-Solsona et al., 2010a; Hernández-Terrones et al., 2011; Hwang et al., 2016; Lubarsky et al., 2018), but has received less attention than ^{222}Rn and Ra isotopes. DSi in groundwater is the product of chemical weathering of rocks and sediments, or dissolution of biogenic opal. Consequently, terrestrial and marine groundwater (or pore water) is often enriched in DSi (Rad et al., 2007; Anschutz et al., 2009) and can further be augmented during the passage through the subterranean estuary (STE) (Moore, 2010; Rahman et al., 2019). Consequently, SGD [including pore water exchange (PEX)] usually contains high DSi concentrations, which qualifies DSi as a useful addition to conventionally used tracers such as ^{222}Rn or Ra (Kim et al., 2005, 2008; Street et al., 2008; Garcia-Solsona et al., 2010b; Hwang et al., 2016; Tamborski et al., 2018). The advantages of DSi as a tracer for SGD include small sampling volumes, low detection limits and high precision measurements. Samples for DSi are easy to store and transport, which makes DSi logistically desirable as a tracer in remote areas with limited infrastructure, where it may be challenging to sample for ^{222}Rn and Ra isotopes. Furthermore, DSi is not prone to degassing, and may thus be a useful tool to compliment ^{222}Rn mass balances in high-energy environments. However, DSi does not behave conservatively in many coastal environments, where it can adsorb onto Fe-oxides or reprecipitates as amorphous Al-Si phases (e.g., Mackin and Aller, 1984). One of the main limitations of DSi as a tracer is that it is used by siliceous plankton (e.g., diatoms, flaggelates, radiolarians and picocyanobacteria) as well as higher trophical levels such as sponges, as a nutrient to build up their hard tissues (Brzezinski, 1985; Krause et al., 2011, 2017; Tréguer and De La Rocha, 2013). The aim of this study is to assess under which conditions DSi can be used as a tracer for SGD. We review the current state of the literature and show two case studies in contrasting geological environments to demonstrate the utility of DSi as a tracer for SGD.

DSi IN GROUNDWATER AND SURFACE WATER

DSi in Groundwater and the Subterranean Estuary

The concentration of DSi in fresh, brackish and marine groundwater is chiefly governed by dissolution rates of minerals in the aquifer and in the sediment (i.e., weathering; **Figure 1**, f) which is usually dependent on the lithology, the subsurface residence time of groundwater and biogeochemical transformations (Bluth and Kump, 1994; Horton et al., 1999; Jacobson et al., 2003; Rahman et al., 2019). Combined, these factors control DSi endmember concentrations in SGD. Indeed, different SGD flow paths (Santos et al., 2012) may lead to unique DSi endmember concentrations. For example, terrestrial groundwater (**Figure 1**, a) can have a different DSi endmember concentration compared to tidally driven marine groundwater (**Figure 1**, b). In either case, differences in DSi concentrations can be attributed to the above mentioned conditions, which are discussed in detail below.

In marine groundwaters, DSi concentrations are dominantly controlled by the dissolution of biogenic silica (e.g., DeMaster, 2002). Based on the dissolution of biogenic silica pore water DSi concentrations can reach 1000–1200 μM under typical pressure and temperature conditions found in marine sediments (e.g., Hurd, 1973; Schink et al., 1975; DeMaster, 2003; Loucaides et al., 2012). Alteration processes like incorporation of Al, adsorption of metals (e.g., Al^{3+} and Fe^{3+}) onto the silica substrate surface, formation of metal oxide coatings, or aging of the substrate inhibit the dissolution of biogenic opal (Van Cappellen and Qiu, 1997; Dixit and Van Cappellen, 2002; Van Cappellen et al., 2002; Michalopoulos and Aller, 2004; Khalil et al., 2007; Loucaides et al., 2010).

In most terrestrial groundwaters, the net silica enrichment is primarily controlled by lithogenic mineral dissolution (e.g., Ehlert et al., 2016), and thus depends on the lithology of the aquifer under study (**Table 1**; Rahman et al., 2019). Silicate mineral dissolution rates vary with pH, temperature, salinity, groundwater flow rates and sediment-water volume ratios (Oelkers and Gislason, 2001; Anschutz et al., 2009; Jeandel and Oelkers, 2015; Morin et al., 2015). Si saturation will be controlled by the type of Si-bearing minerals present. Thus, the maximum attainable DSi concentration in groundwater is a function of the surrounding environment. For example, karstic terrestrial groundwater has relatively low DSi concentration (80 ± 63 μM), reflecting the low Si

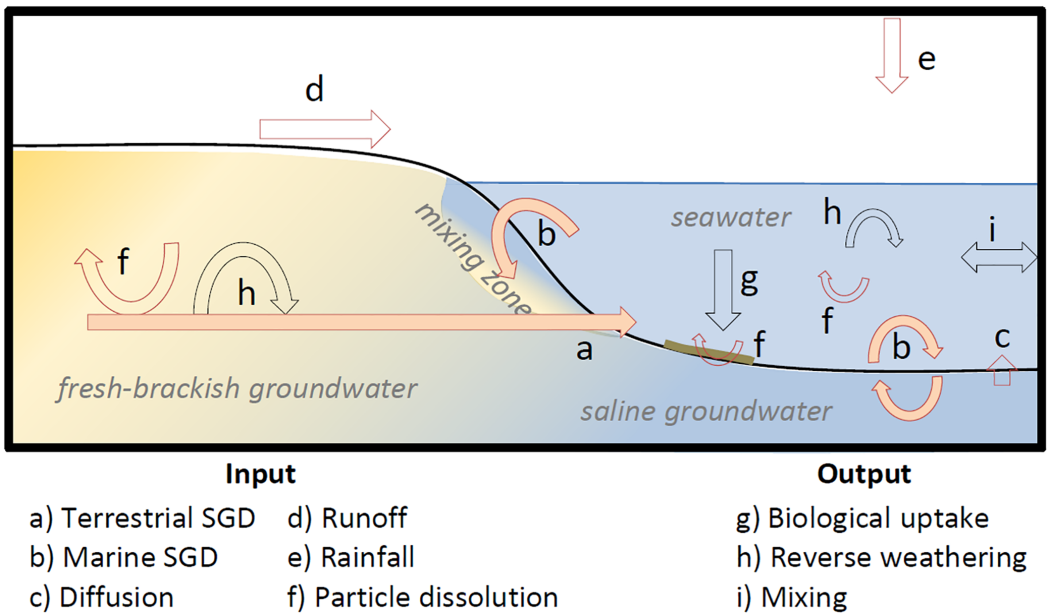

FIGURE 1 | Conceptual figure illustrating different processes governing DSi concentrations in coastal waters and coastal sediments/aquifer. Red arrows represent sources of DSi and black arrows represent sinks of DSi. Orange filled arrows represent hypothetical SGD flow paths, including terrestrial groundwater (a) and marine groundwater (b). Yellow colors represent fresh-brackish waters and blue colors represent saline water. The mixing zone between fresh and saline groundwater is called subterranean estuary (STE). The green line at the seafloor represents biogenic silica which has deposited e.g., after a phytoplankton bloom (Kowalski et al., 2013). The respective processes which lead to an input or output of DSi are labeled in the lower panel. Sources and sinks can vary with respect to the environmental boundary conditions, the size of the arrows is thus not representative for the quantity of their respective fluxes.

content of carbonates, whereas extrusive igneous groundwater is extremely enriched in DSi (604 ± 192 μM) (**Table 1**; Rahman et al., 2019).

Further, DSi concentration in groundwater can be modified during passage though the STE. Non-conservative behavior of DSi in groundwater may be assessed from the observed enrichment or deficit of DSi with respect to two-endmember linear mixing between fresh groundwater and surface marine waters. Whereas carbonate aquifers appear to show no net enrichment of DSi in brackish groundwaters, marine SGD flow paths from extrusive igneous and complex lithologies exhibit average net DSi enrichments of ∼50 μM globally (**Table 1**; Rahman et al., 2019, and references therein). Though there is evidence of non-conservative DSi behavior in aquifers composed of primarily granite (Onodera et al., 2007; Rengarajan and Sarma, 2015; Wang et al., 2015; Lecher et al., 2016), shale (Kim et al., 2005; Lee et al., 2012; Luo et al., 2014; Ye et al., 2016) and sandstone (Weinstein et al., 2011; Sugimoto et al., 2017) lithologies, the data are yet insufficient to constrain net DSi concentrations in marine SGD in these endmember lithologies globally (**Table 1**). At the land-sea transition, dissolution rates of terrestrially derived silicate-bearing mineral phases or silica substrates (e.g., phytoliths) are on average 4–5 times higher in seawater than in freshwater (Loucaides et al., 2008). These findings are consistent with other laboratory studies of basaltic glass or lithogenic particle dissolution in brackish waters (Daux et al., 1997; Advocat et al., 1998; Techer et al., 2001; Jones et al., 2012; Oelkers et al., 2012; Morin et al., 2015), as well as static and flow-through incubations of sediment at the freshwater-seawater transition zone in the STE (Anschutz et al., 2009; Ehlert et al., 2016; Tamborski et al., 2018). Dissolution rates of sediments of different lithologies, at solid surface to volume ratios close to those found in the STE, range from ∼3.4 to 49 mol Si m^{-2} s^{-1} (Techer et al., 2001; Anschutz et al., 2009; Ehlert et al., 2016; Tamborski et al., 2018).

The subsurface residence time of groundwater is directly proportional to the flow velocity and flow path length (i.e., transit time) and is thus tied to DSi enrichments via mineral dissolution kinetics. The longer a parcel of fluid is in contact with Si-bearing minerals, the greater DSi that fluid may obtain from water-rock weathering reactions, until a steady-state or transient steady-state

TABLE 1 | Globally-averaged terrestrial and marine SGD DSi endmember concentrations categorized after lithology, summarized from Rahman et al. (2019).

	Terrestrial SGD DSi [μM]	Marine SGD DSi [μM]
Extrusive Igneous	604 ± 192	56 ± 43
Carbonate	80 ± 63	0
Sandstone	159 ± 80	
Granite	334 ± 255	
Shale	182 ± 91	
Complex lithology	288 ± 245	50 ± 41

Complex lithology is defined as more than one type of major lithology and includes unconsolidated glacial sediments.

is reached between Si dissolution and reprecipitation (Ehlert et al., 2016). In DSi-poor groundwaters, initial dissolution rates are high before Si concentrations stabilize. With longer pore fluid residence times and higher DSi concentrations, dissolution rates decrease (Techer et al., 2001). Coatings or secondary mineral phases form on the substrate, reducing the reactive surface area (Daux et al., 1997; Gislason and Oelkers, 2003). Higher flow velocities can increase dissolution rates as products of the dissolution reaction (i.e., dissolved Si or silicic acid) are transported away from their site of production and the reactions stay far from equilibrium (Anschutz et al., 2009). Due to continuous DSi enrichment in the pore fluid, some portion of the initially released DSi (30 to 60%) will reprecipitate into a secondary mineral phase (e.g., amorphous alumino-silicates), which is dependent on groundwater residence times (Daux et al., 1997; Staudigel et al., 1998). Terrestrial groundwater residence times can vary from days to thousands of years; similarly, marine groundwater residence times can vary from seconds to centuries (Seidel et al., 2015). Knowledge on the time-scale of the flow path under consideration is thus extremely important to evaluate DSi endmember concentrations.

DSi as an Indicator for Groundwater Transport Processes

Dissolved silicon may be used to quantify groundwater residence times when the factors described in section "DSi in Groundwater and the Subterranean Estuary" are considered. Anschutz et al. (2009) investigated the residence time of beach groundwaters based on the kinetics of quartz dissolution in seawater. Intertidal beach sand was incubated with seawater to determine the change in DSi concentration over time. Experiments can be performed under varying conditions, including seawater: sediment ratios, temperature and pH. In addition, incubations can be performed under "static" conditions or with seawater actively circulating with specified flow rates through the sediment. The dissolution rate of silicate minerals can be simply estimated from the linear increase in DSi concentration over time. This methodology has been successfully applied to several sediment types (Anschutz et al., 2009; Charbonnier et al., 2013; Ehlert et al., 2016; Tamborski et al., 2018). Groundwater residence times can be estimated for marine groundwater by assuming that there is no DSi contribution from terrestrial groundwater or from the dissolution of biogenic silica (Ehlert et al., 2016).

Dissolved silicon can also be used to determine if groundwater infiltration or exfiltration occurs within sediments. If the DSi concentration at two distinct depth horizons is known (e.g., 50 and 100 cm), the concentration gradient between both depths can delineate the advective transport of groundwater, assuming that biogeochemical transformations of DSi are negligible between both horizons. The underlying assumption is that in infiltration (recharge) zones, a positive gradient would indicate increasing release of the constituent (DSi) with increasing depth, while in exfiltration (discharge) zones a negative gradient would indicate increasing accumulation of the constituent (DSi) with decreasing depth. With this method, it was possible to visualize in- and exfiltration patterns in the intertidal zone of the beach system on Spiekeroog Island, southern North Sea (Waska et al., 2019).

DSi as a Tracer for SGD in Coastal Waters

If dissolved silicon is used as a tracer for SGD, several processes which affect DSi concentrations have to be considered (**Figure 1**). Inputs can occur from river and surface runoff (F_{runoff}) (**Figure 1**, d), rainfall (F_{rain}) (**Figure 1**, e), dissolution of particles in the water column and surface sediments ($F_{dissolution}$) (**Figure 1**, f), diffusion (F_{diff}) (**Figure 1**, c), and SGD (F_{SGD}) (**Figure 1**, a,b). Output terms include mixing with offshore waters (F_{mix}) (**Figure 1**, i), biological uptake (F_{biol}) (**Figure 1**, g), for example by benthic and pelagic siliceous plankton, and reverse weathering (F_{rev}) (**Figure 1**, h). Assuming steady-state conditions, and that DSi inputs equal DSi outputs, a simple DSi mass balance can be written (Eq. 1).

$$F_{SGD} + F_{diff} + F_{runoff} + F_{rain} + F_{dissolution} = F_{mix} + F_{rev} + F_{biol} \quad (1)$$

In coastal environments many of these processes are often time dependent. Over short time-scales (e.g., tidal cycles) DSi can be considered as a conservative tracer for SGD because dissolution of particles, reverse weathering or biological uptake may be considered negligible with respect to the other noted sources and sinks. In this study, we consequently focus on short time-scales (hours to days). Coastal environments influenced by SGD on such short time-scales include smaller embayments, tidal channels, open beaches or rocky coastlines. Assuming that the previously mentioned processes can be neglected under short time-scales, Eq. 1 simplifies to:

$$F_{SGD} + F_{diff} + F_{runoff} = F_{mix} \quad (2)$$

Note that Eq. 2 is similar to commonly employed ^{222}Rn and Ra mass balances. DSi source and sink terms outlined in Eqs 1 and 2 are discussed in further detail below.

Dissolved silicon inputs from rainfall are usually low when compared to SGD. Concentrations between 0.5 and 15 μM were measured in rainwater in the Yellow Sea and East China Sea (Zhang et al., 2005). In the Mediterranean Sea, concentrations of DSi in rainfall range from below detection limit up to 33 μM, whereas higher concentrations are linked to episodic Saharan dust inputs (Bartoli et al., 2005).

The importance of molecular diffusion as a source of DSi will vary from site to site. Diffusive fluxes (F_{diff}) can be measured using *ex situ* or *in situ* sediment incubation experiments, if bioturbation and bioirrigation can be neglected, for example by inactivation of benthic fauna by asphyxiation (Rutgers Van Der Loeff et al., 1984; Forster and Graf, 1995). Diffusion can also be calculated based on pore water profiles of DSi from Fick's first law (Schink et al., 1974; Oehler et al., 2015; Tamborski et al., 2018).

River and surface runoff (F_{runoff}) can contain significant amounts of DSi as well as amorphous silica and solid phases which can rapidly dissolve upon estuarine mixing (Conley, 1997). Therefore, the amount of DSi transported into the coastal water column by rivers has to be carefully determined, e.g., by

measuring riverine discharge and DSi concentrations, which is also required for other tracers such as ^{222}Rn or Ra. At the global (Dürr et al., 2011; Tréguer and De La Rocha, 2013), regional (Hartmann et al., 2010; Moosdorf et al., 2011), and local (Rad et al., 2007; Schopka and Derry, 2012) scale, DSi fluxes from rivers are well known and measuring methodologies are established. Obviously, close to a river, these fluxes can dominate coastal DSi fluxes. Globally, riverine DSi fluxes amount to 70 t Si per km of coastline, based on riverine Si fluxes of 5.8 Tmol Si/a (Tréguer and De La Rocha, 2013) and a global coastline of 2.3 mio km (Moosdorf et al., 2015). Offshore mixing (F_{mix}) of a tracer can be estimated by different approaches. In an embayment or an estuary where mixing is dominated by tidal forces, offshore mixing can be calculated based on a tidal prism approach (Dyer, 1973). Offshore mixing rates can also directly be measured, for example, by using an Acoustic Doppler Current Profiler (ADCP). Numerical models can be developed to estimate mixing rates and residence times. Alternatively, short-lived Ra and Rn isotopes may be used to estimate mixing with offshore waters (e.g., Burnett and Dulaiova, 2003; Moore et al., 2006). When short time-scale processes are considered (Eq. 2), the mixing loss of DSi must be well-constrained in order to properly balance DSi sources.

If the previously mentioned DSi fluxes (F_{rain}, F_{runoff}, F_{mix}, F_{diff}) into the coastal water column can be quantified or neglected, then the SGD flux can be calculated by dividing the DSi flux from SGD (F_{SGD}) with the DSi concentration in groundwater. Selection of the groundwater endmember should be based on the considerations outlined in section "DSi in Groundwater and the Subterranean Estuary."

CASE STUDIES

Case Study 1: DSi as a Tracer for SGD in a Tropical Volcanic-Carbonate Karstic Region (Southern Java, Indonesia)

The coastline of the tropical karstic region of Gunung Sewu (southern Java) is made of strongly karstified massive coral reef-limestone with intercalated clay and volcanic ash lenses (van Bemmelen, 1949; Flathe and Pfeiffer, 1965; Waltham et al., 1983; Haryono and Day, 2004). Toward the hinterland mountain ranges occur which consist mainly of sediments and volcanic deposits (a detailed geological description and geological map can be found in Oehler et al., 2018). Groundwater flows from several kilometers in the hinterland toward the coast and is enriched in DSi most likely due to the weathering of volcanic material in the hinterland, and the weathering of volcanic ash lenses during transport toward the coast. DSi enriched groundwater thus discharges through intertidal and submarine springs into the coastal ocean (Oehler et al., 2018). The regional lithology is a combination of volcanic and carbonate rocks in the hinterland and dominantly carbonate at the coast, with groundwater DSi concentrations between 200 and 400 μM with a salinity ranging from 0 to 11 (**Figure 2A**, triangles). Surface water samples taken within an embayment which receives groundwater from a single submarine spring and is not affected by surface runoff or river discharge, showed a linear inverse correlation between DSi and salinity (**Figure 2A**, gray dotted line, R^2 = 0.84), indicating the input of DSi from terrestrial SGD. An inverse linear correlation was also observed between $^{224}Ra_{ex}$ and salinity (**Figure 2B**, gray dotted line, R^2 = 0.60), with more scatter between long-lived ^{226}Ra and salinity (**Figure 2C**, gray dotted line, R^2 = 0.03), also indicating inputs of Ra from SGD. Fresh groundwater was low in ^{224}Ra with a concentration of 10.3 dpm 100 L^{-1}, whereas brackish groundwater was enriched in ^{224}Ra with a concentration of up to 38.7 dpm 100 L^{-1} (**Figure 2B**, triangles). ^{226}Ra was slightly enriched in brackish groundwater and highly enriched in fresh groundwater compared to seawater (**Figure 2C**).

Higher DSi concentrations in the coastal water column (139 μM) were observed during low tide and lower concentrations (65 μM) were observed during high tide (**Supplementary Material**). The tidal variations can be used in a tidal prism approach to calculate water residence times (Eq. 3 in the **Supplementary Material**) (Moore et al., 2006), which yielded a water residence time of 0.56 days. The surface water residence time value is reasonable, as the embayment is subject to diurnal tidal variations.

Submarine groundwater discharge fluxes based on the different tracer approaches were calculated based on Eq. 5 (see **Supplementary Material**) and are shown in **Table 2**. We were not able to calculate a SGD flux based on ^{226}Ra, due to the high ^{226}Ra concentrations in seawater (see **Supplementary Material**). The maximum SGD flux derived from DSi (72 cm day^{-1}) was based on the brackish groundwater endmember, and represents brackish SGD. Consequently, these results agree well with the average SGD fluxes based on $^{224}Ra_{ex}$ (65 cm day^{-1}), where the brackish groundwaters were also used as an endmember.

However, coastal water DSi concentrations were slightly lower as it would be expected from theoretical conservative mixing between fresh groundwater and seawater (**Figure 2A**, black dotted line), which indicates either an unknown source of freshwater in the coastal water column which dilutes the DSi signal, or an unknown DSi sink. Freshwater inputs into the coastal water column from rainfall can be neglected, as there was no rainfall within the sampling period. River and surface runoff is minor and can be neglected as a source of DSi as well, which is typical for karstic regions. DSi concentrations in karstic groundwaters can vary over short time scales and the full range of the groundwater DSi endmember may have not been accurately captured in this study, where samples were taken within days. Coastal water DSi concentrations may have also been partially reduced due to an uptake by marine biota (e.g., diatoms), or reverse weathering, which is however, unlikely due to the short coastal water residence times.

Case Study 2: DSi as a Tracer for SGD in a Temperate Coastal Region Protected by Barrier Islands (Spiekeroog, Southern North Sea)

Diatoms are one of the major algae groups present during spring phytoplankton blooms in the North Sea and its surrounding tidal

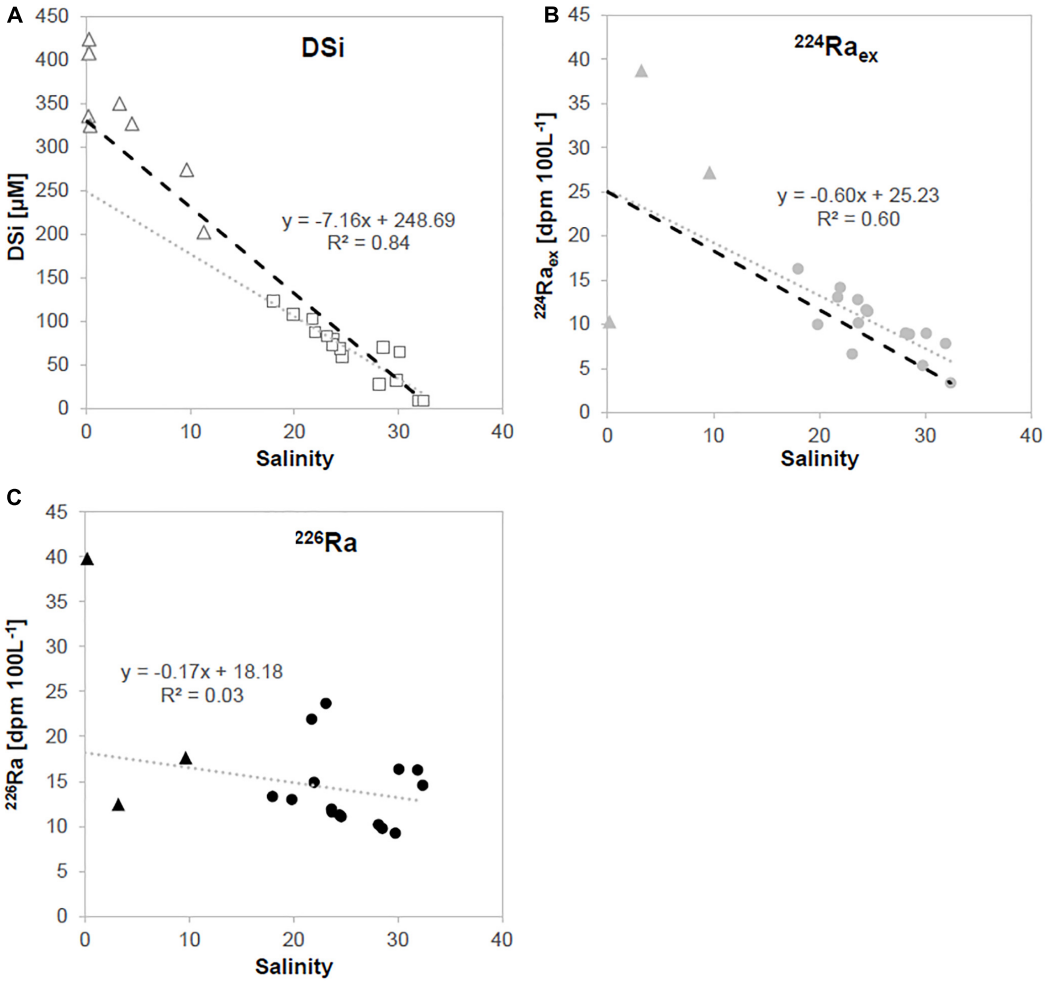

FIGURE 2 | Salinity plotted against **(A)** DSi, **(B)** $^{224}Ra_{ex}$ and **(C)** ^{226}Ra concentrations of water samples taken in an embayment in a karstic region in southern Java. Squares and dots represent surface water column measurements and triangles represent samples taken at coastal and submarine springs. Gray dotted lines show linear correlations of samples taken from the water column, while black dotted lines indicate theoretical conservative mixing between the average groundwater concentration and seawater. Note that only selected spring samples were analyzed for Ra isotopes.

flat system (Reid et al., 1990; Schoemann et al., 1998; Meier et al., 2015; Wiltshire et al., 2015). Diatom growth and the associated DSi uptake control seasonal DSi dynamics in the water column. For example, in the Spiekeroog tidal basin DSi concentrations are high during winter (20–30 µM) and decrease strongly in the water column during the spring diatom bloom reaching concentrations close to zero (**Figure 3**; Grunwald et al., 2010; Beck and Brumsack, 2012). After the bloom, diatoms remain one of the dominant algal groups during the entire growing season (Meier et al., 2015). Furthermore, dinoflagellates, which are adapted to low nutrient concentrations and can have a siliceous skeleton, become important in summer (Meier, 2014; Wiltshire et al., 2015). Both phytoplankton species lead to a continuous DSi consumption until late autumn. The DSi pool in the water column is replenished by discharge of DSi-rich marine groundwater from the surrounding tidal flat sediments where the deposited diatom detritus is degraded (Billerbeck et al., 2006; Beck et al., 2008; Kowalski et al., 2012). Pore water advection in surface sediments (Huettel et al., 1998) leads to the release of DSi-rich pore waters, especially after the spring bloom (DSi up to 400 µM Kowalski et al., 2012). Additionally, SGD from tidal flat margin sediments (Riedel et al., 2010; Moore et al., 2011) lead to the release of groundwater enriched in DSi throughout the whole year (DSi up to 1000 µM Reckhardt et al., 2015).

TABLE 2 | SGD calculations in southern Java based on $^{224}Ra_{ex}$, salinity and DSi mass balances.

	Salinity	DSi [µM]	$^{224}Ra_{ex}$ [dpm 100L^{-1}]
Groundwater	0–11	330 (min 202, max 423)	25.4 (min 10.3, max 38.7)
Coast	25.0	70.6	10.4
Offshore	32.4	8.5	3.3
SGD (cm day^{-1})	54	44 (min 34, max 72)	65 (min 43, max 161)

SGD fluxes are calculated based on average endmember of all coastal springs for $^{224}Ra_{ex}$ and DSi, respectively.

The latter process occurs only around low tide when the tidal flat margins are exposed and is reflected in tidal DSi dynamics in the water column, with highest DSi concentrations around low tide (**Figure 4**; Grunwald et al., 2010). Similar to DSi, SGD transports $^{224}Ra_{ex}$ and ^{222}Rn to the open water column resulting in tidal variations as well (**Figure 4**; Moore et al., 2011; Santos et al., 2015).

The tidal variations in the water column qualify DSi as tracer for SGD because additional DSi is required to obtain the enrichments measured during low tide. Given the low surface freshwater runoff (i.e., by a flood-gate) (Grunwald et al., 2010), the primary DSi source is SGD. Consequently, mass balance models can be developed to estimate SGD fluxes (Eq. 5). For the SGD estimation, a DSi endmember concentration in marine groundwater of 500 μM (Reckhardt et al., 2015) and a DSi concentration difference between tidal basin and nearshore waters of 8 μM (**Figure 4**) was assumed. Mean water volume (105×10^6 m^3) and flushing time (4 days) of the tidal basin was assessed by Stanev et al. (2003) and Moore et al. (2011), respectively. Based on DSi, the SGD flux to the Spiekeroog tidal basin amounts to about 2×10^8 L tidal-cycle^{-1}, which is in the same range of 2–4 $\times 10^8$ L tidal-cycle^{-1} as calculated by Moore et al. (2011) using Ra isotopes. This SGD flux is equivalent to 30 cm day^{-1}, assuming a tidal flat margin length of 59 km for the entire Spiekeroog tidal basin (Moore et al., 2011) and a seepage zone of 25 m (Røy et al., 2008).

We propose that at sites highly controlled by seasonal diatom growth like the coastal region of the southern North Sea, the use of DSi is restricted to certain times of the year. With the onset of the spring diatom bloom until late summer, intensive biological DSi consumption and subsequent dissolution of diatom detritus alter the water column composition (e.g., **Figure 3**). Therefore, we suggest to restrict the use of DSi as tracer for SGD to time spans with low biological activity. $^{224}Ra_{ex}$ may in turn be used as a tracer for SGD independent from the season (**Figure 4**).

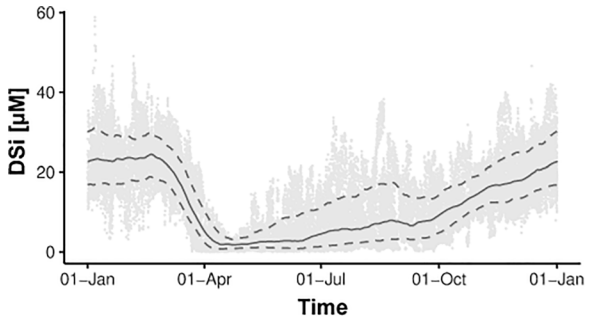

FIGURE 3 | Seasonal DSi dynamics in the water column of the Spiekeroog tidal basin. The solid line indicates the moving average of the time-dependent median including data from 2007 to 2017 and reflects typical seasonal DSi variations occurring every year. The dashed lines show the 10 and 90% quantiles.

DISCUSSION

When and Where Is DSi a Useful Tracer for SGD?

Dissolved silicon can be used as a tracer for terrestrial and marine SGD, as any water which is in contact with a sediment or aquifer matrix will be enriched in DSi with time. Some studies have used DSi as a tracer for SGD in regions impacted by a high terrestrial groundwater flow. These regions include volcanic and/or karstified carbonate rocks where a high terrestrial SGD flow occurs along conduits and cracks. For example, DSi was applied as a tracer for SGD in karstic carbonate regions such as Yucatan (Hernández-Terrones et al., 2011) and Castello, Spain (Garcia-Solsona et al., 2010b), in volcanic regions such as Hawaii (Street et al., 2008; Lubarsky et al., 2018) or Jeju island (Hwang et al., 2005) or in a mixture of volcanic and carbonate lithology's such as in southern Java (this study). Marine SGD is usually depleted in DSi in these regions (e.g., **Table 1**), and therefore DSi will either reflect brackish or fresh discharging groundwater. If brackish SGD discharges into the ocean, DSi can be used to assess the brackish fraction of SGD, in a similar way as Ra isotopes (Garcia-Solsona et al., 2010b). An SGD flux calculated on the basis of a brackish DSi groundwater endmember may thus represent a brackish SGD flux (e.g., as shown in the case study in southern Java). A fresh SGD flux should theoretically be calculated based on the DSi endmember in fresh groundwater, if conservative mixing between fresh groundwater and seawater occurs.

In tropical regions, large amounts of freshwater inputs from surface runoff and rainfall into the coastal water column further limit the applicability of salinity as a tracer for fresh SGD. DSi can consequently be a useful alternative tracer for fresh SGD. While terrestrial SGD is particularly high on small tropical islands (Zektser and Loaiciga, 1993; Moosdorf et al., 2015), only a few studies have been conducted in these regions (e.g., Matson, 1993; Kamermans et al., 2002; Knee et al., 2016; Oehler et al., 2018; Haßler et al., 2019), because they are often remote. In some instances, DSi concentrations and fluxes are reported (e.g., Johnson et al., 2008), but DSi has only rarely been used as a tracer. In southern Java, for example, the logistically challenging infrastructure (e.g., remote beaches, Ra samples needed to be exported) did not allow us to obtain large datasets for Ra (only three groundwater samples). Using DSi as an additional tracer for SGD in this setting thus allowed us to assess SGD fluxes more accurately. The comparably simple methods for measuring DSi combined with its elevated concentrations in groundwater suggest its usability as tracer for SGD in such remote locations.

In environments dominated by permeable sandy sediments DSi can also be used as tracer for SGD, as marine groundwater (or pore water) is highly enriched in DSi, for example reaching concentrations of up to 1000 μM in the tidal flat area of Spiekeroog (Reckhardt et al., 2015). In these regions DSi shows a similar tidal variability as $^{224}Ra_{ex}$, indicating a similar source from SGD (**Figure 4**). SGD fluxes based on DSi are in a similar range as those calculated from ^{224}Ra, indicating its suitability to quantify flux rates. However, high biological uptake rates of DSi (e.g., from pelagic or benthic siliceous phytoplankton) limit the time when DSi can be used as a tracer for SGD to periods

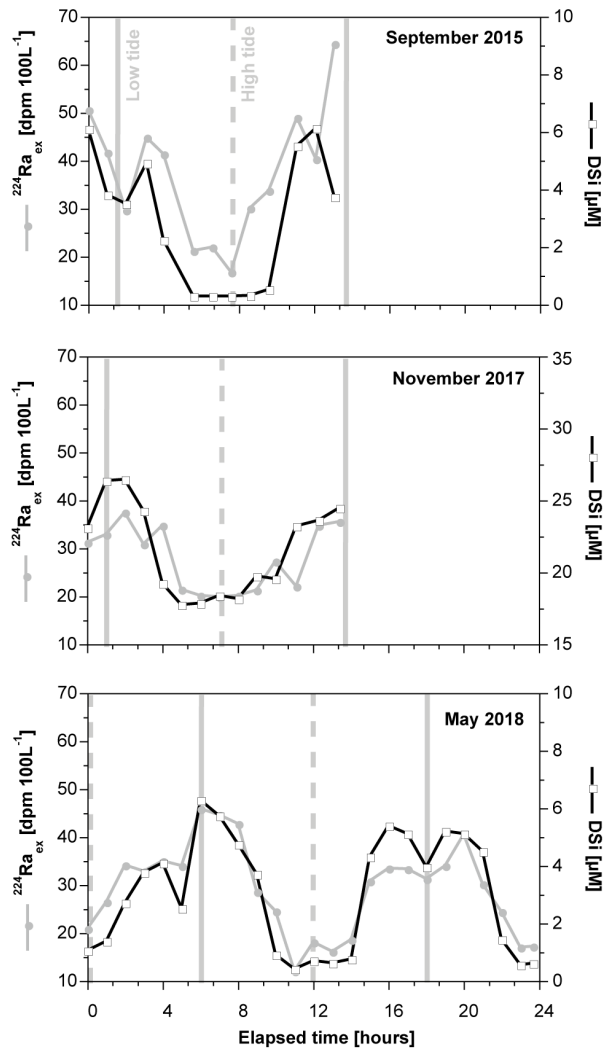

FIGURE 4 | Tidal DSi and $^{224}Ra_{ex}$ dynamics in the water column of the Spiekeroog tidal basin, with highest concentrations/activities around low tide when submarine discharge of DSi/Ra-rich groundwater is highest. The vertical solid and dashed lines indicate low tide and high tide, respectively. The water level changes smoothly depending on the tidal state. In contrast, tidal variations of DSi and $^{224}Ra_{ex}$ show a less smooth pattern because the tidal flat area consists of several tidal flats, which slightly differ in SGD fluxes and DSi endmember concentrations.

when primary productivity is low, for example due to low light availability (**Figure 3**).

Dissolved silicon can also be used in combination with other tracers such as $^{224}Ra_{ex}$ and ^{226}Ra or ^{222}Rn to calculate SGD fluxes and water residence times (e.g., Hwang et al., 2005), an approach which was successfully applied in Yeongil Bay (Kim et al., 2008), Geoje Bay (Hwang et al., 2016) and in Bangdu Bay (Hwang et al., 2005) and might be a useful tool in further SGD studies. DSi can also be useful in SGD studies if groundwater transport processes are investigated. DSi concentration gradients in the sediment can be used to identify exfiltration and infiltration patterns (Waska et al., 2019). Furthermore, if only marine SGD is investigated, simple sediment dissolution experiments can be carried out in order to estimate the residence time of marine groundwater in the sediment based on DSi groundwater concentrations (Anschutz et al., 2009).

When and Where Is DSi Not Applicable as a Tracer for SGD?

The use of DSi as a tracer for SGD is complicated if unknown or unquantifiable sources or sinks of DSi exist. Inputs of particulate Si can occur from rivers and atmospheric deposition, which need to be considered as particles can partly dissolve and release DSi into the water column. Reverse weathering, adsorption to Fe-oxides, precipitation of amorphous Al-Si phases and biological uptake can reduce DSi concentrations in surface sediments and in the water column. In SGD studies over larger spatial (e.g., shelf) or temporal scales (weeks to years) (Lee et al., 2009; Tamborski et al., 2018), the quantification of the previously named DSi sources and sinks and likewise its applicability as a tracer for SGD will become difficult.

Biological uptake depends on various factors such as the growing speed and abundance of DSi incorporating organisms, the availability of other nutrients, temperature and light (e.g., Abreu et al., 1994; DeMaster et al., 1996; Ragueneau et al., 2002; Krause et al., 2011). In many coastal regions, algae blooms such as diatoms follow a seasonal pattern (van Beusekom and Diel-Christiansen, 2009; Grunwald et al., 2010). Using DSi as a tracer for SGD may not be appropriate in these regions if biological uptake of DSi from the water column and pore waters in surface sediments is much higher when compared to inputs via SGD. DSi is for example depleted during spring phytoplankton blooms in the southern North Sea, whereby it acts as a limiting nutrient for primary producers. Biological uptake rates of DSi are consequently high during this time and difficult to quantify. During and after the deposition of diatoms at the seafloor, dissolution rates of biogenic opal in surface sediments are usually high which leads to a high efflux of DSi into the water column (Ehrenhauss et al., 2004; Oehler et al., 2015) and high DSi concentrations in groundwater (or pore water) (Reckhardt et al., 2015). During these times, the end-member concentration of DSi in groundwater will be extraordinarily high and has to be carefully determined. In the southern North Sea it will thus be more difficult to apply DSi as a tracer for SGD during and after phytoplankton blooms in comparison to periods when primary productivity is low (Beusekom and Diel-Christiansen, 2007). In many coastal regions the timing of phytoplankton blooms are well known, and thus appropriate times can be selected during which measurements should be carried out. In addition, it can be useful to determine the phytoplankton community composition and abundance if DSi is used as a tracer for SGD. Similar to other geochemical tracers, DSi cannot be used as a tracer of SGD if the DSi endmember is poorly constrained. Total SGD is composed of several different flow paths driven by a variety of different forcing mechanisms (Santos et al., 2012). In volcanic and karstic environments, defining the SGD DSi endmember may be relatively straightforward (e.g., **Table 1**). But in well-developed carbonate karstic aquifers,

very low DSi concentrations may occur in groundwater, especially under high flow conditions. Furthermore, in lithologic complex environments, DSi endmember concentrations can vary between flow paths. For example, SGD driven by water exchange between a lagoon and the sea will have a unique DSi endmember different from that of seawater circulation through the permeable beach-face (Tamborski et al., 2019). Recently recharged groundwaters will have lower DSi concentrations compared to older, deeper groundwaters.

CONCLUSION

We herein assess DSi as a tracer for SGD and which boundary conditions need to be considered. DSi becomes enriched in groundwater due to biogenic silica dissolution and water-rock interactions, and can reach a transient steady-state equilibrium between dissolution and reprecipitation with time. Therefore, groundwaters and pore waters are usually enriched in DSi when compared to surface waters, which makes DSi a useful tracer for terrestrial and marine SGD. Typical DSi concentrations in terrestrial and marine groundwater can be described depending on lithology of the respective aquifer: extrusive igneous, carbonate, sandstone, granite, shale and complex. Carbonate karst and volcanic regions promote a high terrestrial groundwater flow, where DSi works well as a tracer for terrestrial and brackish SGD. In other regions with complex lithologies (mixtures of sand and clay), such as coastal areas of the North Sea, DSi can be used as a tracer for marine SGD (e.g., forced by tidal pumping), due to the dissolution of lithogenic particles and siliceous ooze in the sediment. One of the largest constraints in using DSi as a tracer for SGD is its non-conservative behavior, especially due to biological uptake by diatoms and other primary producers. Therefore, DSi cannot be used as a tracer for SGD if large amounts of DSi are taken up by algae blooms in the area studied. Determining the phytoplankton community composition and abundance, or a conservative mixing line between salinity and DSi may help researchers to understand if the conditions are suitable to use DSi as a tracer for SGD. Furthermore, DSi can most likely not be used as a tracer for SGD over larger temporal (longer than days) and spatial scales, as it will become difficult to quantify all sources and sinks of DSi over larger scales. DSi can easily be sampled and transported; analyses are in general very cost effective and have a small analytical error. State of the art analytical methods allow precise DSi measurements with small sampling volumes of less than 1 mL. This allows endmember sampling in pore waters and groundwater even on a small vertical scale in the sediment, which has been suggested to be necessary for a representative SGD end-member (Cook et al., 2018). Future SGD studies should consider using DSi as an additional tracer to compliment ^{222}Rn or Ra investigations.

DATA AVAILABILITY

All datasets generated for this study are included in the manuscript and/or the **Supplementary Files**.

AUTHOR CONTRIBUTIONS

MB, RN, CM, BS, and JA collected data for case study 2 and wrote the section "DSi as a Tracer for SGD in a Temperate Coastal Region Protected by Barrier Islands (Spiekeroog, Southern North Sea)." JT and SR contributed with data and interpretation of sections "DSi as an Indicator for Groundwater Transport Processes" and "DSi as a Tracer for SGD in Coastal Waters" and wrote the section "DSi as an Indicator for Groundwater Transport Processes." TO, NM, and BS collected data for section "DSi as a Tracer for SGD in a Tropical Volcanic-Carbonate Karstic Region (Southern Java, Indonesia)." All authors contributed with the interpretation, writing and editing of the manuscript. TO compiled everything and wrote largest parts of sections "Introduction," "DSi as a Tracer for SGD in Coastal Waters," "DSi as a Tracer for SGD in a Tropical Volcanic-Carbonate Karstic Region (Southern Java, Indonesia)," "Discussion" and "Conclusion."

FUNDING

TO, NM, and the presented case study 1 were funded through the BMBF junior research group SGD-NUT (grant #01LN1307A). Open access publication fees are paid by Leibniz-Centre for Tropical Marine Research internal funds. The presented case study 2 was financially supported by the DFG Research Group "BioGeoChemsitry of Tidal Flats", the Ph.D. Research Training Group "The ecology of molecules" funded by the Ministry for Science and Culture of Lower Saxony, and the Institute for Chemistry and Biology of the Marine Environment, University of Oldenburg.

ACKNOWLEDGMENTS

We thank A.-S. Rupp and T. Wischermann for assistance during sampling as well as J. Freund and P. Hähnel for providing **Figure 3**. The crew of the FK Senckenberg is gratefully acknowledged.

SUPPLEMENTARY MATERIAL

The Supplementary Material for this article can be found online at: https://www.frontiersin.org/articles/10.3389/fmars.2019.00563/full#supplementary-material

REFERENCES

Abreu, P. C., Odebrecht, C., and González, A. (1994). Particulate and dissolved phytoplankton production of the patos lagoon estuary, southern Brazil: comparison of methods and influencing factors. *J. Plankton Res.* 16, 737–753. doi: 10.1093/plankt/16.7.737

Advocat, T., Chouchan, J. L., Crovisier, J. L., Guy, C., Daux, V., Jegou, C., et al. (1998). Borosilicate nuclear waste glass alteration kinetics: chemical inhibition and affinity control. *Mater. Res. Soc. Symp. Proc.* 506, 63–70. doi: 10.1557/PROC-506-63

Anschutz, P., Smith, T., Mouret, A., Deborde, J., Bujan, S., Poirier, D., et al. (2009). Tidal sands as biogeochemical reactors. *Estuar. Coast. Shelf Sci.* 84, 84–90. doi: 10.1016/j.ecss.2009.06.015

Bartoli, G., Migon, C., and Losno, R. (2005). Atmospheric input of dissolved inorganic phosphorus and silicon to the coastal northwestern mediterranean sea: fluxes, variability and possible impact on phytoplankton dynamics. *Deep Sea Res. Part I Oceanogr. Res. Pap.* 52, 2005–2016. doi: 10.1016/J.DSR.2005.06.006

Beck, A. J., and Cochran, M. A. (2013). Controls on solid-solution partitioning of radium in saturated marine sands. *Mar. Chem.* 156, 38–48. doi: 10.1016/J.MARCHEM.2013.01.008

Beck, M., and Brumsack, H.-J. (2012). Biogeochemical cycles in sediment and water column of the Wadden Sea: the example spiekeroog Island in a regional context. *Ocean Coast. Manag.* 68, 102–113. doi: 10.1016/j.ocecoaman.2012.05.026

Beck, M., Dellwig, O., Liebezeit, G., Schnetger, B., and Brumsack, H.-J. (2008). Spatial and seasonal variations of sulphate, dissolved organic carbon, and nutrients in deep pore waters of intertidal flat sediments. *Estuar. Coast. Shelf Sci.* 79, 307–316. doi: 10.1016/j.ecss.2008.04.007

Beusekom, J. E. E., and Diel-Christiansen, S. (2007). Global change and the biogeochemistry of the north sea: the possible role of phytoplankton and phytoplankton grazing. *Int. J. Earth Sci.* 98, 269–280. doi: 10.1007/s00531-007-0233-8

Billerbeck, M., Werner, U., Bosselmann, K., Walpersdorf, E., and Huettel, M. (2006). Nutrient release from an exposed intertidal sand flat. *Mar. Ecol. Prog. Ser.* 316, 35–51. doi: 10.3354/meps316035

Bluth, G. J. S., and Kump, L. R. (1994). Lithologic and climatologic controls of river chemistry. *Geochim. Cosmochim. Acta* 58, 2341–2359. doi: 10.1016/0016-7037(94)90015-9

Brzezinski, M. A. (1985). The Si:C:N ratio of marine diatoms: interspecific variability and the effect of some environmental variables. *J. Phycol.* 21, 347–357. doi: 10.1111/j.0022-3646.1985.00347.x

Burnett, W., and Dulaiova, H. (2003). Estimating the dynamics of groundwater input into the coastal zone via continuous radon-222 measurements. *J. Environ. Radioact.* 69, 21–35. doi: 10.1016/s0265-931x(03)00084-5

Burnett, W. C., Bokuniewicz, H., Huettel, M., Moore, W. S., and Taniguchi, M. (2003). Groundwater and pore water inputs to the coastal zone. *Biogeochemistry* 66, 3–33. doi: 10.1023/B:BIOG.0000006066.21240.53

Charbonnier, C., Anschutz, P., Poirier, D., Bujan, S., and Lecroart, P. (2013). Aerobic respiration in a high-energy sandy beach. *Mar. Chem.* 155, 10–21. doi: 10.1016/j.marchem.2013.05.003

Conley, D. J. (1997). Riverine contribution of biogenic silica to the oceanic silica budget. *Limnol. Oceanogr.* 42, 774–777. doi: 10.4319/lo.1997.42.4.0774

Cook, P. G., Rodellas, V., and Stieglitz, T. C. (2018). Quantifying surface water, porewater, and groundwater interactions using tracers: tracer fluxes, water fluxes, and end-member concentrations. *Water Resour. Res.* 54, 2452–2465. doi: 10.1002/2017WR021780

Daux, V., Guy, C., Advocat, T., Crovisier, J.-L., and Stille, P. (1997). Kinetic aspects of basaltic glass dissolution at 90°C: role of aqueous silicon and aluminium. *Chem. Geol.* 142, 109–126. doi: 10.1016/S0009-2541(97)00079-X

DeMaster, D. J. (2002). The accumulation and cycling of biogenic silica in the Southern Ocean: revisiting the marine silica budget. *Deep Sea Res. Part II Top. Stud. Oceanogr.* 49, 3155–3167. doi: 10.1016/S0967-0645(02)00076-0

DeMaster, D. J. (2003). The diagenesis of biogenic silica: chemical transformations occurring in the water column, seabed, and crust. *Treat. Geochimica.* 7, 87–98. doi: 10.1016/B978-0-08-095975-7.00704-X

DeMaster, D. J., Ragueneau, O., and Nittrouer, C. A. (1996). Preservation efficiencies and accumulation rates for biogenic silica and organic C, N, and P in high-latitude sediments: the ross sea. *J. Geophys. Res. Ocean.* 101, 18501–18518. doi: 10.1029/96JC01634

Dixit, S., and Van Cappellen, P. (2002). Surface chemistry and reactivity of biogenic silica. *Geochim. Cosmochim. Acta* 66, 2559–2568. doi: 10.1016/S0016-7037(02)00854-2

Dulaiova, H., Camilli, R., Henderson, P. B., and Charette, M. A. (2010). Coupled radon, methane and nitrate sensors for large-scale assessment of groundwater discharge and non-point source pollution to coastal waters. *J. Environ. Radioact.* 101, 553–563. doi: 10.1016/j.jenvrad.2009.12.004

Dürr, H., Laruelle, G., van Kempen, C., and Slomp, C. (2011). Worldwide typology of nearshore coastal systems: defining the estuarine filter of river inputs to the oceans. *Estuaries Coast.* 34, 441–458. doi: 10.1007/s12237-011-9381-y

Dyer, K. (1973). *Estuaries: a Physical Introduction*. London: John Wiley.

Ehlert, C., Reckhardt, A., Greskowiak, J., Liguori, B. T. P., Böning, P., Paffrath, R., et al. (2016). Transformation of silicon in a sandy beach ecosystem: insights from stable silicon isotopes from fresh and saline groundwaters. *Chem. Geol.* 440, 207–218. doi: 10.1016/J.CHEMGEO.2016.07.015

Ehrenhauss, S., Witte, U., Janssen, F., and Huettel, M. (2004). Decomposition of diatoms and nutrient dynamics in permeable north sea sediments. *Cont. Shelf Res.* 24, 721–737. doi: 10.1016/J.CSR.2004.01.002

Fanning, K. A., Breland, J. A., and Byrne, R. H. (1982). Radium-226 and radon-222 in the coastal waters of west Florida: high concentrations and atmospheric degassing. *Science* 215, 667–670. doi: 10.1126/science.215.4533.667

Flathe, H., and Pfeiffer, D. (1965). Grundzüge der geomorpholgie, geologie und hydrogeologie im karstgebiet gunung sewu (Java, Indonesien). *Geol. Jahrb. B* 83, 533–562.

Forster, S., and Graf, G. (1995). Impact of irrigation on oxygen flux into the sediment: intermittent pumping by callianassa subterranea and "piston-pumping" by *Lanice Conchilega*. *Mar. Biol.* 123, 335–346. doi: 10.1007/bf00353625

Garcia-Solsona, E., Garcia-Orellana, J., Masqué, P., Garcés, E., Radakovitch, O., Mayer, A., et al. (2010a). An assessment of karstic submarine groundwater and associated nutrient discharge to a Mediterranean coastal area (Balearic Islands, Spain) using radium isotopes. *Biogeochemistry* 97, 211–229. doi: 10.1007/s10533-009-9368-y

Garcia-Solsona, E., Garcia-Orellana, J., Masqué, P., Rodellas, V., Mejías, M., Ballesteros, B., et al. (2010b). Groundwater and nutrient discharge through karstic coastal springs (Castelló, Spain). *Biogeosciences* 7, 2625–2638. doi: 10.5194/bg-7-2625-2010

Gislason, S. R., and Oelkers, E. H. (2003). Mechanism, rates, and consequences of basaltic glass dissolution: II. an experimental study of the dissolution rates of basaltic glass as a function of pH and temperature. *Geochim. Cosmochim. Acta* 67, 3817–3832. doi: 10.1016/S0016-7037(00)00176-5

Grunwald, M., Dellwig, O., Kohlmeier, C., Kowalskic, N., Becka, M., Badewiena, T. H., et al. (2010). Nutrient dynamics in a back barrier tidal basin of the Southern North Sea: time-series, model simulations, and budget estimates. *J. Sea Res.* 64, 199–212. doi: 10.1016/j.seares.2010.02.008

Hartmann, J., Jansen, N., Dürr, H. H., Harashima, A., Okubo, K., and Kempe, S. (2010). Predicting riverine dissolved silica fluxes to coastal zones from a hyperactive region and analysis of their first-order controls. *Int. J. Earth Sci.* 99, 207–230. doi: 10.1007/s00531-008-0381-5

Haryono, E., and Day, M. (2004). Landform differentiation within the Gunung Kidul Kegelkarst, Java, Indonesia. *J. Cave Karst Stud.* 66, 62–69.

Haßler, K., Dähnke, K., Kölling, M., Sichoix, L., Nickl, A.-L., and Moosdorf, N. (2019). Provenance of nutrients in submarine fresh groundwater discharge on Tahiti and Moorea, French Polynesia. *Appl. Geochem.* 100, 181–189. doi: 10.1016/J.APGEOCHEM.2018.11.020

Hernández-Terrones, L., Rebolledo-Vieyra, M., Merino-Ibarra, M., Soto, M., Le-Cossec, A., and Monroy-Ríos, E. (2011). Groundwater pollution in a karstic region (NE Yucatan): baseline nutrient content and flux to coastal ecosystems. *Water Air Soil Pollut.* 218, 517–528. doi: 10.1007/s11270-010-0664-x

Horton, T. W., Chamberlain, C. P., Fantle, M., and Blum, J. D. (1999). Chemical weathering and lithologic controls of water chemistry in a high-elevation river system: clark's fork of the yellowstone river, wyoming and montana. *Water Resour. Res.* 35, 1643–1655. doi: 10.1029/1998WR900103

Huettel, M., Ziebis, W., Forster, S., and Luther, G. W. (1998). Advective transport affecting metal and nutrient distributions and interfacial fluxes in permeable sediments. *Geochim. Cosmochim. Acta* 62, 613–631. doi: 10.1016/S0016-7037(97)00371-2

Hurd, D. C. (1973). Interactions of biogenic opal, sediment and seawater in the Central Equatorial Pacific. *Geochim. Cosmochim. Acta* 37, 2257–2282. doi: 10.1016/0016-7037(73)90103-8

Hwang, D., Lee, Y., and Kim, G. (2005). Large submarine groundwater discharge and benthic eutrophication in Bangdu Bay on volcanic Jeju Island, Korea. *Limnol. Oceanogr.* 50, 1393–1403. doi: 10.4319/lo.2005.50.5.1393

Hwang, D.-W., Lee, I.-S., Choi, M., and Kim, T.-H. (2016). Estimating the input of submarine groundwater discharge (SGD) and SGD-derived nutrients in Geoje Bay, Korea using 222Rn-Si mass balance model. *Mar. Pollut. Bull.* 110, 119–126. doi: 10.1016/J.MARPOLBUL.2016.06.073

Jacobson, A. D., Blum, J. D., Chamberlain, C. P., Craw, D., and Koons, P. O. (2003). Climatic and tectonic controls on chemical weathering in the New Zealand Southern Alps. *Geochim. Cosmochim. Acta* 67, 29–46. doi: 10.1016/S0016-7037(02)01053-0

Jeandel, C., and Oelkers, E. H. (2015). The influence of terrigenous particulate material dissolution on ocean chemistry and global element cycles. *Chem. Geol.* 395, 50–66. doi: 10.1016/j.chemgeo.2014.2014.12.001

Johnson, A. G., Glenn, C. R., Burnett, W. C., Peterson, R. N., and Lucey, P. G. (2008). Aerial infrared imaging reveals large nutrient-rich groundwater inputs to the ocean. *Geophys. Res. Lett.* 35:L15606. doi: 10.1029/2008GL034574

Jones, M. T., Pearce, C. R., Jeandel, C., Gislason, S. R., Eiriksdottir, E. S., Mavromatis, V., et al. (2012). Riverine particulate material dissolution as a significant flux of strontium to the oceans. *Earth Planet. Sci. Lett.* 35, 51–59. doi: 10.1016/j.epsl.2012.08.040

Kamermans, P., Hemminga, M. A., Tack, J. F., Mateo, M. Á, Marbà, N., Mtolera, M., et al. (2002). Groundwater effects on diversity and abundance of lagoonal seagrasses in Kenya and on Zanzibar Island (East Africa). *Mar. Ecol. Prog. Ser* 231, 75–83. doi: 10.3354/meps231075

Khalil, K., Rabouille, C., Gallinari, M., Soetaert, K., DeMaster, D. J., and Ragueneau, O. (2007). Constraining biogenic silica dissolution in marine sediments: a comparison between diagenetic models and experimental dissolution rates. *Mar. Chem.* 106, 223–238. doi: 10.1016/j.marchem.2006.12.004

Kim, G., Ryu, J.-W., and Hwang, D.-W. (2008). Radium tracing of submarine groundwater discharge (SGD) and associated nutrient fluxes in a highly-permeable bed coastal zone, Korea. *Mar. Chem.* 109, 307–317. doi: 10.1016/J.MARCHEM.2007.07.002

Kim, G., Ryu, J.-W., Yang, H.-S., and Yun, S.-T. (2005). Submarine groundwater discharge (SGD) into the Yellow Sea revealed by 228Ra and 226Ra isotopes: implications for global silicate fluxes. *Earth Planet. Sci. Lett.* 237, 156–166. doi: 10.1016/J.EPSL.2005.06.011

Knee, K. L., Crook, E. D., Hench, J. L., Leichter, J. J., and Paytan, A. (2016). Assessment of submarine groundwater discharge (SGD) as a source of dissolved radium and nutrients to Moorea (French Polynesia) Coastal Waters. *Estuaries Coast.* 39, 1651–1668. doi: 10.1007/s12237-016-0108-y

Kowalski, N., Dellwig, O., Beck, M., Gräwea, U., Neubertc, N., Näglerc, T. F., et al. (2013). Pelagic molybdenum concentration anomalies and the impact of sediment resuspension on the molybdenum budget in two tidal systems of the North Sea. *Geochim. Cosmochim. Acta* 119, 198–211. doi: 10.1016/J.GCA.2013.05.046

Kowalski, N., Dellwig, O., Beck, M., Grunwald, M., Dürselend, C.-D., Badewienb, T. H., et al. (2012). A comparative study of manganese dynamics in the water column and sediments of intertidal systems of the North Sea. *Estuar. Coast. Shelf Sci.* 100, 3–17. doi: 10.1016/j.ecss.2011.03.011

Krause, J. W., Brzezinski, M. A., Baines, S. B., Collier, J. L., Twining, B. S., and Ohnemus, D. C. (2017). Picoplankton contribution to biogenic silica stocks and production rates in the Sargasso Sea. *Global Biogeochem. Cycles* 31, 762–774. doi: 10.1002/2017GB005619

Krause, J. W., Nelson, D. M., and Brzezinski, M. A. (2011). Biogenic silica production and the diatom contribution to primary production and nitrate uptake in the eastern equatorial Pacific Ocean. *Deep Sea Res. Part II Top. Stud. Oceanogr.* 58, 434–448. doi: 10.1016/J.DSR2.2010.08.010

Lecher, A., and Mackey, K. (2018). Synthesizing the effects of submarine groundwater discharge on marine biota. *Hydrology* 5:60. doi: 10.3390/hydrology5040060

Lecher, A. L., Chien, C.-T., and Paytan, A. (2016). Submarine groundwater discharge as a source of nutrients to the North Pacific and Arctic coastal ocean. *Mar. Chem.* 186, 167–177. doi: 10.1016/J.MARCHEM.2016.09.008

Lee, C. M., Jiao, J. J., Luo, X., and Moore, W. S. (2012). Estimation of submarine groundwater discharge and associated nutrient fluxes in Tolo Harbour, Hong Kong. *Sci. Total Environ.* 433, 427–433. doi: 10.1016/J.SCITOTENV.2012.06.073

Lee, Y.-W., Hwang, D.-W., Kim, G., Lee, W.-C., and Oh, H.-T. (2009). Nutrient inputs from submarine groundwater discharge (SGD) in Masan Bay, an embayment surrounded by heavily industrialized cities, Korea. *Sci. Total Environ.* 407, 3181–3188. doi: 10.1016/J.SCITOTENV.2008.04.013

Loucaides, S., Behrends, T., and Van Cappellen, P. (2010). Reactivity of biogenic silica: surface versus bulk charge density. *Geochim. Cosmochim. Acta* 74, 517–530. doi: 10.1016/j.gca.2009.10.038

Loucaides, S., Van Cappellen, P., and Behrends, T. (2008). Dissolution of biogenic silica from land to ocean: role of salinity and pH. *Limnol. Oceanogr.* 53, 1614–1621. doi: 10.4319/lo.2008.53.4.1614

Loucaides, S., van Cappellen, P., Roubeix, V., Moriceau, B., and Ragueneau, O. (2012). Controls on the recycling and preservation of biogenic silica from biomineralization to burial. *Silicon* 4, 7–22. doi: 10.1007/s12633-011-9092-9

Lubarsky, K. A., Silbiger, N. J., and Donahue, M. J. (2018). Effects of submarine groundwater discharge on coral accretion and bioerosion on two shallow reef flats. *Limnol. Oceanogr.* 63, 1660–1676. doi: 10.1002/lno.10799

Luo, X., Jiao, J. J., Moore, W. S., and Lee, C. M. (2014). Submarine groundwater discharge estimation in an urbanized embayment in Hong Kong via short-lived radium isotopes and its implication of nutrient loadings and primary production. *Mar. Pollut. Bull.* 82, 144–154. doi: 10.1016/J.MARPOLBUL.2014.03.005

Mackin, J. E., and Aller, R. C. (1984). Dissolved Al in sediments and waters of the East China Sea: implications for authigenic mineral formation. *Geochim. Cosmochim. Acta* 48, 281–297. doi: 10.1016/0016-7037(84)90251-5

Matson, E. A. (1993). Nutrient flux through soils and aquifers to the coastal zone of Guam (Mariana Islands). *Limnol. Oceanogr.* 38, 361–371. doi: 10.4319/lo.1993.38.2.0361

Meier, S. (2014). *Spatio Temporal Turnover Of A Phytoplankton Meta Community In a Natural Coastal System*. Ph.D thesis, University of Oldenburg, Oldenburg.

Meier, S., Muijsers, F., Beck, M., Badewien, T. H., and Hillebrand, H. (2015). Dominance of the non-indigenous diatom Mediopyxis helysia in Wadden Sea phytoplankton can be linked to broad tolerance to different Si and N supplies. *J. Sea Res.* 95, 36–44. doi: 10.1016/j.seares.2014.10.001

Michalopoulos, P., and Aller, R. C. (2004). Early diagenesis of biogenic silica in the Amazon delta: alteration, authigenic clay formation, and storage. *Geochim. Cosmochim. Acta* 68, 1061–1085. doi: 10.1016/j.gca.2003.07.018

Moore, W. (2010). The effect of submarine groundwater discharge on the ocean. *Ann. Rev. Mar. Sci.* 2, 59–88. doi: 10.1146/annurev-marine-120308-081019

Moore, W. S., Beck, M., Riedel, T., Rutgers van der Loeff, M., Dellwig, O., et al. (2011). Radium-based pore water fluxes of silica, alkalinity, manganese, DOC, and uranium: a decade of studies in the german wadden sea. *Geochim. Cosmochim. Acta* 75, 6535–6555. doi: 10.1016/J.GCA.2011.08.037

Moore, W. S., Blanton, J. O., and Joye, S. B. (2006). Estimates of flushing times, submarine groundwater discharge, and nutrient fluxes to Okatee Estuary, South Carolina. *J. Geophys. Res.* 111:C09006. doi: 10.1029/2005JC003041

Moore, W. S., and Reid, D. F. (1973). Extraction of radium from natural waters using manganese-impregnated acrylic fibers. *J. Geophys. Res.* 78, 8880–8886. doi: 10.1029/JC078i036p08880

Moosdorf, N., Hartmann, J., and Lauerwald, R. (2011). Changes in dissolved silica mobilization into river systems draining North America until the period 2081–2100. *J. Geochem. Explor.* 110, 31–39. doi: 10.1016/J.GEXPLO.2010.09.001

Moosdorf, N., and Oehler, T. (2017). Societal use of fresh submarine groundwater discharge: an overlooked water resource. *Earth Sci. Rev.* 171, 338–348. doi: 10.1016/J.EARSCIREV.2017.06.006

Moosdorf, N., Stieglitz, T., Waska, H., Dürr, H. H., and Hartmann, J. (2015). Submarine groundwater discharge from tropical islands: a review. *Grundwasser* 20, 53–67. doi: 10.1007/s00767-014-0275-3

Morin, G. P., Vigier, N., and Verney-Carron, A. (2015). Enhanced dissolution of basaltic glass in brackish waters: impact on biogeochemical cycles. *Earth Planet. Sci. Lett.* 417, 1–8. doi: 10.1016/j.epsl.2015.02.005

Oehler, T., Eiche, E., Putra, D., Adyasari, D., Hennig, H., Mallast, U., et al. (2018). Seasonal variability of land-ocean groundwater nutrient fluxes from a tropical karstic region (southern Java, Indonesia). *J. Hydrol.* 565, 662–671. doi: 10.1016/J.JHYDROL.2018.08.077

Oehler, T., Schlüter, M., and Schückel, U. (2015). Seasonal dynamics of the biogenic silica cycle in surface sediments of the Helgoland Mud Area (southern North Sea). *Cont. Shelf Res.* 107, 103–114. doi: 10.1016/j.csr.2015.07.016

Oelkers, E. H., and Gislason, S. R. (2001). The mechanism, rates and consequences of basaltic glass dissolution: i. an experimental study of the dissolution rates of basaltic glass as a function of aqueous al, si and oxalic acid concentration at 25°C and pH = 3 and 11. *Geochim. Cosmochim. Acta* 65, 3671–3681. doi: 10.1016/S0016-7037(01)00664-0

Oelkers, E. H., Jones, M. T., Pearce, C. R., Jeandel, C., Eiriksdottir, E. S., and Gislason, S. R. (2012). Riverine particulate material dissolution in seawater and its implications for the global cycles of the elements. *Comptes Rendus Geosci.* 344, 646–651. doi: 10.1016/j.crte.2012.08.005

Onodera, S., Saito, M., Hayashi, M., and Sawano, M. (2007). Nutrient dynamics with groundwater-seawater interactions in a beach slope of a steep island, western Japan. *IAHS Publ.* 312:150.

Rad, S. D., Allègre, C. J., and Louvat, P. (2007). Hidden erosion on volcanic islands. *Earth Planet. Sci. Lett.* 262, 109–124. doi: 10.1016/j.epsl.2007.07.019

Ragueneau, O., Chauvaud, L., Leynaert, A., Thouzeau, G., Paulet, Y.-M., Bonnet, S., et al. (2002). Direct evidence of a biologically active coastal silicate pump: ecological implications. *Limnol. Oceanogr.* 47, 1849–1854. doi: 10.4319/lo.2002.47.6.1849

Rahman, S., Tamborski, J. J., Charette, M. A., and Cochran, J. K. (2019). Dissolved silica in the subterranean estuary and the impact of submarine groundwater discharge on the global marine silica budget. *Mar. Chem.* 208, 29–42. doi: 10.1016/J.MARCHEM.2018.11.006

Reckhardt, A., Beck, M., Seidel, M., Riedel, T., Wehrmann, A., Bartholom, A., et al. (2015). Carbon, nutrient and trace metal cycling in sandy sediments: a comparison of high-energy beaches and backbarrier tidal flats. *Estuar. Coast. Shelf Sci.* 159, 1–14. doi: 10.1016/j.ecss.2015.03.025

Reid, P. C., Lancelot, C., Gieskes, W. W. C., Hagmeier, E., and Weichart, G. (1990). Phytoplankton of the North Sea and its dynamics: a review. *Netherlands J. Sea Res.* 26, 295–331. doi: 10.1016/0077-7579(90)90094-W

Rengarajan, R., and Sarma, V. V. S. S. (2015). Submarine groundwater discharge and nutrient addition to the coastal zone of the Godavari estuary. *Mar. Chem.* 172, 57–69. doi: 10.1016/J.MARCHEM.2015.03.008

Riedel, T., Lettmann, K., Beck, M., and Brumsack, H.-J. (2010). Tidal variations in groundwater storage and associated discharge from an intertidal coastal aquifer. *J. Geophys. Res.* 115:C04013. doi: 10.1029/2009JC005544

Røy, H., Lee, J. S., Jansen, S., and de Beer, D. (2008). Tide-driven deep pore-water flow in intertidal sand flats. *Limnol. Oceanogr.* 53, 1521–1530. doi: 10.4319/lo.2008.53.4.1521

Rutgers Van Der Loeff, M. M., Anderson, L. G., Hall, P. O., Iversfeldt, A., Josefson, A. B., Sundby, B., et al. (1984). The asphyxiation technique: an approach to distinguishing between molecular diffusion and biologically mediated transport at the sediment-water interface. *Limnol. Oceanogr.* 29, 675–686. doi: 10.4319/lo.1984.29.4.0675

Santos, I. R., Beck, M., Brumsack, H.-J., Maher, D. T., Dittmar, T., Waska, H., et al. (2015). Porewater exchange as a driver of carbon dynamics across a terrestrial-marine transect: insights from coupled 222Rn and pCO2 observations in the German wadden sea. *Mar. Chem.* 171, 10–20. doi: 10.1016/j.marchem.2015.02.005

Santos, I. R., Eyre, B. D., and Huettel, M. (2012). The driving forces of porewater and groundwater flow in permeable coastal sediments: a review. *Estuar. Coast. Shelf Sci.* 98, 1–15. doi: 10.1016/J.ECSS.2011.10.024

Schink, D. R., Fanning, K. A., and Pilson, M. E. Q. (1974). Dissolved silica in the upper pore waters of the Atlantic Ocean floor. *J. Geophys. Res.* 79, 2243–2250. doi: 10.1029/JC079i015p02243

Schink, D. R., Guinasso, N. L., and Fanning, K. A. (1975). Processes affecting the concentration of silica at the sediment-water interface of the Atlantic Ocean. *J. Geophys. Res.* 80, 3013–3031. doi: 10.1029/jc080i021p03013

Schoemann, V., deBarr, H. J. W., de Jong, J. T. M., and Lancelot, C. (1998). Effects of phytoplankton blooms of the cycling of manganese and iron in coastal waters. *Limnol. Oceanogr.* 43, 1427–1441. doi: 10.4319/lo.1998.43.7.1427

Schopka, H. H., and Derry, L. A. (2012). . Chemical weathering fluxes from volcanic islands and the importance of groundwater: the Hawaiian example. *Earth Planet. Sci. Lett.* 339–340, 67–78. doi: 10.1016/j.epsl.2012.05.028

Seidel, M., Beck, M., Greskowiak, J., Riedel, T., Waska, H., Suryaputra, I. G. N. A., et al. (2015). Benthic-pelagic coupling of nutrients and dissolved organic matter composition in an intertidal sandy beach. *Mar. Chem.* 176, 150–163. doi: 10.1016/J.MARCHEM.2015.08.011

Slomp, C., and Van Cappellen, P. (2004). Nutrient inputs to the coastal ocean through submarine groundwater discharge: controls and potential impact. *J. Hydrol.* 295, 64–86. doi: 10.1016/j.jhydrol.2004.02.018

Stanev, E. V., Wolff, J.-O., Burchard, H., Bolding, K., and Flöser, G. (2003). On the circulation in the East Frisian Wadden Sea: numerical modeling and data analysis. *Ocean Dyn.* 53, 27–51. doi: 10.1007/s10236-002-0022-7

Staudigel, H., Yayanos, A., Chastain, R., Davies, G., Verdurmen, E. A. T., Schiffman, P., et al. (1998). Biologically mediated dissolution of volcanic glass in seawater. *Earth Planet. Sci. Lett.* 164, 233–244. doi: 10.1016/S0012-821X(98)00207-6

Street, J. H., Knee, K. L., Grossman, E. E., and Paytan, A. (2008). Submarine groundwater discharge and nutrient addition to the coastal zone and coral reefs of leeward Hawai'i. *Mar. Chem.* 109, 355–376. doi: 10.1016/J.MARCHEM.2007.08.009

Sugimoto, R., Kitagawa, K., Nishi, S., Honda, H., Yamada, M., Kobayashi, S., et al. (2017). Phytoplankton primary productivity around submarine groundwater discharge in nearshore coasts. *Mar. Ecol. Prog. Ser.* 563, 25–33. doi: 10.3354/meps11980

Swarzenski, P. W. (2007). U/Th series radionuclides as coastal groundwater tracers. *Chem. Rev.* 107, 663–674. doi: 10.1021/CR0503761

Tamborski, J., Beek, P., Rodellas, V., Monnin, C., Bergsma, E., Stieglitz, T., et al. (2019). Temporal variability of lagoon–sea water exchange and seawater circulation through a Mediterranean barrier beach. *Limnol. Oceanogr.* 1–22. doi: 10.1002/lno.11169

Tamborski, J., Bejannin, S., Garcia-Orellana, J., Souhaut, M., Charbonnier, C., Anschutz, P., et al. (2018). A comparison between water circulation and terrestrially-driven dissolved silica fluxes to the Mediterranean Sea traced using radium isotopes. *Geochim. Cosmochim. Acta* 238, 496–515. doi: 10.1016/j.gca.2018.07.022

Techer, I., Advocat, T., Lancelot, J., and Liotard, J. M. (2001). Dissolution kinetics of basaltic glasses: control by solution chemistry and protective effect of the alteration film. *Chem. Geol.* 176, 235–263. doi: 10.1016/S0009-2541(00)00400-9

Tréguer, P. J., and De La Rocha, C. L. (2013). The world ocean silica cycle. *Ann. Rev. Mar. Sci.* 5, 477–501. doi: 10.1146/annurev-marine-121211-172346

van Bemmelen, R. (1949). "Geological evolution of the physiographic units-Java," in *The Geology of Indonesia*, Vol. IA, ed. R. W. van Bemmelen, (The Hague: Government Printing Office), 554–559.

van Beusekom, J., and Diel-Christiansen, S. (2009). Global change and the biogeochemistry of the North Sea: the possible role of phytoplankton and phytoplankton grazing. *Int. J. Earth Sci.* 98, 269–280. doi: 10.1007/s00531-007-0233-8

Van Cappellen, P., Dixit, S., and van Beusekom, J. (2002). Biogenic silica dissolution in the oceans: reconciling experimental and field-based dissolution rates. *Global Biogeochem. Cycles* 16, 10–23. doi: 10.1029/2001GB001431

Van Cappellen, P., and Qiu, L. (1997). Biogenic silica dissolution in sediments of the Southern Ocean. I. Solubility. *Deep. Res. Part II Top. Stud. Oceanogr.* 44, 1109–1128. doi: 10.1016/S0967-0645(96)00113-0

Waltham, A., Smart, P., Friederich, H., and Eavis, A. (1983). The caves of Gunung Sewu, Java. *Cave Sci.* 10, 55–96.

Wang, G., Wang, Z., Zhai, W., Moore, W. S., Li, Q., Yan, X., et al. (2015). Net subterranean estuarine export fluxes of dissolved inorganic C, N, P, Si, and total

alkalinity into the Jiulong River estuary, China. *Geochim. Cosmochim. Acta* 149, 103–114. doi: 10.1016/J.GCA.2014.11.001

Waska, H., Greskowiak, J., Ahrens, J., Beck, M., Ahmerkamp, S., and Böning, P. (2019). Spatial and temporal patterns of pore water chemistry in the inter-tidal zone of a high energy beach. *Front. Mar. Sci.* 6:154. doi: 10.3389/fmars.2019.00154

Webster, I. T., Hancock, G. J., and Murray, A. S. (1995). Modelling the effect of salinity on radium desorption from sediments. *Geochim. Cosmochim. Acta* 59, 2469–2476. doi: 10.1016/0016-7037(95)00141-7

Weinstein, Y., Yechieli, Y., Shalem, Y., Burnett, W. C., Swarzenski, P. W., and Herut, B. (2011). What is the role of fresh groundwater and recirculated seawater in conveying nutrients to the Coastal Ocean? *Environ. Sci. Technol.* 45, 5195–5200. doi: 10.1021/es104394r

Wiltshire, K. H., Boersma, M., Carstens, K., Kraberg, A. C., Peters, S., and Scharfe, M. (2015). Control of phytoplankton in a shelf sea: determination of the main drivers based on the helgoland roads time series. *J. Sea Res.* 105, 42–52. doi: 10.1016/j.seares.2015.06.022

Ye, Q., Liu, J., Du, J., and Zhang, J. (2016). Bacterial diversity in submarine groundwater along the coasts of the Yellow Sea. *Front. Microbiol.* 6:1519. doi: 10.3389/fmicb.2015.01519

Zektser, I. S., and Loaiciga, H. A. (1993). Groundwater fluxes in the global hydrologic cycle: past, present and future. *J. Hydrol.* 144, 405–427. doi: 10.1016/0022-1694(93)90182-9

Zhang, J., Zhang, G. S., and Liu, S. M. (2005). Dissolved silicate in coastal marine rainwaters: comparison between the yellow sea and the east china sea on the impact and potential link with primary production. *J. Geophys. Res.* 110:D16304. doi: 10.1029/2004JD005411

Conflict of Interest Statement: The authors declare that the research was conducted in the absence of any commercial or financial relationships that could be construed as a potential conflict of interest.

frontiers in Environmental Science

REVIEW
published: 01 October 2019
doi: 10.3389/fenvs.2019.00141

Submarine Groundwater Discharge: Updates on Its Measurement Techniques, Geophysical Drivers, Magnitudes, and Effects

Makoto Taniguchi[1]*, *Henrietta Dulai*[2], *Kimberly M. Burnett*[3], *Isaac R. Santos*[4,5], *Ryo Sugimoto*[6], *Thomas Stieglitz*[7,8], *Guebuem Kim*[9], *Nils Moosdorf*[10] and *William C. Burnett*[11]

[1] Research Institute for Humanity and Nature, Kyoto, Japan, [2] Department of Earth Sciences, University of Hawaii, Honolulu, HI, United States, [3] University of Hawaii Economic Research Organization, University of Hawaii, Honolulu, HI, United States, [4] National Marine Science Centre, Southern Cross University, Lismore, NSW, Australia, [5] Department of Marine Sciences, University of Gothenburg, Gothenburg, Sweden, [6] Research Center for Marine Bioresources, Fukui Prefectural University, Obama, Japan, [7] Centre for Tropical Water and Aquatic Ecosystem Research, James Cook University, Townsville, QLD, Australia, [8] Aix-Marseille Université, CNRS, IRD, INRA, Coll France, CEREGE, Aix-en-Provence, France, [9] School of Earth & Environmental Sciences/RIO, Seoul National University, Seoul, South Korea, [10] Leibniz Centre for Tropical Marine Research (LG), Bremen, Germany, [11] Department of Earth, Ocean and Atmospheric Science, Florida State University, Tallahassee, FL, United States

OPEN ACCESS

Edited by:
Davide Poggi,
Politecnico di Torino, Italy

Reviewed by:
Henry Bokuniewicz,
The State University of New York (SUNY), United States
Pei Xin,
Hohai University, China

***Correspondence:**
Makoto Taniguchi
makoto@chikyu.ac.jp

Specialty section:
This article was submitted to Water and Wastewater Management, a section of the journal Frontiers in Environmental Science

Received: *30 June 2019*
Accepted: *10 September 2019*
Published: *01 October 2019*

Citation:
Taniguchi M, Dulai H, Burnett KM, Santos IR, Sugimoto R, Stieglitz T, Kim G, Moosdorf N and Burnett WC (2019) Submarine Groundwater Discharge: Updates on Its Measurement Techniques, Geophysical Drivers, Magnitudes, and Effects. Front. Environ. Sci. 7:141. doi: 10.3389/fenvs.2019.00141

The number of studies concerning Submarine Groundwater Discharge (SGD) grew quickly as we entered the twenty-first century. Many hydrological and oceanographic processes that drive and influence SGD were identified and characterized during this period. These processes included tidal effects on SGD, water and solute fluxes, biogeochemical transformations through the subterranean estuary, and material transport via SGD from land to sea. Here we compile and summarize the significant progress in SGD assessment methodologies, considering both the terrestrial and marine driving forces, and local as well as global evaluations of groundwater discharge with an emphasis on investigations published over the past decade. Our treatment presents the state-of-the-art progress of SGD studies from geophysical, geochemical, bio-ecological, economic, and cultural perspectives. We identify and summarize remaining research questions, make recommendations for future research directions, and discuss potential future challenges, including impacts of climate change on SGD and improved estimates of the global magnitude of SGD.

Keywords: submarine groundwater discharge, subterranean estuaries, geophysics, geochemistry, cultural and economic aspects

INTRODUCTION

Some material pathways from land to the sea are obvious while others are not so apparent. Rivers, for example, slowly erode the continents and carry dissolved materials from land to the ocean. This never-ending delivery of dissolved salt to the sea so impressed Joly (1899), University of Dublin, that he calculated that it would take rivers about 90 million years to deliver all the sodium dissolved in the world's oceans. He further speculated that this might be a good approximation for the age of the Earth. Of course, we now know that what he actually estimated was the residence time of sodium. Still, rivers are a major contributor of dissolved materials to the sea. But there are other contributors as well.

Could groundwater play an important role in such land-sea exchange? Terrestrial groundwater flows down-gradient and ultimately discharges into the sea (**Figure 1**). This process, part of what is now called "submarine groundwater discharge" (SGD) has become recognized as an important factor in land-sea exchange. While the presence of submarine springs has been known since the days of the Romans, this "invisible pathway" was neglected scientifically for many years because of the difficulty in assessment and the perception that the process was unimportant. This perception has now changed dramatically. Within the last several years there has emerged a recognition that in some cases, groundwater discharge into the sea may be both volumetrically and chemically important. The earlier views were at least partially driven by the difficulty in measuring such flows. Most large rivers are gauged, and their discharges can often be found online. While there is no direct gauge for SGD, techniques have been worked out over the last few decades that allow us to estimate these flows.

Here we define SGD as "the flow of water through continental and insular margins from the seabed to the coastal ocean, regardless of fluid composition or driving force" (Burnett et al., 2003). Note that we have added the term "insular" to the original definition. As pointed out before (Zektser and Everett, 2000; Moosdorf et al., 2015) islands typically have higher groundwater discharge fluxes per unit area of land mass than continents. Also note that since we view "groundwater" as any water in the saturated zone of geologic material (Freeze and Cherry, 1979), groundwater is here synonymous with pore water. Importantly, SGD includes waters of any salinity. In fact, fresh water from recharged aquifers on land only represents a minor portion of the total flux in many cases. Moore (2010) added a "scale length of meters to kilometers" to the earlier definition in order to separate SGD from microscale processes involving pore water exchange. A reasonable idea as the mechanisms driving the flow are very different. See further discussion on this subject in section Geophysical Processes.

Another term that has become widely used in the field is the "subterranean estuary" (STE; Moore, 1999). Basically, the STE is seen as the mixing zone between groundwater and seawater within a coastal aquifer. Within this zone, reactions occur that can substantially modify the composition of these fluids. So, while one might envision the penetration of seawater and its subsequent discharge back into the sea as "seawater recycling," the geochemical processes within the subterranean estuary may have distinctly altered the composition of the discharging water.

Since there have been a few previous reviews (e.g., Burnett et al., 2003; Moore, 2010) of SGD research, we will limit this overview to updates and refinements since about 2010. We will restrict our coverage to marine settings including the coastal zone, shelf, estuaries, and lagoons. We will include updates concerning measurements, estimates of SGD magnitudes, geochemical/ecological effects, and cultural/economic aspects. While many SGD studies have been concerned with possible chemical/ecological implications, there have also been recent efforts to evaluate the economic and cultural values associated with SGD (e.g., Michael et al., 2017; Moosdorf and Oehler, 2017; Burnett et al., 2018; Pongkijvorasin et al., 2018). There is

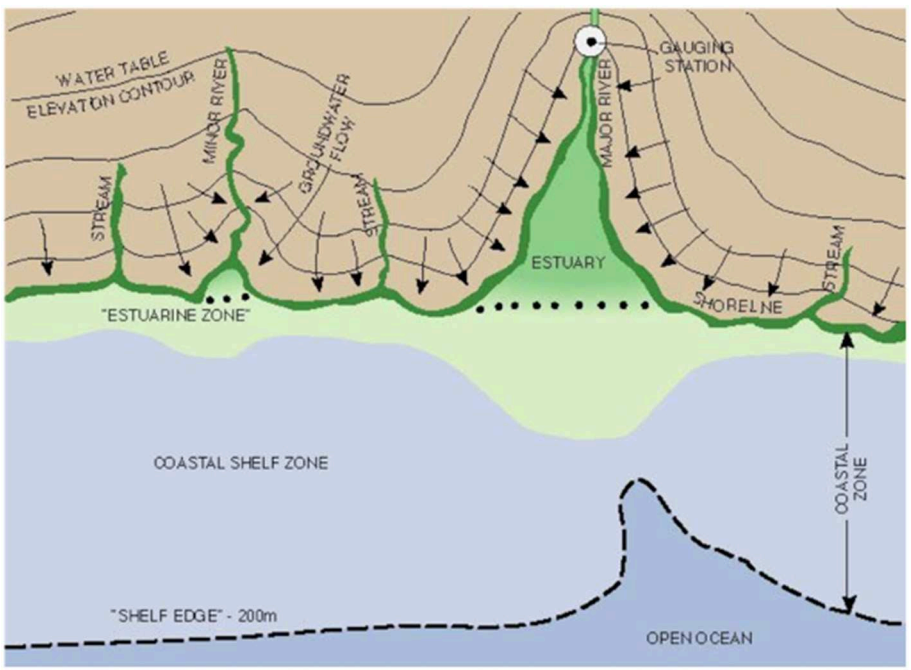

FIGURE 1 | Schematic of the coastal zone showing water table contours and terrestrial groundwater flow paths. This illustrates how groundwater flow driven by hydraulic gradients is focused in river valley estuaries and dispersed at highlands. Note that the groundwater contours and flow paths shown control only the terrestrially-driven flow. Marine, geophysical and biological forces contribute substantially to the total flow through coastal sediments. Also note that the gauging station, located well upstream to eliminate tidal effects, will miss all the groundwater discharged below the gauge (Buddemeier, 1996).

also mounting evidence for the global occurrence of offshore fresh and brackish groundwater reserves underneath continental shelves (Post et al., 2013; Gustafson et al., 2019). Since there is no clear evidence on whether these fossil offshore aquifers are exchanging with the ocean, they are beyond our scope. However, the potential use of these non-renewable reserves as a freshwater resource does provide a clear incentive for future research.

While there was not much scientific work done specifically on SGD prior to the later part of the twentieth century, there were some attempts, many of them related to possible offshore sources of potable water. The lack of interest in the process led Fran Kohout, one of the true pioneers in the field, to comment that "*...these marvels of the sea (submarine springs) are justifiably classified as neglected phenomena of coastal hydrology*" (Kohout, 1966). He reported in that paper that a literature search only succeeded in finding 15 scientifically-oriented studies concerning SGD. Other early contributions included Lee (1977), Bokuniewicz (1980), Johannes (1980), and Valiela and D'Elia (1990) among others. These early researchers had the foresight to see that SGD needed increased attention. In their "Preface to a Special Issue" on groundwater discharge in the journal *Biogeochemistry*, Valiela and D'Elia (1990) commented that "*we are very much in the exploratory stage of this field*." We thus see the period before the mid-1990s as the "*early days*" of SGD research.

Things then started to change quickly. In the proceedings of a Land Ocean Interactions in the Coastal Zone (LOICZ) conference dedicated specifically to SGD ("Groundwater Discharge in the Coastal Zone," Moscow, July 6–10, 1996), it was stated that: *"Measurements or estimates of groundwater and associated chemical fluxes, especially over substantial areas or time periods, are notoriously uncertain"* (Buddemeier, 1996). Around the same time, some very interesting and provocative data started to appear. Based on large enrichments of ^{226}Ra in the shelf waters off South Carolina and Georgia, Moore (1996) concluded that the groundwater flux, largely recirculated seawater, to the shelf must be about 40% of the river flux to the same area. A few months later, Cable et al. (1996) reported that radon (^{222}Rn) was significantly enriched in the inner shelf waters of the northeastern Gulf of Mexico. Using a model based on radon inventories they calculated that within a relatively small region (~620 km^2) there was groundwater (combination of saline and fresh) flow in the range of 180–710 m^3/s. This is roughly equivalent to the outflow from the Apalachicola River, the largest river in Florida. The value of geochemical tracers quickly became apparent and many studies followed. During this period, which we refer to here as the "*developmental period*" from the mid-1990s to mid-2000s, there was substantial progress in this field. During this period there were many site studies, considerable advances in technology, more elaborate modeling efforts, and many new insights into driving forces and magnitudes of SGD. Multiple drivers of SGD became recognized (**Figure 2**). Teams of oceanographers and hydrologists collaborated in meetings and field efforts through sponsorship from the Scientific Committee on Oceanic Research (SCOR), UNESCO and other international agencies (Taniguchi et al., 2002; Burnett et al., 2006). New technologies for measuring geochemical tracers played a key role in getting things moving. For example, Moore and Arnold (1996) developed a coincidence counting system that made determinations of ^{223}Ra and ^{224}Ra much easier and faster. Development of an automated radon-in-water continuous monitoring system greatly simplified radon mapping in the coastal zone (Burnett et al., 2001; Dulaiova et al., 2005). Such technological advances were not limited to geochemical tools. Designs for automated seepage meters based on heat-pulse, dye-dilution, and electromagnetic principles as well as improved electrical resistivity approaches all made substantial contributions (Taniguchi and Fukuo, 1993; Krupa et al., 1998; Paulsen et al., 2001; Sholkovitz et al., 2003; Swarzenski et al., 2006).

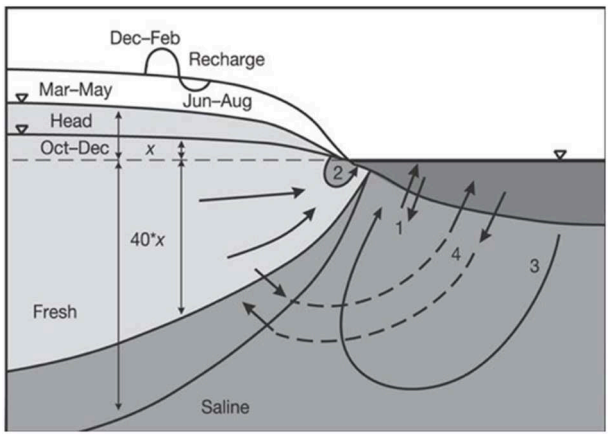

FIGURE 2 | Flow paths and some of the driving forces of SGD. Mechanisms shown include: (1) tidal pumping, (2) nearshore circulation due to tides and waves, (3) saline circulation driven by dispersive entrainment and brackish discharge, and (4) seasonal exchange (Michael et al., 2005).

Beginning around the mid-2000s, we entered into the "*mature stage*" of SGD research. SGD investigations have now advanced from hydrogeologic "curiosities" to mainstream science. The scientific community now recognizes that SGD is not only a function of the terrestrial hydraulic gradient but that marine and other drivers result in substantial flow through coastal and shelf permeable sediments. So, while the water table contours shown in **Figure 1** may describe the terrestrial flow, the total flow in many cases is dominated by seawater infiltration and subsequent circulation through STEs. As pointed out in more recent reviews, the driving forces of SGD and porewater exchange overlap in both time and space (Moore, 2010; Santos et al., 2012b). There is now widespread recognition that SGD plays an important role in the delivery of nutrients and other dissolved materials to the ocean. While SGD remains somewhat invisible, and still represents a challenge to be measured, it is no longer being overlooked.

GEOPHYSICAL ASPECTS

Geophysical Processes

Literature reviews on the physical drivers of porewater exchange (Huettel and Webster, 2000; Huettel et al., 2014) and SGD (Moore, 2010; Santos et al., 2012b; Robinson et al., 2018) are

already available. Here, we summarize recent developments in the field and illustrate the challenges of quantifying the multiple overlapping geophysical drivers of fluid flow (**Figure 3**). SGD and porewater exchange, which we see as different but overlapping processes, are driven by a complex combination of processes occurring over spatial scales ranging from mm to km, and temporal scales ranging from seconds to years (Santos et al., 2012b). Building on Moore's (2010) interpretation of SGD, we use length and time scales as boundaries to distinguish the terms porewater exchange and SGD (see thick line in **Figure 3**). Ours and Moore's (2010) definition of SGD excludes several small spatial and temporal scale processes such

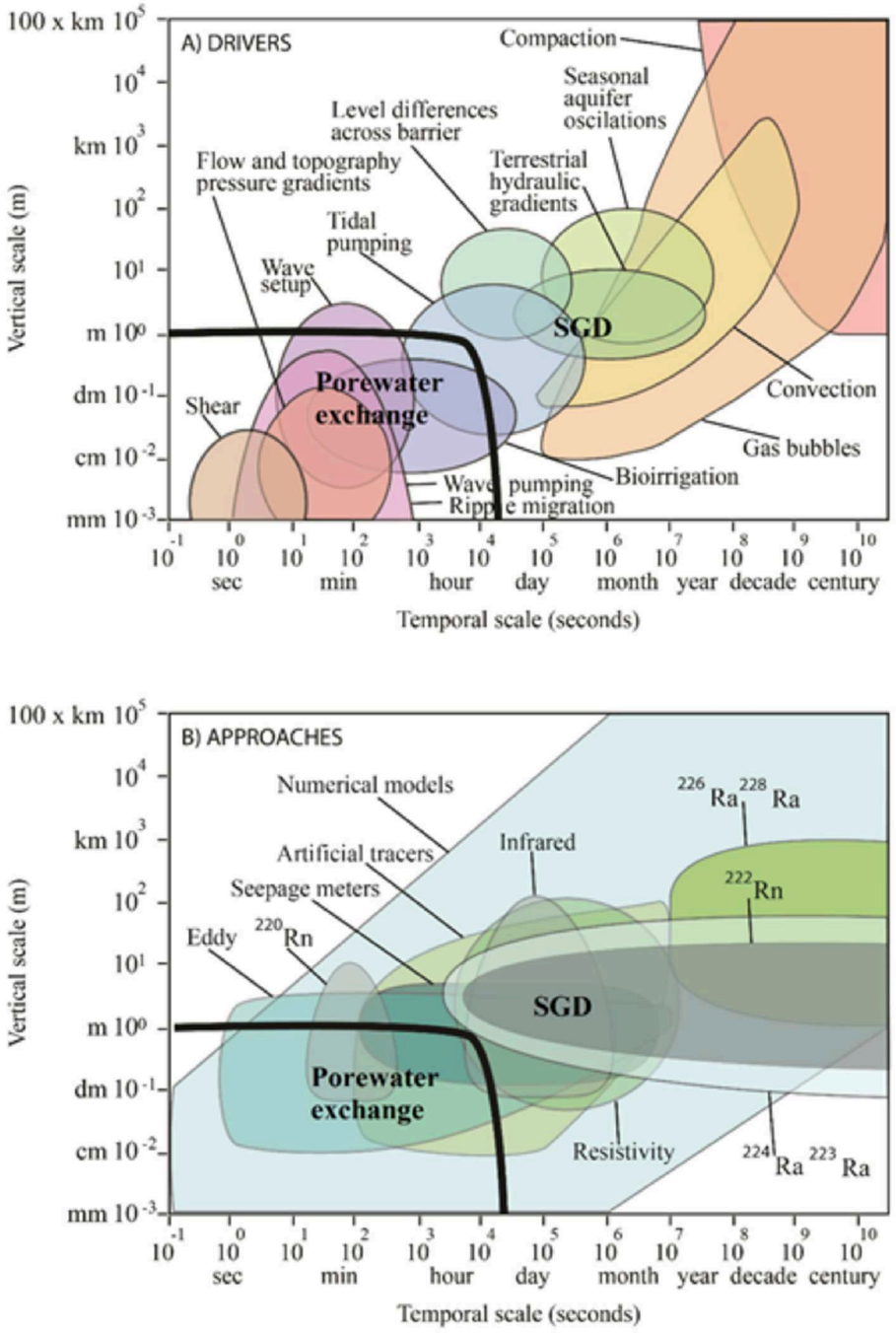

FIGURE 3 | (A) The operating space of the physical processes driving porewater exchange and SGD in coastal systems. The thick black line separates the porewater exchange space (bottom left) from the SGD space according to Moore (2010)'s definition. **(B)** The approaches used to quantify SGD (bottom graph) often capture multiple drivers, preventing a straightforward quantification of individual physical processes.

as wave pumping, flow and topographically-induced pressure gradients, and ripple migration that drive advective porewater exchange on scales of <m and <hour. Other important processes such as tidal pumping, wave setup and bio-irrigation may be considered as porewater exchange and/or SGD depending on the context, measurement technique employed, and environmental implication of interest.

Because different techniques tend to quantify overlapping physical processes, confusion when reporting and interpreting results often prevents straightforward comparisons among different field sites and research groups. Most attempts to quantify different drivers of SGD tend to focus on a separation between fresh SGD driven by terrestrial hydraulic gradients vs. saline SGD driven by multiple marine forces. Similar to porewater exchange (<m scale), saline SGD (>m scale) often has large gross yet zero net water fluxes. Earlier investigations relied on salinity observations of water collected from seepage meters to assess the relative contribution of fresh SGD to total SGD (Michael et al., 2003; Santos et al., 2009) as well as a comparison between Darcy's Law derived fresh SGD vs. total SGD derived from seepage meters (Taniguchi and Iwakawa, 2004) or geochemical tracers (Mulligan and Charette, 2006). More recent investigations have relied on a comparison of salt balance approaches (fresh SGD) vs. geochemical tracers (total SGD). For example, salinity and flow observations were used to infer fresh SGD, while a radium isotope mass balance was used to estimate tidally-driven saline SGD in Australian estuaries (Sadat-Noori et al., 2015, 2017). The different half-lives of radium isotopes have been used to broadly separate SGD from porewater exchange (Tamborski et al., 2017b, 2018).

These investigations provided widespread evidence that the volumetric contribution of fresh SGD is minor compared to saline SGD and porewater exchange at a wide range of field sites. The estimates based on multiple methods also shed light into the physical processes that may be quantified using the different measurement approaches (see overlapping areas in **Figures 3A,B**). Separating the relative contribution of the different physical processes driving saline SGD is important because longer residence times of seawater within sediments will have a greater impact on the geochemical composition of the exchanging seawater (Seidel et al., 2014; Tamborski et al., 2017a). The multiple time scales of marine driving forces are difficult to quantify using geochemical approaches or field observations. As a result, the roles of currents, tides, waves, and density have been explored mostly using numerical models (Li and Barry, 2000; Robinson et al., 2006; Sawyer et al., 2013).

Tidally-driven SGD has been extensively investigated following the discovery of the beach water table over-height or super-elevation (Nielsen, 1990) followed by the discovery of fresh groundwater tubes underlying upper saline plumes in beach aquifers (Robinson et al., 2006). Seawater infiltrating beaches, fractured aquifers and/or marshes at high tide creates a circulation cell that drives the return of seawater to the ocean at low tide on time scales of days to months (Robinson et al., 2009; Wilson et al., 2015; Geng and Boufadel, 2017; Santos et al., 2019). This process can account for a large fraction of SGD on a local scale, releasing solutes from the beach into the ocean. The beach water table over-height is driven by faster aquifer recharge during flood tide than discharge at ebb tide, resulting in a localized increase in beach groundwater level that can retard fresh SGD while enhancing saline SGD (Nielsen, 1999; Li et al., 2000). The upper saline plume commonly found in permeable coastal aquifers (Robinson et al., 2018) can alter density-driven seawater circulation since denser seawater overlying fresh groundwater drives convective exchange (Greskowiak, 2014; Röper et al., 2015).

Wave-driven SGD often overlaps the effects of currents and tides (Xin et al., 2010). While waves are known to play a major role in fluid exchange (Sawyer et al., 2013), field investigations have not been able to fully separate their relative contribution to total SGD. Investigations on wave-driven SGD rely on numerical models usually under ideal, phase-averaged conditions (Robinson et al., 2014). Waves expand the tidally-driven upper saline plume in beaches and enhance total SGD (Xin et al., 2010). The importance of waves driving porewater exchange is highly variable with integrated volumetric exchange rates estimated to exceed tidal pumping by one order of magnitude. During storms, wave pumping can increase by orders of magnitude exceeding all other geophysical drivers of fluid flow across the sediment-water interface (Sawyer et al., 2013). In contrast to the effects of tides that occur primarily in intertidal areas, wave-driven porewater and groundwater flow can also occur in shallow subtidal areas.

The overlapping nature of marine drivers of SGD (i.e., currents, tides, waves, density gradients) complicate the individual quantification of the specific physical drivers of SGD. The residence time of seawater circulation cells in coastal aquifers is quite variable ranging from minutes to hours when driven primarily by currents or waves (Anwar et al., 2014), hours to months when driven by tides in intertidal areas (Seidel et al., 2014) and months to thousands of years when driven by density (Post et al., 2013; Seidel et al., 2015; Michael et al., 2016). The multiple driving forces are not necessarily synergistic or additive (Robinson et al., 2018) and interact non-linearly (King, 2012; Xin et al., 2015). For example, while tidal pumping maximizes density-driven convection in intertidal aquifers, it may decrease terrestrial fresh SGD due to the localized elevation of the water table (Robinson et al., 2007). Overlapping tides and waves in numerical models resulted in lower SGD than when either tides or waves are modeled individually (Xin et al., 2010). SGD also responds to past events creating a memory effect that can modify flow for several weeks (Xin et al., 2014). Delayed SGD related to antecedent storms (Smith et al., 2008; Yu et al., 2017), seasonal changes in the terrestrial hydraulic gradient (Michael et al., 2005), and three-dimensional morphological complexities (Zhang et al., 2016) have been described, adding another dimension to the problem and complicating the assessment of the interactions between multiple forces.

Research about the physical drivers of SGD has been developed mostly in permeable sandy aquifer sites. While muddy sediments are often perceived to be impermeable, secondary permeability created by abundant animal burrows can enable advective flow in muddy mangrove and saltmarsh sediments (Xin et al., 2011; Tait et al., 2016). The burrows can connect underlying sandy aquifers containing fresh groundwater to the

surface (Wilson et al., 2015) and enhance tidally-driven saline SGD (Xin et al., 2011; Stieglitz et al., 2013). Groundwater flows in those systems is three dimensional and highly complex due to the patchy nature of burrows, subtle geomorphological gradients, and heterogeneous sediments and vegetation (Moffett et al., 2012; Wilson and Morris, 2012; Xin et al., 2012). Radon and radium observations in multiple mangrove creeks revealed tidally-driven porewater exchange ranging from 2 to 35 cm/day (Tait et al., 2016, 2017). If extrapolated to the global mangrove area, these exchange rates would be enough to filter the entire continental shelf volume in ∼150 years and are equivalent to ∼1/3 of the annual volume of river water entering the oceans (Tait et al., 2016). Because mangrove and saltmarsh porewaters are often highly enriched in carbon and greenhouse gases (Santos et al., 2019), the input of dissolved carbon to the oceans via mangroves may be comparable to the input from global rivers (Chen et al., 2018b). Therefore, muddy mangrove and saltmarsh systems that are widespread on global shorelines deserve additional attention and may disproportionally contribute to SGD and related biogeochemical inputs to the ocean.

High salinity SGD has also been shown in some deltas. For example, Xu et al. (2013, 2014) used radium isotopes to quantify SGD fluxes in the Yellow River Delta. They estimated a SGD flux of 1.3×10^9 m^3 d^{-1} with a range of 2.8×10^8- 3.0×10^9 m^3 d^{-1}. Even the minimum SGD value was about 3 times higher than the Yellow River discharge at that time. The SGD input of dissolved nutrients was shown to be at least 5 times higher than river input.

Geophysical Methodology

To date, the most commonly applied approaches to quantify SGD fluxes provide estimates over a wide spatial range (**Figure 3**). A significant gap remains between "embayment-scale" or "beach-scale" geochemical flux estimates on one hand, and seepage meter point measurements on the other. Geophysical methods have been increasingly applied in recent years in order to bridge this gap. The most common geophysical tools applied in SGD studies thus far are based on temperature and salinity variations. In contrast to many geochemical tracer approaches, geophysical approaches can discriminate between freshwater and saline components of SGD (e.g., Stieglitz et al., 2008a; Tamborski et al., 2015). Particularly applicable to point sources of freshwater SGD, e.g., karstic or volcanic origin, where considerable spatial contrasts in these parameters exist, these approaches provide a "map," but do not allow for a quantification of SGD fluxes without combining with other methods.

Detection of SGD Sites by Thermal Infrared Sensing

Digital thermal infrared cameras are increasingly accessible in price and size, which has resulted in a significant rise in their application over the past decade. By mapping sea surface temperatures with a thermal infrared (TIR) sensor, plumes of buoyant low-density (fresh/brackish) groundwater can be detected. Locations of groundwater discharge are inferred from temperature anomalies (either low or high), based on the seasonal contrast between groundwater and ocean temperature (e.g., Varma et al., 2010). Often, TIR observations are used as a guide to target subsequent sampling by quantitative methods (e.g., Mulligan and Charette, 2006; Röper et al., 2014). On large spatial scales (km-scale), readily available space borne remote sensing TIR data can be used to identify large SGD inflows sustaining persistent temperature plumes, e.g., in Geographe Bay, Western Australia (Varma et al., 2010), in Java, Indonesia (Oehler et al., 2018), and along the Irish coast (Wilson and Rocha, 2012). TIR cameras are most often mounted on light aircraft (Duarte et al., 2006; Johnson et al., 2008; Lee et al., 2016a; Bejannin et al., 2017) and more recently on drones (e.g., Lee et al., 2016b) with a typical temperature resolution of 0.1°C at a spatial resolution down to 0.5 m (e.g., Johnson et al., 2008; Kelly et al., 2013). An often-overlooked application is the simple handheld use of an infrared camera, which for instance allows the rapid identification of cm-scale groundwater springs at low tide in the intertidal zone (Röper et al., 2014). Some studies suggest that the surface area of a sea surface temperature plume can be used to quantify SGD fluxes (e.g., Kelly et al., 2013; Tamborski et al., 2015). This is based on the assumption that the 3D structure of the plume is known or can be estimated. However, Lee et al. (2016a) illustrate the often non-consistent shape of SGD plumes by multiple aerial surveys over a range of seasons and tidal stages. This inherent limitation of surface remote sensing approaches in oceanography is well-documented (e.g., river plumes, Burrage et al., 2003). While there are inherent limitations in using the non-conservative tracer heat/temperature for SGD studies (SGD is not the only "source" of temperature anomalies), this approach has today become a popular part of the SGD toolkit owing to the availability of affordable sensors. Multispectral and hyperspectral sensors are becoming increasingly accessible and may see wider application in the near future. For example, mapping of turbidity plumes caused by sediment remobilization due to groundwater inflow (Kolokoussis et al., 2011). Sea surface salinity would also be an ideal parameter to map and quantify freshwater inflow, but available operational satellite products (SMOS) to date do not have the appropriate resolution for nearshore processes, and airborne low-frequency microwave radiometer sensors remain rare (e.g., Burrage et al., 2003).

Mapping the Subterranean Estuary With Electrical Ground Conductivity

Early studies of SGD often provided diverse results between "downscaled" geochemical flux estimates and "upscaled" point measurements as, for example, obtained by seepage meters. This is particularly the case where flow patterns are affected by natural or artificial preferential flow paths. While this scale gap remains, it has been significantly reduced over the past decade thanks to advances in a range of additions to the SGD toolkit, including geoelectric methods. When referring to "geoelectric methods," the terms bulk/ground (electrical) ground conductivity, resistivity (the inverse of conductivity), and electrical tomography are used in the literature. They all refer to basically the same approach, albeit using slightly different instrumentation. The electrical conductivity (resistivity) of coastal sediments is a function of the soil porosity (or pore water fraction) and of the salinity (and temperature) of the interstitial water. In SGD studies, spatial variations of pore water salinity close to the fresh-salt interface are significantly

greater than those of porosity. Geoelectric instrumentation consist of an array of multiple electrodes (minimum four), either directly inserted into the ground (e.g., Stieglitz et al., 2008a), deployed on the sediment surface (e.g., Breier et al., 2005; Swarzenski et al., 2006) or, in some cases, towed behind a boat (Manheim et al., 2004; Su et al., 2014). The geometry of the electrode array determines the volume of sediment over which conductivity/resistivity will be averaged (e.g., Stieglitz et al., 2008b; Henderson et al., 2009).

Geoelectric mapping helps to improve SGD field studies by, for example, informing a more representative placement of seepage meters where preferential flow paths persist (Stieglitz et al., 2007, 2008b). It allows upscaling of point measurements to beach-scale fluxes (Stieglitz et al., 2008a), and repeated measurements along the same transects document the temporal variability of the fresh-salt interface and of fresh groundwater and seawater recirculation fluxes (Taniguchi et al., 2008; Bighash and Murgulet, 2015). They can also be used for the establishment of a sub-surface salt balance model from which SGD fluxes can be calculated (Dimova et al., 2011; Bighash and Murgulet, 2015).

Surface-deployed electrodes and an inversion calculation can be used to obtain a 2D resistivity section with a vertical penetration about one order of magnitude less than the horizontal extension of the array (e.g., 10 m depth along a 100 m transect), at a spatial resolution on the order of a few meters. Using this approach, Taniguchi et al. (2006) demonstrated that freshwater SGD rates were highest just landward of the saltwater-freshwater interface on a beach in Japan. Gilfedder et al. (2015) showed that a considerable increase in groundwater flux followed storm events on an Australian coastal wetland. Geoelectrical methods are particularly useful to document the temporal dynamics of SGD fluxes and the freshwater-saltwater interface in the subterranean estuary. For example, resistivity mapping on Ubatuba beach (Brazil) showed that the freshwater–saltwater interface moved offshore during a rising tide, in the opposite direction as would be expected, indicating that preferential flow in the fractured rock aquifer was a more important driver of SGD flux than tidal water level fluctuations at this site (Taniguchi et al., 2008).

While interpretation of *in situ* profile data is straight-forward, uncertainties in both data acquisition (e.g., survey geometry, land topography) and processing (e.g., inversion artifacts, choice of interpolation method) can produce suboptimal results in resistivity inversion calculations of surface arrays (Henderson et al., 2009). These errors can be addressed to some degree by careful ground-truthing (including vertical direct profiling and borehole data) and fine-tuning of the model inversions to the specific characteristics of a field site including sediment type and distribution (Henderson et al., 2009; Johnson et al., 2015). The coupling of geoelectric data and hydrogeological density-driven flow modeling will likely be used more extensively in the future to improve our understanding of the complex and dynamic mixing processes between fresh and saline groundwaters at their interface (Robinson et al., 2006).

Seafloor Mapping and Sub-bottom (seismic) Profiling

Similar to other forms of subsurface fluid flow, SGD can affect seafloor morphology. Acoustic seafloor mapping tools (multibeam echosounders and sidescan sonar) providing high resolution maps of the seafloor have revealed the locations of seafloor structures associated with SGD, e.g., "Wonky Holes" (Stieglitz, unpublished data). These seafloor depressions have a diameter of 10 to 30 m and a depth of up to 4 m below surrounding water depths of around 20 m. These features lie some 10 km offshore from the Great Barrier Reef coastline (Stieglitz and Ridd, 2000; Stieglitz, 2005). Schlüter et al. (2004) and Rousakis et al. (2014) mapped pockmarks in the Baltic and Mediterranean Sea, resulting from the interaction between sediment fluidization and bottom currents and sub-aqueous limestone formation (karstification). The investigation of subsurface geological structures by seismic profiling can be instructive to determine the geological origin of SGD and its flow paths (Evans and Lizarralde, 2003; Viso et al., 2010). For example, seismic profiling data suggests that submarine paleochannels, infilled with permeable sediments and capped with impermeable material provide a hydrological connection of coastal aquifers with offshore discharge sites. Thus, providing preferential flow paths for SGD as interpreted from observations along the Great Barrier Reef (Stieglitz and Ridd, 2000; Stieglitz, 2005) and offshore at Wrightsville Beach, USA (Mulligan et al., 2007). In some cases SGD appears to be controlled by fault lines or fracture patterns (Bokuniewicz et al., 2008). A few examples of results from these approaches are shown in **Figure 4**.

GEOCHEMICAL ASPECTS

Geochemical Processes

The discharge of meteoric groundwater and salty groundwater generally show distinctively different geochemical characteristics. The direct discharge of meteoric groundwater may reflect geochemical characteristics of fresh groundwater, which depend on local hydrogeologic conditions and anthropogenic perturbations. In contrast, the discharge of salty groundwater, which may be composed exclusively of recirculated seawater or a composite of meteoric groundwater and seawater, goes through vigorous biogeochemical alterations in the subterranean estuary (STE) (Santos et al., 2008).

Geochemical processes in the STE are very different from those observed in river estuaries in many respects. The most distinct difference is the fact that the ratio of solid to liquid in a STE is much higher than that in river estuaries. Therefore, reactive elements can be more easily removed, and pH may be enhanced due to the adsorption of H+ on oxide surfaces in an organic-poor STE (Lee and Kim, 2015) or reduced due to production of CO_2 during organic matter respiration (Cyronak et al., 2014). In an organic-rich STE, various re-mineralized components of organic matter, including nutrients, dissolved organic carbon (DOC), dissolved inorganic carbon (DIC), fluorescent dissolved organic matter, and trace elements, are highly enriched and pH is generally lower. The temperature of groundwater is relatively constant compared with surface waters, especially in temperate regions. In addition, STE waters are often

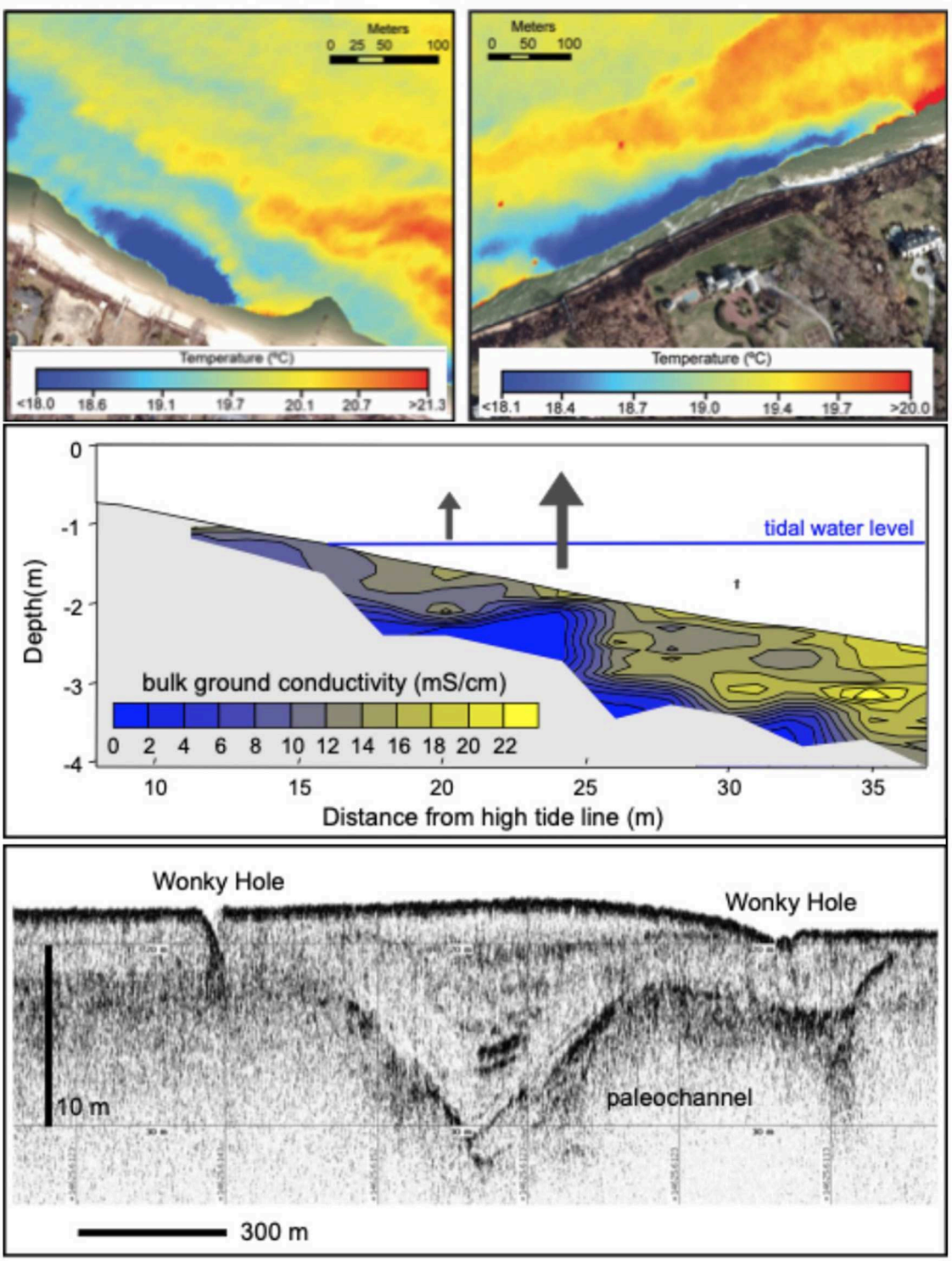

FIGURE 4 | (Top) Airborne Infrared maps from beaches on Long Island (USA) elucidating cold SGD plumes (adapted from Tamborski et al., 2015); **(Center)** bulk ground conductivity transect indicating preferential freshwater SGD flow path. Arrow length indicates SGD flow rates measured with seepage meters at the respective locations (adapted from Stieglitz et al., 2008a); **(Bottom)** Sub-bottom (seismic) profile of a riverine paleochannel and associated Wonky Holes (Great Barrier Reef, Australia) (Stieglitz, unpublished data).

enriched in reduced species [NH_4^+, Fe(II), etc.]. Therefore, the STE has been found to be much more dynamic in terms of biogeochemical alterations, relative to river estuaries.

Amongst chemical species, the fluxes of nutrients via SGD have been studied most extensively since they have significant impacts on marine ecosystems. In a STE, the behavior of N species is very complicated depending on the redox conditions and organic matter re-mineralization. NH_4^+ is often found to be removed by nitrification in oxic conditions (Spiteri et al., 2008; Anwar et al., 2014; Anschutz et al., 2016) or also by adsorption onto particles (Buss et al., 2004; Lorah et al., 2009). Under anoxic conditions, dissolved N can also be removed by forming gaseous species (Kroeger and Charette, 2008; Couturier et al., 2017). Si and P in groundwater can be removed in STE by adsorption, but P can be potentially desorbed from the sediment surface layer under much higher Si concentrations since they compete for the same specific ligand sites including Fe- and Mn-, and Al-oxides (Cho et al., 2019b). However, in organic-rich STEs, all these nutrients are highly enriched by re-mineralization. Recent studies also documented the importance of dissolved organic nitrogen (DON) and phosphorus (DOP) in delivering nutrients through SGD (Kim et al., 2013; Sadat-Noori et al., 2016; Stewart et al., 2018). Therefore, we can conclude that the impact of SGD is very different depending upon the hydrogeological and biogeochemical conditions of the STE.

There have been many upscaling attempts to gauge the magnitude of nutrients fluxes through SGD on basin scales. SGD-driven fluxes of nutrients are generally significant in coastal waters (Kim et al., 2005; Rodellas et al., 2015a; Cho et al., 2018). Recently the global volume of fresh submarine groundwater discharge (FSGD) has been estimated around 1% of river discharge (Luijendijk et al., 2019; Zhou et al., 2019), less than the previously estimated 5–10% (Oki and Kanae, 2006). Consequently, the global fluxes FSGD of DIN, DIP, and DSi through FSGD to the global ocean seem to be below 10% of those from river discharge (Cho et al., 2018 and references therein). However, Cho et al. (2018) showed that the fluxes of DIN, DIP, DSi through total (fresh+saline) groundwater discharge on a global scale were comparable to river inputs. Rahman et al. (2019) also showed a similar result for DSi input via saline SGD, accounting for a 25–30% increase in global estimates of net DSi inputs (riverine, SGD, aeolian, hydrothermal, and seafloor weathering) to the ocean.

SGD may also play an important role for the fluxes of terrestrial carbon to the ocean as a form of DOC or DIC. In addition, a significant amount of marine carbon is also returned back to the ocean by SGD. In general, marine vs. terrestrial sources of DOC and DIC are differentiated by stable carbon isotopes (Gramling et al., 2003). In a STE, DOC is transformed to DIC via microbial processes. DOC and DIC are also formed within a STE by the bacterial degradation of particulate organic carbon (POC). Therefore, many STEs show higher DOC concentrations in groundwater than coastal seawater, indicating that SGD is a potential DOC source to the near-shore ocean (Webb et al., 2019). However, the contribution of SGD to the marine DOC budget remains unknown relative to other sources such as *in-situ* production of DOC in the euphotic zone. Clearly, the importance of SGD on the fluxes of refractory and aged DOC to the ocean should be more extensively evaluated in the future.

Fluxes of DIC were found to be important in many oceanic regions. By considering SGD in the DIC budget in the ocean, the sink or source regions of CO_2 have been re-evaluated (Cai et al., 2003; Dorsett et al., 2011; Liu et al., 2012). The importance of SGD-derived DIC fluxes to the oceans have been particularly emphasized in carbon-rich mangrove forest areas (Chen et al., 2018b) and have been suggested to exceed regional river inputs in Florida (Liu et al., 2012) and in an Australian embayment (Stewart et al., 2015). In addition, DIC concentrations in STEs and their associated contributions to the ocean showed large seasonal variations (Wang et al., 2015). Fluorescent DOM (FDOM), especially humic-like varieties, is generally enriched in STEs, and thus SGD showed a significant influence on the coastal budget of humic-like FDOM (Kim et al., 2013; Suryaputra et al., 2015). Kim and Kim (2017) documented that fresh groundwater in Jeju Island, Korea, generally showed lower DOC due to degradation and higher humic-like FDOM produced from bacterial degradation of labile DOC and POC in aquifers. They suggested that SGD provides an environmental condition favorable for coral ecosystems by reducing UV penetration and DOC concentrations. Therefore, SGD-associated carbon studies should be conducted not only for establishing local/regional carbon budgets but also for understanding marine ecosystem changes and implications for ocean acidification.

Studies of trace element fluxes associated with SGD have shown that many elements exhibit non-conservative behavior within a STE. Although river estuaries are generally sinks of trace elements due to flocculation of particle reactive elements, STEs often display significantly higher trace element concentrations relative to river water or seawater in association with re-mineralization of organic matter, release from oxides, and desorption from sediments (Charette and Sholkovitz, 2006; Santos-Echeandia et al., 2009). Therefore, the behavior of trace elements in STEs is largely dependent on pH, Fe/Mn oxides, and bacterial activities. Due to such a reactive nature of trace elements to particles, colloids play an important role in the delivery of trace elements from STEs to the coastal ocean (Kim and Kim, 2015). In Jeju Island, Korea, Jeong et al. (2012) showed that the change (∼20-fold) in concentrations of trace elements (i.e., Al, Mn, Fe, Co, Ni, and Cu) in the STE resulted in the matching change in inventory of these elements in coastal waters. Although a STE can serve as a significant source for most trace elements which are extremely low in seawater, STEs can be an important sink of conservative elements in seawater by changing redox conditions. For example, forming reduced conditions for U uptake (Charette and Sholkovitz, 2006) and precipitation of Mn oxides for Mo adsorption (Beck et al., 2010). Although a few local or regional studies demonstrated the importance of SGD for the delivery of trace elements to the ocean (Moore, 2010; Jeong et al., 2012; Kim and Kim, 2015; Trezzi et al., 2016), so far the global or basin scale importance is largely unknown. It is particularly important for Fe since the growth of marine planktons could be limited by extremely low-level Fe in seawater, although it is a major element in the earth's crust.

Thus, it is very important to look at the magnitude of SGD-driven dissolved trace elements to the ocean for basin-scale as well as local/regional scales in association with climate and ecosystem changes.

Among trace elements, rare earth elements (REE) associated with SGD have received considerable attention recently. In general, high enrichment of REE, relative to the simple binary mixing of meteoric groundwater and seawater has been observed in STEs, although the STE can also act as a sink for heavy REEs (HREE) owing to adsorption onto Fe oxides (Johannesson et al., 2011). In STEs, light REEs (LREE) are more readily exchangeable on aquifer mineral surfaces than HREEs, and HREEs and middle REEs (MREE) exhibit a greater association with oxide minerals (Willis and Johannesson, 2011; Chevis et al., 2015). Thus, redox conditions along the flow path of groundwater can affect REE concentration and fractionation (Johannesson et al., 2005, 2011; Tang and Johannesson, 2005, 2006). A case study carried out on a sandy STE in Florida (Chevis et al., 2015) showed that advection and bio-irrigation differentially affect REE fluxes to the ocean as fresh groundwater is enriched in HREEs, while marine pore-water is enriched in MREE in association with the reductive dissolution of Fe oxides/oxyhydroxides. Therefore, REE contributions to coastal waters are clearly identified due to large contributions of different REE patterns to coastal waters (Kim and Kim, 2011; Johannesson et al., 2017). Much more extensive studies are necessary to determine SGD's contribution to the budgets and fractionations of REE on basin and global scales.

The compilation of Nd isotopes in the global ocean showed that the traditionally believed main Nd sources, e.g., rivers and atmosphere, cannot explain the large difference in Nd isotope ratios and concentrations in different basins, the so called "Nd paradox." Recent studies showed that SGD can account for the missing Nd source (>90% of the known source; Tachikawa et al., 2003; Johannesson and Burdige, 2007; Chevis et al., 2015). However, much more local and regional evidence are necessary to validate this hypothesis. Besides, large enrichments of alkaline earth elements (Sr, Ba, and Ra and their isotopes) have been successfully utilized to trace SGD to the ocean. SGD inputs of Sr, with less radiogenic Sr than seawater, influence the Sr isotope budget in the ocean, making up 13–31% of the marine Sr isotope budget (Beck et al., 2013). This fluvial input is comparable in magnitude to the flux driven by submarine hydrothermal circulation through mid-ocean ridges. Yet, the use of Sr isotopes as an SGD tracer is still challenging since Sr isotopic composition and distribution of the coastal waters are rather complicated (Huang et al., 2011). Such a complicated pattern seems to be associated with different isotopic ratios from different sources, fractionations along the path, and non-conservative behaviors within the STE (Andersson et al., 1994; Xu and Marcantonio, 2004; Huang and You, 2007). Since Ra isotopes are one of the more useful SGD tracers, more details concerning the Ra isotope applications for flux estimations will be covered in the following methodology section.

Geochemical Methodology

Coastal salinity may seem like an obvious SGD tracer but it has interferences from terrestrial surface runoff and it does not capture the recirculated seawater component of SGD. Therefore, since the 1990's several groundwater tracers have been applied for SGD quantification in addition to, or instead of salinity (**Table 1**). Among others, these include radium, radon, methane, silica, hydrogen, and oxygen stable isotopes of water (Bugna et al., 1996; Cable et al., 1996; Campbell and Bate, 1996; Moore, 1996; Godoy et al., 2013; Rocha et al., 2016). Radon and radium isotopes have been applied most frequently, with 40% of the published 473 SGD articles between 2015 and 2019 applying one or both (Web of Science, 2019). The advantage of radon (^{222}Rn, $T_{1/2}$ = 3.8 days) is that automated measurement methods allow for easy time-series and spatial survey measurements. Due to the large concentration gradient between groundwater and ocean water, its gaseous nature, and relatively short half-life, radon is applicable for assessment of recent and local SGD inputs. Radium analysis of seawater, on the other hand, requires a collection of large volume samples and laboratory or shipboard measurements. However, its great advantage is that radium has four isotopes with half-lives covering a wide range of time scales (^{224}Ra, $T_{1/2}$ = 3.6 days; ^{223}Ra, $T_{1/2}$ = 11.4 days; ^{228}Ra, $T_{1/2}$ = 5.7 years; and ^{226}Ra, $T_{1/2}$ = 1,600 years) thus allowing SGD assessment on multiple spatial and temporal scales. In addition, radium isotopes can be used to estimate water mixing and residence times (Charette et al., 2008). For example, beyond the embayment scale, ocean-basin scale SGD estimates were recently performed using inventories of the relatively long-lived ^{228}Ra (Kwon et al., 2014). Uncertainties are often high for both radon and radium mass balance estimates, largely but not exclusively, because of the difficulty in constraining a value for the groundwater "end-member" (the concentration of the tracer in the discharging groundwater; Burnett et al., 2007; Schubert et al., 2019).

SGD tracer measurement methods have recently been improved to enhance detection limits and make more efficient measurements over longer time periods as well as obtaining finer spatial scale applications. One example of improvement for radium measurements is a large-volume (over 1,500 L/4 h) sampling method using commercially available *in situ* pumps modified to accept MnO_2 coated filter cartridges (Henderson et al., 2013). The method has been applied on continental shelves as well as in open ocean environments and is a promising tool to significantly increase the number of observations of ocean basin-scale radium isotope inventories in the coming years. Improvement in the existing coastal radon detection methods via a commercially available radon-in-air detectors (RAD7, Durridge) was achieved by more efficient gas stripping via improved air-gas exchanger design (Santos et al., 2012a) and use of membrane extractors (Gilfedder et al., 2015). These allow for more powerful and efficient pumping and better radon measurement response rates during coastal surveys. The latter issue was also tackled by Petermann and Schubert (2015), who introduced a methodology to correct radon data collected using an air-water exchanger (RAD-Aqua, Durridge) connected to a RAD-7 radon detector for its response delay when moving

TABLE 1 | Summary of the main geochemical tracers used in SGD related studies.

Tracer	Measurement	Lab/*in situ*	Application	References
Salinity	Conductivity	*In situ*	Fresh water SGD	
^{226}Ra	Gamma-spec	Lab	SGD estimation	Moore, 1996
^{222}Rn	Lucas cells (alpha-scintillation)	Lab	SGD estimation	Cable et al., 1996
^{222}Rn	Automated (RAD-7, alpha-spectrometry)	*In situ*	SGD estimation -temporal -spatial	Burnett et al., 2001; Dulaiova et al., 2005
^{222}Rn	Underwater gamma-spec (HPGe & NaI)	*In situ*	SGD estimation -temporal -spatial	Povinec et al., 2006; Tsabaris et al., 2012; Dulai et al., 2016
^{222}Rn	Automated (RAD-7, alpha-spectrometry)	Lab, *in situ*	STE residence time estimation	Goodridge and Melack, 2014; Oh and Kim, 2016
^{220}Rn	Automated (RAD-7, alpha-spectrometry)	*In situ*	SGD prospecting SGD estimation -temporal -spatial	Chanyotha et al., 2014, 2018; Swarzenski et al., 2016
Methane	Gas chromatography	Lab	SGD estimation	Bugna et al., 1996
Methane	METS membrane diffusion detector TETHYS *in-situ* underwater mass spectrometry	*In situ*	SGD estimation -temporal -spatial	Kim and Hwang, 2002; Dulaiova et al., 2010
^{224}Ra, ^{223}Ra	RaDeCC (alpha-scintillation)	Lab	Water mass mixing, residence times, SGD estimation	Moore and Arnold, 1996; Charette et al., 2008
^{224}Ra/^{228}Th	RaDeCC (alpha-scintillation)	Lab	Porewater exchange	Cai et al., 2014
^{224}Ra, ^{223}Ra	RaDeCC (alpha-scintillation)	Lab	Porewater exchange	Rodellas et al., 2015b
^{228}Ra	Gamma-spectrometry	Lab	Ocean basin scale SGD	Moore et al., 2008; Kwon et al., 2014
^{226}Ra, ^{228}Ra	Large volume pump + gamma spectrometry	Lab	Ocean basin scale SGD	Henderson et al., 2013
^{224}Ra, ^{228}Ra	Underwater gamma-spectrometry	*In situ*	Residence times, SGD estimation	Eleftheriou et al., 2017
fDOM, humification index	Fluorometry	Lab	SGD estimation	Nelson et al., 2015
Silica	Colorimetry	Lab	SGD estimation	Street et al., 2008
δ^{18}O and δ^{2}H	Optical spectroscopy	Lab	SGD estimation	Godoy et al., 2013; Rocha et al., 2016

between high and low radon activity water masses. Schubert et al. (2019) recently suggested additional improvements in the application of radon mass balance approaches that should improve corrections for radon losses from mixing and atmospheric evasion.

Since the "early days" of SGD studies, there has been a natural progression in improving radon measurement methodologies from labor-intensive grab samples collected in the field and analyzed in the lab or on ships (Mathieu et al., 1988), to the use of automated systems such as the RAD-AQUA (Burnett et al., 2001), to completely automated detection systems that can work unattended for months to years. Examples of the latter approach include autonomous water-proofed gamma-spectrometry systems that are passive and do not require power-demanding water pumping (Tsabaris et al., 2012). A mobile underwater *in-situ* gamma-ray spectroscopy system was successfully applied for coastal surveys of radon and ^{224}Ra as a ship-deployed tow system (Patritis et al., 2018) and was also developed for long-term deployment on a permanently moored station where it recorded hourly radon measurements for multiple years (Dulai et al., 2016 and see **Figure 5**). These novel technologies bring the ability to perform longer and higher resolution SGD monitoring in diverse field settings, which will help document trends in SGD in different hydrogeologic and climatic settings, under extreme weather events, excessive groundwater pumping trends, and sea level rise scenarios. Eventually, such systems could be deployed as a global network.

There have been several new SGD tracers introduced recently. Another isotope of radon, ^{220}Rn, also called "thoron," has been used for SGD prospecting, i.e., finding points of discharge as one must be close to a source to detect this very short-lived isotope. In an effort to employ ^{220}Rn as a groundwater tracer, Huxol et al. (2012) showed that while ^{220}Rn is easily detected in soil gas, it is often undetectable in groundwater. This is the case because under saturated conditions, migration of thoron through water is so slow that radioactive decay reduces the concentration to undetectable levels. However, flowing water apparently disturbs the immobile water layers stimulating the transfer of ^{220}Rn to the flowing water phase (Huxol et al., 2013). Thus, while thoron is difficult to detect in groundwater, it does serve as a good groundwater discharge tracer. Chanyotha et al. (2014) found intermittent thoron spikes in a 25-km stretch of a Bangkok canal

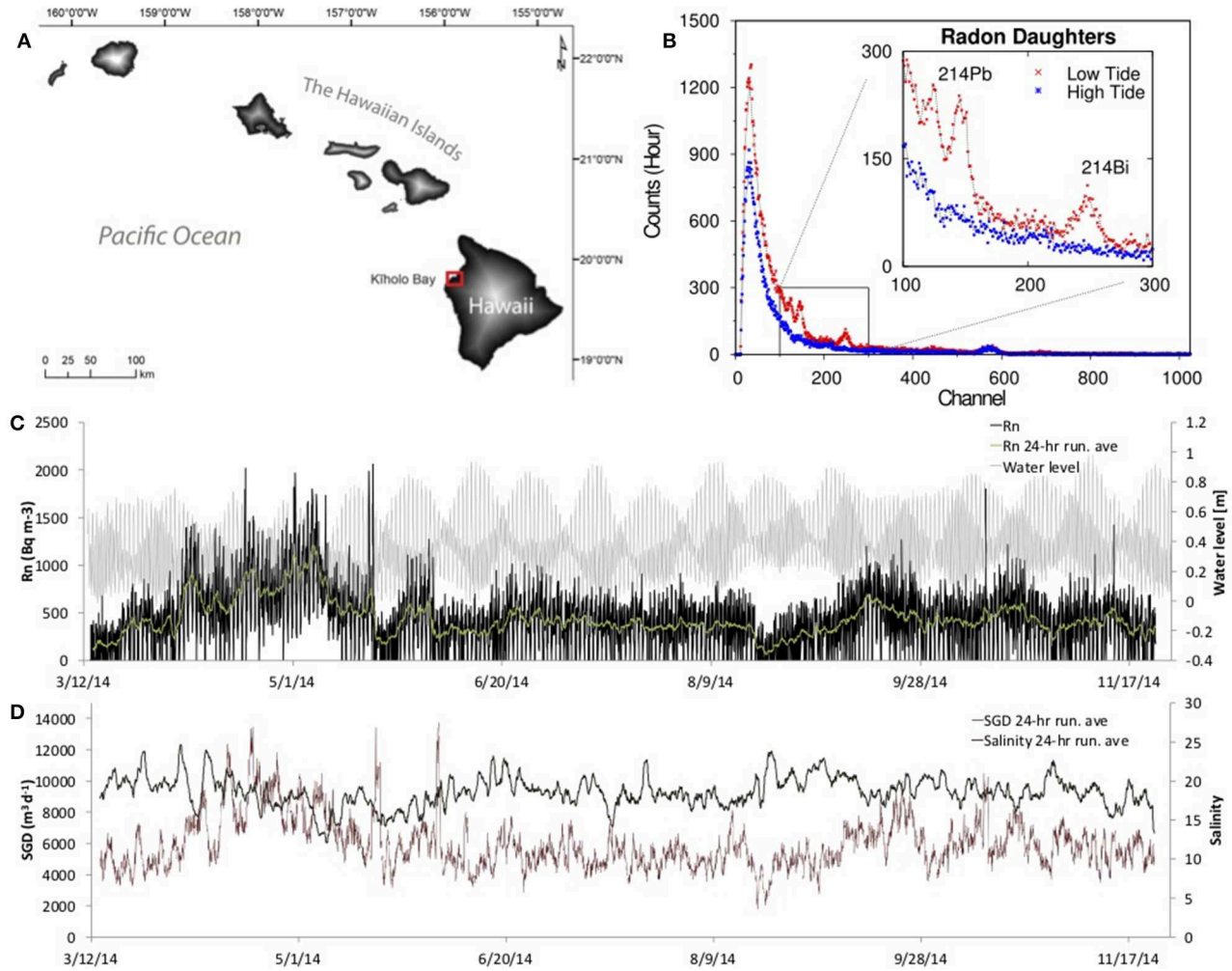

FIGURE 5 | (A) An autonomous gamma-spectrometer [NaI(Tl)] was deployed off the coast of Kiholo Bay, HI, USA. **(B)** Gamma-ray spectra were collected in the surface waters at hourly resolution. **(C)** The spectra during low tide show radon decay products, while at high tide radon and its progenies are diluted to below detection levels. **(D)** Hourly radon measurements over multiple years (a 9-month record shown here) allows us to evaluate SGD dynamics over tidal and seasonal time scales. Data from Dulai et al. (2016).

at essentially the same locations in surveys run along the same line 4 years apart. They also introduced a tool, the "meaningful thoron threshold," that ensures that a positive reading at or above the threshold has a 90% certainty of being a real detect. Thoron was also used in coastal spring discharge monitoring in Hawaii (Swarzenski et al., 2016).

Another natural SGD tracer involves dissolved organic matter (DOM). For example, SGD is often enriched in humic-like fluorescent DOM (Kim and Kim, 2017) and Nelson et al. (2015) demonstrated the utility of using indices of humidification derived from DOM in discharging groundwater as a tracer of SGD dispersal in nearshore waters.

There is renewed interest in the application of other U/Th series radionuclides, for example the $^{224}Ra/^{228}Th$ disequilibrium pair to study SGD and pore-water exchange dynamics (Cai et al., 2014). It has been demonstrated that carefully constructed radon and radium isotope mass-balances with well-defined end-members allow the quantification of and distinction between large-scale SGD and small-scale pore water exchange (Rodellas et al., 2015b; Cook et al., 2018). On a larger-scale form of exchange, radon has been applied to estimate beach pore water residence times and the flushing of a subterranean estuary, which showed positive correlation with tidal amplitudes and associated nutrient and dissolved organic carbon enrichment (Goodridge and Melack, 2014) and strong correlation with seawater intrusion (Oh and Kim, 2016). Radium and radon have also been combined with and used to document SGD-derived greenhouse gas fluxes in for example, a subtropical estuary (Sadat-Noori et al., 2016), the Amazon region (Call et al., 2019), and the Arctic (Lecher et al., 2015).

While geochemical tracers continue to provide valuable information for SGD studies, the most notable trend in the field is the application of multiple techniques that include geochemical tracers, geophysical approaches, direct

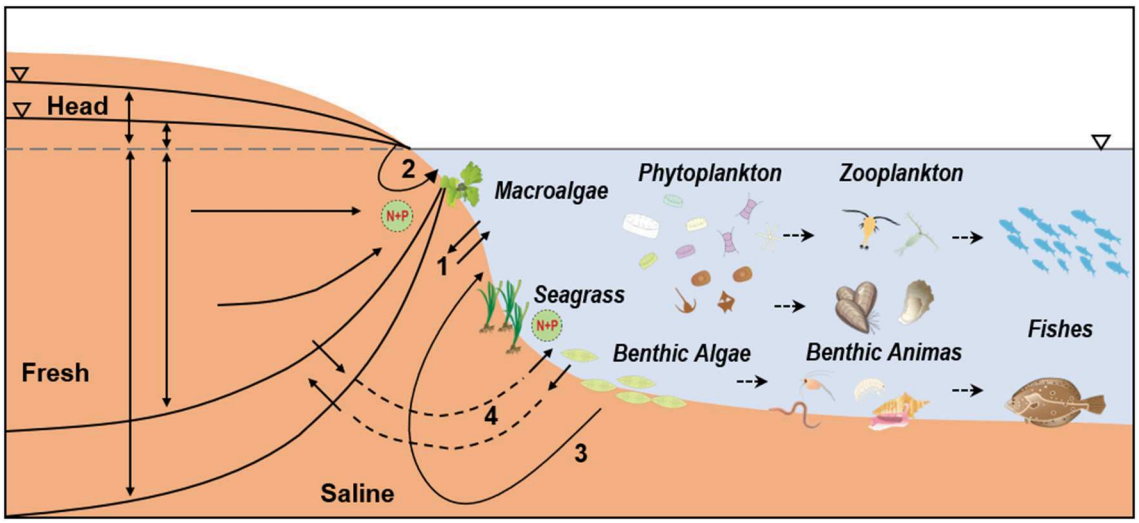

FIGURE 6 | Biological production in coastal ecosystems based on nutrients supplied through SGD. The numbers refer to the driving forces identified in **Figure 2**.

measurements, and hydrological modeling (e.g., Taniguchi et al., 2015). Such applications using multiple approaches decrease the degrees of freedom when interpreting SGD processes in often complex environments.

BIO-ECOLOGICAL IMPACTS

Bio-ecological Processes

Groundwater discharge has been recognized as a mechanism for transporting land-derived materials to the sea. Nutrients, carbon, metals, and other materials, which are dissolved in terrestrial groundwater, can drive bio-ecological processes in coastal seas. These effects are enhanced by recirculated seawater as it reacts within the aquifer sediment (see the Geochemical section). SGD can also act as a conduit of anthropogenic pollutants to coastal regions, and the lower salinity and pH associated with some types of SGD can stress local marine biota (reviewed in Lecher and Mackey, 2018).

Most studies of marine biota with respect to SGD focus on primary producers, because they provide the base of marine ecosystems as well as the chief response to nutrient supply via SGD (**Figure 6**). To date, many studies have revealed that nutrients transported through groundwater can support benthic and water column primary production in various coastal ecosystems. For example, SGD drives benthic primary production in the intertidal zone of the Yellow Sea (Waska and Kim, 2010, 2011). SGD also contributes significantly to reef productivity and/or calcification (Kamermans et al., 2002; Greenwood et al., 2013; McMahon and Santos, 2017). In a coastal water column, phytoplankton community structure was shown to be altered by SGD (Troccoli-Ghinaglia et al., 2010; Blanco et al., 2011; Adolf et al., 2019). More recently, a direct relationship between SGD and *in situ* phytoplankton primary productivity in nearshore coastal areas in Japan was found (Sugimoto et al., 2017). In Mediterranean coastal lagoons, Andrisoa et al. (2019) provided direct evidence for the role of karstic groundwater and porewater fluxes in sustaining primary production. Nutrient addition bioassay experiments support the view that SGD acts as a continual nutrient source (Gobler and Boneillo, 2003; Lecher et al., 2015).

Conversely, excess nutrient loadings via polluted groundwater into coastal seas may cause cultural eutrophication and microalgal blooms. In South Korea, SGD was identified as the most likely nutrient source triggering harmful algal blooms (HABs) and green tides (Hwang et al., 2005; Lee et al., 2009; Kwon et al., 2017; Cho et al., 2019a). In oligotrophic coastal reef environments, significant effects of SGD on marine biota were reported with their magnitudes varying according to land-use practices. The effects were shown to be most intense in locations with high anthropogenic impacts (Amato et al., 2016, 2018). Macroalgal overgrowths of coral reefs worldwide has been associated with nutrient inputs from SGD (Knee and Paytan, 2011). On the other hand, reef structure can also impact the nutrient load discharged into the sea by SGD (Oehler et al., 2019).

In the case of benthic communities, most SGD linkages are reported from intertidal regions. Several patterns have emerged from a limited number of studies suggesting that intertidal fresh SGD can change microbiological communities (Adyasari et al., 2019), determine species diversity, distribution, biomass distribution, and proliferation of benthic animals (e.g., Ouisse et al., 2011; Leitão et al., 2015; Foley, 2018). For example, benthic communities in the vicinity of freshwater SGD are often characterized by reduced species richness and diversity, due to high abundances of a small number of euryhaline/freshwater-tolerant species (Zipperle and Reise, 2005; Dale and Miller, 2008). Intertidal SGD has been associated with a shift in dominant species of macrofauna and meiofauna and can exclude ubiquitous species that are in the surrounding marine environment (Zipperle and Reise, 2005; Welti et al., 2015; Shoji and Tominaga, 2018). SGD might also moderate pore-water

temperatures and provide a refuge in sediment for macrofauna against extreme temperatures (Miller and Ullman, 2004). Overall, intertidal SGD may enhance biodiversity and species richness on a broader spatial scale.

SGD has been believed to contribute to coastal fisheries production including extensive aquaculture (e.g., oyster and mussel) in many locations around the world (Moosdorf and Oehler, 2017; Chen et al., 2018a; Shoji and Tominaga, 2018). Although there was little scientific evidence until recently, a growing body of interdisciplinary work is now demonstrating an ecological linkage between SGD and fisheries resources. For example, the Mediterranean mussel is a highly valuable commercial species. At the Olhos de Aqua beach in Portugal, groundwater inputs were recognized as increasing abundance and body size of these mussels (Piló et al., 2018). Cage experiments of the mussel *Mytilus galloprovincialis* in Salses-Leucate lagoon in France revealed that groundwater discharge provides favorable environmental conditions (i.e., higher temperature and food availability) for faster growth (Andrisoa et al., submitted). This is thought to be the case as groundwater discharge is a major source of nutrients and affects primary production within these ecosystems (Rodellas et al., 2015a; Andrisoa et al., 2019). Along the volcanic coast of northern Japan, fresh groundwater is an important factor providing suitable environment for phytoplankton that drives the high quality of the sessile bivalve *Crasslstrea nippona*, a commercially important local oyster (Hosono et al., 2012). In the Caribbean region, a groundwater-fed inlet provides a habitat for queen conch *Lobatus gigas* populations, which is one of the most important fishery resources in the region (Stieglitz and Dujon, 2017).

An increase of fish abundance and biomass and utilization of nursery areas has been observed in the vicinity of SGD (Hata et al., 2016; Utsunomiya et al., 2017; Starke et al., submitted; Yamane et al., 2019). The first location where an impact of SGD on fish abundance was directly recorded was in Obama Bay, Japan (Utsunomiya et al., 2017). There, the effect of nutrients transported via SGD on the food-chain was highlighted, because primary production was shown to be higher near SGD sites (Sugimoto et al., 2017). Furthermore, in the tidal flat of Seto Inland Sea, Japan, abundant juveniles of the marbles sole *Pseudopleuronectes yokohamae* were found near SGD sites with abundant prey organisms (Hata et al., 2016). Experimental evidence confirmed that the juvenile *P. yokohamae* obtained elevated levels of nutrition in the vicinity of SGD (Fujita et al., 2019). These findings demonstrated that SGD-derived nutrients enhanced marine fish production.

SGD has been shown to influence marine biota across a variety of coastal ecosystems. However, the mechanisms by which SGD affects primary production as well as marine animals differ from one ecosystem to another depending upon the hydrogeographical properties such as type of groundwater discharge (i.e., spring or seepage), location, species present, nutrient content of the groundwater, SGD flux, among other factors (Sugimoto et al., 2017; Shoji and Tominaga, 2018). Additional research is needed for a comprehensive assessment of SGD's impact on marine ecosystems.

Bio-ecological Methodology

Four-decades after Johannes's benchmark paper (Johannes, 1980), several SGD studies confirmed that groundwater is a significant source of nutrients to coastal seas. Although there is no doubt that SGD-derived nutrients contribute to marine organisms and ecosystem functions, evidence of the actual linkage between SGD and marine organisms is limited. Evidence seems best at some specific geological sites (e.g., karstic and volcanic regions) and intertidal sandflats where the discharge of groundwater can be directly viewed (Moosdorf and Oehler, 2017; Lecher and Mackey, 2018). In some cases, gas bubbles and excessive phenomena such as eutrophication and algal blooms are tied to SGD (Knee and Paytan, 2011). The difficulty in making the SGD-ecological linkage may be explained in two ways. First, marine organisms (i.e., microalgae, macroalgae, and animals) living in coastal waters or sediments are subject to various physical and biogeochemical processes that can affect their growth and physiology. In addition, nutrients supplied from multiple sources including rivers, atmospheric deposition, oceanic waters, and organic matter regeneration as well as groundwater inputs complicate an SGD assessment. Second, the pathway of SGD is invisible restricting our investigations in most coastal ecosystems. However, technological advances over the last decade have increased our ability to assess the ecological linkage to SGD in systems from local to shelf scales. Lecher and Mackey (2018) synthesized the effects of SGD on marine biota. Here we focus on how to assess the impact of SGD on marine organisms and ecosystems based on the latest methodological advances (**Table 2**).

Stable nitrogen isotope ratios ($\delta^{15}N$) of primary producers are well-known to be useful in detecting the direct linkage between groundwater inputs and marine organisms when the dissolved inorganic nitrogen (DIN) of groundwater is isotopically distinct from other DIN sources. For example, McClelland and Valiela (1998) demonstrated a strong relationship between increases of $\delta^{15}N$ of NO_3^- in groundwater and increases in $\delta^{15}N$ of various primary producers in several estuaries in Massachusetts. A clear positive relationship between seagrass $\delta^{15}N$ and the estimated groundwater flux was a pioneering work for this approach (Kamermans et al., 2002). To date, several studies have traced the behavior and fate of groundwater DIN using the $\delta^{15}N$ of primary producers, seagrasses, and macroalgae from local to regional scales (e.g., Lapointe et al., 2004, 2015; Derse et al., 2007; Honda et al., 2018; Andrisoa et al., 2019). In comparison to phytoplankton, macroalgae and seagrasses provide a time-integrated view of the N sources. Given that macroalgae directly take up nutrients only from the water column whereas seagrass does so mainly from interstitial waters, macroalgae is considered the more appropriate tool to assess the long-term availability of nitrogen in the overlying water column (Umezawa et al., 2002). In recent studies, researchers have deployed pre-treated macroalgae to assess the time-integrated impacts of SGD on a fine spatial scale. For example, Amato et al. (2016) quantified a groundwater impacted area in Kahului Bay, Hawaii, using the $\delta^{15}N$ of both *in situ* macroalgae collected from intertidal and subtidal zones as well as pre-treated macroalga deployed for a short-term in anchored cages. Similar studies have been

TABLE 2 | Summary of the main bio-ecological parameters used in SGD related studies.

Tracers	Measurement	Lab/*In situ*	Application	References
$\delta^{15}N$ and $\delta^{13}C$	Isotope ratio mass spectrometer (IRMS)	Lab	Tracing nitrogen and carbon flows, food web analysis	McClelland and Valiela, 1998; Hata et al., 2016; Andrisoa et al., 2019
$\delta^{15}N$ of macroalgae deployed in the water	IRMS and macroalgae incubation	Lab + *in situ*	Spatial mapping of SGD impacts on primary producers	Amato et al., 2016
Nutrient	Submersible colorimeter	*In situ*	High resolution monitoring of nutrient	Blanco et al., 2011
Nutrient	Spectrophotometry	Lab	Primary production estimation	Waska and Kim, 2011; Wang et al., 2018
Chlorophyll	Fluorometry	Lab, *in situ*	Biomass of phytoplankton,	Kobayashi et al., 2017; Honda et al., 2018
Photosynthetic pigments	High performance liquid chromatography (HPLC)	Lab	Class differentiation of benthic algae	Waska and Kim, 2010
Phytoplankton	Spectral fluorometry	*In situ*	Class differentiation of phytoplankton	Blanco et al., 2011
Phytoplankton	Flow cytometer	Lab	Size differentiation of phytoplankton	Lecher et al., 2015; Adolf et al., 2019
Phytoplankton	Bottle incubation with nutrient addition	Lab + *in situ*	Growth rate of phytoplankton, Limiting nutrients	Gobler and Boneillo, 2003; Lecher et al., 2015
Phytoplankton	Bottle incubation with enriched $DI^{13}C$ addition	Lab + *in situ*	Primary productivity of phytoplankton	Sugimoto et al., 2017
Dissolved oxygen	Optical oxygen sensor	*In situ*	Net ecosystem production, photosynthesis, respiration	Honda et al., 2018
pCO_2	Non-dispersive infrared sensor	*In situ*	Net ecosystem production, photosynthesis, respiration	Santos et al., 2012a; Maher et al., 2019
Number of benthic animals	Core sampler	*In situ*	Biomass and diversity of animals, Habitat use	Dale and Miller, 2008; Leitão et al., 2015
Number of fish	Net	*In situ*	Biomass and diversity of animals, Habitat use	Hata et al., 2016; Yamane et al., 2019
Behavior of animals	Acoustic telemetry	*In situ*	Habitat use	Stieglitz and Dujon, 2017
Shell length of bivalve	Cage experiment	*In situ*	Growth rate	(Andrisoa et al., submitted)
Total length of fish	Cage experiment	*In situ*	Growth rate	Fujita et al., 2019

done at a fringing coral reef ecosystem of Hawai'i Island (Abaya et al., 2018) and four embayments in Tutuila, American Samoa (Shuler et al., 2019).

However, the exact relationship between algae and SGD is sometimes difficult to interpret because the isotopic composition of the source nitrogen is variable and can cause uncertainty when interpreting the isotope fractionation during the assimilation, especially if more than one form of nitrogen is present (e.g., NO_3^- and NH_4^+), or if more than one source of nitrogen is available (e.g., riverine, groundwater, oceanic, and regenerated nitrogen; Sugimoto et al., 2010, 2014). Thus, the utilization of the $\delta^{15}N$ of primary producers as a proxy for the $\delta^{15}N$ of nutrient sources is difficult unless adequate information is obtained regarding the $\delta^{15}N$ of the various sources. For example, in the Waquoit Bay estuarine system, a comparison of the $\delta^{15}N$ of phytoplankton, NO_3^-, and NH_4^+ revealed that phytoplankton derived 3–47% of their N from groundwater NO_3^-, while the major N source was regenerated NH_4^+ (York et al., 2007).

Along with analyses of $\delta^{15}N$, gradients in the stable carbon isotope ratio ($\delta^{13}C$) between fresh groundwater and marine end members (Gramling et al., 2003) can be utilized to detect the direct linkage between SGD and organisms. For example, the $\delta^{13}C$ signature of macrophyte and phytoplankton in coastal lagoons on the French Mediterranean coastline shows the contribution of karstic groundwater discharge and porewater exchange as significant sources of dissolved inorganic carbon to primary production (Andrisoa et al., 2019). Therefore, these $\delta^{15}N$ and $\delta^{13}C$ signals in primary producers can be traced through some marine food webs. Although there is still no clear evidence,

Hata et al. (2016) suggest that there is a contribution of fresh SGD to local fish production on a tidal flat in Japan.

Biomass, abundance, productivity, physiology, and community structures of marine organisms have been directly assessed along natural gradients of SGD impact as well as compared at both SGD impacted and unimpacted sites. In contrast, visualization approaches using thermal infrared sensing and radon/radium tracing (see Geophysical and Geochemical sections) can be used as a guide for setting up ecological studies. Although the application of TIR imaging for ecological investigations has had limited applications thus far, Miller and Ullman (2004) and Grzelak et al. (2018) clarified a correspondence between the distributions of SGD and benthic organisms using thermal imaging. On the other hand, geochemical tracers such as radium and radon are often used for SGD-ecological studies. For example, Sugimoto et al. (2017) conducted field experiments at three Japanese coastal sites to elucidate the influence of SGD on *in situ* primary productivity of phytoplankton. Before the field experiments, they conducted continuous ^{222}Rn measurement surveys to visualize the spatial variability and gradient of SGD impacts. Consequently, they were able to report clear evidence for a direct association between SGD and coastal primary production. This visualization scheme has been applied in subsequent studies for marine organisms including fish (Utsunomiya et al., 2017). Furthermore, telemetry and biologging approaches for studying animal behavior associated with SGD will be helpful for future studies (Shoji et al., 2017; Stieglitz and Dujon, 2017).

When ^{222}Rn is used as a guide, simultaneous measurements of ^{222}Rn with other biological parameters enable us to assess the input of SGD and the response of marine organisms' activity. At a fringing coral reef in Japan, Blanco et al. (2011) conducted 4-days of continuous monitoring of ^{222}Rn activity, nitrate concentrations and class-differentiated phytoplankton using an automated radon analyzer and submersible sensors. Consequently, they revealed that groundwater-associated NO_3^- discharge drastically increased microalgal productivity and changed the community composition toward a dominance of a particular class. Furthermore, simultaneous measurements of ^{222}Rn with chlorophyll fluorescence, dissolved oxygen and pCO_2 supported a direct linkage between SGD and primary production in time and space at various locations (Kobayashi et al., 2017; Honda et al., 2018; Maher et al., 2019).

Primary production can be estimated by using a nutrient budget method (Waska and Kim, 2011), although estimates of SGD flux and nutrient loading commonly reported in SGD studies may not be appropriate for use as a comparison of nutrient availability for marine biota. In an urbanized embayment in Hong Kong, primary productivity was estimated at 1.5–15 $\times$ 10^6 g C d^{-1}, with 2–53% of the production being supported by SGD-driven PO_4^{3-} flux (Luo et al., 2014). In Daya Bay, China, ∼30% of total primary production was accounted for by SGD based on DIP budgets (Wang et al., 2018). This method can be easily scaled up from a local to a shelf scale. Luo et al. (2018) estimated that new production supported by groundwater-derived DIN constitutes up to about 24% of the total new production in a coastal upwelling shelf system.

Compared to primary producers, research for higher trophic species associated with SGD has just started. In the future, it is essential to clarify the spatial (e.g., local to global scales) and temporal (e.g., diel, seasonal, and decadal) variabilities in the processes relating to how SGD affects coastal fishery resources production. In particular, fish can move to and feed in multiple habitats within a relatively short temporal scale (e.g., tidal and daily scales). In focused flow ("submarine spring") situations, photo series can be used to interpret the behavior of fish at the local scale (Shoji and Tominaga, 2018; Starke et al., submitted). Combinations of hydrographic and geochemical surveys with bio-logging/telemetry approaches and stable isotope analyses together with fish movement and trophic flows in coastal ecosystems would enable accurate estimation of the contribution of SGD to fisheries production.

ECONOMIC AND CULTURAL ASPECTS

Economic Aspects

The presence of SGD in coastal zones, estuaries, and lagoons is associated with a variety of effects and uses, including geochemical and ecological dependencies (Johannes, 1980; Taniguchi et al., 2002; Burnett et al., 2003; Moore, 2010; Hosono et al., 2012), values associated with potable water for domestic use (Duarte et al., 2010; Pongkijvorasin et al., 2010; Burnett et al., 2017, 2018), as well as the historical and cultural importance of SGD-related submarine springs and plumes (Moosdorf and Oehler, 2017; Brosnan et al., 2018). The benefits associated with these uses can be expressed by a variety of metrics, including geochemical characteristics, aerial infrared maps of sea surface temperatures (Johnson et al., 2008), qualitative descriptions of cultural and historical significance (e.g., see next section), as well as economic evaluations of these SGD-related services and outcomes. Appropriate frameworks for deriving these economic estimates are the focus of this section.

Resource economics provides a theoretical framework for considering the economic value of SGD by directly linking groundwater and nearshore resources. Pongkijvorasin et al. (2010) developed a model of coastal groundwater management as a renewable resource and examined economically efficient management in the presence of known marine consequences of SGD. Concern for environmental conditions affecting marine biota controls the optimal steady-state head level of the aquifer. The model was discussed in general terms for any coastal groundwater resource where SGD has an impact on valuable nearshore resources. The authors then applied the model to a case study in Kona Hawai'i, where SGD is being actively studied and where both nearshore ecology and groundwater resources are significant sociopolitical issues. The application incorporated the economic value of SGD by including the market value of a freshwater-dependent marine algae directly in the model's objective function, thereby reducing the economically efficient trajectory of water consumption over time in order to support the growth of this economically and culturally important keystone species.

In a related case study in the same region by Duarte et al. (2010), the authors incorporated the consequences of water

extraction on nearshore resources by imposing a minimum requirement on the growth rate of the valuable marine algae. Efficient pumping rates fluctuate according to various growth requirements on the algae and different assumptions regarding aquifer recharge rates. Given expected growth in future water demand, costly desalination would be required under baseline recharge conditions and a strict minimum standard, and under low recharge conditions regardless of minimum standards of growth. The authors calculated the net present value associated with each scenario (with varying algae growth rates and recharge rates). These values can then be compared, and the differences interpreted as representative of the tradeoff between increased groundwater pumping and the economic value of the nearshore species.

Other studies have taken a more simplified (and static) approach to assessing the economic benefit of groundwater and its related functions, including services by SGD. For example, Burnett et al. (2017) reported results from a choice-based survey and analysis suggesting that residents of Obama City Japan are willing to pay on average JPY 565 (∼$5 USD) per month to maintain the drinking water function and related ecological services of groundwater and SGD in the region. While these stated preference approaches assess values of groundwater and related functions more directly, they are potentially less useful for policy and management than those values derived from dynamic resource management frameworks that include trajectories of efficient resource use over time. In follow-up work in this region, Burnett et al. (2018) developed a model linking groundwater pumping in Obama City to the area's nearshore fishery resource. A decrease in SGD reduces the flow of nitrogen, phosphorus, silica and other nutrients into the ocean, which affects primary production and, ultimately, fishery production. While groundwater is currently being used for domestic use, the economically important nearshore fishery depends on freshwater SGD as a source of nutrients, while the SGD diminishes with increases in pumping. Using a 3D model (MODFLOW) of the groundwater aquifer and fishery catch, market price, and fishing cost data from Obama City, the authors monetized the impact of increased groundwater pumping on the nearshore marine fishery.

Changes in the structure of economies across the world influence the availability of SGD and associated benefits. Hugman et al. (2015) showed how increases in tourism and irrigated agriculture in Portugal influence the distribution of SGD along the coast as well as over time. External pressures on the groundwater aquifer will also affect the economic value associated with SGD. Changes in land use, climate, demand growth, and energy costs will affect future water extraction patterns over space and time, with resulting spatial and temporal implications for SGD and linked coastal and estuarine resources. In the context of the "coastal groundwater squeeze," Michael et al. (2017) describe potential impacts on coastal estuaries and coral reefs (see also Johannes, 1980; Valiela et al., 1990; Amato et al., 2016). Characterizing the linkages between these related systems (e.g., land use to aquifer to SGD to ecosystem) is the first step in developing appropriate frameworks to evaluate economic outcomes associated with adjustments within and between these compartments. As the science relating these interconnected systems improves, so will our ability to express the underlying economic values.

Cultural Aspects

Fresh groundwater flows into the ocean through focused conduits ("submarine springs"), can be visible to the eye and, in some cases, potable. Submarine springs have inspired humans since ancient times. Aside from having important geochemical, biological, and economic importance, sudden occurrences of fresher water in a salty ocean hold cultural, social, and spiritual relevance throughout the world as well.

The cultural relevance of submarine springs is well-documented not only in the literature, but also through legends or places of worship and the naming of historical sites. The links are weakly documented by, for example, temple positions, as seen in Bangkok (Burnett et al., 2009) or on Lombok, Indonesia (Tanah Lot temple: Lubis and Bakti, 2013). Other indications of the cultural importance of submarine springs are place names related to water, such as Olhos de Aqua in Portugal (Carvalho et al., 2013) and local legends, such as the crying Tjilbruke spirit in South Australia (Isaacs, 1979). Because submarine springs are not usually the focus of people researching cultural heritage, little effort has been put into following these links in a structured way. In the following, the cultural relevance of SGD will be exemplified for two locations. This expands on a broader review of the societal use of SGD (Moosdorf and Oehler, 2017).

One of the most characteristic locations where submarine springs have been culturally important is the island of Bahrain. Submarine springs occur off the north side of the island and belong to a large aquifer system under the eastern part of the Arabian Peninsula (Rausch et al., 2014). Since Mesopotamian times (∼3000 BCE), literary texts mentioned the freshwater springs of the island (Crawford, 1998). This renders Bahrain as one of the prime candidates to be "Dilmun" (Bibby and Phillips, 1996; Crawford, 1998). In Sumeran tales, Dilmun is a paradise island where freshwater is plenty, and could possibly be related to the Christian Garden of Eden (Kramer, 1963). Later, in medieval times, the springs were used to refresh water supplies on sailing ships and during military conflicts (cf. Potts, 1985). Until the twentieth century, the water was also sold on land as drinking water (Williams, 1946). These springs, which have a 5000-year history of societal use, have been drying out due to increased on-land pumping of groundwater in recent decades (Taniguchi et al., 2002; Rausch et al., 2014). The consequences of the lost heritage due to the lost springs, which may even have had an impact on the naming of the island (Faroughy, 1951) remains to be discussed.

On the other side of the planet, the first written accords from Rapa Nui (Easter Island) from the Eighteenth century report that the island provides very little freshwater (Martinsson-Wallin and Crockford, 2001). Precipitation infiltrates the permeable volcanic soils immediately and there are no perennial streams on the island (Brosnan et al., 2018). Members of an expedition by the British explorer Captain Cook note that natives drink seawater (Forster et al., 2000)—most likely this refers to them drinking from coastal springs (Brosnan et al., 2018). After the arrival of the Europeans, the native population quickly disappeared so that

no accounts of the prehistoric water usage exist. But remnants of dug wells can be found only right at the coast, which, together with hydrogeological evidence point to fresh or brackish coastal seeps as a main drinking water source throughout the history of the island (Brosnan et al., 2018). While the cultural relevance of these drinking water sources is clear, it is also documented by the distribution of the famous stone monuments on the island, which occur more often close to the coastal seeps (DiNapoli et al., 2019). This leads to the hypothesis that the monuments marked important places, including coastal groundwater seeps (DiNapoli et al., 2019).

These examples showcase the social and historical importance of submarine springs to different cultures. Its relevance can sometimes also be used to qualitatively identify SGD locations, because locals, such as fishermen, often know the locations of submarine springs.

SUMMARY AND REMAINING QUESTIONS

We have updated the state of current research concerning SGD focusing on findings over the last decade, the "mature stage" (after the mid-2000s) of SGD research. Our treatment centered on the updates of measurement techniques, geophysical drivers, magnitudes, and effects.

In terms of *measurement techniques*, technological advances made during the developmental period of SGD research (mid-1990s—mid-2000s) and continuing to this day have had a profound impact on recognizing the scope of SGD. While radon and radium isotopes remain as the most popular geochemical tracers, other possibilities are showing promise. The short-lived isotope of radon (^{220}Rn) can be used for locating sources of SGD. Advances in sub-sea gamma spectrometers allow unattended radon measurements on time scales up to years. In some circumstances DOM, FDOM, Si, and stable isotopes of C and N have proven valuable as SGD tracers. Macroalgae δ^{15}N can be used to assess the long-term time-integrated availability of N from SGD. Interpretations are sometimes difficult because of multiple forms and sources of N. Advances in geoelectric and TIR technologies now allows expanded access to these tools. While these geophysical approaches cannot necessarily measure SGD, they provide useful maps that improve field studies and can be used to document the temporal dynamics of SGD. Coupling geoelectric techniques with hydrological flow modeling should improve our understanding of complex mixing between saline and fresh water SGD. Telemetry and biologging approaches for studying animal behavior associated with SGD will be helpful in future studies.

While many researchers focus mainly on groundwater flow driven by a terrestrial head, SGD is influenced by many *geophysical drivers*. Many of these drivers (tidal pumping, wave setup, etc.) are marine in origin. SGD and porewater exchange are seen as different and overlapping processes. Other drivers (wave pumping, bioturbation, etc.) may produce flow that is considered SGD and/or porewater exchange depending upon the situation and measurement technique. When examined in time and space coordinates, one can differentiate SGD from pore water exchange. Multiple driving forces are not necessarily synergistic or additive and interact in a non-linear fashion. In addition, multiple time scales of overlapping drivers are difficult to study by field observations, so most investigations rely on numerical models.

Recent studies suggest that the *magnitude* of fresh SGD to the ocean is only ∼1% of the annual river discharge. Most previous estimates placed this figure in the 5–10% range. However, while the fresh SGD magnitude is small relative to river discharge, it may still have local impacts. Furthermore, the total (saline + fresh) SGD and its dissolved materials is many times greater than river inputs. While there has been a focus on high-porosity sandy environments in SGD studies, muddy wetlands and marshes can also be important. For example, tidally-driven porewater exchange in mangrove creeks around the world are sufficient to filter the entire continental shelf volume in ∼150 years. Or, said another way, the mangrove creek flow is equivalent to about 1/3 of the global annual river discharge. Muddy coasts thus deserve more attention.

The *effects* on delivery of nutrients and other dissolved materials to the coastal ocean can be profound but depends upon the hydrogeological and biogeochemical conditions of the STE in question. It has been shown in many cases that nutrients transported by SGD can support benthic and water column primary productivity as well as influence the phytoplankton community structure. Of course, an overabundance of nutrients from any source can lead to eutrophication and macroalgal blooms. Intertidal SGD can influence species diversity and biomass distribution of benthic communities. SGD effects on higher trophic levels, including fish, have been documented as well.

While groundwater discharge has traditionally been studied as a geophysical process, SGD is now recognized to have certain *economic and cultural* implications. In order to evaluate the economic value of SGD, one needs to develop a framework to make these estimations. For example, there is a need to characterize the linkages between these interconnected systems: aquifers—land use—SGD—ecosystems in order to evaluate economic outcomes as changes occur within these components. Cultural values come into play as well. Coastal food resources, often influenced by SGD, can have meaningful significance in various cultures. Thus, as SGD changes via groundwater pumping, climate change or other forces, the resource and the community dependent upon that resource are directly and indirectly affected.

Some remaining questions concerning SGD are listed below as suggestions for future research.

a) Spatial and temporal scale issues
   For all the aspects considered here many spatial and temporal scale issues remain to be solved. While we recognize recirculated seawater as the main volumetric component of SGD, what are the time/length scales of the recharging process? How long are the residence times for water and dissolved material circulation in STEs?
b) Climate change impacts on SGD

Predicting the impacts of climate change on SGD is a remaining challenge. Impacts on SGD by sea level rise and changes in precipitation and/or evapotranspiration need to be evaluated. Further collaborations with climate change researchers are essential.

c) Global estimations
While global estimations of SGD and dissolved nutrient inputs associated with SGD have been attempted, uncertainties remain. We can now say with some degree of certainty that fresh groundwater discharge contributes less than a few percent of riverine inputs and saline discharge is several folds higher than rivers. However, more precise evaluations still evade us. Global estimates of SGD-derived fluxes for key elements such as carbon and iron remain unavailable.

d) Muddy shorelines
Most SGD datasets were obtained from sandy shorelines. Muddy saltmarshes and mangroves are widespread along global coastlines but remain understudied. Their muddy soils are often permeable due to abundant animal burrows and can produce extremely high porewater concentrations of carbon and heavy metals. To develop global estimates of groundwater and porewater influences on marine biogeochemical cycles, a stronger focus on mangroves and saltmarshes may be required.

e) Sustainability
SGD is a relatively stable water discharge through a subterranean estuary into the coastal environment. Thus, the "stability" of SGD may be much different from river discharge and shape the environment in a number of ways. Improved understandings of ecosystem functions and linkages to SGD will clarify the corresponding impacts, helping improve management toward a more sustainable coastal environment.

SGD is now recognized as an important pathway between land and sea. In some cases, SGD may be the most important pathway. It has been shown here that SGD has a relationship to other parts of the coastal continuum, and it has relevance from many different points of view. The next steps are to further quantify the interconnected roles allowing one to predict impacts of SGD change within the coastal zone.

AUTHOR CONTRIBUTIONS

MT conceived and initiated this project, provided editing of all sections, and authored the Summary and Remaining Questions portion. HD authored the section on Geochemical Methodology. KB wrote the Economic Aspects section and contributed to editing throughout. IS authored Geophysical Processes. RS wrote the parts entitled Bio-ecological Processes and Bio-ecological Methodology. TS wrote the portion concerning Geophysical Methodology. GK wrote the section on Geochemical Processes. NM authored the Cultural Aspects section. WB wrote the Introduction, parts of the Summary and Remaining Questions and assisted with editing throughout.

ACKNOWLEDGMENTS

All co-authors acknowledge and thank the two reviewers, Henry Bokuniewicz (Stony Brook University) and Pei Xin (Hohai University) for their very constructive advice.

REFERENCES

Abaya, L. M., Wiegner, T. N., Beets, J. P., Colbert, S. L., Kaile'a, M. C., and Kramer, K. L. (2018). Spatial distribution of sewage pollution on a Hawaiian coral reef. *Mar. Pollut. Bull.* 130, 335–347. doi: 10.1016/j.marpolbul.2018.03.028

Adolf, J. E., Burns, J., Walker, J. K., and Gamiao, S. (2019). Near shore distributions of phytoplankton and bacteria in relation to submarine groundwater discharge-fed fishponds, Kona coast, Hawai 'i, USA. *Estuar. Coast. Shelf Sci.* 219, 341–353. doi: 10.1016/j.ecss.2019.01.021

Adyasari, D., Hassenruck, C., Oehler, T., Sabdaningsih, A., and Moosdorf, N. (2019). Microbial community structure associated with submarine groundwater discharge in northern Java (Indonesia). *Sci. Total Environ.* 689, 590–601. doi: 10.1016/j.scitotenv.2019.06.193

Amato, D., Smith, C., and Duarte, T. (2018). Submarine groundwater discharge differentially modifies photosynthesis, growth, and morphology for two contrasting species of gracilaria (rhodophyta). *Hydrology* 5:65. doi: 10.3390/hydrology5040065

Amato, D. W., Bishop, J. M., Glenn, C. R., Dulai, H., and Smith, C. M. (2016). Impact of submarine groundwater discharge on marine water quality and reef biota of Maui. *PLoS ONE* 11:e0165825. doi: 10.1371/journal.pone.0165825

Andersson, P. S., Wasserburg, G., Ingri, J., and Stordal, M. C. (1994). Strontium, dissolved and particulate loads in fresh and brackish waters: the Baltic Sea and Mississippi Delta. *Earth Planet. Sci. Lett.* 124, 195–210. doi: 10.1016/0012-821X(94)00062-X

Andrisoa, A., Stieglitz, T. C., Rodellas, V., and Raimbault, P. (2019). Primary production in coastal lagoons supported by groundwater discharge and porewater fluxes inferred from nitrogen and carbon isotope signatures. *Mar. Chem.* 210, 48–60. doi: 10.1016/j.marchem.2019.03.003

Anschutz, P., Charbonnier, C., Deborde, J., Deirmendjian, L., Poirier, D., Mouret, A., et al. (2016). Terrestrial groundwater and nutrient discharge along the 240-km-long Aquitanian coast. *Mar. Chem.* 185, 38–47. doi: 10.1016/j.marchem.2016.04.002

Anwar, N., Robinson, C., and Barry, D. A. (2014). Influence of tides and waves on the fate of nutrients in a nearshore aquifer: Numerical simulations. *Adv. Water Resour.* 73, 203–213. doi: 10.1016/j.advwatres.2014.08.015

Beck, A. J., Charette, M. A., Cochran, J. K., Gonneea, M. E., and Peucker-Ehrenbrink, B. (2013). Dissolved strontium in the subterranean estuary–implications for the marine strontium isotope budget. *Geochim. Cosmochim. Acta* 117, 33–52. doi: 10.1016/j.gca.2013.03.021

Beck, A. J., Cochran, J. K., and Sañudo-Wilhelmy, S. A. (2010). The distribution and speciation of dissolved trace metals in a shallow subterranean estuary. *Mar. Chem.* 121, 145–156. doi: 10.1016/j.marchem.2010.04.003

Bejannin, S., Van Beek, P., Stieglitz, T., Souhaut, M., and Tamborski, J. (2017). Combining airborne thermal infrared images and radium isotopes to study submarine groundwater discharge along the French Mediterranean coastline. *J. Hydrol.* 13, 72–90. doi: 10.1016/j.ejrh.2017.08.001

Bibby, G., and Phillips, C. (1996). *Looking for Dilmun*. Westminster: Stacey International.

Bighash, P., and Murgulet, D. (2015). Application of factor analysis and electrical resistivity to understand groundwater contributions to coastal embayments in semi-arid and hypersaline coastal settings. *Sci. Total Environ.* 532, 688–701. doi: 10.1016/j.scitotenv.2015.06.077

Blanco, A. C., Watanabe, A., Nadaoka, K., Motooka, S., Herrera, E. C., and Yamamoto, T. (2011). Estimation of nearshore groundwater discharge and its potential effects on a fringing coral reef. *Mar. Pollut. Bull.* 62, 770–785. doi: 10.1016/j.marpolbul.2011.01.005

Bokuniewicz, H. (1980). Groundwater seepage into Great South Bay, New York. *Estuar. Coast. Mar. Sci*. 10, 437–444. doi: 10.1016/S0302-3524(80)80122-8

Bokuniewicz, H., Taniguchi, M., Ishitobi, T., Charrette, M., Allen, M., and Kontar, E. A. (2008). Direct measures of submarine groundwater discharge (SGD) over a fractured rock aquifer in Flamengo Bay Brazil. *Estuar. Coast. Shelf Sci*. 76, 466–472. doi: 10.1016/j.ecss.2007.07.047

Breier, J. A., Breier, C. F., and Edmonds, H. N. (2005). Detecting submarine groundwater discharge with synoptic surveys of sediment resistivity, radium, and salinity. *Geophys. Res. Lett*. 32:23. doi: 10.1029/2005GL024639

Brosnan, T., Becker, M. W., and Lipo, C. P. (2018). *Coastal groundwater discharge and the ancient inhabitants of Rapa Nui (Easter* Island), Chile. *Hydrogeol. J*. 27, 519–34. doi: 10.1007/s10040-018-1870-7

Buddemeier, R. W. (1996). "Groundwater flux to the ocean: definitions, data, applications, uncertainties," in *Groundwater Discharge in the Coastal Zone*, ed. *R. W. Buddemeier (Texel; Moscow: LOICZ/Russian Academy of Sciences),* 16–21.

Bugna, G., Chanton, J. P., Young, J. E., Burnett, W. C., and Cable, P. H. (1996). The importance of groundwater discharge to the methane budgets of nearshore and continental shelf waters of the northeastern Gulf of Mexico. *Geochim. Cosmochim. Acta* 60, 4735–4746. doi: 10.1016/S0016-7037(96)00290-6

Burnett, K., Wada, C. A., Endo, A., and Taniguchi, M. (2017). The economic value of groundwater in Obama. *J. Hydrol.* 11, 44–52. doi: 10.1016/j.ejrh.2015.10.002

Burnett, K., Wada, C. A., Taniguchi, M., Sugimoto, R., and Tahara, D. (2018). Evaluating the tradeoffs between groundwater pumping for snow-melting and nearshore fishery productivity in Obama city, Japan. *Water* 10:1556. doi: 10.3390/w10111556

Burnett, W. C., Aggarwal, P. K., Aureli, A., Bokuniewicz, H., Cable, J. E., Charette, M. A., et al. (2006). Quantifying submarine groundwater discharge in the coastal zone via multiple methods. *Sci. Total Environ*. 367, 498–543 doi: 10.1016/j.scitotenv.2006.05.009

Burnett, W. C., Bokuniewicz, H., Huettel, M., Moore, W. S., and Taniguchi, M. (2003). Groundwater and pore water inputs to the coastal zone. *Biogeochemistry* 66, 3–33. doi: 10.1023/B:BIOG.0000006066.21240.53

Burnett, W. C., Chanyotha, S., Wattayakorn, G., Taniguchi, M., Umezawa, Y., and Ishitobi, T. (2009). Underground sources of nutrient contamination to surface waters in Bangkok, Thailand. *Sci. Total Environ*. 407, 3198–3207. doi: 10.1016/j.scitotenv.2008.11.006

Burnett, W. C., Kim, G., and Lane-Smith, D. (2001). A continuous radon monitor for assessment of radon in coastal ocean waters. *J. Radioanal. Nucl. Chem*. 249, 167–172. doi: 10.1023/A:1013217821419

Burnett, W. C., Santos, I. R., Weinstein, Y., Swarzenski, P. W., and Herut, B. (2007). "Remaining uncertainties in the use of Rn-222 as a quantitative tracer of submarine groundwater discharge," in *Proceedings of Symposium HS1001 at IUGG2007* International Association of Hydrological Sciences (IAHS) Publ. 312, A New Focus on Groundwater-Seawater Interactions (Perugia), 109–118.

Burrage, D. M., Heron, M. L., Hacker, J. M., Miller, J. L., Stieglitz, T. C., Steinberg, C. R., et al. (2003). Structure and influence of tropical river plumes in the Great Barrier Reef: application and performance of an airborne sea surface salinity mapping system. *Remote Sens. Environ*. 85, 204–220. doi: 10.1016/S0034-4257(02)00206-7

Buss, S. R., Herbert, A. W., Morgan, P., Thornton, S. F., and Smith, J. W. N. (2004). A review of ammonium attenuation in soil and groundwater. *Q. J. Eng. Geol. Hydrogeol*. 37, 347–359. doi: 10.1144/1470-9236/04-005

Cable, J. E., Burnett, W. C., Chanton, J. P., and Weatherly, G. (1996). Modeling groundwater flow into the ocean based on ^{222}Rn. *Earth Planet. Sci. Lett*. 144, 591–604. doi: 10.1016/S0012-821X(96)00173-2

Cai, P., Shi, X., Moore, W. S., Peng, S., Wang, G., and Dai, M. (2014). 224Ra:228Th disequilibrium in coastal sediments: Implications for solute transfer across the sediment–water interface. *Geochim. Cosmochim. Acta* 125, 68–84. doi: 10.1016/j.gca.2013.09.029

Cai, W.-J., Wang, Y., Krest, J., and Moore, W. S. (2003). The geochemistry of dissolved inorganic carbon in a surficial groundwater aquifer in North Inlet, South Carolina, and the carbon fluxes to the coastal ocean. *Geochim. Cosmochim. Acta* 67, 631–639. doi: 10.1016/S0016-7037(02)01167-5

Call, M., Santos, I. R., Dittmar, T., De Rezende, C. E., Asp, N. E., and Maher, D. T. (2019). High pore-water derived CO2 and CH4 emissions from a macro-tidal mangrove creek in the Amazon region. *Geochim. Cosmochim. Acta* 247, 106–120. doi: 10.1016/j.gca.2018.12.029

Campbell, E. E., and Bate, G. C. (1996). Groundwater as a possible controller of surf diatom biomass. *Rev. Chil. Hist. Nat*. 69, 503–510.

Carvalho, L. F., Rocha, C., Fleming, A., Veiga-Pires, C., and Anibal, J. (2013). Interception of nutrient rich submarine groundwater discharge seepage on European temperate beaches by the acoel flatworm, Symsagittifera roscoffensis. *Mar. Pollut. Bull*. 75, 150–156. doi: 10.1016/j.marpolbul.2013.07.045

Chanyotha, S., Kranrod, C., Burnett, W. C., Lane-Smith, D., and Simko, J. (2014). Prospecting for groundwater discharge in the canals of Bangkok via natural radon and thoron. *J. Hydrol*. 519, 1485–1492. doi: 10.1016/j.jhydrol.2014.09.014

Chanyotha, S., Sola, P., Kritsananuwat, R., Lane-Smith, D., and Burnett, W. C. (2018). Improved measurements of thoron (^{220}Rn) in natural waters. *J. Radioanal. Nucl. Chem*. 318, 777–784. doi: 10.1007/s10967-018-6110-z

Charette, M. A., Moore, W. S., and Burnett, W. C. (2008). "Uranium- and thorium-series nuclides as tracers of submarine groundwater discharge," in *U-Th Series Nuclides in Aquatic Systems*, eds S. Krishnaswami and J. *Kirk Cochran (Amsterdam; Elsevier),* 155–191. doi: 10.1016/S1569-4860(07)00005-8

Charette, M. A., and Sholkovitz, E. R. (2006). Trace element cycling in a subterranean estuary: Part 2. Geochemistry of the pore water. *Geochim. Cosmochim. Acta* 70, 811–826. doi: 10.1016/j.gca.2005.10.019

Chen, X., Lao, Y., Wang, J., Du, J., Liang, M., and Yang, B. (2018a). Submarine groundwater-borne nutrients in a tropical bay (Maowei Sea, China) and their impacts on the oyster aquaculture. *Geochem. Geophys. Geosyst*. 19, 932–951. doi: 10.1002/2017GC007330

Chen, X., Zhang, F., Lao, Y., Wang, X., Du, J., and Santos, I. R. (2018b). Submarine groundwater discharge-derived carbon fluxes in mangroves: an important component of blue carbon budgets? *J. Geophys. Res*. 123, 6962–6979. doi: 10.1029/2018JC014448

Chevis, D. A., Johannesson, K. H., Burdige, D. J., Cable, J. E., Martin, J. B., and Roy, M. (2015). Rare earth element cycling in a sandy subterranean estuary in Florida, USA. *Mar. Chem*. 176, 34–50. doi: 10.1016/j.marchem.2015.07.003

Cho, H. M., Kim, G., Kwon, E. Y., Moosdorf, N., Garcia-Orellana, J., and Santos, I. R. (2018). Radium tracing nutrient inputs through submarine groundwater discharge in the global ocean. *Sci. Rep*. 8:2439. doi: 10.1038/s41598-018-20806-2

Cho, H. M., Kim, G., and Shin, K. H. (2019a). Tracing nitrogen sources fueling coastal green tides off a volcanic island using radon and nitrogen isotopic tracers. *Sci. Total Environ*. 665, 913–919. doi: 10.1016/j.scitotenv.2019.02.212

Cho, H. M., Kim, J. H., and Kim, G. (2019b). Desorption of phosphate on sandy sediments by silicate in groundwater. *Geochim. Cosmochim. Acta* 257, 184–190. doi: 10.1016/j.gca.2019.05.003

Cook, P. G., Rodellas, V., and Stieglitz, T. C. (2018). Quantifying surface water, porewater, and groundwater interactions using tracers: tracer fluxes, water fluxes, and end-member concentrations. *Water Resour. Res*. 54, 2452–2465. doi: 10.1002/2017WR021780

Couturier, M., Tommi-Morin, G., Sirois, M., Rao, A., Nozais, C., and Chaillou, G. (2017). Nitrogen transformations along a shallow subterranean estuary. *Biogeosciences* 14, 3321–3336. doi: 10.5194/bg-14-3321-2017

Crawford, H. E. W. (1998). *Dilmun and Its Gulf Neighbours*. Cambridge: Cambridge University Press.

Cyronak, T., Santos, I. R., Erler, D. V., Maher, D. T., and Eyre, B. D. (2014). Drivers of pCO_2 variability in two contrasting coral reef lagoons: the influence of submarine groundwater discharge. *Global Biogeochem. Cycles* 28, 398–414. doi: 10.1002/2013GB004598

Dale, R. K., and Miller, D. C. (2008). Hydrologic interactions of infaunal polychaetes and intertidal groundwater discharge. *Mar. Ecol. Prog. Ser*. 363, 205–215. doi: 10.3354/meps07455

Derse, E., Knee, K. L., Wankel, S. D., Kendall, C., Berg, C. J., and Paytan, A. (2007). Identifying sources of nitrogen to Hanalei Bay, Kauai, utilizing the nitrogen isotope signature of macroalgae. *Environ. Sci. Technol*. 41, 5217–5223. doi: 10.1021/es0700449

Dimova, N. T., Swarzenski, P. W., Dulaiova, H., and Glenn, C. R. (2011). Utilizing multichannel electrical resistivity methods to examine the dynamics of the fresh water-seawater interface in two Hawaiian groundwater systems. *J. Geophys. Res*. 117:C02012. doi: 10.1029/2011JC007509

DiNapoli, R. J., Lipo, C. P., Brosnan, T., Hunt, T. L., Hixon, S., Morrison, A. E., et al. (2019). Rapa Nui (Easter Island) monument (ahu) locations explained by freshwater sources. *PLoS ONE* 14:e0210409. doi: 10.1371/journal.pone.0210409

Dorsett, A., Cherrier, J., Martin, J. B., and Cable, J. E. (2011). Assessing hydrologic and biogeochemical controls on pore-water dissolved inorganic carbon cycling in a subterranean estuary: a 14C and 13C mass balance approach. *Mar. Chem.* 127, 76–89. doi: 10.1016/j.marchem.2011.07.007

Duarte, T. K., Hemond, H. F., Frankel, D., and Frankel, S. (2006). Assessment of submarine groundwater discharge by handheld aerial infrared imagery: case study of Kaloko fishpond and bay, Hawai'i. *Limnol. Oceanogr.* 4, 227–236. doi: 10.4319/lom.2006.4.227

Duarte, T. K., Pongkijvorasin, S., Roumasset, J., Amato, D., and Burnett, K. (2010). Optimal management of a Hawaiian Coastal Aquifer with nearshore marine Ecological Interactions. *Water Resour. Res.* 46:W11545. doi: 10.1029/2010WR009094

Dulai, H., Kamenik, J., Waters, C. A., Kennedy, J., Babinec, J., Jolly, J., et al. (2016). Autonomous long-term gamma-spectrometric monitoring of submarine groundwater discharge trends in Hawaii. *J. Radioanal. Nucl. Chem.* 307, 1865–1870. doi: 10.1007/s10967-015-4580-9

Dulaiova, H., Camilli, R., Henderson, P. B., and Charette, M. A. (2010). Coupled radon, methane and nitrate sensors for large-scale assessment of groundwater discharge and non-point source pollution to coastal waters. *J. Environ. Radioactiv.* 101, 553–563. doi: 10.1016/j.jenvrad.2009.12.004

Dulaiova, H., Peterson, R., Burnett, W. C., and Lane-Smith, D. (2005). A multi-detector continuous monitor for assessment of ^{222}Rn in the coastal ocean. *J. Radioanal. Nucl. Chem.* 263, 361–365. doi: 10.1007/s10967-005-0595-y

Eleftheriou, G., Tsabaris, C., Patiris, D. L., Androulakaki, E. G., and Vlastou, R. (2017). Estimation of coastal residence time of submarine groundwater discharge using radium progenies. *Appl. Radiat. Isotopes* 121, 44–50 doi: 10.1016/j.apradiso.2016.12.021

Evans, R. L., and Lizarralde, D. (2003). Geophysical evidence for karst formation associated with offshore groundwater transport: an example from North Carolina. *Geochem. Geophys Geosyst.* 4:8. doi: 10.1029/2003GC000510

Faroughy, A. (1951). *The Bahrein Islands*. New York, NY: Verry, Fisher & Co., Inc.

Foley, L. J. (2018). Karst-channelled intertidal submarine groundwater discharge (SGD) conditions the form of the rock pool sessile assemblage. *Estuar. Coast. Shelf Sci.* 213, 236–244. doi: 10.1016/j.ecss.2018.08.014

Forster, G., Thomas, N., and Berghof, O. (2000). *A Voyage Round the World*. Honolulu, HI: University of Hawai'i Press.

Freeze, R. A., and Cherry, J. A. (1979). *Groundwater*. Englewood Cliffs, NJ: Prentice-Hall Inc.

Fujita, K., Shoji, J., Sugimoto, R., Nakajima, T., Honda, H., Takeuchi, M., et al. (2019). Increase in fish production through bottom-up trophic linkage in coastal waters induced by nutrients supplied via submarine groundwater. *Front. Environ. Sci.* 7:82. doi: 10.3389/fenvs.2019.00082

Geng, X., and Boufadel, M. C. (2017). The influence of evaporation and rainfall on supratidal groundwater dynamics and salinity structure in a sandy beach. *Water Resour. Res.* 53, 6218–6238. doi: 10.1002/2016WR020344

Gilfedder, B. S., Frei, S., Hofmann, H., and Cartwright, I. (2015). Groundwater discharge to wetlands driven by storm and flood events: Quantification using continuous Radon-222 and electrical conductivity measurements and dynamic mass-balance modelling. *Geochim. Cosmochim. Acta* 165, 161–177. doi: 10.1016/j.gca.2015.05.037

Gobler, C. J., and Boneillo, G. E. (2003). Impacts of anthropogenically influenced groundwater seepage on water chemistry and phytoplankton dynamics within a coastal marine system. *Mar. Ecol. Prog. Ser.* 255, 101–114. doi: 10.3354/meps255101

Godoy, J. M., Souza, T. A., Godoy, M. L. D. P., Moreira, I., Carvalho, Z. L., Lacerda, L. D., et al. (2013). Groundwater and surface water quality in a coastal bay with negligible fresh groundwater discharge: Arraial do Cabo, Brazil. *Mar. Chem.* 156, 85–97. doi: 10.1016/j.marchem.2013.05.004

Goodridge, B. M., and Melack, J. M. (2014). Temporal evolution and variability of dissolved inorganic nitrogen in beach pore water revealed using radon residence times. *Environ. Sci. Technol.* 48, 14211–14218. doi: 10.1021/es504017j

Gramling, C., McCorkle, D., Mulligan, A., and Woods, T. J. L. (2003). A carbon isotope method to quantify groundwater discharge at the land-sea interface. *Limnol. Oceanogr.* 48, 957–970. doi: 10.4319/lo.2003.48.3.0957

Greenwood, J. E., Symonds, G., Zhong, L., and Lourey, M. (2013). Evidence of submarine groundwater nutrient supply to an oligotrophic barrier reef. *Limnol. Oceanogr.* 58, 1834–1842. doi: 10.4319/lo.2013.58.5.1834

Greskowiak, J. (2014). Tide-induced salt-fingering flow during submarine groundwater discharge. *Geophys. Res. Lett.* 41, 6413–6419. doi: 10.1002/2014GL061184

Grzelak, K., Tamborski, J., Kotwicki, L., and Bokuniewicz, H. (2018). Ecostructuring of marine nematode communities by submarine groundwater discharge. *Mar. Environ. Res.* 136, 106–119. doi: 10.1016/j.marenvres.2018.01.013

Gustafson, C., Key, K., and Evans, R. L. (2019). Aquifer systems extending far offshore on the U.S. *Atlantic margin. Sci. Rep.* 9:8709. doi: 10.1038/s41598-019-44611-7

Hata, M., Sugimoto, R., Hori, M., Tomiyama, T., and Shoji, J. (2016). Occurrence, distribution and prey items of juvenile marbled sole *Pseudopleuronectes yokohamae* around a submarine groundwater seepage on a tidal flat in southwestern Japan. *J. Sea Res.* 111, 47–53. doi: 10.1016/j.seares.2016.01.009

Henderson, P. B., Morris, P. J., Moore, W. S., and Charette, M. A. (2013). Methodological advances for measuring low level radium isotopes in seawater. *J. Radioanal. Nucl. Chem.* 296, 357–362. doi: 10.1007/s10967-012-2047-9

Henderson, R. D., Day-Lewis, F. D., Abarca, E., Harvey, C. F., Karam, H. N., Liu, L., et al. (2009). Marine electrical resistivity imaging of submarine groundwater discharge: Sensitivity analysis and application in Waquoit Bay, Massachusetts, USA. *Hydrogeol. J.* 18, 173–185. doi: 10.1007/s10040-009-0498-z

Honda, H., Sugimoto, R., Kobayahsi, S. (2018). "Submarine groundwater discharge and its influence on primary production in Japanese coasts: Case study in Obama Bay," in *The Water-Energy-Food Nexus. Human-Environmental Security in the Asia-Pacific Ring of Fire*, eds A. Endo and T. Oh (Singapore: Springer), 101–115.

Hosono, T., Ono, M., Burnett, W. C., Tokunaga, T., Taniguchi, M., and Akimichi, T. (2012). Spatial distribution of submarine groundwater discharge and associated nutrients within a local coastal area. *Environ. Sci. Technol.* 46, 5319–5326. doi: 10.1021/es2043867

Huang, K. F., and You, C. F. (2007). Tracing freshwater plume migration in the estuary after a typhoon event using Sr isotopic ratios. *Geophys. Res. Lett.* 34, 2403–2408. doi: 10.1029/2006GL028253

Huang, K. F., You, C. F., Chung, C. H., and Lin, I. T. (2011). Nonhomogeneous seawater Sr isotopic composition in the coastal oceans: a novel tool for tracing water masses and submarine groundwater discharge. *Geochem. Geophys. Geosyst.* 12:3372. doi: 10.1029/2010GC003372

Huettel, M., Berg, P., and Kostka, J. E. (2014). Benthic exchange and biogeochemical cycling in permeable sediments. *Annu. Rev. Mar. Sci.* 6, 23–51. doi: 10.1146/annurev-marine-051413-012706

Huettel, M., and Webster, I. T. (2000). "Porewater flow in permeable sediments." in *Benthic Boundary Layer: Transport Processes and Biochemistry*, eds B. P. Boudreau and B. B. Jørgensen (Oxford: Oxford Press), 144–179.

Hugman, R., Stigter, T. Y., Monteiro, J. P., Costa, L., and Nunes, L. M. (2015). Modeling the spatial and temporal distribution of coastal groundwater discharge for different water use scenarios under epistemic uncertainty: case study in South Portugal. *Environ. Earth Sci.* 73, 2657–2669. doi: 10.1007/s12665-014-3709-4

Huxol, S., Brennwald, M. S., Hoehn, E., and Kipfer, R. (2012). On the fate of ^{220}Rn in soil material in dependence of water content: implications from field and laboratory experiments. *Chem. Geol.* 298–299, 116–122. doi: 10.1016/j.chemgeo.2012.01.002

Huxol, S., Brennwald, M. S., and Kipfer, R. (2013). Processes controlling ^{220}Rn concentrations in the gas and water phases of porous media. *Chem. Geol.* 335, 87–92. doi: 10.1016/j.chemgeo.2012.10.049

Hwang, D. W., Lee, Y. W., and Kim, G. (2005). Large submarine groundwater discharge and benthic eutrophication in Bangdu Bay on volcanic Jeju Island, Korea. *Limnol. Oceanogr.* 50, 1393–1403. doi: 10.4319/lo.2005.50.5.1393

Isaacs, J. (1979). *Australian Dreaming: 40,000 Years of Aboriginal History*. Sydney, NSW; New York, NY: Lansdowne Press.

Jeong, J., Kim, G., and Han, S. (2012). Influence of trace element fluxes from submarine groundwater discharge (SGD) on their inventories in coastal waters off volcanic island, Jeju, Korea. *Appl. Geochem.* 27, 37–43. doi: 10.1016/j.apgeochem.2011.08.014

Johannes, R. E. (1980). The ecological significance of the submarine discharge of groundwater. *Mar. Ecol. Prog. Ser.* 3, 365–373. doi: 10.3354/meps003365

Johannesson, K. H., and Burdige, D. J. (2007). Balancing the global oceanic neodymium budget: evaluating the role of groundwater. *Earth Planet. Sci. Lett.* 253, 129–142. doi: 10.1016/j.epsl.2006.10.021

Johannesson, K. H., Chevis, D. A., Burdige, D. J., Cable, J. E., Martin, J. B., and Roy, M. (2011). Submarine groundwater discharge is an important net source of light and middle REEs to coastal waters of the Indian River Lagoon, Florida, USA. *Geochim. Cosmochim. Acta* 75, 825–843. doi: 10.1016/j.gca.2010.11.005

Johannesson, K. H., Cortés, A., Ramos Leal, J. A., Ramírez, A. G., and Durazo, J. (2005). "Geochemistry of rare earth elements in groundwaters from a Rhyolite Aquifer, Central México," in *Rare Earth Elements in Groundwater Flow Systems. Water Science and Technology Library, Vol. 51*, ed K. H. Johannesson (Dordrecht: Springer), 188–222.

Johannesson, K. H., Palmore, C. D., Fackrell, J., Prouty, N. G., Swarzenski, P. W., Chevis, D. A., et al. (2017). Rare earth element behavior during groundwater–seawater mixing along the Kona Coast of Hawaii. *Geochim. Cosmochim. Acta* 198, 229–258. doi: 10.1016/j.gca.2016.11.009

Johnson, A. G., Glenn, C. R., Burnett, W. C., Peterson, R. N., and Lucey, P. G. (2008). Aerial infrared imaging reveals large nutrient-rich groundwater inputs to the ocean. *Geophys. Res. Lett.* 35:L15606. doi: 10.1029/2008GL034574

Johnson, C. D., Swarzenski, P. W., Richardson, C. M., Smith, C. G., Kroeger, K. D., and Ganguli, P. M. (2015). Ground-truthing electrical resistivity methods in support of submarine groundwater discharge studies: examples from Hawaii, Washington, and California. *J. Environ. Eng. Geophys.* 20, 81–87. doi: 10.2113/JEEG20.1.81

Joly, J. (1899). *An Estimate of the Geological Age of the Earth*. Dublin: Scientific Transactions of the Royal Dublin Society.

Kamermans, P., Hemminga, M. A., Tack, J. F., Mateo, M. A., Marb,à, N., and Mtolera, M. (2002). Groundwater effects on diversity and abundance of lagoonal seagrasses in Kenya and on Zanzibar Island (East Africa). *Mar. Ecol. Prog. Ser.* 231, 75–83. doi: 10.3354/meps231075

Kelly, J. L., Glenn, C. R., and Lucey, P. G. (2013). High-resolution aerial infrared mapping of groundwater discharge to the coastal ocean. *Limnol. Oceanogr.* 11, 262–277. doi: 10.4319/lom.2013.11.262

Kim, G., Hwang, D.-W. (2002). Tidal pumping of groundwater into the coastal ocean revealed from submarine 222Rn and CH4 monitoring. *Geophys. Res. Lett.* 29, 23–27. doi: 10.1029/2002GL015093

Kim, G., Ryu, J. W., Yang, H. S., and Yun, S. T. (2005). Submarine groundwater discharge (SGD) into the Yellow Sea revealed by 228Ra and 226Ra isotopes: Implications for global silicate fluxes. *Earth Planet. Sci. Lett.* 237, 156–166. doi: 10.1016/j.epsl.2005.06.011

Kim, I., and Kim, G. (2011). Large fluxes of rare earth elements through submarine groundwater discharge (SGD) from a volcanic island, Jeju, Korea. *Mar. Chem.* 127, 12–19. doi: 10.1016/j.marchem.2011.07.006

Kim, I., and Kim, G. (2015). Role of colloids in the discharge of trace elements and rare earth elements from coastal groundwater to the ocean. *Mar. Chem.* 176, 126–132. doi: 10.1016/j.marchem.2015.08.009

Kim, J., and Kim, G. (2017). Inputs of humic fluorescent dissolved organic matter via submarine groundwater discharge to coastal waters off a volcanic island (Jeju, Korea). *Sci. Rep.* 7:7921. doi: 10.1038/s41598-017-08518-5

Kim, T. H., Kwon, E., Kim, I., Lee, S. A., and Kim, G. (2013). Dissolved organic matter in the subterranean estuary of a volcanic island, Jeju: importance of dissolved organic nitrogen fluxes to the ocean. *J. Sea Res.* 78, 18–24. doi: 10.1016/j.seares.2012.12.009

King, J. N. (2012). Synthesis of benthic flux components in the Patos Lagoon coastal zone, Rio Grande do Sul, Brazil. *Water Resour. Res.* 48:W12530. doi: 10.1029/2011WR011477

Knee, K., and Paytan, A. (2011). 4.08 submarine groundwater discharge: a source of nutrients, metals, and pollutants to the Coastal Ocean. *Treat. Estuar. Coast. Sci.* 4, 205–234. doi: 10.1016/B978-0-12-374711-2.00410-1

Kobayashi, S., Sugimoto, R., Honda, H., Miyata, Y., Tahara, D., Tominaga, O., et al. (2017). High-resolution mapping and time-series measurements of 222Rn concentrations and biogeochemical properties related to submarine groundwater discharge along the coast of Obama Bay, a semi-enclosed sea in Japan. *Prog. Earth Planet. Sci.* 4:6. doi: 10.1186/s40645-017-0124-y

Kohout, F. A. (1966). Submarine springs: a neglected phenomenon of coastal hydrology. *Hydrology* 26, 391–413.

Kolokoussis, P., Karathanassi, V., Rokos, D., Argialas, D., Karageorgis, A. P., and Georgopoulos, D. (2011). Integrating thermal and hyperspectral remote sensing for the detection of coastal springs and submarine groundwater discharges. *Int. J. Remote Sens.* 32, 8231–8251. doi: 10.1080/01431161.2010.533209

Kramer, S. N. (1963). *The Sumerians: Their History, Culture, and Character*. Chicago, IL: University of Chicago Press.

Kroeger, K. D., and Charette, M. A. (2008). Nitrogen biogeochemistry of submarine groundwater discharge. *Limnol. Oceanogr.* 53, 1025–1039. doi: 10.4319/lo.2008.53.3.1025

Krupa, S. L., Belanger, T. V., Heck, H. H., Brok, J. T., and Jones, B. J. (1998). Krupaseep - the next generation seepage meter. *J. Coast Res.* 25, 210–213.

Kwon, E. Y., Kim, G., Primeau, F., Moore, W. S., Cho, H-M, DeVries, T., et al. (2014). Global estimate of submarine groundwater discharge based on an observationally constrained radium isotope model. *Geophys. Res. Lett.* 42, 8438–8444. doi: 10.1002/2014GL061574

Kwon, H. K., Kang, H., Oh, Y. H., Park, S. R., and Kim, G. (2017). Green tide development associated with submarine groundwater discharge in a coastal harbor, Jeju, Korea. *Sci Rep.* 7:6325. doi: 10.1038/s41598-017-06711-0

Lapointe, B. E., Barile, P. J., and Matzie, W. R. (2004). Anthropogenic nutrient enrichment of seagrass and coral reef communities in the Lower Florida Keys: discrimination of local versus regional nitrogen sources. *J. Exp. Mar. Biol. Ecol.* 308, 23–58. doi: 10.1016/j.jembe.2004.01.019

Lapointe, B. E., Herren, L. W., Debortoli, D. D., and Vogel, M. A. (2015). Evidence of sewage-driven eutrophication and harmful algal blooms in Florida's Indian River Lagoon. *Harmful Algae* 43, 82–102. doi: 10.1016/j.hal.2015.01.004

Lecher, A., and Mackey, K. (2018). Synthesizing the effects of submarine groundwater discharge on Marine Biota. *Hydrology* 5:60. doi: 10.3390/hydrology5040060

Lecher, A. L., Kessler, J. D., Sparrow, K. J., Kodovska, F. G.-T., Dimova, N., Murry, J., et al. (2015). Methane transport through submarine groundwater discharge to the North Pacific and Arctic Ocean at two Alaskan sites. *Limnol. Oceanogr.* 61, S344–55. doi: 10.1002/lno.10118

Lee, D. R. (1977). A device for measuring seepage flux in lakes and estuaries. *Limnol. Oceanogr.* 22, 140–147. doi: 10.4319/lo.1977.22.1.0140

Lee, E., Kang, K. M., Hyun, S. P., Lee, K. Y., Yoon, H., Ha, K., et al. (2016a). Submarine groundwater discharge revealed by aerial thermal infrared imagery: a case study on Jeju Island, Korea. *Hydrol. Process.* 30, 3494–3506. doi: 10.1002/hyp.10868

Lee, E., Yoon, H., Hyun, S. P., Burnett, W. C., Koh, D. C., Kang, K. M., et al. (2016b). Unmanned aerial vehicles (UAVs)-based thermal infrared (TIR) mapping, a novel approach to assess groundwater discharge into the coastal zone. *Limnol. Oceanogr.* 14, 725–735. doi: 10.1002/lom3.10132

Lee, J., and Kim, G. (2015). Dependence of pH in coastal waters on the adsorption of protons onto sediment minerals. *Limnol. Oceanogr.* 60, 831–839. doi: 10.1002/lno.10057

Lee, Y. W., Hwang, D. W., Kim, G., Lee, W. C., and Oh, H. T. (2009). Nutrient inputs from submarine groundwater discharge (SGD) in Masan Bay, an embayment surrounded by heavily industrialized cities, Korea. *Sci. Total Environ.* 407, 3181–3188. doi: 10.1016/j.scitotenv.2008.04.013

Leitão, F., Encarnação, J., Range, P., Schmelz, R. M., Teodósio, M. A., and Chícharo, L. (2015). Submarine groundwater discharges create unique benthic communities in a coastal sandy marine environment. *Estuar. Coast. Shelf Sci.* 163, 93–98. doi: 10.1016/j.ecss.2015.06.007

Li, L., and Barry, D. A. (2000). Wave-induced beach groundwater flow. *Adv. Water Res.* 23, 325–337. doi: 10.1016/S0309-1708(99)00032-9

Li, L., Barry, D. A., Stagnitti, F., Parlange, J. Y., and Jeng, D. S. (2000). Beach water table fluctuations due to spring-neap tides: moving boundary effects. *Adv. Water Res.* 23, 817–824. doi: 10.1016/S0309-1708(00)00017-8

Liu, Q., Dai, M., Chen, W., Huh, C. A., Wang, G., Charette, M. A., et al. (2012). How significant is submarine groundwater discharge and its associated dissolved inorganic carbon in a river-dominated shelf system? *Biogeosciences* 9, 1777–1795. doi: 10.5194/bg-9-1777-2012

Lorah, M. M., Cozzarelli, I. M., and Böhlke, J. K. (2009). Biogeochemistry at a wetland sediment–alluvial aquifer interface in a landfill leachate plume. *J. Contamin. Hydrol.* 105, 99–117. doi: 10.1016/j.jconhyd.2008.11.008

Lubis, R. F., and Bakti, H. (2013). Mata Air Tawar Di Tengah Laut. *Geomagz* 3, 38–42.

Luijendijk, E., Gleeson, T., and Moosdorf, N. (2019). The flow of fresh groundwater and solutes to the World's oceans and coastal ecosystems. *EarthArXiv*. doi: 10.31223/osf.io/sw8r4

Luo, X., Jiao, J. J., Liu, Y., Zhang, X., Liang, W., and Tang, D. (2018). Evaluation of water residence time, submarine groundwater discharge, and maximum new production supported by groundwater borne nutrients in a coastal upwelling shelf system. *J. Geophys. Res*. 123, 631–655. doi: 10.1002/2017JC013398

Luo, X., Jiao, J. J., Moore, W. S., and Lee, C. M. (2014). Submarine groundwater discharge estimation in an urbanized embayment in Hong Kong via short-lived radium isotopes and its implication of nutrient loadings and primary production. *Mar. Pollut. Bull.* 82, 144–154. doi: 10.1016/j.marpolbul.2014.03.005

Maher, D. T., Call, M., Macklin, P., Webb, J. R., and Santos, I. R. (2019). Hydrological versus biological drivers of nutrient and carbon dioxide dynamics in a Coastal Lagoon. *Estuar. Coasts*. 42, 1015–1031. doi: 10.1007/s12237-019-00532-2

Manheim, F. T., Krantz, D. E., and Bratton, J. F. (2004). Studying ground water under Delmarva coastal bays using electrical resistivity. *Groundwater* 42, 1052–1068. doi: 10.1111/j.1745-6584.2004.tb02643.x

Martinsson-Wallin, H., and Crockford, S. J. (2001). Early Settlement of Rapa Nui (Easter Island). *Asian Perspect*. 40, 244–278. doi: 10.1353/asi.2001.0016

Mathieu, G. G., Biscaye, P. E., Lupton, R. A., and Hammond, D. E. (1988). System for measurement of 222Rn at low levels in natural waters. *Health Phys*. 55, 989–992. doi: 10.1097/00004032-198812000-00015

McClelland, J. W., and Valiela, I. (1998). Linking nitrogen in estuarine producers to land-derived sources. *Limnol. Oceanogr.* 43, 577–585. doi: 10.4319/lo.1998.43.4.0577

McMahon, A., and Santos, I. R. (2017). Nitrogen enrichment and speciation in a coral reef lagoon driven by groundwater inputs of bird guano. *J. Geophys. Res.* 122, 7218–7236. doi: 10.1002/2017JC012929

Michael, H. A., Lubetsky, J. S., and Harvey, C. F. (2003). Characterizing submarine groundwater discharge: a seepage meter study in Waquoit Bay, Massachusetts. *Geophys. Res. Lett*. 30, 1297–1301. doi: 10.1029/2002GL016000

Michael, H. A., Mulligan, A. E., and Harvey, C. F. (2005). Seasonal oscillations in water exchange between aquifers and the coastal ocean. *Nature* 436, 1145–1148. doi: 10.1038/nature03935

Michael, H. A., Post, V. E. A., Wilson, A. M., and Werner, A. D. (2017). Science, society, and the coastal groundwater squeeze. *Water Res. Res.* 53, 2610–2617. doi: 10.1002/2017WR020851

Michael, H. A., Scott, K. C., Koneshloo, M., Yu, X., Khan, M. R., and Li, K. (2016). Geologic influence on groundwater salinity drives large seawater circulation through the continental shelf. *Geophys. Res. Lett*. 43, 782–791. doi: 10.1002/2016GL070863

Miller, D. C., and Ullman, W. J. (2004). Ecological consequences of ground water discharge to Delaware Bay, United States. *Groundwater* 42, 959–970. doi: 10.1111/j.1745-6584.2004.tb02635.x

Moffett, K. B., Gorelick, S. M., McLaren, R. G., and Sudicky, E. A. (2012). Salt marsh ecohydrological zonation due to heterogeneous vegetation-groundwater-surface water interactions. *Water Resour. Res.* 48:W02516. doi: 10.1029/2011WR010874

Moore, W. S. (1996). Large groundwater inputs to coastal waters revealed by ^{226}Ra enrichments. *Nature* 380, 612–614. doi: 10.1038/380612a0

Moore, W. S. (1999). The subterranean estuary: a reaction zone of ground water and sea water. *Mar. Chem*. 65, 111–126. doi: 10.1016/S0304-4203(99)00014-6

Moore, W. S. (2010). The effect of submarine groundwater discharge on the ocean. *Annu. Rev. Mar. Sci*. 2, 59–88. doi: 10.1146/annurev-marine-120308-081019

Moore, W. S., and Arnold, R. (1996). Measurement of ^{223}Ra and ^{224}Ra in coastal waters using a delayed coincidence counter. *J. Geophys. Res*. 101, 1321–1329. doi: 10.1029/95JC03139

Moore, W. S., Sarmiento, J. L., and Key, R. M. (2008). Submarine groundwater discharge revealed by ^{228}Ra distribution in the upper Atlantic. *Nat. Geosci*. 1, 309–311. doi: 10.1038/ngeo183

Moosdorf, N., and Oehler, T. (2017). Societal use of fresh submarine groundwater discharge: An overlooked water resource. *Earth Sci. Rev*. 171, 338–348. doi: 10.1016/j.earscirev.2017.06.006

Moosdorf, N., Stieglitz, T., Waska, H., Durr, H. H., and Hartmann, J. (2015). Submarine groundwater discharge from tropical islands: a review. *Grundwasser* 20, 53–67. doi: 10.1007/s00767-014-0275-3

Mulligan, A. E., and Charette, M. A. (2006). Intercomparison of submarine groundwater discharge estimates from a sandy unconfined aquifer. *J. Hydrol.* 327, 411–425. doi: 10.1016/j.jhydrol.2005.11.056

Mulligan, A. E., Evans, R. L., and Lizarralde, D. (2007). The role of paleochannels in groundwater/seawater exchange. *J. Hydrol*. 335, 313–329. doi: 10.1016/j.jhydrol.2006.11.025

Nelson, C. N., Donahue, M. J., Dulaiova, H., Goldberg, S. J., La Valle, F. F., Lubarsky, K., et al. (2015). Fluorescent dissolved organic matter as a multivariate biogeochemical tracer of submarine groundwater discharge in coral reef ecosystems. *Mar. Chem. 177*, 232–243. doi: 10.1016/j.marchem.2015.06.026

Nielsen, P. (1990). Tidal dynamics of the water table in beaches. *Water Resour. Res*. 26, 2127–2134. doi: 10.1029/WR026i009p02127

Nielsen, P. (1999). Groundwater dynamics and salinity in coastal barriers. *J. Coastal Res*. 15, 732–740.

Oehler, T., Bakti, H., Lubis, R. F., Purwoarminta, A., Delinom, R., and Moosdorf, N. (2019). Nutrient dynamics in submarine groundwater discharge through a coral reef (western Lombok, Indonesia). *Limnol. Oceanogr*. doi: 10.1002/lno.11240. [Epub ahead of print].

Oehler, T., Eiche, E., Putra, D., Adyasari, D., Hennig, H., Mallast, U., et al. (2018). Seasonal variability of land-ocean groundwater nutrient fluxes from a tropical karstic region (southern Java, Indonesia). *J. Hydrol*. 565, 662–671. doi: 10.1016/j.jhydrol.2018.08.077

Oh, Y. H., and Kim, G. (2016). Large scale seasonal changes in the recharge of seawater in a subterranean estuary revealed by a radon tracer. *Hydrol. Process*. 30, 2525–2532. doi: 10.1002/hyp.10807

Oki, T., and Kanae, S. (2006). Global hydrological cycles and world water resources. *Science* 313, 1068–1072. doi: 10.1126/science.1128845

Ouisse, V., Riera, P., Migné, A., Leroux, C., and Davoult, D. (2011). Freshwater seepages and ephemeral macroalgae proliferation in an intertidal bay: I Effect on benthic community structure and food web. *Estuar. Coast. Shelf Sci*. 91, 272–281. doi: 10.1016/j.ecss.2010.10.034

Patritis, D. L., Tsabaris, C., Schmidt, M., Karageorgis, A. P., Prospathopoulos, A. M., Alexakis, S., et al. (2018). Mobile underwater in stitu gammas ray spectroscopy to localize groundwater emanation from pockmarks in the Eckernforde bay, Germany. *Appl. Radiat. Isotopes* 140, 305–313. doi: 10.1016/j.apradiso.2018.07.037

Paulsen, R. J., Smith, C. F., O'Rourke, D., and Wong, T. (2001). Development and evaluation of an ultrasonic ground water seepage meter. *Groundwater* 39, 904–911. doi: 10.1111/j.1745-6584.2001.tb02478.x

Petermann, E., and Schubert, M. (2015). Quantification of the response delay of mobile radon-in-air detectors applied for detecting short-term fluctuations of radon-in-water concentrations. *Eur. Phys. J. Spec. Top*. 224, 697–707. doi: 10.1140/epjst/e2015-02400-5

Piló, D., Barbosa, A. B., Teodósio, M. A., Encarnação, J., Leitão, F., Range, P., et al. (2018). Are submarine groundwater discharges affecting the structure and physiological status of rocky intertidal communities? *Mar. Environ. Res*. 136, 158–173. doi: 10.1016/j.marenvres.2018.02.013

Pongkijvorasin, S., Burnett, K., and Wada, C. A. (2018). Joint management of an interconnected coastal aquifer and invasive tree. *Ecol. Econ*. 146, 125–135. doi: 10.1016/j.ecolecon.2017.10.011

Pongkijvorasin, S., Roumasset, J., Duarte, T., and Burnett, K. (2010). Renewable resource management with stock externalities: coastal aquifers and submarine groundwater discharge. *Res. Energy Econ*. 32, 277–291. doi: 10.1016/j.reseneeco.2009.09.001

Post, V. E., Groen, J., Kooi, H., Person, M., Ge, S., and Edmunds, W. M. (2013). Offshore fresh groundwater reserves as a global phenomenon. *Nature* 504, 71–78. doi: 10.1038/nature12858

Potts, D. T. (1985). Reflections on the history and archaeology of Bahrain. *J. Am. Orient. Soc*. 105, 675–710. doi: 10.2307/602727

Povinec, P. P., Comanducci, J.-F., Levy-Palomo, I., and Oregioni, B. (2006). Monitoring of submarine groundwater discharge along the Donnalucata coast in the south-eastern Sicily using underwater gamma-ray spectrometry. *Continent. Shelf Res*. 26, 874–884. doi: 10.1016/j.csr.2005.12.009

Rahman, S., Tamborski, J. J., Charette, M. A., and Cochran, J. K. (2019). Dissolved silica in the subterranean estuary and the impact of submarine groundwater discharge on the global marine silica budget. *Mar. Chem*. 208, 29–42. doi: 10.1016/j.marchem.2018.11.006

Rausch, R., Dirks, H., Kallioras, A., and Schuth, C. (2014). The Riddle of the springs of dilmun-does the Gilgamesh Epic tell the truth? *Groundwater* 52, 640–644. doi: 10.1111/gwat.12214

Robinson, C., Brovelli, A., Barry, D. A., and Li, L. (2009). Tidal influence on BTEX biodegradation in sandy coastal aquifers. *Adv. Water Res.* 32, 16–28. doi: 10.1016/j.advwatres.2008.09.008

Robinson, C., Gibbes, B., and Li, L. (2006). Driving mechanisms for groundwater flow and salt transport in a subterranean estuary. *Geophys. Res. Lett.* 33:L03402. doi: 10.1029/2005GL025247

Robinson, C., Li, L., and Barry, D. A. (2007). Effect of tidal forcing on a subterranean estuary. *Adv. Water Res.* 30, 851–865. doi: 10.1016/j.advwatres.2006.07.006

Robinson, C., Xin, P., Li, L., and Barry, D. A. (2014). Groundwater flow and salt transport in a subterranean estuary driven by intensified wave conditions. *Water Resour. Res.* 50, 1–17. doi: 10.1002/2013WR013813

Robinson, C. E., Xin, P., Santos, I. R., Charette, M. A., Li, L., and Barry, D. A. (2018). Groundwater dynamics in subterranean estuaries of coastal unconfined aquifers: Controls on submarine groundwater discharge and chemical inputs to the ocean. *Adv. Water Res.* 115, 315–331. doi: 10.1016/j.advwatres.2017.10.041

Rocha, C., Veiga-Pires, C., Scholten, J., Knoeller, K., Gröcke, D. R., Carvalho, L., et al. (2016). Assessing land–ocean connectivity via submarine groundwater discharge (SGD) in the Ria Formosa Lagoon (Portugal): combining radon measurements and stable isotope hydrology. *Hydrol. Earth Syst. Sci.* 20, 3077–3098. doi: 10.5194/hess-20-3077-2016

Rodellas, V., Garcia-Orellana, J., Masqué, P., Feldman, M., and Weinstein, Y. (2015a). Submarine groundwater discharge as a major source of nutrients to the Mediterranean Sea. *Proc. Natl. Acad. Sci. U.S.A.* 112, 3926–3930. doi: 10.1073/pnas.1419049112

Rodellas, V., Garcia-Orellana, J., Trezzi, G., Masque, P., Berdalet, E., Bokuniewicz, H. J., et al. (2015b). "Seasonal cycles in radium fluxes to a Mediterranean Bay: submarine groundwater discharge vs porewater advection," in *2015 Aquatic Sciences Meeting. Program Book* (Granada), 64.

Röper, T., Greskowiak, J., and Massmann, G. (2014). Detecting small groundwater discharge springs using handheld thermal infrared imagery. *Groundwater* 52, 936–942. doi: 10.1111/gwat.12145

Röper, T., Greskowiak, J., and Massmann, G. (2015). Instabilities of submarine groundwater discharge under tidal forcing. *Limnol. Oceanogr.* 60, 22–28. doi: 10.1002/lno.10005

Rousakis, G., Karageorgis, A. P., and Georgiou, P. (2014). Geological structure and seabed morphology of the Stoupa submarine groundwater discharge system, Messinia, Greece. *Environ. Earth Sci.* 71, 5059–5069. doi: 10.1007/s12665-013-2910-1

Sadat-Noori, M., Maher, D. T., and Santos, I. R. (2016). Groundwater discharge as a source of dissolved carbon and greenhouse gases in a subtropical estuary. *Estuar. Coasts* 39, 639–656. doi: 10.1007/s12237-015-0042-4

Sadat-Noori, M., Santos, I. R., Sanders, C. J., Sanders, L. M., and Maher, D. T. (2015). Groundwater discharge into an estuary using spatially distributed radon time series and radium isotopes. *J. Hydrol.* 528, 703–719. doi: 10.1016/j.jhydrol.2015.06.056

Sadat-Noori, M., Santos, I. R., Tait, D. R., Reading, M. J., and Sanders, C. J. (2017). High porewater exchange in a mangrove-dominated estuary revealed from short-lived radium isotopes. *J. Hydrol.* 553, 188–198. doi: 10.1016/j.jhydrol.2017.07.058

Santos, I. R., Burnett, W. C., Chanton, J., Dimova, N., and Peterson, R. (2009). Land or ocean?: assessing the driving forces of submarine groundwater discharge at a coastal site in the Gulf of Mexico. *J. Geophys. Res.* 114:C04012. doi: 10.1029/2008JC005038

Santos, I. R., Burnett, W. C., Chanton, J., Mwashote, B., Suryaputra, I. G. N. A., and Dittmar, T. (2008). Nutrient biogeochemistry in a Gulf of Mexico subterranean estuary and groundwater-derived fluxes to the coastal ocean. *Limnol. Oceanogr.* 53, 705–718. doi: 10.4319/lo.2008.53.2.0705

Santos, I. R., Eyre, B. D., and Huettel, M. (2012b). The driving forces of porewater and groundwater flow in permeable coastal sediments: a review. *Estuar. Coast. Shelf Sci.* 98, 1–15. doi: 10.1016/j.ecss.2011.10.024

Santos, I. R., Maher, D. T., and Eyre, B. D. (2012a). Coupling automated radon and carbon dioxide measurements in coastal waters. *Environ. Sci. Technol.* 46, 7685–7691. doi: 10.1021/es301961b

Santos, I. R., Maher, D. T., Larkin, R., Webb, J. R., and Sanders, C. J. (2019). Carbon outwelling and outgassing vs. burial in an estuarine tidal creek surrounded by mangrove and saltmarsh wetlands. *Limnol. Oceanogr.* 64, 996–1013. doi: 10.1002/lno.11090

Santos-Echeandia, J., Prego, R., Cobelo-García, A., and Millward, G. E. (2009). Porewater geochemistry in a Galician Ria (NW Iberian Peninsula): implications for benthic fluxes of dissolved trace elements (Co, Cu, Ni, Pb, V, Zn). *Mar. Chem.* 117, 77–87. doi: 10.1016/j.marchem.2009.05.001

Sawyer, A. H., Shi, F., Kirby, J. T., and Michael, H. A. (2013). Dynamic response of surface water-groundwater exchange to currents, tides, and waves in a shallow estuary. *J. Geophys. Res. C* 118, 1749–1758. doi: 10.1002/jgrc.20154

Schlüter, M., Sauter, E. J., Andersen, C. E., Dahlgaard, H., and Dando, P. R. (2004). Spatial distribution and budget for submarine groundwater discharge in Eckernförde Bay (Western Baltic Sea). *Limnol. Oceanogr.* 49, 157–167. doi: 10.4319/lo.2004.49.1.0157

Schubert, M., Petermann, E., Stollberg, R., Gebel, M., Scholten, J., Knöller, K., et al. (2019). Improved approach for the investigation of submarine groundwater discharge by means of radon mapping and radon mass balancing. *Water* 11:749. doi: 10.3390/w11040749

Seidel, M., Beck, M., Greskowiak, J., Riedel, T., Waska, H., Suryaputra, I. G. N. A., et al. (2015). Benthic-pelagic coupling of nutrients and dissolved organic matter composition in an intertidal sandy beach. *Mar. Chem.* 176, 150–163. doi: 10.1016/j.marchem.2015.08.011

Seidel, M., Beck, M., Riedel, T., Waska, H., Suryaputra, I. G. N. A., Schnetger, B., et al. (2014). Biogeochemistry of dissolved organic matter in an anoxic intertidal creek bank. *Geochim. Cosmochim. Acta* 140, 418–434. doi: 10.1016/j.gca.2014.05.038

Shoji, J., Mitamura, H., Ichikawa, K., Kinoshita, H., and Arai, N. (2017). Increase in predation risk and trophic level induced by nocturnal visits of piscivorous fishes in a temperate seagrass bed. *Sci. Rep.* 7:3895. doi: 10.1038/s41598-017-04217-3

Shoji, J., and Tominaga, O. (2018). "Relationships between submarine groundwater discharge and coastal fisheries as a water-food nexus," in *The Water-Energy-Food Nexus*, eds A. Endo and T. Oh (Singapore: Springer), 117–131.

Sholkovitz, E. R., Herbold, C., and Charette, M. A. (2003). An automated dye-dilution based seepage meter for the time-series measurement of submarine groundwater discharge. *Limnol. Oceanogr. Methods* 1, 16–28. doi: 10.4319/lom.2003.1.16

Shuler, C. K., Amato, D. W., Veronica Gibson, V., Baker, L., Olguin, A. N., and Dulai, H. (2019). Assessment of terrigenous nutrient loading to coastal ecosystems along a human land-use gradient, Tutuila, American Samoa. *Hydrology* 6:18. doi: 10.3390/hydrology6010018

Smith, C. G., Cable, J. E., and Martin, J. B. (2008). Episodic high intensity mixing events in a subterranean estuary: effects of tropical cyclones. *Limnol. Oceanogr.* 53, 666–674. doi: 10.4319/lo.2008.53.2.0666

Spiteri, C., Slomp, C. P., Tuncay, K., and Meile, C. (2008). Modeling biogeochemical processes in subterranean estuaries: effect of flow dynamics and redox conditions on submarine groundwater discharge of nutrients. *Water Res. Res.* 44:W02430. doi: 10.1029/2008WR006997

Stewart, B., Bryan, K. R., Pilditch, C. A., and Santos, I. R. (2018). Submarine groundwater discharge estimates using radium isotopes and related nutrient inputs into Tauranga Harbour (New Zealand). *Estuar. Coasts* 41, 384–403. doi: 10.1007/s12237-017-0290-6

Stewart, B. T., Santos, I. R., Tait, D., Macklin, P. A., and Maher, D. T. (2015). Submarine groundwater discharge and associated fluxes of alkalinity and dissolved carbon into Moreton Bay (Australia) estimated via radium isotopes. *Mar. Chem.* 174, 1–12. doi: 10.1016/j.marchem.2015.03.019

Stieglitz, T. (2005). Submarine groundwater discharge into the near-shore zone of the Great Barrier Reef, Australia. *Mar. Pollut. Bull.* 51, 51–59. doi: 10.1016/j.marpolbul.2004.10.055

Stieglitz, T., Clark, J. F., and Hancock, G. J. (2013). The mangrove pump: The tidal flushing of animal burrows in a tropical mangrove forest determined from radionuclide budgets. *Geochim. Cosmochim. Acta* 102, 12–22. doi: 10.1016/j.gca.2012.10.033

Stieglitz, T., Rapaglia, J., and Bokuniewicz, H. (2008a). Estimation of submarine groundwater discharge from bulk ground electrical conductivity measurements. *J. Geophys. Res.* 113:C08007. doi: 10.1029/2007JC004499

Stieglitz, T., and Ridd, P. (2000). "Submarine groundwater discharge from paleochannels?: 'Wonky Holes' on the inner shelf of the great barrier reef, Australia," in *Hydro 2000: Interactive Hydrology; Proceedings* (Perth, WA), 189–194.

Stieglitz, T., Taniguchi, M., and Neylon, S. (2008b). Spatial variability of submarine groundwater discharge, Ubatuba, Brazil. *Estuar. Coast. Shelf Sci.* 76, 493–500. doi: 10.1016/j.ecss.2007.07.038

Stieglitz, T. C., and Dujon, A. M. (2017). A groundwater-fed coastal inlet as habitat for the Caribbean queen conch Lobatus gigas an acoustic telemetry and space use analysis. *Mar. Ecol. Prog. Ser.* 571, 139–152. doi: 10.3354/meps12123

Stieglitz, T. C., Rapaglia, J., and Krupa, S. C. (2007). An effect of pier pilings on nearshore submarine groundwater discharge from a (partially) confined aquifer. *Estuar. Coasts* 30, 543–550. doi: 10.1007/BF03036520

Street, J. H., Knee, K. L., Grossman, E. E., and Paytan, A. (2008). Submarine groundwater discharge and nutrient addition to the coastal zone and coral reefs of leeward Hawaii. *Mar. Chem.* 109, 355–376. doi: 10.1016/j.marchem.2007.08.009

Su, N., Burnett, W. C., MacIntyre, H. L., Liefer, J. D., Peterson, R. N., and Viso, R. (2014). Natural radon and radium isotopes for assessing groundwater discharge into Little Lagoon, Alabama: implications for harmful algal blooms. *Estuar. Coasts* 37, 893–910. doi: 10.1007/s12237-013-9734-9

Sugimoto, R., Kasai, A., Miyajima, T., and Fujita, K. (2010). Modeling phytoplankton production in Ise Bay, Japan: Use of nitrogen isotopes to identify dissolved inorganic nitrogen sources. *Estuar. Coast. Shelf Sci.* 86, 450–466. doi: 10.1016/j.ecss.2009.10.011

Sugimoto, R., Kitagawa, K., Nishi, S., Honda, H., Yamada, M., and Kobayashi, S. (2017). Phytoplankton primary productivity around submarine groundwater discharge in nearshore coasts. *Mar. Ecol. Prog. Ser.* 563, 25–33. doi: 10.3354/meps11980

Sugimoto, R., Sato, T., Yoshida, T., and Tominaga, O. (2014). Using stable nitrogen isotopes to evaluate the relative importance of external and internal nitrogen loadings on phytoplankton production in a shallow eutrophic lake (Lake Mikata, Japan). *Limnol. Oceanogr.* 59, 37–47. doi: 10.4319/lo.2014.59.1.0037

Suryaputra, I. G. N. A., Santos, I. R., Huettel, M., Burnett, W. C., and Dittmar, T. (2015). Non-conservative behavior of fluorescent dissolved organic matter (FDOM) within a subterranean estuary. *Continent. Shelf Res.* 110, 183–190. doi: 10.1016/j.csr.2015.10.011

Swarzenski, P. W., Burnett, W. C., Greenwood, W. J., Herut, B., Peterson, R., Dimova, N., et al. (2006). Combined time-series resistivity and geochemical tracer techniques to examine submarine groundwater discharge at Dor Beach, Israel. *Geophys. Res. Lett.* 33:L24405. doi: 10.1029/2006GL028282

Swarzenski, P. W., Dulaiova, H., Kroeger, K. D., Smith, C. G., Dimova, N., Storlazzi, C. D., et al. (2016). Observations of offshore groundwater flow: Kahekili Beach Park submarine springs, Maui, Hawaii. *J. Hydrol.* 11, 147–165. doi: 10.1016/j.ejrh.2015.12.056

Tachikawa, K., Athias, V., and Jeandel, C. (2003). Neodymium budget in the modern ocean and paleo-oceanographic implications. *J. Geophys. Res.* 108:3254. doi: 10.1029/1999JC000285

Tait, D. R., Maher, D. T., Macklin, P. A., and Santos, I. R. (2016). Mangrove pore water exchange across a latitudinal gradient. *Geophys. Res. Lett.*43, 3334–3341. doi: 10.1002/2016GL068289

Tait, D. R., Maher, D. T., Sanders, C. J., and Santos, I. R. (2017). Radium-derived porewater exchange and dissolved N and P fluxes in mangroves. *Geochim. Cosmochim. Acta* 200, 295–309. doi: 10.1016/j.gca.2016.12.024

Tamborski, J., Bejannin, S., Garcia-Orellana, J., Souhaut, M., Charbonnier, C., Anschutz, P., et al. (2018). A comparison between water circulation and terrestrially-driven dissolved silica fluxes to the Mediterranean Sea traced using radium isotopes. *Geochim. Cosmochim. Acta* 238, 496–515. doi: 10.1016/j.gca.2018.07.022

Tamborski, J. J., Cochran, J. K., and Bokuniewicz, H. J. (2017a). Application of 224Ra and 222Rn for evaluating seawater residence times in a tidal subterranean estuary. *Mar. Chem.* 189, 32–45. doi: 10.1016/j.marchem.2016.12.006

Tamborski, J. J., Cochran, J. K., and Bokuniewicz, H. J. (2017b). Submarine groundwater discharge driven nitrogen fluxes to Long Island Sound, NY: Terrestrial vs. marine sources. *Geochim. Cosmochim. Acta* 218, 40–57. doi: 10.1016/j.gca.2017.09.003

Tamborski, J. J., Rogers, A. D., Bokuniewicz, H. J., Cochran, J. K., and Young, C. R. (2015). Identification and quantification of diffuse fresh submarine groundwater discharge via airborne thermal infrared remote sensing. *Remote Sens. Environ.* 171, 202–217. doi: 10.1016/j.rse.2015.10.010

Tang, J., and Johannesson, K. H. (2005). "Rare earth element concentrations, speciation, and fractionation along groundwater flow paths: the carrizo sand (Texas) and upper floridan aquifers," in *Rare Earth Elements in Groundwater Flow Systems*, Vol. 51. Water Science and Technology Library, ed K. H. Johannesson (Dordrecht: Springer), 223–251.

Tang, J., and Johannesson, K. H. (2006). Controls on the geochemistry of rare earth elements along a groundwater flow path in the Carrizo Sand aquifer, Texas, USA. *Chem. Geol.* 225, 156–171. doi: 10.1016/j.chemgeo.2005.09.007

Taniguchi, M., Burnett, W. C., Cable, J. E., and Turner, J. V. (2002). Investigation of submarine groundwater discharge. *Hydrol. Process.* 16, 2115–2129. doi: 10.1002/hyp.1145

Taniguchi, M., and Fukuo, Y. (1993). Continuous measurements of groundwater seepage using an automatic seepage meter. *Groundwater* 31, 675–679. doi: 10.1111/j.1745-6584.1993.tb00601.x

Taniguchi, M., Ishitobi, T., and Shimada, J. (2006). Dynamics of submarine groundwater discharge and freshwater-seawater interface. *J. Geophys. Res.* 111:C01008. doi: 10.1029/2005JC002924

Taniguchi, M., and Iwakawa, H. (2004). Submarine groundwater discharge in Osaka Bay, Japan. *Limnology* 5, 25–32. doi: 10.1007/s10201-003-0112-3

Taniguchi, M., Ono, M., and Takahashi, M. (2015). Multi-scale evaluations of submarine groundwater discharge. *Proc. IAHS* 365, 66–71. doi: 10.5194/piahs-365-66-2015

Taniguchi, M., Stieglitz, T., and Ishitobi, T. (2008). Temporal variability of water quality of submarine groundwater discharge in Ubatuba, Brazil. *Estuar. Coast. Shelf Sci.* 76, 484–492. doi: 10.1016/j.ecss.2007.07.019

Trezzi, G., Garcia-Orellana, J., Rodellas, V., Santos-Echeandia, J., Tovar-Sánchez, A., Garcia-Solsona, E., et al. (2016). Submarine groundwater discharge: A significant source of dissolved trace metals to the North Western Mediterranean Sea. *Mar. Chem.* 186, 90–100. doi: 10.1016/j.marchem.2016.08.004

Troccoli-Ghinaglia, L., Herrera-Silveira, J. A., Comín, F. A., and Díaz-Ramos, J. R. (2010). Phytoplankton community variations in tropical coastal area affected where submarine groundwater occurs. *Continent. Shelf Res.* 30, 2082–2091. doi: 10.1016/j.csr.2010.10.009

Tsabaris, C., Patritis, D. L., Karageorgis, A. P., Eleftheriou, G., Papadopoulos, V. P., Georgopoulos, D., et al. (2012). *In-situ* radionuclide characterization of a submarine groundwater discharge site at Kalogria Bay, Stoupa, Greece. *J. Environ. Radioactiv.* 108, 50–59. doi: 10.1016/j.jenvrad.2011.08.005

Umezawa, Y., Miyajima, T., Yamamuro, M., Kayanne, H., and Koike, I. (2002). Fine-scale mapping of land-derived nitrogen in coral reefs by 15N in macroalgae. *Limnol. Oceanogr.* 47, 1405–1416. doi: 10.4319/lo.2002.47.5.1405

Utsunomiya, T., Hata, M., Sugimoto, R., Honda, H., Kobayashi, S., Miyata, Y., et al. (2017). Higher species richness and abundance of fish and benthic invertebrates around submarine groundwater discharge in Obama Bay, Japan. *J. Hydrol.* 11, 139–146. doi: 10.1016/j.ejrh.2015.11.012

Valiela, I., Costa, J., Foreman, K., Teal, J. M., Howes, B., and Aubrey, D. (1990). Transport of groundwater-borne nutrients from watersheds and their effects on coastal waters. *Biogeochemistry* 10, 177–197. doi: 10.1007/BF00003143

Valiela, I., and D'Elia, C. (1990). Groundwater inputs to coastal waters. *Biogeochemistry* 10, 175–335. doi: 10.1007/BF00003142

Varma, S., Turner, J., and Underschultz, J. (2010). Estimation of submarine groundwater discharge into Geographe Bay, Bunbury, Western Australia. *J. Geochem. Expl.* 106, 197–210. doi: 10.1016/j.gexplo.2010.02.003

Viso, R., McCoy, C., Gayes, P., and Quafisi, D. (2010). Geological controls on submarine groundwater discharge in Long Bay, South Carolina (USA). *Continent. Shelf Res.* 30, 335–341. doi: 10.1016/j.csr.2009.11.014

Wang, G., Wang, Z., Zhai, W., Moore, W. S., Li, Q., Yan, X., et al. (2015). Net subterranean estuarine export fluxes of dissolved inorganic C, N, P, Si, and total alkalinity into the Jiulong River estuary, China. *Geochim. Cosmochim. Acta* 149, 103–114. doi: 10.1016/j.gca.2014.11.001

Wang, X., Li, H., Zheng, C., Yang, J., Zhang, Y., and Zhang, M. (2018). Submarine groundwater discharge as an important nutrient source influencing nutrient structure in coastal water of Daya Bay, China. *Geochim. Cosmochim. Acta* 225, 52–65. doi: 10.1016/j.gca.2018.01.029

Waska, H., and Kim, G. (2010). Differences in microphytobenthos and macrofaunal abundances associated with groundwater discharge in the intertidal zone. *Mar. Ecol. Prog. Ser.* 407, 159–172. doi: 10.3354/meps08568

Waska, H., and Kim, G. (2011). Submarine groundwater discharge (SGD) as a main nutrient source for benthic and water-column primary production in a large intertidal environment of the Yellow Sea. *J. Sea Res.* 65, 103–113. doi: 10.1016/j.seares.2010.08.001

Webb, J. R., Santos, I. R., Maher, D. T., Tait, D. R., Cyronak, T., Sadat-Noori, M., et al. (2019). Groundwater as a source of dissolved organic matter to coastal waters: Insights from radon and CDOM observations in 12 shallow coastal systems. *Limnol. Oceanogr.* 64, 182–196. doi: 10.1002/lno.11028

Welti, N., Gale, D., Hayes, M., Kumar, A., Gasparon, M., Gibbes, B., et al. (2015). Intertidal diatom communities reflect patchiness in groundwater discharge. *Estuar. Coast. Shelf Sci.* 163, 116–124. doi: 10.1016/j.ecss.2015.06.006

Williams, M. O. (1946). Bahrein: port of pearls and petroleum. *Natl. Geogr. Mag.* 89, 198–210.

Willis, S. S., and Johannesson, K. H. (2011). Controls on the geochemistry of rare earth elements in sediments and groundwaters of the Aquia aquifer, Maryland, USA. *Chem. Geol.* 285, 32–49. doi: 10.1016/j.chemgeo.2011.02.020

Wilson, A., and Morris, J. (2012). The influence of tidal forcing on groundwater flow and nutrient exchange in a salt marsh-dominated estuary. *Biogeochemistry* 108, 27–38. doi: 10.1007/s10533-010-9570-y

Wilson, A. M., Evans, T. B., Moore, W. S., Schutte, C. A., and Joye, S. B. (2015). What time scales are important for monitoring tidally influenced submarine groundwater discharge? Insights from a salt marsh. *Water Resour. Res.* 51, 4198–4207. doi: 10.1002/2014WR015984

Wilson, J., and Rocha, C. (2012). Regional scale assessment of submarine groundwater discharge in Ireland combining medium resolution satellite imagery and geochemical tracing techniques. *Remote Sens. Environ.* 119, 21–34. doi: 10.1016/j.rse.2011.11.018

Xin, P., Kong, J., Li, L., and Barry, D. A. (2012). Effects of soil stratigraphy on pore-water flow in a creek-marsh system. *J. Hydrol.* 475, 175–187. doi: 10.1016/j.jhydrol.2012.09.047

Xin, P., Robinson, C., Li, L., Barry, D. A., and Bakhtyar, R. (2010). Effects of wave forcing on a subterranean estuary. *Water Resour. Res.* 46:W12505. doi: 10.1029/2010WR009632

Xin, P., Wang, S. S. J., Lu, C., Robinson, C., and Li, L. (2015). Nonlinear interactions of waves and tides in a subterranean estuary. *Geophys. Res. Lett.* 42, 2277–2284. doi: 10.1002/2015GL063643

Xin, P., Wang, S. S. J., Robinson, C., Li, L., Wang, Y.-G., and Barry, D. A. (2014). Memory of past random wave conditions in submarine groundwater discharge. *Geophys. Res. Lett.* 41, 2401–2410. doi: 10.1002/2014GL059617

Xin, P., Yuan, L. R., Li, L., and Barry, D. A. (2011). Tidally driven multiscale pore water flow in a creek-marsh system. *Water Resour. Res.* 47:W07534. doi: 10.1029/2010WR010110

Xu, B., Burnett, W. C., Dimova, N., Diao, S., Mi, T., Jiang, X., et al. (2013). Hydrodynamics in the Yellow River Estuary via radium isotopes: ecological perspectives. *Continent. Shelf Res.* 66, 19–28. doi: 10.1016/j.csr.2013.06.018

Xu, B., Xia, D., Burnett, W. C., Dimova, N. T., Wang, H., Zhang, L., et al. (2014). Natural ^{222}Rn and ^{220}Rn indicate the impact of the Water-Sediment Regulation Scheme (WSRS) on submarine groundwater discharge in the Yellow River Estuary, China. *Appl. Geochem.* 51, 79–85. doi: 10.1016/j.apgeochem.2014.09.018

Xu, Y., and Marcantonio, F. (2004). Speciation of strontium in particulates and sediments from the Mississippi River mixing zone. *Geochim. Cosmochim. Acta* 68, 2649–2657. doi: 10.1016/j.gca.2003.12.016

Yamane, K., Murase, I., Shirafuji, N., Hayashi, A., Nagakura, Y., and Watanabe, Y. (2019). Nursery habitat use for larval and juvenile Pacific herring Clupea pallasii in Miyako Bay on the Pacific coast of northern Japan. *Fish. Sci.* 85, 407–416. doi: 10.1007/s12562-019-01301-7

York, J. K., Tomasky, G., Valiela, I., and Repeta, D. J. (2007). Stable isotopic detection of ammonium and nitrate assimilation by phytoplankton in the Waquoit Bay estuarine system. *Limnol. Oceanogr.* 52, 144–155. doi: 10.4319/lo.2007.52.1.0144

Yu, X., Xin, P., Lu, C., Robinson, C., Li, L., and Barry, D. A. (2017). Effects of episodic rainfall on a subterranean estuary. *Water Resour. Res.* 53, 5774–5787. doi: 10.1002/2017WR020809

Zektser, I. S., and Everett, L. G. (2000). *Groundwater and the Environment: Applications for the Global Community*. Boca Raton, FL: Lewis Publishers. doi: 10.1201/9781420032895

Zhang, Y., Li, L., Erler, D. V., Santos, I., and Lockington, D. (2016). Effects of alongshore morphology on groundwater flow and solute transport in a nearshore aquifer. *Water Resour. Res.* 52, 990–1008. doi: 10.1002/2015WR017420

Zhou, Y., Sawyer, A. H., David, C. H., and Famiglietti, J. S. (2019). Fresh submarine groundwater discharge to the near-global coast. *Geophys. Res. Lett.* 46, 5855–5863. doi: 10.1029/2019GL082749

Zipperle, A., and Reise, K. (2005). Freshwater springs on intertidal sand flats cause a switch in dominance among polychaete worms. *J. Sea Res.* 54, 143–150. doi: 10.1016/j.seares.2005.01.003

Conflict of Interest: The authors declare that the research was conducted in the absence of any commercial or financial relationships that could be construed as a potential conflict of interest.

frontiers in Environmental Science

ORIGINAL RESEARCH
published: 17 October 2019
doi: 10.3389/fenvs.2019.00162

Submarine Groundwater Discharge and Stream Baseflow Sustain Pesticide and Nutrient Fluxes in Faga'alu Bay, American Samoa

Eric M. Welch[1], *Henrietta Dulai*[1,2]*, *Aly El-Kadi*[1,2] *and Christopher K. Shuler*[1,2]

[1] Department of Earth Sciences, School of Ocean Earth Science and Technology, University of Hawaiĭ Mānoa, Honolulu, HI, United States, [2] Water Resources Research Center, University of Hawai'i Mānoa, Honolulu, HI, United States

It is increasingly recognized that groundwater discharge in the form of stream baseflow and submarine groundwater discharge (SGD) plays an important role in contaminant transport. This study seeks to demonstrate the importance of groundwater flow for the distribution and transport of selected pesticides and nutrients in the Faga'alu aquifer on the island of Tutuila in American Samoa. Field measurements, including seepage runs and analysis of stream and groundwater for pesticides and nutrients, were combined with hydrological modeling. Selected analytes were glyphosate (GLY), dichlorodiphenyl-trichloroethane (DDT), imidacloprid, and azoxystrobin for pesticides and chemical species of nitrogen, phosphate, and silicate for nutrients. Hydrological flow and transport models of the aquifer were built to simulate groundwater flow and to provide estimates of GLY and dissolved inorganic nitrogen (DIN) fluxes. Stream baseflow was responsible for 59% and SGD for 41% of groundwater flow to the bay, which totaled 6,550 ± 980 m^3/d in the dry season when surface runoff was negligible. DDT was found in 85% and GLY in 100% of tested samples. SGD and baseflow thus delivered 9 ± 2 g/d of DDT, 0.9 ± 0.2 g/d of GLY, 570 ± 100 g/d of DIN and 840 ± 110 g/d of dissolved inorganic phosphorus (DIP) into Faga'alu Bay. While all pesticide levels are below environmental limits, their presence in baseflow and SGD, which discharge continuously year-round, result in sustained fluxes of GLY and DDT to the reef. The presence of DDT in groundwater decades after its last application confirms its long-term environmental persistence.

Keywords: submarine groundwater discharge, stream baseflow, pesticides, nutrients, water quality, hydrological model, groundwater hydrology

OPEN ACCESS

Edited by:
Alberto Tiraferri, Politecnico di Torino, Italy

Reviewed by:
Jordi Garcia-Orellana, Autonomous University of Barcelona, Spain
Henry Bokuniewicz, The State University of New York (SUNY), United States

***Correspondence:**
Henrietta Dulai
hdulaiov@hawaii.edu

Specialty section:
This article was submitted to Water and Wastewater Management, a section of the journal Frontiers in Environmental Science

Received: *29 June 2019*
Accepted: *30 September 2019*
Published: *17 October 2019*

Citation:
Welch EM, Dulai H, El-Kadi A and Shuler CK (2019) Submarine Groundwater Discharge and Stream Baseflow Sustain Pesticide and Nutrient Fluxes in Faga'alu Bay, American Samoa. Front. Environ. Sci. 7:162. doi: 10.3389/fenvs.2019.00162

INTRODUCTION

There is mounting evidence that populated Pacific islands struggle with water quality problems that affect human as well as ecosystem health (Mosley and Aalbersberg, 2003; Bolabola, 2007; Erler et al., 2018). Typically, population density is highest along coastlines, where centralized sanitary systems serve only a small fraction of the population and decentralized agriculture leaves room for unregulated practices, resulting in nutrient, pathogen, and pesticide pollution. While issues related to rising human population have been recognized for decades, such as water pollution

and ecosystem health decline, the contributions from individual pollution sources and pathways of contaminants are diverse and still, at best, under investigation (Mosley and Aalbersberg, 2003; Craig et al., 2005). For example, in the U.S. territory of American Samoa, anthropogenic contaminants from point, and non-point sources such as onsite sewage disposal systems (OSDS), piggeries, and agriculture, have been a widespread problem (Vaouli et al., 2010). As 90% of the municipal water on the densely populated island is sourced from groundwater, the concern over polluted drinking water resources has become a serious issue (Shuler et al., 2017). Additional concern is that pollution from groundwater propagates to streams and coastline as well (Shuler et al., 2019). Groundwater discharge to streams and the coastal ocean is often hard to quantify and is the subject of this study, which focuses on the Faga'alu watershed on the island of Tutuila, American Samoa (**Figure 1A**). The benthic ecosystem in Faga'alu Bay is classified as one of the most impacted on the island (Houk et al., 2005; Tuitele et al., 2014) and it has been labeled a priority remediation watershed by the U.S. Coral Reef Task Force (Messina and Biggs, 2016).

Coral reefs support large biodiversity (Nyström et al., 2000), however, anthropogenic pollution from terrestrial sources makes reefs less resilient and more susceptible to diseases (Bruno et al., 2003). Although surface runoff collects and distributes large amounts of dissolved and suspended particulate contaminants to the coastal region (Polidoro et al., 2017), the contributions of submarine groundwater discharge (SGD) to the coastal contaminant budget is becoming more widely accepted as important, if not dominant (Johannes and Hearn, 1985; Dulai et al., 2016). Submarine groundwater discharge refers to the flow of groundwater across the land-ocean interface, which can carry dissolved compounds and often serves as an important pathway of contaminants from coastal aquifers into the ocean (Rodellas et al., 2015). SGD results from underflow, which collects solutes from the surrounding aquifer material and overlaying land-use as it moves downstream, eventually discharging at the coast when it crosses the land-ocean boundary. Studies in similar coastal volcanic geological settings (e.g., Korea, Japan, New Zealand) have found SGD to play a major role in overall water and contaminant budget (Kim et al., 2003; Hosono et al., 2012; Stewart et al., 2018). Stream baseflow, another process addressed in this study, results from underflow entering a stream where groundwater level and streambed conductivity are higher (Larkin, 1988). Stream baseflow is a connection between surface and groundwater systems and has been shown to affect stream water quality (Miller et al., 2016) and in case of small island watersheds, also coastal water quality.

Nutrient fluxes have been the focus of many SGD studies because they are widely known to leach into the water table and to be carried by groundwater flow to the coastline (Richardson et al., 2015; Amato et al., 2016; Shuler et al., 2019). Pesticides also commonly leach into and may be dispersed in aquifers (i.e., Schuette, 1998), although their mobility is species dependent and is usually lower than those of nutrients (Davidson, 1995). Chemical and physical properties such as solubility, adsorption, degradation, and volatilization determine the potential of pesticides to contaminate groundwater (Chin and Weber, 1988; Davidson, 1995). Many studies have described pesticide movement in groundwater (e.g., Zhang et al., 2009; Rendón-von Osten and Dzul-Caamal, 2017), including the presence of the ubiquitous herbicide glyphosate (Magga et al., 2008) but few have documented their transport across the land-ocean interface to the coastal ocean through SGD (Gallagher et al., 1996; Almasri, 2008).

Glyphosate has become the most heavily used herbicide in the world since its introduction as a key ingredient in the popular Roundup formula in 1974 (Benbrook, 2016). Its heavy use in both agricultural plots and roadside-to-backyard domestic settings and its mobility makes it an ideal tracer to demonstrate the chemical connection between land applications and receiving water bodies. This study thus used glyphosate as a tracer to demonstrate the role of groundwater in the transport of pesticides to streams and the coastal ocean. Other pesticides surveyed in this study include the insecticide dichlorodiphenyl-trichloroethane (DDT) along with its breakdown product dichlorodiphenyl-dichloroethylene (DDE) (from here on both collectively referred to as "DDT"), the insecticide imidacloprid, and the fungicide azoxystrobin. Application of DDT has not been legal in American Samoa since 1972, after the U.S. EPA officially banned the compound due to its adverse effects on wildlife and potential threat to human health (Lallanilla, 2019). The insecticide, however, was sprayed heavily across the island in the mid-twentieth century and is still persistent thanks to its long residence time in the environment (Travis et al., 1946; NPIC Oregon State University, 1999). Also quantified in this study were nutrient fluxes, in order to provide comparison to other island studies (e.g., Glenn et al., 2013; Shuler et al., 2019).

Field observations of contaminant concentrations and previously published land-use data were integrated with hydrological modeling to characterize groundwater fluxes and associated selected pesticide and nutrient fluxes in the Faga'alu aquifer on the island of Tutuila, in American Samoa. The modular 3-dimensional MODFLOW model (Harbaugh et al., 2000) was utilized to estimate fresh SGD and baseflow contribution while the multi-species transport model MT3DMS (Zheng and Wang, 1999) was used to model contaminant transport. The goal of the model simulation was to quantify relative contributions of the multiple glyphosate and dissolved inorganic nitrogen (DIN) sources to SGD and baseflow fluxes, including OSDS and piggeries as well as urban and agricultural non-point pollution sources. Groundwater contribution to the overall water and contaminant budget of the watershed via stream baseflow and SGD was assessed, and hypothetical scenarios focusing on changes in land-use and contaminant inputs were run to assess potential remediation actions to help develop better pollution management practices.

STUDY AREA

American Samoa

The largest island in American Samoa, Tutuila (14.3258° S, 170.7325° W) lies within the South Pacific Convergence Zone (SPCZ). Rainfall varies geographically across the island, ranging from 3,000 to 6,000 mm/year (Craig, 2002). Wet season is

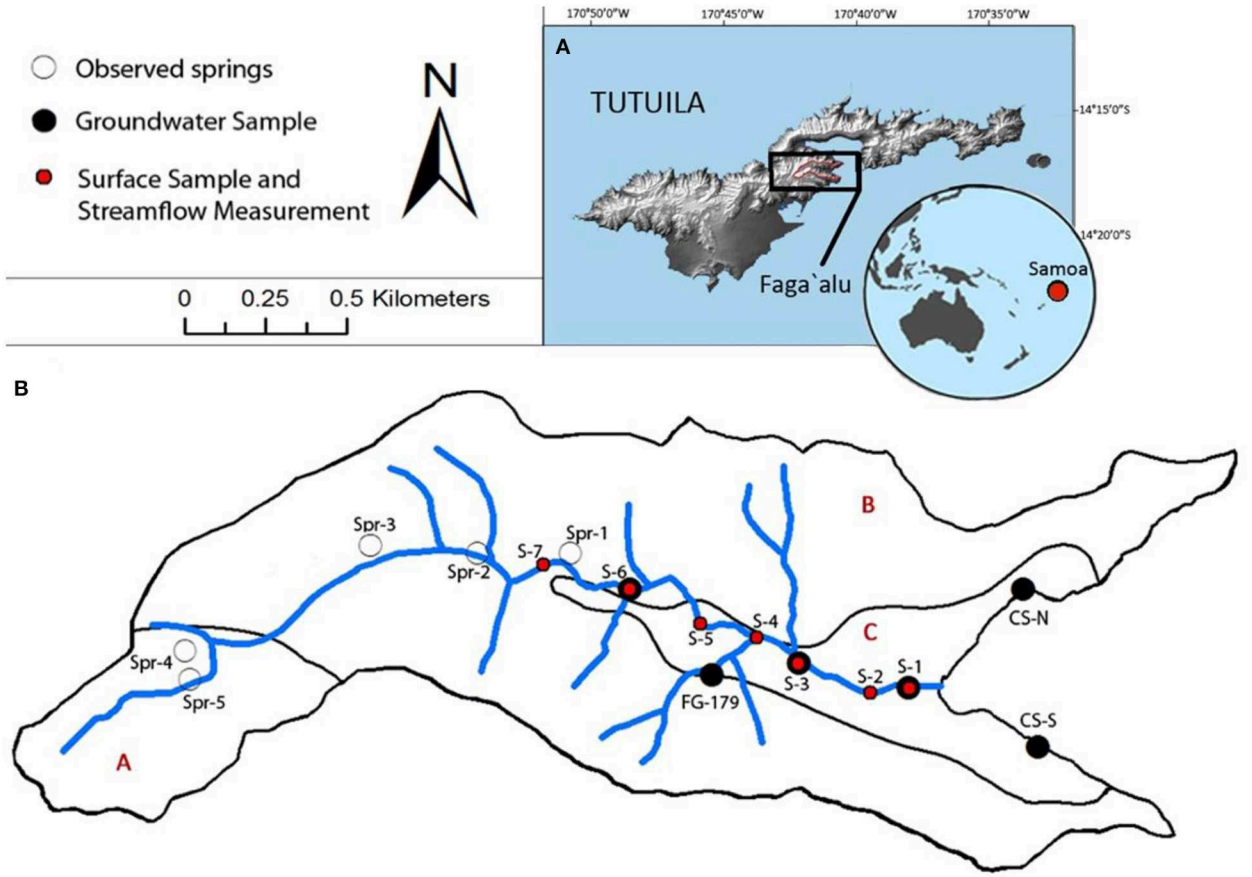

FIGURE 1 | (A) The Faga'alu watershed is located in the central-south sector of Tutuila, American Samoa. **(B)** Sampling locations are depicted in the detailed map of the watershed, which is divided into primary geologic units: **(A)** Pago Volcanic Series, intra-caldera, trachyte plugs, and dikes, **(B)** Pago Volcanic Series, intra-caldera, **(C)** Beach sand and silty/clay alluvium (Stearns, 1944). Indicated are sampling sites of groundwater (black circles: well FG-179, shallow stream bank and coastal springs sampled using push point samplers 0.8 m below ground surface), stream water (red circles, also locations of seepage runs and ^{222}Rn measurements), and mountain springs used as observation points for groundwater head level calibration (hollow circles).

between October and May, and the dry season is from June to September (Craig et al., 2005). Tutuila's mountainous terrain is a result of eroded shield volcanoes (Stearns, 1944). Alluvial valleys have been carved over time from erosion and are spaced along the island coastline (Stearns, 1944; Izuka et al., 2007). The 2 km^2 Faga'alu watershed contains the Faga'alu Stream (3 km), with headwaters on the slopes of Matafao Mountain running down an alluvial valley, and emptying into the Faga'alu Bay of the outer Pago Harbor (Messina and Biggs, 2016). The undisturbed upper watershed is steeply sloped and forested, while the Faga'alu village lies on the lower alluvial plain. The valley slopes are comprised of dense basaltic rocks, which also underlie the alluvial deposits of silty and sandy clay loams of >50 m thickness on the lower plain where human development is highest (Messina and Biggs, 2016). One groundwater well, managed by the American Samoa Power Authority (ASPA) is used as a municipal water source, and is located halfway up the developed area, near the boundary where the alluvium intersects the basalt (**Figure 1B**). Alluvium thickness at the well is ∼25 m (ASPA drilling logs, personal communication). No documented descriptions of the aquifer's hydrogeologic properties in Faga'alu exist. Although small perched bodies of groundwater have been documented in American Samoa (i.e., at Ototole and Olosega; Davis, 1963), none have yet been confirmed in Faga'alu.

Agriculture, both conventional and agroforestry, is widespread in American Samoa, and represents one of the major nutrient and pesticide sources (Misa and Vargo, 1993). Pigs are the most prevalent form of livestock raised on Tutuila, and are a source of organic matter, pathogens, and excess nitrogen (Zennaro, 2007). Cesspools are the prime method of human wastewater management, used in over 5,500 homes on the island, and contribute a significant amount of excess nitrogen into the water table (NOAA/EPA, 2003; Shuler et al., 2017). A fringing coral reef exists at the shoreline and extends 50–400 m offshore in Faga'alu Bay. Water quality of the bay is currently of major concern due to turbid, nutrient-enriched waters (Messina and Biggs, 2016; McCormick, 2017; Vargas-Angel and Schumacher, 2018; Shuler et al., 2019).

METHODS

Sample Collection and Analysis

Groundwater samples were collected at six sites (three from stream bank sediments, two from coastal springs, and one from the only existing public well in the watershed, **Figure 1B**) in August 2016 during the dry season. Surface samples were taken at seven sites in the stream. Water from the well (screened from 20 to 32 m depth) was collected from a wellhead collection port while stream bank groundwater and spring sites were sampled using push-point samplers (MHE Products) and a peristaltic pump from 0.4–0.6 m depth below ground surface. All samples were filtered on-site with a 0.45 μm hydrophilic polyethersulfone capsule filter. Nutrients were collected in acid-washed high density polyethylene (HDPE) bottles. Pesticides were collected in combusted glass amber vials to prevent photodegradation. Once collected, all samples were chilled and then refrigerated for short-term storage. Water for radon analysis was collected in 250 mL glass bottles with no headspace. A YSI multiparameter sonde (6600 V2-2 model) was used to measure temperature, salinity, and dissolved oxygen *in situ* in each sample.

A seepage run, where streamflow was measured at seven stations along the main channel, was performed under baseflow conditions on the same day and locations as sample collection (**Figure 1B**). The SonTek FlowTracker Handheld Acoustic Doppler Velocimeter was used to measure streamflow. Samples were analyzed for radon (^{222}Rn) at each surface and groundwater site to identify groundwater contribution and hyporheic exchange, thus identifying gaining and losing sections of the stream (Burnett and Dulaiova, 2003; Dulaiova et al., 2006). Radon samples were analyzed the day of collection (**Supplementary Table 1**) using a Rad-H_2O instrument (Durridge).

Water samples were analyzed for their nutrient concentrations of total dissolved nitrogen (TDN), phosphate (PO_4^{3-}), nitrate and nitrite (N+N), ammonium ($NH_4^+ + NH_3$ from here on referred to as NH_4^+), and silicate ($Si(OH)_4$) at the University of Hawai'i SOEST Laboratory for Analytical Biogeochemistry. Dissolved inorganic nitrogen (DIN) concentrations were calculated as the sum of the measured N+N and NH_4^+ values. Pesticide analysis included GLY, DDT, imidacloprid, and azoxystrobin. An enzyme linked immunosorbent assay (ELISA) (Abraxis LLC) analysis was performed for the four chosen pesticides. The colored wells were analyzed in a spectrophotometric microplate reader (Abraxis, Model 4303) at a wavelength of 450 nm to obtain concentration values. The minimum detection limits for GLY, DDT, imidacloprid, and azoxystrobin were 50, 370, 6, and 9 ng/L, respectively (www.abraxiskits.com). Relative uncertainty of GLY concentrations based on field and method duplicates derived via the ELISA test was 10–22%. Relative uncertainty of DDT was 10–16%. Nutrient uncertainties, expressed as absolute errors were 17 μg/L for TDN, 0.3 μg/L for PO_4^{3-}, 8 μg/L N+N, 2 μg/L NH_4^+, 56 μg/L $Si(OH)_4$. Radon relative uncertainties derived from counting statistics were 10–30% at 1-sigma.

Modeling Approaches

Water flow and contaminant transport were modeled using the MODFLOW (Harbaugh et al., 2000) and MT3DMS (Zheng and Wang, 1999) models, respectively. The MODFLOW model was used to predict groundwater levels and water fluxes necessary for transport modeling via MT3DMS. The Groundwater Modeling System (GMS) software (https://www.aquaveo.com) served as a graphical interface in building the conceptual models. MODFLOW was calibrated using (1) stream baseflow from seepage runs taken during sample collection and (2) water table head levels obtained from the well and elevations of groundwater springs documented during this study. The elevations of the observed mountain springs were utilized as water levels where the groundwater spring represents an intersection of the top of the water table and the land's surface. This relies on the assumption that the observed spring is fed by a saturated zone that is hydraulically connected to the aquifer. Field-based groundwater levels and baseflow fluxes were utilized through both iterative and automatic approaches in calibrating MODFLOW. The iterative approach was used initially to constrain hydraulic conductivity, while the automatic approach via the PEST code (Doherty and Hunt, 2010) was used to refine the conductivity estimates. MT3DMS was used to model contaminant transport in the aquifer through convection, dispersion, adsorption and decay. MT3DMS was calibrated through an iterative approach to match observed against modeled GLY and DIN concentrations. A flow chart relating the models and their respective inputs and outputs can be found in **Supplementary Figure 1**.

Groundwater Flow Model

The MODFLOW-2000 (McDonald and Harbaugh, 1988) numerical model comprised of 4221 active cells (38 × 30 m) across two vertical layers. The top layer covered the zone between mean sea level (MSL) and the terrain elevation, while the lower layer covered MSL to 500 m below MSL. Recharge was based on estimates from the Soil and Water Assessment Tool (SWAT) model created by Leta et al. (2017), with daily recharge ranging from 1.8 to 3.5 mm/d across the watershed. Other data were sourced from available geographical information system data that included stream, well, geologic units, and domain boundary data. A pumping rate of 163.53 m^3/d was assigned to the well based on data provided by American Samoa Power Authority (ASPA).

The six observation points for head level were supplemented by stream baseflow discharge rates, which were obtained from the seepage run measurements. The zonal parameter estimation method via PEST software (Kennedy, 2012; MODFLOW-PEST Pilot Points, 2016) was incorporated in the calibration process to obtain the best fit between measurements and model values. Conductivity-calibration zones were set based on known geological units (**Figure 1B**). The model was considered adequately calibrated when residuals for head and discharge were minimized to within 10% of maximum observed values.

Pesticide and Nutrient Fluxes in Baseflow and SGD

To separately estimate baseflow from high level and coastal aquifer portions of the watershed in the model, MODFLOW stream arcs were divided into upper and lower reaches (boundary set at S-5, **Figure 1B**). To obtain the respective mass

TABLE 1 | Groundwater nutrient and pesticide concentrations.

Sample site	Type	Glyphosate (ng/L)	DDT/DDE (ng/L)	TDN (μg/L)	PO_4 (μg/L)	$Si(OH)_4$ (μg/L)	N+N (μg/L)	NH_4^+ (μg/L)	DIN (μg/L)
S-1	Stream bank	90	1,220	70	160	16,620	20	65	90
S-3	Stream bank	80	1,310	90	180	15,630	50	15	70
S-6	Stream bank	180	<	110	100	16,390	70	2	70
FG-179	Well	160	880	170	260	20,200	90	20	110
CS-N	Coastal spring	160	2,070	340	110	6,910	250	7	260
CS-S	Coastal spring	300	1,510	140	50	1,940	90	6	100

< indicates below detection limits.

flux rate, pesticide and nutrient concentrations from stream bank groundwater samples were multiplied by the modeled groundwater flow estimates for each segment.

SGD fluxes at the land-ocean interface were determined by summing up flow through coastal grid cells in three sections of the model: (1) the northern coastline, (2) the central coastline, and (3) the southern coastline. The central coastal segment representing the region from the stream mouth to S-1, was excluded from SGD and was included in stream baseflow instead. Pesticide and nutrient concentrations at the northern and southern coastal springs were used to represent their respective segment of the coast, while S-1 was used for the central coastal segment. To estimate the flux rates, the respective contaminant concentrations were multiplied by the estimated SGD flow for the corresponding coastal segment.

Contaminant Transport Model

An MT3DMS transport model was developed to simulate the advective and dispersive transport and transformation of contaminants through the aquifer. In addition to hydrologic data carried over from the hydrogeologic model, new parameters were incorporated in the transport model, including porosity, longitudinal dispersivity, dispersivity-anisotropy ratios, and DIN and GLY attenuation and decay coefficients. A sensitivity analysis test was run to determine which parameters most affected the calibration (**Supplementary Figure 2**) and adjustments were made to find the optimal match between the modeled and observed values (**Supplementary Table 2**). The simulation-time was about 55 years to obtain a steady-state condition for each contaminant.

Glyphosate served as the representative pesticide to trace movement through the aquifer. GLY concentrations were added in the model based on annual applied concentrations by agricultural activities derived from literature values (**Supplementary Table 3**), which were added as recharge concentrations. GLY, however, is not only used for agriculture, but also for smaller-scale applications along roadsides and in residential yards for weed control (Tang et al., 2015). As an approximation, and due to the lack of information, half the concentration applied to agricultural plots in the model was assumed to pertain to the domestic zones. A literature-based sorption coefficient (1.64×10^{-5} m^3/mg) as well as decay rate constant (based on half-lives ranging from 91 to 197 days) were used in the model to represent natural degradation of GLY (Schuette, 1998; Henderson et al., 2010).

DIN loading rates were estimated for each endmember using attenuation rates specific to each source (**Supplementary Table 3**). Mass loading rates were applied to the point sources of cesspools and piggeries, while annual application concentrations were applied to non-point source agricultural N-inputs. A fixed level of N was additionally added into all non-agricultural domains to represent natural background levels of DIN (Shuler et al., 2017). Fluxes of DIN and GLY for ocean and stream segments of interest were then determined by the calibrated transport model.

Contaminant Source Contributions

The calibrated MT3DMS model was used to run several hypothetical land-use scenarios for DIN and GLY source contributions throughout the watershed. Each source of DIN was individually assessed for its relative contributions to the total N flux via baseflow and SGD. A scenario was then run when cesspools were improved (i.e., converted to septic systems) by doubling their DIN attenuation efficiency, which was simulated by halving the DIN concentration that entered the aquifer from each OSDS unit (**Supplementary Table 3**). To determine how the rates of agricultural or domestic GLY affect concentration at each observation point, scenarios were run to simulate each source individually. Two additional scenarios were run where the application amount of GLY was halved in the developed zones and then in all the application zones to simulate improved practices if half of the currently used herbicide was applied. These scenarios may give insight to what could be accomplished in the future to improve water quality of the stream and coastline.

RESULTS

Water Quality Results

Overall, 100% of Faga'alu samples had detectable levels of GLY and 85% had DDT. Groundwater GLY concentrations ranged between 80 and 300 ng/L and averaged 160 ± 80 ng/L. Stream bank groundwater samples had relatively higher value furthest upstream at S-6 (180 ng/L), and lower values at S-3 (80 ng/L) and S-1 (90 ng/L). The well (FG-179) had a concentration of 160 ng/L and the northern and southern coastal springs were 160 and 300 ng/L, respectively (**Table 1, Figure 2A**). Glyphosate in surface samples at the seven stream sites ranged between 60

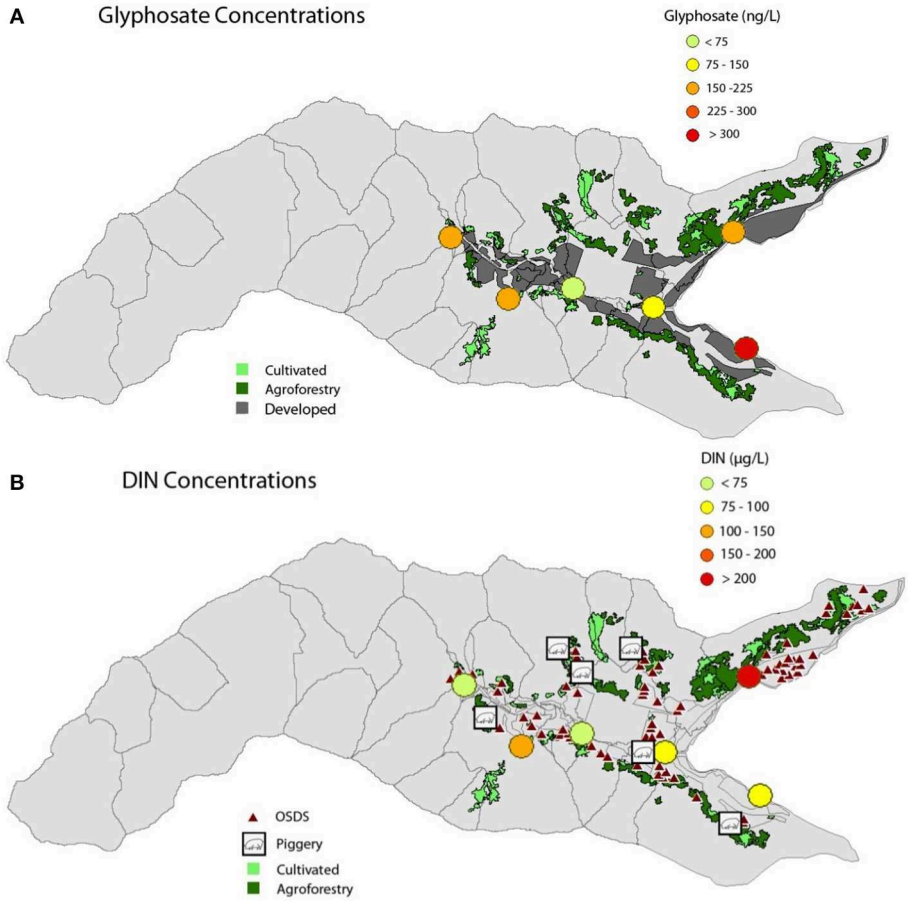

FIGURE 2 | (A) GLY and **(B)** DIN concentrations at the six groundwater sampling sites in Faga'alu, shown with related point source and land-use contributors—cultivated (light green polygons), agroforestry (dark green polygons), OSDS units (triangles), piggeries (square icons), and unpaved developed/residential land (dark gray).

and 230 ng/L with an average of 140 ± 70 ng/L (**Table 2**). Higher concentrations were found in the upper four sites (S-4 to S-7), averaging 180 ± 40 ng/L, the lower three stream samples (S-1 to S-3) averaged 80 ± 20 ng/L. When comparing the concentrations at sites which had both surface and groundwater samples (S-1, S-3, S-6), GLY was comparable in surface water to groundwater (S-1 80 vs. 90 ng/L, S-3 90 vs. 80 ng/L, S-6 200 vs. 180 ng/L).

DDT was ubiquitously present in groundwater samples, ranging from below detection limit to 2,070 ng/L with an average of 1,400 ± 690 ng/L. In surface waters, DDT ranged from below detection limit at S-5 to 2,030 ng/L at S-7 with an average of 1,240 ± 720 ng/L (**Tables 1**, **2**). The other two tested pesticides, imidacloprid and azoxystrobin, were not detected in any of the Faga'alu samples, and will not be discussed further.

DIN in Faga'alu groundwater ranged between 60 and 250 µg/L and averaged 110 ± 70 µg/L, with generally higher concentrations toward the coastal areas (**Figure 2B**). Stream bank groundwater samples had lower DIN than the coastal springs and the well (**Table 1**). DIN in stream surface waters were comparable to groundwater concentrations across the watershed, with a range from 60 to 140 µg/L and an average of 80 ± 30 µg/L. Ammonium did show notable differences, as it averaged 4 ± 2 µg/L in surface water compared to 19 ± 23 µg/L in groundwater samples with a maximum of 130 µg/L at S-1. This is expected because of limited oxygen present in streambank groundwater as opposed to the oxygenated stream.

Phosphate concentrations ranged from 50 to 260 µg/L in groundwater samples with an average of 140 ± 70 µg/L, and ranged from 80 to 120 µg/L with an average of 110 ± 10 µg/L in the surface water samples. Silica showed a relatively even distribution across stream bank groundwater and stream surface samples, averaging 16,210 ± 6,970 µg/L and 16,480 ± 300 µg/L, respectively, but showed much more diluted values at the northern and southern coastal springs (6,910 and 1,940 µg/L, respectively). The well had $Si(OH)_4$ concentrations of 20,200 µg/L.

Groundwater Flow Model Results

The final calibrated MODFLOW model had a root mean squared residual (RMSR) of 12 m for head and a RMSR of 256 m^3/d for discharge. The model was considered satisfactorily calibrated

TABLE 2 | Stream discharge measurements and surface sample nutrient and pesticide concentrations.

Sample site	Type	Discharge (m^3/d)	Glyphosate (ng/L)	DDT/DDE (ng/L)	TDN (μg/L)	PO_4 (μg/L)	$Si(OH)_4$ (μg/L)	N+N (μg/L)	NH_4^+ (μg/L)	DIN (μg/L)
S-1	Stream	3,630	80	840	180	110	16,890	130	8	140
S-2	Stream	2,900	60	1,850	130	120	16,770	70	2	70
S-3	Stream	2,290	90	1,380	120	120	16,730	60	3	60
S-4	Stream	2,370	140	840	120	110	16,000	70	4	70
S-5	Stream	1,970	230	<	130	110	16,260	90	3	90
S-6	Stream	2,530	200	1,720	120	100	16,390	80	2	80
S-7	Stream	2,390	170	2,030	120	80	16,300	80	3	80

< indicates below detection limits.

TABLE 3 | Observed and modeled groundwater head levels of the calibrated MODFLOW model with relative error.

Observation point	Observed head level (m)	Modeled head level (m)	Relative error (%)
Well FG-179	3	6	+156
Spring-1	42	69	+63
Spring-2	109	112	+3
Spring-3	160	162	+1
Spring-4	253	255	+1
Spring-5	250	264	+5
Root mean squared residual		12 m	

TABLE 4 | Observed streamflow under baseflow conditions assuming no additional surface runoff contribution, in comparison to modeled baseflow results.

Sample site	Observed discharge (m^3/d)	Modeled discharge (m^3/d)	Relative error (%)
S-7	2,390	2,100	−12
S-6	2,530	2,370	−7
S-5	1,970	2,440	24
S-4	2,370	2,460	4
S-3	2,290	2,490	9
S-2	2,890	2,500	−14
S-1	3,630	3,240	11
Root mean squared residual		260 m^3/d	

Flow from tributaries was not quantified and was neglected. Uncertainty on observed discharge is 12.5% derived from flow measurement (7.5%, Huhta and Sloat, 2007) and estimate of stream cross section (10%).

when the RMSR (head+flow) was 2.31 and the coefficients of determination (r^2) were 0.99 for head and 0.82 for flow (**Tables 3**, **4**).

The modeled freshwater SGD from the coastline of the entire bay was 2,680 ± 290 m^3/d, while the modeled stream baseflow was 3,870 ± 430 m^3/d. Both estimates have 11% uncertainty assigned based on the relative error derived for baseflow (**Table 4**). The high-level aquifer baseflow in the upper reach of the stream contributed 63% of the stream's flow, while the lower reach contributed 37%, which reflects gaining stretches both upstream and near the coast. The field-based seepage run and radon concentration trends verified this pattern of gaining stretches of the stream (**Supplementary Figure 3**). Radon concentrations in stream bank groundwater were higher where baseflow was present, suggesting radon rich groundwater upwelling as opposed to intrusion of low-radon hyporheic flow. Accordingly, stream radon levels were also highest at sections predicted to be gaining reaches. While these observations are only qualitative, they confirm the model predicted patterns of surface water groundwater exchange. According to the model, most of the watershed's SGD came from the central coastline of the bay (69%), while the northern and southern coastlines contributed 18 and 13%, respectively (**Figure 3**). The modeled combined flow of groundwater to Faga'alu Bay under baseflow conditions, delivered by the combination of stream baseflow and freshwater SGD was thus 6,550 ± 980 m^3/d (**Table 5**).

Contaminant Transport Model Results

The results of MT3DMS model are shown in **Supplementary Table 4**, where calibration was performed using GLY and DIN as tracers for agricultural, domestic and mass loading pathways within the watershed. For DIN, most sites were underestimated in the model in comparison to the measured values (1–91% relative error). The MT3DMS model was considered acceptable when the mean absolute error (MAE) of the total modeled vs. observed DIN values fell within 15% of the maximum observed DIN concentration (250 μg/L) and obtained an r^2 of 0.66. Modeled glyphosate levels had an MAE of 125 ng/L, producing a low r^2 value (0.024). The model produced estimates that were within an order of magnitude of the observed concentrations but did not capture GLY in the upper watershed (S-6) and therefore was only used as a screening tool to make qualitative assessments of GLY distribution and to compare various land-use scenarios. Fluxes of GLY and DIN determined using the MT3DMS model are listed in **Supplementary Table 5** along with those estimated using the MODFLOW derived water fluxes multiplied by field observations.

Land-Use Contaminant Source Scenarios

From all the considered N-sources piggeries contributed 6% of the total DIN, agriculture contributed a very small fraction (<1%), and OSDS units added the largest fraction, 90% of DIN concentrations recorded at the observation points. Natural N which was added into each polygon resulted in a 4%

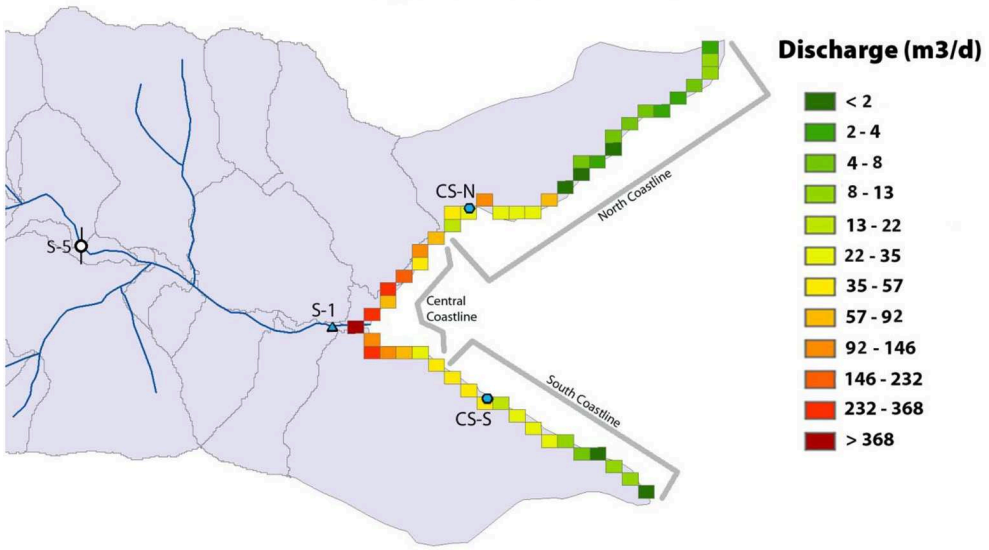

FIGURE 3 | MODFLOW model derived SGD fluxes show larger groundwater discharge to the central portion of the bay, with diminishing fluxes outward toward the northern and southern ends of the bay. Grid cells belonging to the northern, central, and southern sectors of the coastline as well as coastal springs (CS-N, S-1, and CS-S) are shown.

contribution to the total concentration at our observation sites (**Supplementary Table 6**). The scenario where OSDS N-attenuation efficiency was doubled, resulted in 46% less DIN at the observation points, significantly reducing the amount of this anthropogenic pollutant discharging into the stream and the coastal ocean.

Agricultural inputs represented 28.5% and domestic GLY application contributed 71.5% of the total GLY observed at the sampling points, despite half as much GLY assumed to be applied for domestic uses. This is partially a result of the proximity of domestic applications to the stream but also an artifact of the model not capturing GLY groundwater concentrations at the gaining section of the stream at station S-6. In absence of available information, this study did not include any major agricultural or domestic GLY sources in the upper watershed despite elevated GLY being recorded consistently in groundwater and the stream. As domestic GLY applications delivered high concentrations at the stream and coastal observation points, a scenario was run where it was assumed that people used half of the glyphosate in the domestic zones. The concentrations at the observation points dropped by 37% in this scenario. When GLY application rates were cut by half in agricultural zones, the total concentrations entering our observation sites dropped an additional 13%, to total a 50% decrease.

DISCUSSION

Contaminant Concentrations and Fluxes

Pesticides

Gaining sections of the stream were identified via multiple methods (seepage run, radon, hydrological model), where all methods were in good agreement that there was baseflow contribution from the high level as well as basal aquifers. GLY was observed in all groundwater samples and an important factor that seemed to drive stream GLY concentrations was the presence of baseflow in gaining reaches. Station S-6 marks the upper boundary of the village and there is a small plot of agriculture adjacent to it, with a quarry just upstream. Seepage runs and elevated stream and groundwater Rn showed the stream to be gaining water from the underlying aquifer in this region. Groundwater at S-6 was higher in GLY than any other stream bank station. Surface stations S-5, 6, 7 were also all higher in GLY than any other sections of the stream. In contrast, S-3, located downstream of the upper watershed in the losing reach of the stream had the lowest concentration of all sites (80 and 90 ng/L GLY in ground- and surface water, respectively).

The well and northern coastal spring (both 160 ng/L) are each downslope of agricultural plots, possibly contributing to their glyphosate load. The southern coastal spring probably integrates inputs from multiple sources, including agriculture as well as domestic uses and had the highest recorded concentrations (300 ng/L). Observed concentrations and transport model results suggest that because of their proximity to the stream, applications on domestic properties have the potential to deliver GLY to the stream sites in addition to the larger but more distant agricultural inputs. This can be attributed to GLY breakdown within the aquifer and its sorption to soil and so nearby applications to be more influential. For example, S-1 (90 and 80 ng/L GLY in ground- and surface water, respectively) in the lower village lies farthest from any significant agricultural plots, but lies within the central part of the village on a gaining section of the stream. Here, possible GLY application sites include roadsides and yards in upstream homes where herbicides containing glyphosate may

be applied to control unwanted weeds, although contributions from upstream agricultural plots via deeper groundwater flow lines cannot be ruled out.

Glyphosate levels in Faga'alu stream and groundwater were orders of magnitude lower than the Maximum Contaminant Level (MCL) of 700,000 ng/L in drinking water (EPA, 2009) or environmental limits (mg/L; EPA, 1993). GLY concentrations found across the watershed were comparable to findings elsewhere, such as a study in Catalonia by Sanchis et al. (2012) which found average GLY to be 200 ng/L in groundwater. GLY concentrations in groundwater in Canada were reported at 660 ng/L (Van Stempvoort et al., 2014, 2016), even higher levels were recorded in a study in Mexico (440 to 1410 ng/L, Rendón-von Osten and Dzul-Caamal, 2017). In Faga'alu, groundwater flow was responsible for 0.54 ± 0.09 and 0.34± 0.08 g/d of GLY discharge via baseflow and fresh SGD, respectively.

The relatively uniform distribution of DDT reflects its method of island-wide application several decades ago (NPIC Oregon State University, 1999). Its presence in stream bank groundwater and coastal springs so long after its last application is notable, which reflects its persistent nature as it is adsorbed onto soils and slowly leaches into groundwater. Whitall and Holst (2015) reported sediment DDT concentrations of up to 2.3 ng/g in Faga'alu watershed, suggesting that sediments are likely to be a reservoir of DDT from which groundwater may mobilize it. In this study, Faga'alu had similar concentration ranges of DDT in both surface and groundwater. DDT fluxes to the reef were determined to be 5.3 ± 0.8 and 3.7 ± 0.6 g/d via baseflow and SGD, respectively (**Table 5**). DDT concentrations of up to 2,000 ng/L were observed in both stream and groundwater samples, nearly half of the water quality limit of 5,000 ng/L (EPA, 2016).

Nitrogen

Nitrite, nitrate, and ammonium concentrations (**Tables 1**, **2**) were all orders of magnitude below recommended US limits [drinking water MCLs of nitrite 1 mg/L, nitrate 10 mg/L (EPA, 2009), ammonium environmental limit 0.25–32.3 mg/L Oregon Department of Human Services, 2000]. Measured nutrient concentrations followed land-use and groundwater flow patterns across the watershed with increasing concentrations downstream of the agricultural and populated areas in the watershed. In the samples, between 65 and 100% of TDN consisted of DIN, and thus both followed a similar distribution pattern. N+N represented between 20 and 70% of DIN, with NH_4^+ representing the rest. The northern coastal spring (CS-N) had the highest DIN (250 μg/L) and TDN (340 μg/L) concentrations, likely a result of the high density of OSDS units along the coast, along with large agricultural plots up the slope of the adjacent ridge. As the transport model predicts, OSDS is likely the primary contributor of DIN in Faga'alu groundwater with as much as 90% of groundwater DIN originating from them.

Although N+N generally contributed more to DIN than did NH_4^+ in Faga'alu samples, the stream bank sample at S-1 had lower N+N than NH_4^+, which can likely be explained by anoxic organic rich estuarine sediments. Additionally at site S-1, DIN was 72% higher in the surface samples than groundwater samples. At other sites, surface stream DIN levels were all comparable to the stream bank groundwater.

Of the sites sampled, the highest concentrations of N were observed at the two coastal springs and the well. This is not surprising, as coastal springs integrate all upstream inputs and are also a site of converging shallow and deeper groundwater flow lines. This also highlights the point this study is making, that SGD should be considered in coastal nutrient budgets, as it is a point of source and flow convergence and an important nutrient pathway to the coastal ocean.

Phosphate and Silicate

As phosphate acts as an essential constituent of organisms, the EPA has no set MCL for drinking water (Oram, 2014a). In freshwater bodies, phosphate is usually a limiting nutrient, thus in excess can lead to accelerated eutrophication, leading to algal blooms and lower dissolved oxygen. The EPA has set the maximum acceptable stream PO_4^{3-} concentration to 100 μg/L (Oram, 2014b). Four of the six stream bank groundwater and five of the seven stream surface sites sampled exceeded this amount (**Tables 1**, **2**) suggesting that groundwater contribution likely plays an important role in driving these elevated PO_4^{3-} concentrations. Specifically, the well (FG-179) had the highest concentration of phosphate (260 μg/L), possibly due to the accumulation of upslope agricultural inputs in the deep groundwater, but more likely the longer groundwater pathways obtaining enriched P from natural rock weathering. It has been shown that DIP in volcanic aquifers can naturally be elevated (Porder and Ramachandran, 2013), so it is possible that natural sources (i.e., basalt weathering) are responsible for the elevated groundwater PO_4 concentrations.

Silicate in groundwater reflects water-rock interactions, as Si dissolves from silica-rich minerals within the underlying rocks. Silica content is also directly proportional to groundwater residence times within the rocks in the aquifer (Pradeep et al., 2016). This is often reflected in deeper-sourced groundwater over shallow-sourced water (Khan et al., 2015). This seems to be the case in Faga'alu, as the highest concentration of $Si(OH)_4$ was found in the well (FG-179), which is sourced from the deepest groundwater in the study. The coastal springs showed the lowest $Si(OH)_4$ values, as they were diluted by the ocean. The range of $Si(OH)_4$ concentrations in groundwater was 1,940–20,200 μg/L, with a mean concentration of 12,950 ± 6970 μg/L. The stream bank sites average, however, was <2% different from the surface stream sample average concentration. This confirms active surface water-groundwater interactions in the stream.

Evaluation of the Groundwater Flow Model

It should be noted that MODFLOW and related simulation software assumes validity of the continuum approach implying that aquifers can be treated as porous media (Bear, 1979). Such an approach defines a representative elementary volume (REV) that is large enough to represent the medium properties, such as porosity or hydraulic conductivity, but still small enough to be considered as a point in the mathematical formulation of the water flow process. In practical terms, field measurements are considered as average values over the REV. In a case where significant preferential flow exists, for example due to the

TABLE 5 | Modeled groundwater discharge via stream baseflow and fresh SGD, and their associated pesticide and nutrient fluxes based on observed concentrations in each representative section of the watershed.

	Modeled baseflow			Measured baseflow	Modeled fresh SGD				Measured fresh SGD (Shuler et al., 2019)	Baseflow + fresh SGD modeled Flux
	Upper reach	Lower reach	Baseflow sum		North	Central	South	SGD Sum		
Discharge (m^3/d)	2,440 ± 580	1,430 ± 160	3,870 ± 260	3,630	480 ± 50	1,840 ± 200	360 ± 40	2,680 ± 300	2,820-11,730	6,550 ± 980
Discharge (m^3/m/d)	1.08	1.94	1.29		0.64	3.68	0.56	1.42		
GLY (g/d)	0.43 ± 0.12	0.11 ± 0.02	0.54 ± 0.09	0.28	0.07 ± 0.02	0.16 ± 0.04	0.11 ± 0.02	0.34 ± 0.08		0.88 ± 0.23
DDT (g/d)	3.5 ± 1.0	1.8 ± 0.3	5.3 ± 0.8	4.4	1.0 ± 0.2	2.2 ± 0.4	0.5 ± 0.1	3.7 ± 0.6		9.0 ± 2.0
DIN (g/d)	170 ± 40	100 ± 10	270 ± 30	300	120 ± 20	150 ± 20	30 ± 10	300 ± 40		570 ± 100
TDN (g/d)	270 ± 70	110 ± 20	370 ± 40	250	160 ± 20	130 ± 20	50 ± 10	340 ± 50		710 ± 140
PO_4 (g/d)	240 ± 60	240 ± 30	480 ± 30	590	50 ± 10	300 ± 30	20 ± 2	370 ± 40		840 ± 110
$Si(OH)_4$ (g/d)	39,880 ± 9,570	23,120 ± 2540	63,000 ± 4,170	60,300	3,320 ± 370	30,580 ± 3,370	700 ± 80	34,600 ± 3,800		97,600 ± 12,530
N+N (g/d)	170 ± 40	40 ± 10	210 ± 20	50	120 ± 20	20 ± 3	30 ± 4	170 ± 20		380 ± 70
NH_4^+ (g/d)	5 ± 1	60 ± 10	65 ± 8	245	5 ± 1	125 ± 20	2.0 ± 0.3	132 ± 20		200 ± 40

Contributions from the lower and upper reaches of the stream are summed for total stream-derived fluxes into the bay while contributions from the north, central, and southern coastlines of the bay are summed for bay-wide fresh SGD-derived fluxes. The final column shows the total combined modeled flux for each contaminant derived from fresh groundwater (baseflow + SGD).

existence of large size fractures, applicability of porous media models will be questionable. Two interacting flow systems would exist in this case with Darcyan and non-Darcyan flows in the porous media and fractures, respectively (Bear, 1979). Modeling efforts will thus be complicated by requiring data about the location, size, and properties of the fractures. Volcanic aquifers may include conduits, fractures, dikes, and other features. However, many modeling studies completed in American Samoa, Hawaii, and other Pacific Islands have successfully utilized porous media models in managing groundwater resources (e.g., Oki, 2005; Izuka et al., 2007; Whittier et al., 2010; Gingerich and Engott, 2012). In this regard, hydraulic conductivity is typically calibrated for various geologic units integrating smaller-scale heterogeneities within the aquifer. In our case, although all calibrated head elevations of the modeled water table lie within 10% of total head values in the watershed, two sites (Spring-1 and the well) had a high relative error of 60 to 150%, respectively (**Table 3**). The poor match at these sites is likely the result of unknown small-scale hydrogeological properties of the subsurface.

For our purposes of estimating baseflow and SGD, the model adequately estimated discharge observations and gave us confidence in its applicability to study contaminant fluxes. The modeled stream baseflow measurements matched the observations to an average of 11%, with absolute error ranging from 90 to 464 m^3/d across the sites. The RMSR of 256 m^3/d falls well below 10% of the total modeled stream baseflow (3,870 m^3/d). The modeled baseflow entering the bay at the lowest stream station, S-1 overestimated the total measured surface flow by only 11 %. Additionally, Faga'alu Stream gauge measurements from August 10th, 2016 recorded a total streamflow of 3,830 m^3/d, with baseflow delineated at 3,670 m^3/d on the day of the seepage run (https://github.com/cshuler/ASPA-UH_Stream_REPO), only 5% relative error compared to the modeled flow. Contrary to observations, however, the model did not calculate any of the sections to be losing water to the aquifer. Every reach of stream calculated in the model was gaining from the last (**Table 4**), while the seepage run identified the presence of both gaining and losing sections. Specifically, between site S-6 to S-5, discharge dropped by over 550 m^3/d, while the model predicted a 67 m^3/d increase in flow. Such a discrepancy is again most likely due to simplifications in the conceptual model that do not accurately capture the true geologic features of the site. Our study approach was therefore to combine field observations and modeling to derive contaminant transport pathways.

The MODFLOW-derived groundwater fluxes were compared to the measured values collected during a previous study in 2014-2015 (Shuler et al., 2019), which consisted of baseflow separation and indirect measurement of SGD entering the bay calculated by a ^{222}Rn mass balance (Shuler et al., 2019). Groundwater flow as a sum of SGD and stream baseflow was 5,500–14,400 m^3/d (Shuler et al., 2019) by comparison to 6,550 $\pm$ 980 m^3/d in this 2016 study. Although both measurements occurred during American Samoa's dry season under baseflow conditions, some variability in the elevation of the water table due to seasonal conditions likely exists. This study's estimate is on the lower end but within the range of the previously published results. The shore length-normalized fresh SGD rates of 0.6 to 3.7 m^3/m/d (**Table 5**) are comparable to rates found at other volcanic island settings such as Jeju, Hawaii, Japan, and New Zealand (Kim et al., 2003; Hosono et al., 2012; Dulai et al., 2016; Stewart et al., 2018). In such settings reported fresh SGD rates can be up to 100 m^3/m/d and it is interesting that a relatively wet place such as Tutuila is on the lower end of the spectrum of observed fresh SGD rates. Otherwise, fresh SGD volume of ~2,000 m^3/d discharging to the whole Faga'alu Bay is comparable to similarly-sized embayments, see for example synthesis of previous work in Hawaii Islands by Kelly et al. (2019).

Nearly as much water was delivered to the bay via SGD (41%) as from the stream (59%) during baseflow conditions, making SGD a considerable fraction of the daily water and solute load in the dry season. The central coastline of the bay contributed more SGD than both the north and south coasts combined. Other studies similarly found elevated groundwater discharge to occur in estuaries of streams and rivers (e.g., Buddemeier, 1996; Dulaiova et al., 2006). The northern coastline contributed slightly more SGD than the southern shore, which agrees with overall SGD distribution patterns in Faga'alu found by Shuler et al. (2019). This agreement supports that the water fluxes determined by the model can justifiably be used to estimate contaminant transport. It is, however, important to point out that the study only addresses a one-time observation during dry season, so it should not be extrapolated to annual average conditions. At the same time, SGD and baseflow are a continuous year-round input to the coastline so the results presented are minimum contaminant fluxes. Land-based pollution runoff probably increases when surface runoff is present in the wet season.

The approach only estimated freshwater SGD, which is considered the major pathway of terrestrial contaminants and probably captures GLY fluxes appropriately. DIN however may also be contributed by the saline component of SGD as demonstrated elsewhere. Mulligan and Charette (2006) showed that ammonium may be produced in the subterranean estuary (STE) by remineralization processes and released within the salinity transition zone. At the same time nitrate removal by denitrification in the STE may attenuate the terrestrial DIN flux. This study did not investigate nutrient transformation and attenuation within the salinity transition zone, instead it uses nutrient concentrations past the STE sampled at the groundwater discharge point. Likewise, due to lack of information on the salinity transition zone, this study did not develop a density-dependent groundwater model to account for salt-fresh water interaction at the land-ocean interface. Density effects were ignored due to the lack of salinity data but future studies could explore the role of the STE for contaminant attenuation and SGD via density dependent groundwater models such as SEAWAT.

Groundwater-Derived Contaminant Fluxes Based on Observed Concentrations and Model-Derived Groundwater Fluxes

SGD from the central coast delivered the most contaminants across the land-ocean interface, with the exception of TDN and

N+N (**Table 5**), the majority of which, according to the model were delivered from the northern shoreline. This assumes that CS-N TDN levels are valid for the whole northern section of the coastline. The upper stream reach contributed much more discharge than the lower reach. Likewise, contaminant fluxes entering the stream from baseflow were higher in the upper reach, partly because of higher concentrations, also because of much higher water discharge. The only exception to this was DIP, which was distributed equally, and ammonium, which had over 10 times higher concentrations in the lower reach although it may be oxidized during discharge. Field observations and modeled groundwater discharge in this study estimated that SGD contributes a comparable amount of DIN, DDT and GLY as the stream. The combined total flux of each contaminant entering the bay each day via fresh SGD and baseflow thus has the potential to greatly influence water quality and reef health in this designated priority watershed.

Evaluation of the Contaminant Transport Model

MODFLOW derived groundwater flow was utilized in MT3DMS to determine contaminant flow. Observations at one well and five stream sites (6 GLY, 6 DIN) were evaluated in the transport model. Limitations of the study were the low number of observations and that concentrations at each site could fluctuate greatly over seasons and years, so we are reporting results as "per day" and concentrations and fluxes represent dry season estimates. Additionally, in contrast to groundwater flow models, porous-media transport models are less accurate under the assumption of continuous media where preferential flow can prevail due to fractures (e.g., Glenn et al., 2013). Another uncertainty in this study is the absence of actual site-specific chemical application rates and attenuation coefficients of nutrients and pesticides. Given such difficulties, we were able to obtain model estimates that matched observations to within an order-of-magnitude for both GLY and DIN concentrations at all sites. Such uncertainties support the use of this model primarily as a screening tool in demonstrating the importance of groundwater fluxes and predicting scenarios involving variables relative to one another, rather than for precise quantitative analysis (Zheng et al., 2012). Future studies should emphasize a wider spatial and temporal distribution of sampling sites as well as identify application rates of fertilizers and herbicides along with OSDS and piggery mass loading rates, rather than relying on literature data.

Toward using the model as a screening tool, a sensitivity analysis was performed. Dispersivity played the largest factor in affecting end concentrations of both solutes at all sites, whereas porosity specifically affected GLY concentrations more than DIN (**Supplementary Figure 2**). Sensitivity to anisotropy ratios was most noticeable at the northern coastal spring (CS-N). Extremely high fluxes of DIN appear in this northern coastal sector compared to other regions of the watershed with similar OSDS density, which might be the result of how PEST zonally estimated hydraulic conductivity in this location.

The solute fluxes derived from the transport model fell within the same order of magnitude as the values estimated by MODFLOW's derived groundwater discharges and observed concentrations (**Supplementary Table 5**). The MT3DMS model underestimated GLY fluxes and overestimated DIN fluxes, due to inconsistencies in the modeled upper reach of the stream. Fluxes based on MODFLOW estimates are thus more realistic than those based on MT3DMS estimates, considering the model limitations discussed above.

Scenarios of GLY and DIN Source Variability and Resulting Fluxes in the Watershed

Scenarios were run using the transport model to look for relative contributions of each point and non-point source to dissolved contaminant loads. The transport model predicted that 90% of groundwater DIN is being contributed to the observation points by OSDS input. As these are installed below ground, possibly interacting with the water table, OSDS have the most direct nutrient loading pathway. The other 10% of DIN transported in the aquifer according to the model is contributed mostly by piggeries and natural sources. The trends are not valid across the entire watershed though, for example, piggeries are estimated to contribute 20% DIN in the southern coastal spring (CS-S), indicating that the model predicts the nearby piggery to play a larger role at this site than piggeries on average at other sample sites. Fertilizer application was the source of only <1% of DIN contribution estimated by the model to arrive at our observation points. In Hawai'i, it has been found that very small fractions of agricultural DIN leach into groundwater in the root zone of plants (El-Kadi and Yabusaki, 1996), which could explain why fertilizer N shows such small contribution to the DIN inventory in the model. Watering techniques and high precipitation could also inhibit fertilizer's capability to make it into the groundwater by creating a surface runoff to the nearest surface water body. However, other studies attribute heavy agriculture to play a larger role in groundwater nutrient budgets and coastal SGD N-fluxes (e.g., Amato et al., 2016).

In a study that looked at watershed nutrient sources on the same island but a different watershed, Shuler et al. (2017) showed that OSDS contributed 60 ± 7% of the DIN flux. The fraction of groundwater-derived DIN estimated by this study's MT3DMS model (90%) would thus fall a bit higher. The piggery contribution was 20 ± 6% in comparison to 6% in this study. The agricultural N inputs were 9 ± 4% in Shuler et al. study 2017 in comparison to <1% in Faga'alu. While the absolute fractions were different between the two studies and watersheds, the relative role of each source was similar, OSDS being the dominant DIN contributor.

Scenarios of improved OSDS installations and decreased pesticide-use were run to predict the impact of changes in land-use management practices on groundwater quality. When DIN mass loading rates were halved for each OSDS-unit, simulating a 2-fold improvement to the assumed cesspools that occupy

the lower Faga'alu watershed, the average DIN concentrations of the observation points improved by 46%. Thus, upgrading many of the current cesspools in the watershed to septic systems could provide a considerable improvement in future groundwater quality, due to more effective nitrogen attenuation and resulting smaller amounts of nutrients leaching into the coastal waters.

Glyphosate-use scenarios were performed to see the relative contributions from domestic and agricultural inputs. The results show that degradation of GLY may influence which sources contribute the most to the observation sites. According to the model, the domestic inputs, which were modeled with half the initial concentrations as the agricultural zones, delivered a significant amount of the herbicide to the observation points. This indicates that proximity to the stream may be an important factor in glyphosate contamination. Agricultural GLY may be more diluted and degraded before reaching observation points within the village.

Scenarios were thus run with (1) half the domestic input of GLY and (2) with half the total GLY (domestic and agricultural) applied. The first scenario lowered average concentrations by 37% across the watershed, and the second scenario lowered GLY arrival another 13%, to a total of 50%. This shows that improving application techniques or limiting the use of GLY-based herbicides near the stream and coastline could significantly lower the amount of the herbicide in discharging groundwater (**Supplementary Table 6**). It should be noted that assumptions about application rates, geographical distribution of application, and degradation rates were made. Finally, as mentioned previously, the underlying geology and soil properties may play a role in the attenuation of glyphosate and their heterogeneity may have not been captured in the model.

Potential Threat to the Reef Ecosystem

Glyphosate is the most common ingredient in top-selling herbicides around the world today (e.g., Roundup), and its harmful effects have been discussed, specifically in regards to its carcinogenic nature to humans (Tarazona et al., 2017). There are a few studies that reported on the effects of GLY on aquatic ecosystems (e.g., Diu, 2016; Pérez et al., 2017). According to our study, 880 ± 230 mg/d of GLY is entering Faga'alu Bay, with near-ocean groundwater concentrations reaching values likely similar to those measured in coastal springs (160 to 300 ng/L). In a study by Diu (2016) focusing on coral exposed to different concentrations of GLY, the herbicide was generally found not to have harmful effects on reef fertilization or settlement. Only in contained studies, at concentrations above 690,000 ng/L does GLY affect coral fertilization (Diu, 2016), which is three orders of magnitude higher than what was found in Faga'alu coastal springs. The GLY that enters Faga'alu Bay each day via baseflow and coastal SGD is likely diluted relatively quickly as it enters a large body of water and mixes offshore. Gallagher et al. (1996) found low concentrations of pesticides across coastal sites in Virginia, but detected none in the offshore surface water or sediment samples. The chronic effects of the GLY itself are suggested not to be a factor on reef health, as its dilution and degradation are relatively rapid in open water (Schuette, 1998). With a half-life ranging from 47 to 267 days, depending on the type of microbial communities present (Mercurio et al., 2014), GLY is not known to bioaccumulate in organisms as it has low lipid solubility (Schuette, 1998). Diu (2016), however, found that lower fertilization rates in coral can be attributed to the runoff of Roundup (Monsanto®) into marine environments. Despite GLY itself not being detrimental to reef health, in combination with other chemicals (e.g., Roundup solution), the formulation is likely to present increased toxicity to the reef (Diu, 2016). Thus, monitoring GLY fluxes in stream and across the land-ocean interface from Roundup application may still be of importance in Faga'alu.

The insecticide DDT has a much longer residence time than glyphosate and is able to bioaccumulate in the tissues of organisms. Studies have shown that DDT likely has an effect on the calcification of adult corals and other calcifying organisms in the reef community (Kwok, 2015; Porter et al., 2018), similar to the effects it had on the calcium-related eggshell thickness of bird eggs in early studies (Porter and Wiemeyer, 1969; Peakall, 1970). The fact that 9,000 ± 2,000 mg of DDT is contributed to Faga'alu Bay via stream baseflow and SGD each day, highlights its persistence and ubiquity in the environment decades after its ban (EPA, 2016). Despite that it is no longer sprayed, DDT's long half-life allows it to accumulate in the ecosystem. DDT has the potential to chronically affect growth and reproduction of marine organisms within the reef as its daily load into the bay has spanned several decades, and may continue for several more. This study sheds light on groundwater fluxes of DDT into the bay but it should be noted that it has multiple other pathways. Thanks to its high sorption coefficient DDT sorbs to soil and sediment particles (Magga et al., 2008) and can readily get transported by stream suspended loads and also released by sediment resuspension in the bay. A study in coastal California demonstrated that sediment resuspension resulted in DDT release and contaminant levels in the water column closely correlated to sediment DDT levels (Zeng and Venkatesan, 1999). Studying DDT in tissues of organisms in the future would thus be beneficial to understanding the long-term effects the insecticide is having in Faga'alu Stream and Bay.

Total N entering Faga'alu Bay via baseflow and SGD together is 710 ± 140 g/d and total P is 840 ± 110 g/d. Elevated nutrient concentrations have already been documented in Faga'alu Bay in other studies (Whitall and Holst, 2015; Shuler et al., 2019). In American Samoa, the National Coastal Condition Report (Colianni et al., 2012) determined cut-points for coastal DIN at <500 μg/L, and all groundwater and stream DIN measured in our study were lower than that. For DIP, the cut-point of fair condition is <70 μg/L of P, which is exceeded by all but three stream and groundwater samples. In addition, corals are sensitive to excess nutrients, and levels above 14 μg/L-N (DIN) and 3 μg/L-P can be considered unhealthy for a reef ecosystem, as it may promote more algal growth (Goreau and Thacker, 1994; Mosley et al., 2005). These high levels of nutrients can lead to eutrophication in the bay, upsetting the delicate balance of the reef ecosystem. Excess algae can smother the corals and block sunlight from reaching important photosynthetic organisms, and can promote the spread of harmful bacteria

(Coral Reef Alliance, 2019). Thus, in the case of Faga'alu, a reduction in nutrient fluxes could be beneficial to the bay. As this study demonstrates, groundwater quality directly affects coastal nutrient levels, and the nutrient fluxes from baseflow and SGD should be considered when nutrient pathways into the reef are evaluated.

CONCLUSIONS

This study further implicates the importance of the role of fresh SGD and baseflow to overall water and contaminant fluxes in coastal aquifers with volcanic geologic properties. By integrating observed groundwater contaminant concentrations with a hydrogeological model of Faga'alu Watershed in American Samoa, relative SGD and baseflow fluxes of pesticides and nutrients were determined for each sector of coastline and reach of stream. Although flow rates modeled in this study are only calibrated against a snapshot of observations, the model-estimated contributions reasonably captured groundwater flow in comparison to a study from a previous dry season (Shuler et al., 2019). The model predicted the central coastline to be contributing the most SGD to Faga'alu Bay and the upper reach of the stream was contributing the most baseflow. Under baseflow conditions SGD flux was 41% of the total fresh groundwater flow to the bay and stream baseflow was responsible for 59%. It is evident that groundwater plays a significant role in water and solute transport to the bay, especially during the dry season of July through September.

Clearly, a more robust modeling approach would be based on year-round observations capturing seasons and extreme weather conditions as well as based on geographically extended hydrogeological observations. In addition, as a next step, a hydrological model capturing the salinity transition zone and total SGD would help further in interpreting nutrient cycling and fluxes across the land-ocean interface.

Field investigation confirmed pesticides to be present in the groundwater, and by combining their measured concentrations with model-derived groundwater discharge, fluxes across the land-ocean interface were slightly <1 g of GLY to the bay each day and nearly 9 g/d of DDT. The continued flux of these chemicals could have chronic effects on reef health and should be investigated in more detail. Nutrient fluxes were 710 ± 140 g of TDN and 840 ± 110 g of DIP per day where 90% of TDN was estimated to be derived from OSDS. Although concentrations of N at any individual sampling site did not exceed EPA recommended values, concentrations of DIP were above the acceptable limits (Oram, 2014b) in many locations.

Better land-use practices, specifically reducing the amount of applied pesticides and improving the wastewater infrastructure can help reduce the leaching of pesticides and nutrients into groundwater. Models like the one developed here but perfected with more observations could be applied for optimization of elimination of pollution sources that have the largest impact. As Faga'alu has been designated a priority watershed in monitoring reef health, it is important to consider not only contaminants entering the bay via surface pathways, but also as demonstrated by this study, to consider groundwater transport via SGD and stream baseflow as pathways for pesticides and nutrients into the bay.

DATA AVAILABILITY STATEMENT

All datasets generated for this study are included in the manuscript/**Supplementary Files**.

AUTHOR CONTRIBUTIONS

HD and AE-K contributed conception and design of the study. EW and CS designed and performed the field-based aspects of the study. HD and EW performed the laboratory analysis. AE-K and EW developed the hydrological models. EW wrote the first draft of the manuscript. HD, AE-K, and CS wrote sections of the manuscript. All authors contributed to manuscript revision, read and approved the submitted version.

FUNDING

Funding for this project was provided to HD by the USGS Water Resources Research Institute Program (WRRIP) project number 2016AS455B and the Hawai'i EPSCoR Program funded by the National Science Foundation's Research Infrastructure Improvement (RII) OIA-1557349, to AE-K from the Pacific Regional Integrated Sciences and Assessments (Pacific RISA), NOAA Climate Program Office project number NA15OAR4310146, and to EW from the University of Hawaii Undergraduate Research Opportunities Program (UROP).

ACKNOWLEDGMENTS

The authors acknowledge continued support from the American Samoa Environmental Protection Agency, the American Samoa Power Authority, the NOAA AS office, American Samoa Community College, and the Coral Reef Advisory Group for providing essential logistical assistance on Tutuila and enabling the field component of this work. The authors would also like to thank the village of Faga'alu, the Pulenuu of Faga'alu, and others who generously provided access to study sites. We would like to thank Dr. Mark Schmaedick and Dr. Ian Gurr at the American Samoa Community College Land Grant for their time and expertise when developing research methods used in this study. We thank Drs. Olkeba Tolessa Leta, Trent Biggs, and Alex Messina for collaboration support, advice, and feedback at various stages of the study. This is contributed paper WRRC-CP-2020-04 of the Water Resources Research Center, and SOEST publication # 10802 at the University of Hawaii at Manoa, Honolulu, Hawaii.

SUPPLEMENTARY MATERIAL

The Supplementary Material for this article can be found online at: https://www.frontiersin.org/articles/10.3389/fenvs.2019.00162/full#supplementary-material

REFERENCES

Almasri, M. N. (2008). Assessment of intrinsic vulnerability to contamination for Gaza coastal aquifer, Palestine. *J. Environ. Manage.* 88, 577–593. doi: 10.1016/j.jenvman.2007.01.022

Amato, D. W., Bishop, J. M., Glenn, C. R., Dulai, H., and Smith, C. M. (2016). Impact of submarine groundwater discharge on marine water quality and reef biota of Maui. *PLoS ONE* 11:e0165825. doi: 10.1371/journal.pone.0165825

Bear, J. (1979). *Hydraulics of Groundwater, McGraw-Hill Series in Water Resources and Environmental Engineering*. New York, NY: McGraw-Hill.

Benbrook, C. M. (2016). Trends in glyphosate herbicide use in the United States and globally. *Environ. Sci. Eur.* 28:3. doi: 10.1186/s12302-016-0070-0

Bolabola, A. (2007). "Pollution a growing concern in Fiji Waters," in *Pacific Islands Report, Pacific Islands Development Program*. Available online at: www.pireport.org/articles/2007/07/05/pollution-growing-concern-fiji-waters

Bruno, J. F., Petes, L. E., Harvell, C. D., and Hettinger, A. (2003). Nutrient enrichment can increase the severity of coral diseases. *Ecol. Lett.* 6, 1056–1061. doi: 10.1046/j.1461-0248.2003.00544.x

Buddemeier, R. W. (1996). "Groundwater flux to the ocean: definitions, data, applications, uncertainties," in *LOICZ Reports Studies 8*, 16–21.

Burnett, W. C., and Dulaiova, H. (2003). Estimating the dynamics of groundwater input into the coastal zone via continuous radon-222 measurements. *J. Environ. Radioact.* 69, 21–35. doi: 10.1016/S0265-931X(03)00084-5

Chin, Y.-P., and Weber, W. J. (1988). *The Interaction of Hydrophobic Organic Compounds with Natural Solids and Dispersed Organic Polymers* (ProQuest Dissertations and Theses). Web.

Colianni, G., Aquarone, M., Balthis, L., Bourgeois, P., Casey, J., Cooksey, C., et al. (2012). *National Coastal Condition Report IV*. Environmental Protection Agency, Office of Water and Office of Research and Development. Available online at: https://www.epa.gov/sites/~production/files/2014-10/documents/0_nccr_4_report_508_bookmarks.pdf

Coral Reef Alliance (2019). *Clean Water for Reefs*. Available online at: https://coral.org/what-we-do/clean-water-for-reefs/.

Craig, P. (2002). *Natural History Guide to American Samoa: A Collection of Articles*. Pago Pago, American Samoa: National Park Service and the Dept. of Marine and Wildlife Resources.

Craig, P., DiDonato, G., Fenner, D., and Hawkins, C. (2005). "The state of coral reef ecosystems of American Samoa," in *The State of Coral Reef Ecosystems of the United States and Pacific Freely Associated States,* ed J. Waddell (Silver Spring, MD: NOAA Technical Memorandum NOS NCCOS 11. NOAA/NCCOS Center for Coastal Monitoring and Assessment's Biogeography Team), 312–337.

Davidson, J. H. (1995). *South Dakota Groundwater Protection Law*. University of Arkansas System Division of Agriculture.

Davis, D. A. (1963). *Ground-Water Reconnaissance of American Samoa*. Washington, DC: US Government Printing Office.

Diu, S. (2016). *Trouble in Paradise: The Effect of Glyphosate and Roundup Toxicity on Coral Fertilization and Settlement* (Master's thesis). Princeton University. Available online at: https://dataspace.princeton.edu/jspui/handle/88435/dsp01sj139440v

Doherty, J. E., and Hunt, R. J. (2010). *Approaches to Highly Parameterized Inversion: A Guide to Using PEST for Groundwater-Model Calibration*. Reston, VA: US Department of the Interior; US Geological Survey. doi: 10.3133/sir20105169

Dulai, H., Kleven, A., Ruttenberg, K., Briggs, R., and Thomas, F. (2016). "Evaluation of submarine groundwater discharge as coastal nutrient source and its role in coastal groundwater quality and quantity," in *Emerging Issues in Groundwater Resources, Advances in Water Security,* ed A. Fares (Springer International Publishing), 187–221. doi: 10.1007/978-3-319-32008-3_8

Dulaiova, H., Burnett, W. C., Wattayakorn, G., and Sojisuporn, P. (2006). Are groundwater inputs into river-dominated areas important? The Chao Phraya River—Gulf of Thailand. *Limnol. Oceanogr.* 51, 2232–2247. doi: 10.4319/lo.2006.51.5.2232

El-Kadi, A., and Yabusaki, K. (1996). *Assessment of Nutrient Use and Nitrate Contamination in Central Oahu, Hawai'i*. Water Resources Research Center, University of Hawai'i at Mānoa. Honolulu, HI: WRRC unedited report.

EPA (1993). *Reregistration Eligibility Decision (RED): Glyphosate; EPA-738-R-93-014*. Washington, DC: U.S. Environmental Protection Agency, Office of Prevention, Pesticides, and Toxic Substances, Office of Pesticide Programs, U.S. Government Printing Office.

EPA (2009). *National Primary Drinking Water Regulations*. Environmental Protection Agency, Office of Groundwater and Drinking Water, 816-F-09-004. Available online at: https://www.epa.gov/sites/production/files/2016-06/documents/npwdr_complete_table.pdf.

EPA (2016). *DDT- A Brief History and Status*. Environmental Protection Agency. Available online at: https://19january2017snapshot.epa.gov/ingredients-used-pesticide-products/ddt-brief-history-and-status_html.

Erler, D. V., Shepherd, B., Linsley, B., and Lough, J. M. (2018). Coral skeletons record increasing agriculture-related groundwater nitrogen inputs to a South Pacific reef over the past century. *Geophys. Res. Lett.* 45, 8370–8378. doi: 10.1029/2018GL078656

Gallagher, D. L., Dietrich, A. M., Reay, W. G., Hayes, M. C., and Simmons, G. M. Jr. (1996). Ground water discharge of agricultural pesticides and nutrients to estuarine surface water. *Groundwater Monit. Remediat.* 16, 118–129. doi: 10.1111/j.1745-6592.1996.tb00579.x

Gingerich, S. B., and Engott, J. A. (2012). Groundwater Availability in the Lahaina District, West Maui, Hawai'i. U.S. Geological Survey Report. doi: 10.3133/sir20125010

Glenn, C. R., Whittier, R. B., Dailer, M. L., Dulaiova, H., El-Kadi, A. I., Fackrell, J., et al. (2013). *Lahaina Groundwater Tracer Study–Lahaina, Maui, Hawaii*. Final Report, Honolulu, HI: Hawaii DOH.

Goreau, T. J., and Thacker, K. (1994). "Coral Reefs, Sewage, and Water Quality Standards," in *Caribbean Water and Wastewater Association Conference* (Kingston).

Harbaugh, A. W., Banta, E. R., Hill, M. C., and McDonald, M. G. (2000). MODFLOW-2000, The U. S. Geological Survey Modular Ground-Water Model-User Guide to Modularization Concepts and the Ground-Water Flow Process. Open-file Report. U. S. Geological Survey 92, 134. doi: 10.3133/ofr200092

Henderson, A. M., Gervais, J. A., Luukinen, B., Buhl, K., Stone, D., Strid, A., et al. (2010). *Glyphosate Technical Fact Sheet*. Corvallis, OR:National Pesticide Information Center; Oregon State University Extension Services.

Hosono, T., Ono, M., Burnett, W. C., Tokunaga, T., Taniguchi, M., and Akimichi, T. (2012). Spatial distribution of submarine groundwater discharge and associated nutrients within a local coastal area. *Environ. Sci. Technol.* 46, 5319–5326. doi: 10.1021/es2043867

Houk, P., Didonato, G., Iguel, J., and Van Woesik, R. (2005). Assessing the effects of non-point source pollution on American Samoa's coral reef communities. *Environ. Monit. Assess.* 107, 11–27. doi: 10.1007/s10661-005-2019-4

Huhta, C., and Sloat, J. (2007). *Discharge Uncertainty Calculations Using a SonTek FlowTracker*. SonTek/YSI Inc. Available online at: www.sontek.com.

Izuka, S. K., Perreaultm, J. A., and Presley, T. K. (2007). Areas Contributing Recharge to Wells in the Tafuna-Leone Plain, Tutuila, American Samoa. No. 2007-5167. Geological Survey (US).

Johannes, R. E., and Hearn, C. J. (1985). The effect of submarine groundwater discharge on nutrient and salinity regimes in a coastal lagoon off Perth, Western Australia. *Estuarine Coast. Shelf Sci.* 21, 789–800. doi: 10.1016/0272-7714(85)90073-3

Kelly, J. L., Dulai, H., Glenn, C. R., and Lucey, P. G. (2019). Integration of aerial infrared thermography and in situ radon-222 to investigate submarine groundwater discharge to Pearl Harbor, Hawaii, USA. *Limnol. Oceanogr.* 64, 238–257 doi: 10.1002/lno.11033

Kennedy, J. (2012). *A Closer Look at Parameter Estimation (PEST) for Visual MODFLOW Flex 2012.2*. Waterloo Hydrogeologic, Nova Metrix, LLC. Available online at: www.waterloohydrogeologic.com/2012/12/05/a-closer-look-at-parameter-estimation-pest-for-visual-modflow-flex-20122/.

Khan, A., Umar, R., and Khan, H. H. (2015). Significance of silica in identifying the processes affecting groundwater chemistry in parts of Kali watershed, Central Ganga Plain, India. *Appl. Water Sci.* 5, 65–72. doi: 10.1007/s13201-014-0164-z

Kim, G., Lee, K. K., Park, K. S., Hwang, D. W., and Yang, H. S. (2003). Large submarine groundwater discharge (SGD) from a volcanic island. *Geophys. Res. Lett.* 30:2098. doi: 10.1029/2003GL018378

Kwok, C. K. (2015). Spatial and temporal signatures of heavy metals in Hong Kong corals and the responses of their life history stages to heavy metal and organic pollutions (Diss). The Chinese University of Hong Kong, Hong Kong.

Lallanilla, M. (2019). *What is the Story About the Banned Pesticide DDT?* The Spruce, Dotdash. Availabale online at: www.thespruce.com/what-is-ddt-history-impacts-1708897.

Larkin, R. G. (1988). *Hydrogeologic Controls on Underflow in Alluvial Valleys: Implications for Texas Water Law*.

Leta, O. T., Dulai, H., El-Kadi, A. I., Messina, A. M., and Biggs, T. W. (2017). "Assessing sediment yield and the effect of best management practices on sediment yield reduction for Tutuila island, American Samoa," in *Final Paper # H31H-1600, Presented at the 2017 AGU Fall Meeting* (New Orleans, LA).

Magga, Z., Tzovolou, D. N., Theodoropoulou, M. A., Dalkarani, T., Pikios, K., and Tsakiroglou, C. D. (2008). Soil column experiments used as a means to assess transport, sorption, and biodegradation of pesticides in groundwater. *J. Environ. Sci. Health Part B* 43, 732–741. doi: 10.1080/03601230802388868

McCormick, G. R. (2017). *Water quality and sources of nutrient loads in watersheds of American Samoa* (Dissertation). San Diego State University, San Diego, CA, United States.

McDonald, M. G., and Harbaugh, A. W. (1988). *A Modular Three-Dimensional Finite-Difference Ground-Water Flow Model. Vol. 6*. Reston, VA: US Geological Survey.

Mercurio, P., Flores, F., Mueller, J. F., Carter, S., and Negri, A. P. (2014). Glyphosate persistence in seawater. *Marine Pollut. Bull.* 85, 385–390. doi: 10.1016/j.marpolbul.2014.01.021

Messina, A. M., and Biggs, T. W. (2016). Contributions of human activities to suspended sediment yield during storm events from a small, steep, tropical watershed. *J. Hydrol.* 538, 726–742. doi: 10.1016/j.jhydrol.2016.03.053

Miller, M. P., Buto, S. G., Susong, D. D., and Rumsey, C. (2016). The importance of base flow in sustaining surface water flow in the Upper Colorado River Basin. *Water Resour. Res.* 52, 3547–3562. doi: 10.1002/2015WR017963

Misa, M. M., and Vargo, A. M. (1993). "Indigenous agroforestry in American Samoa," in *Proceedings of the Workshop on Research Methodologies and Applications for Pacific Island Agroforestry; July 16-20, 1990; Kolonia, Pohnpei, Federated States of Micronesia. Gen. Tech. Rep. PSW-GTR-140*, Vol. 140, eds B. Raynor, and R. R. Bay (Pacific Southwest Research Station, Forest Service, US Department of Agriculture), 83.

MODFLOW-PEST Pilot Points (2016). *Aquaveo, GMS 10.1 Tutorial*.

Mosley, L., Singh, S., and Aalbersberg, B. (2005). Water Quality Monitoring in Pacific Island Countries. SOPAC Technical Reports 381, 42.

Mosley, L. M., and Aalbersberg, W. G. L. (2003). Nutrient levels in sea and river water along the 'Coral Coast'of Viti Levu, Fiji. *S. Pac. J. Nat. Appl. Sci.* 21, 35–40. doi: 10.1071/SP03007

Mulligan, A. E., and Charette, M. A. (2006). Intercomparison of submarine groundwater discharge estimates from a sandy unconfined aquifer. *J. Hydrol.* 327, 411–425. doi: 10.1016/j.jhydrol.2005.11.056

NOAA/EPA (2003). American Samoa Coastal Nonpoint Program NOAA/EPA Decisions on Conditions of Approval. American Samoa Decision Document.

NPIC and Oregon State University (1999). *DDT [General Fact Sheet]*. Retrieved from: http://npic.orst.edu/factsheets/ddtgen.pdf.

Nyström, M., Folke, C., and Moberg, F. (2000). Coral reef disturbance and resilience in a human-dominated environment. *Trends Ecol. Evol.* 15, 413–417. doi: 10.1016/S0169-5347(00)01948-0

Oki, D. S. (2005). Numerical Simulation of the Effects of Low-Permeability Valley-Fill Barriers and the Redistribution of Ground-Water Withdrawals in the Pearl Harbor Area, Oahu, Hawaii. U.S. Geological Survey Scientific Investigations Report 2005-5253, 111. doi: 10.3133/sir20055253

Oram, B. (2014a). *Phosphates in the Environment.* Water Research Center, Water Research Watershed Center. Available online at: www.water-research.net/index.php/glossary.

Oram, B. (2014b). *Water Quality Terms Glossary*. Water Research Center, Water Research Watershed Center. Available online at: www.water-research.net/index.php/glossary.

Oregon Department of Human Services (2000). *Ammonia- Health Effects Information.* Environmental Toxicology Section, Office of Environmental Public Health, Technical Bulletin. Available online at: https://www.oregon.gov/oha/PH/HealthyEnvironments/DrinkingWater/Monitoring/Documents/health/ammonia.pdf.

Peakall, D. B. (1970). p, p'-DDT: Effect on calcium metabolism and concentration of estradiol in the blood. *Science* 168, 592–594. doi: 10.1126/science.168.3931.592

Pérez, D. J., Okada, E., Menone, M. L., and Costa, J. L. (2017). Can an aquatic macrophyte bioaccumulate glyphosate? Development of a new method of glyphosate extraction in *Ludwigia peploides* and watershed scale validation. *Chemosphere* 185, 975–982. doi: 10.1016/j.chemosphere.2017.07.093

Polidoro, B. A., Comeros-Raynal, M. T., Cahill, T., and Clement, C. (2017). Land-based sources of marine pollution: Pesticides, PAHs and phthalates in coastal stream water, and heavy metals in coastal stream sediments in American Samoa. *Marine Pollut. Bull.* 116, 501–507. doi: 10.1016/j.marpolbul.2016.12.058

Porder, S., and Ramachandran, S. (2013). The phosphorus concentration of common rocks—a potential driver of ecosystem P status. *Plant Soil* 367, 41–55. doi: 10.1007/s11104-012-1490-2

Porter, R. D., and Wiemeyer, S. N. (1969). Dieldrin and DDT: effects on sparrow hawk eggshells and reproduction. *Science* 165, 199–200. doi: 10.1126/science.165.3889.199

Porter, S. N., Humphries, M. S., Buah-Kwofie, A., and Schleyer, M. H. (2018). Accumulation of organochlorine pesticides in reef organisms from marginal coral reefs in South Africa and links with coastal groundwater. *Marine Pollut. Bull.* 137, 295–305. doi: 10.1016/j.marpolbul.2018.10.028

Pradeep, K., Nepolian, M., Anandhan, P., Chandran, Kaviyarasan, R., Prasanna, M. V., et al. (2016). "A study on variation in dissolved silica concentration in groundwater of hard rock aquifers in Southeast coast of India," in *IOP Conference Series: Materials Science and Engineering*, Vol. 121. No. 1. (IOP Publishing). doi: 10.1088/1757-899X/121/1/012008

Rendón-von Osten, J., and Dzul-Caamal, R. (2017). Glyphosate residues in groundwater, drinking water and urine of subsistence farmers from intensive agriculture localities: a survey in Hopelchén, Campeche, Mexico. *Int. J. Environ. Res. Public Health* 14:595. doi: 10.3390/ijerph14060595

Richardson, C. M., Dulai, H., and Whittier, R. B. (2015). Sources and spatial variability of groundwater-delivered nutrients in Maunalua Bay, O'ahu, Hawai 'i. *J. Hydrol.* 11, 178–193. doi: 10.1016/j.ejrh.2015.11.006

Rodellas, V., Garcia-Orellana, J., Masqué, P., Feldman, M., and Weinstein, Y. (2015). Submarine groundwater discharge as a major source of nutrients to the Mediterranean Sea. *Proc. Nat. Acad. Sci.* 112, 3926–3930. doi: 10.1073/pnas.1419049112

Sanchis, J., Kantiani, L., Llorca, M., Rubio, F., Ginebreda, A., Fraile, J., et al. (2012). Determination of glyphosate in groundwater samples using an ultrasensitive immunoassay and confirmation by on-line solid-phase extraction followed by liquid chromatography coupled to tandem mass spectrometry. (Report). *Anal. Bioanal. Chem.* 402, 2335–2345. doi: 10.1007/s00216-011-5541-y

Schuette, J. (1998). Environmental fate of glyphosate. *Environ. Monit. Pest Manage.* 1, 1–13.

Shuler, C. K., Amato, D. W., Gibson, V., Baker, L., Olguin, A. N., Dulai, H., et al. (2019). Assessment of terrigenous nutrient loading to coastal ecosystems along a human land-use gradient, Tutuila, American Samoa. *Hydrogeology* 6:18. doi: 10.3390/hydrology6010018

Shuler, C. K., El-Kadi, A., Dulaiova, H., Glenn, C. R., and Fackrell J. K. (2017). Source partitioning of anthropogenic groundwater nitrogen in a mixed-use landscape, Tutuila, American Samoa. *Hydrogeol. J.* 25, 2419–2434. doi: 10.1007/s10040-017-1617-x

Stearns, H. T. (1944). *Geology of the Samoan Islands. GSA Bull.* 55, 1279–1332. doi: 10.1130/GSAB-55-1279

Stewart, B. T., Bryan, K. R., Pilditch, C. A., and Santos, I. R. (2018). Submarine groundwater discharge estimates using radium isotopes and related nutrient inputs into Tauranga Harbour (New Zealand). *Estuaries Coasts* 41, 384–403. doi: 10.1007/s12237-017-0290-6

Tang, B., Boënne, W., Desmet, N., Seuntjens, P., Bronders, J., and van Griensven, A. (2015). Quantification and characterization of glyphosate use and loss in a residential area. *Sci. Total Environ.* 517, 207–214. doi: 10.1016/j.scitotenv.2015.02.040

Tarazona, J. V., Court-Marques, D., Tiramani, M., Reich, H., Pfeil, R., Istace, F., et al. (2017). Glyphosate toxicity and carcinogenicity: a review of the scientific

basis of the European Union assessment and its differences with IARC. *Arch. Toxicol.*91, 2723–2743. doi: 10.1007/s00204-017-1962-5

Travis, B. V., Maple, J. D., Hurlbut, H. S., and Husman, C. N. (1946). Cub airplanes in the South Pacific for application of DDT. *J. Econ. Entomol.* 39, 726–728. doi: 10.1093/jee/39.6.726

Tuitele, C., Buchan, E. L., Regis, J., Wiles, P., and Ilaoa, N (2014). *Territory of American Samoa Integrated Water Quality Monitoring and Assessment Report.* Hawaii: American Samoa Environmental Protection Agency, Pago Pago, American Samoa, Nimbus Environmental Services.

Van Stempvoort, D. R., Roy, J. W., Brown, S. J., and Bickerton, G. (2014). Residues of the herbicide glyphosate in riparian groundwater in urban catchments. *Chemosphere* 95, 455–463. doi: 10.1016/j.chemosphere.2013.09.095

Van Stempvoort, D. R., Spoelstra, J., Senger, N. D., Brown, S. J., Post, R., and Struger, J. (2016). Glyphosate residues in rural groundwater, Nottawasaga River Watershed, Ontario, Canada. *Pest Manage. Sci.* 72, 1862–1872. doi: 10.1002/ps.4218

Vaouli, E., Tuiteli, C., Buchan, E. L., Regis, J., Wiles, P., and Ilaoa, N. (2010). Territory of American Samoa Integrated Water Quality Monitoring and Assessment Report 2010. ASEPA.

Vargas-Angel, B., and Schumacher, B. (2018). *Baseline Surveys for Coral Reef Community Structure and Demographics in Vatia and Faga'alu Bay, American Samoa.* NOAA.

Whitall, D. R., and Holst, S. (2015). *Pollution in Surface Sediments in Faga'alu Bay, Tutuila, American Samoa*. NOAA Technical Memorandum NOS NCCOS 201. Silver Spring, MD, 54. doi: 10.7289/V5/TM-NOS-NCCOS-201

Whittier, R., Rotzoll, K., Dhal, S., El-Kadi, A. I., Ray, C., and Chang, D. (2010). Groundwater source assessment program for the state of Hawaii, USA: Methodology and example application. *Hydrogeology* 18, 711–723. doi: 10.1007/s10040-009-0548-6

Zeng, E. Y., and Venkatesan, M. I. (1999). Dispersion of sediment DDTs in the coastal ocean off southern California. *Sci. Total Environ.* 229, 195–208. doi: 10.1016/S0048-9697(99)00064-9

Zennaro, B. (2007). *Regulating illegal piggery waste runoff. ArcNews Online*. ESRI. Available online at: https://www.esri.com/news/arcnews/fall07articles/regulating-illegal.html.

Zhang, P., Aagaard, P., Nadim, F., Gottschalk, L., and Haarstad, K. (2009). Sensitivity analysis of pesticides contaminating groundwater by applying probability and transport methods. *Integr. Environ. Assess. Manage.* 5, 414–425. doi: 10.1897/IEAM_2008-087.1

Zheng, C., Hill, M. C., Cao, G., and Ma, R. (2012). MT3DMS: model use, calibration, and validation. *Trans. ASABE* 55, 1549–1559. doi: 10.13031/2013.42263

Zheng, C., and Wang, P. P. (1999). *MT3DMS: A Modular Three-Dimensional Multispecies Transport Model for Simulation of Advection, Dispersion, and Chemical Reactions of Contaminants in Groundwater Systems; Documentation and User's Guide*. Tuscaloosa, AL: Alabama University.

Conflict of Interest: The authors declare that the research was conducted in the absence of any commercial or financial relationships that could be construed as a potential conflict of interest.

frontiers in Marine Science

ORIGINAL RESEARCH
published: 03 December 2019
doi: 10.3389/fmars.2019.00753

Enhanced Growth Rates of the Mediterranean Mussel in a Coastal Lagoon Driven by Groundwater Inflow

Aladin Andrisoa[1], Franck Lartaud[2], Valentí Rodellas[1], Ingrid Neveu[2] and Thomas C. Stieglitz[1,3]*

[1] Aix-Marseille Université, CNRS, IRD, INRA, Coll France, CEREGE, Aix-en-Provence, France, [2] Sorbonne Université, CNRS, Laboratoire d'Ecogéochimie des Environnements Benthiques (LECOB), UMR 8222, Observatoire Océanologique de Banyuls, Banyuls-sur-Mer, France, [3] Centre for Tropical Water and Aquatic Ecosystem Research TropWATER, James Cook University, Townsville, QLD, Australia

Groundwater discharge is today recognized as an important pathway for freshwater, nutrients and other dissolved chemical substances to coastal systems. While its effect on supporting primary production in coastal ecosystems is increasingly recognized, its impact on growth of animals at higher trophic level (primary and secondary consumers) is less well documented. Here, we investigate the impact of groundwater discharge on the growth of the Mediterranean mussel (*Mytilus galloprovincialis*) in a coastal lagoon. Growth rates and condition index (tissue weight/shell weight) of mussels growing at groundwater-exposed sites and at a control site in Salses-Leucate lagoon (France) were measured. The mussels in this lagoon produce circadian (daily rhythm) growth increments in their shell, as opposed to semi-diurnal increments in tidally influenced systems. Mussels from groundwater-influenced sites have higher growth rate and condition index compared to those from a control site. Importantly, growth rates from groundwater-influenced sites are amongst the highest rates reported for the Mediterranean region (41 ± 9 $\mu m\ d^{-1}$). The higher growth rates at groundwater-influenced sites are likely a consequence of both the higher winter temperatures of lagoon water as a result of groundwater discharging with relatively constant temperatures, and the groundwater-driven nutrient supply that increase the food availability to support mussel growth. Overall, this study demonstrates that groundwater discharge to Mediterranean lagoons provides favorable environmental conditions for fast growth of mussels of high commercial-quality.

Keywords: groundwater discharge, coastal lagoon, *Mytilus galloprovincialis*, Mediterranean mussel, growth rate, condition index

OPEN ACCESS

Edited by:
Alberto Basset, University of Salento, Italy

Reviewed by:
Ryo Sugimoto, Fukui Prefectural University, Japan
Paulo Vasconcelos, Portuguese Institute of Ocean and Atmosphere (IPMA), Portugal

****Correspondence:***
Aladin Andrisoa
andrisoa@cerege.fr

Specialty section:
This article was submitted to Marine Ecosystem Ecology, a section of the journal Frontiers in Marine Science

Received: *22 January 2019*
Accepted: *19 November 2019*
Published: *03 December 2019*

Citation:
Andrisoa A, Lartaud F, Rodellas V, Neveu I and Stieglitz TC (2019) Enhanced Growth Rates of the Mediterranean Mussel in a Coastal Lagoon Driven by Groundwater Inflow. Front. Mar. Sci. 6:753. doi: 10.3389/fmars.2019.00753

INTRODUCTION

Coastal lagoons are highly productive ecosystems, supporting a wide range of ecosystem services such as aquaculture, fishery, tourism and others (Newton et al., 2014; Riera et al., 2018; Velasco et al., 2018). They are very dynamic environments controlled by physical processes under both marine and terrestrial influence (Kjerfve, 1994). These ecosystems are threatened by climatic and anthropogenic disturbances such as land use change, coastal erosion, sedimentation and excessive

nutrient loading (De Wit et al., 2005; Aliaume et al., 2007; Anthony et al., 2009). Whilst the role of surface waters (rivers, streams, runoff, etc.) in supporting biological production in coastal ecosystems has been extensively documented (Middelburg and Nieuwenhuize, 2001; Liu et al., 2010; Bianchi et al., 2014; Cloern et al., 2014), groundwater discharge is only more recently being recognized as an important pathway of nutrients for coastal systems (Slomp and Van Cappellen, 2004; Moore, 2010; Null et al., 2012).

In the Mediterranean Sea, which is an oligotrophic basin characterized by limited surface water inputs, groundwater discharge is a major source of nutrients to coastal systems and may thus affect the primary production in the ecosystems (Herrera-Silveira, 1998; Basterretxea et al., 2010; Tovar-Sánchez et al., 2014; Rodellas et al., 2015). However, the impacts of groundwater discharge are not limited to nutrient loading: a wide range of organisms also respond to changes in water salinity, light penetration into water column, pH and turbulence (Short and Burdick, 1996; Troccoli-Ghinaglia et al., 2010; Lee et al., 2017). For example, groundwater input has been demonstrated to increase meiofauna diversity (Encarnação et al., 2015) and the abundance and body size of Mediterranean mussels (Piló et al., 2018) in Olhos de Agua beach in Portugal, and enhance species richness, abundance and biomass of fishes and invertebrates in Japanese coastal waters, where high groundwater-borne nutrient concentrations have been reported (Hata et al., 2016; Utsunomiya et al., 2017). Conversely, groundwater discharge reduces coral species diversity in coastal systems due to lower salinity (Lirman et al., 2003; Amato et al., 2016). While some studies document the effect of groundwater discharge on primary producers in coastal ecosystems (e.g., Herrera-Silveira, 1998; Charette et al., 2001; Andrisoa et al., 2019), the impact of groundwater discharge on the growth of animals such as mussels and fish species remains largely unstudied (Hata et al., 2016; Piló et al., 2018).

In this study, we assess the effects of groundwater discharge on the growth of the Mediterranean mussel (*Mytilus galloprovincialis*), which is a commercially important species in the Mediterranean region. Typical for bivalves, mussels sequentially deposit new shell layers during their growth. The shell growth patterns are controlled by both environmental and physiological factors such as temperature, salinity, food availability, tides, day/night cycles and biological clocks (Evans, 1972; Richardson, 1988; Jones et al., 1989; Sato, 1997; Schöne et al., 2004). We here investigate the variations in growth rate and condition index (tissue dry weight/shell dry weight) of mussels growing in the groundwater-fed Salses-Leucate lagoon (France) and examine the role of environmental parameters in mussel growth in this natural environment.

MATERIALS AND METHODS

Study Sites

Salses-Leucate lagoon is located on the southwestern French Mediterranean coast. The region experiences rainfall during fall and spring (500 mm per year) with little rain during summer, and is characterized by strong northwesterly winds, regularly exceeding 10 m s^{-1}, which play an important role in the hydrodynamics of the lagoon (e.g., Stieglitz et al., 2013; Rodellas et al., 2018).

Groundwater discharges directly into the lagoon from two karstic springs, Font Estramar and Font Dame, with mean water flows of 3.0×10^5 m^3 d^{-1} and 2.0×10^5 m^3 d^{-1}, respectively (Fleury et al., 2007; **Figure 1**). The lagoon is permanently connected with the Mediterranean Sea by three large artificial openings in the eastern part of the lagoon, through which lagoon water efficiently exchanges on a continuous basis. A recent study showed that nutrient inputs driven by the discharge of the two karstic springs are the main source of nitrogen for primary producers in the western basin (Andrisoa et al., 2019). A few small intermittent streams deliver freshwater to the lagoon from the catchment area only during high-rainfall periods.

Installation of Mussel Cages and Monitoring of Environmental Parameters

Three different locations in the western basin of Salses-Leucate lagoon were selected to evaluate the influence of groundwater inputs on mussel growth: two groundwater-influenced sites, located close to the karstic springs of Font Dame and Font Estramar, respectively, and a control site (Port Fitou) far from the groundwater sources and representative for average lagoon conditions (**Figure 1**). At each location, thirty to sixty (naturally present) specimens of Mediterranean mussels

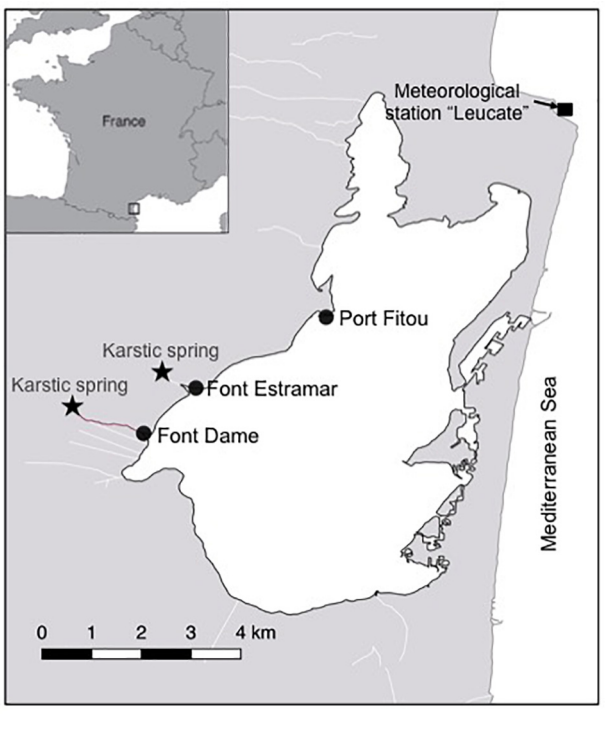

FIGURE 1 | Salses-Leucate lagoon location on the French Mediterranean coastline. The groundwater-influenced sites (Font Dame and Font Estramar) and control site (Port Fitou) are shown, as well as the groundwater springs and the meteorological station.

M. galloprovincialis were collected on 10 October 2016 at Font Dame and Font Estramar sites and 17 February 2017 at Port Fitou (**Table 1**). The initially selected lagoon control sites (i.e., deep cages) were not appropriate due to large salinity variability, requiring a new control site (Port Fitou) installed only 4 month after the beginning of the experiments. New specimens were collected on 27 June 2017 at Font Dame sites but not at Font Estramar sites. Shell length of each individual was measured and specimens were immersed in a calcein solution of 150 mg/L for 1 h. The fluorescent marker calcein is incorporated into growing calcium carbonate structures (Moran, 2000), and used for identification and measurement of growth of various calcifying species (Mahé et al., 2010; Lartaud et al., 2013; Nedoncelle et al., 2013). Sodium bicarbonate (105 g) was added to the solution to adjust the pH to 8.2 and to enhance the solubility of calcein. After shell marking, the calcein-marked mussels were returned to their original location by placing them in cages (25 × 12 cm). At a mean water depth of ca. 70 cm at both Font Dame and Font Estramar sites, cages were installed at 50 cm (surface cage) and 20 cm (bottom cage) above the bottom, experiencing different conditions in the periodically stratified water column due to fresh groundwater inflow. One cage was installed at Port Fitou (vertical homogeneity of the water column). As the mussels were returned to their respective original habitat, it is reasonable to assume that they tolerate the environmental conditions and that growth is not affected by the experimental setup. The calcein-marked mussels were periodically sampled from the cages between November 2016 and January 2018 (**Table 1**).

CTD loggers (Solinst LTC Levelogger and NKE S2T600) were installed with all the mussel cages at the three sites to monitor temperature, salinity, and water level variations. Water level was corrected for atmospheric pressure. Loggers were protected with copper mesh to avoid biofouling of the sensors, and were regularly cleaned (once every 1–2 months). Precipitation, wind and atmospheric pressure data at the nearby meteorological station "Leucate" were extracted from the French meteorological service (Météo France).

Sample Preparation

In the laboratory, mussel samples were cleaned to remove all epibionts and other attached organisms. The shell total length was measured along the maximum growth axis using a caliper. The shells were carefully opened and tissues removed. The shell and the flesh of each individual were dried at 60°C overnight and weighted separately.

For the sclerochronological analysis, the right valve of each shell was cut along the maximum growth axis and perpendicular to the growth lines with a Buehler Isomet low-speed saw, using a 0.3 mm thick diamond wafering blade (**Figure 2a**). The section was mounted on a glass slide using Epoxy Araldite 2020 resin (**Figure 2b**). A thin section (0.8 mm) of shell was cut along the maximum growth axis, ground with 80, 180, 400, and 800 *SiC* grit, polished with 3, 1 and 0.3 μm Al_2O_3 powder and rinsed with deionized water following the protocol in Nedoncelle et al. (2013). In order to resolve growth patterns in the shells (**Figure 2c**), polished sections were etched in a Mutvei's solution composed of 500 mL 1% acetic acid, 500 mL 25% glutaraldehyde, and 5 g alcian blue powder for 1 h at 37–40°C (Schöne et al., 2005a) (**Figure 2d**). Etched samples were immediately rinsed with deionized water and dried.

Condition Index

The condition index (C.I.) is defined as the ratio between the flesh (tissue) dry weight and the shell dry weight (Eq. 1). This index is commonly used to assess the health and the quality of

TABLE 1 | The shell length mean (Mean ± SD) and range (Min–Max), and the number (*n*) of mussels installed/collected from the cages with collection date from the different stations in Salses-Leucate lagoon: FDS: Font Dame Surface, FDD: Font Dame Deep, FES: Font Estramar Surface, FED: Font Estramar Deep, and PF: Port Fitou.

	Date	FDS	FDD	FES	FED	PF
Installation	10/10/2016	49 ± 16 (21–78, *n* = 30)	58 ± 8 (43–79, *n* = 29)	51 ± 11 (22–67, *n* = 40)	38 ± 6 (22–52, *n* = 76)	
	17/02/2017	–	–	–	–	58 ± 6 (46–78, *n* = 33)
	27/06/2017	40 ± 11 (20–82, *n* = 63)	46 ± 10 (29–80, *n* = 30)	–	–	–
Collection	24/11/2016	59 ± 10 (49–77, *n* = 6)	66 ± 11 (55–82, *n* = 5)	56 ± 4 (51–61, *n* = 5)	47 ± 3 (44–51, *n* = 6)	–
	14/01/2017	63 ± 7 (54–74, *n* = 6)	63 ± 6 (53–71, *n* = 7)	56 ± 11 (27–69, *n* = 10)	39 ± 3 (36–42, *n* = 10)	–
	27/03/2017	59 ± 7 (52–70, *n* = 5)	61 ± 5 (53–67, *n* = 6)	56 ± 4 (51–60, *n* = 6)	44 ± 3 (41–49, *n* = 7)	63 ± 8 (57–77, *n* = 7)
	27/06/2017	52 ± 10 (38–68, *n* = 15)	–	–	–	65 ± 7 (56–70, *n* = 10)
	29/11/2017	54 ± 13 (37–82, *n* = 15)	57 ± 13 (49–81, *n* = 8)	–	–	63 ± 4 (57–67, *n* = 5)
	29/01/2018	43 ± 4 (38–50, *n* = 10)	53 ± 10 (39–66, *n* = 5)	–	–	60 ± 11 (46–79, *n* = 10)

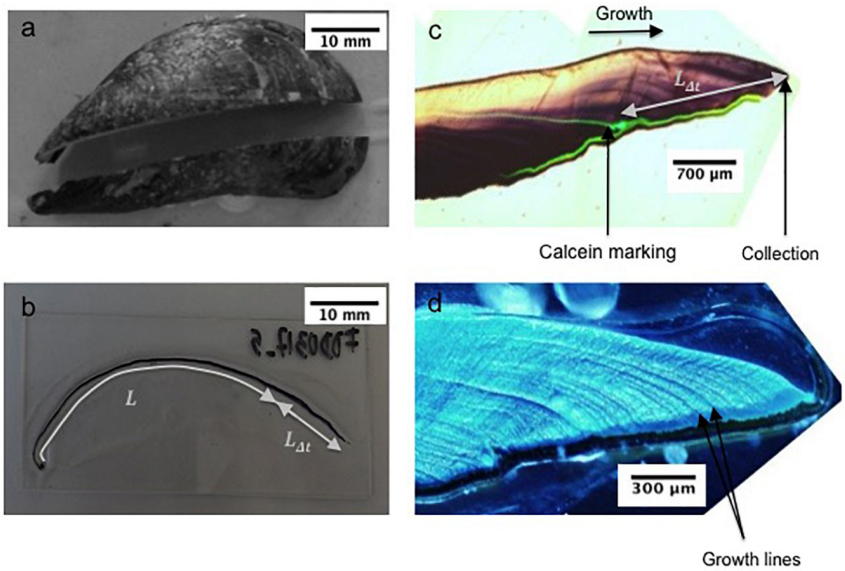

FIGURE 2 | (a) Mussel section along the maximum growth axis, **(b)** section mounted on glass slide showing the shell length ($L_t = L + L_{\Delta t}$), **(c)** shell under natural light showing the calcein marking, and **(d)** the shell under fluorescent light showing growth increments.

the mussel for scientific and commercial purposes (Lucas and Beninger, 1985; Yildiz et al., 2006; Peharda et al., 2007). It is particularly important in quality assessment and marketing value of bivalves – the higher the proportion of tissue, the better the commercial value (Župan and Šarić, 2014).

$$C.I. = \frac{Tissue\ dry\ weight}{Shell\ dry\ weight}\ x\ 100 \quad (1)$$

Growth Analyses

In order to identify the growth lines marked with calcein, the cross-sections (on the glass slide) were viewed under epifluorescent microscope at magnification 4X (OLYMPUS BX61) and digitized with an OLYMPUS DP 72 camera at the Observatoire Oceanologique de Banyuls-sur-Mer, France (BIOPIC platform). Mutvei-treated sections were analyzed under reflecting light using the same microscope and camera. Growth analyses were carried out on mounted photographs using image processing software Adobe Photoshop and Image J. The distance between the calcein mark and the ventral edge of the shell ($L_{\Delta t}$) was measured to allow an estimation of the growth rate during the period held in the cages (**Figure 2c**). The number of growth increments was counted to estimate the growth periodicity. The width of growth increments was measured to assess the relation between growth and environmental parameters. In some cases, the growth pattern was not well revealed by the Mutvei etching, which may lead to an underestimation of growth increments and an overestimation of the increment width (Nedoncelle et al., 2013). We focused our analysis on the shells with clear growth increments. The periodicities in shell growth were estimated by Fast Fourier Transform (FFT) (Welch, 1967; Walker, 1996).

Growth Curves

The growth rate of individual mussels was modeled using the Von Bertalanffy growth equation as described in Nedoncelle et al. (2013):

$$L_t = L_\infty(1 - exp^{[-K(t-t_0)]}) \quad (2)$$

where L_t is the shell total length (mm), measured along the maximal growth axis (**Figure 2b**); L_∞ is the asymptotic theoretical shell length (mm); K represents the growth coefficient (year^{-1}); and t_0 is the time constant obtained from the minimum size at mussel settlement (L_0) (L_0 and t_0 are assumed to be zero in our calculations; Ramón et al., 2007). For each individual, L_t was measured and the shell portion $L_{\Delta t}$ determined from the distance between the calcein mark and the ventral edge of the shell (**Figure 2b**).

The linear regression between the total shell length (L_t) and L allows to define the Ford-Walford y-intercept a and regression slope b used to calculate the Von Bertalanffy parameters K and L_∞ (Nedoncelle et al., 2013):

$$L_t = a + b^*L \quad (3)$$

$$K = -\ln(b)/\Delta t \quad (4)$$

$$L_\infty = a/(1-b) \quad (5)$$

The growths of mussels from different sites were compared using commonly used indices of growth performance: the phi-prime index (φ') and the index P, calculated from the Von Bertalanffy growth parameters K and L_∞ (e.g., Brey, 1999; Ragonese et al., 2012):

$$\varphi' = \log_{10}(K) + 2^*\log_{10}(L_\infty) \quad (6)$$

$$P = \log_{10}(K^*L_\infty) \quad (7)$$

Statistical Analyses

Data normality and homogeneity of variances were tested with Shapiro–Wilk and Levene's tests, respectively. All statistical analyses were considered at $\alpha = 0.05$ level. Analysis of Variance (one-way ANOVA) was used to assess the differences in condition indices between sites Font Dame Surface, Font Dame Deep, Font Estramar Surface, Font Estramar Deep and Port Fitou. We used *t*-test statistics to determine if there were significant differences in condition indices, growth rates, salinity and water temperature between groundwater-influenced sites (Font Dame Surface, Font Dame Deep, Font Estramar Surface, Font Estramar Deep, which were pooled together for this comparison) and the control site (Port Fitou). The differences between surface cages (Font Dame Surface and Font Estramar Surface) and bottom cages (Font Dame Deep and Font Estramar Deep) were also tested using *t*-test statistics.

RESULTS

Condition Index

The average condition indices estimated from the sampled mussels during the study period were 8.8 ± 2.3% (n = 50) at Font Dame Surface, 9.9 ± 2.3% (n = 26) at Font Dame Deep, 9.5 ± 3.3% (n = 20) at Font Estramar Surface, 8.8 ± 2.2% (n = 23) at Font Estramar Deep and 5.8 ± 1.4% (n = 30) at Port Fitou. The condition index varied significantly between sites (ANOVA: $F = 5.32$, $p < 0.05$) with significantly higher indices at the groundwater-influenced sites over the control site (*t*-test: $t = 5.93$, $p < 0.05$) (**Figure 3A**).

Shell Growth Rate

The mean growth rates for sampled mussels were 48.2 ± 6.0 μm d^{-1} (n = 31) at Font Dame Surface, 32.8 ± 5.0 μm d^{-1} (n = 17) at Font Dame Deep, 38.8 ± 7.7 μm d^{-1} (n = 13) at Font Estramar Surface, 36.4 ± 5.0 μm d^{-1} (n = 13) at Font Estramar Deep and 27.7 ± 2.5 μm d^{-1} (n = 8) at Port Fitou (**Figure 3B**). Similar to the condition index, the growth rate of mussels from the groundwater-influenced sites (mean = 40.9 ± 9.2 μm d^{-1}) was significantly higher than that of the control site (27.7 ± 2.5 μm d^{-1}) (*t*-test: $t = 5.24$, $p < 0.05$). At the groundwater-influenced sites (Font Dame and Font Estramar), the growth rates were significantly higher for the mussels from the surface than those from the bottom (*t*-test: $t = 3.97$, $p < 0.05$) with the highest rate observed at Font Dame Surface.

Growth Curves

The Von Bertalanffy growth curves derived from *M. galloprovincialis* collected in Salses-Leucate lagoon at the groundwater-influenced sites (combined data from Font Dame Surface, Font Dame Deep, Font Estramar Surface and Font Estramar Deep; n = 79, size range = 26.5–81.5 mm) and at the control site (n = 11, size range = 56.0–68.0 mm) are presented in **Figure 4**, together with curves obtained for the same species growing at other coastal Mediterranean sites. Overall, the growth rates of *M. galloprovincialis* from Salses-Leucate lagoon (groundwater-influenced sites: $K = 0.54$, $L_\infty = 75.0$ mm; control site: $K = 0.46$, $L_\infty = 63.9$ mm) are among the highest reported for this species in the Mediterranean region, particularly for the groundwater-influenced sites (**Table 2**; **Figure 4**). As commonly observed, the results indicated a fast growth rate at a younger age and a decrease in growth rates as the shell approaches its maximum size (**Figure 4**). Individuals collected from the groundwater-influenced sites showed higher total growth rates than individual from the control site. For instance, after 3 years, mussels from the groundwater-influenced sites reached 60 mm while those from the control site reached only 48 mm. Furthermore, the growth performance indices at the groundwater influenced sites ($\varphi' = 3.48$, $P = 1.61$) and the control site ($\varphi' = 3.27$, $P = 1.47$) were also among the highest reported to date for this species in the Mediterranean region (**Table 2**).

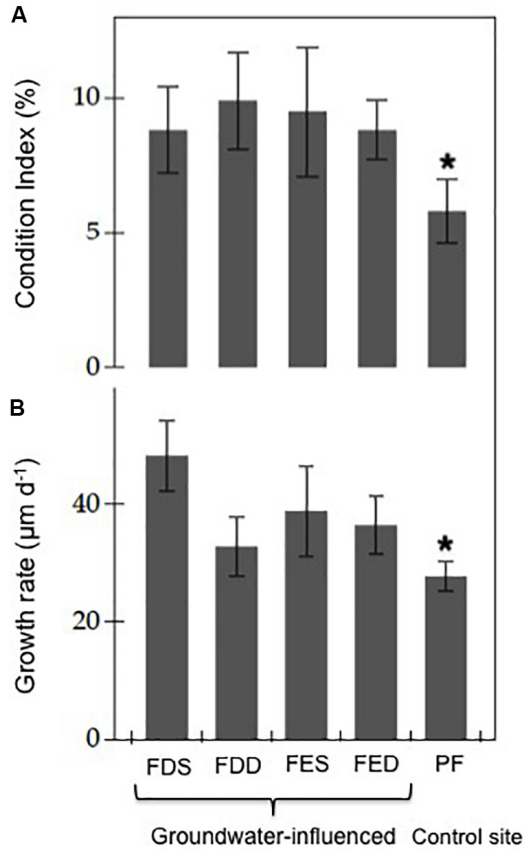

FIGURE 3 | (A) Mean (±SD) condition indices and **(B)** growth rate in groundwater-influenced sites (FDS: Font Dame Surface, FDD: Font Dame Deep, FES: Font Estramar Surface and FED: Font Estramar Deep) and the control site (PF: Port Fitou) in Salses-Leucate lagoon. The asterisk indicates that p is less than 0.05 for the Student's *t*-test between groundwater-influenced sites and control site (condition index: groundwater influenced-sites n = 119, control site n = 30, *t*-test, $t = 5.93$, $p < 0.05$; growth rate: groundwater influenced-sites n = 74, control site n = 8, *t*-test, $t = 5.24$, $p < 0.05$).

TABLE 2 | The Von Bertalanffy growth parameters and the growth performance indices values of *M. galloprovincialis* from this study and other coastal systems in the Mediterranean region.

References	Sites	K	L_∞ (mm)	φ'	P
This study	GW-influenced sites	0.54	75.0	3.48	1.61
	Control site	0.46	63.9	3.27	1.47
Posa and Tursi, 1991	Semi-enclosed basin, Italy	0.09	62.1	2.54	0.75
	Coastal basin, Italy	0.10	58.7	2.54	0.77
Sarà et al., 2012	Coastal bay, Italy	0.03	51.3	1.90	0.19
Ramón et al., 2007	Coastal bay, Spain	0.76	85.0	3.74	1.81
Ceccherelli and Rossi, 1984	Coastal lagoon, Italy	0.66	85.9	3.69	1.75
Abada-Boujemaa, 1996	Coastal area, Algeria	0.31	64.0	3.10	1.30

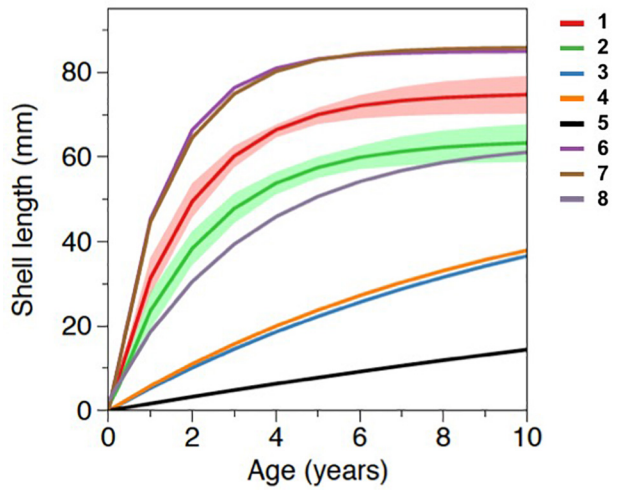

FIGURE 4 | Von Bertalanffy growth curves of *Mytilus galloprovincialis* from the groundwater-influenced sites and the control site in Salses-Leucate lagoon and from other coastal systems in the Mediterranean region with **1**: groundwater-influenced sites in this study (K = 0.54, L_∞ = 75.0); **2**: control site in this study (K = 0.46, L_∞ = 63.9); **3**: semi-enclosed basin in Italy (K = 0.09, L_∞ = 62.1, Posa and Tursi, 1991); **4**: coastal basin in Italy (K = 0.10, L_∞ = 58.7, Posa and Tursi, 1991); **5**: coastal bay in Italy (K = 0.03, L_∞ = 51.3, Sarà et al., 2012); **6**: coastal bay in Spain (K = 0.76, L_∞ = 85.0, Ramón et al., 2007), **7**: coastal lagoon in Italy (K = 0.66, L_∞ = 85.9, Ceccherelli and Rossi, 1984), and **8**: coastal area in Algeria (K = 0.31, L_∞ = 64.0, Abada-Boujemaa, 1996). Shaded areas represent the standard deviations of data obtained in the present study.

Growth Increments

Mussels growing in Salses-Leucate lagoon formed growth increment with daily (circadian) rhythm. Among the shells showing clear growth pattern, the average number of increments were 0.9 ± 0.2 (n = 17), 0.7 ± 0.1 (n = 15), 0.8 ± 0.2 (n = 9), 0.8 ± 0.1 (n = 9), and 0.7 ± 0.1 (n = 6) per day in Font Dame Surface, Font Dame Deep, Font Estramar Surface, Font Estramar Deep and Port Fitou, respectively. For instance, a mussel collected at Font Estramar Surface formed 93 growth increments during 96 days. The number of increments was consistently lower than the number of days.

Sclerochronological profiles showed a large variability in increment width for a given shell. The periodicities in increments width were estimated by FFT analyses. The analyzed shells exhibited similar patterns and, as an example, three shells (one each site) are presented in **Figure 5**. The FFT analyses revealed peaks at low frequency corresponding to periodicities of 12.7, 11.2, and 11.3 increments for the shells S1 (FDS0118-3), S2 (FDD0118-4), and S3 (PF0118-3), respectively. Considering the near-daily rhythm of the growth increment, the peaks correspond thus to a period of 11–13 days (near-fortnightly period). The power spectrum for the three shells also showed peaks at high frequencies corresponding to the periods of approximately 3 and 5 days.

Environmental Parameters

Time Series Variations

The daily precipitation in Salses-Leucate lagoon ranged between 0.0 and 70.2 mm with a maximum value recorded shortly after the calcein marking (13 October 2016) (**Figure 6a**). High rainfall events coincided overall with high wind events and occurred chiefly between January and April. The region is characterized by frequent strong winds generally blowing from the northwest. Southeasterly winds also arrive from the Mediterranean Sea but they are less frequent. The wind speed recorded varied between 1.6 and 18.0 m s^{-1} with an average value of 5.8 ± 2.8 m s^{-1} (**Figure 6b**).

Lagoon water levels at Font Dame, Font Estramar and Port Fitou showed similar patterns. They are principally controlled by precipitations as well as winds (Ladagnous and Le Bec, 1997). The water level generally increased with increasing precipitation and wind speed (**Figure 6c**). The average water levels were 0.7 ± 0.1, 0.8 ± 0.2, and 1.0 ± 0.1 m in Font Dame, Font Estramar and Port Fitou, respectively, indicating that the installed cages (at 0.2 and 0.5 m from the sediment-water interface) were rarely exposed.

The water temperature showed overall similar patterns at the study sites with seasonal minimum values observed in winter and maximum values in summer overlaid by daily variations (**Figure 6d**). From February 2017 to January 2018 (data available at all sites), the water temperatures were significantly higher at groundwater-influenced sites (mean values in FDS = 18.1 ± 5.1, FDD = 18.1 ± 6.0, FES = 20.5 ± 4.8, and FED = 20.1 ± 5.1°C) than at Port Fitou (mean = 17.3 ± 6.7°C) (t-test: t = 2.34, $p < 0.05$). Furthermore, for the total period of data collection (October 2016 – January 2018), the water temperatures were significantly higher at the surface (FDS = 16.7 ± 5.1°C; FES = 16.5 ± 5.5°C) than at the bottom (FDD = 16.5 ± 5.5°C; FED = 15.8 ± 5.9°C) (t-test: t = 1.38, $p < 0.05$).

The salinity was highly variable at the groundwater-influenced sites (Font Dame and Font Estramar) and no clear pattern was observed (**Figure 6e**), with salinity ranges of 9.0–35.8 (FDS), 7.4–44.4 (FDD), 10.2–36.8 (FES), and 10.0–40.7 (FED). In contrast, salinity in Port Fitou was relatively stable with seasonal values ranging between 26.2 and 41.8, showing small daily variations and a seasonal pattern with maximum values

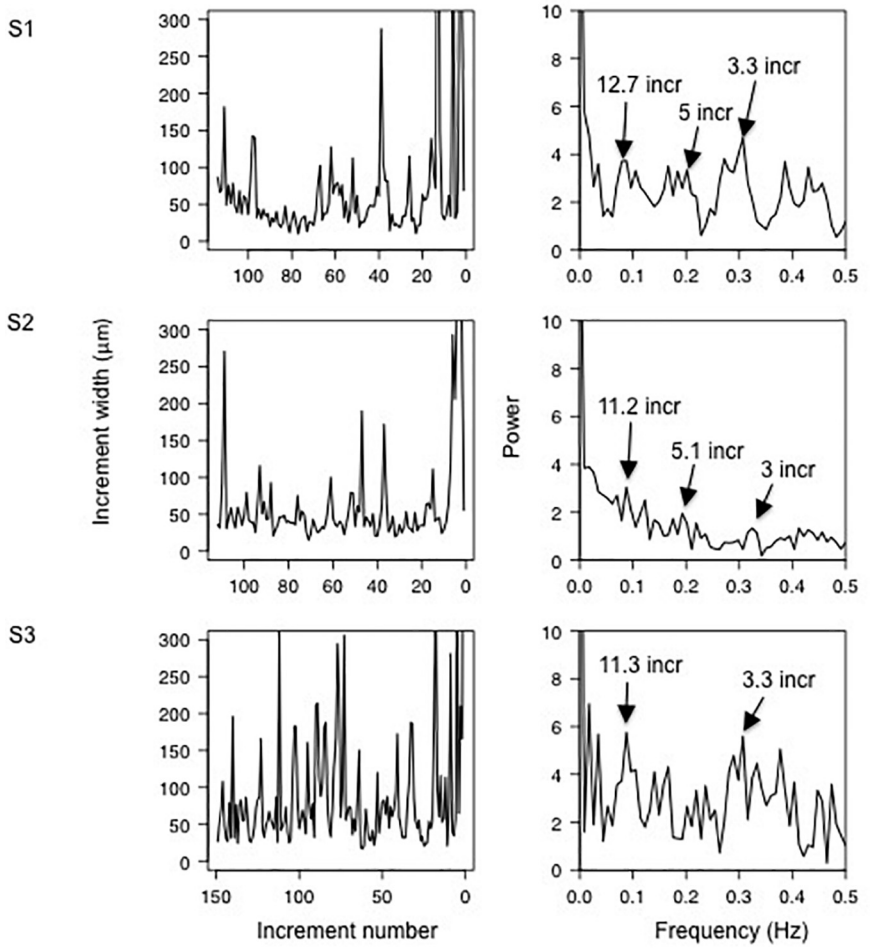

FIGURE 5 | (Left panel) increment number from the calcein mark **(right side)** to the collection **(left side)** for three representative *Mytilus galloprovincialis* shells S1 (FDS0118-3), S2 (FDD0118-4), and S3 (PF0118-3) between June 2017 and January 2018. **(Right panel)** Fast Fourier Transform showing the periodicities of the increment width.

recorded at the end of summer (consistent with an increase of evaporation and a decrease of freshwater inputs). The salinity at Port Fitou was overall considerably higher than that observed at the groundwater-influenced sites, reflecting average lagoon conditions (t-test: $t = 37.95$, $p < 0.05$).

Spectral Analyses

At both groundwater-influenced sites, spectral analyses of parameters in bottom and surface waters showed similar patterns and periodicities, and thus here we present surface water data only. The FFT analyses of the temperature data showed overall well-defined peaks centered at 12 h, 1 and 13 days for surface waters at the three study sites (Font Dame, Font Estramar, and Port Fitou) except for Font Estramar at the low frequency (**Figures 7A–C**). For salinity, peaks were also observed at 12 h, 1 and 13 days for the site Font Dame while no clear peaks were observed at Font Estramar and Port Fitou (**Figures 7D–F**). Periodicities of 12 h and 11 days were exhibited for the water depth at Font Dame and Port Fitou while at Font Estramar the water depth followed periodicities of 12 and 24 h (**Figures 7G–I**). The FFT analyses for the wind speed showed clear peaks at 1 and 2.6 days (**Figure 7J**).

DISCUSSION

Periodicity in Shell Growth and Environmental Influences

The growth increment count demonstrates that *M. galloprovincialis* in Salses-Leucate lagoon forms growth increment on a near-daily basis (circadian rhythm). Generally, growth patterns reported in mytilid species refer rather to tidal cycles (Langton, 1977; Richardson, 1989; Buschbaum and Saier, 2001; Zaldibar et al., 2004) and circa-tidal periodicity has been observed in several bivalves (Pannella and Macclintock, 1968; Evans, 1972; Richardson, 1988; Schöne et al., 2003; Miyaji et al., 2007; Connor and Gracey, 2011). For instance, Richardson (1989) showed that *M. edulis* growing under tidally submerged conditions exhibits a clearly defined growth pattern coinciding

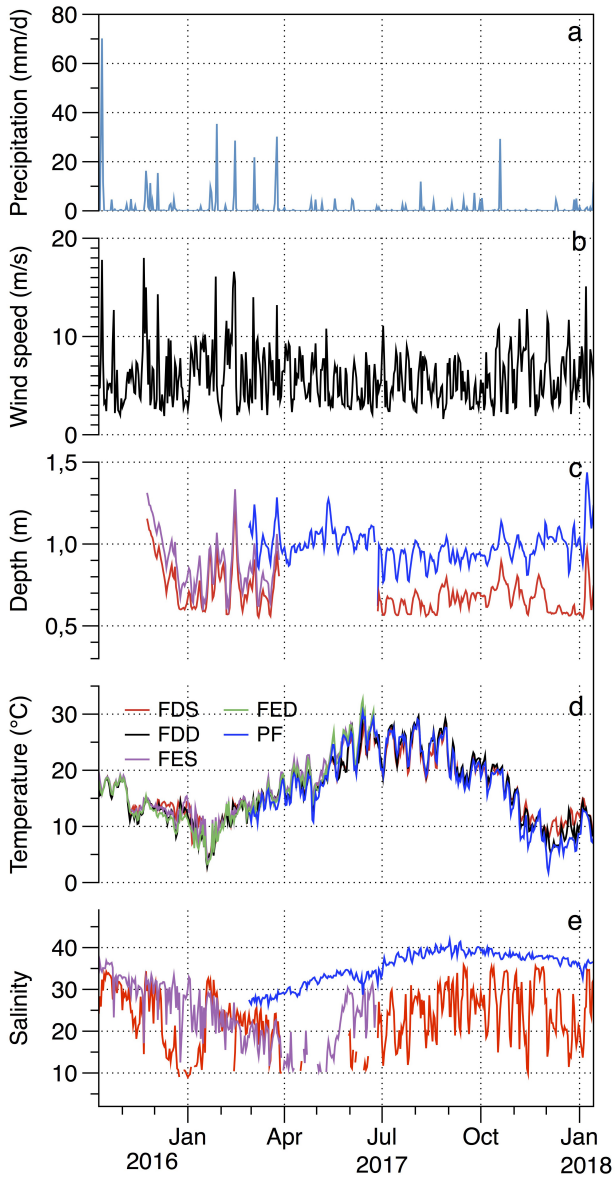

FIGURE 6 | Temporal variations between October 2016 and January 2018 in **(a)** precipitation, **(b)** wind speed, **(c)** water depth, **(d)** temperature, and **(e)** salinity in Salses-Leucate lagoon: Font Dame Surface (FDS), Font Dame Deep (FDD), Font Estramar Surface (FES), Font Estramar Deep (FED), and Port Fitou (PF). The salinity data shows large variability and presents similar seasonal pattern for surface and bottom cages. For clarity, we present the surface water salinity only.

with the number of emersions. In Salses-Leucate lagoon, tidal variations are relatively small (<0.05 m) as a consequence of the small tidal cycles in the Mediterranean Sea and the restricted exchange between the lagoon and sea, and thus tidal cycles have a negligible influence on mussel growth patterns. The circadian rhythm observed in mussels from Salses-Leucate lagoon has been reported in other bivalve mollusks (Pannella and Macclintock, 1968; Richardson, 1988; Parsons et al., 1993; Chauvaud et al., 2005), and is often related to cycles governed by biological clocks (Pittendrigh and Daan, 1976; Schöne, 2008; Connor and Gracey, 2011). The biology of most organisms is closely related to the changes in their environmental conditions, which often present clear daily patterns of, mainly, temperature and light. As a consequence, bivalves and other organisms have developed behavioral and physiological daily patterns (Connor and Gracey, 2011). As commonly observed in coastal environments, temperature, salinity, water depth, and wind speed variations in Salses-Leucate lagoon exhibit daily periodicity, suggesting that these environmental factors contribute to the daily pattern of mussel growth in the lagoon.

Although the growth pattern is oriented toward a daily pattern, the number of growth increments counted in the shell was generally slightly lower than the number of days, suggesting that either growth halts during some part of the study period or that the growth pattern was not well revealed by the Mutvei etching, resulting in a potential underestimation of the number of growth increments (Nedoncelle et al., 2013). Similar observations have been reported previously for *Arctica islandica* (Witbaard et al., 1994; Schöne et al., 2005b), *Pecten maximus* (Chauvaud et al., 2005), and *Phacosoma japonicum* (Tanabe, 2007). They observed that the number of growth increment formed during a limited interval of time is (sometimes significantly) lower than the number of days (or tides) at the study sites. Winter growth cessation is indeed common in bivalves (Jones and Quitmyer, 1996; Tanabe, 2007; Okaniwa et al., 2010), because the production of shell carbonate ceases below species-specific growth temperature thresholds. For instance, *Margaritifera margaritifera* in northern Sweden stops producing shell carbonate below 5°C (Schöne, 2008) while *M. galloprovincialis* from Tokyo Bay, Japan, stops growing or barely grows for water temperature between 8 and 14°C (Okaniwa et al., 2010). Growth cessation may also occur all year round as a result of an abrupt change in the environmental conditions due to strong wind events, drop in salinity and/or phytoplankton bloom (due to toxicity or clogging of the gill system) (Page and Hubbard, 1987; Chauvaud et al., 1998; Schöne, 2008; Okaniwa et al., 2010). The observed discrepancy in days and growth increments in this study is small in comparison to those observed at many other sites, likely due to the comparatively stable environmental conditions in the lagoon, but nevertheless suggests that the conditions temporarily cause either a complete cessation of growth during specific days or a desynchronization in the circadian rhythm of growth increment deposition (Chauvaud et al., 2005).

Aside from the (near-) daily cycles, the spectral analysis of the increment width shows spectral peaks at frequencies corresponding to periods of 11–13 days (**Figure 5**) The temperature, salinity and water depth patterns also exhibit periodicity of approximately 11–13 days, suggesting a spring-neap cycle influence on the growth of *M. galloprovincialis* in Salses-Leucate lagoon. Tidal patterns in (non-lagoonal) bivalves are widespread and are expressed by thin increments altering with groups of relatively thick ones, forming periodic pattern of 13–14 days, corresponding to the fortnightly spring-neap tide cycles (Evans, 1972; Richardson, 1989; Miyaji et al., 2007), and suggested to be related to valve activity and/or current velocity

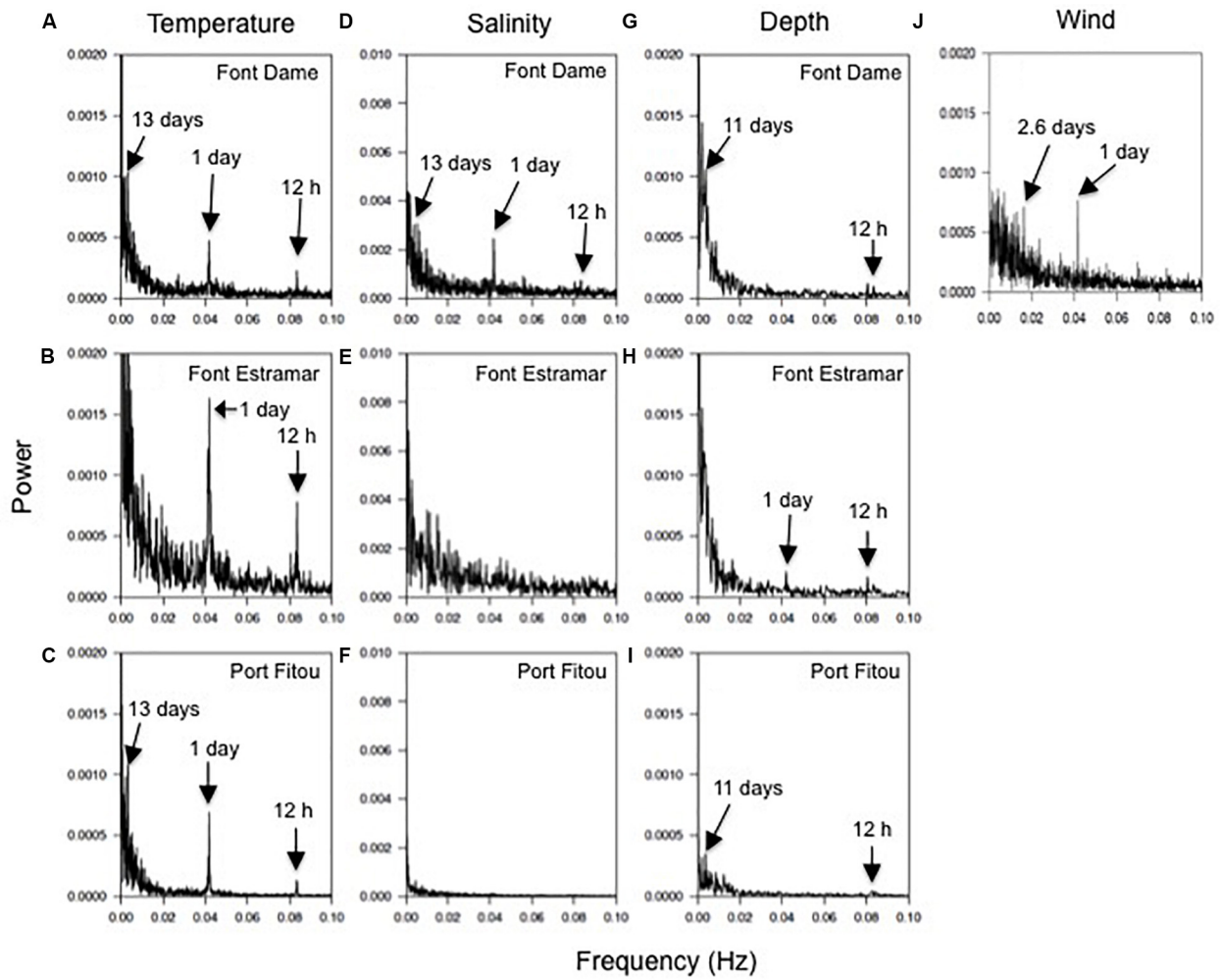

FIGURE 7 | (A–C) Fast Fourier Transformations of the temperature, **(D–F)** salinity and **(G–I)** water depth at Font Dame (FD), Font Estramar (FE) and Port Fitou (PF), and **(J)** the wind speed at the study. Arrows indicate peaks of the power spectrum.

changes modifying the food availability (Clark, 2005; Lartaud et al., 2010; Tran et al., 2011). Whilst spring-neap cycles can affect groundwater discharge rate in tidal systems (e.g., Kim and Hwang, 2002; Taniguchi et al., 2002; Sieyes et al., 2008), this is unlikely the case in Salses-Leucate lagoon due to the quasi-negligible tidal amplitude. However, spring-neap cycles are likely affecting the exchange between the lagoon and the Mediterranean Sea (Sylaios et al., 2006), and may therefore play a role in controlling the temperature, salinity, water depth and eventually the nutrient supply in Salses-Leucate lagoon.

The origin of the periodicity of approximately 3 and 5 days in the increment growth remains uncertain (**Figure 5**). It may be related to frequent wind events, which show a periodicity of 2.6 days (close to the 3–5 days periodicities of the growth increments), and thus drive the circulation within the lagoon and exchange with the sea, thereby controlling environmental factors in the lagoon (**Figure 6**). For instance, southeasterly winds favor the input of seawater in the lagoon while northwesterly winds reduce its input. Furthermore, wind-driven circulation of lagoon water through sediments is recognized as an important source of nutrient in coastal lagoons (Rodellas et al., 2018). This "wind-driven" nutrient supply may increase phytoplankton abundance, which in turn may control mussel growth, albeit with a small temporal lag governed by primary production timescales.

Growth of *M. galloprovincialis* in the Mediterranean Region

The Von Bertalanffy curves show that the growth rates of *M. galloprovincialis* from Salses-Leucate lagoon are among the highest rates recorded for this species in the Mediterranean region (**Figure 4**). This clearly indicates that Salses-Leucate lagoon is well suitable for the growth of *M. galloprovincialis*. The time required to grow to a length of 30 mm (ca. 1 year) is significantly shorter than that reported for the same species from the coastal bay of Mare Grande and the semi-enclosed basin of Mare Piccolo (Italy) of approximately 7 years (Posa and Tursi, 1991) or longer in the Gulf of Castellammare (Sarà et al., 2012).

The growth rates of *M. galloprovincialis* observed in this study (particularly from the groundwater-influenced sites) are only a little below those reported from the coastal lagoon of Sacca di Scardovari on the Adriatic coast (Ceccherelli and Rossi, 1984) and Fangar Bay in Spain (Ramón et al., 2007). The Sacca di Scardovari lagoon and Fangar Bay are both located at the mouth of big rivers (Po River and Ebro River, respectively), and thus these areas are likely receiving nutrient inputs from rivers. Moreover, these areas are well known for agricultural activities, which may also be a relevant source of nutrients (Busch, 2013; Di Giuseppe et al., 2014). Despite the seasonal variations in water temperature in Salses-Leucate lagoon, the water temperature ranges (Median = 16.0°C, Q1 = 12.3°C and Q3 = 20.4°C) includes the optimal temperature range for growth of *M. galloprovincialis* (17–20°C) (Blanchette et al., 2007).

Role of Groundwater Discharge

Mytilus galloprovincialis at the groundwater influenced sites shows higher growth rate and condition index compared to that of the control site, suggesting that groundwater influenced sites are favorable for their growth (**Figures 3**, **4**). Three compounding effects of groundwater inputs to coastal areas can explain the differences between mussel growth at groundwater-influenced and non-influenced sites, i.e., groundwater-driven variations in (i) temperature, (ii) nutrient availability, and (iii) salinity.

(i) Despite the seasonal variations of water temperature in the lagoon (**Figure 6d**), the average water temperature at the groundwater-influenced sites is significantly higher than the temperature at the control site. Since temperatures in groundwater sources are relatively constant throughout the year (17–19°C), groundwater inputs in winter (when lagoon waters temperatures "elsewhere" are below 10°C) produce an increase of lagoon water temperatures at the groundwater-influenced sites. The higher growth rate and condition index observed at the groundwater-influenced sites may thus (at least in part) be related to this groundwater-driven increase in temperature (Schöne et al., 2002, 2005b).

(ii) In addition to water temperature, food availability is a major factor controlling shell growth and condition indices. Bivalve growth increases with increasing phytoplankton abundance (Page and Hubbard, 1987; Sato, 1997), with food availability controlling 64–70% of the variation in growth of *M. galloprovincialis* (His et al., 1989). Sato (1997) demonstrated that growth of bivalve *Phacosoma japonica* in Ariake Bay (Japan) is also primarily influenced by food availability. High phytoplankton abundance has been directly linked to groundwater input in several costal systems worldwide (Valiela et al., 1990; McClelland et al., 1997; Herrera-Silveira, 1998). A recent study demonstrates that groundwater discharge from Font Dame and Font Estramar sustains primary production of the lagoon investigated here (Andrisoa et al., 2019). Indeed, the concentrations of particulate organic nitrogen in Salses-Leucate lagoon [which is dominated by phytoplankton in this lagoon (Carlier et al., 2009)], are higher in groundwater-influenced sites (62 ± 40 μg N L^{-1}) than in the control site (52.8 ± 21.9 μg N L^{-1}) (A. Andrisoa, unpublished data). The high nutrient concentrations driven by groundwater inputs likely favor phytoplankton growth at the groundwater-influenced sites, which is readily available for mussel growth at these sites.

(iii) Groundwater from Font Dame and Font Estramar discharges substantial amounts of freshwater into Salses-Leucate lagoon, considerably affecting the salinity at the groundwater-influenced sites. Salinity is one of the dominant environmental factors controlling growth. Generally, *M. galloprovincialis* exhibits highest growth at salinity 35 (His et al., 1989). Typical responses of mussels to lower salinity include reduced feeding activity, slower growth and valve closure (Navarro, 1988; Riisgård et al., 2012). For example, due to low salinities in the Baltic Sea (salinity between 6 and 8 in the northern part), mussels are dwarfed in this area (Kautsky, 1982; Vuorinen et al., 2002). Similarly, Riisgård et al. (2012) showed that mussels growing at salinity 10 have slower growth rates than those growing at salinity 30. However, acclimation to reduced salinities may take place, and mussels are able to adjust growth at changing salinities (Davenport, 1979; Qiu et al., 2002). The higher mussel growth rates measured at the groundwater-influenced sites despite lower salinity suggest that mussels growing there are either acclimated to low salinity environments or that salinity has a less important effect on mussel growth compared to temperature and food availability in this lagoonal environment. Also note that salinity at the groundwater-influenced sites is highly variable (**Figure 6e**), which may cause stress to the animals. Many bivalves can tolerate small changes in salinity, but salinity outside their acceptable range may negatively affect their growth (Peteiro et al., 2018).

It should be noted that due to sampling constraints (see section Materials and Methods), specimens from different sites were not sampled for exactly the same periods. This could have implications for our results since both growth rates and condition indices highly reflect species reproductive dynamics. Growth rates and condition indices are generally lower during the resting phase (usually from November to February) and higher during gonad maturation and ripening (from April to October) (e.g., Karayücel and Ye, 2010; Vural et al., 2015). Mussels from Font Dame and Port Fitou were studied throughout almost a year, thus covering the different phases of the reproductive cycle, therefore the comparison between groundwater-influenced and control sites must be considered robust. However, specimens from Font Estramar site were monitored from October 2016 to late March 2017 only, and therefore biased toward winter months. Considering the expected lower growth rates in winter periods, the results obtained from the groundwater-influenced site Font Estramar are likely an underestimation of mussel growth rate and condition index in the annual cycle. Further, mussels at the control site Port Fitou were naturally present in a narrower range size than at the groundwater sites, potentially biasing the results. A transplantation of specimen from other

sites to cover the same size distribution would likely have introduced an unknown, potentially large bias. Despite these experimental limitations, mussel growth rates and condition indices at groundwater influenced sites are significantly higher than those estimated at control site.

The growth rates of mussels in the upper (shallower) cages are slightly higher than those of bottom cages (**Figure 3B**). Despite the shallow water depth (≈0.8 m), the water column at the groundwater-influenced sites is generally stratified (except during wind events). The upper cages are relatively more influenced by lower-density groundwater inputs (mean salinity FDS = 21.8 ± 7.1; FES = 24.3 ± 7.0) in comparison to the bottom cages (mean salinity FDD = 27.6 ± 6.5; FED = 27.2 ± 6.1). Thus, temperatures and nutrient concentrations are expected to be higher in surface waters than in bottom waters as a consequence of groundwater inputs, favoring mussel growth rates in the upper cages. The high light availability and temperatures driven by direct solar radiation in surface waters may also favor phytoplankton and thus mussel growth. Higher growth rate of mussels in surface waters than in deeper layers has previously been reported and attributed either to differences in temperature (Fuentes et al., 2000) or the high availability of phytoplankton (Page and Hubbard, 1987). In addition, the lower growth rates observed in the bottom cages may partially result from siltation. Sediment resuspension occurs often in the study area due to frequent wind events and may explain in part the difference in growth observed between upper and lower cages. Silts and clay can clog the gills of mussels, interfere with filter feeding and affect indirectly by reducing light availability for phytoplankton, inhibiting the growth of bivalves (Bricelj et al., 1984; Box and Mossa, 1999).

Economic Implications

The Mediterranean mussel (*M. galloprovincialis*) is a highly valuable commercial species. The world production of mussels from aquaculture reach an annual value of 1.2 million tons corresponding to an economic value of over 500 million United States dollars (Okumuş et al., 2014). About 80.000 tons are produced annually in France (Župan and Šarić, 2014), and in Thau lagoon (a neighboring site on the French Mediterranean coast), annual mussel production is estimated at 5.400 tons (Gangnery et al., 2004). In particular the competitive price compared to other bivalves makes mussels a sought after seafood (Orban et al., 2002). However, in recent years, the production of mussel is leveling off due to reduced number of suitable coastal sites for high productivity mussel farming, as consequences of human activities (Cataudella et al., 2015). The results of this study clearly show that coastal sites influenced by groundwater inputs represent ideal environments for mussel growth (and thus potential mussel farming), resulting in higher growth rates (1.5 cm yr^{-1}) and condition index. Higher condition index indicates high quality of a marketed product, i.e., better health status and fatness, especially during the periods of gonad maturation and ripening. Mussel aquaculture is traditionally placed in coastal waters with large primary productivity (e.g., Peharda et al., 2007). Results from this study suggest that groundwater-influenced sites can offer environmental conditions well suited for mussel aquaculture, and therefore, it may be economically profitable to farm mussels in groundwater-influenced areas.

CONCLUSION

M. galloprovincialis in Salses-Leucate lagoon produce circadian (daily rhythm) shell growth increments and have amongst the highest growth rates to date reported for the Mediterranean region. In Salses-Leucate lagoon, mussels from groundwater-influenced sites have higher growth rate and condition index compared to those from a control site (chiefly influenced by seawater), demonstrating that groundwater inflows are favorable for mussel growth. Groundwater discharging to coastal areas is characterized by relatively constant temperatures and is an important source of nutrients, providing thus significant food resources to filter feeders like mussels. This study indicates that higher temperature and food availability associated with groundwater inputs may explain the fast growth rate of *M. galloprovincialis* at groundwater-influenced sites in Salses-Leucate lagoon, and thus provides direct evidence for the "downstream" ecological impacts of groundwater discharge on this commercially important species.

Identifying suitable sites for profitable production is a considerable challenge in mussel aquaculture. Groundwater-influenced sites are suitable sites for mussel farming, particularly in oligotrophic waters like the Mediterranean Sea. In addition to its increasingly recognized ecological role, this study suggests that groundwater inputs to coastal areas can have non-negligible economic effects on fisheries products in coastal socio-ecosystems.

ETHICS STATEMENT

In this work invertebrates (mussels) are investigated. No ethics approval is required or available for this work in France.

AUTHOR CONTRIBUTIONS

TS conceived and led the study. FL, AA, and TS designed the experiments. IN and VR contributed to laboratory and field work, respectively. All authors contributed to the manuscript writing.

FUNDING

This research was supported by the French National Research Agency (ANR) through ANR @RAction chair medLOC (ANR-14-ACHN-0007-01 – project leader TS). AA was partially supported by Labex OT-Med (ANR-11-LABEX-0061), and VR acknowledges support from the European Union's Horizon 2020 Research and Innovation Program under the Marie Skłodowska-Curie Grant Agreement No 748896.

ACKNOWLEDGMENTS

We thank Michel and Henry Comte (Salses-le-Château), L. Fonbonne (Rivage Leucate), R de Wit (MARBEC Montpellier), A. Fiandrino, M. David, and D. Munaron (IFREMER Sete), V. Bailly Comte (BRGM Montpellier), and P. Cook (Flinders University) for sharing their expert knowledge on regional lagoon and groundwater processes. The community from "Le domaine de Pedros" facilitated access to Fitou. We acknowledge the facilities of Biology platform of imaging and cytometry (BioPIC) from Banyuls Oceanographical Observatory, and thank the reviewers for their thorough and constructive comments on the manuscript.

REFERENCES

Abada-Boujemaa, Y. M. (1996). *Cinétique, Croissance, Production et Composition Biochimique des deux bivalves Mytilidés: Perna perna* (.) et *Mytilus galloprovincialis (Lmk) du Littoral Algérois*. France: Muséum National d'Histoire Naturelle.

Aliaume, C., Do Chi, T., Viaroli, P., and Zaldívar, J. M. (2007). Coastal lagoons of Southern Europe: recent changes and future scenarios. *Trans. Waters Monogr.* 1, 1–12.

Amato, D. W., Bishop, J. M., Glenn, C. R., Dulai, H., and Smith, C. M. (2016). Impact of submarine groundwater discharge on marine water quality and Reef Biota of Maui. *PLoS One* 11:e0165825. doi: 10.1371/journal.pone.0165825

Andrisoa, A., Stieglitz, T. C., Rodellas, V., and Raimbault, P. (2019). Primary production in coastal lagoons supported by groundwater discharge and porewater fluxes inferred from nitrogen and carbon isotope signatures. *Mar. Chem.* 210, 48–60. doi: 10.1016/j.marchem.2019.03.003

Anthony, A., Atwood, J., August, P., Byron, C., Cobb, S., Foster, C., et al. (2009). Coastal lagoons and climate change: ecological and social ramifications in US Atlantic and Gulf coast ecosystems. *Ecol. Soc.* 14:8.

Basterretxea, G., Tovar-Sanchez, A., Beck, A. J., Masqué, P., Bokuniewicz, H. J., Coffey, R., et al. (2010). Submarine groundwater discharge to the coastal environment of a Mediterranean island (Majorca, Spain): ecosystem and biogeochemical significance. *Ecosystems* 13, 629–643. doi: 10.1007/s10021-010-9334-5

Bianchi, T., Allison, M., and Cai, W.-J. (2014). *Biogeochemical Dynamics at Major River-Coastal Interfaces: Linkages with Global Change*. Cambridge: Cambridge University Press.

Blanchette, C. A., Helmuth, B., and Gaines, S. D. (2007). Spatial patterns of growth in the mussel, *Mytilus californianus*, across a major oceanographic and biogeographic boundary at Point Conception, California, USA. *J. Exp. Mar. Biol. Ecol.* 340, 126–148. doi: 10.1016/j.jembe.2006.09.022

Box, J. B., and Mossa, J. (1999). Sediment, land use, and freshwater mussels: prospects and problems. *J. North Am. Benthol. Soc.* 18, 99–117. doi: 10.2307/1468011

Brey, T. (1999). Growth performance and mortality in aquatic macrobenthic invertebrates. *Adv. Mar. Biol.* 35, 153–243.

Bricelj, V. M., Malouf, R. E., and de Quillfeldt, C. (1984). Growth of juvenile *Mercenaria mercenaria* and the effect of resuspended bottom sediments. *Mar. Biol.* 84, 167–173. doi: 10.1007/BF00393001

Busch, J. A. (2013). *Phytoplankton Dynamics and Bio-Optical Variables Associated with Harmful Algal Blooms in Aquaculture Zones*. PhD thesis, Bremen University.

Buschbaum, C., and Saier, B. (2001). Growth of the mussel *Mytilus edulis* L. in the Wadden Sea affected by tidal emergence and barnacle epibionts. *J. Sea Res.* 45, 27–36. doi: 10.1016/S1385-1101(00)00061-7

Carlier, A., Riera, P., Amouroux, J., Bodiou, J., Desmalades, M., and Grémare, A. (2009). Spatial heterogeneity in the food web of a heavily modified Mediterranean coastal lagoon: stable isotope evidence. *Aquat. Biol.* 5, 167–179. doi: 10.3354/ab00147

Cataudella, S., Crosetti, D., Massa, F., General Fisheries Commission for the Mediterranean Food and Agriculture Organization of the United Nations, and Food and Agriculture Organization of the United Nations, (2015). *Mediterranean Coastal Lagoons: Sustainable Management and Interactions Among Aquaculture, Capture Fisheries and the Environment*. Rome: Food abd Agriculture Organization of the United Nations.

Ceccherelli, V. U., and Rossi, R. (1984). Settlement, growth and production of the mussel *Mytilus galloprovincialis*. *Mar. Ecol. Prog. Ser.* 16, 173–184. doi: 10.3354/Meps016173

Charette, M. A., Buesseler, K. O., and Andrews, J. E. (2001). Utility of radium isotopes for evaluating the input and transport of groundwater-derived nitrogen to a Cape Cod estuary. *Limnol. Oceanogr.* 46, 465–470. doi: 10.4319/lo.2001.46.2.0465

Chauvaud, L., Lorrain, A., Dunbar, R. B., Paulet, Y.-M., Thouzeau, G., Jean, F., et al. (2005). Shell of the Great Scallop *Pecten maximus* as a high-frequency archive of paleoenvironmental changes: GREAT SCALLOP *Pecten maximus*. *Geochem. Geophys. Geosystems* 6, 1–15. doi: 10.1029/2004GC000890

Chauvaud, L., Thouzeau, G., and Paulet, Y.-M. (1998). Effects of environmental factors on the daily growth rate of *Pecten maximus* juveniles in the Bay of Brest (France). *J. Exp. Mar. Biol. Ecol.* 227, 83–111. doi: 10.1016/S0022-0981(97)00263-3

Clark, G. R. (2005). Daily growth lines in some living Pectens (Mollusca: Bivalvia), and some applications in a fossil relative: time and tide will tell. *Palaeogeogr. Palaeoclimatol. Palaeoecol.* 228, 26–42. doi: 10.1016/j.palaeo.2005.03.044

Cloern, J. E., Foster, S. Q., and Kleckner, A. E. (2014). Phytoplankton primary production in the world's estuarine-coastal ecosystems. *Biogeosciences* 11:25. doi: 10.5194/bg-11-2477-2014

Connor, K. M., and Gracey, A. Y. (2011). Circadian cycles are the dominant transcriptional rhythm in the intertidal mussel *Mytilus californianus*. *Proc. Natl. Acad. Sci. U.S.A.* 108, 16110–16115. doi: 10.1073/pnas.1111076108

Davenport, J. (1979). The isolation response of mussels (*Mytilus edulis* L.) exposed to falling sea-water concentrations. *J. Mar. Biol. Assoc. U. K.* 59, 123–132. doi: 10.1017/S0025315400043423

De Wit, R., Leibreich, J., Vernier, F., Delmas, F., Beuffe, H., Maison, , Ph, et al. (2005). Relationship between land-use in the agro-forestry system of les Landes, nitrogen loading to and risk of macro-algal blooming in the Bassin d'Arcachon coastal lagoon (SW France). *Estuar. Coast. Shelf Sci.* 62, 453–465. doi: 10.1016/j.ecss.2004.09.007

Di Giuseppe, D., Bianchini, G., Vittori Antisari, L., Martucci, A., Natali, C., and Beccaluva, L. (2014). Geochemical characterization and biomonitoring of reclaimed soils in the Po River Delta (Northern Italy): implications for the agricultural activities. *Environ. Monit. Assess.* 186, 2925–2940. doi: 10.1007/s10661-013-3590-8

Encarnação, J., Leitão, F., Range, P., Piló, D., Chícharo, M. A., and Chícharo, L. (2015). Local and temporal variations in near-shore macrobenthic communities associated with submarine groundwater discharges. *Mar. Ecol.* 36, 926–941. doi: 10.1111/maec.12186

Evans, J. W. (1972). Tidal Growth Increments in the Cockle *Clinocardium nuttalli*. *Science* 176, 416–417. doi: 10.1126/science.176.4033.416

Fleury, P., Bakalowicz, M., and de Marsily, G. (2007). Submarine springs and coastal karst aquifers: a review. *J. Hydrol.* 339, 79–92. doi: 10.1016/j.jhydrol.2007.03.009

Fuentes, J., Gregorio, V., Giráldez, R., and Molares, J. (2000). Within-raft variability of the growth rate of mussels, *Mytilus galloprovincialis*, cultivated in the Ría de Arousa (NW Spain). *Aquaculture* 189, 39–52. doi: 10.1016/s0044-8486(00)00357-4

Gangnery, A., Bacher, C., and Buestel, D. (2004). Application of a population dynamics model to the Mediterranean mussel, *Mytilus galloprovincialis*, reared in Thau Lagoon (France). *Aquaculture* 229, 289–313. doi: 10.1016/S0044-8486(03)00360-0

Hata, M., Sugimoto, R., Hori, M., Tomiyama, T., and Shoji, J. (2016). Occurrence, distribution and prey items of juvenile marbled sole *Pseudopleuronectes yokohamae* around a submarine groundwater seepage on a tidal flat in southwestern Japan. *J. Sea Res.* 111, 47–53. doi: 10.1016/j.seares.2016.01.009

Herrera-Silveira, J. A. (1998). Nutrient-phytoplankton production relationships in a groundwater-influenced tropical coastal lagoon. *Aquat. Ecosyst. Health Manag.* 1, 373–385. doi: 10.1016/s1463-4988(98)00015-3

His, E., Robert, R., and Dinet, A. (1989). Combined effects of temperature and salinity on fed and starved larvae of the mediterranean mussel *Mytilus galloprovincialis* and the Japanese oyster *Crassostrea gigas*. *Mar. Biol.* 100, 455–463. doi: 10.1007/BF00394822

Jones, D. S., Arthur, M. A., and Allard, D. J. (1989). Sclerochronological records of temperature and growth from shells of *Mercenaria mercenaria* from Narragansett Bay. *Rhode Island. Mar. Biol.* 102, 225–234. doi: 10.1007/bf00428284

Jones, D. S., and Quitmyer, I. R. (1996). Marking time with bivalve shells: oxygen isotopes and season of annual increment formation. *PALAIOS* 11, 340–346. doi: 10.2307/3515244

Karayücel, S., and Ye, M. (2010). Growth and production of raft cultivated mediterranean mussel (*Mytilus galloprovincialis* Lamarck, 1819) in Sinop, Black Sea. *Turk. J. Fish. Aqua. Sci.* 10, 09–17.

Kautsky, N. (1982). Growth and size structure in a baltic *Mytilus edulis* population. *Mar. Biol.* 68, 117–133. doi: 10.1007/BF00397599

Kim, G., and Hwang, D.-W. (2002). Tidal pumping of groundwater into the coastal ocean revealed from submarine 222Rn and CH4 monitoring. *Geophys. Res. Lett.* 29, 23–21. doi: 10.1029/2002GL015093

Kjerfve, B. (1994). *Coastal Lagoon Processes*. Amsterdam: Elsevier.

Ladagnous, H., and Le Bec, C. (1997). *Lagune de Salses-Leucate. I-Analyse bibliographique*. Available at: https://archimer.ifremer.fr/doc/00073/18422/.

Langton, R. W. (1977). Digestive rhythms in the mussel *Mytilus edulis*. *Mar. Biol.* 41, 53–58. doi: 10.1007/BF00390581

Lartaud, F., Chauvaud, L., Richard, J., Toulot, A., Bollinger, C., Testut, L., et al. (2010). Experimental growth pattern calibration of Antarctic scallop shells (*Adamussium colbecki,* Smith 1902) to provide a biogenic archive of high-resolution records of environmental and climatic changes. *J. Exp. Mar. Biol. Ecol.* 393, 158–167. doi: 10.1016/j.jembe.2010.07.016

Lartaud, F., Pareige, S., de Rafelis, M., Feuillassier, L., Bideau, M., Peru, E., et al. (2013). A new approach for assessing cold-water coral growth in situ using fluorescent calcein staining. *Aquat. Living Resour.* 26, 187–196. doi: 10.1051/alr/2012029

Lee, E., Shin, D., Hyun, S. P., Ko, K.-S., Moon, H. S., Koh, D.-C., et al. (2017). Periodic change in coastal microbial community structure associated with submarine groundwater discharge and tidal fluctuation. *Limnol. Oceanogr.* 62, 437–451. doi: 10.1002/lno.10433

Lirman, D., Orlando, B., Maciá, S., Manzello, D., Kaufman, L., Biber, P., et al. (2003). Coral communities of Biscayne Bay, Florida and adjacent offshore areas: diversity, abundance, distribution, and environmental correlates. *Aquat. Conserv. Mar. Freshw. Ecosyst.* 13, 121–135. doi: 10.1002/aqc.552

Liu, K.-K., Atkinson, L., Quiñones, R., and Talaue-McManus, L. (eds) (2010). *Carbon and Nutrient Fluxes in Continental Margins*. Berlin: Springer.

Lucas, A., and Beninger, P. G. (1985). The use of physiological condition indices in marine bivalve aquaculture. *Aquaculture* 44, 187–200. doi: 10.1016/0044-8486(85)90243-1

Mahé, K., Bellamy, E., Lartaud, F., and de Rafélis, M. (2010). Calcein and manganese experiments for marking the shell of the common cockle (*Cerastoderma edule*): tidal rhythm validation of increments formation. *Aquat. Living Resour.* 23, 239–245. doi: 10.1051/alr/2010025

McClelland, J. W., Valiela, I., and Michener, R. H. (1997). Nitrogen-stable isotope signatures in estuarine food webs: a record of increasing urbanization in coastal watersheds. *Limnol. Oceanogr.* 42, 930–937. doi: 10.4319/lo.1997.42.5.0930

Middelburg, J., and Nieuwenhuize, J. (2001). Nitrogen isotope tracing of dissolved inorganic nitrogen behaviour in tidal estuaries. *Estuar. Coast. Shelf Sci.* 53, 385–391. doi: 10.1006/ecss.2001.0805

Miyaji, T., Tanabe, K., and Schöne, B. R. (2007). Environmental controls on daily shell growth of *Phacosoma japonicum* (Bivalvia: Veneridae) from Japan. *Mar. Ecol. Prog. Ser.* 336, 141–150. doi: 10.3354/meps336141

Moore, W. S. (2010). The effect of submarine groundwater discharge on the ocean. *Annu. Rev. Mar. Sci.* 2, 59–88. doi: 10.1146/annurev-marine-120308-081019

Moran, A. L. (2000). Calcein as a marker in experimental studies newly-hatched gastropods. *Mar. Biol.* 137, 893–898. doi: 10.1007/s002270000390

Navarro, J. M. (1988). The effects of salinity on the physiological ecology of *Choromytilus chorus* (Molina, 1782)(Bivalvia: Mytilidae). *J. Exp. Mar. Biol. Ecol.* 122, 19–33. doi: 10.1016/0022-0981(88)90209-2

Nedoncelle, K., Lartaud, F., de Rafelis, M., Boulila, S., and Le Bris, N. (2013). A new method for high-resolution bivalve growth rate studies in hydrothermal environments. *Mar. Biol.* 160, 1427–1439. doi: 10.1007/s00227-013-2195-7

Newton, A., Icely, J., Cristina, S., Ana, B., Ana Cristina, C., Franciscus, C., et al. (2014). An overview of ecological status, vulnerability and future perspectives of European large shallow, semi-enclosed coastal systems, lagoons and transitional waters. *Estuar. Coast. Shelf Sci.* 140, 95–122. doi: 10.1016/j.ecss.2013.05.023

Null, K. A., Dimova, N. T., Knee, K. L., Esser, B. K., Swarzenski, P. W., Singleton, M. J., et al. (2012). Submarine groundwater discharge-derived nutrient loads to san francisco bay: implications to future ecosystem changes. *Estuar. Coast.* 35, 1299–1315. doi: 10.1007/s12237-012-9526-7

Okaniwa, N., Miyaji, T., Sasaki, T., and Tanabe, K. (2010). Shell growth and reproductive cycle of the Mediterranean mussel *Mytilus galloprovincialis* in Tokyo Bay, Japan: relationship with environmental conditions. *Plankton Benthos Res.* 5, 214–220. doi: 10.3800/pbr.5.214

Okumuş, Ý, Başçinar, N., and Özkan, M. (2014). The effects of phytoplankton concentration, size of mussel and water temperature on feed consumption and filtration rate of the mediterranean mussel (*Mytilus galloprovincialis* Lmk). *Turk. J. Zool.* 26, 167–172.

Orban, E., Di Lena, G., Nevigato, T., Casini, I., Marzetti, A., and Caproni, R. (2002). Seasonal changes in meat content, condition index and chemical composition of mussels (*Mytilus galloprovincialis*) cultured in two different Italian sites. *Food Chem.* 77, 57–65. doi: 10.1016/s0308-8146(01)00322-3

Page, H. M., and Hubbard, D. M. (1987). Temporal and spatial patterns of growth in mussels Mytilus edulis on an offshore platform: relationships to water temperature and food availability. *J. Exp. Mar. Biol. Ecol.* 111, 159–179. doi: 10.1016/0022-0981(87)90053-0

Pannella, G., and Macclintock, C. (1968). Biological and environmental rhythms reflected in molluscan shell growth. *J. Paleontol.* 42, 64–80. doi: 10.1017/S0022336000061655

Parsons, G. J., Robinson, S. M. C., Roff, J. C., and Dadswell, M. J. (1993). Daily growth rates as indicated by valve ridges in postlarval giant scallop (*Placopecten magellanicus*) (Bivalvia: Pectinidae). *Can. J. Fish. Aquat. Sci.* 50, 456–464. doi: 10.1139/f93-053

Peharda, M., Župan, I., Bavčević, L., Frankić, A., and Klanjšček, T. (2007). Growth and condition index of mussel *Mytilus galloprovincialis* in experimental integrated aquaculture. *Aquac. Res.* 38, 1714–1720. doi: 10.1111/j.1365-2109.2007.01840.x

Peteiro, L. G., Woodin, S. A., Wethey, D. S., Costas-Costas, D., Martínez-Casal, A., Olabarria, C., et al. (2018). Responses to salinity stress in bivalves: evidence of ontogenetic changes in energetic physiology on Cerastoderma edule. *Sci. Rep.* 8:8329. doi: 10.1038/s41598-018-26706-9

Piló, D., Barbosa, A. B., Teodósio, M. A., Encarnação, J., Leitão, F., Range, P., et al. (2018). Are submarine groundwater discharges affecting the structure and physiological status of rocky intertidal communities? *Mar. Environ. Res.* 136, 158–173. doi: 10.1016/j.marenvres.2018.02.013

Pittendrigh, C. S., and Daan, S. (1976). A functional analysis of circadian pacemakers in nocturnal rodents. *J. Comp. Physiol.* 106, 333–355. doi: 10.1007/BF01417860

Posa, D., and Tursi, A. (1991). Growth Models of *Mytilus galloprovincialis* lamarck on the mar grande and on the mar Piccolo of Taranto (Southern Italy). *Stat. Appl.* 3, 135–143.

Qiu, J.-W., Tremblay, R., and Bourget, E. (2002). Ontogenetic changes in hyposaline tolerance in the mussels *Mytilus edulis* and *M. trossulus*: implications for distribution. *Mar. Ecol. Prog. Ser.* 228, 143–152. doi: 10.3354/meps228143

Ragonese, S., Vitale, S., Mazzola, S., Pagliarino, E., and Bianchini, M. L. (2012). Behavior of some growth performance indexes for exploited Mediterranean hake. *Acta Adriat. Int. J. Mar. Sci.* 53, 105–123.

Ramón, M., Fernández, M., and Galimany, E. (2007). Development of mussel (*Mytilus galloprovincialis*) seed from two different origins in a semi-enclosed Mediterranean Bay (N.E. Spain). *Aquaculture* 264, 148–159. doi: 10.1016/j.aquaculture.2006.11.014

Richardson, C. A. (1988). Tidally produced growth bands in the subtidal bivalve *Spisula Subtruncata* (Da Costa). *J. Molluscan Stud.* 54, 71–82. doi: 10.1093/mollus/54.1.71

Richardson, C. A. (1989). An analysis of the microgrowth bands in the shell of the common mussel *Mytilus Edulis*. *J. Mar. Biol. Assoc. U. K.* 69, 477–491. doi: 10.1017/S0025315400029544

Riera, R., Tuset, V. M., Betancur, R.-R., Lombarte, A., Marcos, C., and Pérez-Ruzafa, A. (2018). Modelling alpha-diversities of coastal lagoon fish assemblages from the Mediterranean Sea. *Prog. Oceanogr.* 165, 100–109. doi: 10.1016/j.pocean.2018.05.003

Riisgård, H. U., Bøttiger, L., and Pleissner, D. (2012). Effect of salinity on growth of mussels, *Mytilus edulis*, with special reference to great belt (Denmark). *Open J. Mar. Sci.* 02:167. doi: 10.4236/ojms.2012.24020

Rodellas, V., Garcia-Orellana, J., Masqué, P., Feldman, M., and Weinstein, Y. (2015). Submarine groundwater discharge as a major source of nutrients to the Mediterranean Sea. *Proc. Natl. Acad. Sci.* 112, 3926–3930. doi: 10.1073/pnas.1419049112

Rodellas, V., Stieglitz, T. C., Andrisoa, A., Cook, P. G., Raimbault, P., Tamborski, J. J., et al. (2018). Groundwater-driven nutrient inputs to coastal lagoons: the relevance of lagoon water recirculation as a conveyor of dissolved nutrients. *Sci. Total Environ.* 642, 764–780. doi: 10.1016/j.scitotenv.2018.06.095

Sarà, G., Reid, G. K., Rinaldi, A., Palmeri, V., Troell, M. A. L. M., and Kooijman, S. (2012). Growth and reproductive simulation of candidate shellfish species at fish cages in the Southern Mediterranean: dynamic Energy Budget (DEB) modelling for integrated multi-trophic aquaculture. *Aquaculture* 32, 259–266. doi: 10.1016/j.aquaculture.2011.10.042

Sato, S. (1997). Shell microgrowth patterns of bivalves reflecting seasonal change in phytoplankton abundance. *Paleontol. Res.* 1, 260–266.

Schöne, B., Tanabe, K., Dettman, D., and Sato, S. (2003). Environmental controls on shell growth rates and δ18O of the shallow-marine bivalve mollusk Phacosoma japonicum in Japan. *Mar. Biol.* 142, 473–485. doi: 10.1007/s00227-002-0970-y

Schöne, B. R. (2008). The curse of physiology—challenges and opportunities in the interpretation of geochemical data from mollusk shells. *Geo-Mar. Lett.* 28, 269–285. doi: 10.1007/s00367-008-0114-6

Schöne, B. R., Dunca, E., Fiebig, J., and Pfeiffer, M. (2005a). Mutvei's solution: an ideal agent for resolving microgrowth structures of biogenic carbonates. *Palaeogeogr. Palaeoclimatol. Palaeoecol.* 228, 149–166. doi: 10.1016/j.palaeo.2005.03.054

Schöne, B. R., Houk, S. D., FreyreCastro, A. D., Fiebig, J., Oschmann, W., Kroncke, I., et al. (2005b). Daily Growth Rates in Shells of *Arctica islandica*: assessing sub-seasonal environmental controls on a long-lived Bivalve Mollusk. *PALAIOS* 20, 78–92. doi: 10.2110/palo.2003.p03-101

Schöne, B. R., Freyre Castro, A. D., Fiebig, J., Houk, S. D., Oschmann, W., and Kröncke, I. (2004). Sea surface water temperatures over the period 1884–1983 reconstructed from oxygen isotope ratios of a bivalve mollusk shell (Arctica islandica, southern North Sea). *Palaeogeogr. Palaeoclimatol. Palaeoecol.* 212, 215–232. doi: 10.1016/j.palaeo.2004.05.024

Schöne, B. R., Goodwin, D. H., Flessa, K. W., Dettman, D. L., and Roopnarine, P. D. (2002). Sclerochronology and growth of the bivalve mollusks Chione (Chionista) fluctifraga and C. (Chionista) cortezi in the northern Gulf of California. *Mexico. Veliger* 45, 45–54.

Short, F. T., and Burdick, D. M. (1996). Quantifying eelgrass habitat loss in relation to housing development and nitrogen loading in Waquoit Bay. *Massachusetts. Estuar.* 19, 730–739. doi: 10.2307/1352532

Sieyes, N. R., de Yamahara, K. M., Layton, B. A., Joyce, E. H., and Boehm, A. B. (2008). Submarine discharge of nutrient-enriched fresh groundwater at Stinson Beach, California is enhanced during neap tides. *Limnol. Oceanogr.* 53, 1434–1445. doi: 10.4319/lo.2008.53.4.1434

Slomp, C. P., and Van Cappellen, P. (2004). Nutrient inputs to the coastal ocean through submarine groundwater discharge: controls and potential impact. *J. Hydrol.* 295, 64–86. doi: 10.1016/j.jhydrol.2004.02.018

Stieglitz, T. C., van Beek, P., Souhaut, M., and Cook, P. G. (2013). Karstic groundwater discharge and seawater recirculation through sediments in shallow coastal Mediterranean lagoons, determined from water, salt and radon budgets. *Mar Chem.* 156, 73–84. doi: 10.1016/j.marchem.2013.05.005

Sylaios, G. K., Tsihrintzis, V. A., Akratos, C., and Haralambidou, K. (2006). Quantification of water, salt and nutrient exchange processes at the mouth of a Mediterranean coastal lagoon. *Environ. Monit. Assess.* 119, 275–301. doi: 10.1007/s10661-005-9026-3

Tanabe, K. (2007). Age and growth rate determinations of an intertidal bivalve, Phacosoma japonicum, using internal shell increments. *Lethaia* 21, 231–241. doi: 10.1111/j.1502-3931.1988.tb02075.x

Taniguchi, M., Burnett, W. C., Cable, J. E., and Turner, J. V. (2002). Investigation of submarine groundwater discharge. *Hydrol. Process.* 16, 2115–2129. doi: 10.1002/hyp.1145

Tovar-Sánchez, A., Basterretxea, G., Rodellas, V., Sánchez-Quiles, D., García-Orellana, J., Masqué, P., et al. (2014). Contribution of groundwater discharge to the coastal dissolved nutrients and trace metal concentrations in majorca island: karstic vs detrital systems. *Environ. Sci. Technol.* 48, 11819–11827. doi: 10.1021/es502958t

Tran, D., Nadau, A., Durrieu, G., Ciret, P., Parisot, J.-P., and Massabuau, J.-C. (2011). Field chronobiology of a molluscan bivalve: how the moon and sun cycles interact to drive oyster activity rhythms. *Chronobiol. Int.* 28, 307–317. doi: 10.3109/07420528.2011.565897

Troccoli-Ghinaglia, L., Herrera-Silveira, J. A., Comín, F. A., and Díaz-Ramos, J. R. (2010). Phytoplankton community variations in tropical coastal area affected where submarine groundwater occurs. *Cont. Shelf Res.* 30, 2082–2091. doi: 10.1016/j.csr.2010.10.009

Utsunomiya, T., Hata, M., Sugimoto, R., Hinda, H., Kobayashi, S., Miyata, J., et al. (2017). Higher species richness and abundance of fish and benthic invertebrates around submarine groundwater discharge in Obama Bay. *Japan. J. Hydrol. Reg. Stud.* 11, 139–146. doi: 10.1016/j.ejrh.2015.11.012

Valiela, I., Costa, J., Foreman, K., Teal, J. M., Howes, B., and Aubrey, D. (1990). Transport of groundwater-borne nutrients from watersheds and their effects on coastal waters. *Biogeochemistry* 10, 177–197. doi: 10.1007/bf00003143

Velasco, A. M., Pérez-Ruzafa, A., Martínez-Paz, J. M., and Marcos, C. (2018). Ecosystem services and main environmental risks in a coastal lagoon (Mar Menor, Murcia, SE Spain): the public perception. *J. Nat. Conserv.* 43, 180–189. doi: 10.1016/j.jnc.2017.11.002

Vuorinen, I., Antsulevich, A. E., and Maximovich, N. V. (2002). Spatial distribution and growth of the common mussel *Mytilus edulis* L. in the archipelago of SW-Finland, northern Baltic Sea. *Boreal Environ. Res.* 7, 41–52.

Vural, P., Yildiz, H., and Acarli, S. (2015). Growth and survival performances of Mediterranean mussel (*Mytilus galloprovincialis*, Lamarck, 1819) on different depths in Cardak lagoon, Dardanelles. *Mar. Sci. Tech. Bull.* 4, 7–12.

Walker, J. (1996). *Fast Fourier Transforms*. Boca Raton, FL: CRC Press.

Welch, P. (1967). The use of fast Fourier transform for the estimation of power spectra: a method based on time averaging over short, modified periodograms. *IEEE Trans. Audio Electroacoustics* 15, 70–73. doi: 10.1109/TAU.1967.1161901

Witbaard, R., Jenness, M. I., Van Der Borg, K., and Ganssen, G. (1994). Verification of annual growth increments in *Arctica islandica* L. from the North Sea by means of oxygen and carbon isotopes. *Neth. J. Sea Res.* 33, 91–101. doi: 10.1016/0077-7579(94)90054-X

Yildiz, H., Mustafa, P., and Musa, B. (2006). Condition indices of Mediterranean Mussels (*Mytilus galloprovincialis* L. 1819) growing on suspended ropes in Dardanelles. *J. Food Technol.* 4, 221–224.

Zaldibar, B., Cancio, I., and Marigómez, I. (2004). Circatidal variation in epithelial cell proliferation in the mussel digestive gland and stomach. *Cell Tissue Res.* 318, 395–402. doi: 10.1007/s00441-004-0960-0

Župan, I., and Šarić, T. (2014). Growth and condition index – two important factors in mussel farming. *Meso Prvi Hrvat. Èasopis O Mesu XVI* 275:259.

Conflict of Interest: The authors declare that the research was conducted in the absence of any commercial or financial relationships that could be construed as a potential conflict of interest.

frontiers in Marine Science

ORIGINAL RESEARCH
published: 21 January 2020
doi: 10.3389/fmars.2019.00809

Enhanced Productivity and Fish Abundance at a Submarine Spring in a Coastal Lagoon on Tahiti, French Polynesia

Claudia Starke[1,2]*, *Werner Ekau*[1] *and Nils Moosdorf*[1,3]

[1] Leibniz Centre for Tropical Marine Research (ZMT), Bremen, Germany, [2] Institute of Marine Ecosystem and Fishery Science (IMF), Hamburg, Germany, [3] Institute of Geosciences, University of Kiel, Kiel, Germany

Submarine groundwater discharge (SGD), the direct discharge of groundwater into the sea, is abundant around the globe. Fresh SGD can occur as focused flow in submarine springs. However, little is known on the impact of submarine springs on marine organisms. For a better understanding of the interaction between SGD and its surrounding organisms, the impact of SGD on the abundance of fish was investigated in a coastal lagoon of Tahiti, French Polynesia. The study is based on the assumption of an enhanced biological production due to increased amounts of nutrient input caused by terrestrial groundwater supply into the sea. Biofouling processes and zooplankton samples were used as indicators for elevated nutrient input due to submarine springs. The main objective was to investigate the effect on the abundance of fish assuming a higher fish abundance possibly caused by a bottom-up control. Presented data show a significantly higher abundance around a submarine spring as well as significantly larger growth of algal turfs exposed to groundwater discharge. Zooplankton evaluations suggest slightly higher abundances around the submarine spring. The results suggest elevated nutrient concentrations transmitted by submarine springs may cause a bottom-up control resulting in a higher abundance of fish around the investigated submarine spring.

Keywords: submarine groundwater discharge, *in situ* primary productivity, nutrient input, fish abundance, bottom-up control

OPEN ACCESS

Edited by:
Makoto Taniguchi, Research Institute for Humanity and Nature, Japan

Reviewed by:
Francesco Tiralongo, Ente Fauna Marina Mediterranea (EFMM), Italy
Henry Bokuniewicz, The State University of New York (SUNY), United States

***Correspondence:**
Claudia Starke
starkeclaudia82@gmail.com

Specialty section:
This article was submitted to Marine Ecosystem Ecology, a section of the journal Frontiers in Marine Science

Received: *16 January 2019*
Accepted: *16 December 2019*
Published: *21 January 2020*

Citation:
Starke C, Ekau W and Moosdorf N (2020) Enhanced Productivity and Fish Abundance at a Submarine Spring in a Coastal Lagoon on Tahiti, French Polynesia. Front. Mar. Sci. 6:809. doi: 10.3389/fmars.2019.00809

INTRODUCTION

Scientific interest in submarine groundwater discharge (SGD), the direct discharge of groundwater to the coastal waters, has strongly increased over the past years, highlighting its influence on coastal nutrient budgets (Moore, 2010; Moosdorf et al., 2015), global water budgets (Burnett et al., 2003; Kwon et al., 2014), and global biogeochemical cycles (Slomp and Van Cappellen, 2004; Cole et al., 2007; Beusen et al., 2013; Cho et al., 2018). Its effect on marine flora and fauna in turn has been studied rarely (e.g., Fujita et al., 2019; Lilkendey et al., 2019). These recent studies point towards a bottom-up influence of SGD on fish abundance and fitness.

We present a detailed photographic study of fish at a submarine spring site located in a coastal lagoon of Tahiti, French Polynesia accompanied by observations on nutrients, primary (biofouling) and secondary production (zooplankton).

Due to their location between continental and marine ecosystems, coastal lagoons are often described as boundary environments (Sarno et al., 1993). Their prevailing sedimentary deposition

in tropical zones is often characterized by the accumulation of calcium carbonate remains and calcium carbonate producing organisms (Duck and da Silva, 2012). Determined by the local climate conditions and the degree of hydrological access salinity values can alternate from freshwater to hypersaline (Kjerfve, 1986). Coastal lagoons are highly productive ecosystems with water depths that rarely exceed a few meters (Kjerfve, 1986). The coastal lagoon presented in this study (Trou de Lagon) exhibits several SGD spots of which we used two for our investigations.

Submarine groundwater discharge consists of two main fractions: recirculated seawater and terrestrial groundwater discharging into the ocean (Burnett et al., 2003). The latter, here called "fresh SGD" referring to the fresh fraction of the often brackish actual discharge, is an important pathway of terrestrial pollutants including nutrients, trace metals, pharmaceuticals, various pollutants and other terrestrial substances into the coastal ocean (Knee and Paytan, 2011). Fresh SGD can discharge diffusely, e.g., from a coarse grained coastal sediment, in a focused way from conduits (here called "submarine springs") (Slomp and Van Cappellen, 2004). Submarine springs generally influence their surrounding environment, by changing salinity, temperature, nutrient and sediment concentrations (Miller and Ullman, 2004; Oehler et al., 2018) or by creating morphological features on the sea floor (Stieglitz and Ridd, 2000). Ecological impacts of SGD were mostly derived from postulating an impact from elevated nutrient content (e.g., Johannes, 1980; Miller and Ullman, 2004; Slomp and Van Cappellen, 2004; Tait et al., 2014).

Direct impacts of terrestrial groundwater inflow through elevated nutrient concentrations was reported to enhance biological production as well as species diversity of coastal ecosystems in a limited number of studies (Lecher and Mackey, 2018). However, fishermen in many regions all over the world observe higher fish abundance around submarine springs and attribute the flourishing influence to the freshwater (Moosdorf and Oehler, 2017). This effect was scientifically confirmed only in locations in Japan reporting significantly higher abundances or biomass of fish (Utsunomiya et al., 2015; Hata et al., 2016; Shoji and Tominaga, 2018; Fujita et al., 2019). In Mauritius, a positive effect of fresh SGD on fitness of juvenile fish was observed (Lilkendey et al., 2019).

As changes in ecosystems are often based on alterations in nutrient fluxes, Johannes (1980) argued that ignoring SGD may lead to profound misinterpretation of ecological data in terms of coastal pollution, benthic zonation and productivity. His data indicated that SGD locally delivers several times more nitrate to coastal waters at the assessed location than river runoff does. This is supported by other authors, partly associated with harmful algae blooms, at various locations (e.g., Laroche et al., 1997; Paerl, 1997; Gobler and Sañudo-Wilhelmy, 2001; Smith and Swarzenski, 2012; Liu et al., 2017). Paytan et al. (2006) reported enhanced anthropogenic nutrient loads from SGD is also likely to contribute to reef degradation.

Few authors reported on nutrient fluxes delivered by SGD on marine biota. For example, macrophyte tissue reflecting δ15N of SGD showing higher nitrogen concentrations, larger leaves and blades, reduced macrophytes biodiversity and higher biomass (Kamermans et al., 2002; Umezawa et al., 2002; Lapointe et al., 2005; Amato et al., 2016). Studies lacking δ15N data but conducted in known SGD areas also show these tendencies as e.g., in the most investigated green macroalgae *Ulva*. Williams and Carpenter (1988) worked on the productivity of small micro filamentous epilithic algae, so called "algal turfs", resulting in a significantly higher primary production per unit chlorophyll-a of ammonium treated algal turfs. The bryozoan *Pentapora fascialis* also showed changes of colony growth, size, and mortality around SGD (Novosel et al., 2005; Cocito et al., 2006).

According to Liu et al. (2017) environmental factors influencing zooplankton abundance and diversity are mainly chlorophyll-a concentration, temperature and salinity. As SGD influences these factors and as zooplankton is highly depending on primary producers, zooplankton is here used as an indicator for SGD and its influence on higher trophic levels. In the present study, primarily mesozooplankton will be investigated. Based on the key role of zooplankton in early life history of fish Liu et al. (2017) pointed out that changes in zooplankton abundance as well as in its composition have significant impacts on the recruitment and dynamics of fish.

The present study investigates the effect of a submarine spring on the abundance of fish in a coastal lagoon of Tahiti, French Polynesia, assuming a bottom-up control caused by elevated nutrient concentrations from a submarine spring.

MATERIALS AND METHODS

To investigate the abundance of fish a stationary photo sampling was performed. To visualize the nutrient input and emphasize the effect on primary- and secondary production a short-term *in situ* biofouling experiment as well as a zooplankton sampling of small sampling size were conducted. These two parameters were used as indicator of elevated nutrient concentrations released by the submarine groundwater spring at Trou de Lagon.

Study Site

Experiments were performed from 20th February until 3rd March 2017. Tahiti is a volcanic island located at 17° 24′ S and 149° 07′ W (**Figure 1**). It is part of the so called Society Island archipelago, with a surface of 1042 km^2 (Rougerie et al., 1997). The island is composed mainly of basaltic material (Frouin, 2000) and surrounded by an almost continuous barrier reef disconnected from the coastline by a narrow lagoon of 100 to 800 m width and a rather small tide-range of about ±0.15 m (Rougerie et al., 1997).

The climate of Tahiti Island is influenced by the Southern Oscillation. Trade winds blow primarily from the northeast during summer (rainy season) and southeast during winter. The mean rainfall is 150 cm y^{-1} and the air temperature generally between 20–33°C. Tahiti is located in the western area of the south pacific gyre with sea surface temperatures between 26–30°C and sea surface salinity values of 35.5–36.3. The high salinity values are caused by the negative P-E differentials leading to

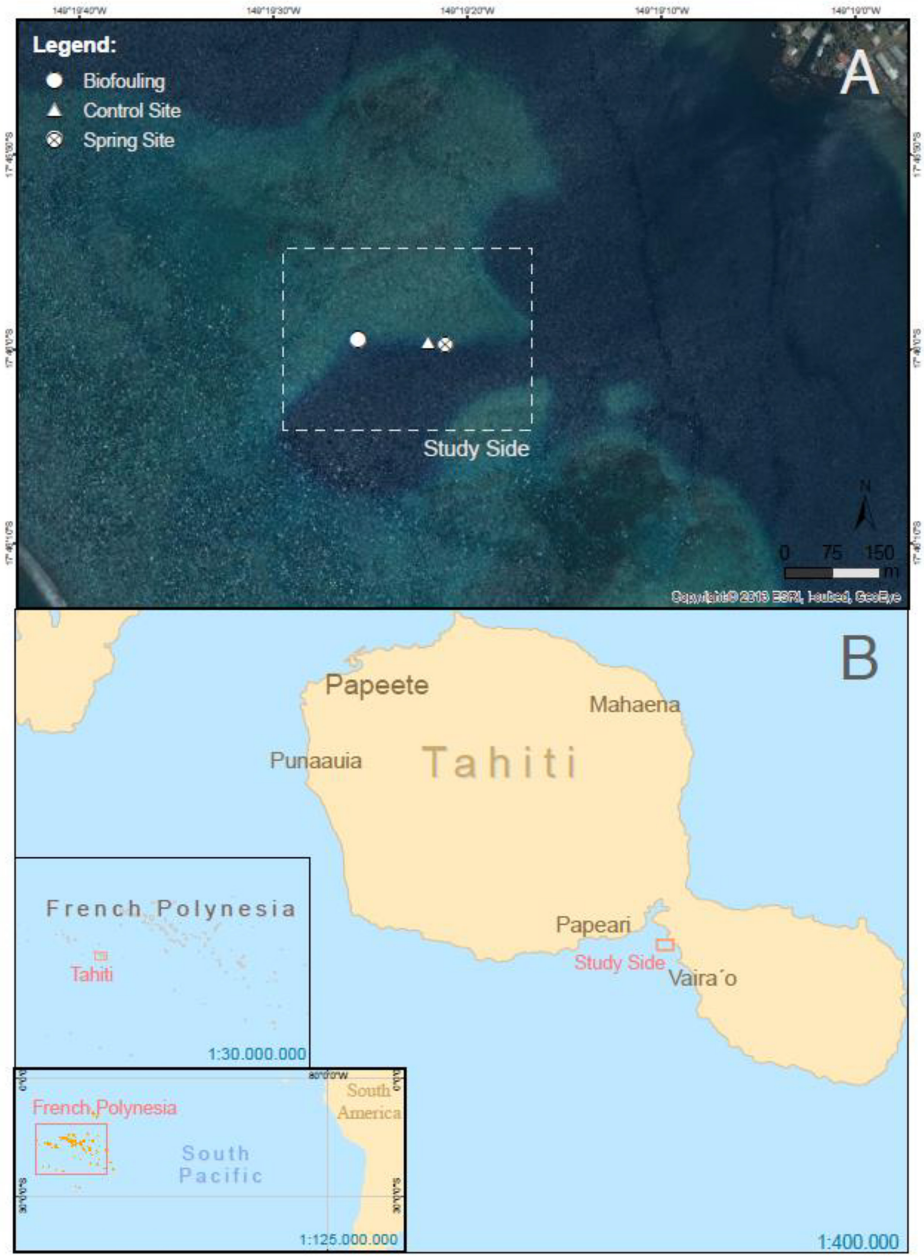

FIGURE 1 | Location of Tahiti, French Polynesia **(B)** and sampling site **(A)**.

increasing surface salinity whereas values may decrease during rainy season (Delcroix and Hénin, 1991; Rougerie et al., 1997).

Tahiti generally consists of two major volcanoes called Tahiti-Nui (the bigger part of the island) and Tahiti-Iti (the smaller part of the island) which are aligned in NW-SW (Duncan et al., 1994). The study site is called Trou du Lagon which is located on Tahiti-Iti in a low populated area. One of the main food production in form of agriculture and livestock cultivation is located in the region of Afaahiti-Taravao, Papeari, and Vairao at the isthmus of the island which is the transition from Tahiti-Nui to Tahiti-Iti (Cunningham, 1961). The study site is located directly within this area which leads to the assumption that the elevated nutrient concentrations are caused by the agriculture and livestock production.

Trou de Lagon is an oval basin in shape (**Figure 1A**) with depths from two to thirty meters enclosed in a shallow water body connected to the lagoon. The sampling area ranges about 200 m × 200 m around the sampling sites with three submarine springs in 11.6, 5.5, and 3.5 m water depth. The springs are of small size and do not exhibit any expression at the water surface. The distance to the shore line is about 850 m, the distance to the reef about 800 m. As Tahiti is a volcanic island, the substrate is

basalt, which is mostly covered by corals, due to the oligotrophic water conditions, the lack of sediments and the nearby barrier reef. The *in situ* biofouling and photo sampling experiments were performed at two different springs at the same study site during the same time. While no direct geochemical characterization of the springs is available, given the geology of the island and the SGD from Tahiti in general (cf. Haßler et al., 2019) two springs that close to each other can be expected to originate from the same aquifer and behave similarly. The sampling was performed at 17° 46'S and 149° 19'W in about 130 m distance to each other. The study site exhibits very little disturbances due to divers or fishermen.

Physical and Chemical Parameters

To demonstrate the presence of submarine discharge, water samples were taken directly from the discharge spot using falcon tubes. The sampling was performed daily during the stationary photo sampling and once during the biofouling experiment. The sampling solely provided salinity data as temperature adapted too quickly to the ambient seawater temperature. To estimate the groundwater discharge temperature of the submarine spring at Trou de Lagon temperature was measured manually at different accessible groundwater discharge spots within the eulittoral zone around the island. These measurements were performed by using a rod-thermometer. Nitrate and phosphate concentrations of the spring at Trou de Lagon were taken from Haßler et al. (2019), who performed a field study in January 2016.

Biofouling Process

In order to indicate the assumed elevated primary production a short-term *in situ* experiment was conducted. A total of 26 plastic panels of ten by ten centimeters size were strung on a rope and tied around corals in 3.5 m depth, through the submarine spring (**Figures 2**, **3**). The objective was to expose the central panels to the submarine spring to monitor the biofouling process caused by the spring, and observe the range of influence to both sides of the spring. The panels on the outer parts of the line exposed to fully marine seawater were used as control panels. For identification purposes, the groundwater exposed panels were marked with cable ties. For further evaluations, all panels were distinguished in spring and control panels.

After 10 days, the panels were taken out of the water and dried for several days not exposed to direct sunlight. To analyze, front and back side of each panel were scanned by using an Epson Perfection V330 photo scanner. All scans were cropped at a height of seven centimeters to cut out the rope influenced part of the panels. Within this part most of the settlement took place but the focus of analysis was on the panels' surfaces. The cropping and all further analyses were performed by using the software ImageJ (Version 1.51 f). To finally quantify the amount of settlement as percentage of covered area, a scale was entered using the *Set Scale* function. Therefore, a line of known distance on one of the panels was used as scale reference. The Type of Image was set on *RGB Color* and the *Color Threshold* function was used. To define the areas of settlement the *Color Space* was set on *HSB,* which are the three properties to describe a color (Hue, Saturation and Brightness). On an interval of 0–255, given by ImageJ, thresholds were set by trial and error and applied for all panels equally. The hue was set from 0 to 115, saturation from 26 to 255 and brightness from 115 to 255. Applying these settings, the areas of investigation were defined in red (**Figure 4**, right) to finally determine the settled areas in percent by using the function *Analyze Particles*. The front and back sides of all 26 panels were evaluated separately to gain two separate datasets which can be considered as replicates. In total, five panels where marked as groundwater discharge exposed and eleven as seawater exposed (control).

Zooplankton Abundance

As a further indicator of elevated nutrient concentrations, a zooplankton sampling of small sampling size was performed. The sampling was carried out by using an APSTEIN plankton net of 55 μm mesh size and a unscrewable net beaker (sampling container) within a water column of 5 m. A total of twelve hauls was performed, six hauls around the submarine spring within a radius of about 3 m and six at the control site. Each haul was performed from the boat in the same way. After each haul, the inside of the net was rinsed with filtered sea water (55 μm) in order to collect the entire sample in the sampling

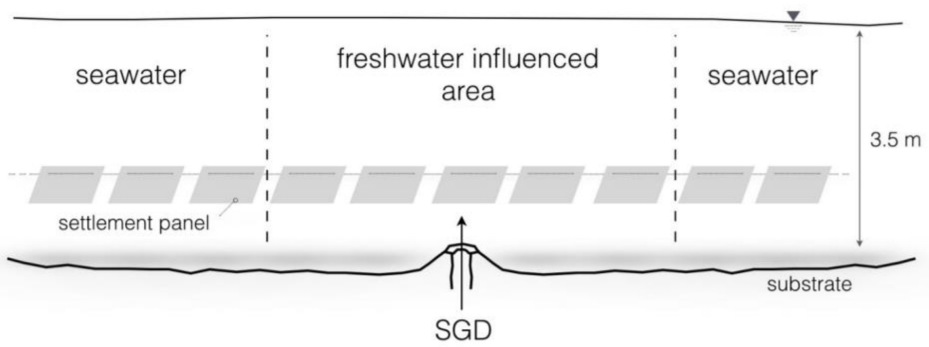

FIGURE 2 | Experimental design of the 10-day *in situ* biofouling experiment in 3.5 m water depth. In total 26 settlement panels were used, five panels exposed to the submarine spring and twenty-one to seawater.

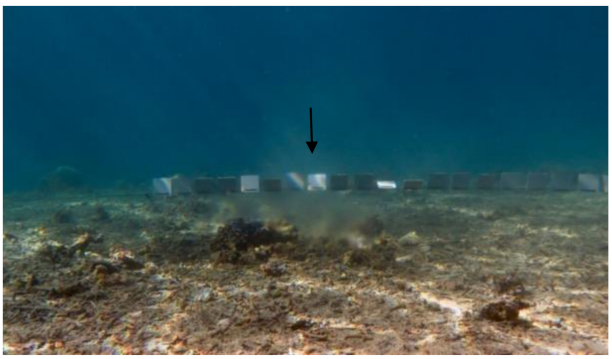

FIGURE 3 | Settlement panels (10 × 10 cm) stringed on a rope and fastened across the submarine spring (↓).

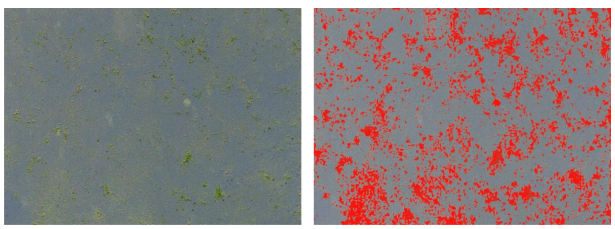

FIGURE 4 | One of 26 settlement panels exposed to the submarine spring (left: settled areas in green, yellowish; right: identical areas in red to quantify the proportion of settlement in percent by using ImageJ).

container. After rinsing, the container was unscrewed and the content transferred in 50 ml Kautex container by using a funnel and a squeeze bottle with filtered sea water (55 µm). Each sample was preserved in 60% alcohol and stored in a fridge at six degrees Celsius until analysis.

To analyze the zooplankton abundance the hardware Hydroptic ZooScan ZSCA02 together with the software Vuescan (Version 8.4.57), ZooProcess and Plankton Identifier was used, following the procedure described by Gorsky et al. (2010). To determine the zooplankton abundance each sample was first transferred into a sieve of 55 µm mesh size to separate it from the alcohol. To scan the isolated sample, it was poured directly into a transparent frame (15 cm × 24 cm) inserted in the scanning cell. The frame includes a 5-mm step. De-ionized water was poured up to the edge of the step beforehand to avoid forming a meniscus on the periphery of the image. To obtain one vignette (image) of each single individual overlapping organisms and organisms touching the side of the frame were physically separated from each other or from the frame before digitizing. Organisms touching the sides of the frame are automatically removed from the data set (Gorsky et al., 2010). The density of individuals was below 1000–1500 organisms within the scanning area which is sufficient to reduce overlapping organisms (Gorsky et al., 2010). To recheck that organisms are not overlapping, each scan was reviewed and overlapping individuals separated manually by using the software ImageJ. Each 16-bit raw image was normalized and converted into an 8-bit full gray scale image and processed by subtracting the background and removing the frame edges. The rolling ball method (Sternberg, 1983) provided by the ZooProcess software was used for background subtraction.

For automatic classification (Plankton Identifier) of objects across all scanned images into major groups a learning file of selected categories was used. The learning file contained vignettes of single objects of different taxonomic groups. Each folder within the learning file represented one taxonomic group. Additional folders of abiotic objects as e.g., fibers, bubbles as well as blurry objects were also part of the learning file. To reduce the error rates all automatically classified objects were re-validated manually, and any misidentified objects were moved to the appropriate taxonomic group. The final images are digitized with 96-dpi and pixels of 24284 – 15296 in size with a pixel resolution of 10.58 µm. These 8-bit gray level images require about 350 MB storage and can be handled easily by regular PC ìs (**Figure 5**). Finally, the zooplankton was classified into six major groups above genus level (Copepods, Appendicularia, Chaetognatha, Malacostraca, Polychaeta, and fish eggs). The classification on a species level is not feasible using the software Plankton Identifier. The abundance was calculated for each haul per site as well as for each of the six groups per site given in the number of individuals per volume of water (Ind. L^{-1}).

Stationary Photo Sampling

To investigate the effect of the submarine spring on the abundance of fish, a 10-day stationary photo sampling was implemented. Two GoProHero4 cameras were mounted on the bottom of the reef, one camera in about one meter distance to the submarine spring in 5.5 m depth recording the presence of fish around the submarine spring. The second camera was installed in 5.4 m depth as a control. The control site was chosen in a way that the surrounding area was ideally of the same structure and certainly not influenced by the submarine spring. The distance between both cameras was 56 m. In order to install the cameras two small camera mounts were built to guarantee a secure hold as well as to reduce possible thievery (**Figure 6**). Recorded were images instead of videos in order to enhance the battery capacity. The cameras were set to take images at an interval of one shot per minute. The change of batteries and memory cards took place once a day at 7:30 AM. In consequence, the daily recording started at the same time and ended with the complete battery discharge. Status lights and sounds were deactivated. In order to extend the batteries capacity each camera was equipped with one GoPro battery BacPac. By using the battery packs, images were taken up to 10 h per day, resulting in about 400 to 600 pictures per day. To evaluate the photo sampling the number of fish at the spring and control site images was counted manually. To visualize a potential difference in quantity straightforward as well as to compare the obtained data easier, the number of fish recorded in the images were grouped in categories. For example, one up to five fish, six up to ten fish. Species were not identified. Distant fish in the very depth of the images were neglected during the counting process. In total 7206 Images were evaluated with 3603 images per site (**Figure 7**).

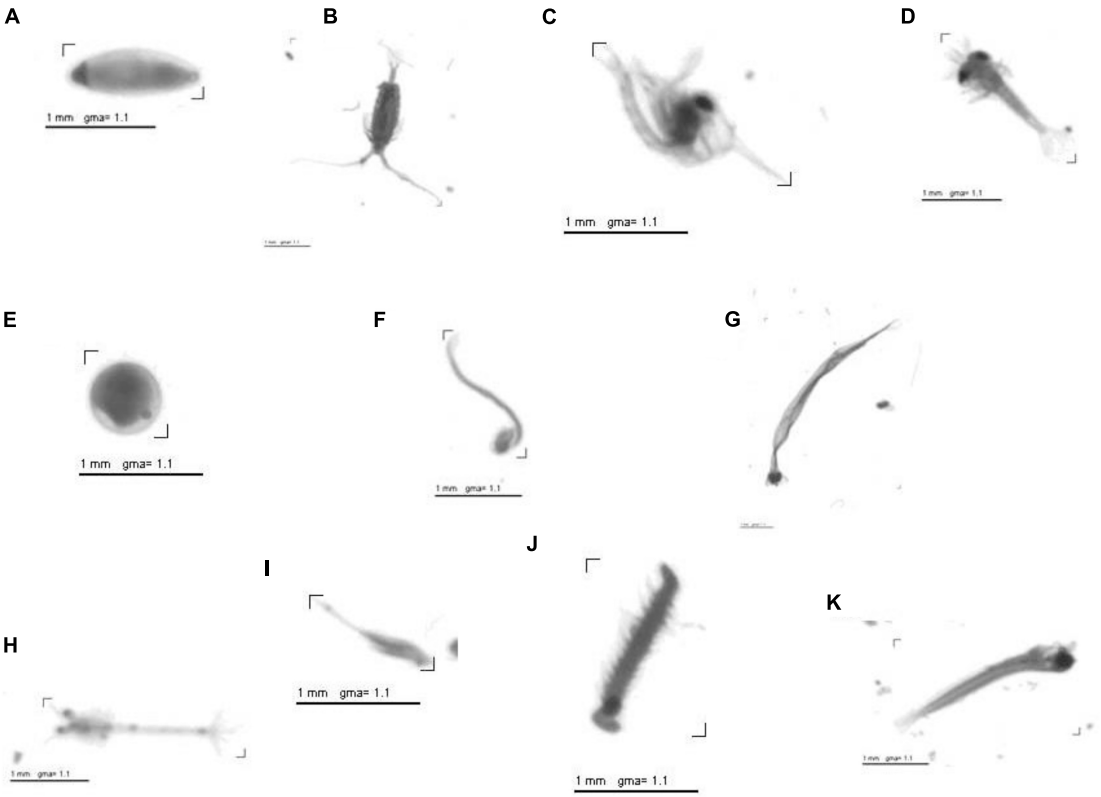

FIGURE 5 | Examples of scanned objects (vignettes) **(A)** Ostracoda (Oligostraca), **(B)** Calanoida (Copepoda), **(C)** Zoea (Decapoda), **(D)** Zoea (Decapoda), **(E)** Egg, **(F)** Appendicularia (Tunicata), **(G)** Chaetognatha (Metazoa), **(H)** Zoea (Decapoda), **(I)** Harpacticoida (Copepod), **(J)** Polychaeta (Annelida), **(K)** Fish Larvae.

Statistics

The Statistical analysis was carried out by using the software R-Studio (Version 1.0.143). The assumptions of normal distributed data and homoscedasticity were tested by graphical and numeric methods. The type of distribution was investigated by plotting normal q-q plots, histograms as well as by performing the Shapiro–Wilk test. Homoscedasticity was verified by the *F*-test. Log transformations were applied when the assumptions of normal distribution and homoscedasticity were not fulfilled. The subsequent hypotheses testing was carried out either by using the parametric two sampled *T*-test or the non-parametric Mann–Whitney*U*-test depending on whether the assumptions were fulfilled. The frequencies of counted categorized fish were analyzed by applying the Chi–squared Test of homogeneity. Therefore, the data was displayed in a contingency table. Based on this table the test evaluates the distribution of frequencies compared to the expected frequency (Köhler et al., 2012). The test was applied on the same number of images at both sites at the respective days. The data set consists of one factor (site) with two factor levels (spring and control) and one response variable depending on which data set was tested (settlement, abundance, counts).

FIGURE 6 | Installation built for the stationary photo sampling (left: metal loops fixed onto a metal plate to interlock the GoPro camera housing; right: mounting process of the metal construction as fixation for the 10-day photo sampling).

RESULTS

Physical and Chemical Parameters

The manually measured groundwater spring temperatures at different submarine springs within the eulittoral zone around the island were between 23.0 and 24.0°C whereas at Trou de Lagon the temperature at the control site (seawater) of the photo sampling was between 29.2 and 30.2°C. The salinity values at the photo sampling and biofouling experiment resulted in

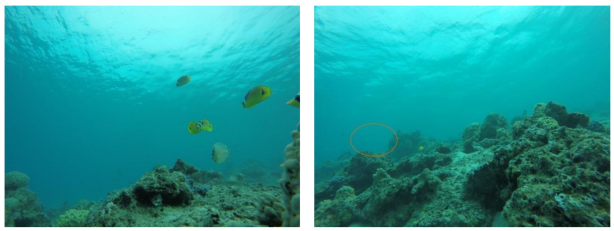

FIGURE 7 | Example of higher fish abundance regarding three-dimensionality and different substrate manifestation in the depth of the images [left: spring site with less substrate, right: control site with more pronounced substrate and a higher number of fish in the depth of the image (orange circle)].

salinities between 18.5 and 26.5 (still mixed with seawater) at the submarine spring and between 35.4 and 35.9 at the control site. The nutrient concentration of the submarine spring at Trou de Lagon was measured in 2016, resulting in concentrations of 5.7 mmol m^{-3} NO_x and 3.7 mmol m^{-3} PO_4. Concentrations in seawater sampled at a control site were below 0.4 mmol m^{-3} PO_4 and below 0.3 mmol m^{-3} NO_x (Haßler et al., 2019).

Biofouling Process

The settlement of algal turf on the groundwater exposed settlement panels was significantly higher compared to the seawater exposed panels (non-parametric Mann–Whitney *U*-test, $p = 0.004$ and $p = 0.030$ on panel front and back sides, respectively). The panels exposed to the submarine spring exhibit elevated settlement compared to the seawater exposed control panels. The largest amount of settlement in area percent of the submarine spring exposed panels is located above the total amount of settlement of the seawater exposed panels (**Figure 8**). The groundwater exposed panels displayed a median settlement of 6.5% whereas the seawater exposed panels exhibit a median settlement of 2.7%. The panel front sides were settled more intensively (medians 10.3 and 3.6% for groundwater and seawater exposed panels, respectively) than the back sides (medians 3.7 and 2.1% on groundwater and seawater exposed panels). The median settlement area thus increased by factor 2.4 of the groundwater exposed panels (2.8 at the front sides, 1.8 at the back sides). From **Figure 9** it can be seen that related to the center of the spring the increasing biofouling process exhibited a shift to the right of front and back sides, respectively.

Zooplankton

The total zooplankton abundance of six hauls at Trou de Lagon was slightly higher around the submarine spring (2.57 Ind. L^{-1} ± 0.10 Ind. L^{-1}) than at the control site (2.36 Ind. L^{-1} ± 0.16 Ind. L^{-1}). The median abundance was with 0.46 Ind. L^{-1} around the submarine spring and 0.33 Ind. L^{-1} at the control site slightly higher around the spring. The most abundant taxa at both sites were Copepoda followed by Appendicularia, Chaetognatha, Malacostraca, Polychaeta, and fish eggs. Copepoda were taken here as a proxy for elevated nutrient concentrations. The total copepod abundance was 1.97 Ind. L^{-1} ± 0.09 Ind. L^{-1} around the submarine spring and 1.82 Ind. L^{-1} ± 0.14 Ind. L^{-1} at the control site. The median copepod abundance of six hauls was 0.35 Ind. L^{-1} around the submarine spring and 0.25 Ind. L^{-1} at the control site.

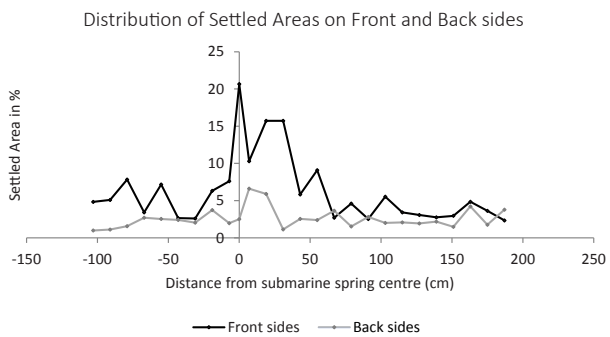

FIGURE 9 | Biofouling processes of 26 settlement panels exposed to a submarine spring and the seawater control section. The biofouling process on the front and the back sides of the settlement panels are illustrated separately. Each data point is one panel in the same distance to the submarine spring as in the field experiment.

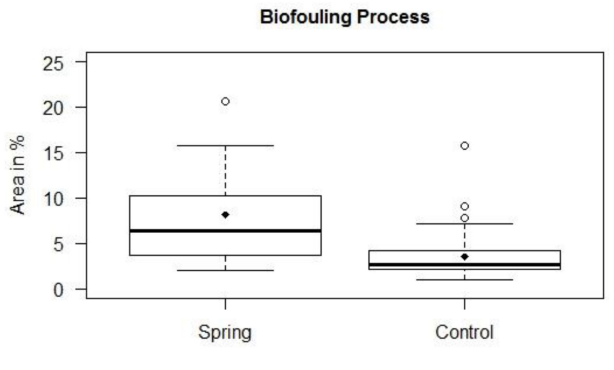

FIGURE 8 | Biofouling processes of settlement panels exposed to a submarine spring and a control section of seawater.

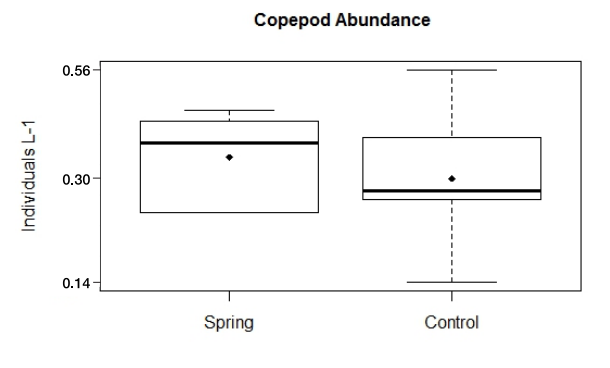

FIGURE 10 | Copepod abundances sampled within a diameter of six meters around a submarine spring and a seawater control site.

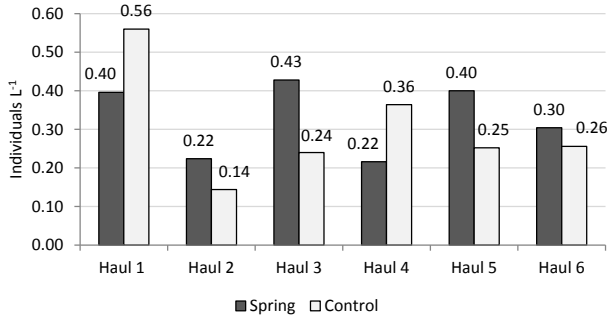

FIGURE 11 | Copepod abundances sampled at the submarine spring site within a diameter of six meters around the submarine spring and the seawater control site.

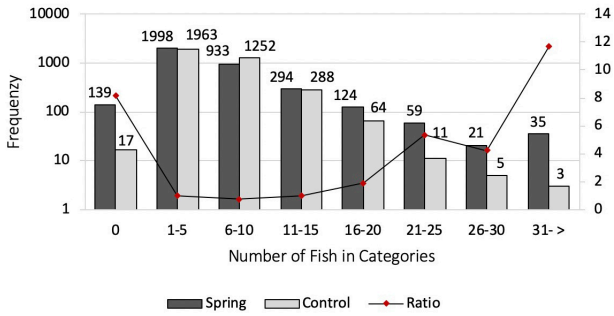

FIGURE 12 | Categorized frequencies of counted fish around a submarine spring and a seawater control site. The secondary axis depicts the ratio Spring/Control. Note that the left (Frequency) axis is on logarithmic scale while the right (Ratio) axis is linear.

The evaluation of Copepod abundances per haul (**Figures 10**, **11**) resulted in slightly higher abundances around the submarine spring in four out of six hauls (two, three, five, and six) compared to the control sites. However, the applied non-parametric Mann–Whitney *U*-test did not result in a significantly higher copepod abundance ($p = 0.7$) around the submarine spring compared to the control site.

Stationary Photo Sampling

With the stationary photo sampling we analyzed the number of fish around a submarine spring and a control site. The number of fish, here presented in frequencies of counted categories, declined stronger at the control site compared to the submarine spring site (**Figure 12**). Five out of seven categories were counted more frequent at the submarine spring site compared to the control site. Categories of zero fish and six until ten fish were counted more frequent at the control site. The frequency distribution of counted categories (**Figure 12**) follows more or less a Poisson distribution. The factor results of spring and control site presents the increase in categories of higher number of fish (**Figure 12**, secondary axis). Category 0 was counted more often by factor 8.2, category 1–5 by factor 1.0, category 6–10 by factor 0.7, category 11–15 by factor 1.0, category 16–20 by factor 1.9, category 21–25 by factor 5.4, category 26–30 by factor 4.2, category 31 → by factor 11.7. Despite the eight times more frequent category of zero fish and the similar outcome of category 1–5, 6–10, and 11–15 fish the evaluation resulted in a higher presence of fish at the submarine spring site. According to the Chi–Square test of homogeneity the frequencies of counted categories significantly differ ($p < 0.001$) from one another in favor of the submarine spring site.

DISCUSSION

The presence of the submarine springs was confirmed visually, in salinity and temperature measurements. The temperatures of the submarine springs at Trou de Lagon are assumed to be equivalent to the manually measured temperatures at the different groundwater discharge spots within the eulittoral zone around the island. The salinity differences between the submarine spring site and control site underscore the effect of the submarine spring on the environmental parameters. The remaining low salinity values of the spring site are caused by the immediate mixing of ground and seawater whilst discharging. Nitrogen and phosphorus concentrations were elevated at the submarine spring sites compared to samples of seawater at a control site (Haßler et al., 2019). The reduced salinity within the spring as well as the nutrient concentrations support our hypothesis of fresh SGD as a source of nutrient enrichment at the groundwater discharge site.

Data regarding species diversity of Tahiti lagoons are scarce. Studies on macrobenthic communities were mostly undertaken of soft bottom communities at the most populated region of the island nearby Papeete or Faaa Airport (e.g., Frouin and Hutchings, 2001). The authors described the resulting biomass and species diversity as low in comparison with most other areas within the South Pacific Ocean. Some fish species identified in the context of this study are: different types of Holothuroidea; Chaetodontidae: *Chaetodon ornatissmus, Chaetodon mertensii, Chaetodon unimaculatus, Focipiger flavissimus, Forcipiger flavissimus*; Balistidae: *Odonus niger, Balistapus undulatus, Rhinecanthus aculeatus, Balistoides viridescens*; Scaridae: *Scarus oviceps*; Aulostomidae: *Aulostomus chinensis*; Pomacanthidae: *Centropyge flavissima, Pygoplites diacanthus*; Pomacentridae: *Chromis margaritifer*; Labridae: *Thalassoma hardwicke, Halichoeres trimaculatus; Acanthuridae: Zebrasoma scopas, Acanthurus triostegus* the latter is often found grazing on hard substrate near freshwater discharge where certain algae grow (Kuiter and Tonozuka, 2001).

The frequency of counted categories of larger fish groups was significantly higher at the submarine groundwater spring site. Our hypothesis of a higher presence of fish around submarine springs can thus be confirmed for the site of the present study. While categories including small groups of fish were counted in similar frequencies at both sites, categories of larger

groups were counted significantly more often at the submarine spring site (**Figure 12**). Despite the possibility, that factors such as wind stress or waves may have certain influence, that we could not control or measure in this study, we conclude that the main cause for the increased abundance of fish around the spring is the elevated nutrient inflow by groundwater discharge enhancing primary production leading to a higher availability of prey.

An adaptation to changing environmental conditions as e.g., the seahorse *Hippocampus guttulatus* in Tiralongo and Baldacconi (2014) is not considered as the nutrient input at Trou de Lagon is punctual and thus avoidable. Fish at Trou de Lagon are assumed to prefer the proximity of the spring due to higher availability of nutrients and prey. Tiralongo and Baldacconi (2014) worked on a *H. guttulatus* population found in the Mar Piccolo of Taranto (Ionian Sea) known for its substantial pollution and oscillations of environmental parameters. This declining and endangered species, inhabit preferably seagrass and macroalgal meadows. Yet, the population is well adapted to the highly polluted environment showing a clear preference to artificial hard substrate over the usual seagrass. The authors' assumption of the abundant population is lacking fishing pressure and good availability of food caused by the artificial eutrophication. However, it is questionable whether this result can be linked to the present study. Fish at Trou de Lagon inhabit a general oligotrophic environment being attracted by a submarine spring carrying higher nutrient concentrations, whereas *H. guttulatus* inhabit a highly eutrophic environment but mainly found in the western part of the lagoon, which is in direct contact with the open sea allowing a water exchange.

Apart from nutrient input also temperature should be considered to effect the distribution of fish around the study sites. Groundwater discharge temperatures in lower latitudes generally tends to be lower than its ambient seawater (Shaban et al., 2005; Ka'eo Duarte et al., 2006; Johnson et al., 2008). As dissolved oxygen (DO) increases with lower temperature and salinity values, here caused by the submarine spring, it might also influence the abundance of fish around submarine springs although the observed flow rate at Trou de Lagon is low. Salinity and temperature values could not be measured precisely as ground and seawater mixed immediately during the sampling.

A variability in refuge possibilities due to higher manifestation of substrate between sites was tried to rule out by the camera set up. Recorded were image sections with approximately the same amount of substrate within close proximity to the camera at both sites (spring and control). However, a difference in substrate manifestation took place at the very far back of the control site images.

A higher abundance of fish due to recruitment after spawning depending on seasonal variations of temperature, inducing algal blooms in spring or autumn, were excluded as the climate is tropical with only two distinct seasons. However, it is worth mentioning that instead of seasonal variations in temperature as in higher latitudes other variations as rain and dry season do have an effect on reproduction (Flecker and Feifarek, 1994) and may influence processes. Furthermore, seasonal variation is not assumed to cause such selective higher fish abundance.

The significantly higher abundance of fish is suggested to be the result of nutrient inflow by the groundwater discharge enhancing primary production as presented in the short-term biofouling experiment.

Lapointe (1997) found epilithic algal communities such as algal turfs as well as macroalgae and coralline algae increasing with increasing nutrient concentrations. During our short-term biofouling experiment, a visible settlement of small filamentous sessile algae took place, which was significantly higher on the groundwater compared to the seawater exposed panels. The biofouling process on the front sides was higher compared to the back sides of the settlement panels. The latter might be a result of the light exposure with a higher light irradiation on the front sides caused by the alignment to the sun. The back sides of the panels were aligned in south-eastern direction receiving light irradiation for a fractional amount of the day, whereas the front sides where aligned more in direction north-west receiving light irradiation during almost the entire daytime. The extent of biofouling along the transect (**Figure 9**) exhibited a shift of elevated settlement to the right which might be caused by slight currents moving the mixing plume to the right or the freshwater exposed panels have not been marked precisely.

The result of the biofouling experiment supports the previously assumed higher productivity due to elevated nutrient concentrations around SGD sites (e.g., Williams and Carpenter, 1988; Lapointe, 1997; Novosel et al., 2005; Cocito et al., 2006). Factors such as wave energy, exposure to winds or regional advection as causes of the different manifestation in settlement between ground and seawater exposed panels are excluded. These factors would in contrast cause a mixing of fresh and seawater during short or long term events neutralizing the groundwater effect rather leading to a homogeneous algal turf manifestation.

The total zooplankton abundance at the groundwater discharge site was just slightly and insignificantly higher compared to the control site. The overall abundance was very low at both sites, based on the in general oligotrophic tropic waters of low production (Dias et al., 2015). An even lower total abundance of 0.068 Ind. L^{-1} was found by Carleton and Doherty (1998) in a lagoon of Tuamotu Archipelago, located within the same archipelago as Tahiti. As expected the most abundant taxon at both sampling sites were Copepods which are the most important grazer of nano- and microplankton and the main diet of planktivorous fish.

The outcome of the present work is in line with results from Obama Bay, Japan, showing a significantly higher abundance of fish at a groundwater discharge site (Utsunomiya et al., 2015). Also, a significantly higher abundances of turban snail, hermit crabs and gammarids were reported at the groundwater discharge site (Utsunomiya et al., 2015). The authors assumed the higher abundance of fish might be the result of the 18 times higher gammarid abundance being the major prey for these fish. The higher abundance of fish around the submarine spring at Trou de Lagon may thus be the result of a bottom-up control as hypothesized.

Diversity of fish species was not evaluated in the frame of this work, as a proper identification of species could not be performed by using the recorded images. Obstacles were e.g., the distance of fish to the camera, turbidity or the salinity gradient blurring the sight. The proportion of juvenile and adult fish could not be estimated on the basis of the implemented sampling. Therefore, a 3D video-based technique (Neuswanger et al., 2016) should be considered for further investigations.

Difficulties which occurred during the image evaluation should be taken into account for further investigations. Difficulties in counting fish occurred for example due to the three-dimensionality of the water body, changing image sections caused by the daily change of batteries, different manifestations of substrate as well as rapidly changing turbidity. The three-dimensionality of the water body made it difficult to count as the distances to the actual study site cannot be estimated precisely. In addition with different substrate complexity the counting involves subjective decisions. More substrate causes more shelter and nutrition for fish. A varying amount of substrate between two sites may also influence the abundance of fish (McClanahan, 1994; Gratwicke and Speight, 2005) which may be an additional variable besides the submarine spring. The cameras were set up in a way to record the same amount of substrate image sections at both sites. A little higher substrate complexity occurred in the distance of the control site images. To overcome this obstacle distant fish in the very depth of the images were neglected during the counting process as they were basically out of the study site clearly evident by very small sizes and blurriness caused by the distance. Double counting of fish was minimized by recounting.

While there are abundant research questions that need answering regarding the impact of submarine springs on flora and fauna, the here presented results are the first to show that submarine springs do attract fish in tropical settings. This result is assumed to be induced by the nutrient inflow of the submarine spring as presented in our *in situ* biofouling experiment.

DATA AVAILABILITY STATEMENT

The datasets generated for this study can be found as Starke et al. (2018).

AUTHOR CONTRIBUTIONS

CS planned and carried out the experiments, analyzed the data, and wrote the manuscript with support of WE and NM. WE and NM supervised the project and provided critical feedback and helped to shape the research, analysis, and manuscript.

FUNDING

This study was funded through German Federal Ministry of Education and Research (BMBF) Grant #01LN1307A to NM.

ACKNOWLEDGMENTS

We would like to thank Kathrin Haßler from Leibniz Centre for Tropical Marine Research (ZMT), Bremen, Germany for providing us with the nutrient concentration data of Trou de Lagon, Lionel Hertrich, and Isabelle Klein from Tahiti Iti Diving Centre for their support during the *in situ* implementation process. Also, Till Oehler and Stefanie Bröhl (ZMT) for their support in organizational and technical issues.

REFERENCES

Amato, D. W., Bishop, J. M., Glenn, C. R., Dulai, H., and Smith, C. M. (2016). Impact of submarine groundwater discharge on marine water quality and Reef Biota of Maui. *PLoS One* 11:e0165825. doi: 10.1371/journal.pone.0165825

Beusen, A. H. W., Slomp, C. P., and Bouwman, A. F. (2013). Global land-ocean linkage: direct inputs of nitrogen to coastal waters via submarine groundwater discharge. *Environ. Res. Lett.* 8:034035. doi: 10.1088/1748-9326/8/3/034035

Burnett, W. C., Bokuniewicz, H., Huettel, M., Moore, W. S., and Taniguchi, M. (2003). Groundwater and pore water inputs to the coastal zone. *Biogeochemistry* 66, 3–33. doi: 10.1023/B:BIOG.0000006066.21240.53

Carleton, J. H., and Doherty, P. J. (1998). Tropical zooplankton in the highly-enclosed lagoon of Taiaro Atoll (Tuamotu Archipelago, French Polynesia). *Coral Reefs* 17, 29–35. doi: 10.1007/s003380050090

Cho, H.-M., Kim, G., Kwon, E. Y., Moosdorf, N., Garcia-Orellana, J., and Santos, I. R. (2018). Radium tracing nutrient inputs through submarine groundwater discharge in the global ocean. *Sci. Rep.* 8:2439. doi: 10.1038/s41598-018-20806-2

Cocito, S., Novosel, M., Pasarić, Z., and Key, M. M. (2006). Growth of the bryozoan *Pentapora Fascialis* (Cheilostomata, Ascophora) around submarine freshwater springs in the Adriatic Sea. *Linzer Biol. Beitr.* 38, 15–24.

Cole, J. J., Prairie, Y. T., Caraco, N. F., McDowell, W. H., Tranvik, L. J., Striegl, R. G., et al. (2007). Plumbing the global carbon cycle: integrating inland waters into the terrestrial carbon budget. *Ecosystems* 10, 172–185. doi: 10.1007/s10021-006-9013-8

Cunningham, G. (1961). Food for Tahiti. *Econ. Geogr.* 37, 347–352. doi: 10.2307/141998

Delcroix, T., and Hénin, C. (1991). Seasonal and interannual variations of sea surface salinity in the Tropical Pacific Ocean. *J. Geophys. Res.* 96, 22135–22150. doi: 10.1029/91JC02124

Dias, C. O., Araujo, A. V., Vianna, S. C., Loureiro Fernandes, L. F., Paranhos, R., Suzuki, M. S., et al. (2015). Spatial and temporal changes in biomass, production and assemblage structure of mesozooplanktonic copepods in the Tropical South-West Atlantic Ocean. *J. Mar. Biol. Assoc. United Kingdom* 95, 483–496. doi: 10.1017/S0025315414001866

Duck, R. W., and da Silva, J. F. (2012). Coastal lagoons and their evolution: a hydromorphological perspective. *Estuar. Coast. Shelf. Sci.* 110, 2–14. doi: 10.1016/j.ecss.2012.03.007

Duncan, R. A., Fisk, M. R., White, W. M., and Nielsen, R. L. (1994). Tahiti: geochemical evolution of a French Polynesian Volcano. *J. Geophys. Res.* 99, 24341–24357. doi: 10.1029/94jb00991

Flecker, A. S., and Feifarek, B. (1994). Disturbance and the temporal variability of invertebrate assemblages in two andean streams. *Freshw. Biol.* 31, 131–142. doi: 10.1111/j.1365-2427.1994.tb00847.x

Frouin, P. (2000). Effects of anthropogenic disturbances of tropical soft-bottom benthic communities. *Mar. Ecol. Prog. Ser.* 194, 39–53. doi: 10.3354/meps194039

Frouin, P., and Hutchings, P. (2001). Macrobenthic communities in a tropical lagoon (Tahiti, French Polynesia, central Pacific). *Coral Reefs* 19, 277–286. doi: 10.1007/PL00006961

Fujita, K., Shoji, J., Sugimoto, R., Nakajima, T., Honda, H., Takeuchi, M., et al. (2019). Increase in fish production through bottom-up trophic linkage in coastal waters induced by nutrients supplied *via* submarine groundwater. *Front. Environ. Sci.* 7.

Gobler, C. J., and Sañudo-Wilhelmy, S. A. (2001). Temporal variability of groundwater seepage and brown tide blooms in a long island embayment. *Mar. Ecol. Prog. Ser.* 217, 299–309. doi: 10.3354/meps217299

Gorsky, G., Ohman, M. D., Picheral, M., Gasparini, S., Stemmann, L., Romagnan, J. B., et al. (2010). Digital zooplankton image analysis using the zooscan integrated system. *J. Plankt. Res.* 32, 285–303. doi: 10.1093/plankt/fbp124

Gratwicke, B., and Speight, M. R. (2005). The relationship between fish species richness, abundance and habitat complexity in a range of shallow tropical marine habitats. *J. Fish Biol.* 66, 650–667. doi: 10.1111/j.1095-8649.2005.00629.x

Hata, M., Sugimoto, R., Hori, M., Tomiyama, T., and Shoji, J. (2016). Occurrence, distribution and prey items of juvenile marbled sole *Pseudopleuronectes Yokohamae* around a submarine groundwater seepage on a tidal flat in Southwestern Japan. *J. Sea Res.* 111, 47–53. doi: 10.1016/j.seares.2016.01.009

Haßler, K., Dähnke, K., Kölling, M., Sichoix, L., Nickl, A. L., and Moosdorf, N. (2019). Provenance of nutrients in submarine fresh groundwater discharge on Tahiti and Moorea, French Polynesia. *Appl. Geochem.* 100, 181–189. doi: 10.1016/j.apgeochem.2018.11.020

Johannes, R. E. (1980). The ecological significance of the submarine discharge of groundwater. *Mar. Ecol. Prog. Ser.* 3, 365–373. doi: 10.3354/meps003365

Johnson, A. G., Glenn, C. R., Burnett, W. C., Peterson, R. N., and Lucey, P. G. (2008). Aerial infrared imaging reveals large nutrient-rich groundwater inputs to the ocean. *Geophys. Res. Lett.* 35:L15606. doi: 10.1029/2008GL034574

Ka'eo Duarte, T., Hemond, H. F., Frankel, D., and Frankel, S. (2006). Assessment of submarine groundwater discharge by handheld aerial infrared imagery: case study of Kaloko Fishpond and Bay, Hawai'i. *Limnol. Oceanogr.* 4, 227–236. doi: 10.4319/lom.2006.4.227

Kamermans, P., Hemminga, M. A., Tack, J. F., Mateo, M. A., Marbà, N., Mtolera, M., et al. (2002). Groundwater effects on diversity and abundance of lagoonal seagrasses in Kenya and on Zanzibar Island (East Africa). *Mar. Ecol. Prog. Ser.* 231, 75–83. doi: 10.3354/meps231075

Kjerfve, B. (1986). "Comparative oceanography of coastal lagoons," in *Estuarine Variability*, ed. D. A. Wolfe (New York, NY: Academic Press), 63–81. doi: 10.1016/B978-0-12-761890-6.50009-5

Knee, K. L., and Paytan, A. (2011). *Submarine Groundwater Discharge. Treatise on Estuarine and Coastal Science*. Amsterdam: Elsevier, 205–233. doi: 10.1016/B978-0-12-374711-2.00410-1

Köhler, W., Schachtel, G., and Voleske, P. (2012). "Biostatistik," in *Eine Einführung für Biologen und Agrarwissenschaftler*, Berlin: Springer-Verlag.

Kuiter, R. H., and Tonozuka, T. (2001). "Pictorial guide to indonesian reef fishes. Part 3. Jawfishes - Sunfishes, Opistognathidae - Molidae," in *Zoonetics*. Australia, Ref. No. 48637, 623–893.

Kwon, E. Y., Kim, G., Primeau, F., Moore, W. S., Cho, H.-M., DeVries, T., et al. (2014). Global estimate of submarine groundwater discharge based on an observationally constrained radium isotope model. *Geophys. Res. Lett.* 41, 8438–8444. doi: 10.1002/2014GL061574

Lapointe, B. E. (1997). Nutrient thresholds for bottom-up control of macroalgal blooms on Coral Reefs in Jamaica and Southeast Florida. *Limnol. Oceanogr.* 42, 1119–1131. doi: 10.4319/lo.1997.42.5_part_2.1119

Lapointe, B. E., Barile, P. J., Littler, M. M., and Littler, D. S. (2005). Macroalgal blooms on southeast florida coral reefs. *Harmful Algae* 4, 1106–1122. doi: 10.1016/j.hal.2005.06.002

Laroche, J., Nuzzi, R., Waters, R., Wyman, K., Falkowski, P., and Wallace, D. (1997). Brown tide blooms in long island's coastal waters linked to interannual variability in groundwater flow. *Global Change Biol.* 3, 397–410. doi: 10.1046/j.1365-2486.1997.00117.x

Lecher, A., and Mackey, K. R. M. (2018). Synthesizing the effects of submarine groundwater discharge on marine biota. *Hydrology* 5:60. doi: 10.3390/hydrology5040060

Lilkendey, J., Pisternick, T., Neumann, S. I., Dumur Neelayya, D., Bröhl, S., Neehaul, Y., et al. (2019). Fresh submarine groundwater discharge augments growth in a reef fish. *Front. Mar. Sci.* 6.

Liu, J., Su, N., Wang, X., and Du, J. (2017). Submarine groundwater discharge and associated nutrient fluxes into the southern yellow sea: a case study for semi-enclosed and oligotrophic seas-implication for green tide bloom. *J. Geophys. Res. Oceans* 122, 139–152. doi: 10.1002/2016JC012282

McClanahan, T. R. (1994). Kenyan coral reef lagoon fish: effects of fishing, substrate complexity, and Sea Urchins. *Coral Reefs* 13, 231–241. doi: 10.1007/BF00303637

Miller, D. C., and Ullman, W. J. (2004). Ecological consequences of ground water discharge to Delaware Bay, United States. *Ground Water* 42, 959–970. doi: 10.1111/j.1745-6584.2004.tb02635.x

Moore, W. S. (2010). The effect of submarine groundwater discharge on the ocean. *Annu. Rev. Mar. Sci.* 2, 59–88. doi: 10.1146/annurev-marine-120308-081019

Moosdorf, N., and Oehler, T. (2017). Societal use of fresh submarine groundwater discharge: an overlooked water resource. *Earth Sci. Rev.* 171, 338–348. doi: 10.1016/j.earscirev.2017.06.006

Moosdorf, N., Stieglitz, T., Waska, H., Dürr, H. H., and Hartmann, J. (2015). Submarine groundwater discharge from tropical islands: a review. *Grundwasser* 20, 53–67. doi: 10.1007/s00767-014-0275-3

Neuswanger, J. R., Wipfli, M. S., Rosenberger, A. E., and Hughes, N. F. (2016). Measuring fish and their physical habitats: versatile 2D and 3D video techniques with user-friendly software. *Can. J. Fish. Aquat. Sci.* 73, 1861–1873. doi: 10.1139/cjfas-2016-0010

Novosel, M., Olujic, G., Cocito, S., and Pozar-Domac, A. (2005). "Submarine freshwater springs in the adriatic sea: a unique habitat for the Bryozoan *Pentapora fascialis*," in *Proceedings of the 13th International Conference of the International Bryozoology Association* (Chile: IBA).

Oehler, T., Eiche, E., Putra, D., Adyasari, D., Hennig, H., Mallast, U., et al. (2018). Seasonal variability of land-ocean groundwater nutrient fluxes from a Tropical Karstic Region (Southern Java, Indonesia). *J. Hydrol.* 565, 662–671. doi: 10.1016/j.jhydrol.2018.08.077

Paerl, H. W. (1997). Coastal eutrophication and harmful algal blooms: importance of atmospheric deposition and groundwater as 'new' nitrogen and other nutrient sources. *Limnol. Oceanogr.* 42, 1154–1165. doi: 10.4319/lo.1997.42.5_part_2.1154

Paytan, A., Shellenbarger, G. G., Street, J. H., Gonneea, M. E., Davis, K., Young, M. B., et al. (2006). Submarine groundwater discharge: an important source of new inorganic nitrogen to coral reef ecosystems. *Limnol. Oceanogr.* 51, 343–348. doi: 10.4319/lo.2006.51.1.0343

Rougerie, F., Fichez, R., and Déjardin, P. (1997). Geomorphology and hydrogeology of selected islands of French Polynesia: Tikehau (Atoll) and Tahiti (Barrier Reef). Geology and hydrogeology of carbonate islands. *Dev. Sedimentol.* 54, 475–502. doi: 10.1016/s0070-4571(04)80037-2

Sarno, D., Zingone, A., Saggiomo, V., and Carrada, G. (1993). Phytoplankton biomass and species composition in a Mediterranean coastal lagoon. *Hydrobiologia* 271, 27–40. doi: 10.1007/BF00005692

Shaban, A., Khawlie, M., Abdallah, C., and Faour, G. (2005). Geologic controls of submarine groundwater discharge: application of remote sensing to North Lebanon. *Environ. Geol.* 47, 512–522. doi: 10.1007/s00254-004-1172-3

Shoji, J., and Tominaga, O. (2018). "Relationships between submarine groundwater discharge and coastal fisheries as a water-food Nexus," in *The Water-Energy-Food Nexus*, eds A. Endo, and T. Oh (Singapore: Springer), 117–131. doi: 10.1007/978-981-10-7383-0_9

Slomp, C. P., and Van Cappellen, P. (2004). Nutrient inputs to the coastal ocean through submarine groundwater discharge: controls and potential impact. *J. Hydrol.* 295, 64–86. doi: 10.1016/j.jhydrol.2004.02.018

Smith, C. G., and Swarzenski, P. W. (2012). An investigation of submarine groundwater-borne nutrient fluxes to the west florida shelf and recurrent harmful algal blooms. *Limnol. Oceanogr.* 57, 471–485. doi: 10.4319/lo.2012.57.2.0471

Starke, C., Ekau, W., and Moosdorf, N. (2018). "Impact of submarine groundwater discharge on fish and zooplankton abundances and on early biofouling processes in a coastal la goon of Tahiti, French Polynesia," in *Leibniz-Zentrum für Marine Tropenforschung*, Bremen, Germany: PANGAEA. Available at: https://doi.org/10.1594/PANGAEA.888416.

Sternberg, S. R. (1983). Biomedical image processing. *Computer* 16, 22–34. doi: 10.1109/MC.1983.1654163

Stieglitz, T., and Ridd, P. (2000). "Submarine groundwater discharge from paleochannels?: 'Wonky Holes' on the Inner Shelf of the Great Barrier Reef, Australia," in *Proceedings of the international conference on Hydro 2000: Interactive Hydrology* (Barton: Institution of Engineers).

Tait, D. R., Erler, D. V., Santos, I. R., Cyronak, T. J., Morgenstern, U., and Eyre, B. D. (2014). The influence of groundwater inputs and age on nutrient dynamics in a Coral Reef Lagoon. *Mar. Chem.* 166, 36–47. doi: 10.1016/j.marchem.2014.08.004

Tiralongo, F., and Baldacconi, R. (2014). A conspicuous population of the long-snouted seahorse, *Hippocampus guttulatus* (Actinopterygii: Syngnathiformes: Syngnathidae), in a highly polluted mediterranean coastal lagoon. *Acta Ichthyol. Piscatoria* 44, 99–104. doi: 10.3750/AIP2014.44.2.02

Umezawa, Y., Miyajima, T., Yamamuro, M., Kayanne, H., and Koike, I. (2002). Fine-scale mapping of land-derived nitrogen in coral reefs by δ 15 N in Macroalgae. *Limnol. Oceanogr.* 47, 1405–1416. doi: 10.4319/lo.2002.47.5.1405

Utsunomiya, T., Hata, M., Sugimoto, R., Honda, H., Kobayashi, S., Miyata, Y., et al. (2015). Higher species richness and abundance of fish and benthic invertebrates around submarine groundwater discharge in Obama Bay, Japan. *J. Hydrol. Reg. Stud.* 11, 139–146. doi: 10.1016/j.ejrh.2015.11.012

Williams, S. L., and Carpenter, R. C. (1988). Nitrogen-limited primary productivity of coral reef algal turfs: potential contribution of ammonium excreted by *Diadema Antillarum*. *Mar. Ecol. Prog. Ser.* 47, 145–152. doi: 10.3354/meps047145

Conflict of Interest: The authors declare that the research was conducted in the absence of any commercial or financial relationships that could be construed as a potential conflict of interest.

frontiers in Environmental Science

ORIGINAL RESEARCH
published: 18 February 2020
doi: 10.3389/fenvs.2019.00205

Nutrient Fluxes Associated With Submarine Groundwater Discharge From Karstic Coastal Aquifers (Côte Bleue, French Mediterranean Coastline)

Simon Bejannin[1], Joseph James Tamborski[1†], Pieter van Beek[1*], Marc Souhaut[1], Thomas Stieglitz[2], Olivier Radakovitch[2,3], Christelle Claude[2], Pascal Conan[4], Mireille Pujo-Pay[4], Olivier Crispi[4], Emilie Le Roy[1†] and Claude Estournel[1]*

[1] LEGOS, Laboratoire d'Etudes en Géophysique et Océanographie Spatiales UMR 5566 (Université de Toulouse, CNES, CNRS, IRD, UPS), Observatoire Midi Pyrénées, Toulouse, France, [2] Aix-Marseille Univ, CNRS, IRD, INRA, Coll France, CEREGE, Aix-en-Provence, France, [3] IRSN (Institut de Radioprotection et de Sûreté Nucléaire), PSE-ENV/SRTE/LRTA, Saint-Paul-Lez-Durance, France, [4] Laboratoire d'Océanographie Biologique, Sorbonne Université, UPMC, CNRS, UMR 7621, Laboratoire Arago, Banyuls-sur-Mer, France

Determination of submarine groundwater discharge (SGD) from karstic coastal aquifers is important to constrain hydrological and biogeochemical cycles. However, SGD quantification using commonly employed geochemical methods can be difficult to constrain under the presence of large riverine inputs, and is further complicated by the determination of the karstic groundwater endmember. Here, we investigated a coastal region where groundwater discharges from a karstic aquifer system using airborne thermal infrared mapping and geochemical sampling conducted along offshore transects. We report radium data (^{223}Ra, ^{224}Ra, ^{228}Ra) that we used to derive fluxes (water, nutrients) associated with terrestrial groundwater discharge and/or seawater circulation through the nearshore permeable sediments and coastal aquifer. Field work was conducted at different periods of the year to study the temporal variability of the chemical fluxes. Offshore transects of ^{223}Ra and ^{224}Ra were used to derive horizontal eddy diffusivity coefficients that were subsequently combined with surface water nutrient gradients ($NO_2^- + NO_3^-$, DSi) to determine the net nutrient fluxes from SGD. The estimated DSi and ($NO_2^- + NO_3^-$) fluxes are 6.2 ± 5.0 *10^3 and 4.0 ± 2.0 *10^3 mol d^{-1} per km of coastline, respectively. We attempted to further constrain these SGD fluxes by combining horizontal eddy diffusivity and ^{228}Ra gradients. However, SGD endmember selection in this area (terrestrial groundwater discharge vs. porewater) adds further uncertainty to the flux calculation and thus prevented us from calculating a reliable flux using this latter method. Additionally, the relatively long half-life of ^{228}Ra (5.75 y) makes it sensitive to specific circulation patterns in this coastal region, including sporadic intrusions of Rhône river waters that impact both the ^{228}Ra and nutrient surface water distributions. We show that SGD nutrient fluxes locally reach up to 20 times the nutrient fluxes from a small river (Huveaune River). On a regional

OPEN ACCESS

Edited by:
Henrietta Dulai, University of Hawaii at Manoa, United States

Reviewed by:
Aaron Beck, Geomar Helmholtz Center for Ocean Research Kiel, Germany
Kimberly Null, Moss Landing Marine Laboratories, United States

***Correspondence:**
Joseph James Tamborski
jtamborski@whoi.edu
Pieter van Beek
vanbeek@legos.obs-mip.fr

†Present address:
Joseph James Tamborski and Emilie Le Roy, Department of Marine Chemistry and Geochemistry, Woods Hole Oceanographic Institution, Woods Hole, MA, United States

Specialty section:
This article was submitted to Water and Wastewater Management, a section of the journal Frontiers in Environmental Science

Received: *31 May 2019*
Accepted: *20 December 2019*
Published: *18 February 2020*

Citation:
Bejannin S, Tamborski JJ, van Beek P, Souhaut M, Stieglitz T, Radakovitch O, Claude C, Conan P, Pujo-Pay M, Crispi O, Le Roy E and Estournel C (2020) Nutrient Fluxes Associated With Submarine Groundwater Discharge From Karstic Coastal Aquifers (Côte Bleue, French Mediterranean Coastline). Front. Environ. Sci. 7:205. doi: 10.3389/fenvs.2019.00205

scale, DSi fluxes driven by SGD vary between 0.1 and 1.4% of the DSi inputs of the Rhône River, while the ($NO_2^- + NO_3^-$) fluxes driven by SGD on this 22 km long coastline are between 0.1 and 0.3% of the Rhône River inputs, the largest river that discharges into the Mediterranean Sea. Interestingly, the nutrient fluxes reported here are similar in magnitude compared with the fluxes quantified along the sandy beach of La Franqui, in the western Gulf of Lions (Tamborski et al., 2018), despite the different lithology of the two areas (karst systems vs. unconsolidated sediment).

Keywords: submarine groundwater discharge, Mediterranean sea, radium isotopes, thermal infrared remote sensing, nutrient fluxes, GEOTRACES

INTRODUCTION

Submarine Groundwater Discharge (SGD) is now recognized as a vector for many chemical elements that impact the biogeochemistry and ecology of the coastal seas (Moore, 1996; Charette and Buesseler, 2004; Slomp and Van Cappellen, 2004; Burnett et al., 2006). SGD can facilitate phytoplankton development in coastal areas (Paytan et al., 2006) or may play a role in eutrophication of coastal seas, including in some cases harmful algal blooms (Gobler and Sañudo-Wilhelmy, 2001). SGD includes (i) the discharge of terrestrial groundwater to the sea and (ii) the circulation of seawater through the coastal aquifer and permeable coastal sediments (Burnett et al., 2003; Moore, 2010). The mixing zone between groundwater and seawater is defined as the subterranean estuary (Moore, 1999), a geochemically reactive subsurface zone where many chemical species are modified by biogeochemical reactions and water-rock interactions. Although, SGD has been shown to supply essential nutrients (Charette et al., 2001; Slomp and Van Cappellen, 2004; Hwang et al., 2005; Knee et al., 2010; Beusen et al., 2013; Tamborski et al., 2017) and trace elements to the coastal sea (Jeong et al., 2012; Trezzi et al., 2017), relatively few studies have been conducted on nutrient fluxes driven by SGD in the Mediterranean Sea (Garcia-Solsona et al., 2010; Weinstein et al., 2011; Tovar-Sánchez et al., 2014; Rodellas et al., 2015, 2017; Tamborski et al., 2018). In particular, little information is available on the nutrient fluxes associated with SGD along the French Mediterranean coastline (Rodellas et al., 2017; Tamborski et al., 2018), despite the presence of several well-known karstic springs (Arfib et al., 2006; Fleury et al., 2007; Stieglitz et al., 2013; Bejannin et al., 2017).

Karstic springs may contribute groundwater to the coastal ocean from different geological sources over different temporal and spatial scales; thus, evaluation of SGD from coastal karst aquifers remains a significant challenge (Montiel et al., 2018). Karst aquifers may respond rapidly to even minor precipitation events, and this rapid flushing can result in significant export events (Fleury et al., 2007). Certain karstic springs may continuously flow in the absence of rainfall, as is the case of the brackish Port-Miou spring, one of the largest groundwater springs that enter the Mediterranean Sea (Arfib and Charlier, 2016). Evaluation of nutrient loads via karst SGD is therefore critical in semi-arid, oligotrophic regions like the Mediterranean Sea (Tovar-Sánchez et al., 2014). Ra isotopes have proved to be useful tracers of SGD from coastal karst aquifers, particularly in the Mediterranean Sea (Ollivier et al., 2008; Garcia-Solsona et al., 2010; Mejías et al., 2012; Tovar-Sánchez et al., 2014; Baudron et al., 2015; Rodellas et al., 2015; Montiel et al., 2018; Tamborski et al., 2018).

A recent study in the Mediterranean Sea reported SGD-driven nutrient estimates based on a basin-wide ^{228}Ra mass balance (Rodellas et al., 2015). The ^{228}Ra inventory, after considering known ^{228}Ra sources and ^{228}Ra sinks, is divided by the ^{228}Ra submarine groundwater endmember activity to determine a SGD flux. Importantly, Rodellas et al. (2015) note that ^{228}Ra SGD endmembers reported throughout the Mediterranean Basin span a wide-range, from 10^2 to 10^5 dpm m^{-3}. This example illustrates the complexity in determining the submarine groundwater endmember, particularly in karst environments. It is thus important to also conduct studies at regional- and local-scales (i) to better constrain the processes involved in the transfer of chemical species between land and the coastal seas and (ii) to elucidate spatial and temporal variability associated with these fluxes.

In this study, we investigated the karstic coastline of the Côte Bleue region located west of the city of Marseille, France. This coastline is located east of the Rhône river plume, where riverine nutrient inputs support 23–69% of the primary production of the Gulf of Lions (Ludwig et al., 2009). This coastline is of specific interest since it may exhibit significant transfer of water and associated solutes toward the sea through terrestrial groundwater discharge, as is the case in other karstic systems worldwide (Garcia-Solsona et al., 2010; Pavlidou et al., 2014; Tovar-Sánchez et al., 2014). SGD may constitute an additional input of nutrients that contributes to sustain the primary production in the coastal sea. Here, we investigated the entire Côte Bleue coastline (22 km), in order to evaluate if coastal sections without springs could also contribute as a nutrient source. In addition, we focused on the temporal variability of these fluxes. We thus conducted offshore transects of radium isotopes that were used to derive horizontal eddy diffusivity coefficients (K_h), that were subsequently combined with surface water nutrient gradients (DSi, $NO_2^- + NO_3^-$) in order to determine the net nutrient flux from SGD. Offshore transects of ^{228}Ra were also investigated with the aim to derive SGD-driven nutrient fluxes by combining K_h and ^{228}Ra gradients with the SGD endmember. Fluxes were investigated over a 1-year period (April 2016, October 2016, December 2016, and March 2017).

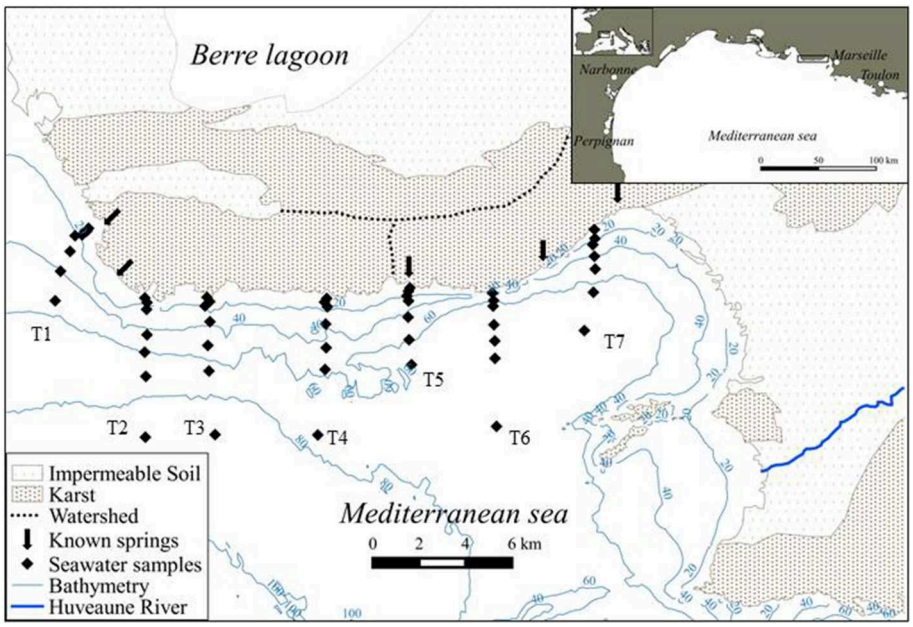

FIGURE 1 | Location of the study site, Côte Bleue, a karstic coastline that is situated in south-eastern France. Previous hydrogeological characterizations (based on Carte Hydrogéologique des Bouches du Rhône, 1972, BRGM) are reported. The location of the offshore transects (T1 to T7) are shown, with diamonds indicating the surface water samples. Arrows indicate the presence of known springs along this coastline.

MATERIALS AND METHODS

Study Site

Côte Bleue is a 22 km long stretch of karstic coastline situated along the French Mediterranean Sea, within the Gulf of Lions. It is located 15 km east of the Rhône River, the largest river discharging into the French Mediterranean Sea, and is 15 km west of the Huveaune River, a small river discharging in Marseille (**Figure 1**). The steep rocky coast hosts a series of coves (Calanques), which shelter small harbors and beaches. Submarine flow paths and springs are known to exist from its three watersheds (**Figure 1**; Carte Hydrogéologique des Bouches du Rhône, 1972, BRGM). Little quantitative information exists on groundwater discharge magnitude, its seasonality and associated solute fluxes. This area receives little to no rain during the summer (from June to September) with low precipitation rates throughout the year (**Figure S1**). The total precipitation recorded during the 2 years of this study (2016–2017) is 632 mm (meteociel.fr). The water depth in this area is 6–20 m at 100 m offshore and 70–80 m depth at 8 km offshore (**Figure 1**). There are no permanent riverine inputs along Côte Bleue. The land and sea adjacent to the coast are protected areas (Natura 2000) and are subject to biologic monitoring (Jouvenel et al., 2004); fishing and diving is banned in the area. Artificial reefs have been installed to improve fish populations (Jensen et al., 2012).

The hydrodynamical regime of the Gulf of Lions is very complex (Millot, 1990). The main general circulation feature that influences the Gulf of Lions is the Northern Current (NC) that flows along the continental slope from east to west (Millot, 1990; see e.g., Figure 1 of Gatti et al., 2006). The NC was shown to occasionally intrude on the shelf (Petrenko, 2003). Maps of horizontal currents in the eastern part of the Gulf of Lions indicate a predominant westward/northwestward flow offshore Côte Bleue (Pairaud et al., 2011). However, these patterns were found further offshore compared to the coastal region that was investigated in the present study. No information is thus available on the circulation patterns in the first 8 km along the coastline. West of Côte Bleue, the circulation pattern generally drives the Rhône river plume westward and therefore the Rhône river plume does not impact the investigated region. In some rare cases, however, the shelf waters in the area of Marseille were shown to be influenced by Rhône river intrusion that may impact the biogeochemical patterns in the area (Gatti et al., 2006; Fraysse et al., 2014).

Field Methods

For reconnaissance of SGD locations, airborne thermal infrared (temperature) and in-water radon mapping were carried out. Airborne thermal infrared images were acquired on 20 September 2012 using a FLIR Systems ThermaCAM SC 3000 along the coast. Detailed information on the flight acquisition is presented in Bejannin et al. (2017). Groundwater temperature tends to follow the average annual air temperature; thus, surface water temperature may be qualitatively used to identify coastal areas potentially impacted by groundwater discharge. Images were acquired in the morning (7:30 a.m.) to provide the largest relative temperature difference between suspected discharging groundwater and ambient surface waters. Thermal infrared images were mosaicked and manually georeferenced against satellite imagery (Google Earth) for visualization.

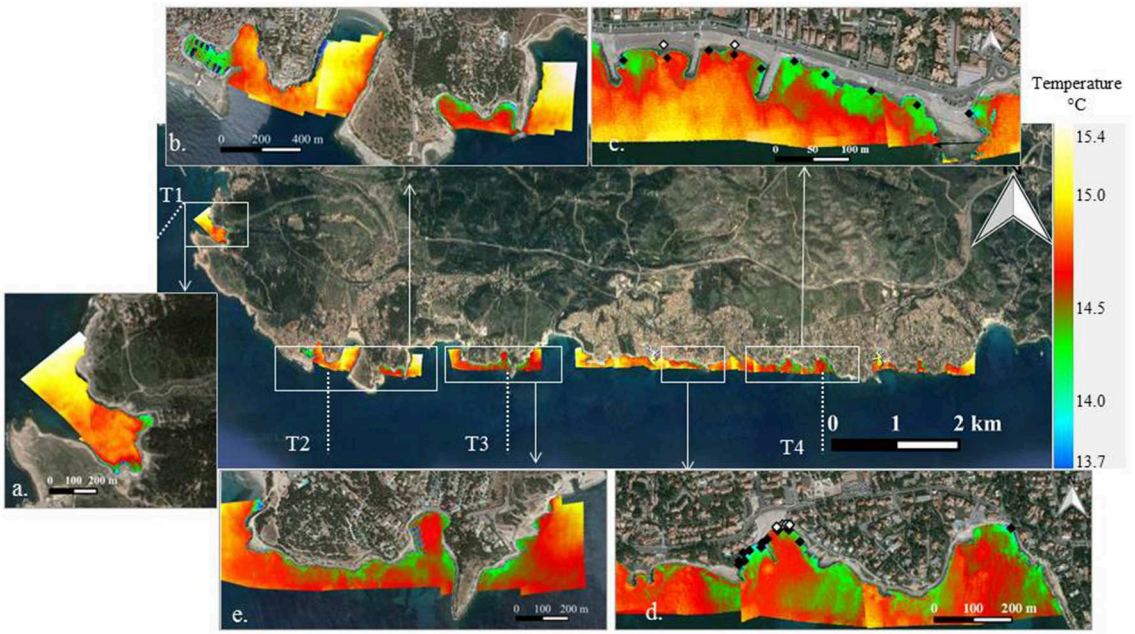

FIGURE 2 | Thermal infrared imagery acquired along Côte Bleue on 20/09/2012 at 7:40 a.m. In the insets that show different zooms of the coastline **(a–e)**, the sampling locations of the nearshore water and porewater samples are displayed on the TIR images. Black diamonds denote nearshore water samples and white diamonds denote porewater samples. It is important to note that the water sample collection and the thermal infrared overflight were not conducted at the same time.

Radon mapping of surface waters was measured *in situ* on 27–28 October 2016 using two Rn-in-air detectors (RAD7-Durridge, Co. Inc.) routed simultaneously through an air-water exchanger in order to locate potential sites of terrestrial groundwater discharge (Burnett and Dulaiova, 2003; Dulaiova et al., 2005; Stieglitz et al., 2013; Cockenpot et al., 2015). Surface water was pumped from 0.5 m depth at a constant flow rate of 2.5 L min^{-1} and filtered through an 80 μm cartridge while continuously moving along the coastline. Data integration of the run was fixed to 15 min, and the system was equilibrated at least for 30 min before the start. We considered that one integrated measurement corresponds to the activity of the water collected 15 min earlier. The distance between each point ranged between 200 and 400 m. The western transect was done from east to west (day 1), and the eastern one from west to east (day 2). In both cases, this direction affected the measurement due to the delay necessary for the equilibration time from high to low activity (Stieglitz et al., 2010). All activities were corrected from temperature, humidity (using the Durridge software) and salinity.

Data from the airborne thermal infrared imagery and continuous ^{222}Rn survey were used to select nearshore and offshore transect sampling stations (**Figures 1**, **2**). Nearshore surface water samples (∼20 L; within 5 m of the shoreline) and porewater samples (∼2–5 L) for Ra isotopes were collected using either a submersible pump or a manual hand pump. These samples were collected in the bay heading transect 1 (Laurons Bay) and in the areas where thermal infrared temperature anomalies exist (**Figure 2**). Three brackish karstic springs were sampled in May 2017 in a small bay (Laurons bay) at transect 1 by scuba divers. Additional porewater samples were collected from hand-dug bore holes which intersected the saturated zone of the beach for areas where there was permeable sediment (**Figure 2**). Seawater samples (∼100 L; from 100 m to 8.5 km offshore) were collected along offshore transects (**Figure 1**) using a submersible pump on board the R/V Antedon II. Various transects and coastal water samples were collected on April 28, October 26–27, December 7–8 in 2016, and on March 20–22 in 2017. Seven shore-perpendicular transects were investigated over these four campaigns (**Figure 1**); only transect T4 was sampled during all four seasonal campaigns (chiefly due to weather constraints). This includes transects conducted offshore sites of known or potential karstic springs and sites where no groundwater discharge exists. Salinity was recorded *in situ* during the sampling operations using the shipboard CTD for the seawater samples, and a handheld WTW^{TM} probe (Xylem) for the nearshore samples. Water samples for nutrients were collected during each cruise using a submersible pump and filtered in the field (0.45 μm).

Laboratory Methods

Water samples for Ra isotopes were passed through MnO_2-coated acrylic fibers ("Mn-fiber") at a flow rate <1 L min^{-1} to ensure a 100% yield of Ra extraction onto the fiber (Moore and Reid, 1973). Once back in the laboratory, the fibers were rinsed three times with Ra-free deionized water and dried with compressed air until a water:fiber ratio of 1:1 was reached (Sun and Torgersen, 1998). Short-lived ^{223}Ra and ^{224}Ra activities were determined using a Radium Delayed Coincidence Counter (RaDeCC; Moore and Arnold, 1996). Detector efficiencies and error propagation calculations were calculated after Moore

(2008) and Garcia-Solsona et al. (2008). A first counting session was run after sample collection to determine the total ^{224}Ra and ^{223}Ra activities. For high activity samples, another counting session was run after 1 week to determine the total ^{223}Ra activity. The Mn-fibers were analyzed again 3 weeks after sampling to determine the ^{224}Ra activities supported by ^{228}Th. These supported activities were then subtracted to the total ^{224}Ra activities to determine excess ^{224}Ra (denoted $^{224}Ra_{ex}$). Select samples were counted at least 1 year after sampling to determine ^{228}Ra activities using RaDeCC via ^{228}Th ingrowth, following Moore (2008). Select samples (T1 and T7 for all cruises) were additionally analyzed for ^{228}Ra using the low-background gamma detectors at the LAFARA underground laboratory in Ferrières, French Pyrénées (van Beek et al., 2010, 2013). Prior to gamma analysis, the Mn-fibers were dried, pressed using a hydraulic press at 20 metric tons, placed into plastic boxes and vacuum sealed into bags to prevent from any Rn loss. A semi-planar detector (ORTEC/AMETEK; van Beek et al., 2013) was used to determine ^{228}Ra activities from an average of the ^{228}Ac photo-peaks (338, 911, and 969 keV).

Nutrient samples were filtered at 0.45 μm, immediately poisoned with $HgCl_2$ (10 μg L^{-1}) and stored at 4°C in the dark. In the laboratory, nitrate (NO_3^-), nitrite (NO_2^-), phosphate (PO_4^{3-}) and dissolved silica (DSi) concentrations were measured on a continuous flow autoanalyzer Technicon® AutoAnalyzer II at LOMIC, Banyuls-sur-Mer (Aminot and Kérouel, 2004). The analytical precision of NO_3^-, NO_2^-, PO_4^{3-}, and DSi is ±0.02, ±0.01, ±0.02, and ±0.05 μM, respectively.

Water and Solute Flux Estimations

Several methods based on the use of geochemical tracers (i.e., radium isotopes and radon) are used to quantify SGD fluxes (Burnett et al., 2006), including isotope mass balances and gradient flux calculations. The radium quartet (^{223}Ra, $t_{1/2}$ = 11.4 d; ^{224}Ra, $t_{1/2}$ = 3.66 d; ^{226}Ra, $t_{1/2}$ = 1,600 y; ^{228}Ra, $t_{1/2}$ = 5.75 y), as well as ^{222}Rn ($t_{1/2}$ = 3.83 d), have been widely used to study SGD worldwide (Moore, 1996; Charette et al., 2001; Paytan et al., 2006; Rodellas et al., 2015; Tamborski et al., 2015). These radionuclides are produced within an aquifer by the decay of their sediment-bound U/Th series parent nuclide. Production near the mineral surface provides sufficient energy to recoil the daughter isotope into the surrounding pore fluid (Swarzenski, 2007). Ra isotopes tend to be adsorbed onto sediments at low ionic strengths (i.e., freshwater); however, Ra isotopes are desorbed and released into the surrounding pore fluid under brackish conditions (Webster et al., 1995). Ra isotope activities are typically 2–3 orders of magnitude greater in brackish groundwaters than in surface waters; thus, Ra isotopes are powerful tracers of SGD inputs to the sea. The range of half-lives (from days to thousands of years) of these isotopes allows for the quantification of SGD flow-paths which may occur over a wide-range of time scales (Moore, 1996; Charette et al., 2001).

SGD fluxes of conservative chemical elements can be quantified by combining horizontal eddy diffusivity coefficients K_h (derived from short-lived Ra isotopes) and offshore gradients of the elements under consideration (Moore, 2000a; Windom et al., 2006). This method provides a direct estimate of the chemical flux, and the knowledge of the SGD endmember is not required, which is an advantage since the endmember is not always easy to determine. However, the calculation is only valid when the chemical element under consideration behaves conservatively in seawater, that is, it is not significantly impacted by biological or geochemical processes within the time-frame of the coastal water residence time. Further, this assumes that the chemical element gradient is derived solely from SGD. Alternatively, K_h can be combined to the offshore gradient of ^{228}Ra (or ^{226}Ra) and the calculated ^{228}Ra SGD flux can then be converted into a chemical flux by multiplying the ^{228}Ra flux by the chemical element/^{228}Ra ratio in the SGD endmember. Such a calculation implies that the SGD endmember is well-constrained for ^{228}Ra and the chemical element of interest. Both methods have been widely used to derive SGD fluxes (Charette et al., 2001; Hancock et al., 2006; Niencheski et al., 2007; Knee et al., 2011; Li and Cai, 2011).

The principal method used here to derive SGD-driven nutrient fluxes combines horizontal eddy diffusivity coefficients (K_h; determined by short-lived Ra surface water gradients) with surface water nutrient gradients (section Nutrient Mixing Model). As a comparison, SGD-driven nutrient fluxes were determined by combining horizontal eddy diffusivity coefficients with surface water ^{228}Ra gradients and nutrient endmember concentrations (when it was applicable; section ^{228}Ra Mixing Model).

Nutrient Mixing Model

Surface water ^{223,224}Ra activities are used to estimate the exchange rate between the Côte Bleue coastline and the coastal sea. If horizontal dispersion can be approximated by a diffusive process, then a one-dimensional model can be applied, assuming that advection is negligible and conditions are in steady-state (Moore, 2000a):

$$\frac{dA}{dt} = K_h \frac{\partial^2 A}{\partial d^2} - \lambda A \quad (1)$$

where A is the radium isotope activity, K_h is the horizontal eddy diffusivity coefficient (m^2 s^{-1}), d is the distance offshore and λ is the decay constant of the Ra isotope used. Assuming steady state, the solution of Equation (1) is:

$$A_d = A_0 \exp(-d\sqrt{\frac{\lambda}{K_h}}) \quad (2)$$

where A_d is the Ra isotope activity at the distance d from the coast and A_0 is the radium activity at the boundary ($d = 0$). The horizontal eddy diffusivity coefficient (K_h) can thus be estimated from a plot of $\ln(^{224}Ra_{ex})$ as a function of offshore distance (Moore, 2000a). K_h is then calculated from the estimate of the slope of the linear regression ($K_h = \lambda/m^2$ where m is the slope of the linear regression). Horizontal eddy diffusivity coefficients (m^2 s^{-1}) were calculated for each campaign. The horizontal eddy diffusivity coefficient uncertainty was determined from the error associated with the slope of the ln(Ra) vs. offshore distance relationship, which includes the analytical uncertainty of the Ra

measurement (Garcia-Solsona et al., 2008). The uncertainty of K_h is thus:

$$\Delta(\mathrm{K_h}) = 2\mathrm{K_h}\frac{\Delta \mathrm{m}}{\mathrm{m}} \quad (3)$$

where $\Delta(K_h)$ is the uncertainty associated with K_h, m is the slope of the linear relationship ln(Ra) vs. offshore distance and Δm is the error determined using Origin Software.

The horizontal eddy diffusivity coefficients obtained for each campaign are then multiplied by the observed surface water nutrient gradient to calculate the SGD-driven nutrient flux. The offshore nutrient gradient (μmol L^{-1} km^{-1}) is defined as the slope of the plot of a nutrient concentration as a function of offshore distance. A nutrient flux (μmol s^{-1} km^{-1}) is calculated by multiplying the horizontal eddy diffusivity coefficient with the nutrient gradient by the depth of the water layer impacted by SGD (i.e., terrestrial groundwater inputs and also potentially circulation of seawater through the sediment). This thickness was determined from the CTD vertical profiles acquired at each sampling station and from several vertical profiles of Ra isotopes (**Table S1**). A range of 5–10 m depth was used in the calculations. This calculation assumes that nutrient uptake and utilization is negligible over the time-scale of offshore water transport, and that the surface water Ra and nutrient gradients are solely derived from SGD. Uncertainty in the nutrient flux was propagated as the uncertainty of the horizontal eddy diffusivity coefficients and the uncertainty of the slope of the nutrient concentration surface water gradient. The assumptions used in the model are the following: (i) we neglect advection; (ii) the source term for Ra and nutrients is the coastline ($d = 0$); and (iii) nutrient consumption is assumed to be negligible. These assumptions are further discussed in section Mixing Model: K_h * Nutrient Offshore Gradient.

^{228}Ra Mixing Model

SGD-driven nutrient fluxes were also calculated using the observed surface water ^{228}Ra gradient for each transect, as a comparison to the above approach (Moore, 2000a; Charette et al., 2007). The horizontal eddy diffusivity coefficient is multiplied by the ^{228}Ra surface water gradient and the layer depth impacted by SGD to determine a ^{228}Ra flux (dpm d^{-1} km^{-1}), assuming that the observed ^{228}Ra is derived from SGD. The volumetric SGD flux is estimated by dividing the ^{228}Ra flux by the ^{228}Ra activity of the SGD endmember. The nutrient flux can finally be estimated by multiplying this water flux with the nutrient concentration of the endmember. We choose the average ^{228}Ra activity and nutrient concentrations of the three brackish springs sampled in Laurons bay as the SGD endmember. The SGD endmember must be well-characterized in this approach, which can introduce additional uncertainty; this is further discussed in section ^{228}Ra Gradient Method.

SYMPHONIE Model

Simulations of oceanic circulation in the Gulf of Lions have been conducted using the SYMPHONIE model (Marsaleix et al., 2008, 2019). This model has been widely used to study the Rhône plume in situations of realistic forcing by wind and river discharge (Estournel et al., 2001; Reffray et al., 2004) and more broadly the circulation over the entire Gulf of Lions (Estournel et al., 2003; Petrenko et al., 2008). The model configuration is based on a bipolar grid with a resolution of about 375 m on the Gulf of Lions shelf gradually increasing further offshore. This simulation is embedded in a configuration of the whole Mediterranean. The meteorological forcing is calculated with bulk formulas based on the hourly outputs of the ECMWF weather forecast model. The daily flow of the Rhône and the main rivers of the Gulf of Lions is extracted from the HYDRO database (www.hydro.eaufrance.fr). The simulation runs from July 2011 to April 2017. Daily averages of salinity and current are stored and presented here.

RESULTS

Reconnaissance of SGD Sites

There are several cooler surface water temperature plumes (~14°C) with respect to the warmer, ambient seawater (>15°C) identified by the previous airborne thermal infrared survey (**Figure 2**). Locations of cooler surface water temperatures may be influenced by groundwater inputs, as groundwater temperatures reflect the mean annual air temperature (Anderson, 2005). However, it cannot be excluded that other processes may also impact the temperature of surface waters in such coastal environments at this time of the day (e.g., cooling of shallow nearshore waters during the night; impact of waves, etc.). There are several small, low temperature plumes in bays in front of transects 1, 2, and 3 (**Figures 2a,b,e**). Finally, several plumes are visible at two locations where the coastline transitions to a beach near transect 4 (Sausset-les-Pins and Carry-le-Rouet, **Figures 2c,d**, respectively). For Sausset-les-Pins (**Figure 2d**), several plumes are visible between jetties, while no temperature differences are visible on other parts of the coastline. For Carry-le-Rouet (**Figure 2c**), the plumes are located throughout the coastline. These two locations were further investigated with salinity and radium isotope measurements (see below) to validate that the surface water temperature signatures were impacted by SGD. It is important to note that the airborne TIR flight (2012) was not conducted at the same time as the water sampling campaigns (2016–2017).

Two zones of surface water enrichments (>1 km of shoreline length) of ^{222}Rn were observed (**Figure 3**). The local ^{222}Rn enrichments reach activities up to two orders of magnitude higher (370–2,150 dpm 100 L^{-1}) than other *in situ* measurements taken along the coast (<370 dpm 100L^{-1}), indicating two prominent locations of SGD that include the Laurons bay west of Côte Bleue (T1) and Niolon bay (T7) east of Côte Bleue. These two areas correspond to sites where springs are known to discharge into the coastal seas and where large fractures exist, as noted by geological maps (**Figure 1**). A slight increase in ^{222}Rn is also observed near transect 3, consistent with the previous airborne temperature signatures (**Figure 2**).

^{223}Ra and $^{224}Ra_{ex}$ activities were highest closest to the shoreline and decreased in activity with increasing distance offshore, with significant temporal variability (**Figure 4**; ^{223}Ra not shown). Transect 4 was sampled during all campaigns; the sample collected closest to the shoreline shows large differences

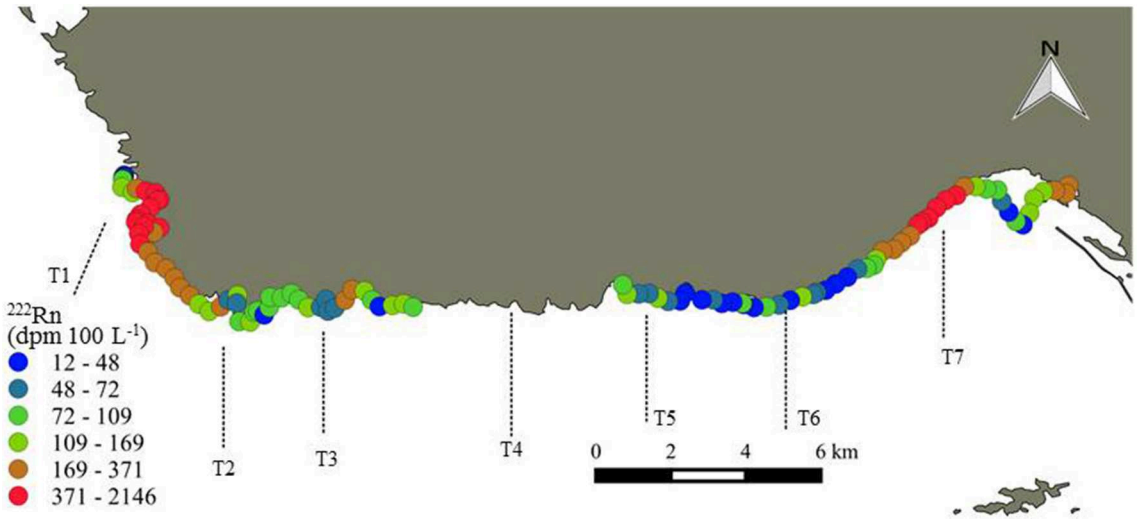

FIGURE 3 | Radon activities (dpm 100 L^{-1}) acquired from a continuous shoreline survey on 27–28 October 2016. The dotted lines represent the location of the offshore surface water transects. Note that the color scale is not linear.

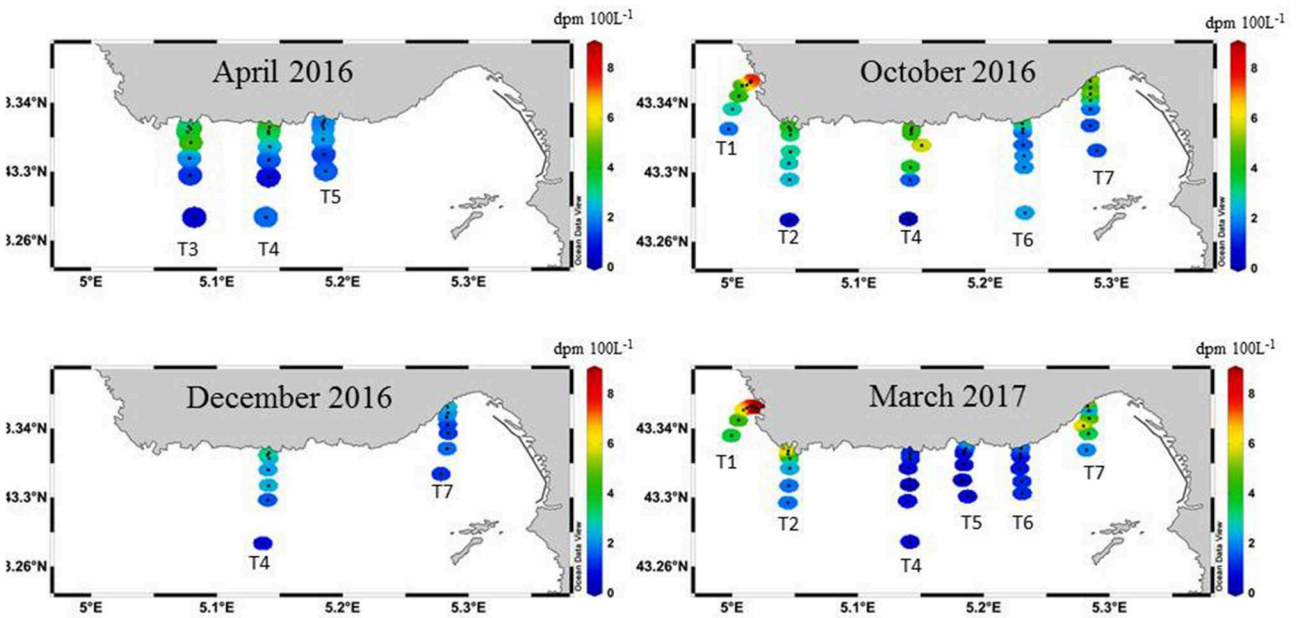

FIGURE 4 | $^{224}Ra_{ex}$ activities (dpm 100 L^{-1}) determined in surface waters along the transects off Côte Bleue in April 2016, October 2016, December 2016, and March 2017. The same color scale is used for the four panels.

in activity, with a maximum value in October (4.8 dpm 100 L^{-1}) and a minimum value in March (1.0 dpm 100 L^{-1}). During October 2016 and March 2017, the highest observed Ra activities were observed for the western most and the eastern most transects (**Figure 4**), which coincides with the shoreline areas where the ^{222}Rn signal was the highest (**Figure 3**). However, T1 was not sampled in April and December 2016 and T7 was not sampled in April 2016. The sampling stations farthest from the coast (~6–8 km) have $^{224}Ra_{ex}$ activities ranging from below detection limit (i.e., no excess ^{224}Ra) to 3.6 dpm 100 L^{-1}, with an average (±STD) value of 1.3 (±0.9) dpm 100 L^{-1} ($n = 16$; **Table 1**). The ^{228}Ra activities in the coastal seas (<8 km) range between 1.7 and 24 dpm 100 L^{-1}, with a mean value of 4.2 ± 2.3 dpm 100 L^{-1} ($n = 98$; **Table 1**), indicating that these coastal waters are enriched in ^{228}Ra with respect to open Mediterranean seawaters (typically 1–2.5 dpm 100 L^{-1}; Schmidt and Reyss, 1996; van Beek et al., 2009; Rodellas et al., 2015).

Surface water samples collected in several locations of cooler surface water temperatures within the first 5 m of the shoreline, as identified by the previous airborne TIR flight (**Figure 2**), display

TABLE 1 | Average ± standard deviation of salinity and Ra isotopes in seawater (from 100 m to 8 km offshore), nearshore water (within 5 m offshore), karstic springs and minimum—maximum values of salinity, and Ra isotopes for shallow porewater (0.5 m depth) sampled from April 2016, October 2016, December 2016, and March 2017.

Sample type	Sampling month	*n*	Salinity	^{223}Ra dpm 100 L^{-1}	^{224}Ra$_{ex}$ dpm 100 L^{-1}	^{228}Ra dpm 100 L^{-1}
Seawater	Apr-16	21	38.0 ± 0.3	0.3 ± 0.1	2.3 ± 1.3	4.0 ± 4.0
	Oct-16	36 (32)	38.2 ± 0.1	0.4 ± 0.2	3.4 ± 1.9	3.3 ± 1.6
	Dec-16	14	–	0.2 ± 0.1	1.5 ± 0.7	3.6 ± 0.8
	Mar-17	46 (31)	38.1 ± 0.4	0.3 ± 0.3	2.9 ± 3.5	4.0 ± 1.2
	Average	117 (98)	38.1 ± 0.3	0.3 ± 0.2	2.9 ± 2.5	4.2 ± 2.3
Coastal water	Oct-16	9	37.1 ± 0.7	2.2 ± 1.7	31 ± 51	5.4 ± 2.6
	Dec-16	14	21.8 ± 0.4	0.7 ± 0.5	8.1 ± 3.3	4.5 ± 0.8
	Mar-17	18 (15)	37.7 ± 1.3	2.6 ± 3.4	45 ± 83	4.7 ± 0.9
	Average	41 (38)	37.7 ± 0.9	1.1 ± 0.8	11 ± 5.0	4.8 ± 1.4
Porewater	Oct-16	2	17.8–37.5	2.4–13.1	21–278	5.9–82
	Dec-16	5	18.2–38.1	6–39	28–212	2.1–16
	Mar-17	5 (3)	13.7–38.1	3.6–18.4	39–324	2.4–18
	Average	13 (11)	13.7–38.1	2–39	21–324	2.1–82
Karstic spring	Average (May-17)	3 (3)	27.0 ± 0.9	37 ± 25	1,485 ± 658	826 ± 45

*Shallow porewater and coastal water sample locations are presented in **Figure 2**; seawater sample locations are presented in **Figure 1**. Numbers within brackets are the number of samples analyzed for ^{228}Ra.*

a salinity of 37.7 ± 0.9, which is not significantly different from offshore seawater (salinity = 38.1 ± 0.3; **Table 1**). The salinity measurements conducted in nearshore waters, therefore, do not confirm that the TIR plumes could be related to terrestrial groundwater inputs. These samples display relatively higher short-lived Ra activities (**Table 1**). ^{228}Ra activities in nearshore water samples (along the beach) and seawater samples (up to 8.5 km) were similar, with activities of 4.8 (±1.4) and 4.2 (±2.3) dpm 100 L^{-1}, respectively. Shallow porewater samples (0.5 m) taken along the coastline were reduced in salinity (29.3 ± 9.7; minimum = 13.7) and higher in short-lived Ra activities, reflecting influence of a terrestrial groundwater endmember (**Figure 5**). ^{223}Ra and ^{224}Ra$_{ex}$ activities were between 2–39 and 21–324 dpm 100 L^{-1} in porewaters while ^{228}Ra activities were 2.1–203 dpm 100 L^{-1} (**Figure 5**). Finally, three karstic springs that discharge in Laurons bay at transect T1 showed average ^{223}Ra, ^{224}Ra$_{ex}$, and ^{228}Ra activities of 37 (±25), 1,485 (±658), and 826 (±45) dpm 100 L^{-1}, respectively ($n = 3$; **Table 1**).

Taken together, these lines of evidence suggest that the chemical enrichments observed along this 22 km coastline (^{223}Ra, ^{224}Ra$_{ex}$, ^{228}Ra, and ^{222}Rn; **Table 1**) are driven by SGD. This includes the discharge of terrestrial groundwater (e.g., via ^{222}Rn) and, although it is predominantly a rocky coast, a component of seawater circulation through permeable sediment, as evidenced by the porewaters collected in several beaches (**Figure 5**).

Nutrient Concentrations

Average (±STD) nutrient concentrations for nearshore waters (<5 m offshore) and seawater samples are reported in **Table 2**, as well as minimum and maximum values of nutrient concentrations for shallow porewaters. During October 2016, nearshore waters (taken in areas of previously identified thermal infrared anomalies) had an average (±STD) concentration of 0.1 (±0.1) μM PO_4^{3-}, 5.8 (±11.5) μM DSi, and 3.8 (±6.9) μM $NO_2^- + NO_3^-$ (sum of NO_2^- and NO_3^-, hereafter NO_3^- as this sum is >80% of NO_3^- on average). Nearshore waters sampled during December 2016 had lower nutrient concentrations than the samples collected in October, with average values of 0.03 (±0.02), 1.1 (±0.4), and 0.8 (±0.3) μM for PO_4^{3-}, DSi and NO_3^-, respectively. In general, offshore seawater samples collected were greatest for PO_4^{3-}, DSi, and NO_3^- during April and March, while average concentrations were lower in December and October. In general, the concentrations of DSi and NO_3^- decreased with increasing salinity, and thus distance offshore, similar to ^{223}Ra and ^{224}Ra$_{ex}$ (**Figures 4–6**). Most PO_4^{3-} concentrations in seawater were below the method detection limit (0.01 μM).

Porewater concentrations were approximately one order of magnitude higher than coastal surface waters, with values between 0.01 and 4.0 μM for PO_4^{3-}, 1.9 and 133 μM for DSi, and 22 and 194 μM for NO_3^- over the sampled salinity gradient (**Figure 6**). The variable average nutrient concentrations between sampling months (**Table 2**) may reflect changes in porewater salinity, rather than a seasonal endmember (**Figure 6**). The average NO_3^- and DSi concentrations of the springs sampled in Laurons bay in front of transect T1 are 2.3 (±3.3) 113 (±40) μM, respectively ($n = 3$; mean salinity of 27). PO_4^{3-} was not analyzed for these springs.

DISCUSSION

Estimate of the SGD Fluxes

Determination of the Horizontal Eddy Diffusivity Coefficients K_h

All of the surface water transects were used to estimate horizontal eddy diffusivity coefficients, K_h (**Figure 7**). We do not observe any significant difference between the ^{223}Ra and ^{224}Ra$_{ex}$ derived

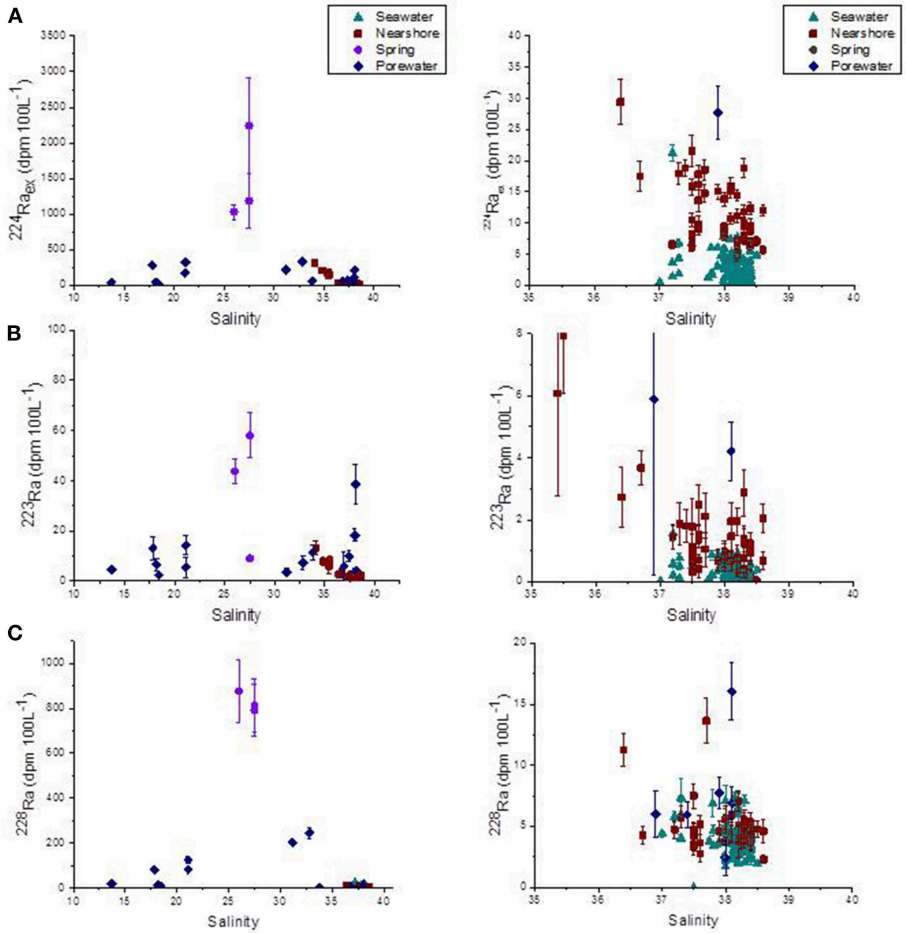

FIGURE 5 | (A) $^{224}Ra_{ex}$ (dpm 100 L^{-1}), **(B)** ^{223}Ra (dpm 100 L^{-1}), and **(C)** ^{228}Ra (dpm 100 L^{-1}) along Côte Bleue as a function of salinity, for all sampling dates. Samples are categorized by water types (karstic spring, porewater, nearshore water within 5 m from the shoreline and seawater from 100 m to 8 km offshore). Right-hand side panels are zooms between salinity 35 and 40.

K_h. Here, we choose to report the K_h values derived from the $^{224}Ra_{ex}$ activities that display lower uncertainties (**Figure 7**). The slopes (together with their associated uncertainty) of the linear relationships between ln(^{224}Ra) and offshore distance are reported for each campaign on **Figure 7**, together with the correlation coefficients r and p-values. For a given season, the $^{224}Ra_{ex}$ activities reported for the different transects are similar and decrease with increasing offshore distance. Therefore, we report a single K_h value for each season that is deduced from the slope of the linear relationship (following Equation 2). In doing so, the number of data points is increased and the significance of the correlation coefficient is thus improved. We calculate the error of the slope, which we use to determine the uncertainty on the K_h estimate, unlike many studies that report K_h values without considering any associated uncertainty (Moore, 2000a; Tamborski et al., 2018). Note that in March 2017, two different trends were observed (transects T1, T2, T7 showing higher Ra activities than transects T4, T5, T6). In this latter case, two K_h estimates were determined from the two trends (**Figure 7**). However, the slopes obtained are the same (within error bars) and therefore the K_h estimates are not significantly different. This suggests that the two trends observed in March 2017 were not the result of different offshore mixing characteristics but are rather explained by differences in the absolute Ra activities at the coast (i.e., higher ^{224}Ra activities in March 2017 for T1 and T7 that are located offshore of springs, but also for T2). The significance of the correlation coefficients suggests that the offshore dispersion of the Ra activities may indeed be approximated by a 1D diffusive mixing model. However, we have no *in situ* information that would support the assumption of negligible advection.

The mean K_h for the two transects sampled in April 2016 is 39 (±22) m^2 s^{-1} (**Table 3**). In October 2016, 5 transects were investigated and the mean K_h is 96 (±44) m^2 s^{-1}. The highest K_h was estimated for December 2016, with a K_h of 184 (±112) m^2 s^{-1}, which could be related to the winter conditions (increased mixing). In March 2017, the K_h values associated with the two groups of transects were 56 (±42) and 52 (±35) m^2 s^{-1}, for transects T1, T2, T7, and transects T4, T5, T6, respectively. The K_h values do not exhibit a significant temporal variability when considering their associated uncertainties.

TABLE 2 | Average ± standard deviation of nutrient concentrations in seawater (from 100 m to 8 km offshore), nearshore water (within 5 m offshore), karstic springs and minimum—maximum values for shallow porewater (0.5 m depth) sampled from April 2016, October 2016, December 2016, and March 2017, and karstic springs (Laurons bay).

Sample type	Sampling month	*n*	PO_4^{3-} μM	$Si(OH)_4$ μM	$NO_2^- + NO_3^-$ μM
Seawater	Apr-16	21	0.04 ± 0.02	2.1 ± 0.5	1.3 ± 0.5
	Oct-16	36	0.02 ± 0.02	1.4 ± 0.3	0.3 ± 0.2
	Dec-16	14	0.02 ± 0.02	1.5 ± 0.4	0.7 ± 0.3
	Mar-17	46	0.03 ± 0.02	1.6 ± 0.5	1.5 ± 0.5
	Average	117	0.02 ± 0.02	1.6 ± 0.5	1.0 ± 0.7
Coastal water	Oct-16	9	0.09 ± 0.10	5.8 ± 11.5	3.8 ± 6.9
	Dec-16	14	0.03 ± 0.02	1.1 ± 0.4	0.8 ± 0.3
	Mar-17	18	0.08 ± 0.13	7.0 ± 15.4	1.7 ± 2.5
	Average	41	0.06 ± 0.09	4.2 ± 10.8	1.8 ± 3.8
Porewater	Oct-16	2	1.1–2.0	87–109	44–194
	Dec-16	5	0.01–4.0	2–58	2–56
	Mar-17	5	0.3–1.2	6–133	22–41
	Average	12	0.01–4.0	2–133	22–194
Karstic spring	May-17	3	–	82–157	0.02–4.26
	Average	3	–	113 ± 40	

Mixing Model: K_h * Nutrient Offshore Gradient

For numerous transects, there is no significant nutrient gradient (for example, no DSi gradient for T5 in April 2016; **Figure 8A**); in this case, a slope is not reported and the nutrient flux is not estimated with this method. Statistically significant surface water gradients (and gradient uncertainties) are reported in **Figure 8** for DSi, and in **Figure 9** for NO_3^-. Surface water DSi and NO_3^- gradients, with estimated uncertainties, are summarized by sampling season in **Table 3**. It bears mention that NO_3^- gradients may not capture the complete dissolved inorganic nitrogen gradient, which may comprise a significant pool of NH_4^+. We do not report PO_4^{3-} gradients, as the concentration of PO_4^{3-} is very low and uniform in the Mediterranean seawater samples (**Table 2**).

$^{224}Ra_{ex}$-derived horizontal eddy diffusivity coefficients (K_h; **Figure 7**) were thus multiplied by (statistically significant) surface water nutrient gradients (**Figures 8**, **9**; **Table 3**) and the water depth impacted by SGD (5–10 m). Corresponding DSi fluxes varied between 0.9 (±0.9)−1.7 (±1.8) $*10^3$ mol d^{-1} km^{-1} of shoreline and 6.3 (±4.5)−13 (±9.4) $*10^3$ mol d^{-1} km^{-1} of shoreline, estimated in April 2016 and December 2016, respectively (**Figure 10**). NO_3^- fluxes were between 0.5 (±0.4)−1.1 (±0.7) $*10^3$ and 3.4 (±3.5)−6.9 (±6.9) $*10^3$ mol d^{-1} km^{-1} of shoreline for the same seasons (**Figure 10**).

April 2016 exhibited the lowest mean DSi flux, with only one statistically significant seawater DSi transect (T4; **Figure 10**). In comparison, the monthly average DSi fluxes were maximum in October and December 2016. We do observe significant temporal variability among individual transects that were repeatedly sampled (transects 4 and 7). DSi fluxes were four times higher in October than in April for transect 4, and up to 8 times higher in December for that same transect. Temporal variability in nutrient flux for these repeated transects may be driven by temporally variable precipitation. The total precipitation registered (during 4 days) 12 days before the December sampling equaled 88 mm while 33 mm of rainfall was registered (during 4 days) 11 days prior to the October sampling. Monthly averaged NO_3^- fluxes are similar between the different sampling periods (**Figure 10**; **Table 3**). NO_3^- fluxes estimated for transect 4 were similar in April and October. The average (±STD) DSi and NO_3^- fluxes, for all the transects in which a nutrient gradient was estimated, equal to 6.2 (±5.0) $*10^3$ and 4.0 (±2.0) $*10^3$ mol d^{-1} km^{-1}, respectively (**Figure 10**; **Table 3**).

It remains to be seen if SGD is the sole source of the observed nutrient gradients. Nutrient inputs from the Rhône River, the largest river that enters the Mediterranean Sea and whose river mouth is 15 km from the western shoreline of Côte Bleue, may be deflected eastward toward Côte Bleue on rare occasions (Gatti et al., 2006; Fraysse et al., 2014). Surface salinity maps have been generated using the SYMPHONIE model to study the fate of the Rhône river plume into the Gulf of Lions at the dates of the sampling campaigns. The plume was usually deflected toward the West (April 2016, October 2016, December 2016). In contrast, intrusion of Rhône river water (eastward transport) was observed on 15–16 March 2017 (that is, 1 week before the March 2017 sampling campaign), with diluted river waters reaching the entire Côte Bleue coastline (**Figure 11**). On 21 and 22 March, the impact of river waters was less important, with the exception of the western Côte Bleue that was still potentially impacted by these waters (**Figure 11**). The intrusion of Rhône river waters may thus have impacted the nutrient and Ra distributions offshore Côte Bleue during the March 2017 campaign. There are no other known nutrient sources along Côte Bleue. On the other hand, interpretation of offshore nutrient gradients (or lack thereof) is subject to a sound understanding of the uptake rate of inorganic nutrients in the water column, in addition to other known nutrient sources and sinks. As shown in Monterey Bay, nutrient loads driven by SGD can be quickly utilized by phytoplankton (Lecher et al., 2015). Along Côte Bleue, the apparent surface water ages derived from $^{224}Ra/^{228}Ra$ activity ratios (Moore, 2000b) range from several days (open coastline) to ca. ten days in semi-enclosed bays like Laurons bay located in front of T1. Nutrient uptake cannot be excluded over this time scale and could impact the offshore nutrient gradient. Thus, we rely on several different methods (e.g., Radon survey; ^{228}Ra offshore gradients), in addition to the nutrient gradient method, to constrain SGD along Côte Bleue.

^{228}Ra Gradient Method

The regional view of the entire dataset is that the ^{228}Ra activities do not decrease with increasing distance offshore (**Figure 12**). Only two transects among the 16 transects investigated here display statistically significant offshore ^{228}Ra gradients ($p < 0.01$) and we thus derived SGD fluxes from these data only. The ^{228}Ra gradient for T7 in December 2016 is −0.164 (±0.065) dpm 100 L^{-1} km^{-1} while the ^{228}Ra gradient for T5 in March 2017 is −0.225 (±0.058) dpm 100 L^{-1} km^{-1}. The ^{228}Ra fluxes are estimated by combining these gradients with the ^{224}Ra-derived

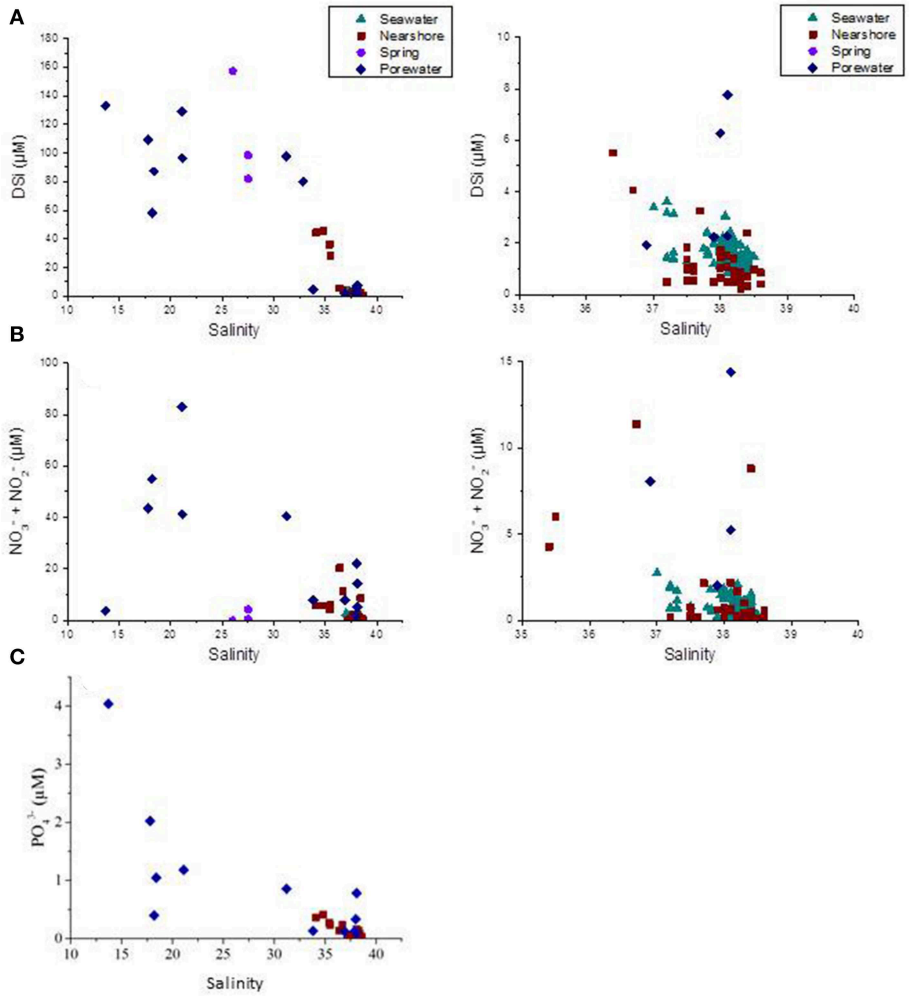

FIGURE 6 | (A) DSi (µM), **(B)** $NO_2^- + NO_3^-$ (µM), and **(C)** PO_4^{3-} (µM) along Côte Bleue as a function of salinity, for all sampling dates. Samples are categorized by water types (karstic spring, porewater, nearshore water within 5 m from the shoreline, and seawater from 100 m to 8 km offshore). Right-hand side panels are zooms between salinity 35 and 40.

horizontal eddy diffusivity coefficient corresponding to the appropriate month (section Determination of the Horizontal Eddy Diffusivity Coefficients K_h). The ^{228}Ra fluxes are thus 2.6 (±1.9) *10^8 and 1.8 (±0.8) *10^8 dpm d^{-1} km^{-1} for December (T7) and March (T5), respectively.

This method requires the use of the SGD endmember to determine the volumetric SGD flux (obtained by dividing the ^{228}Ra fluxes by the ^{228}Ra activity of the endmember). The nutrient flux can finally be estimated by multiplying this water flux with the nutrient concentration of the endmember. This makes this method particularly sensitive to the endmember, which is not easy to define in this region (spring at its outlet vs. porewater; **Figures 5**, **6**). Using the karstic springs as an endmember (^{228}Ra of 826 ± 45 dpm 100 L^{-1}; $n = 3$), this yields a volumetric SGD flux for T7 in December 2016 of 1.6 (±1.2)−3.2 (±2.3) *10^4 m^3 d^{-1} km^{-1} using an impacted layer of 5 and 10 m, respectively. The volumetric SGD fluxes for T5 in March 2017 are 0.7 (±0.5)−1.4 (±1.0) *10^4 m^3 d^{-1} km^{-1}, respectively. Using the mean DSi concentration in the spring (113 µM), the DSi fluxes thus estimated are 1.8 (±1.4)−3.6 (±2.9) *10^3 mol d^{-1} km^{-1} for T7 in December and 0.8 (±0.6)−1.6 (±1.2) *10^3 mol d^{-1} km^{-1} for T5 in March (for 5 and 10 m impacted depths, respectively). These estimations are on the same order of magnitude as the estimations reported in section Mixing Model: K_h * Nutrient Offshore Gradient (**Figure 10**). Using the NO_3^- concentrations of the brackish springs (2.4 ± 2.6 µM; two springs considered out of the three), the NO_3^- fluxes estimated from the ^{228}Ra gradient are 0.04 (±0.06)−0.08 (±0.10) *10^3 and 0.02 (±0.03)−0.03 (±0.04) *10^3 mol d^{-1} km^{-1} for T7 and T5, respectively. The estimations of NO_3^- fluxes are lower than the estimations made in section Mixing Model: K_h * Nutrient Offshore Gradient. Note that the NO_3^- concentrations of the brackish springs are surprisingly low (2.4 ± 2.6 µM) compared to other Mediterranean karstic springs (e.g., Rodellas et al., 2015). This pattern could explain the NO_3^- fluxes being lower than the estimations made in section Mixing Model: K_h * Nutrient

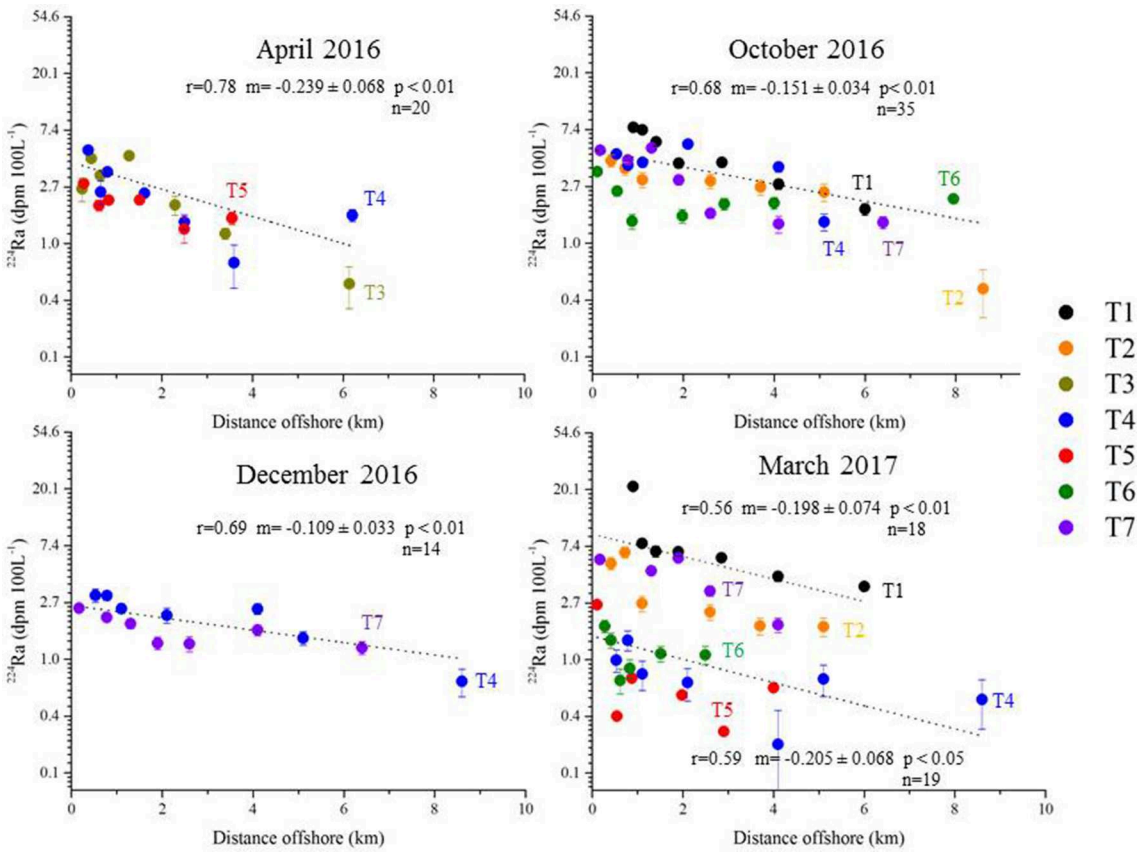

FIGURE 7 | Plot of ln $^{224}Ra_{ex}$ (dpm 100 L^{-1}) as a function of distance offshore. The transects are arranged by sampling date (April 2016, October 2016, December 2016, and March 2017). Each transect is presented by a unique color. For each season, we report the correlation coefficient *r*, slope *m* (and associated uncertainty), *p*-value, and the number of values (*n*) used to build the linear regression.

TABLE 3 | Monthly averaged horizontal eddy diffusivity coefficients (K_h; m^2 s^{-1}), nutrient gradients (μmol L^{-1} km^{-1}) and nutrient fluxes (mol d^{-1} km^{-1}) along Côte Bleue.

Sampling time	K_h (^{224}Ra)	DSi gradient	$NO_2^- + NO_3^-$ gradient	DSi flux	$(NO_2^- + NO_3^-)$ flux
	m^2 s^{-1}	μmol L^{-1} km^{-1}		mol d^{-1} km^{-1}	
Apr-16	39 ± 22	−0.05 ± 0.04	−0.09 ± 0.04	1.7E+03 ± 1.8E+03	3.2E+03 ± 2.3E+03
Oct-16	96 ± 44	−0.08 ± 0.03	−0.04 ± 0.03	6.4E+03 ± 3.8E+03	3.7E+03 ± 2.7E+03
Dec-16	184 ± 112	−0.08 ± 0.03	−0.04 ± 0.03	1.3E+04 ± 9.0E+03	6.9E+03 ± 6.9E+03
Mar-17	54 ± 38	−0.07 ± 0.01	−0.05 ± 0.02	3.5E+03 ± 2.5E+03	2.2E+03 ± 1.8E+03
Average				6.2E+03 ± 5.0E+03	4.0E+03 ± 2.0E+03

The flux estimations reported here were made using 10 m as the water depth impacted by SGD.

Offshore Gradient and questions the validity of the NO_3^- endmember used for this method. The spring endmember may be dominated by NH_4^+, which we did not measure in this study.

Alternatively, considering the maximum NO_3^- concentrations of the porewater samples (83 μM corresponding to S = 21.1, with a ^{228}Ra activity of 125 dpm 100 L^{-1}; **Table S1**) as the endmember leads to NO_3^- fluxes of 8.7 (±6.4)−17 (±13) *10^3 and 3.8 (±2.8)−7.7 (±5.5) *10^3 mol d^{-1} km^{-1} for T7 and T5, respectively. These estimations are in better agreement, but greater than the estimations of section Mixing Model: K_h * Nutrient Offshore Gradient (**Figure 10**). Using the maximum DSi concentration of the porewater samples (133 μM corresponding to a salinity of 13.7; with a ^{228}Ra activity of 18.2 dpm 100 L^{-1}) as the endmember leads to DSi fluxes of 95 (±69)−190 (±150) *10^3 mol d^{-1} km^{-1} of shoreline and 42 (±30)−84 (±65) *10^3 mol d^{-1} km^{-1} for T7 and T5, respectively (calculated for 5 and 10 m layers). Considering this porewater DSi endmember leads to estimates that are one to two orders of magnitude higher than the estimate reported in section Mixing Model: K_h * Nutrient Offshore Gradient. This highlights

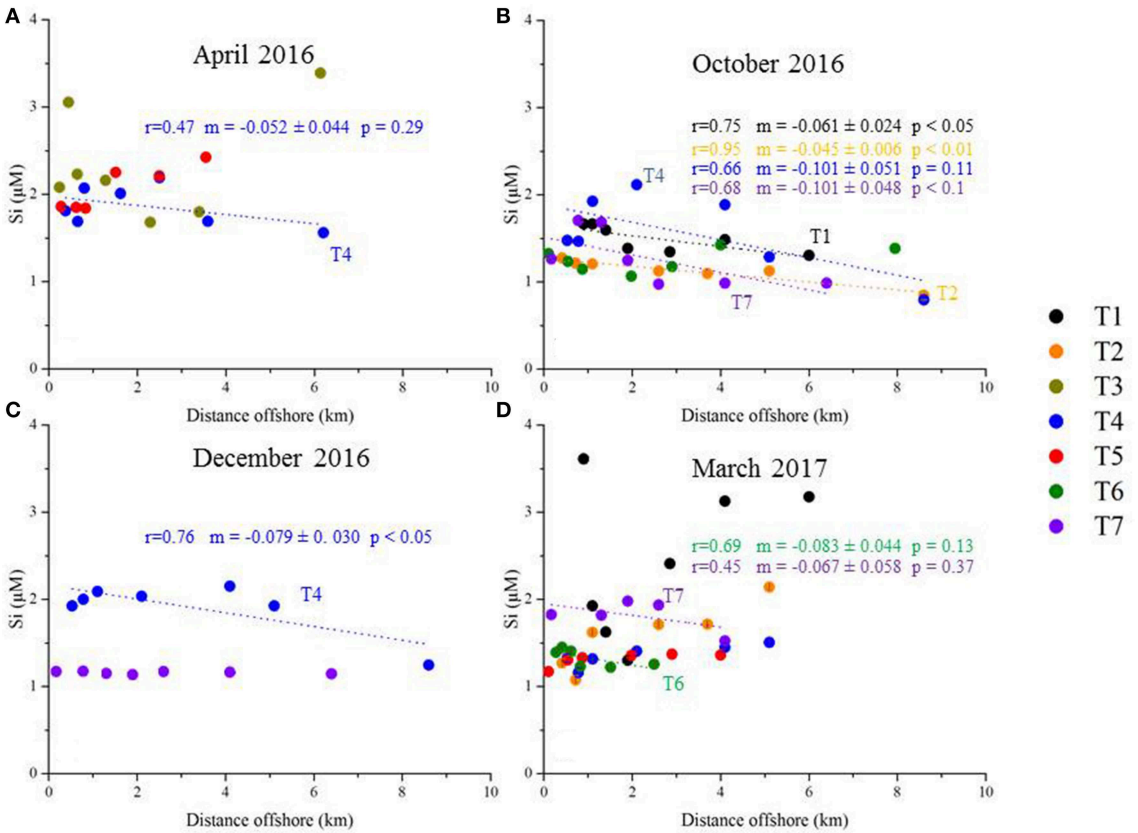

FIGURE 8 | Plot of DSi (µM) as a function of distance offshore. The transects are arranged by sampling date [**(A)** April 2016, **(B)** October 2016, **(C)** December 2016, and **(D)** March 2017]. Each transect is presented as a unique color. The dotted lines represent the linear regressions with significant *p*-values. The correlation coefficient *r*, slope *m* (and associated uncertainty), and *p*-values are listed for each transect (same color code as the transect symbols).

the importance of properly selecting the SGD endmember in determining nutrient fluxes from offshore ^{228}Ra gradients.

We should be able to estimate an SGD-driven PO_4^{3-} flux using this method, whereas we could not from the method used in section Mixing Model: K_h * Nutrient Offshore Gradient because there was no observable surface water PO_4^{3-} gradient. Considering the maximum PO_4^{3-} concentrations of the porewater samples (4.04 µM; **Table 2**), PO_4^{3-} fluxes are 0.8 (±0.7)−1.6 (±1.4) *10^2 and 0.4 (±0.3)−0.7 (±0.6) *10^2 mol d^{-1} km^{-1} for T7 and T5, respectively. PO_4^{3-} was not measured in the karstic springs sampled in the bay at the head of transect 1. In comparison, Tamborski et al. (2018) estimated an SGD-driven DIP flux along the sandy, alluvial shoreline of La Palme lagoon of 0.2 (±0.1) *10^2 mol d^{-1} km^{-1} of shoreline.

In the following, we prefer to rely on the flux estimates determined by combining horizontal eddy diffusivity coefficients with surface water nutrient gradients (section Mixing Model: K_h * Nutrient Offshore Gradient), particularly because knowledge of the SGD endmember is not requisite for this method. In addition, the ^{228}Ra distribution during the different campaigns did not show a decreasing trend with increasing distance offshore, which prevented us from using the ^{228}Ra mixing model for the majority of the sampling campaigns. The Rhône River mouth is located 15 km west of Côte Bleue and represents the largest freshwater input into the Mediterranean Sea (mean flow of 1,700 m^3 s^{-1}; Pont et al., 2002). The river plume is usually deflected westward (Estournel et al., 2001). However, Gatti et al. (2006) and Fraysse et al. (2014) showed that intrusion of Rhône river diluted waters could in some cases reach the Bay of Marseille, as a consequence of different physical processes (e.g., wind stress; presence of mesoscale eddy). In particular, the combination of an intrusion event with southeastern winds is expected to impact the Côte Bleue coastline (Fraysse et al., 2014). Such intrusion was shown to impact the biogeochemical functioning of the coastal waters by transporting large quantities of nutrients into the bay. Because ^{228}Ra displays a relatively long half-life (5.75 y), its distribution offshore of Côte Bleue may thus be impacted by sporadic intrusions of Rhône River waters. In March 2017, the ^{228}Ra activities are especially high at T1 near the coastline (∼25 dpm 100 L^{-1}; **Figure 12**). During that same campaign, the nutrient concentrations were also high in the coastal waters. The transects located along the western half of the Côte Bleue coastline showed elevated NO_3^- concentrations during this period (T1–T4; **Figure 9**). As discussed above (section Mixing Model: K_h * Nutrient Offshore Gradient), the surface salinity maps generated using the SYMPHONIE model indicate intrusion

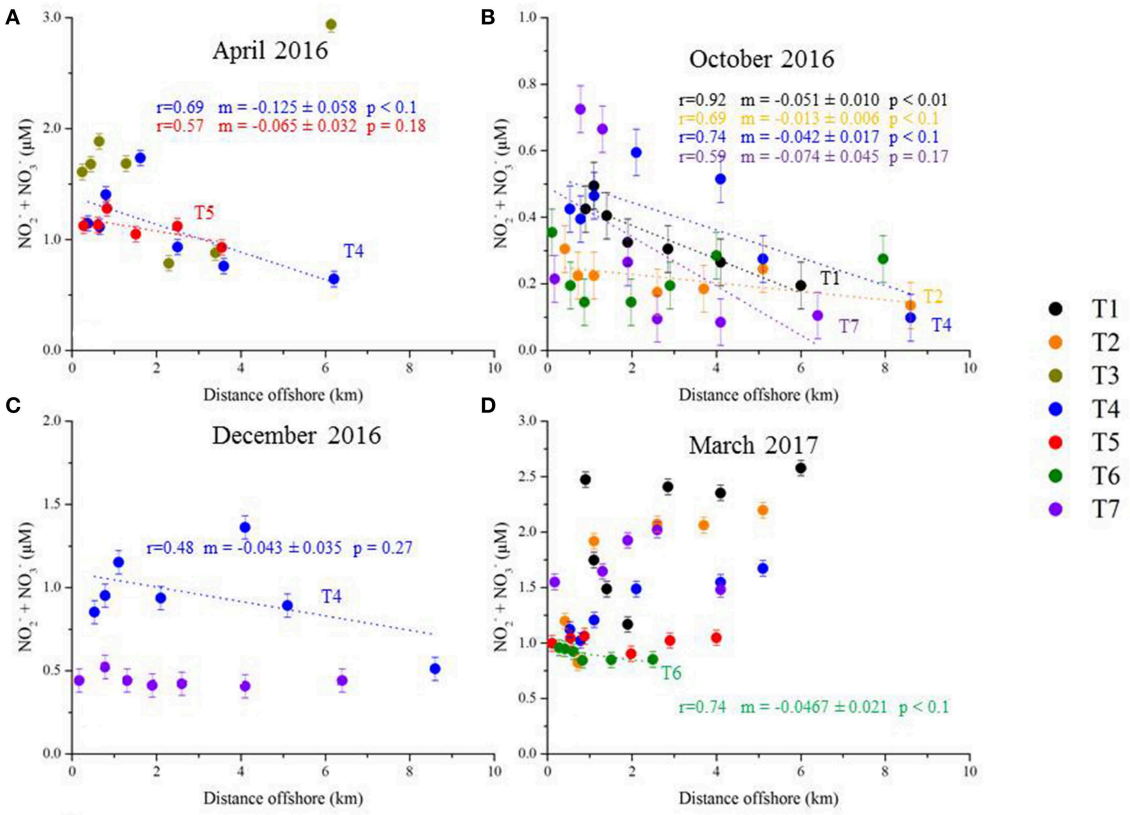

FIGURE 9 | Plot of $NO_2^- + NO_3^-$ (µM) as a function of distance offshore. The transects are arranged by sampling date [**(A)** April 2016, **(B)** October 2016, **(C)** December 2016, and **(D)** March 2017]. Each transect is presented as a unique color. The dotted lines represent the linear regressions with significant *p*-values. The regression coefficient *r*, slope *m* (and associated uncertainty), and *p*-values are listed for each transect (same color code as the transect symbols). Note that the plots have different y-axes scale.

of Rhône river waters that reached the entire Côte Bleue coastline on 15–16 March 2017 (**Figure 11**). One week later, on 21 and 22 March (March campaign), the western part of Côte Bleue is still impacted by these waters (**Figure 11**), which likely explain the observed nutrient and ^{228}Ra patterns. The vertical profiles of salinity (**Figure S2**) indicate waters with lower salinity (<38) at T1, T2, and T4 during the March 2017 campaign that support this hypothesis. ^{224}Ra, with its shorter half-life (3.66 d), may be less impacted by such intrusions that occur on average 7.6 times per year (Fraysse et al., 2014), unless sampling is performed just after an intrusion event. This is an additional argument to determine SGD from the method that combines K_h with the gradient of the chemical element of interest, rather than the method using the ^{228}Ra gradient.

Significance of the SGD Fluxes

Tamborski et al. (2018) estimated DSi and DIN fluxes along La Palme lagoon, a sandy alluvial stretch of the French Mediterranean coastline, of (2.4 ± 1.4) *10^3 mol Si d^{-1} km^{-1} and (5.7 ± 3.2) *10^3 mol N d^{-1} km^{-1} of shoreline into the Mediterranean Sea (**Figure 13**). These fluxes are similar in magnitude to the DSi and DIN fluxes reported here (**Figure 10**) despite the different lithology of the two areas (unconsolidated sediment vs. karst systems). For the entire Mediterranean basin, Rodellas et al. (2015) reported DSi and DIN fluxes of (0.1–27) *10^3 mol d^{-1} km^{-1} of shoreline and (0.1–64) *10^3 mol d^{-1} km^{-1} of shoreline, respectively, in relative agreement with the fluxes estimated here (**Figure 13**). Our estimations are on the same order of magnitude as other karst aquifer SGD studies in the Mediterranean Sea. Weinstein et al. (2011) estimate a terrestrial SGD flux discharging in Dor Bay, southeastern Mediterranean Sea, of 1.5 *10^3 and 1.4 *10^3 mol d^{-1} km^{-1} of DSi and DIN, respectively. In different coves along Majorca Island, SGD supplies a DSi flux ranging from 22 to 13,000 mol d^{-1} km^{-1} and DIN fluxes of 21 to 6,500 mol d^{-1} km^{-1} (Tovar-Sánchez et al., 2014). These examples suggest that Côte Bleue is similar to other Mediterranean karstic areas.

We estimated nutrient fluxes supplied by local rivers using river gauging stations (hydro.eaufrance.fr) and monthly chemical elements analyses (sierm.eaurmc.fr), where the nutrient flux is equivalent to the river discharge multiplied by the nutrient concentration. Here, we first compared the nutrient flux driven by SGD to the Huveaune River (flowing in Marseille; **Figure 1**) using the gauging station (Y4424040) in Aubagne and the

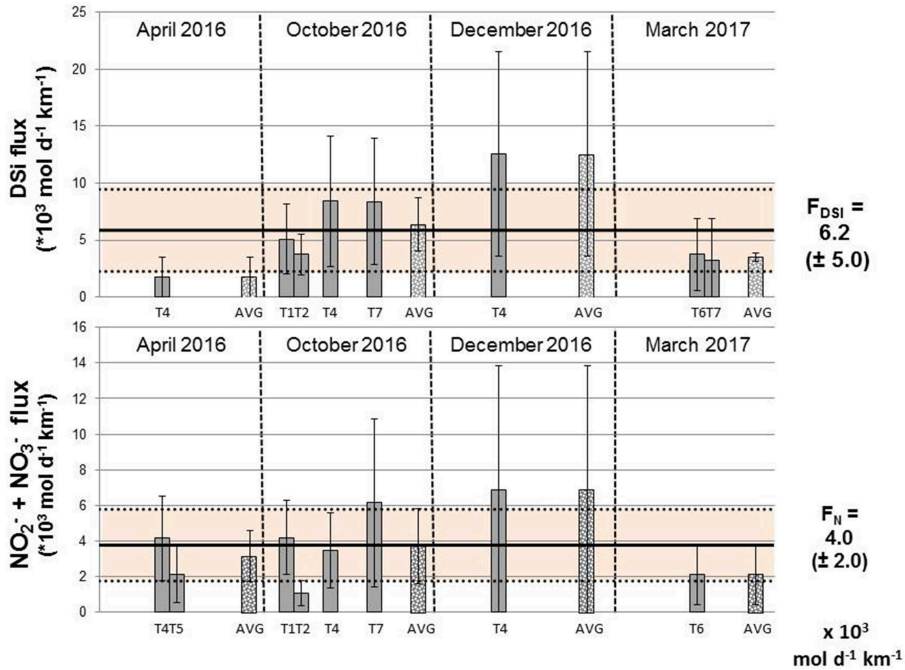

FIGURE 10 | Fluxes of DSi and NO_3^- (mol d^{-1} km^{-1}) estimated along Côte Bleue for each transect using Ra isotopes (K_h*nutrient gradient). The mean fluxes (±standard deviation) are also reported for each season (April 2016, October 2016, December 2016, and March 2017) and are denoted AVG.

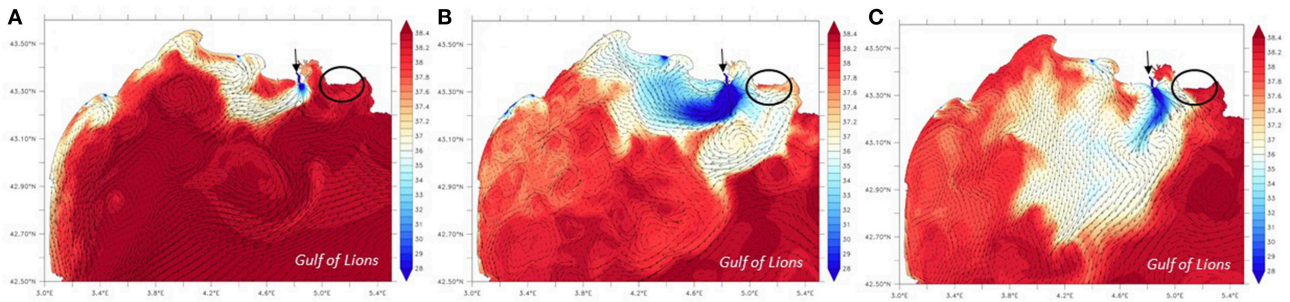

FIGURE 11 | Daily-averaged surface salinity and current simulated with the SYMPHONIE model for: **(A)** 27 October 2016, **(B)** 16 March 2017, **(C)** 22 March 2017. Note the change in the isocontours spacing at 37. These figures illustrate two different patterns for the Rhône river plume that enters into the Gulf of Lions: in most cases, the Rhône river waters are transported westward (October 2016 situation as an example) and in some rare cases, they are deflected eastward toward the Côte Bleue coastline (March 2017 situation). The arrow locates the Rhône river and the open circle indicates the Côte Bleue coastline.

chemical analyses station (06198100) in Marseille. It is important to note that the Huveaune River is over 15 km away from the eastern section of our study site; these waters do not impact our investigated shorelines. We then compared SGD fluxes in Côte Bleue to the largest river discharging in the French Mediterranean Sea: The Rhône River. We use the gauging station in Tarascon (Station: V7200015) and the chemical analyses made in Roquemaure, the most downstream sampling station (Station: 06121500). We compared these river fluxes to the SGD-driven NO_3^- and DSi fluxes estimated from the method described in section Mixing Model: K_h * Nutrient Offshore Gradient. The SGD-driven nutrient fluxes are multiplied by the coastal length of Côte Bleue impacted by terrestrial SGD; here we take a shoreline length of 5 km, where the coastal ^{222}Rn activities were the highest (**Figure 3**). Note that these fluxes will represent upper limits, as the mean SGD-driven nutrient fluxes are estimated only for transects in which we observed significant offshore gradients.

SGD represents between 3 and 22 times the DSi and NO_3^- fluxes driven by the Huveaune River, with significant temporal variability (**Table 4**). While the DSi flux driven by SGD is 4 times greater than the DSi flux driven by the Huveaune River in March 2017, SGD is 22 times greater than the river fluxes in December 2016. NO_3^- fluxes follow the same pattern, with SGD-driven fluxes slightly higher than the Huveaune river flux in March 2017 and reaching 5 times the river flux in October 2016. In comparison, the DSi fluxes driven by SGD is only between 0.1

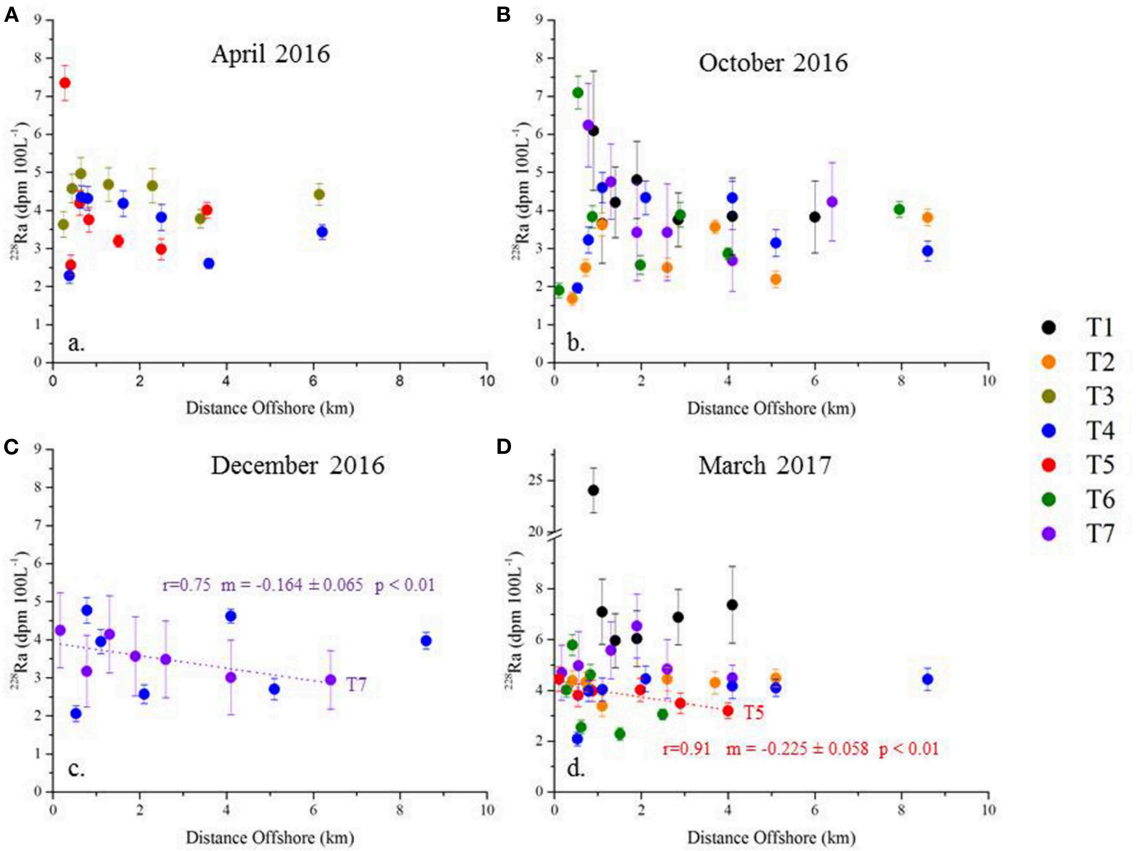

FIGURE 12 | Plot of ^{228}Ra (dpm 100 L^{-1}) as a function of distance offshore. The transects are arranged by sampling date [**(A)** April 2016, **(B)** October 2016, **(C)** December 2016, and **(D)** March 2017]. Each transect is presented as a unique color. Note that the plots have different y-axes scale. The dotted lines represent the linear regressions with significant *p*-values.

and 1.4% of the DSi fluxes driven by the Rhône River (**Table 4**). The NO_3^- flux driven by SGD is only between 0.1 and 0.3% of the Rhône River NO_3^- inputs (**Table 4**). Nutrient inputs of SGD may still be significant compared to the Rhône River, as SGD is the only terrestrial input of nutrients to Côte Bleue when the Rhône River plume does not enter the Bay of Marseille and Côte Bleue.

CONCLUSION

Characterization of water and nutrient fluxes from coastal karst aquifers remains a significant challenge (Montiel et al., 2018). We used two different geochemical tracer methods to estimate SGD fluxes along a karst coastline (Côte Bleue, French Mediterranean Sea) where the presence of terrestrial groundwater discharge was suspected from the thermal infrared signature of nearshore waters and from a radon survey that was conducted along the coastline. Horizontal eddy diffusivity coefficients (K_h), derived from offshore $^{224}Ra_{ex}$ transects, combined with offshore nutrient gradients provided the most consistent flux results, as we could derive SGD nutrient fluxes for almost all the investigated transects during all sampling periods. Knowledge of the SGD endmember is not required for this method, which constitutes a strong advantage in such an area where the endmember is difficult to constrain. This method is only applicable when the chemical element of interest behaves conservatively within the timeframe of coastal mixing processes, and when there is no significant external nutrient (or Ra) sources. In contrast, offshore ^{228}Ra gradients combined with K_h yielded significant flux estimations for only 2 of the investigated transects (out of 16, over 4 seasons). This approach is also disadvantageous for Côte Bleue in that it requires a well-constrained SGD endmember, which is difficult to determine in this specific region (karstic spring vs. porewaters).

The ^{228}Ra and nutrient distributions observed during March 2017 suggest that the coastal waters may have been impacted by the intrusion of Rhône River diluted waters that were deflected eastward, a phenomenon that only occurs ∼8 times a year (Fraysse et al., 2014), further complicating the use of long-lived ^{228}Ra as a tracer for SGD along Côte Bleue. This is in contrast with the dominant situation when the plume is deflected westward and therefore does not impact the investigated region. The Rhône River constitutes the largest nutrient source to the Gulf of Lions and can support 23–69% of the primary production (Ludwig et al., 2009). We estimate that SGD along Côte Bleue

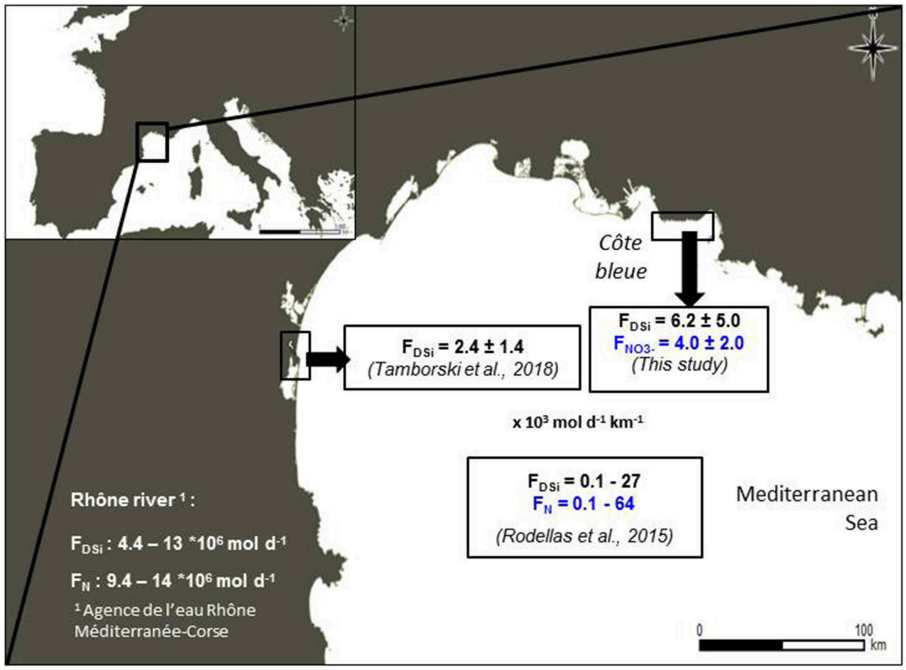

FIGURE 13 | DSi and NO_3^- fluxes determined in this study along Côte Bleue. As a comparison, we report the (i) DSi fluxes determined by Tamborski et al. (2018) offshore La Franqui coastline (western Gulf of Lions), (ii) the DSi and N fluxes determined by Rodellas et al. (2015) using a Ra mass balance applied to the entire Mediterranean Sea (the fluxes reported on the figure have been normalized to the Mediterranean shore length −64,000 km—according to Rodellas et al., 2015), and (iii) the DSi and N fluxes associated with the Rhône river.

TABLE 4 | Estimation of nutrient fluxes (mol d^{-1}) driven by SGD, the Huveaune River and the Rhône River in April, October, and December 2016, and March 2017.

		SGD (*10^3 mol d^{-1})	Huveaune river (*10^3 mol d^{-1})	Rhône river (*10^6 mol d^{-1})
DSi	Apr-16	9 ± 9	1.7	13
	Oct-16	32 ± 12	1.4	5.3
	Dec-16	63 ± 45	2.9	4.4
	Mar-17	17 ± 2	4.4	6.5
$NO_3^- + NO_2^-$	Apr-16	16 ± 7	5.4	14
	Oct-16	19 ± 11	3.9	9.4
	Dec-16	34 ± 35	10.1	10
	Mar-17	11 ± 9	13.3	14

*DSi and NO_3^- fluxes reported here were estimated using Ra isotopes (K_h * nutrient gradients) considering 10 m as the water depth impacted by SGD. Note than the Rhône River fluxes are reported in 10^6 mol d^{-1}.*

supplies ≤1% of the DSi and NO_3^- inputs of the Rhône River. However, in the absence of eastward deflected Rhône River diluted waters, SGD is the only known nutrient source to the nearshore area of Côte Bleue. It is interesting to note that the nutrient fluxes reported here are similar in magnitude compared with the fluxes quantified along the sandy beach of La Franqui, in the western Gulf of Lions (Tamborski et al., 2018), despite the different lithology of the two areas (karst systems vs. unconsolidated sediment). We recommend that multiple methods be used in future studies investigating SGD and nutrient cycling from coastal karst aquifers.

DATA AVAILABILITY STATEMENT

All datasets generated for this study are included in the article/**Supplementary Material**.

AUTHOR CONTRIBUTIONS

SB, JT, MS, and PB analyzed the samples for radium isotopes. OR, CC, and TS conducted the radon surveys (*in situ* analysis). SB, JT, PB, MS, TS, OR, CC, and EL contributed to the collection of samples at sea or along the coastline. OC, PC, and MP-P analyzed the nutrient concentrations. SB, JT, TS, and PB computed the TIR images. SB, JT, and PB calculated the SGD fluxes based on the radium isotopes. SB, JT, PB, TS, OR, CC, PC, and MP-P contributed to the interpretation of the data. SB, JT, PB, TS, OR, and PC contributed to the writing of the manuscript. CE generated the salinity and circulation maps using the SYMPHONIE model and contributed to the sections related to the interpretation of these maps.

FUNDING

The Ph.D. thesis fellowship of SB and the postdoctoral fellowship of JT were supported by FEDER funded by Europe and Région

Occitanie Pyrénées-Méditerranée (SELECT project). This project was funded by (i) ANR-MED-SGD (ANR-15-CE01-0004; PB) and (ii) CNES for funding the airborne TIR images acquired in 2012 as part of the Geomether project (PI: Pascal Allemand, PB being responsible for the acquisition of TIR images in that project).

ACKNOWLEDGMENTS

We thank Virginie Sanial for her participation to the survey that allowed us to acquire airborne TIR images. We thank captain and crew of RV Antédon II for help during sampling at sea. We thank Dorian Guillemain, Nagib Bhairy, Deny Malengros, and Christian Grenz at MIO for providing the CTD data. We thank M. Plantevin at Saumaty harbor. We thank European Union and Région Occitanie Pyrénées-Méditerranée for supporting the LAFARA underground laboratory through a FEDER funding (SELECT project). We are grateful to EDF (Electricité De France) for allowing us to run our germanium detectors in the tunnel of Ferrières, Ariège. We thank Caroline Ulses and Ivane Pairaud for constructive discussions. We thank the two reviewers and the associate editor Henrietta Dulai for their constructive comments that allowed us to improve the quality of the paper.

SUPPLEMENTARY MATERIAL

The Supplementary Material for this article can be found online at: https://www.frontiersin.org/articles/10.3389/fenvs.2019.00205/full#supplementary-material

Figure S1 | Daily precipitation recorded at Marseille-Marignane airport (data from meteociel.fr). Periods when field work was conducted are indicated by vertical gray lines.

Figure S2 | Vertical profiles of salinity (CTD data) obtained at all transects investigated in March 2017.

Table S1 | ^{223}Ra, ^{224}Ra$_{ex}$, ^{228}Ra activities, and $NO_3^- + NO_2^-$, DSi concentrations determined in water samples collected offshore Côte Bleue, in nearshore waters, in porewaters and in springs (in April 2016, October 2016, December 2016, and March 2017). Shallow porewater and coastal water sample locations are presented in **Figure 2**; seawater sample locations are presented in **Figure 1**. The vertical profiles built in March 2017 are in bold. Porewater samples are underlined in gray.

REFERENCES

Aminot, A., and Kérouel, R. (2004). *Hydrologie des Écosystèmes Marins: Paramètres et Analyses, Edn*. (Ifremer), 336.

Anderson, M. P. (2005). Heat as a ground water tracer. *Ground Water* 43, 951–968. doi: 10.1111/j.1745-6584.2005.00052.x

Arfib, B., Cavalera, T., and Gilli, E. (2006). Influence de l'hydrodynamique sur l'intrusion saline en aquifère karstique côtier. *Comptes Rendus Geosci*. 338, 757–767. doi: 10.1016/j.crte.2006.07.001

Arfib, B., and Charlier, J.-B. (2016). Insights into saline intrusion and freshwater resources in coastal karstic aquifers using a lumped Rainfall-Discharge-Salinity model (the Port-Miou brackish spring, SE France). *J. Hydrol.* 540, 148–161. doi: 10.1016/j.jhydrol.2016.06.010

Baudron, P., Cockenpot, S., Lopez-Castejon, F., Radakovitch, O., Gilabert, J., Mayer, A., et al. (2015). Combining radon, short-lived radium isotopes and hydrodynamic modeling to assess submarine groundwater discharge from an anthropized semiarid watershed to a Mediterranean lagoon (Mar Menor, SE Spain). *J. Hydrol.* 525, 55–71. doi: 10.1016/j.jhydrol.2015.03.015

Bejannin, S., van Beek, P., Stieglitz, T., Souhaut, M., and Tamborski, J. (2017). Combining airborne thermal infrared images and radium isotopes to study submarine groundwater discharge along the French Mediterranean coastline. *J. Hydrol. Reg. Stud.* 13, 72–90. doi: 10.1016/j.ejrh.2017.08.001

Beusen, A. H. W., Slomp, C. P., and Bouwman, A. F. (2013). Global land–ocean linkage: direct inputs of nitrogen to coastal waters via submarine groundwater discharge. *Environ. Res. Lett*. 8:034035. doi: 10.1088/1748-9326/8/3/034035

Burnett, W. C., Aggarwal, P. K., Aureli, A., Bokuniewicz, H., Cable, J. E., Charette, M. A., et al. (2006). Quantifying submarine groundwater discharge in the coastal zone via multiple methods. *Sci. Total Environ.* 367, 498–543. doi: 10.1016/j.scitotenv.2006.05.009

Burnett, W. C., Bokuniewicz, H., Huettel, M., Moore, W. S., and Taniguchi, M. (2003). Groundwater and pore water inputs to the coastal zone. *Biogeochemistry* 66, 3–33. doi: 10.1023/B:BIOG.0000006066.21240.53

Burnett, W. C., and Dulaiova, H. (2003). Estimating the dynamics of groundwater input into the coastal zone via continuous radon-222 measurements. *J. Environ. Radioactiv.* 69, 21–35. doi: 10.1016/S0265-931X(03)00084-5

Charette, M. A., and Buesseler, K. O. (2004). Submarine groundwater discharge of nutrients and copper to an urban subestuary of Chesapeake Bay (Elizabeth River). *Limnol. Oceanogr.* 49, 376–385. doi: 10.4319/lo.2004.49.2.0376

Charette, M. A., Buesseler, K. O., and Andrews, J. E. (2001). Utility of radium isotopes for evaluating the input and transport of groundwater-derived nitrogen to a Cape Cod estuary. *Limnol. Oceanogr.* 46, 465–470. doi: 10.4319/lo.2001.46.2.0465

Charette, M. A., Gonneea, M. E., Morris, P. J., Statham, P., Fones, G., Planquette, H., et al. (2007). Radium isotopes as tracers of iron sources fueling a Southern Ocean phytoplankton bloom. *Deep Sea Res. Part II Top. Stud. Oceanogr.* 54, 1989–1998. doi: 10.1016/j.dsr2.2007.06.003

Cockenpot, S., Claude, C., and Radakovitch, O. (2015). Estimation of air water gas exchange coefficient in a shallow lagoon based on ^{222}Rn mass balance. *J. Environ. Radioactiv.* 143, 58–69. doi: 10.1016/j.jenvrad.2015.02.007

Dulaiova, H., Peterson, R., Burnett, W. C., and Lane-Smith, D. (2005). A multi-detector continuous monitor for assessment of ^{222}Rn in the coastal ocean. *J. Radioanal. Nucl. Chem.* 263, 361–363. doi: 10.1007/s10967-005-0063-8

Estournel, C., Broche, P., Marsaleix, P., Devenon, J. L., Auclair, F., and Vehil R. (2001). The Rhone River plume in unsteady conditions: numerical and experimental results. *Estuarine Coast. Shelf. Sci.* 53, 25–38. doi: 10.1006/ecss.2000.0685

Estournel, C., Durrieu de Madron, X., Marsaleix, P., Auclair, F., Julliand, C., and Vehil, R. (2003). Observation and modelisation of the winter coastal oceanic circulation in the Gulf of Lions under wind conditions influenced by the continental orography (FETCH experiment). *J. Geophys. Res.* 108:8059. doi: 10.1029/2001JC000825

Fleury, P., Bakalowicz, M., and de Marsily, G. (2007). Submarine springs and coastal karst aquifers: a review. *J. Hydrol.* 339, 79–92. doi: 10.1016/j.jhydrol.2007.03.009

Fraysse, M., Pairaud, I., Ross, O. N., Faure, V. M., and Pinazo, C. (2014). Intrusion of Rhone River diluted water into the Bay of Marseille: generation processes and impacts on ecosystem functioning. *J. Geophys. Res. Oceans* 119, 6535–6556. doi: 10.1002/2014JC010022

Garcia-Solsona, E., Garcia-Orellana, J., Masqué, P., and Dulaiova, H. (2008). Uncertainties associated with ^{223}Ra and ^{224}Ra measurements in water via a Delayed Coincidence Counter (RaDeCC). *Mar. Chem.* 109, 198–219. doi: 10.1016/j.marchem.2007.11.006

Garcia-Solsona, E., Garcia-Orellana, J., Masqué, P., Rodellas, V., Mejías, M., Ballesteros, B., et al. (2010). Groundwater and nutrient discharge through karstic coastal springs (Castello, Spain). *Biogeosciences* 7, 2625–2638. doi: 10.5194/bg-7-2625-2010

Gatti, J. Petrenko, A., Devenon, J.-L., Leredde, Y., and Ulses, C. (2006), The Rhone river dilution zone present in the northeastern shelf of the Gulf of Lion in December 2003. *Cont. Shelf Res.* 26, 1794–1805, doi: 10.1016/j.csr.2006.05.012

Gobler, C., and Sañudo-Wilhelmy, S. (2001). Effects of organic carbon, organic nitrogen, inorganic nutrients, and iron additions on the growth of

phytoplankton and bacteria during a brown tide bloom. *Mar. Ecol. Prog. Ser.* 209, 19–34. doi: 10.3354/meps209019

Hancock, G. J., Webster, I. T., and Stieglitz, T. C. (2006). Horizontal mixing of Great Barrier Reef waters: offshore diffusivity determined from radium isotope distribution. *J. Geophys. Res.* 111:C12019. doi: 10.1029/2006JC003608

Hwang, D.-W., Kim, G., Lee, Y.-W., and Yang, H.-S. (2005). Estimating submarine inputs of groundwater and nutrients to a coastal bay using radium isotopes. *Mar. Chem.* 96, 61–71. doi: 10.1016/j.marchem.2004.11.002

Jensen, A., Collins, K., and Lockwood, A. P. (2012). *Artificial Reefs in European Seas*. Springer Science and Business Media.

Jeong, J., Kim, G., and Han, S. (2012). Influence of trace element fluxes from submarine groundwater discharge (SGD) on their inventories in coastal waters off volcanic island, Jeju, Korea. *Appl. Geochem.* 27, 37–43. doi: 10.1016/j.apgeochem.2011.08.014

Jouvenel, J.-Y., Bachet, F., Harmenin, J.-G., and Bellan-Santini, D. (2004). "Suivi biologique d'une réserve marine de la Côte Bleue (Golfe de Marseille, Méditerranée, France)," in *Colloque ≪Importance de La Recherche Dans Les Aires Protégées: Des Fondements à La Gestion≫, Organisé En Guadeloupe Par La SNPN, 5-7 Juin 2002* (Paris: Société nationale de protection de la nature et d'acclimatation de France).

Knee, K. L., Garcia-Solsona, E., Garcia-Orellana, J., Boehm, A. B., and Paytan, A. (2011). Using radium isotopes to characterize water ages and coastal mixing rates: a sensitivity analysis. *Limnol. Oceanogr. Methods* 9, 380–395. doi: 10.4319/lom.2011.9.380

Knee, K. L., Street, J. H., Grossman, E. E., Boehm, A. B., and Paytan, A. (2010). Nutrient inputs to the coastal ocean from submarine groundwater discharge in a groundwater-dominated system: relation to land use (Kona coast, Hawaii, U.S.A.). *Limnol. Oceanogr.* 55, 1105–1122. doi: 10.4319/lo.2010.55.3.1105

Lecher, A. L., MacKay, K., Kudela, R., Ryan, J., Fisher, A., Murray, J., et al. (2015). Nutrient loading through submarine groundwater discharge and phytoplankton growth in Monterey Bay, CA. *Environ. Sci. Technol.* 49, 6665–6673. doi: 10.1021/acs.est.5b00909

Li, C., and Cai, W.-J. (2011). On the calculation of eddy diffusivity in the shelf water from radium isotopes: high sensitivity to advection. *J. Mar. Syst.* 86, 28–33. doi: 10.1016/j.jmarsys.2011.01.003

Ludwig, W., Dumont, E., Meybeck, M., and Heussner, S. (2009). River discharges of water and nutrients to the Mediterranean and Black Sea: major drivers for ecosystem changes during past and future decades? *Prog. Oceanogr.* 80, 199–217. doi: 10.1016/j.pocean.2009.02.001

Marsaleix, P., Auclair, F., Floor, J. W., Herrmann, M. J., Estournel, C., Pairaud, I., et al. (2008). Energy conservation issues in sigma-coordinate free-surface ocean models. *Ocean Model.* 20, 61–89. doi: 10.1016/j.ocemod.2007.07.005

Marsaleix, P., Michaud, H., and Estournel, C. (2019). 3D phase-resolved wave modelling with a non-hydrostatic ocean circulation model. *Ocean Model.* 136, 28–50. doi: 10.1016/j.ocemod.2019.02.002

Mejías, M., Ballesteros, B. J., Antón-Pacheco, C., Domínguez, J. A., Garcia-Orellana, J., and Garcia-Solsona, E., et al. (2012). Methodological study of submarine groundwater discharge from a karstic aquifer in the Western Mediterranean Sea. *J. Hydrol.* 464–465, 27–40. doi: 10.1016/j.jhydrol.2012.06.020

Millot, C. (1990). The Gulf of Lions' hydrodynamics. *Cont. Shelf Res.* 10, 885–894. doi: 10.1016/0278-4343(90)90065-T

Montiel, D., Dimova, N., Andreo, B., Prioeto, J., García-Orellana, J., and Rodellas, V. (2018). Assessing submarine groundwater discharge (SGD) and nitrate fluxes in highly heterogeneous coastal karst aquifers: challenges and solutions. *J. Hydrol.* 557, 222–242. doi: 10.1016/j.jhydrol.2017.12.036

Moore, W. S. (1996). Using the radium quartet for evaluating groundwater input and water exchange in salt marshes. *Geochim. Cosmochim. Acta* 60, 4645–4652. doi: 10.1016/S0016-7037(96)00289-X

Moore, W. S. (1999). The subterranean estuary: a reaction zone of ground water and sea water. *Mar. Chem.* 65, 111–125. doi: 10.1016/S0304-4203(99)00014-6

Moore, W. S. (2000a). Determining coastal mixing rates using radium isotopes. *Cont. Shelf Res.* 20, 1993–2007. doi: 10.1016/S0278-4343(00)00054-6

Moore, W. S. (2000b). Ages of continental shelf waters determined from ^{223}Ra and ^{224}Ra. *J. Geophys. Res. Oceans* 105, 22117–22122. doi: 10.1029/1999JC000289

Moore, W. S. (2008). Fifteen years experience in measuring ^{224}Ra and ^{223}Ra by delayed-coincidence counting. *Mar. Chem.* 109, 188–197. doi: 10.1016/j.marchem.2007.06.015

Moore, W. S. (2010). The effect of submarine groundwater discharge on the ocean. *Annu. Rev. Mar. Sci.* 2, 59–88. doi: 10.1146/annurev-marine-120308-081019

Moore, W. S., and Arnold, R. (1996). Measurement of ^{223}Ra and ^{224}Ra on coastal waters using a delayed coincidence counter. *J. Geophys. Res. Oceans* 101, 1321–1329. doi: 10.1029/95JC03139

Moore, W. S., and Reid, D. F. (1973). Extraction of radium from natural waters using manganese-impregnated acrylic fibers. *J. Geophys. Res.* 78, 8880–8886. doi: 10.1029/JC078i036p08880

Niencheski, L. F. H., Windom, H. L., Moore, W. S., and Jahnke, R. A. (2007). Submarine groundwater discharge of nutrients to the ocean along a coastal lagoon barrier, Southern Brazil. *Mar. Chem.* 106, 546–561. doi: 10.1016/j.marchem.2007.06.004

Ollivier, P., Claude, C., Radakovitch, O., and Hamelin, B. (2008). TIMS measurements of 226Ra and 228Ra in the Gulf of Lion, an attempt to quantify submarine groundwater discharge. *Mar. Chem.* 109, 337–354. doi: 10.1016/j.marchem.2007.08.006

Pairaud, I. L., Gatti, J., Bensoussan, N., Verney, R., and Garreau, P. (2011). Hydrology and circulation in a coastal area off Marseille: validation of a nested 3D model with observations. *J. Mar. Syst.* 88, 20–33. doi: 10.1016/j.jmarsys.2011.02.010

Pavlidou, A., Papadopoulos, V. P., Hatzianestis, I., Simboura, N., Patiris, D., and Tsabaris, C. (2014). Chemical inputs from a karstic submarine groundwater discharge (SGD) into an oligotrophic Mediterranean coastal area. *Sci. Total Environ.* 488–489, 1–13. doi: 10.1016/j.scitotenv.2014.04.056

Paytan, A., Shellenbarger, G. G., Street, J. H., Gonneea, M. E., Davis, K., and Young, M. B., et al. (2006). Submarine groundwater discharge: an important source of new inorganic nitrogen to coral reef ecosystems. *Limnol. Oceanogr.* 51, 343–348. doi: 10.4319/lo.2006.51.1.0343

Petrenko, A. (2003), Variability of circulation features in the Gulf of Lion NW Mediterranean Sea. Importance of inertial currents. *Oceanol. Acta* 26, 323–338. doi: 10.1016/S0399-1784(03)00038-0

Petrenko, A., Dufau, C., and Estournel, C. (2008). Barotropic eastward currents in the western Gulf of Lion, north-western Mediterranean Sea, during stratified conditions. *J. Mar. Syst.* 74, 406–428. doi: 10.1016/j.jmarsys.2008.03.004

Pont, D., Simonnet, J.-P., and Walter, A. V. (2002), Medium-term changes in suspended sediment delivery to the ocean: consequences of catchment heterogeneity and river management (Rhône River, France). *Estuarine Coastal Shelf Sci.* 54, 1–18, doi: 10.1006/ecss.2001.0829

Reffray, G., Fraunié, P., and Marsaleix, P. (2004). Secondary flows induced by wind forcing in the Rhône region of freshwater influence. *Ocean Dyn.* 54, 179–196. doi: 10.1007/s10236-003-0079-y

Rodellas, V., Garcia-Orellana, J., Masqué, P., Feldman, M., and Weinstein, Y. (2015). Submarine groundwater discharge as a major source of nutrients to the Mediterranean Sea. *Proc. Natl. Acad. Sci. U.S.A.* 112, 3926–3930. doi: 10.1073/pnas.1419049112

Rodellas, V., Garcia-Orellana, J., Trezzi, G., Masqué, P., Stieglitz, T. C., Bokuniewicz, H., et al. (2017). Using the radium quartet to quantify submarine groundwater discharge and porewater exchange. *Geochim. Cosmochim. Acta* 196, 58–73. doi: 10.1016/j.gca.2016.09.016

Schmidt, S., and Reyss, J.-L. (1996). Radium as internal tracer of Mediterranean Outflow Water. *J. Geophys. Res.* 101, 3589–3596.

Slomp, C. P., and Van Cappellen, P. (2004). Nutrient inputs to the coastal ocean through submarine groundwater discharge: controls and potential impact. *J. Hydrol.* 295, 64–86. doi: 10.1016/j.jhydrol.2004.02.018

Stieglitz, T., van Beek, P., Souhaut, M., and Cook, P. (2013). Groundwater discharge Karstic groundwater discharge and seawater recirculation through sediments in shallow coastal Mediterranean lagoons, determined from water, salt and radon budgets. *Mar. Chem.* 156, 73–84 doi: 10.1016/j.marchem.2013.05.005

Stieglitz, T. C., Cook, P. G., and Burnett, W. C. (2010). Inferring coastal processes from regional-scale mapping of ^{222}Radon and salinity: examples from the Great Barrier Reef, Australia. *J. Environ. Radioact.* 101, 544–552. doi: 10.1016/j.jenvrad.2009.11.012

Sun, Y., and Torgersen, T. (1998). The effects of water content and Mn-fiber surface conditions on ^{224}Ra measurement by ^{220}Rn emanation. *Mar. Chem.* 62, 299–306. doi: 10.1016/S0304-4203(98)00019-X

Swarzenski, P. W. (2007). U/Th series radionuclides as coastal groundwater tracers. *Chem. Rev.* 107, 663–674. doi: 10.1021/cr0503761

Tamborski, J., Bejannin, S., Garcia-Orellana, J., Souhaut, M., Charbonnier, C., Anschutz, P., et al. (2018). A comparison between water circulation and terrestrially-driven dissolved silica fluxes to the Mediterranean Sea traced using radium isotopes. *Geochim. Cosmochim. Acta* 238, 496–515. doi: 10.1016/j.gca.2018.07.022

Tamborski, J. J., Cochran, J. K., and Bokuniewicz, H. J. (2017). Submarine groundwater discharge driven nitrogen fluxes to Long Island Sound, NY: terrestrial vs. marine sources. *Geochim. Cosmochim. Acta* 218, 40–57. doi: 10.1016/j.gca.2017.09.003

Tamborski, J. J., Rogers, A. D., Bokuniewicz, H. J., Cochran, J. K., and Young, C. R. (2015). Identification and quantification of diffuse fresh submarine groundwater discharge via airborne thermal infrared remote sensing. *Remote Sens. Environ*. 171, 202–217. doi: 10.1016/j.rse.2015.10.010

Tovar-Sánchez, A., Basterretxea, G., Rodellas, V., Sánchez-Quiles, D., García-Orellana, J., Masqué, P., et al. (2014). Contribution of groundwater discharge to the coastal dissolved nutrients and trace metal concentrations in Majorca Island: Karstic vs Detrital systems. *Environ. Sci. Technol*. 48, 11819–11827. doi: 10.1021/es502958t

Trezzi, G., Garcia-Orellana, J., Rodellas, V., Masqué, P., Garcia-Solsona, E., and Andersson, P. S. (2017). Assessing the role of submarine groundwater discharge as a source of Sr to the Mediterranean Sea. *Geochim. Cosmochim. Acta* 200, 42–54. doi: 10.1016/j.gca.2016.12.005

van Beek, P., Souhaut, M., Lansard, B., Bourquin, M., Reyss, J.-L., von Ballmoos, P., et al. (2013). LAFARA: a new underground laboratory in the French Pyrénées for ultra low-level gamma-ray spectrometry. *J. Environ. Radioact*. 116, 152–158. doi: 10.1016/j.jenvrad.2012.10.002

van Beek, P., Souhaut, M., and Reyss, J.-L. (2010). Measuring the radium quartet (^{228}Ra, ^{226}Ra, ^{224}Ra, ^{223}Ra) in seawater samples using gamma spectrometry. *J. Environ. Radioact.* 101, 521–529. doi: 10.1016/j.jenvrad.2009.12.002

van Beek, P., Sternberg, E., Reyss, J.-L., Souhaut, M., Robin, E., and Jeandel, C. (2009). ^{228}Ra/^{226}Ra and ^{226}Ra/Ba ratios in the Western Mediterranean Sea: barite formation and transport in the water column. *Geochim. Cosmochim. Acta* 73, 4720–4737 doi: 10.1016/j.gca.2009.05.063

Webster, I. T., Hancock, G. J., and Murray, A. S. (1995). Modelling the effect of salinity on radium desorption from sediments. *Geochim. Cosmochim. Acta* 59, 2469–2476. doi: 10.1016/0016-7037(95)00141-7

Weinstein, Y., Yechieli, Y., Shalem, Y., Burnett, W. C., Swarzenski, P. W., and Herut, B. (2011). What is the role of fresh groundwater and recirculated seawater in conveying nutrients to the Coastal Ocean? *Environ. Sci. Technol*. 45, 5195–5200. doi: 10.1021/es104394r

Windom, H. L., Moore, W. S., Niencheski, L. F. H., and Jahnke, R. A. (2006). Submarine groundwater discharge: a large, previously unrecognized source of dissolved iron to the South Atlantic Ocean. *Mar. Chem*. 102, 252–266. doi: 10.1016/j.marchem.2006.06.016

Conflict of Interest: The authors declare that the research was conducted in the absence of any commercial or financial relationships that could be construed as a potential conflict of interest.

frontiers in Environmental Science

ORIGINAL RESEARCH
published: 17 July 2020
doi: 10.3389/fenvs.2020.00108

Radium Mass Balance Sensitivity Analysis for Submarine Groundwater Discharge Estimation in Semi-Enclosed Basins: The Case Study of Long Island Sound

Joseph Tamborski[1,2,3], J. Kirk Cochran[4], Henry Bokuniewicz[4], Christina Heilbrun[4], Jordi Garcia-Orellana[5,6], Valentí Rodellas[5] and Robert Wilson[4]*

[1] Department of Geosciences, Stony Brook University, Stony Brook, NY, United States, [2] Department of Marine Chemistry & Geochemistry, Woods Hole Oceanographic Institution, Woods Hole, MA, United States, [3] Centre for Water Resources Studies, Dalhousie University, Halifax, NS, Canada, [4] School of Marine and Atmospheric Sciences, Stony Brook University, Stony Brook, NY, United States, [5] ICTA, Institut de Ciència i Tecnologia Ambientals, Universitat Autònoma de Barcelona, Bellaterra, Spain, [6] Department de Física, Universitat Autònoma de Barcelona, Bellaterra, Spain

OPEN ACCESS

Edited by:
Makoto Taniguchi, Research Institute for Humanity and Nature, Japan

Reviewed by:
Vhahangwele Masindi, Council for Scientific and Industrial Research (CSIR), South Africa
Henrietta Dulai, University of Hawai'i at Mānoa, United States

***Correspondence:**
Joseph Tamborski
jtamborski@whoi.edu

Specialty section:
This article was submitted to Water and Wastewater Management, a section of the journal Frontiers in Environmental Science

Received: *13 June 2019*
Accepted: *23 June 2020*
Published: *17 July 2020*

Citation:
Tamborski J, Cochran JK, Bokuniewicz H, Heilbrun C, Garcia-Orellana J, Rodellas V and Wilson R (2020) Radium Mass Balance Sensitivity Analysis for Submarine Groundwater Discharge Estimation in Semi-Enclosed Basins: The Case Study of Long Island Sound. Front. Environ. Sci. 8:108. doi: 10.3389/fenvs.2020.00108

Estimation of submarine groundwater discharge (SGD) to semi-enclosed basins by Ra isotope mass balance is herein assessed. We evaluate ^{224}Ra, ^{226}Ra, and ^{228}Ra distributions in surface and bottom waters of Long Island Sound (CT-NY, United States) collected during spring 2009 and summer 2010. Surface water and bottom water Ra activities display an apparent seasonality, with greater activities during the summer. Long-lived Ra isotope mass balances are highly sensitive to boundary fluxes (water flux and Ra activity). Variation (50%) in the ^{224}Ra, ^{226}Ra, and ^{228}Ra offshore seawater activity results in a 63–74% change in the basin-wide ^{226}Ra SGD flux and a 58–60% change in the ^{228}Ra SGD flux, but only a 4–9% change in the ^{224}Ra SGD flux. This highlights the need to accurately constrain long-lived Ra activities in the inflowing and outflowing water, as well as water fluxes across boundaries. Short-lived Ra isotope mass balances are sensitive to internal Ra fluxes, including desorption from resuspended particles and inputs from sediment diffusion and bioturbation. A 50% increase in the sediment diffusive flux of ^{224}Ra, ^{226}Ra, and ^{228}Ra results in a ∼30% decrease in the ^{224}Ra SGD flux, but only a ∼6–10% decrease in the ^{226}Ra and ^{228}Ra SGD flux. When boundary mixing is uncertain, ^{224}Ra is the preferred tracer of SGD if sediment contributions are adequately constrained. When boundary mixing is well-constrained, ^{226}Ra and ^{228}Ra are the preferred tracers of SGD, as sediment contributions become less important. A three-dimensional numerical model is used to constrain boundary mixing in Long Island Sound (LIS), with mean SGD fluxes of $1.2 \pm 0.9 \times 10^{13}$ L y^{-1} during spring 2009 and $3.3 \pm 0.7 \times 10^{13}$ L y^{-1} during summer 2010. The SGD flux to LIS during summer 2010 was one order of magnitude greater than the freshwater inflow from the Connecticut River. The maximum marine SGD-driven N flux is $14 \pm 11 \times 10^{8}$ mol N y^{-1} and rivals the N load of the Connecticut River.

Keywords: radium isotopes, submarine groundwater discharge, porewater exchange, nitrogen, Long Island Sound

INTRODUCTION

Submarine groundwater discharge (SGD) is a component of the hydrologic cycle and can act as an important vector for the transport of nutrients, carbon, trace elements, and pollutants to the coastal ocean (Moore, 2010; Knee and Paytan, 2011). SGD includes both terrestrial, meteorically-derived groundwater driven by a positive onshore hydraulic gradient and marine (i.e., saline) groundwater, driven by a variety of physical forcing mechanisms including density, tide, and wave driven flow (Santos et al., 2012). Naturally occurring radium isotopes are powerful tracers of SGD, as brackish groundwaters are typically enriched in dissolved Ra isotopes by several orders of magnitude over seawater (Swarzenski, 2007; Charette et al., 2008). The Ra quartet spans a wide range of half-lives (^{223}Ra = 11.4 d, ^{224}Ra = 3.66 d, ^{226}Ra = 1600 y, and ^{228}Ra = 5.75 y) and has thus been applied to trace and quantify inputs of SGD to the ocean on a variety of scales (Moore, 2010). For a given area, evaluation of the Ra source terms (e.g., rivers, particle desorption, diffusion, and bioirrigation), and Ra sinks (e.g., mixing, radioactive decay) can be used to quantify SGD. A Ra flux supplied by SGD is typically invoked to explain any imbalance between Ra sink and Ra source fluxes. Consequently, a SGD-driven Ra flux can be converted to a volumetric water flow with a proper characterization of the SGD endmember Ra activity. Multiple Ra isotopes are often used to quantify SGD; however, differences between short-lived and long-lived Ra isotope mass balances are often poorly constrained or not fully understood (Moore et al., 2006; Beck et al., 2007, 2008; Garcia-Solsona et al., 2008; Knee et al., 2016; Tamborski et al., 2017b).

Each Ra isotope is sensitive to different source and sink terms, reflecting the time-scale of a particular process with respect to the Ra isotope half-life. For example, short-lived ^{223}Ra and ^{224}Ra are more rapidly lost via radioactive decay, while long-lived ^{226}Ra and ^{228}Ra are not. Thus, the water column inventory of ^{223}Ra and ^{224}Ra must be well constrained to evaluate these short half-life tracers. Furthermore, flow paths of varying time-scales may have unique short-lived and long-lived Ra activities, and thus these isotopes may trace different SGD and porewater exchange flow paths (Rodellas et al., 2017). In addition, different geological matrices can have unique ratios of uranium (^{223}Ra, ^{226}Ra), and thorium (^{224}Ra, ^{228}Ra) series isotopes, thus enabling the identification of different geologic sources (Charette et al., 2008; Swarzenski, 2007).

This article synthesizes sediment, surface water, bottom water and groundwater Ra isotope data that has been previously collected in the semi-enclosed tidal estuary of Long Island Sound (LIS; Krishnaswami et al., 1982; Copenhaver et al., 1993; Turekian et al., 1996; Garcia-Orellana et al., 2014; Bokuniewicz et al., 2015; Tamborski et al., 2017a,b). In addition, we present new data on long-lived ^{226}Ra and ^{228}Ra, previously collected during 2009 and 2010. Here, we use short-lived ^{224}Ra and long-lived ^{226,228}Ra to quantify total SGD to LIS by mass balance. The main objective of this article is to evaluate the sensitivity of SGD estimated from Ra isotope mass balances. We evaluate Ra source and sink terms, and provide general recommendations on best-practices for Ra mass balances in semi-enclosed basins for future studies. We conclude with a revised estimate of SGD-driven NO_3^- loadings to LIS.

MATERIALS AND METHODS

Study Site

Long Island Sound is a tidal estuary bound by New York City at its western end, the southern shore of Connecticut at its northern boundary and the northern shore of Long Island (NY) at its southern boundary (**Figure 1**). At the beginning of the 20th century, urbanization, and pollution from the Metropolitan New York area led LIS to be nicknamed the "urban sea" (Koppelman et al., 1976; Latimer et al., 2013). Bottom-water hypoxia and eutrophication have been linked to excess nitrogen inputs from wastewater, sewage effluent, river inputs, and groundwater (NYSDEC and CTDEP, 2000). Indeed, Long Island's coastal embayments are vulnerable to excess nitrogen loading from submarine groundwater inputs (Bokuniewicz, 1980; Capone and Bautista, 1985). However, the volume of total SGD to LIS is not well known, despite increasing recognition of this important pollutant pathway.

The volume of terrestrial SGD to LIS from both Connecticut and New York shorelines is generally well constrained from hydrogeologic models (Buxton and Modica, 1992; Scorca and Monti, 2001; Suffolk County, 2015). Ra isotope mass balances in LIS' smaller embayment, Smithtown Bay (Bokuniewicz et al., 2015; Tamborski et al., 2017b), and for the entire LIS (Garcia-Orellana et al., 2014) all suggest that total SGD is dominated by marine groundwater inputs. Tamborski et al. (2017b) found that SGD within the first 200 m of the shoreline, determined from short-lived radionuclide mass balances, was up to ∼55% greater than SGD estimates determined from long-lived radionuclides and physical seepage meter measurements. To explain this difference, they suggested that wave and tidal circulation SGD flow paths captured short-lived radionuclide fluxes due to their faster regeneration rates within sediments, while these flow paths would not capture ^{226}Ra and ^{228}Ra. Interestingly, the total SGD flux to Smithtown Bay determined by Bokuniewicz et al. (2015) from ^{224}Ra, which includes inputs to the entire bay, was one to three orders of magnitude greater than the total SGD flux within the first 200 m of the shoreline. This led Tamborski et al. (2017b) to hypothesize that there may be additional, deeper SGD flow paths farther offshore in Smithtown Bay and LIS, from either the deeper Magothy aquifer or seawater circulation through offshore permeable sediments driven by density-forcing mechanisms, in addition to short-scale circulation fluxes driven by bioturbation and wave pumping.

Analytical Methods

Surface and deep-water samples from LIS were collected aboard the *R/V Seawolf* during 24–30 April 2009, 29 July–04 August 2009, and 03–12 August 2010. These samples, along with an analysis of the short-lived Ra isotopes, are described in Garcia-Orellana et al. (2014). Separately, groundwaters were collected from intertidal cluster wells from a coastal bluff and a barrier beach subterranean estuary, during spring and

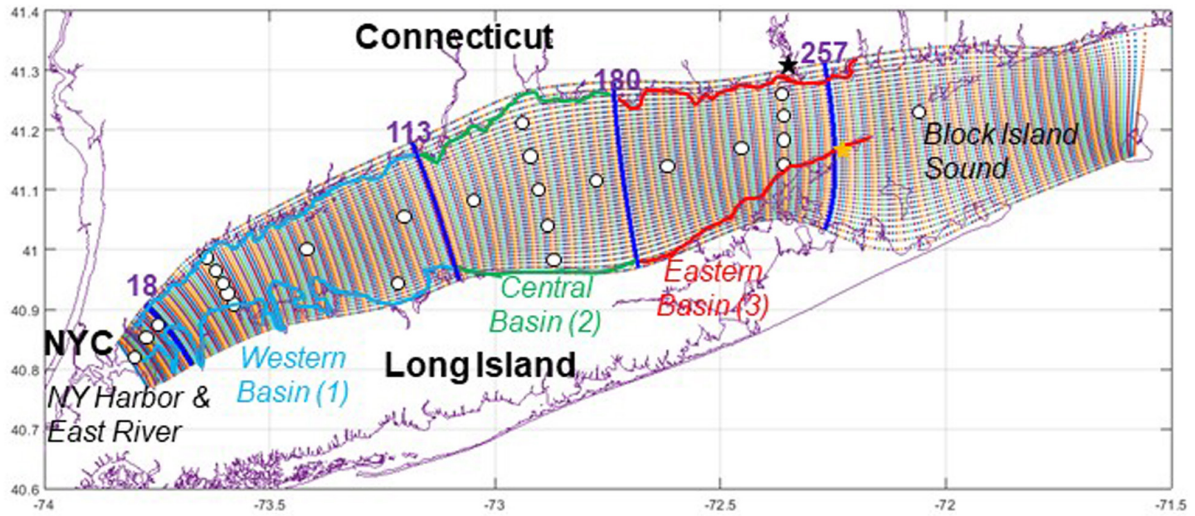

FIGURE 1 | The study site of Long Island Sound, bound between Long Island (NY), and Connecticut. Surface and bottom sampling stations are indicated by white circles. The mouth of the Connecticut River is indicated by a black star; Orient Point is indicated by an orange star. Long Island Sound is subdivided into the western (light blue), central (green), and eastern (red) basins, after Garcia-Orellana et al. (2014). Purple numbers correspond to the cross-section numbers in **Table 1**. Mean water exchange transports through cross-sections 18 113, 180, and 257 (N-S oriented dark blue lines) are derived from the three-dimensional model of Crowley (2005); the two-dimensional grid used in the model calculations is shown for reference and overlaps the land-ocean boundary.

summer 2014 and 2015. Additional coastal stations were sampled via drive-point piezometer at the low tide shoreline. These groundwater samples, including an analysis of the Ra quartet, are described in Tamborski et al. (2017a).

Briefly, water samples (seawater = 20–60 L; groundwater = 1–4 L) were filtered through MnO_2 impregnated acrylic fibers at a flow rate of <1 L min^{-1} to quantitatively extract dissolved Ra from solution onto the fiber. Short-lived ^{223}Ra and ^{224}Ra were measured using a Radium Delayed Coincidence Counter (RaDeCC; Moore and Arnold, 1996) immediately after sample collection. An additional count was performed 1 month after sample collection to measure ^{228}Th, to determine the amount of unsupported (excess) ^{224}Ra. Subsequently, the Mn-fibers were leached in a HCl and Hydroxylamine hydrochloride mixture and Ra was co-precipitated with $BaSO_4$. Precipitates were removed from the leachate, stored in glass vials and sealed for >3 weeks. Samples were counted on a Canberra Intrinsic Ge well detector, where the activity of long-lived ^{226}Ra and ^{228}Ra was determined from the 352 keV (^{214}Pb) and 911 keV (^{228}Ac) photopeaks, respectively. Gamma counting efficiencies were determined from NBS Standard Reference Material 4350B.

Estimates of Water Transport

LIS is made up of three basins (western, central, and eastern); water flux between basins and within LIS's boundaries were estimated to evaluate Ra mixing. Crowley (2005) determined that the transport through cross-sections to the west of Orient Point had a long term mean of 2.05 × 10^{13} L y^{-1} throughout the LIS basin (section 257; **Figure 1**), as determined from three-dimensional numerical simulations of circulation with meteorological and boundary sea-level forcing. The cross-sectionally-averaged transport exhibited significant temporal variability which was spatially coherent, with residence times on the order of several weeks to 2 months (Crowley, 2005). The differences in cross-sectionally-averaged transport can be attributed to localized effects of river discharge and to storage of water between sections. Water exchange fluxes were derived from the model of Crowley (2005) at cross-sections that approximately separate LIS into its three unique basins (western, central, and eastern; **Figure 1**) over a period between 2009 and 2010. Long term mean exchange transports through cross-sections exhibit an east to west net transport (**Table 1**). Note that these mean exchange transports have a standard error on the order of 10% because of the large temporal variability in the exchange. The mean surface freshwater inflow to the entire basin is on the order 1.34 × 10^{13} L y^{-1}, of which the Connecticut River at the far end of the Sound contributes approximately 1.19 × 10^{13} L y^{-1}, depending upon the seasonal conditions. The exchange transports at section 257 are corrected to accommodate the surface freshwater inflow between sections 18 and 257 (**Figure 1**). It should be noted that section 257 is located approximately at the longitudinal position of the Connecticut River, and that recent dye simulations emphasize that much of the Connecticut River waters exit to the east (Jia and Whitney, 2019).

RESULTS AND DISCUSSION

Ra Distribution

Long-lived ^{226}Ra and ^{228}Ra activities generally increased from east to west in LIS (**Table 2**). Compared to surface waters, deep-water Ra activities were greater on average for the western basin and similar to surface waters for the central and eastern basins (**Table 2**). Surface and deep-water Ra activities generally

TABLE 1 | Cross-sectional mean water exchange transports and standard error of the means, arranged by westerly flow (Qwest), and easterly flow (Qeast).

Cross-section #	$Q_{west} \pm SE \times 10^{14}$ L y^{-1}	$Q_{east} \pm SE \times 10^{14}$ L y^{-1}
18	0.65 ± 0.13	0.46 ± 0.12
113	3.14 ± 0.28	2.86 ± 0.28
180	3.46 ± 0.43	3.30 ± 0.39
257	5.95 ± 0.56	5.70 ± 0.50
257 (Corrected)	5.86 ± 0.56	5.80 ± 0.56

*Cross-section numbers correspond to the sections depicted on **Figure 1**.*

increased with decreasing salinity (**Figure 2**) and displayed an apparent seasonality, with greater activities during summer over spring (**Table 2** and **Figure 2**). During summer 2010, reduced bottom water salinity and elevated Ra activities suggest SGD was occurring several kilometers offshore.

Intertidal groundwater samples collected along the north-shore of Long Island (Tamborski et al., 2017a) spanned a wide salinity range (**Table 3**), with maximum Ra activities at a salinity of ∼18.6 (^{226}Ra = 106 dpm 100 L^{-1}; ^{228}Ra = 1650 dpm 100 L^{-1}; **Figure 2**). The mean (±standard deviation) ^{228}Ra/^{226}Ra activity ratio of Long Island marine groundwater was 7.5 ± 3.3 (salinity = 26.6 ± 1.0; n = 44). Marine groundwaters from the Connecticut shoreline had a ^{228}Ra/^{226}Ra activity ratio of 13.8 ± 4.1 (salinity = 28.4 ± 1.3; n = 5; **Table 3**). Connecticut fresh groundwaters, sampled from inland wells, had ^{228}Ra/^{226}Ra activity ratios between 0.2–1.4 (Krishnaswami et al., 1982; Copenhaver et al., 1993). This is in marked contrast to the ^{228}Ra/^{226}Ra activity ratio of the Connecticut River (∼3; Dion, 1983) and East River (3.8–4.1; Turekian et al., 1996). ^{228}Ra and ^{226}Ra activities of surface and bottom water samples, and activity ratios of possible sources, are presented in **Figure 3**.

Ra Mass Balance

Long-lived ^{226}Ra and ^{228}Ra mass balances for LIS were constructed after the short-lived ^{224}Ra mass balance developed by Garcia-Orellana et al. (2014) for spring 2009 and summer 2010, for the entire LIS basin. We have further developed Ra mass balances for each individual basin (western, central, and eastern; **Figure 1**). The Ra mass balances have been updated to reflect new terms, as described below. Briefly, a surface and deep box Ra inventory (dpm) is calculated for the western, central, and eastern basins of LIS (**Table 4**). The Ra inventory is calculated as the product of the water volume within each basin and the mean Ra activity of the basin. The Ra mass balance is written as:

$$J_{out} + J_{decay} = J_{in} + J_{river} + J_{desorp} + J_{diffusion} + J_{SGD} \quad (1)$$

Where the left-hand side represents Ra sinks and the right-hand side represents Ra sources. The Ra mass balance includes loss from mixing (J_{out}) and radioactive decay (J_{decay}). Ra sources include mixing (J_{in}), riverine input (J_{river}), the desorption of Ra from resuspended particles (J_{desorp}), molecular diffusion and bioturbation ($J_{diffusion}$), and SGD (J_{SGD}). Each term in Eq. 1 is assessed for ^{224}Ra, ^{226}Ra, and ^{228}Ra for the western, central, eastern, and total basins during spring 2009 and summer 2010, thus resulting in 24 unique Ra mass balances. All Ra mass balances are summarized in the **Supplementary Material** (**Supplementary Table S1**). Each term in Eq. 1 is described in further detail below, including a sensitivity analysis on the final estimated Ra flux supplied by SGD (section "Mass balance sensitivity").

Boundary Fluxes

Boundary fluxes determined from a three-dimensional numerical model (section "Estimates of water transport") are used to quantify the exchange of water and Ra isotopes between New York Harbor and the East River with the western basin of LIS (section 18), between the western basin and the central basin of LIS (section 113), between the central basin and the eastern basin of LIS (section 180), and between the eastern basin of LIS and Block Island Sound (section 257; **Table 1** and **Figure 1**). We use the same boundary flux for spring 2009 and summer 2010, although we acknowledge that there may be minor differences in seasonal water volume and thus exchange. Ra mixing fluxes (J_{in} and J_{out}) are calculated from the sectional mean water exchange transports and the associated endmember Ra activity. Because there is a net east to west water transport in LIS (**Table 1**), we use the mean deep-water Ra activities (**Table 2**) to represent Ra mixing from east to west. Mean Ra surface water activities (**Table 2**) are used to represent Ra mixing from west to east, for each respective basin under consideration. Boundary fluxes are summarized in **Figure 4**.

The ^{224}Ra, ^{226}Ra, and ^{228}Ra activities of the East River are, respectively, taken as 9 dpm 100 L^{-1} (Garcia-Orellana et al., 2014), 10.7 dpm 100 L^{-1} (Li et al., 1977), and 64 dpm 100 L^{-1} (Turekian et al., 1996) for both seasons. Block Island Sound seawater was previously sampled for long-lived Ra at 5 m and 25 m depth during summer 1991 (St101; Turekian et al., 1996). This same station was sampled during spring 2009 in this study. We use a ^{224}Ra, ^{226}Ra, and ^{228}Ra activity of 3.6, 5.3, and 29 dpm 100 L^{-1}, respectively, for spring 2009 and activities of 3.6, 8.5, and 47 dpm 100 L^{-1}, respectively, for summer 2010. It is important to note that only one sample is used to characterize the Ra endmember for each of these mixing input terms.

The Connecticut River is the largest river entering LIS. Connecticut River discharge was estimated as the mean discharge over the two-week period preceding each seasonal LIS survey, based on the average residence time of the eastern basin (Crowley, 2005). The Connecticut River discharge is taken as 2.52 × 10^{13} L y^{-1} during spring 2009 and 0.68 × 10^{13} L y^{-1} during summer 2010 from the USGS gaging station at Middle Haddam (ID 01193050). Note that the spring 2009 and summer 2010 Connecticut River discharges were, respectively, above and below the mean annual river discharge (∼1.2 × 10^{13} L y^{-1}). The Connecticut River is only considered in the eastern basin and total basin Ra mass balances. Several other rivers enter LIS from both Long Island (e.g., Nissequogue River) and Connecticut (e.g., Housatonic River, Thames River) shorelines, which together account for a cumulative discharge on the order of ∼0.4 × 10^{13} L y^{-1} (Koppelman et al., 1976); here we assume that one third of this water flux enters each of the three LIS basins. The riverine Ra flux to LIS (J_{river}) is calculated as the product of the river discharge to each basin and the dissolved Ra

TABLE 2 | Mean ^{226}Ra and ^{228}Ra activities in the three basins of Long Island Sound during spring 2009, summer 2009, and summer 2010, arranged by surface and deep-water samples.

	^{226}Ra Surface	^{228}Ra Surface	*n* (surface)	^{226}Ra Deep	^{228}Ra Deep	*n* (deep)
	(dpm 100 L^{-1})			(dpm 100 L^{-1})		
Spring 2009						
Western Basin	9.3 ± 1.4	61 ± 12	9	10.1 ± 1.3	71 ± 7	7
Central Basin	10.0 ± 0.8	58 ± 4	7	10.0 ± 0.9	52 ± 9	6
Eastern Basin	7.3 ± 1.9	39 ± 19	6	6.6 ± 1.3	33 ± 13	5
Mean	9.0 ± 1.8	54 ± 16	22	9.0 ± 2.0	54 ± 18	18
Summer 2009						
Western Basin	12.9 ± 3.2	97 ± 21	4	14.1 ± 1.2	104 ± 7	4
Central Basin	9.8 ± 1.3	57 ± 19	3	9.8 ± 1.4	56 ± 11	3
Eastern Basin	9.2 ± 0.6	50 ± 4	4	9.6 ± 0.6	41 ± 9	4
Mean	10.7 ± 2.7	69 ± 26	11	11.3 ± 2.4	68 ± 29	11
Summer 2010						
Western Basin	11.5 ± 2.6	80 ± 22	7	14.1 ± 0.6	98 ± 12	6
Central Basin	11.1 ± 0.7	73 ± 9	6	11.9 ± 1.4	72 ± 11	6
Eastern Basin	10.0 ± 1.3	69 ± 12	5	9.8 ± 0.9	48 ± 6	5
Mean	10.9 ± 1.9	75 ± 17	18	12.1 ± 2.0	74 ± 23	17

activity of the Connecticut River mouth (**Figure 1**). Surface water salinity at the station sampled near the mouth of the Connecticut River was ∼28; therefore, the Ra flux estimated here intrinsically includes the desorption of Ra from suspended riverine particles. This calculation assumes that the Ra endmember at the mouth of the Connecticut River is representative of all rivers entering LIS, as done by Turekian et al. (1996); riverine fluxes are summarized in **Figure 4**.

Internal Fluxes

The desorption of long-lived ^{226}Ra and ^{228}Ra from resuspended particles (J_{desorp}) throughout LIS is negligible due to the slow regeneration time of ^{226}Ra and ^{228}Ra in sediments. The desorption of ^{224}Ra is estimated from suspended particle concentrations for spring 2009 (1.5 ± 1.3 mg L^{-1}) and summer 2010 (4.0 ± 2.5 mg L^{-1}), and a surface-exchangeable ^{224}Ra activity of 0.75 dpm g^{-1}. Desorption of ^{224}Ra from tidally resuspended particles is 1.6 ± 1.4 × 10^4 dpm m^{-2} y^{-1} for spring 2009 and 4.4 ± 2.7 × 10^4 dpm m^{-2} y^{-1} for summer 2010 (Garcia-Orellana et al., 2014; **Figure 4**).

Sediment diffusion and bioturbation have been shown to be an important source of short-lived Ra isotopes to LIS, due to their relatively rapid regeneration rates within sediments (Garcia-Orellana et al., 2014). This source term should be relatively less important for the long-lived Ra isotopes, due to their slower regeneration rates in sediments. Tamborski et al. (2017b) conducted sediment core incubation experiments (at 20°C and 3°C; oxic, and hypoxic conditions) to determine the sediment flux of long-lived Ra isotopes for a sandy (intertidal) core and a silty (offshore) core from LIS. ^{228}Ra sediment fluxes in LIS were previously determined from the disequilibrium between solid-phase ^{228}Ra and its parent ^{232}Th (Cochran, 1979; Turekian et al., 1996), which integrates over several half-lives of ^{228}Ra and thus represents a mean-annual ^{228}Ra flux. Each of these methods includes a Ra flux from both molecular diffusion and bioirrigation. These various flux estimates were averaged together for coarse-grained sediments and fine-grained sediments. Fluxes were further separated by temperature (warm = summer; cold = early spring) and oxygen content (hypoxic = summer; oxic = early spring) to differentiate between spring and summer conditions (**Table 5**). Sediment-mediated ^{228}Ra and ^{226}Ra inputs were calculated using a LIS bottom surface area of 0.90 × 10^9 m^2, 1.08 × 10^9 m^2, and 0.96 × 10^9 m^2 for the western, central and eastern basins. Further, we assume a fine-grained and coarse-grained surficial sediment distribution for the western (70% fine, 30% coarse), central (50% fine, 50% coarse), and eastern (0% fine, 100% coarse) basins following Poppe et al. (2000). Sediment Ra fluxes are summarized in **Figure 4**.

Assuming steady-state, the radioactive decay of ^{224}Ra and ^{228}Ra is calculated as the product of the respective Ra inventory for each basin and the Ra isotope decay constant (0.189 d^{-1} for ^{224}Ra and 0.121 y^{-1} for ^{228}Ra). Decay of ^{226}Ra is negligible due to its long half-life (**Figure 4**). The excess Ra inventory in each basin (Σ Ra sinks – Σ Ra sources; Eq. 1) is presumed to be balanced by SGD (J_{SGD}). A negative SGD flux implies either that Ra sources approximately balance Ra sinks (within the propagated uncertainties), or that one (or more) known Ra flux is improperly characterized. SGD-derived Ra fluxes are converted into volumetric water flows by dividing the Ra flux by the Ra activity of the SGD endmember, sampled from intertidal wells and shoreline piezometer stations along both NY and CT shorelines (Garcia-Orellana et al., 2014; Tamborski et al., 2017a). Selection of the SGD Ra endmember is discussed below (section "SGD volumetric water flow to Long Island Sound").

Mass Balance Sensitivity

Analysis of Ra sources and sinks reveals that boundary fluxes dominate the long-lived Ra isotopes while sediment contributions (diffusion and desorption) and radioactive decay

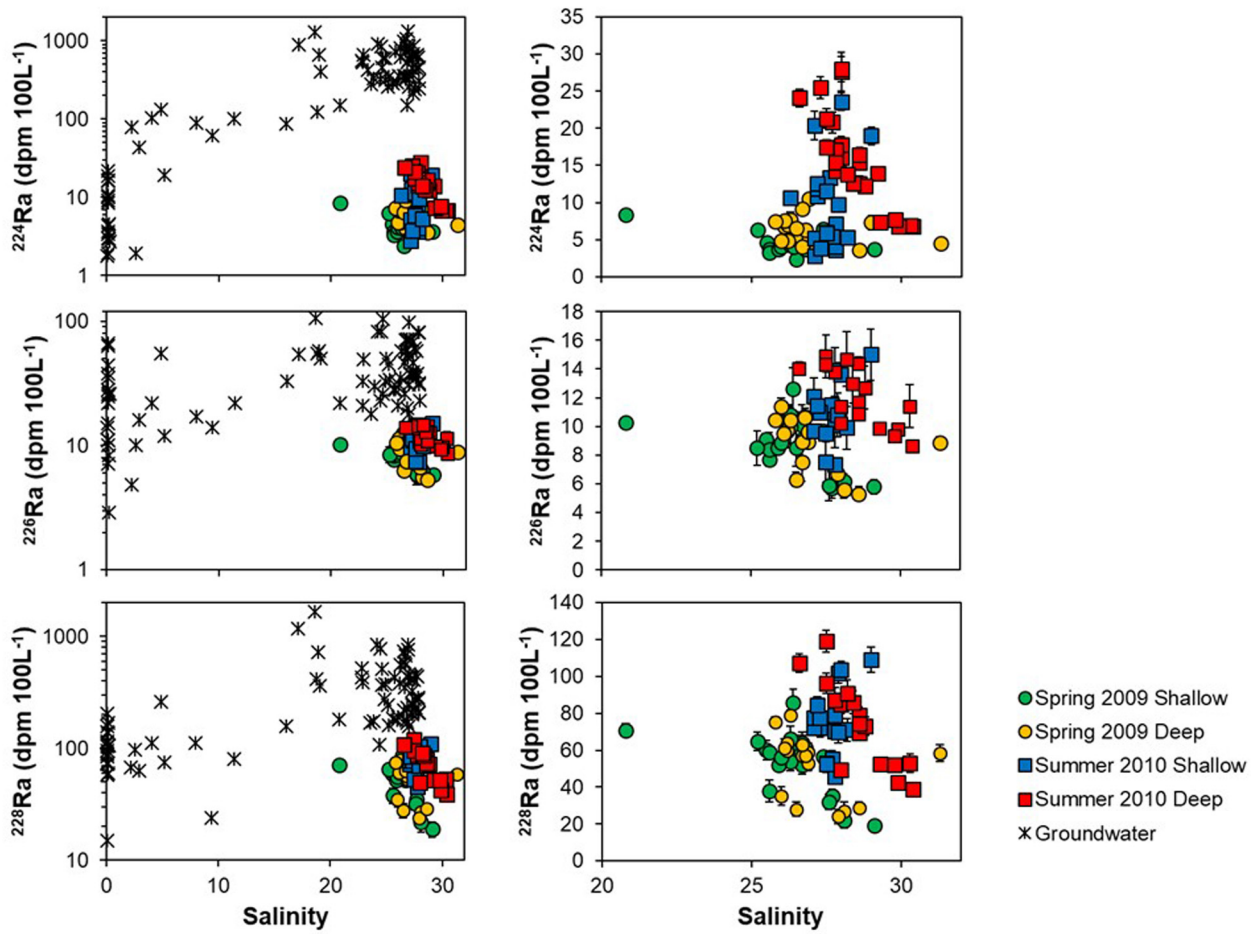

FIGURE 2 | Dissolved Ra vs salinity for Long Island Sound surface waters, bottom waters, and groundwaters. Surface and bottom water samples are presented in the right-hand panels for improved visualization and are arranged by season, from Garcia-Orellana et al. (2014). Groundwater samples are from intertidal cluster wells and shoreline piezometer stations on Long Island (Tamborski et al., 2017a) and Connecticut (Garcia-Orellana et al., 2014).

TABLE 3 | Summary of groundwater Ra endmembers from Long Island (LI) and Connecticut (CT) shorelines.

Groundwater source	Salinity	^{224}Ra dpm 100 L^{-1}	^{226}Ra dpm 100 L^{-1}	^{228}Ra dpm 100 L^{-1}	^{228}Ra/^{226}Ra	*n*
LI fresh groundwater*	0.1 ± 0.0	8 ± 6	25 ± 18	104 ± 45	6.2 ± 5.0	17
LI brackish groundwater*	15.5 ± 8.4	346 ± 340	36 ± 26	359 ± 390	9.0 ± 5.1	27
LI marine groundwater*	26.6 ± 1.0	523 ± 260	47 ± 21	344 ± 177	7.5 ± 3.3	44
CT fresh groundwaterˆ	<1	n/a	44 ± 36	27 ± 17	0.8 ± 0.5	7
CT marine groundwaterˆˆ	28.4 ± 1.3	356 ± 45	28 ± 8	381 ± 123	13.8 ± 4.1	5

*Groundwater samples are classified by salinity: fresh groundwater = 0–1; brackish groundwater = 4–24; and marine groundwater = 25–28. Error bars indicate ± 1 standard deviation from the mean. Note that brackish groundwaters from Connecticut are not included in this analysis. *Groundwaters from Tamborski et al. (2017a). ˆGroundwaters from Copenhaver et al. (1993) and Krishnaswami et al. (1982). ˆˆGroundwaters from Garcia-Orellana et al. (2014) and analyzed in this study.*

dominate the short-lived Ra isotopes (**Figure 4**). Ra mass balance sensitivity to each of these terms is discussed below.

Sediment diffusion, bioirrigation, and desorption support ∼50% of the ^{224}Ra inventory for LIS but only ∼6% of the ^{226}Ra inventory and ∼10–20% of the ^{228}Ra inventory (**Figure 4**). The ^{224}Ra sediment flux is constrained from sediment incubation experiments from five different locations (Garcia-Orellana et al., 2014); the ^{228}Ra sediment flux is constrained from four sediment incubations and two estimates from ^{228}Ra:^{232}Th disequilibrium (Cochran, 1979; Turekian et al., 1996). Is this representative of the entirety of LIS? Few Ra-based SGD studies capture sediment-mediated Ra inputs from more than a few measurements (Beck et al., 2007, 2008; Garcia-Solsona et al., 2008; Rodellas et al., 2012, 2015; Cai et al., 2014; Tamborski et al., 2017b).

The molecular diffusive flux of Ra from shallow porewater to overlying seawater is governed by the Ra concentration gradient between porewater and seawater (Fick's first law). Bioturbation and bioirrigation can further facilitate Ra transport by enhancing the effective sediment surface-area, thus complicating diffusive flux estimates. Due to its short half-life, ^{224}Ra regenerates rapidly in sediments from the decay of its particle-reactive parent ^{228}Th. The activity of ^{230}Th and ^{232}Th (the parents of ^{226}Ra and ^{228}Ra) are similar in LIS sediments, resulting in similar production rates in muddy and sandy sediments (Cochran, 1979). Therefore, seasonal redox changes may affect the diffusive flux of short-lived and long-lived Ra isotopes differently, as the redox interface migrates between bottom waters and the shallow subsurface (Garcia-Orellana et al., 2014). This seasonal control impacts Ra diffusion and more importantly, the influence of the benthic fauna, which are presumed to be less active during colder periods. We have attempted to capture this variability by using different sediment incubations for spring and summer conditions (**Table 5**).

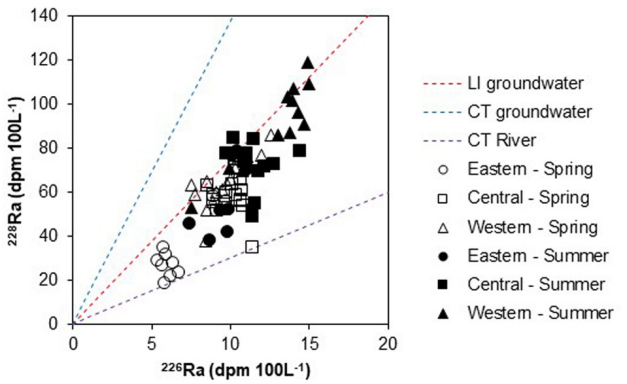

FIGURE 3 | Cross-plot of ^{228}Ra and ^{226}Ra activities in shallow and deep waters collected from Long Island Sound, arranged by sampling season. Note that error bars are generally smaller than the symbol size. Dashed lines indicate the ^{228}Ra/^{226}Ra activity ratio of possible Ra sources. Data sources: Connecticut River (AR = 3; Dion, 1983); Connecticut marine groundwater (AR = 14 ± 4; this study); and Long Island marine groundwater (AR = 8 ± 3; Tamborski et al., 2017a).

Are the incubations used to quantify diffusion and bioirrigation from sediments accurate? ^{228}Ra fluxes for muddy LIS sediments, determined from the deficit of solid-phase ^{228}Ra relative to its parent ^{232}Th (Cochran, 1979; Turekian et al., 1996), are in general agreement with ^{228}Ra fluxes determined from sediment chamber incubations (33–82 dpm m^{-2} d^{-1} vs 12–207 dpm m^{-2} d^{-1}). The solid-phase ^{228}Ra:^{232}Th approach integrates over the half-life of ^{228}Ra, therein representing a mean-annual ^{228}Ra flux; therefore, these estimates seem reasonable at the seasonal time-scale considered here. A recent study found the traditional sediment incubation approach for ^{224}Ra flux determination to be similar to ^{224}Ra fluxes determined from ^{224}Ra:^{228}Th disequilibrium (Shi et al., 2018). Thus, it seems that the incubations used to quantify the Ra flux from diffusion and bioirrigation are accurate, although it remains to be seen how representative these several cores are for the entirety of LIS. A 50% increase in the diffusive flux of ^{224}Ra, ^{226}Ra, and ^{228}Ra, while keeping all other parameters equal (Eq. 1), results in a ∼30% decrease

TABLE 4 | ^{226}Ra (top) and ^{228}Ra (bottom) inventories in western, central and eastern LIS in spring 2009 and summer 2010.

	Basin	Water volume (×10^{12} L)	Spring 2009		Summer 2010	
			Mean ^{226}Ra activity (dpm 100 L^{-1})	^{226}Ra inventory (×10^{11} dpm)	Mean ^{226}Ra activity (dpm 100 L^{-1})	^{226}Ra inventory (×10^{11} dpm)
Surface	Eastern basin	3.40	7.3 ± 1.9	2.5 ± 0.7	10.0 ± 1.3	3.4 ± 0.5
	Central basin	2.90	10.0 ± 0.8	2.9 ± 0.2	11.1 ± 0.7	3.2 ± 0.2
	Western basin	1.87	9.3 ± 1.4	1.8 ± 0.3	11.5 ± 2.6	2.1 ± 0.5
Deep	Eastern basin	18.8	6.6 ± 1.3	12.3 ± 2.4	9.8 ± 0.9	18.5 ± 1.7
	Central basin	17.6	10.0 ± 0.9	17.7 ± 1.5	11.9 ± 1.4	20.9 ± 2.4
	Western basin	7.42	10.1 ± 1.3	7.5 ± 1.0	14.1 ± 0.6	10.5 ± 0.5
Total		52.0		45 ± 3		59 ± 3
			Spring 2009		Summer 2010	
			Mean ^{228}Ra activity (dpm 100 L^{-1})	^{228}Ra inventory (×10^{12} dpm)	Mean ^{228}Ra activity (dpm 100 L^{-1})	^{228}Ra inventory (×10^{12} dpm)
Surface	Eastern basin	3.40	39.2 ± 18.6	1.3 ± 0.6	68.9 ± 11.9	2.3 ± 0.4
	Central basin	2.90	58.5 ± 4.2	1.7 ± 0.1	73.2 ± 9.0	2.1 ± 0.3
	Western basin	1.87	61.4 ± 12.5	1.2 ± 0.2	80.1 ± 22.4	1.5 ± 0.4
Deep	Eastern basin	18.8	33.3 ± 12.7	6.3 ± 2.4	47.7 ± 6.0	9.0 ± 1.1
	Central basin	17.6	52.4 ± 9.0	9.2 ± 1.6	71.7 ± 11.1	12.6 ± 2.0
	Western basin	7.42	70.8 ± 7.2	5.3 ± 0.3	97.7 ± 11.8	7.3 ± 0.9
Total		52.0		25 ± 3		35 ± 3

TABLE 5 | Summary of ^{226}Ra and ^{228}Ra sediment fluxes in Long Island Sound.

Season	Sediment conditions	^{226}Ra (dpm m^{-2} d^{-1})	^{228}Ra (dpm m^{-2} d^{-1})
Spring	Fine-grained Oxic	28 ± 14	207 ± 104
	Coarse-grained Cold	3 ± 2	16 ± 8
Summer	Fine-grained Hypoxic	1 ± 1	42 ± 26*
	Coarse-grained Warm	8 ± 4	39 ± 20

*^{224}Ra fluxes were determined for each LIS basin and are summarized in Garcia-Orellana et al. (2014). Data Sources: Tamborski et al. (2017b); *Average of Cochran (1979); Turekian et al. (1996), and Tamborski et al. (2017b).*

in the ^{224}Ra SGD flux to LIS, but only a ∼6% and ∼10% decrease in the ^{226}Ra and ^{228}Ra SGD flux, respectively (total-basin mass balances). More realistic is a decrease in the ^{226}Ra and ^{228}Ra sediment diffusive flux. Many studies neglect diffusion of long-lived Ra isotopes altogether (Rama and Moore, 1996; Beck et al., 2007, 2008). Indeed, exclusion of this term would result in a 6–7% increase in the ^{226}Ra SGD flux and a 10–18% increase in the ^{228}Ra SGD flux (total-basin mass balances).

Desorption of ^{226}Ra and ^{228}Ra from resuspended sediments is assumed negligible. Desorption of ^{224}Ra from resuspended sediments is estimated to account for 14–19% of the total ^{224}Ra inventory for the total-basin mass balance. Rodellas et al. (2015) note that it is difficult to accurately constrain the Ra flux from resuspended sediments, which can be a significant Ra source in embayments with fine-grained sediments. The surface-exchangeable ^{224}Ra estimated for LIS (0.75 dpm g^{-1}) is based on shallow porewater (0–2 cm) ^{224}Ra activities from two sediment cores (Garcia-Orellana et al., 2014) and a mean K_d for Ra of 50 L kg^{-1} (Cochran, 1979; Sun and Torgersen, 2001). Even more difficult to constrain is the rate at which sediments are resuspended to release ^{224}Ra into the water column. Here, sediments are assumed to be resuspended on tidal time-scales. This term represents the second largest source of uncertainty in the ^{224}Ra mass balance (**Figure 4**). A 50% increase in the ^{224}Ra desorption flux, while keeping all other parameters equal (Eq. 1), results in a ∼14–19% decrease in the ^{224}Ra SGD flux to LIS (total-basin mass balances).

With respect to the loss by radioactive decay, the basin-wide ^{224}Ra inventory is more sensitive to this term than are the long-lived Ra inventories. Indeed, decay of ^{224}Ra dominates over mixing losses, regardless of the basin or season (**Figure 4**). This implies that a large number of water column samples are necessary to accurately capture the (near) instantaneous ^{224}Ra inventory. The ^{224}Ra inventory integrates over the half-life of ^{224}Ra, such that this inventory will accurately reflect the times of the year when the sampling was conducted, but this inventory may not be representative of a seasonal or annual ^{224}Ra flux. Importantly, this suggests that multiple sampling campaigns are necessary to capture any seasonality in the ^{224}Ra inventory for SGD flux determination. Fortunately, ^{224}Ra decay is the simplest flux term to constrain, as it is only dependent upon measuring ^{224}Ra concentration. This is the opposite case for long-lived ^{226}Ra and ^{228}Ra, where a lower number of water column samples may be adequate to capture the long-lived Ra water column inventory, while mixing terms must be well-constrained. Seasonality in long-lived Ra sources and sinks may be difficult to resolve with these isotopes because they integrate over long temporal scales.

Multiple water column Ra samples are required at the boundaries (East River and Block Island Sound in this case) to accurately constrain the boundary mixing Ra flux (**Figure 4**). The boundary water flux may be difficult to quantify in environments where numerical models or instrument deployment (e.g., ADCP) are unavailable. The ^{224}Ra inventory will be less sensitive to boundary mixing when the time-scale of mixing is sufficiently large with respect to the half-life of ^{224}Ra (**Figure 4**). Western and eastern basin long-lived Ra isotope mass balances for spring 2009 reveal that Ra sources approximately balance Ra sinks, without the need to invoke SGD. However, the uncertainties on these mass balances are quite large, owing to the uncertainty of the mixing endmember activity (East River for the western basin and Block Island Sound for the eastern basin). The Ra flux into LIS from mixing with the East River (J_{river}) and Block Island Sound (J_{in}) were each determined from one sampling station (Li et al., 1977; Turekian et al., 1996). A 50% change in the East River ^{224}Ra, ^{226}Ra, and ^{228}Ra activity, while keeping all other parameters equal (Eq. 1), results in only a 1–2% change in the ^{224}Ra SGD flux, and a 6–10% change in both the ^{226}Ra and ^{228}Ra SGD fluxes (total-basin mass balances). This is minor in comparison to the Ra flux exchanged between Block Island Sound. A 50% change in the Block Island Sound ^{224}Ra, ^{226}Ra, and ^{228}Ra activity, while keeping all other parameters equal (Eq. 1), results in only a 4–9% change in the ^{224}Ra SGD flux, but a 63–74% change in the ^{226}Ra SGD flux and a 58–60% change in the ^{228}Ra SGD flux. This highlights the critical importance of accurately determining boundary water fluxes and endmember activities, especially for the long-lived Ra isotopes (**Table 1**).

The western and eastern basin Ra activities are properly characterized (**Table 2**); thus, the central basin Ra mass balances are more adequately constrained for mixing compared to the total-basin mass balances. We emphasize that, by capturing mixing gains and losses, the central basin Ra mass balances adequately characterize the Ra-derived SGD flux, regardless of the Ra isotope used (**Figure 4**). We note that the real water exchange uncertainties may be higher than what is determined from the numerical model (**Table 1**); uncertainty in determining boundary mixing will produce large uncertainties in the long-lived Ra SGD fluxes.

The Magnitude and Significance of Submarine Groundwater Discharge to Long Island Sound

Endmember Mixing Model: An Alternative Approach to Estimate SGD

Results from the Ra mass balance in LIS reveal that SGD estimates derived from long-lived Ra isotopes are highly sensitive to boundary exchange processes (**Figure 4**). Potential uncertainties on the estimation of these boundary exchange fluxes might thus compromise the SGD estimates. An endmember mixing model

is an alternative approach to estimate the importance of SGD as a source of ^{226}Ra and ^{228}Ra to LIS, as proposed by Moore (2003). In order to simplify the system, and considering that other sources such as rivers, desorption, diffusion and decay are less important (**Figure 4**), we assume that long-lived Ra isotopes in LIS are exclusively supplied by SGD and open ocean water through boundary exchange. This approach is therefore qualitative and serves to constrain the relative magnitude of SGD only as a comparison to the mass balance. Coastal groundwater endmembers from Long Island and Connecticut shorelines have relatively distinct ^{228}Ra/^{226}Ra ratios (**Table 3** and **Figure 3**) and are thus treated as separate sources of Ra. We may thus approximate the relative contribution of Ra measured in LIS from Long Island groundwater (f_{LI}), Connecticut groundwater (f_{CT}), and seawater (f_{sea}) using a three-endmember mixing model (Moore, 2003):

$$f_{sea} + f_{LI} + f_{CT} = 1 \quad (2)$$

$$^{228}Ra_{sea} * f_{sea} + {}^{228}Ra_{LI} * f_{LI} + {}^{228}Ra_{CT} * f_{CT} = {}^{228}Ra_{measured} \quad (3)$$

$$^{226}Ra_{sea} * f_{sea} + {}^{226}Ra_{LI} * f_{LI} + {}^{226}Ra_{CT} * f_{CT} = {}^{226}Ra_{measured} \quad (4)$$

where Ra_{measured} is the measured ^{226,228}Ra activity of LIS. The three-endmember mixing model is only applied to bottom water samples from the western and eastern basins, in order to reduce riverine contributions and uncertainty in selecting a proper seawater (i.e., boundary) endmember. For the eastern basin, the seawater endmember is taken as the seasonal deep-water Ra activity of Block Island Sound. For the western basin, the seawater endmember is taken as the seasonal deep-water Ra activity of the central basin (**Table 2**). We note that the relatively large standard deviation of the endmember ^{228}Ra/^{226}Ra ratios (**Table 3**) reflects natural variability in endmember composition and thus produces considerable uncertainties in the endmember mixing models (∼30%), such that these results should be interpreted as qualitative only.

On average, Long Island groundwater contributed to 5% (spring 2009), and 6% (summer 2010) of the measured eastern basin Ra activities, with negligible contributions from Connecticut groundwater. In contrast, Long Island and Connecticut groundwaters contributed approximately equal Ra proportions to the western basin during summer 2010 (4 and 5%, respectively), while Connecticut dominated western inputs during spring 2009 (10%) with negligible inputs from Long Island. Multiplying these percentages by the volume of water in LIS (5.20×10^{13} L; **Table 4**) and dividing by a residence time of 60 days (Crowley, 2005) results in an SGD flux on the order of $\sim$1–3 $\times$ 10^{13} L y^{-1}. While this is a clear simplification of the system and thus the results can only be used in a qualitative manner, this independent approach helps constrain the relative magnitude of SGD to LIS and further helps to constrain the groundwater Ra endmember. These qualitative results demonstrate that ≥90% of the long-lived Ra isotopes in LIS are derived from boundary exchange, highlighting the critical importance of properly characterizing boundary endmembers and water exchange transports. Therefore, when boundary exchange mixing is not well constrained, it is not recommended to use ^{226}Ra and ^{228}Ra to quantify SGD in semi-enclosed basins.

SGD Volumetric Water Flow to Long Island Sound

The Ra mass balances indicate a significant amount of ^{224}Ra, ^{226}Ra, and ^{228}Ra unaccounted for, that must be balanced by inputs from SGD (**Figure 4**). The SGD Ra flux to each basin is converted into a water flow by dividing by the SGD Ra endmember activity. Results from the three-endmember mixing analysis (section "Endmember mixing model: An alternative approach to estimate SGD") reveals SGD from Connecticut is insignificant in the eastern basin and is dominated by Long Island marine groundwater; thus, Long Island groundwater is used as the Ra endmember for the eastern basin (**Table 3**). The western basin was impacted by Connecticut groundwater during spring 2009, and therefore we use the mean Connecticut marine groundwater Ra activity as an endmember during spring. In contrast, the western basin was impacted by approximately equal proportions of Long Island and Connecticut groundwater during summer 2010, and therefore an average of each endmember is used. For the central basin, we simply use an average of the Long Island and Connecticut marine groundwater Ra activities (salinity 25–28) for SGD flux determination (**Table 3**). SGD determination is highly sensitive to the selection of the groundwater endmember (Cook et al., 2018); endmember sensitivity is not evaluated in this study. Ra activities in the SGD endmembers are assumed to be constant throughout the year and therefore we only consider seasonal differences in SGD flux (Luek and Beck, 2014). Marine groundwater ^{224}Ra activities from LIS are not seasonal (Tamborski et al., 2017a), as ^{224}Ra will be quickly regenerated within shallow marine sediments, integrating all SGD flow paths. Seasonality in marine SGD to LIS may be driven, in part, by seasonal differences in density-dependent dispersive mixing within permeable sediments (Tamborski et al., 2017a), and movement of the freshwater-saltwater interface in response to regional precipitation (Michael et al., 2005; Tamborski et al., 2017b).

Volumetric SGD flows are summarized in **Figure 5**. Averaging all three Ra isotope mass balances for the total LIS basin (±standard deviation) results in an SGD flux of $1.2 \pm 0.9 \times 10^{13}$ L y^{-1} during spring 2009 and $3.8 \pm 0.7 \times 10^{13}$ L y^{-1} during summer 2010. These estimates are within the range of estimates qualitatively determined from the three-endmember mixing model and slightly lower than the ^{224}Ra-derived SGD flux of 3.2–7.4 $\times$ 10^{13} L y^{-1}, previously estimated by Garcia-Orellana et al. (2014). As noted above, the long-lived Ra isotope mass balances are significantly impacted by boundary mixing (section "Mass balance sensitivity"). The central basin Ra mass balances accurately constrain the ^{226}Ra and ^{228}Ra endmember activities of the western and eastern basins (**Table 2**), which account for the ^{226,228}Ra mixing sources and sinks, assuming that the water flow estimations are accurate (**Table 1**). The average SGD flux to the central basin of LIS is $1.1 \pm 0.8 \times 10^{13}$ L y^{-1} during spring 2009 and $1.9 \pm 0.9 \times 10^{13}$ L y^{-1} during summer 2010,

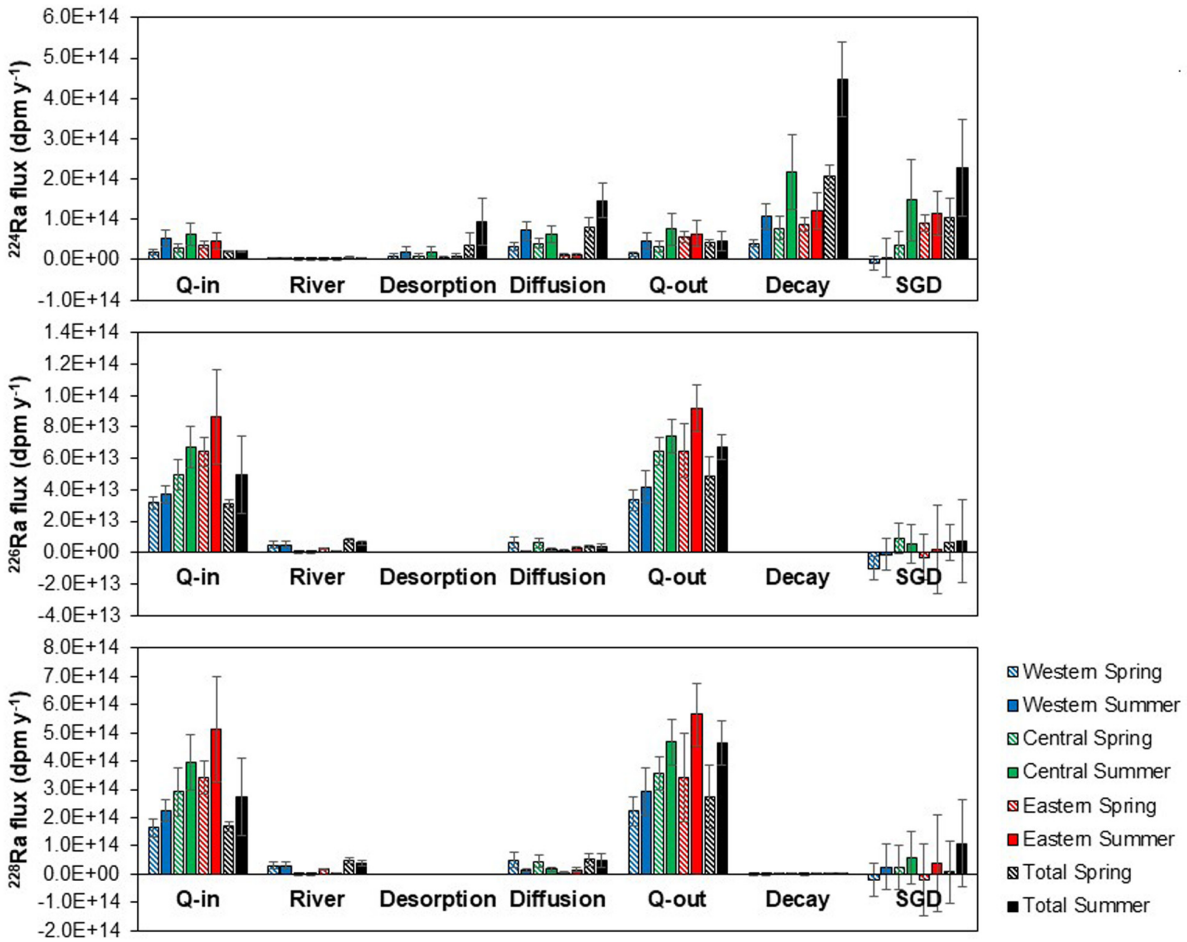

FIGURE 4 | Summary of ^{224}Ra (top), ^{226}Ra (middle), and ^{228}Ra (bottom) sources and sinks to Long Island Sound, arranged by basin and season. A negative SGD flux implies either that Ra sources approximately balance Ra sinks (within the propagated uncertainties), or that one (or more) known Ra flux is improperly characterized.

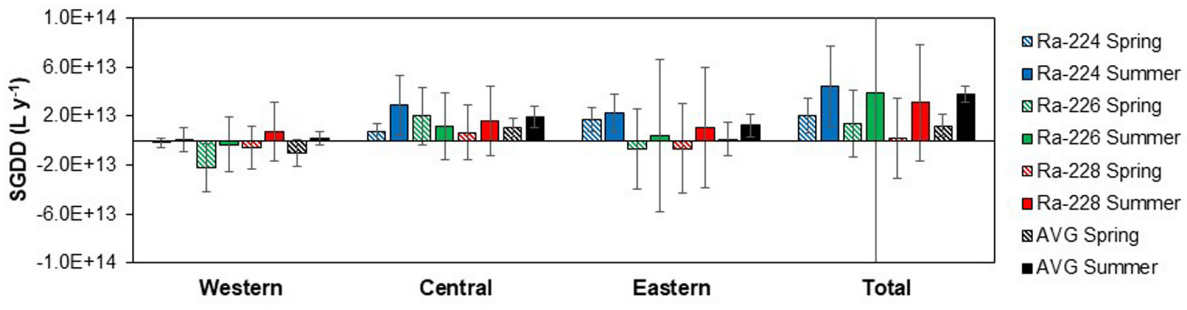

FIGURE 5 | Summary of Ra-derived SGD estimates to Long Island Sound, arranged by basin and season. The average spring and summer values (black) represent an average (±standard deviation) of all three Ra isotopes. A negative SGD flux implies either that Ra sources approximately balance Ra sinks (within the propagated uncertainties), or that one (or more) known Ra flux is improperly characterized.

or ∼50% of the SGD flux determined from the basin-wide mass balances during summer 2010. For just the central basin, the total SGD flux during spring 2009 and summer 2010 was equivalent to 45% and 280% of the freshwater inflow from the Connecticut River (2.52 and 0.68 $\times$ 10^{13} L y^{-1} during April 2009 and August 2010, respectively). Given the number of variables (Eq. 1), it is remarkable that the three different Ra isotopes converge on similar SGD values to LIS, despite relatively large uncertainties over two different seasons (**Figure 5**).

Nitrogen Loads

Excess nitrogen loading stimulates phytoplankton growth and can lead to adverse ecological conditions in LIS. Nitrogen loads from wastewater effluent and the Connecticut River are typically assumed to be the dominant sources of N to LIS (NYSDEC and CTDEP, 2000; Suffolk County, 2015). However, recent work suggests that SGD may rival the N load of wastewater effluent and rivers to LIS (Tamborski et al., 2017b). The mixing zone between groundwater and seawater in the coastal aquifer, i.e., the subterranean estuary, is critically important for controlling a variety of chemical reactions, which can add or remove chemical elements from the system (Moore, 1999). In the subterranean estuary, nitrogen in groundwater can be removed by biological processes including denitrification, or groundwater nitrogen may merely be diluted by mixing with seawater (Kroeger and Charette, 2008). Conversely, nitrate can be generated as a product of organic matter remineralization, when seawater rich in organic matter infiltrates into permeable sediments from waves and tidal forcing mechanisms. Below, we provide a revised estimate of the SGD-driven N load to LIS during spring and summer conditions, using our revised Ra isotope mass balances (**Figure 5**).

Marine SGD includes circulating seawater flow paths driven by physical forcing mechanisms, including density-driven flow and tidal pumping (Santos et al., 2012); importantly, marine SGD is separate from terrestrial (i.e., meteoric, fresh) groundwater in the ensuing analysis. Tamborski et al. (2017b) estimated a marine SGD NO_3^- endmember of 23 ± 13 μM during spring and 37 ± 29 μM during summer. This endmember is a non-conservative N enrichment, corrected for binary mixing between seawater and terrestrial groundwaters. Stable isotope analyses of $^{15}N\text{-}NO_3^-$ and $^{18}O\text{-}NO_3^-$ suggest that the marine SGD NO_3^- is derived from the remineralization of organic matter within the subterranean estuary, rather than from an atmospheric or anthropogenic source. The marine SGD flux to LIS is estimated as the total SGD flux (total-basin = $1.2 \pm 0.9 \times 10^{13}$ L y^{-1} during spring 2009 and $3.8 \pm 0.7 \times 10^{13}$ L y^{-1} during summer 2010) corrected for fresh groundwater contributions, estimated from numerical models (Scorca and Monti, 2001). As a first-order approximation, the marine SGD-driven NO_3^- flux is $2.8 \pm 2.7 \times 10^8$ mol N y^{-1} for spring 2009 and $14 \pm 11 \times 10^8$ mol N y^{-1} for summer 2010. Just considering the central basin of LIS, where SGD estimates are the most accurate (**Figure 5**), the marine SGD-driven NO_3^- flux is $2.6 \pm 2.3 \times 10^8$ mol N y^{-1} for spring 2009 and $7.1 \pm 6.4 \times 10^8$ mol N y^{-1} for summer 2010. We note that more work is required to fully constrain the spatial and temporal variability of the marine SGD NO_3^- endmember for the entire LIS basin. This first-order marine SGD NO_3^- flux is approximately two orders of magnitude greater than the N flux determined within the first 200 m of the Smithtown Bay shoreline by Tamborski et al. (2017b). Importantly, this suggests that SGD supplies a N load nearly equivalent to that of the Connecticut River and wastewater effluent, such that N loss via burial or denitrification may be greater than currently estimated (Vlahos et al., 2020). The mean annual $NO_3^- + NO_2^-$ load of the Connecticut River, measured at Middle Haddam (approximately 97% of the Connecticut River drainage area) is $4.5–4.7 \times 10^8$ mol N y^{-1}, and comprises 42–49% of the total N flux of the Connecticut River (Mullaney et al., 2018). The N load from wastewater treatment plants to LIS is approximately 5.6×10^8 mol N y^{-1} (NYSDEC and CTDEP, 2000), although this load is in decline due to improving wastewater treatment conditions (Suffolk County, 2015). Importantly, these lines of evidence suggest that far more attention should be paid to monitoring SGD-driven N loads to LIS.

CONCLUSION

Physical measurements and hydrologic models often fail to capture total SGD (Burnett et al., 2006). Ra isotopes integrate over a larger spatial area, making their use to quantify SGD a popular tool among scientists. In certain large-scale embayments like LIS, the monitoring of SGD and its associated chemical load to the sea is equally as important as monitoring riverine fluxes. However, long-term SGD monitoring is seldom performed, due to the unforeseen nature of SGD and its broad difficulty in quantification. A sensitivity analysis of Ra isotope mass balances to the semi-enclosed LIS basin reveals:

1. The selection and interpretation of the Ra isotope used will ultimately depend on the target process and flow path of interest. The different ingrowth rates of the Ra quartet enable tracing different time-scale processes. Short-lived Ra isotopes may trace short-scale length processes (Santos et al., 2012), such as wave-pumping, that are not fully captured by long-lived Ra isotopes (Rodellas et al., 2017).
2. Short-lived Ra mass balances are highly sensitive to sediment (diffusion and desorption) fluxes, but are less significantly impacted by boundary mixing (scale-dependent). When mixing is uncertain, ^{224}Ra is the preferred tracer of SGD. Studies using short-lived Ra mass balances should direct their attention toward accurately constraining sediment Ra contributions. The advantage of short-lived Ra isotopes is that their major sink is radioactive decay (scale-dependent); thus, an adequate sampling strategy can reasonably constrain the short-lived Ra inventory with minor uncertainty. Short-lived Ra mass balances can provide a reasonable first-order approximation of SGD if the Ra inventory is well-constrained and sediment contributions are minor.
3. A large number of water column samples are necessary to accurately capture the (near) instantaneous short-lived Ra inventory. The ^{224}Ra inventory integrates over the half-life of ^{224}Ra, such that this inventory will accurately reflect the times of the year when the sampling was conducted. The ^{224}Ra inventory may not be representative of a seasonal or annual ^{224}Ra flux associated with SGD, suggesting that multiple sampling campaigns are necessary to capture any seasonality in the ^{224}Ra inventory for SGD flux determination. A lower number of water column samples may be adequate to capture the long-lived Ra water column inventory; however, a greater number of samples are required to evaluate spatial variability.

4. Long-lived Ra mass balances are highly sensitive to fluxes represented by exchange at the boundaries of the system. Studies using long-lived Ra mass balances in semi-enclosed environments should direct their attention toward accurately constraining mixing gains and losses. This requires characterization of long-lived Ra activities in the inflowing and outflowing water, as well as flows of water across the boundaries. Water exchange across boundaries must be well-constrained in order to minimize the final uncertainty of the Ra SGD flux.
5. Long-term SGD monitoring using short-lived Ra isotopes will require frequent water column surveys to accurately constrain the short-lived Ra inventory. Long-term SGD monitoring using long-lived Ra isotopes should focus sampling efforts on accurately constraining mixing gains and losses.

SGD to the central basin of LIS is estimated as $1.1 \pm 0.8 \times 10^{13}$ L y^{-1} during spring 2009 and $1.9 \pm 0.9 \times 10^{13}$ L y^{-1} during summer 2010, equivalent to 45 and 280% of the freshwater inflow of the Connecticut River during the same time period. This SGD flux supplies a bioavailable N load of $2.6–7.1 \times 10^{8}$ mol N y^{-1}, similar to that of the Connecticut River (Mullaney et al., 2018). Long-term SGD monitoring is required to fully understand the magnitude and temporal variability of SGD-driven N loads to LIS.

DATA AVAILABILITY STATEMENT

All datasets generated for this study are included in the article/**Supplementary Material**.

AUTHOR CONTRIBUTIONS

JC, HB, and JG-O developed the seawater sampling strategy. JG-O, VR, JC, and CH were responsible for seawater sample collection. JT developed the groundwater sampling strategy and was responsible for groundwater and sediment core sample collection. JT, JC, JG-O, and CH were responsible for radium analyses. RW produced water exchange estimates from the model of Crowley (2005). JT developed and wrote the manuscript, with the assistance of JC, HB, JG-O, VR, CH, and RW. All authors contributed to the article and approved the submitted version.

FUNDING

This project has been funded by New York Sea Grant projects (R/CCP-16 and R/CMC-12). This research is contributing to the ICTA-UAB Unit of Excellence "María de Maeztu" (MDM-2015-0552) and MERS (2017 SGR – 1588, Generalitat de Catalunya). VR acknowledges financial support from the Beatriu de Pinós postdoctoral program of the Catalan Government (2017-BP-00334).

ACKNOWLEDGMENTS

We thank David Bowman and the crews of the R/V *Seawolf* for their assistance in sampling.

SUPPLEMENTARY MATERIAL

The Supplementary Material for this article can be found online at: https://www.frontiersin.org/articles/10.3389/fenvs.2020.00108/full#supplementary-material

TABLE S1 | Summary of Ra isotope mass balances, arranged by basin and season.

REFERENCES

Beck, A. J., Rapaglia, J. P., Cochran, J. K., and Bokuniewicz, H. J. (2007). Radium mass-balance in Jamaica Bay, NY: evidence for a substantial flux of submarine groundwater. *Mar. Chem.* 106, 419–441. doi: 10.1016/j.marchem.2007.03.008

Beck, A. J., Rapaglia, J. P., Cochran, J. K., Bokuniewicz, H. J., and Yang, S. (2008). Submarine groundwater discharge to Great South Bay, NY, estimated using Ra isotopes. *Mar. Chem.* 109, 279–291. doi: 10.1016/j.marchem.2007.07.011

Bokuniewicz, H. (1980). Groundwater seepage into Great South Bay, New York. *Estuar. Coast. Mar. Sci.* 10, 437–444. doi: 10.1016/S0302-3524(80)80122-8

Bokuniewicz, H., Cochran, J. K., Garcia-Orellana, J., Valenti, R., Wallace, D. J., Christina, H., et al. (2015). Intertidal percolation through beach sands as a source of 224,223Ra to Long Island Sound, New York and Connecticut, United States. *J. Mar. Res.* 73, 123–140. doi: 10.1357/002224015816665570

Burnett, W. C., Aggarwal, P. K., Aureli, A., Bokuniewicz, H., Cable, J. E., Charette, M. A., et al. (2006). Quantifying submarine groundwater discharge in the coastal zone via multiple methods. *Sci. Total Environ.* 367, 498–543. doi: 10.1016/j.scitotenv.2006.05.009

Buxton, H. T., and Modica, E. (1992). Patterns and rates of groundwater flow on Long Island. New York. *Ground Water* 30, 857–866. doi: 10.1111/j.1745-6584.1992.tb01568.x

Cai, P., Shi, X., Moore, W. S., Peng, S., Wang, G., and Dai, M. (2014). 224Ra:228Th disequilibrium in coastal sediments: implications for solute transfer across the sediment-water interface. *Geochim. Cosmochim. Acta* 125, 68–84. doi: 10.1016/j.gca.2013.09.029

Capone, D. G., and Bautista, M. F. (1985). A groundwater source of nitrate in nearshore marine sediments. *Nature* 313, 214–216. doi: 10.1038/313214a0

Charette, M. A., Moore, W. S., and Burnett, W. C. (2008). "Uranium- and thorium-series nuclides as tracers of submarine groundwater discharge," in *U-Th Series Nuclides in Aquatic Systems*, eds S. Krishnaswami, and J. K. Cochran, (Amsterdam: Elsevier), 155–192.

Cochran, J. K. (1979). *The Geochemistry of 226Ra and 228Ra in Marine Deposits*. Ph.D. Thesis, Yale University, New Haven, CT.

Cook, P. G., Rodellas, V., and Stieglitz, T. (2018). Quantifying surface water, porewater and groundwater interactions using tracers: tracer fluxes, water fluxes, and end-member concentrations. *Water Resour. Res.* 54, 2452–2465. doi: 10.1002/2017WR021780

Copenhaver, S. A., Krishnaswami, S., Turekian, K. K., Epler, N., and Cochran, J. K. (1993). Retardation of 238U and 232Th decay chain radionuclides in Long Island and Connecticut aquifers. *Geochim. Cosmochim. Acta* 57, 597–603. doi: 10.1016/0016-7037(93)90370-c

Crowley, H. (2005). *The Seasonal Evolution of Thermohaline Circulation in Long Island Sound*. Ph.D. thesis, Stony Brook University, Stony Brook, NY.

Dion, E. P. (1983). *Trace Elements and Radionuclides in the Connecticut River and Amazon River Estuary*. Ph.D. Thesis, Yale University, New Haven, CT.

Garcia-Orellana, J., Cochran, J. K., Bokuniewicz, H., Daniel, J. W. R., Rodell, V., Heilbrun, C., et al. (2014). Evaluation of 224Ra as a tracer for submarine groundwater discharge in Long Island Sound (NY). *Geochim. Cosmochim. Acta* 141, 314–330. doi: 10.1016/j.gca.2014.05.009

Garcia-Solsona, E., Masqué, P., Garcia-Orellana, J., Rapaglia, J., Beck, A. J., Cochran, J. K., et al. (2008). Estimating submarine groundwater discharge around Isola La Cura, northern Venice Lagoon (Italy), by using the radium quartet. *Mar. Chem.* 109, 292–306. doi: 10.1016/j.marchem.2008.02.007

Jia, Y., and Whitney, M. W. (2019). Summertime Connecticut River Water Pathways and Wind Impacts. *JGR Oceans* 124, 1897–1914. doi: 10.1029/2018JC014486

Knee, K. L., Crook, E. D., Hench, J. L., Leichter, J. J., and Paytan, A. (2016). Assessment of submarine groundwater discharge (SGD) as a source of dissolved radium and nutrients to Moorea (French Polynesia) coastal waters. *Estuar. Coasts* 39, 1651–1668. doi: 10.1007/s12237-016-0108-y

Knee, K. L., and Paytan, A. (2011). "Submarine groundwater discharge: a source of nutrients, metals and pollutants to the coastal ocean," in *Treatise on Estuarine and Coastal Science*, Vol. 4, eds E. Wolanski, and D. S. McLusky (Waltham: Academic Press), 205–233.

Koppelman, L. E., Weyl, P. K., Gross, M. G., and Davies, D. S. (1976). *Urban Sea: Long Island Sound*. Westport, CT: Praeger Publishers.

Krishnaswami, S., Graustein, W. C., and Turekian, K. K. (1982). Radium, thorium and radioactive lead isotopes in groundwaters: application to the in situ determination of adsorption-desorption rate constants and retardation factors. *Water Resour. Res.* 18, 1633–1675.

Kroeger, K. D., and Charette, M. A. (2008). Nitrogen biogeochemistry of submarine groundwater discharge. *Limnol. Oceanogr.* 53, 1025–1039. doi: 10.4319/lo.2008.53.3.1025

Latimer, J., Tedesco, M., Swanson, R., Yarish, C., Stacey, P., and Garza, C. (2013). *Long Island Sound: Prospects for the urban sea*. Berlin: Springer.

Li, Y.-H., Mathieu, G., Biscaye, P., and Simpson, H. J. (1977). The flux of 226Ra from estuarine and continental shelf sediments. *Earth Planet. Sci. Lett.* 37, 237–241. doi: 10.1016/0012-821x(77)90168-6

Luek, J. L., and Beck, A. J. (2014). Radium budget of the York River estuary (VA, USA) dominated by submarine groundwater discharge with a seasonally variable groundwater end-member. *Mar. Chem.* 165, 55–65. doi: 10.1016/j.marchem.2014.08.001

Michael, H. A., Mulligan, A. E., and Harvey, C. F. (2005). Seasonal oscillations in water exchange between aquifers and the coastal ocean. *Nature* 436, 1145–1148. doi: 10.1038/nature03935

Moore, W. S. (1999). The subterranean estuary: a reaction zone of ground water and sea water. *Mar. Chem.* 65, 111–125. doi: 10.1016/S0304-4203(99)00014-6

Moore, W. S. (2003). Sources and fluxes of submarine groundwater discharge delineated by radium isotopes. *Biogeochemistry* 66, 75–93. doi: 10.1023/B:BIOG.0000006065.77764.a0

Moore, W. S. (2010). "The effect of submarine groundwater discharge on the ocean," in *Annual Review of Marine Science*, (Palo Alto: Annual Reviews), 59–88.

Moore, W. S., and Arnold, R. (1996). Measurement of Ra-223 and Ra-224 in coastal waters using a delayed coincidence counter. *J Geophys Res* 101, 1321–1329. doi: 10.1029/95JC03139

Moore, W. S., Blanton, J. O., and Joye, S. B. (2006). Estimates of flushing times, submarine groundwater discharge, and nutrient fluxes to Okatee Estuary, South Carolina. *J. Geophys. Res.* 111:C090006. doi: 10.1029/2005JC003041

Mullaney, J. R., Martin, J. W., and Morrison, J. (2018). *Nitrogen Concentrations and Loads for the Connecticut River at Middle Haddam, Connecticut, Computed with the use of Autosampling and Continuous Measurements Of Water Quality for Water Years 2009 to 2014*. U.S. Geological Survey Scientific Investigations Report 2018–5006. (Reston, VI: USGS), doi: 10.3133/sir20185006

NYSDEC and CTDEP (2000). *A Total Maximum Daily Load Analysis to Achieve Water Quality Standards for Dissolved Oxygen in Long Island Sound*. Albany, NY: NYSDEC, 55.

Poppe, L. J., Knebel, H. J., and Mlodzinska, Z. J. (2000). Distribution of surficial sediment in Long Island Sound and adjacent waters: texture and total organic carbon. *J. Coast Res.* 16, 567–574.

Rama, and Moore, W. S. (1996). Using the radium quartet for evaluating groundwater input and water exchange in salt marshes. *Geochim. Cosmochim. Acta* 60, 4645–4652. doi: 10.1016/s0016-7037(96)00289-x

Rodellas, V., Garcia-Orellana, J., Garcia-Solsona, E., Masqué, P., Domínguez, J. A., Ballesteros, B. J., et al. (2012). Quantifying groundwater discharge from different sources into a Mediterranean wetland by using 222Rn and Ra isotopes. *J. Hydrol.* 466–467, 11–22. doi: 10.1016/j.jhydrol.2012.07.005

Rodellas, V., Garcia-Orellana, J., Masqué, P., and Font-Muñoz, J. S. (2015). The influence of sediment sources on radium-derived estimates of submarine groundwater discharge. *Mar. Chem.* 171, 107–117. doi: 10.1016/j.marchem.2015.02.010

Rodellas, V., Garcia-Orellana, J., Trezzi, G., Masque, P., Steiglitz, T. C., Bokuniewicz, H., et al. (2017). Using the radium quartet to quantify submarine groundwater discharge and porewater exchange. *Geochim. Cosmochim. Acta* 196, 58–73. doi: 10.1016/j.gca.2016.09.016

Santos, I. R., Eyre, B. D., and Huettel, M. (2012). The driving forces of porewater and groundwater flow in permeable coastal sediments: a review. *Estuar. Coast. Shelf Sci.* 98, 1–15. doi: 10.1016/j.ecss.2011.10.024

Scorca, M. P., and Monti, J. (2001). *Estimates of Nitrogen Loads Entering Long Island Sound from Ground Water and Streams on Long Island, New York, 1985-96*. Coram, N.Y: U.S. Dept. of the Interior, U.S. Geological Survey.

Shi, X., Mason, R. P., and Charette, M. A. (2018). Mercury flux from salt marsh sediments: Insights from a comparison between 224Ra/228Th disequilibrium and core incubation methods. *Geochim. Cosmochim. Acta* 222, 569–583. doi: 10.1016/j.gca.2017.10.033

Suffolk County (2015). *Suffolk County Comprehensive Water Resources Management Plan*. Reston, VI: USGS.

Sun, Y., and Torgersen, T. (2001). Adsorption-desorption reactions and bioturbation transport of ^{224}Ra in marine sediments: a one-dimensional model with applications. *Mar. Chem.* 74, 227–243. doi: 10.1016/S0304-4203(01)00017-2

Swarzenski, P. W. (2007). U/Th series radionuclides as coastal groundwater tracers. *Chem. Rev.* 107, 663–674. doi: 10.1021/cr0503761

Tamborski, J. J., Cochran, J. K., and Bokuniewicz, H. J. (2017a). Application of 224Ra and 222Rn for evaluating seawater residence times in a tidal subterranean estuary. *Mar. Chem.* 189, 32–45. doi: 10.1016/j.marchem.2016.12.006

Tamborski, J. J., Cochran, J. K., and Bokuniewicz, H. J. (2017b). Submarine groundwater discharge driven nitrogen fluxes to Long Island Sound, NY: terrestrial vs. marine sources. *Geochim. Cosmochim. Acta* 218, 40–57. doi: 10.1016/j.gca.2017.09.003

Turekian, K. K., Tanaka, N., and Turekian, V. C. (1996). Transfer rates of dissolved tracers through estuaries based on 228Ra: a study of Long Island Sound. *Cont. Shelf Res.* 16, 863–873. doi: 10.1016/0278-4343(95)00039-9

Vlahos, P., Whitney, M. M., Menniti, C., Mullaney, J. R., Morrison, J., and Jia, Y. (2020). Nitrogen budgets of the Long Island Sound estuary. *Estuar. Coast. Shelf Sci.* 232:10693. doi: 10.1016/j.ecss.2019.106493

Conflict of Interest: The authors declare that the research was conducted in the absence of any commercial or financial relationships that could be construed as a potential conflict of interest.

frontiers in Environmental Science

ORIGINAL RESEARCH
published: 11 August 2020
doi: 10.3389/fenvs.2020.00126

Investigating Boron Isotopes for Identifying Nitrogen Sources Supplied by Submarine Groundwater Discharge to Coastal Waters

Joseph Tamborski[1,2], Caitlin Brown[3†], Henry Bokuniewicz[4], J. K. Cochran[4] and E. T. Rasbury[3]*

[1] Woods Hole Oceanographic Institution, Woods Hole, MA, United States, [2] Centre for Water Resources Studies, Dalhousie University, Halifax, NS, Canada, [3] Department of Geosciences, Stony Brook University, Stony Brook, NY, United States, [4] School of Marine and Atmospheric Sciences, Stony Brook University, Stony Brook, NY, United States

OPEN ACCESS

Edited by:
Ryo Sugimoto,
Fukui Prefectural University, Japan

Reviewed by:
David Widory,
Université du Québec à Montréal, Canada
Vhahangwele Masindi,
Council for Scientific and Industrial Research (CSIR), South Africa

***Correspondence:**
Henry Bokuniewicz
henry.bokuniewicz@stonybrook.edu

†Present address:
Caitlin Brown,
US Environmental Protection Agency, Boston, MA, United States

Specialty section:
This article was submitted to Water and Wastewater Management, a section of the journal Frontiers in Environmental Science

Received: 24 October 2019
Accepted: 16 July 2020
Published: 11 August 2020

Citation:
Tamborski J, Brown C, Bokuniewicz H, Cochran JK and Rasbury ET (2020) Investigating Boron Isotopes for Identifying Nitrogen Sources Supplied by Submarine Groundwater Discharge to Coastal Waters. Front. Environ. Sci. 8:126. doi: 10.3389/fenvs.2020.00126

Stable isotopes of oxygen, nitrogen, and boron were used to identify the sources of nitrate (NO_3^-) in submarine groundwater discharge (SGD) into a large tidal estuary (Long Island Sound, NY, United States). Potential contaminants such as manure, septic waste and fertilizer overlap in $\delta^{15}N$ and $\delta^{18}O$ but have been shown to have distinctive $\delta^{11}B$ in non-coastal settings. Two distinct subterranean estuaries were studied with different land-use up gradient, representative of (1) mixed medium-density residential housing and (2) agriculture. These sites have overlapping $\delta^{15}N$ and $\delta^{18}O$ measurements in NO_3^- and are unable to discriminate between different N sources. Boron isotopes and concentrations are measurably different between the two sites, with little overlap. The subterranean estuary impacted by mixed medium-density residential housing shows little correlation between $\delta^{11}B$ and [B] or between $\delta^{11}B$ and salinity, demonstrating that direct mixing relationships between fresh groundwater and seawater were unlikely to account for the variability. No two sources could adequately characterize the $\delta^{11}B$ of this subterranean estuary. Groundwater N at this location should be derived from individual homeowner cesspools, although measured septic waste has much lower $\delta^{11}B$ compared to the coastal groundwaters. This observation, with no trend in $\delta^{11}B$ with [B] indicates multiple sources supply B to the coastal groundwaters. The agricultural subterranean estuary displayed a positive correlation between $\delta^{11}B$ and [B] without any relationship with salinity. Binary mixing between sea spray and fertilizer can reasonably explain the distribution of B in the agricultural subterranean estuary. Results from this study demonstrate that $\delta^{11}B$ can be used in combination with $\delta^{15}N$ to trace sources of NO_3^- to the subterranean estuary if source endmember isotopic signatures are well-constrained, and if the influence of seawater on $\delta^{11}B$ signatures can be minimized or easily quantified.

Keywords: submarine groundwater discharge, boron, nitrogen, nitrate, fertilizer, wastewater, septic waste

INTRODUCTION

Submarine groundwater discharge (SGD) is an important vector for the delivery of nutrients to the coastal ocean (e.g., Taniguchi et al., 2019). While once thought to be a relatively minor component of the overall coastal nitrogen budget, studies have shown that non-point-sources of diffuse SGD can supply as much nitrogen into coastal waters as rivers (Slomp and Van Cappellen, 2004; Kroeger and Charette, 2008; Rodellas et al., 2015). The extent of SGD's effect on coastal water quality has been difficult to establish because SGD consists of a fresh groundwater component and a seawater component that mix in a biogeochemically reactive subterranean estuary (STE; Moore, 1999; Burnett et al., 2003; Slomp and Van Cappellen, 2004). The terrestrial, fresh component of SGD (FSGD) represents a source of new N to coastal waters and, if significant, can help sustain primary production and even coastal algal blooms (Gobler and Sanudo-Wilhelm, 2001), thus fueling coastal eutrophication (Paerl, 1995; Howarth and Marino, 2006).

Isotopes of N and O in nitrate (NO_3^-) have a proven utility in sorting out the sources of nitrogen delivered to groundwaters (Aravena et al., 1993; Bateman and Kelly, 2007; Bannon and Roman, 2008; Kendall et al., 2008). In particular, δ^{15}N-NO_3^- and δ^{18}O-NO_3^- can distinguish between NO_3^- fertilizers, atmospheric NO_3^-, manure and sewage-derived NO_3^- (Kendall, 1998; Kendall et al., 2008). However, the overlapping δ^{15}N signatures of soil N, animal and human waste, and nitrification of NH_4^+ in fertilizer and precipitation, as well as the biological modification of nitrogen and oxygen isotopes, can limit their utility in fully identifying anthropogenic sources of nitrogen. In addition, the speciation and attenuation of nitrogen may be modified in the STE before it reaches the coastal ocean (Kroeger and Charette, 2008; Erler et al., 2014). For example, changes in dissolved oxygen (DO) in groundwater may cause changes in N and O isotopic composition by nitrifying NH_4^+ to NO_3^- or denitrifying NO_3^- to N_2. NH_4^+ volatilization and nitrogen remineralization may also alter N speciation (Charbonnier et al., 2013) and isotopic composition. Therefore, the groundwater isotopic signatures of N and O of an inland groundwater source may differ from that delivered to the coastal ocean, making it difficult to track anthropogenic sources of NO_3^- through the STE (Anschutz et al., 2016). The addition of other tracers may be useful in resolving these problems, including boron (B) isotopes.

Boron is added to groundwater both naturally and with contaminants such as NO_3^- in association with borate minerals used in fertilizers and detergents through septic systems or sewage (Barth, 1998; Vengosh, 1998; Vengosh et al., 1999). B is added to groundwater naturally via precipitation and water-rock interactions that include sorption reactions with clay minerals and iron hydroxides (Demetriou and Pashalidis, 2012). Anthropogenic sources of B to groundwaters include fertilizers and septic systems or sewage (Vengosh et al., 1999). Plants require B as an essential micronutrient for growth and therefore borate minerals are commonly added to commercial fertilizers (Shireen et al., 2018). Detergents and household cleaning products contain elevated [B] that is subsequently transported to septic systems.

Boron is highly soluble in groundwater and is therefore a co-migrant of groundwater NO_3^-, including fertilizer and septic sources. B is not removed by wastewater treatment nor is it affected by processes that alter N concentration, such as nitrification and denitrification; however, B speciation is controlled by pH. At low pH boric acid (BOH_3) is the dominant species, while at high pH borate (BOH_4^-) dominates, with a pKa of 9.2 in fresh water (McPhail et al., 1972). There is an isotope fractionation between these species that makes borate isotopically enriched in ^{10}B. Boric acid is conservative, but borate has a strong affinity for positively charged particle surfaces (e.g., clays) because of its negative charge (Palmer et al., 1987). This can result in changes in the isotope ratio as B can be fractionated by processes such as adsorption and desorption of borate onto iron oxides and clay minerals (McPhail et al., 1972; Goldberg and Glaubig, 1985; Glavee et al., 1995; Lemarchand et al., 2007; Demetriou and Pashalidis, 2012). However, these processes are pH dependent, where adsorption is greatest at pH 9 and decreases to less than 10% adsorption at pH 5 and lower (Bloesch et al., 1987; De La Fuente and Camacho, 2009; Demetriou and Pashalidis, 2012). The large relative mass differences between ^{11}B and ^{10}B means that isotope fractionation leads to a wide range of isotopic values in nature. The combined use of δ^{11}B and δ^{15}N to trace NO_3^- sources has been successfully applied in terrestrial and aquatic environments (Komor, 1997; Widory et al., 2004, 2005, 2013; Seiler, 2005; Bronders et al., 2012; Lindenbaum, 2012; Briand et al., 2013, 2017; Eppich et al., 2013; Saccon et al., 2013; Ransom et al., 2016; Guinoiseau et al., 2018; Kruk et al., 2020); however, the use of δ^{11}B and δ^{15}N has yet to be tested in the STE of coastal systems.

Site Description

Long Island Sound (LIS) is a coastal estuary that lies between the south shore of Connecticut and the north shore of Long Island, NY, United States (**Figure 1**). The southern shoreline of LIS is cut into an unconfined, unconsolidated, sole-source aquifer (the Upper Glacial Aquifer) of glacial deposits with a hydraulic conductivity between 7 and 70 m d^{-1} (Buxton and Modica, 1992). The hydraulic gradient has been estimated to be 0.001 (McClymonds and Franke, 1972) with a vertical hydraulic gradient between 0.02 and 0.08 in the upper meter of sediment at the shoreline. Under these conditions, significant SGD has been documented along the shores of LIS (Durand, 2014; Garcia-Orellana et al., 2014; Bokuniewicz et al., 2015; Young et al., 2015; Tamborski et al., 2017a,b). FSGD-driven N loads to Smithtown Bay ($1–13*10^6$ mol N y^{-1}), an embayment of LIS, rivals that of the local Nissequogue River ($4–10*10^6$ mol N y^{-1}) and has been implicated as the primary new N source to LIS (Tamborski et al., 2017a).

This study focuses on two distinct STE's along the north shore of Long Island at Callahans Beach (adjacent to Smithtown Bay) and at Iron Pier Beach (on the North Fork of Long Island; **Figure 1**). Anthropogenic contaminant sources including cesspools, septic systems and fertilizers are implicated in

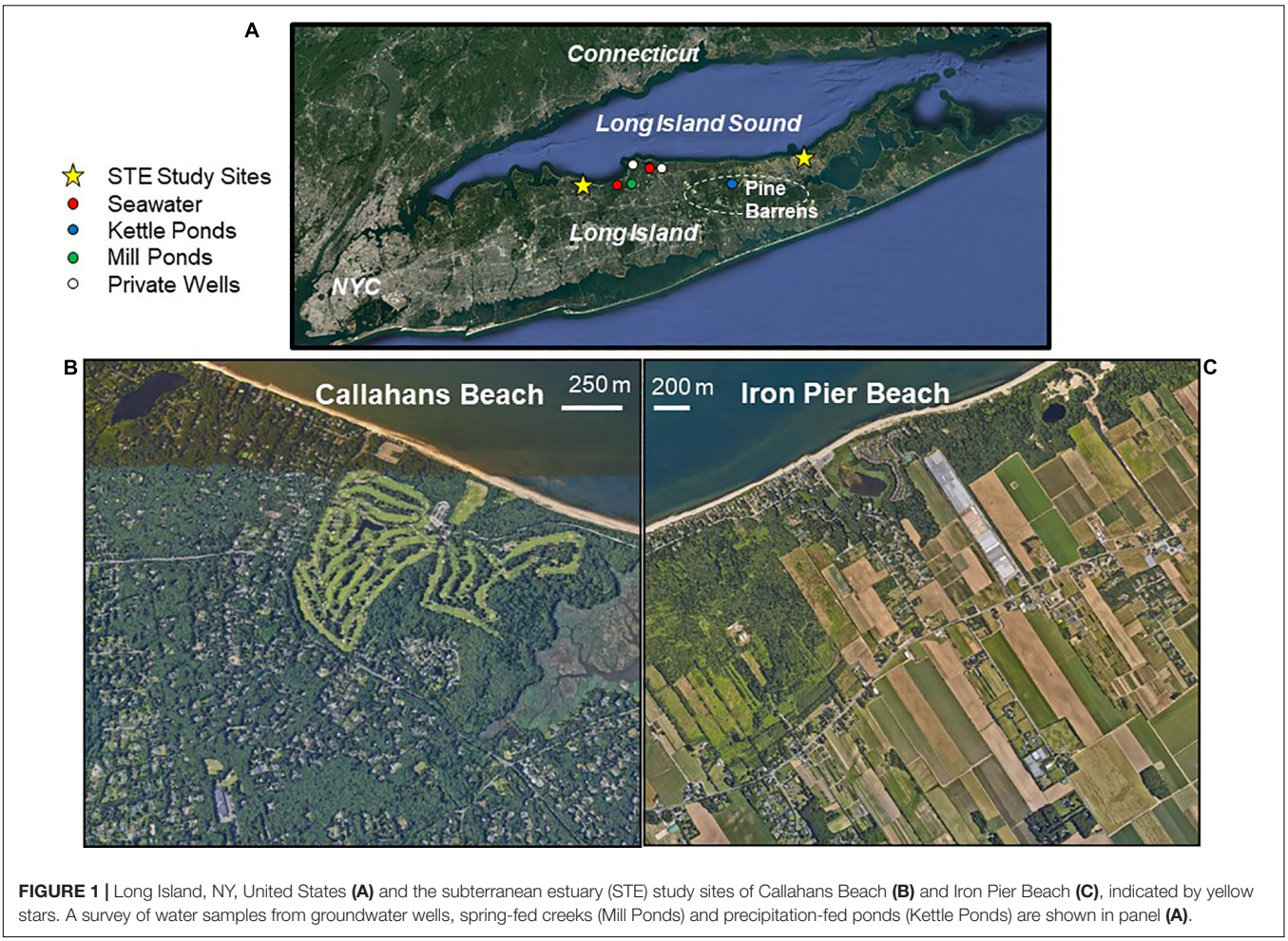

FIGURE 1 | Long Island, NY, United States **(A)** and the subterranean estuary (STE) study sites of Callahans Beach **(B)** and Iron Pier Beach **(C)**, indicated by yellow stars. A survey of water samples from groundwater wells, spring-fed creeks (Mill Ponds) and precipitation-fed ponds (Kettle Ponds) are shown in panel **(A)**.

producing elevated NO_3^- levels seen in Long Island's unconfined Upper Glacial Aquifer (Bellone, 2015). Land cover within the watershed of Callahans Beach is composed of medium-density residential housing (2770 people km^{-2}; town of Fort Salonga); the beach itself is directly down-gradient from a golf course (**Figure 1**). This site has been well studied (Tamborski et al., 2015, 2017a,b) and was chosen to represent a shoreline impacted by mixed anthropogenic N sources (fertilizer, manure and/or septic); there was no evidence of groundwater denitrification or nitrogen attenuation in the STE (Tamborski et al., 2017a). At Callahans Beach, SGD rates vary tidally and can reach 50 cm d^{-1} near low tide (Tamborski et al., 2015). Land cover within the watershed of Iron Pier Beach is predominantly used for agriculture and this lower population density site (470 people km^{-2}; town of Northville) was chosen to represent a shoreline impacted by a fertilizer N source. At Iron Pier Beach, SGD was measured at rates up to 75 cm d^{-1} via manual seepage meter measurements (Brown, 2018). Identifying the sources of nitrogen in groundwater is of particular importance to managers here because an effort to reduce nitrogen in Suffolk County, NY, United States, called "Reclaim our Water Initiative," is predicated on nitrogen pollution from septic systems (Suffolk County Government, 2019).

MATERIALS AND METHODS

Field Methods

Multi-level cluster wells were installed above the spring high tide elevation at Callahans Beach in 2014 at depths of 3.0 m, 5.0 m, 6.0 m, and 7.0 m below surface, and at Iron Pier Beach at 1.5 m, 3.0 m, and 4.5 m depths in 2017 using a track-mounted Geoprobe. Multi-level cluster-well installation at Callahans Beach is described in Tamborski et al. (2017b). Groundwater was collected from cluster wells monthly at both sites using a peristaltic pump, from June to December 2017, for nutrient analyses. Temperature, conductivity, salinity, DO, ORP and pH were measured in the field using a YSI-566 multi-probe. Groundwater samples for N, O, and B isotopic analysis were collected from June through October. Water samples for nutrient concentrations and N and O isotopes were filtered in the field (0.2 μm), collected in 15 mL falcon tubes and kept on ice. Samples were frozen upon returning to the lab and kept frozen until analyzed. The water samples for B isotope analysis were filtered in the field (0.2 μm), collected in 50 mL polypropylene centrifuge tubes and were kept refrigerated until analyzed.

A variety of possible endmembers were sampled to further constrain potential B sources. To estimate the contribution

of B from seawater, we analyzed coastal seawater samples (n = 10) from Port Jefferson Harbor (**Figure 1**). Precipitation was collected from acid cleaned rain gauges on four separate occasions (at Stony Brook University). Surface waters were collected from protected precipitation-fed lakes (i.e., kettle ponds; Pine Barrens region; n = 3) and spring-fed ponds (Mill Pond and Setauket Pond; n = 8). Private wells (n = 5) in Smithtown and Old Field were sampled at the houses before the filter (which was disconnected). Septic waste (n = 3) was collected from private residences on Long Island with a peristaltic pump from a pump chamber (immediately downfield from the septic tank prior to the drain-field) and stored in 1 L plastic containers with no processing (e.g., no filtering, pH adjustment). All surface and groundwater samples were collected in acid cleaned 50 mL polypropylene bottles. The bottles were rinsed with the water that was being collected and then collected to avoid air space. Temperature, DO, and salinity were measured at the time of collection. Samples were prepared for B analyses in the same way that SGD samples described above were prepared.

Analytical Methods & Endmember Experiments

In order to obtain $\delta^{11}B$ and to estimate how much [B] could be expected from commercial products, tap water was used to leach five commonly applied fertilizers, one manure sample purchased locally and one locally collected Canada goose dropping. The tap water represents water that would be used for irrigation of lawns, making the leach a more realistic value for what might be delivered to groundwater. The fertilizers and manure were put in 50 mL centrifuge tubes up to the 5 mL mark, filled to the 50 mL mark with tap water and placed on a shaker table at room temperature for several hours.

Boron concentrations were measured with an Agilent 7500cx Quadrupole ICP-MS using a standard bracketing routine with background subtraction. After concentrations were established, approximately 250 ng of B was separated from the matrix using Amberlite IRA 743, a B-specific resin. Samples were adjusted to a pH of ∼9 before adding to the columns, washed with pH 9 adjusted DI water, and eluted with 2% nitric acid following a modified procedure from Lemarchand et al. (2002). Boron isotope ratios were measured using a Nu Instruments Plasma II multi-collector ICP-MS using a standard bracketing routine that included a background between each sample and standard. These background measurements were averaged and subtracted from the sample and standards before using the average of bracketing standards (NBS 951, which is taken as 0‰) to calculate $\delta^{11}B$. Measurement precision is between 0.5 and 1.0‰. Archived groundwater samples from Callahans Beach, collected during July 2014 and May 2015, were additionally analyzed for [B] and $\delta^{11}B$.

Coastal groundwater samples for nitrate concentration analysis were prepared using a modified vanadium (III) reduction procedure (Miranda et al., 2001; Doane and Howarth, 2003). Samples for the analysis of ammonium were prepared and analyzed using a mixed-reagent method (Presley and Claypool, 1971). Nutrient (NO_3^- and NH_4^+) concentrations were measured spectrophotometrically on a BPPBABTECH Omega series microplate reader. $\delta^{15}N\text{-}NO_3^-$ and $\delta^{18}O\text{-}NO_3^-$ were measured at the stable isotope facility at the University of California, Davis by bacterial denitrification assay. Isotope ratios were measured on a ThermoFinnigan GasBench + PreCon trace-gas concentration system interfaced to a ThermoScientific Delta V Plus isotope-ratio mass spectrometer with measurement precision of 0.4‰ for $\delta^{15}N\text{-}NO_3^-$ and 0.5‰ for $\delta^{18}O\text{-}NO_3^-$. Nitrogen isotopes are referenced to air while oxygen isotopes are referenced to Vienna Standard Mean Ocean Water (VSMOW). Nitrite was removed prior to analysis (Granger and Sigman, 2009). November and December groundwater samples were not analyzed for $\delta^{15}N\text{-}NO_3^-$ and $\delta^{18}O\text{-}NO_3^-$.

RESULTS

Possible Sources – Boron

Natural Sources

The survey of local water sources reveals a range in [B] and large variability in $\delta^{11}B$ (**Table 1**). Rainwater varied from 6 to 13 ppb with a $\delta^{11}B$ between 12.7 and 33.4‰ (**Table 1**). Kettle ponds in the Pine Barrens region, which is a protected part of the Long Island watershed without farming and residences (**Figure 1**), demonstrated similar [B] as the rainwater samples (6–8 ppb) and somewhat higher $\delta^{11}B$ values (27.5 to 32.7‰; **Table 1**). These protected ponds are fed by precipitation and should therefore represent the average annual precipitation $\delta^{11}B$ and [B] endmember.

Private wells to depths of 30 and 90 m in the Upper Glacial aquifer (town of Old Field; **Figure 1**) give a range of [B] of 18–47 ppb and a range of $\delta^{11}B$ of 19.6 to 36.6‰ (**Table 1**). In contrast, one well from the town of Smithtown (Metcalf) was higher in [B] (67 ppb) and lower in $\delta^{11}B$ (11‰; **Table 1**). Water collected along two spring-fed creeks (Setauket Mill Pond and Stony Brook Mill Pond) were enriched in [B] (17–25 ppb) and isotopically low ($\delta^{11}B$ = 9.0–15.8‰; Setauket Pond 2E; **Table 1**) as compared to inland groundwaters. A total of 10 coastal seawater samples were collected along the shoreline of Port Jefferson Harbor; the mean (± standard deviation) $\delta^{11}B$ is 39.4 ± 0.2‰ for a [B] of 3580 ppb and a salinity of 27 psu.

Anthropogenic and Animal Sources

The public water supply is used for agricultural and homeowner irrigation; therefore, tap water was used to leach a variety of fertilizers and manure samples. The tap water has relatively low [B] (11 ppb) and elevated $\delta^{11}B$ (34.9‰; **Table 1**). Leaching with tap water produced a range of [B] and while it is understood that farming and lawn practices are not mimicked by our leaching experiments and attenuation is expected, the $\delta^{11}B$ values are used in ensuing mixing models (see section "Identifying Potential Sources of Groundwater Nitrate Using Boron Stable Isotopes"). The differences in [B] availability through these qualitative leaching experiments provides order of magnitude concentrations and shows differences among the various potential B sources. The $\delta^{11}B$ values for five commonly applied commercial fertilizers (Scotts Thick'R Lawn, Holly Tone,

TABLE 1 | Summary of B concentration and δ^{11}B isotopic values for natural waters, including precipitation, protected precipitation-fed lakes, spring-fed ponds, groundwater wells, public tap water, and seawater.

Sample type	δ^{11}B (‰)	B (ppb)	Lat	Lon
Precipitation				
SBU Rain 1	12.7	13	40.9570	−73.1251
SBU Rain 2	33.4	6	40.9570	−73.1251
SBU Rain 3	21.3	9	40.9570	−73.1251
SBU Rain 4	15.6	7	40.9570	−73.1251
Precipitation-fed lakes (protected)				
Lake Panamoka	27.5	7	40.9217	−72.8543
Ridge Lake	30.9	8	40.9169	−72.8568
Tarkill Pond	32.7	6	40.9167	−72.8551
Spring-fed ponds				
Stony Brook Mill Pond 1	15.8	24	40.9149	−73.1468
Stony Brook Mill Pond 2	14.2	25	40.9145	−73.1461
Setauket Pond 2A	10.9	24	40.9464	−73.1152
Setauket Pond 2C	9.5	28	40.9441	73.1158
Setauket Pond 2D	10.8	25	40.9452	−73.1152
Setauket Pond 2E	9.0	17	40.9452	−73.1152
Groundwater wells				
Metcalf (Smithtown)	11.0	67	40.9589	−73.0069
29B Fuller (Old Field)	19.6	47	40.9560	−73.1289
21A Johnson (Old Field)	36.6	18	40.9568	−73.1288
Johnson #2 (Old Field)	36.6	20	40.9570	−73.1283
33B Wooton (Old Field)	36.0	26	40.9570	−73.1283
Public (tap) water	34.9	11		
Seawater				
Port Jefferson Harbor (n = 10)	39.4	3580	40.9664	−73.0781

TABLE 2 | Summary of potential contaminant endmember δ^{11}B isotopic values analyzed, including fertilizers, animals waste and septic waste.

Sample type	δ^{11}B (‰)	B (ppb)
Fertilizers		
Scotts Thick'R Lawn™	12.6	349
Holly Tone™	7.4	4000
10–10–10	11.9	1310
5–10–5	4.9	2500
Milorganite™	−4.4	405
Animal waste		
Commercial manure	25.9	92
Goose droppings	25.8	75
Septic waste		
59R Sewage	−0.2	1275
9B Sewage	2.5	250
CSH Sewage	2.1	105

10–10–10, 5–10–5, and Milorganite™) analyzed ranged from −4.4 to 12.6‰ (**Table 2**). In contrast, commercial manure (animal source unknown) was higher in δ^{11}B (25.9‰), and similar to that of Canada goose manure collected from Stony Brook University's campus (25.8‰; **Table 2**). The δ^{11}B of three septic samples ranged between −0.2 and 2.5‰ (**Table 2**). Milorganite™ is the heat-treated residue from microbes that were used to break up solids in the public wastewater treatment for the city of Milwaukee, likely accounting for its similar composition (−4.4‰) to the septic samples. These analyses were conducted to better understand potential B endmembers, and N isotope values were not measured.

Subterranean Estuary Groundwaters – Concentrations

Callahans Beach

Groundwater salinity remained constant at depth (≤0.3 psu) and waters were well-oxygenated (with dissolved oxygen, [DO] > 5 mg L^{-1}) at Callahans Beach (**Table 3**). DO was variable with depth and was generally lower in August and September than it was in the other 4 months. Groundwater pH generally increased with depth but showed some variability being lower in July (4.77–4.98) than at other times (4.80–5.89). [B] did not show a statistically significant correlation with salinity (R^2 = 0.22, excluding a high outlier from 6 m depth in July) or with NO_3^- concentrations (**Table 3** and **Figure 2**). B concentrations were variable with depth for each month, ranging from 14 to 47 ppb, with one elevated salinity sample at 73 ppb (**Table 3**). NO_3^- concentrations in groundwater from Callahans Beach ranged from 3.7 to 19.3 mg L^{-1} (as NO_3^-) with a mean (± standard deviation) of 12.7 ± 4.6 mg L^{-1} (**Table 3** and **Figure 2B**). NO_3^- concentrations were elevated during June through September and decreased from October through December 2017. NH_4^+ was present at trace levels through the summer and increased slightly in November and December. These differences may have been driven by changes in regional precipitation. October 2017 had about 150 mm of total rainfall, while November and December 2017 had about 50 mm of total rainfall. Tamborski et al. (2017a) monitored these same wells over a 12-month period (2014–2015), during which NH_4^+ concentrations were negligible and NO_3^- was the dominant form of inorganic N.

Iron Pier Beach

At Iron Pier Beach, groundwater salinity was relatively constant with depth (<0.5 psu), with slightly elevated salinities in July (<2 psu; **Table 4**). DO generally decreased with depth but all samples were well-oxygenated (>5 mg L^{-1}); DO was slightly higher in summer than in winter. There was variability in pH with depth and pH was lower in June (4.98–5.07) than at other times of the year (5.10–5.92). On average, B concentrations at Iron Pier Beach were higher than those at Callahans Beach (16–98 ppb), variable with depth and were not correlated with salinity (**Table 4** and **Figure 2A**). NO_3^- concentrations were consistently higher at Iron Pier Beach than those at Callahans Beach. The mean (± standard deviation) groundwater NO_3^- concentration was 28.2 ± 9.3 mg L^{-1} with a range of 9.3 to 52.6 mg L^{-1}. NO_3^- concentrations showed no seasonal differences and generally increased with depth, with minor amounts of NH_4^+ (**Table 4**).

Subterranean Estuary Groundwaters – Stable Isotopes

Groundwater samples from Callahans Beach collected in 2017 gave δ^{15}N-NO_3 values that ranged from 1.9‰ to

TABLE 3 | Callahans Beach coastal groundwater samples collected in 2017.

Well	Date	Depth	T	Salinity	DO	pH	ORP	NO_x	NH_4^+	B	$\delta^{15}N$	$\delta^{18}O$	$\delta^{11}B$
		m	°C		mg L^{-1}		mV	mg L^{-1}	mg L^{-1}	ppb	‰ - air	‰ - VSMOW	‰
CH2	Jun-17	−3	na	na	na	4.98	83	19.3	0.0	27	3.6	2.2	33.0
CH3	Jun-17	−5	na	na	na	5.22	73	18.0	0.0	27	3.8	0.0	29.0
CH4	Jun-17	−6	na	na	na	5.38	48	18.0	0.0	26	3.8	−0.1	23.7
CH5	Jun-17	−7	na	na	na	5.34	61	9.1	0.0	26	3.8	−0.1	37.1
CH2	Jun-17	−3	17.1	0.28	9.4	4.80	216	16.1	0.0	24	3.2	−0.4	31.1
CH3	Jul-17	−5	16.4	0.27	10.0	4.77	209	14.6	0.0	24	3.6	0.6	25.9
CH4	Jul-17	−6	17.3	9.36	8.8	4.80	197	16.7	0.0	73	3.6	1.1	42.2
CH5	Jul-17	−7	16.4	0.29	9.5	4.79	202	6.4	0.0	24	4.2	0.6	36.5
CH2	Aug-17	−3	25.6	0.28	5.7	5.29	256	10.7	0.0	26	4.0	1.3	32.0
CH3	Aug-17	−5	23.9	0.24	6.8	5.59	253	15.8	8.3	28	3.9	0.3	32.0
CH4	Aug-17	−6	23.1	0.26	6.5	5.66	272	17.1	0.0	27	3.1	1.0	27.8
CH5	Aug-17	−7	na	0.24	6.4	5.55	257	7.9	0.0	27	4.6	0.5	39.6
CH2	Sep-17	−3	14.4	0.22	8.3	5.45	293	13.5	0.0	47	4.1	1.2	39.6
CH3	Sep-17	−5	14.4	0.22	8.0	5.53	308	15.1	0.0	27	4.2	1.3	35.9
CH4	Sep-17	−6	14.1	0.21	7.6	5.87	346	16.0	0.0	27	2.8	1.3	41.9
CH5	Sep-17	−7	14.1	0.22	8.0	5.68	336	3.9	0.0	26	4.7	0.9	29.6
CH2	Oct-17	−3	19.0	0.21	7.7	5.46	253	15.0	0.0	25	4.1	0.2	37.6
CH3	Oct-17	−5	21.2	0.22	6.5	5.42	264	14.0	0.0	19	4.0	1.0	31.4
CH4	Oct-17	−6	20.0	0.22	7.8	5.60	238	17.3	0.0	16	1.9	1.5	40.2
CH5	Oct-17	−7	18.7	0.23	6.7	5.56	250	4.8	0.0	22	4.6	1.1	27.6
CH2	Nov-17	−3	7.4	0.25	9.5	5.40	341	12.0	0.0	19	na	na	39.7
CH3	Nov-17	−5	6.2	0.26	9.0	5.68	289	12.6	3.2	16	na	na	34.4
CH4	Nov-17	−6	5.8	0.27	9.2	5.70	308	3.7	2.4	15	na	na	42.5
CH5	Nov-17	−7	6.1	0.27	9.9	5.89	325	12.3	0.7	17	na	na	29.2
CH2	Dec-17	−3	4.8	0.29	10.0	5.87	266	13.8	0.2	17	na	na	36.3
CH3	Dec-17	−5	5.0	0.29	9.2	5.67	291	12.4	0.5	18	na	na	30.7
CH4	Dec-17	−6	4.3	0.31	9.8	5.86	238	3.5	0.7	14	na	na	27.0
CH5	Dec-17	−7	4.5	0.29	9.3	5.72	308	15.0	0.8	18	na	na	39.1

na, not analyzed.

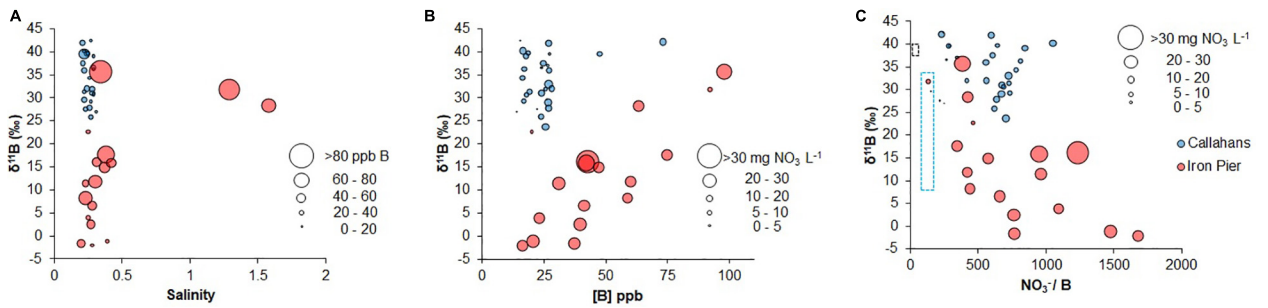

FIGURE 2 | (A) Coastal groundwater salinity vs. $\delta^{11}B$ with point size reflecting B concentration **(A)**; B concentration vs. $\delta^{11}B$ with point size reflecting NO_3^- concentration **(B)** and NO_3/B vs. $\delta^{11}B$ with point size reflecting NO_3^- concentration **(C)**. The range of seawater (~0.5 mg N L^{-1}) and precipitation (~1 mg N L^{-1}) in panel **(C)** are represented by dashed black and blue rectangles, respectively.

4.7‰ and $\delta^{18}O\text{-}NO_3$ values that ranged from −0.4‰ to 2.2‰ (**Figure 3A**). $\delta^{15}N\text{-}NO_3$ was slightly lower at 6 m depth (sample ID = CH4) than at other depths during August, September, and October (**Table 3**). $\delta^{18}O\text{-}NO_3$ values were generally variable at depth without an obvious trend. The $\delta^{11}B$ of groundwater at Callahans Beach ranged from 23.7‰ to 42.5‰ with a concurrent change at 6 m depth (**Table 3**). $\delta^{11}B$ was significantly higher from July to October, but lower during June, and showed no trend with NO_3^- concentrations (**Figure 2B**).

Iron Pier Beach groundwaters had a similar range of $\delta^{15}N\text{-}NO_3$ values (0.5‰ to 5.0‰) as Callahans Beach (**Figure 3A**). $\delta^{15}N\text{-}NO_3$ values at Iron Pier Beach generally increased with depth (**Table 4**), while $\delta^{18}O\text{-}NO_3$ values were highest at a depth of 3 m. $\delta^{11}B$ values were generally lower at Iron Pier Beach than groundwater samples from Callahans Beach and ranged from −2.1‰ to 35.7‰ (**Table 4** and **Figure 2**) and displayed a significant positive correlation with B concentration (R^2 = 0.56; **Figure 2B**). Groundwater NO_3/B ratios were significantly greater than seawater and precipitation endmembers for both sites (**Figure 2C**), demonstrating a significant input of anthropogenic NO_3^- to the STE.

DISCUSSION

Subsurface Processes and Variability

Groundwater pH was low at both sites (**Tables 3**, **4**) and was not correlated with [B] or $\delta^{11}B$. Therefore, B isotopic signatures are unlikely to be affected by sorption and should only reflect nitrogen source compositions or mixing processes. Coastal groundwaters at both sites were well oxygenated (**Tables 3**, **4**); despite this, denitrification may occur in sedimentary anoxic micro-sites (Brandes and Devol, 1997). There was no evidence of denitrification in the STE (**Figure 3A**), assuming that denitrification results in a $\delta^{18}O$ to $\delta^{15}N$ ratio of 2:1 (Kendall et al., 2008). This is further supported by comparing $\delta^{15}N$ with $\ln[NO_3^-]$ and $1/[NO_3^-]$ (**Figure 4**). Denitrification should result in trends distinctive from that induced by binary mixing. The narrow range of $\delta^{15}N$ for the coastal groundwaters coupled with overlapping signatures of $\delta^{15}N$ in potential endmembers (**Figure 3A**) precludes using N alone to untangle mixing sources (**Figure 4**).

There were no seasonal changes in $\delta^{15}N\text{-}NO_3^-$ and $\delta^{18}O\text{-}NO_3^-$ at Iron Pier Beach, but there were differences with depth (**Table 4**). The groundwater at 1.5 m depth had a lower δ^{15} N value relative to the other groundwater samples at Iron Pier Beach. Lower isotope values for samples at 1.5 m depth may be explained by nitrification processes within the STE where oxic conditions are persistent (Kroeger and Charette, 2008), especially at this shallow depth. Alternatively, differences may be related to geologic heterogeneity. At Callahans Beach, fresh groundwaters at 6 m depth were lower in $\delta^{15}N\text{-}NO_3^-$ with variable $\delta^{11}B$, compared to shallower and deeper groundwaters (**Table 3**). This depth horizon is geologically distinct from neighboring sediments. Indeed, Tamborski et al. (2017b) observed significant radon, radium, and dissolved Mn^{2+} enrichments at this depth horizon. Geologic heterogeneity can act to both modify groundwater flow paths and enhance biogeochemical transformations within the STE (Heiss et al., 2020). However, denitrification cannot explain the differences in $\delta^{15}N\text{-}NO_3^-$ and $\delta^{18}O\text{-}NO_3^-$ compositions (**Figures 3A**, **4**). In the ensuing analysis, we thus interpret changes in stable isotopes to reflect changes in groundwater N (and B) sources, rather than from a biogeochemical process or cycle, unless explicitly stated.

Potential Sources of Groundwater Nitrate Using Nitrate Stable Isotopes

The nitrogen and oxygen isotope values of NO_3^- in groundwater from Callahans Beach show no seasonal trends (**Table 3**). The samples from this study are similar in $\delta^{15}N\text{-}NO_3^-$ to previously measured values at that site from 2014 and 2015 (Tamborski et al., 2017a); however, the 2017 samples span a much narrower range in $\delta^{18}O\text{-}NO_3$ (**Figure 3A**). Samples from both Callahans Beach and Iron Pier Beach plot in the overlapping fields of nitrification of NH_4^+ in fertilizer and precipitation, soil NH_4^+, manure and septic waste (**Figure 3A**). Previous studies at Callahans Beach attributed the $\delta^{15}N$ and $\delta^{18}O$ of groundwater NO_3^- to either nitrification of septic waste, or to mineral fertilizer (Tamborski et al., 2017a). Studies of drinking supply well samples collected in Northport, a sewered community to the southwest of Callahans

TABLE 4 | Iron Pier Beach coastal groundwater samples collected in 2017.

Well	Date	Depth m	T °C	Salinity	DO mg L^{-1}	pH	ORP mV	NO_x mg L^{-1}	NH_4^+ mg L^{-1}	B ppb	$\delta^{15}N$ ‰ - air	$\delta^{18}O$ ‰ -VSMOW	$\delta^{11}B$ ‰
IP1	Jun-17	1.5	18.4	0.23	12.9	4.98	54	29.9	0.0	31	0.5	1.9	11.4
IP2	Jun-17	3	19.4	0.20	9.4	5.41	77	28.6	0.0	37	3.8	6.7	−1.6
IP3	Jun-17	4.5	18.4	0.31	10.3	5.07	105	52.6	0.1	43	4.7	−0.2	16.1
IP1	Jul-17	1.5	18.6	1.29	9.8	5.87	170	12.4	0.0	92	0.6	1.9	31.9
IP2	Jul-17	3	16.8	1.58	10.1	5.57	147	26.6	0.0	63	3.6	6.5	28.3
IP3	Jul-17	4.5	16.5	0.37	10.2	5.35	123	26.8	0.0	47	4.4	1.1	14.9
IP2	Aug-17	3	19.1	0.28	6.9	5.64	288	27.1	0.0	16	3.7	7.0	−2.1
IP3	Aug-17	4.5	18.0	0.28	7.6	5.68	319	27.0	0.1	41	4.0	3.7	6.6
IP1	Oct-17	1.5	15.6	0.25	8.4	5.82	184	25.2	0.0	23	0.8	2.7	3.9
IP2	Oct-17	3	12.5	0.23	8.4	5.59	230	25.8	0.0	59	3.2	6.2	8.3
IP3	Oct-17	4.5	12.6	0.34	7.8	5.72	120	37.7	0.0	98	5.0	0.9	35.7
IP1	Nov-17	1.5	8.2	0.25	9.3	5.10	250	9.3	0.8	20	na	na	22.7
IP2	Nov-17	3	7.8	0.27	8.7	5.72	302	30.1	0.0	40	na	na	2.5
IP3	Nov-17	4.5	7.4	0.38	8.6	5.92	321	25.7	0.0	75	na	na	17.6
IP1	Dec-17	1.5	7.4	0.30	9.6	5.72	262	25.2	0.0	60	na	na	11.8
IP2	Dec-17	3	7.1	0.39	8.9	5.84	3	30.2	0.2	20	na	na	−1.1
IP3	Dec-17	4.5	7.1	0.42	9.0	5.90	260	39.9	0.5	42	na	na	15.9

na, not analyzed.

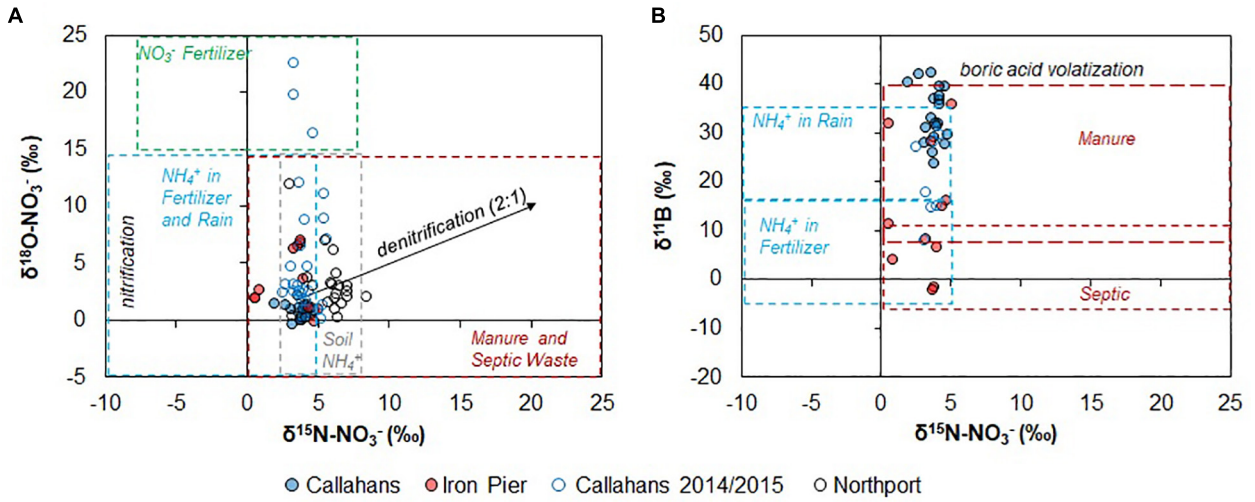

FIGURE 3 | (A) δ^{15}N-NO_3 vs. δ^{18}O-NO_3 of coastal groundwater samples. Callahans 2014/2015 data from Tamborski et al. (2017a). Northport data from Bleifuss et al. (2000). Source fields modified from Kendall et al. (2008). **(B)** δ^{15}N-NO_3 vs. δ^{11}B. The δ^{15}N-NO_3 source fields are from Kendall et al. (2008) and the δ^{11}B ranges are based on a survey of possible sources on Long Island as well as the ranges reported by Vengosh et al. (1994, 1999), Bassett et al. (1995); Komor (1997), Seiler (2005), Widory et al. (2005), Tirez et al. (2010), and Eppich et al. (2013). Only select samples from Callahans 2014/2015 are included (salinity ≤ 0.3).

Beach, have NO_3^- concentrations less than 10 mg L^{-1} (Bleifuss et al., 2000). These sewered community groundwaters have higher δ^{15}N-NO_3^- values compared with those from Iron Pier and Callahans Beach (hollow black circles; **Figure 3A**). The δ^{15}N-NO_3^- and δ^{18}O-NO_3^- values from the Northport supply wells were attributed to nitrification of NH_4^+ in fertilizer, with small inputs from septic waste (Bleifuss et al., 2000); we note that the soil NH_4^+ and manure/septic waste source fields also overlap in δ^{15}N-NO_3^- for these supply well samples (**Figure 3A**).

Residences in the watershed of Callahans Beach are unsewered and use individual, homeowner septic systems for wastewater disposal (i.e., cesspools); thus, a septic waste N signature is expected for Callahans Beach. Callahans Beach is located immediately down-gradient of a golf course, and in the vicinity of communities that fertilize their lawns (**Figure** 1), and so a N and B source from fertilizers is also expected. Based on the δ^{15}N-NO_3^- and δ^{18}O-NO_3^- data and the endmember source fields identified in Kendall et al. (2008), it is unclear what the dominant source of NO_3^- is to the groundwaters of the Callahans Beach STE (**Figure 3A**). Iron Pier Beach is located down-gradient from agricultural fields, so a fertilizer source for the NO_3^- was expected. Based on δ^{15}N-NO_3^- and δ^{18}O-NO_3^- is unclear, however, if the Iron Pier Beach samples are sourced from nitrification of NH_4^+ in fertilizer and precipitation, soil NH_4^+, manure or septic waste.

Identifying Potential Sources of Groundwater Nitrate Using Boron Stable Isotopes

Stable isotope measurements of δ^{15}N-NO_3^- and δ^{18}O-NO_3^- are unable to discriminate NO_3^- sources in the STE, despite local knowledge of each study site's primary NO_3^- sources. Comparison of δ^{15}N and δ^{11}B values has allowed the discrimination of anthropogenic NO_3^- sources in other terrestrial and aquatic-based studies (Komor, 1997; Widory et al., 2004, 2005, 2013; Seiler, 2005; Bronders et al., 2012; Lindenbaum, 2012; Briand et al., 2013, 2017; Eppich et al., 2013; Saccon et al., 2013; Guinoiseau et al., 2018; Kruk et al., 2020). Callahans Beach and Iron Pier Beach have distinct land-use patterns within their respective coastal watersheds (**Figure 1**). *A posteriori* knowledge of each site, and of the Long Island region (Bellone, 2015), provides a unique opportunity to compare "known" nitrogen sources to those estimated from δ^{11}B and δ^{15}N-NO_3^- versus δ^{18}O-NO_3^-.

Endmember Mixing and N Sources

Comparison between δ^{11}B and δ^{15}N provides qualitative information on potential groundwater N sources (**Figure 3B**). Endmember source fields of δ^{11}B from this study (**Tables 1**, **2**), with additional constraints as summarized by Eppich et al. (2013), suggests that groundwater NO_3^- for Iron Pier Beach is derived from either nitrification of NH_4^+ in fertilizer or septic waste. In contrast, groundwater NO_3^- at Callahans Beach is interpreted to reflect either nitrification of NH_4^+ in precipitation or an animal manure source. Precipitation can supply, at most, 1 mg L^{-1} of NO_3^- to the groundwater system of Long Island; therefore, precipitation is not the primary source of the observed N concentrations (**Table 3**) or δ^{11}B (**Figures 2C**, **5**). Binary mixing models were used to investigate theoretical mixing between different sources of B in the STE. Assuming that B is not attenuated by *in situ* biogeochemical processes, then mixing between two different endmembers may be quantitatively approximated as:

$$[B] = C_1^* X + C_2^* (1 - X) \quad (1)$$

$$\delta^{11}B = ((\delta^{11}B_1^*C_1^*X) + (\delta^{11}B_2^*C_2^*(1 - X))) / (C_1^*X + C_2^*(1 - X)) \quad (2)$$

where X is the fraction of endmember 1 in the coastal groundwater, C_1 and $\delta^{11}B_1$ are the concentration and isotope composition of endmember 1 and C_2 and $\delta^{11}B_2$ are the concentration and isotope composition of endmember 2. Estimated endmembers (**Figure 5**) were used to investigate potential mixing relationships between natural sources (precipitation or seawater) with contaminant sources B (fertilizer, septic waste or animal waste). We note that endmember mixing models may be improved with a Bayesian statistical analysis, which accounts for the degree of overlap and uncertainty of different sources (Ransom et al., 2016); however, a more comprehensive analysis of potential endmembers is required here. The two different subterranean estuaries studied have relatively distinct ranges of $\delta^{11}B$ (**Figure 2**) and therefore we treat each site as a separate system in the ensuing discussion.

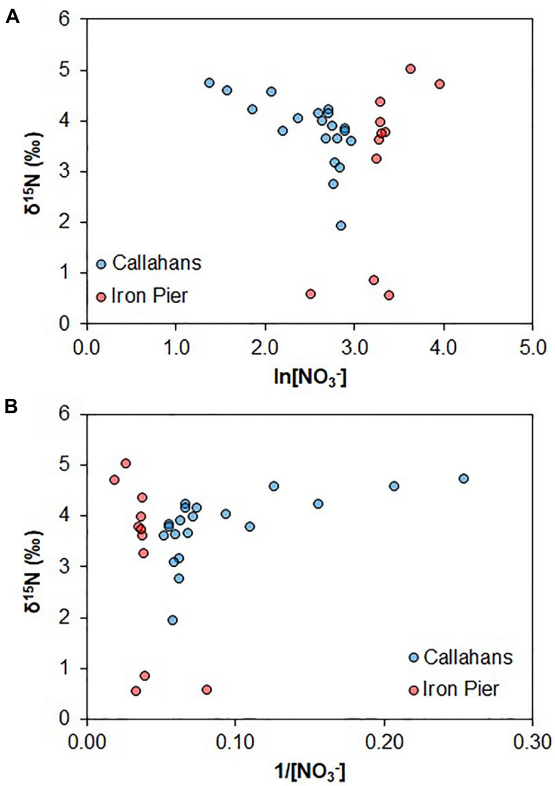

FIGURE 4 | Natural logarithm of NO_3^- vs. $\delta^{15}N$ **(A)** and $1/[NO_3^-]$ vs. $\delta^{15}N$ **(B)** of coastal groundwater samples.

Iron Pier Beach

Agriculture dominates the lower population density (470 people km^{-2}) watershed of Iron Pier Beach. Groundwater NO_3^- at this site should be derived from mineral fertilizers. Fresh groundwater samples from Iron Pier Beach are systematically lower in $\delta^{11}B$ compared to Callahans Beach (**Figure 2**). Iron Pier groundwater $\delta^{11}B$ increases nearly linearly with increasing B concentration (**Figure 2B**), suggesting that binary mixing occurred between an isotopically enriched B source and an isotopically depleted, lower [B] source. Precipitation has isotopically high $\delta^{11}B$ but is too low in [B] to explain the higher $\delta^{11}B$ values of the Iron Pier groundwater (**Figure 5**). Animal manure is an alternative endmember; however, three coastal groundwater samples are higher in $\delta^{11}B$ than the two measured manure samples (**Figure 5**). Either two samples are insufficient to adequately characterize the $\delta^{11}B$ of animal manure (Eppich et al., 2013), or this is not an appropriate endmember for this site.

Seawater has elevated $\delta^{11}B$ and [B] and may therefore constitute one endmember for Iron Pier Beach (**Figure 5**). Groundwater salinities are on the order of 0.3 psu (**Table 4**); direct mixing between a contaminant endmember and seawater (25–28 psu) would mean that seawater contributes between 1 and 2% of the observed salinity. This amount of seawater [B] could be

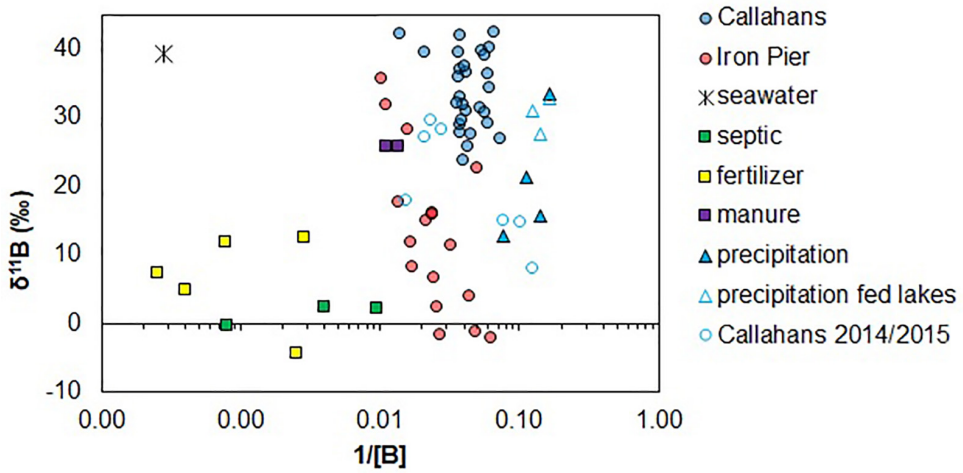

FIGURE 5 | Log of 1/B vs. $\delta^{11}B$ of coastal groundwater samples and different endmembers analyzed in this study.

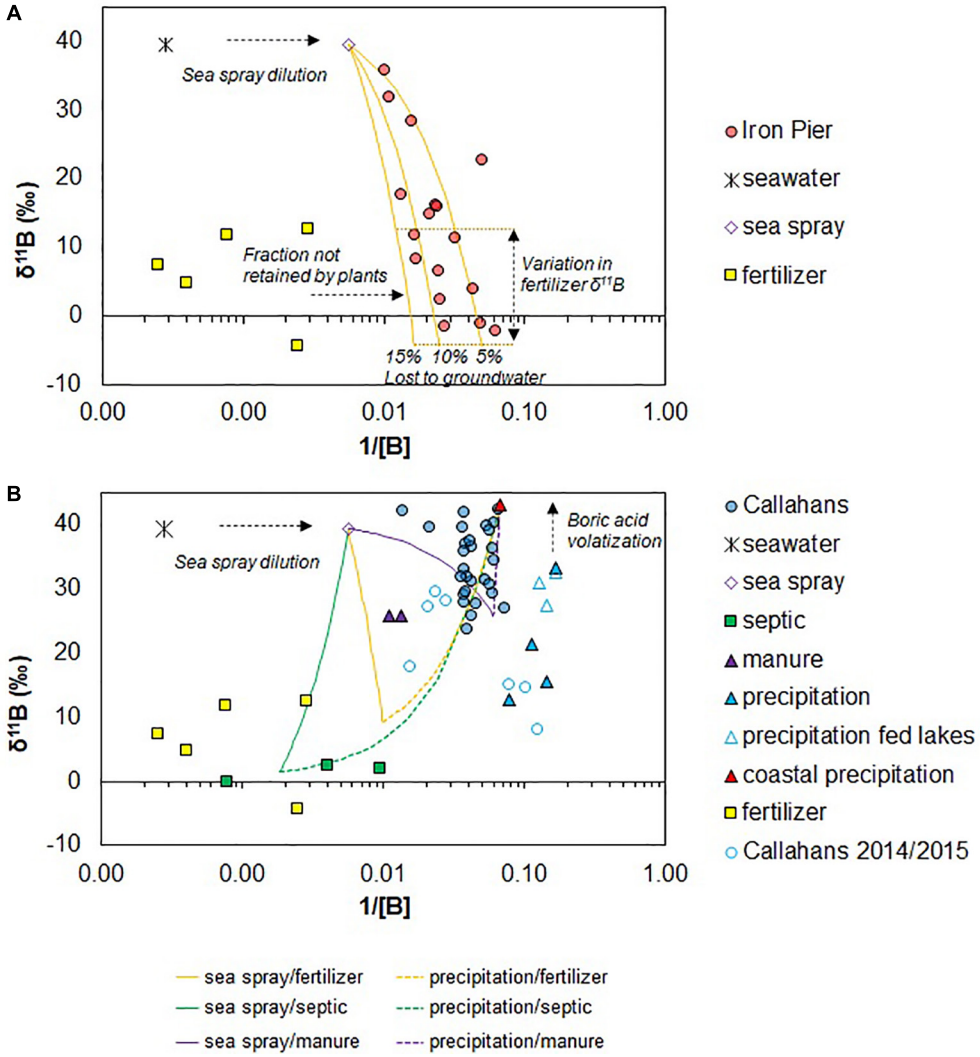

FIGURE 6 | Log of 1/B vs. δ^{11}B of coastal groundwater samples from Iron Pier Beach **(A)** and Callahans Beach **(B)**. In panel **(A)**, theoretical mixing between sea spray and fertilizer (orange curves) assumes that sea spray constitutes 5% of the B concentration of seawater, and that B retention from plants is between 85 and 95% of the applied fertilizer load. The horizontal orange dashed lines indicate the range of fertilizer δ^{11}B (Milorganite^{TM} [–4.4‰] to Scotts Thick'R Lawn^{TM} [12.6‰]) over a B concentration range of 20–60 ppb. In panel **(B)**, the dashed curves show mixing between coastal precipitation with possible contaminant endmembers, and solid curves show mixing between sea spray and possible contaminant endmembers, including fertilizer (9‰), septic waste (1.5‰) and animal manure (26‰). Coastal precipitation is set as the highest observed δ^{11}B signature for Callahans Beach (15 ppb, 42.5‰). Manure B concentrations are 20% of the laboratory leached concentration. Fertilizer δ^{11}B is the average of analyzed fertilizer leaches, excluding Milorganite^{TM}; septic waste δ^{11}B is the average of the analyzed septic waste samples (**Table 2**).

delivered via sea spray that is diluted by rainfall. Septic waste and fertilizer endmembers (**Table 2**) are isotopically light enough to serve as the second endmember for Iron Pier Beach. However, B concentrations of the leaches are 1–3 orders of magnitude higher (lower 1/B; **Figure 5**) than the isotopically lowest δ^{11}B groundwater sample (16 ppb; −2.1‰; **Table 4**). The [B] of the fertilizers determined from the leaching experiments are not representative of a natural system. Borate minerals are added to commercial fertilizers because B is an essential micro-nutrient for plant growth (Shireen et al., 2018); therefore, a significant fraction of the B from a fertilizer application should be retained by the plant-root system. Further, the leaching experiment used a small amount of water so the leach is much more concentrated than what would be found in irrigation water even if the plant roots were inefficient at utilizing the B.

Theoretical mixing between highly diluted sea spray and fertilizers reasonably explains the coastal groundwater B data of Iron Pier Beach (**Figure 6A**). These mixing curves represent an isotopically light fertilizer (**Table 2**) assuming that 5, 10 or 15% of the applied B is lost to the groundwater system. Note that a higher δ^{11}B signature for fertilizer (12.6‰) would simply shift these mixing curves upward toward higher δ^{11}B values, assuming that B concentration ranges remain the same (**Figure 6A**). Given these assumptions, groundwater N at Iron Pier Beach must be

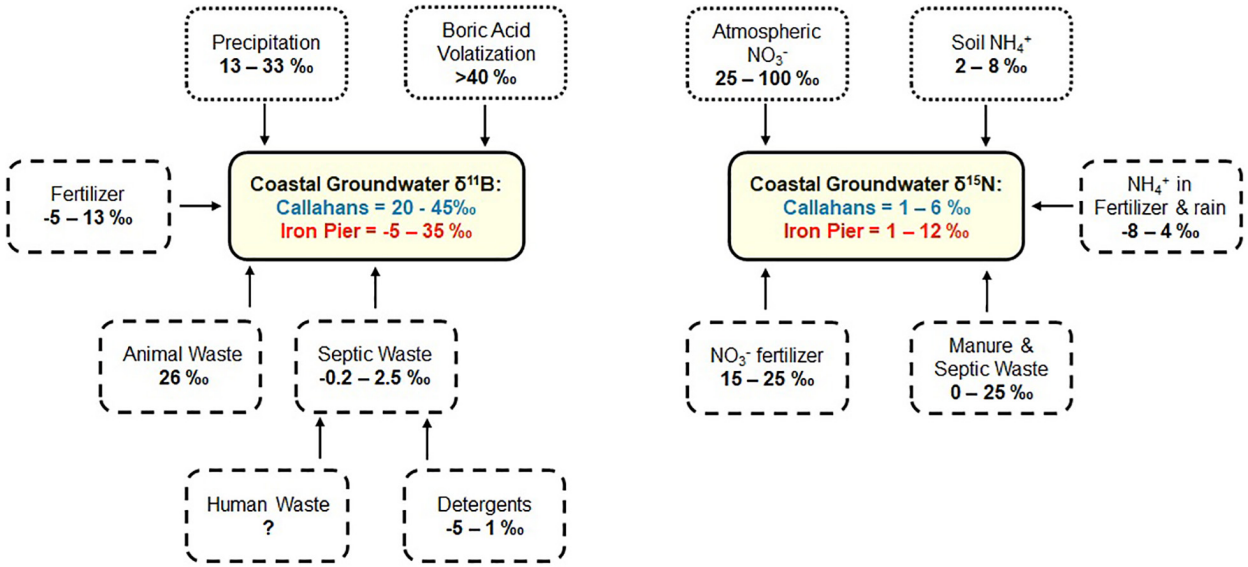

FIGURE 7 | Summary of $\delta^{11}B$ (left) and $\delta^{15}N$ (right) endmember isotope ratios of coastal groundwaters. Dotted boxes reflect natural sources or processes. Dashed boxes reflect anthropogenic contaminant sources. $\delta^{11}B$ ratios constrained from **Tables 1**, **2**. $\delta^{15}N$ ratios from Kendall et al. (2008).

predominantly sourced from nitrification of NH_4^+ in fertilizer (**Figures 3B**, **6A**), consistent with our working knowledge of this agricultural coastal system. Notably though, there is no trend in NO_3^- with [B] (**Figure 2B**), and therefore a simple two-component mix cannot explain the source of NO_3^- at Iron Pier Beach using N alone (**Figure 4**).

Callahans Beach

Callahans Beach is directly down-gradient from medium-density residential housing (2770 people km^{-2}) and a public golf course. Groundwater NO_3^- at this site should be derived from septic (i.e., cesspool) waste, with minor contributions from fertilizers. The coastal groundwater $\delta^{11}B$ of Callahans Beach reflects a much heavier $\delta^{11}B$ source compared to measured septic waste (−0.2 – 2.5‰) and fertilizer (**Table 2**). Anthropogenic B compounds used in detergents and cleaning products have a $\delta^{11}B$ signature between −5 and 1‰ (Vengosh et al., 1999), such that the $\delta^{11}B$ signature of the measured septic waste may be dominated by detergents, rather than human waste.

The highest $\delta^{11}B$ signatures (>39‰) suggest a contribution of B from seawater, although coastal groundwater salinities are low (<0.3) and do not show a trend with [B] or $\delta^{11}B$ (**Figure 2A**). Sea spray was invoked as the isotopically high $\delta^{11}B$ endmember for Iron Pier Beach (**Figure 6A**). At Callahans Beach, B concentrations are systematically lower than Iron Pier Beach, and so despite appreciably high $\delta^{11}B$ signatures, [B] cannot be explained by sea spray alone. $\delta^{11}B$ signatures higher than seawater isotope values may be derived from boric acid volatilization of seawater (Chetelat et al., 2005). The highest $\delta^{11}B$ we measured for rainwater is 33.4‰ (**Table 1**), but coastal precipitation can be much heavier (Chetelat et al., 2005). Therefore, we suggest that the high $\delta^{11}B$ endmember of Callahans Beach results from boric acid volatilization of seawater, resulting in a higher $\delta^{11}B$ coastal precipitation endmember (**Figure 6B**). The highest $\delta^{11}B$ value for Callahans Beach, 42.5‰ (CH4, November 2017; **Table 3**) has relatively low NO_3^- concentrations (3.7 mg NO_3^- L^{-1} or 0.84 mg N L^{-1}), similar to the N concentration of regional precipitation (Suffolk County Government, 2019). In the ensuing analysis, this sample is assumed to represent the B endmember of regional coastal precipitation.

Mixing relationships between sea spray and coastal precipitation were examined with respect to septic waste (1.5‰), animal manure (26‰) and fertilizer (9‰; **Figure 6B**). Sea spray B concentrations were assumed to represent 5% of measured seawater concentrations. Notably, because there is little change in [B] for a large range in $\delta^{11}B$, no single mixing curve will fit all of the Callahans Beach data. Therefore, it is not possible to demonstrate with certainty using B whether the N source is derived from fertilizer or septic waste (via individual homeowner cesspools). However, the range of values demonstrates that there is not one single endmember, consistent with our knowledge that groundwater NO_3^- within this watershed is derived from multiple non-point sources.

Coastal groundwaters collected during 2014 and 2015 are distinct in $\delta^{18}O\text{-}NO_3^-$ and $\delta^{11}B$ compared to samples from the same wells collected during 2017 (**Figure 3**). The B signatures of several 2015 samples match precipitation endmember B signatures, suggesting that recently recharged groundwaters obtain B and N from precipitation (**Figure 6A**). Importantly, this data demonstrates annual variability in groundwater flow and contaminant transport to LIS. While coastal groundwaters collected throughout 2017 showed relatively higher values of $\delta^{11}B$, it remains to be seen how contaminant delivery varies over longer time periods for this sole-source, unconfined aquifer.

Synthesis and Conceptual Model

In the coastal systems studied here, B and NO_3^- are added to the groundwater system in different ways, and are impacted by precipitation and seawater (sea spray versus boric acid volatilization) differently (**Figure 7**). Precipitation and seawater both have relatively low N concentrations (<1 mg L^{-1}). Seawater is a distinct endmember, due to its high [B] and its isotopically high $\delta^{11}B$ signature (**Figure 7**). Boric acid volatilization of seawater produces isotopically high B, and thus gives a very distinctive low B concentration endmember for coastal precipitation. It is interesting that two subterranean estuaries from similar settings have distinct sources of 'uncontaminated' waters. One has to consider differences in pathways for B from both fertilizer and septic waste. In the case of fertilizer, plants use B as a micro-nutrient, and so the concentration of B that is added to the groundwater system will be lower than what was applied to the land surface. In contrast, [B] in septic waste does not change. Therefore, homeowner cesspools likely reflect different sources of B and NO_3^- to the groundwater system (**Figure 7**). Septic waste $\delta^{11}B$ integrates multiple contaminant sources, including detergents, commercial cleaning products and human waste. Given the low $\delta^{11}B$ signature of septic waters (**Table 2**), B in detergents must dominate the B signature of septic waste. In contrast, human waste is the primary N source in septic waste and therefore B and N are decoupled in septic systems (**Figure 7**). Importantly, there is no relationship between B and NO_3^- concentrations in either of the studied subterranean estuaries (**Figure 2**).

CONCLUSION

Application of boron isotopes in coastal settings is vulnerable to the influence of seawater (via sea spray), which has orders of magnitude higher boron concentrations compared to various contaminant sources. Identification and discrimination of NO_3^- and B sources in coastal settings thus requires (1) adequate characterization of local sources (both natural waters and contaminants) and (2) an understanding of biogeochemical processes within the STE. Coastal groundwaters are collected from beaches in SGD studies to integrate terrestrial groundwater flow paths over the entirety of the coastal watershed and to account for any biogeochemical processes (i.e., denitrification) in the STE that would influence N concentration and speciation prior to discharge. The advantage of collecting coastal groundwater to account for N transformation may thus hinder the utility of B as an auxiliary N source tracer if seawater significantly modifies subsurface geochemical signatures. The results from this study demonstrate the utility of multi-isotope tracing techniques to identify N sources in polluted coastal aquifers. Future studies should explicitly measure isotopic values of different possible endmembers in order to constrain local variability in N and B sources.

DATA AVAILABILITY STATEMENT

The datasets generated for this study are available on request to the corresponding author.

AUTHOR CONTRIBUTIONS

CB and JT collected the field data under the supervision of HB, JC, and ER. Boron isotopes were analyzed in the lab of ER. All authors participated in the data analysis and interpretation.

FUNDING

This research was funded by New York Sea Grant projects R/CMC-13 and R/CMC-13-NYCT. The MC-ICP-MS used for this work was funded through NSF-MRI 0959524.

ACKNOWLEDGMENTS

JT acknowledges funding from the Canada First Research Excellence Fund, through the Ocean Frontier Institute. Katie Wooton, Deanna Downs, and Brooke Peritore (Stony Brook University FIRST lab) performed all of the boron isotope analyses for the fresh waters and potential contaminant endmembers.

REFERENCES

Anschutz, P., Charbonnier, C., Deborde, J., Deirmendjian, L., Poirier, D., Mouret, A., et al. (2016). Terresrial groundwater and nutrient discharge along the 240-km-long aquitanian coast. *Mar. Chem.* 185, 38–47. doi: 10.1016/j.marchem.2016.04.002

Aravena, R., Evans, M. L., and Cherry, J. A. (1993). Stable isotopes of oxygen and nitrogen in source identification of nitrate from septic systems. *Ground Water* 31, 180–186. doi: 10.1111/j.1745-6584.1993.tb01809.x

Bannon, R. O., and Roman, C. T. (2008). Using stable isotopes to monitor anthropogenic nitrogen inputs to estuaries. *Ecol. Appl.* 18, 22–30. doi: 10.1890/06-2006.1

Barth, S. (1998). Application of boron isotopes for tracing sources of anthropogenic contamination in groundwater. *Water Resour.* 32, 685–690. doi: 10.1016/s0043-1354(97)00251-0

Bassett, R. L., Buszka, P. M., Davidson, G. R., and Chong-Diaz, D. (1995). Identification of groundwater solute sources using boron isotopic composition. *Environ. Sci. Technol.* 29, 2915–2922. doi: 10.1021/es00012a005

Bateman, A. S., and Kelly, S. D. (2007). Fertilizer nitrogen isotope signatures. *Isotop. in Environ. Health Stud.* 43, 237–247. doi: 10.1080/10256010701550732

Bellone, S. (2015). *Suffolk County Comprehensive Water Resources Management Plan*. Suffolk County, NY: Department of Health Services.

Bleifuss, P., Hanson, G., and Schoonen, M. (2000). *Tracing Sources of Nitrate in the Long Island Aquifer System, SUNY-Stony Brook*. Ph.D. Thesis, SUNY Stony Brook, New York, NY.

Bloesch, P., Bell, L., and Hughes, J. (1987). Adsorption and desorption of boron by goethite. *Soil Res.* 25, 377–390.

Bokuniewicz, H. J., Cochran, J. K., Garcia-Orellana, J., Rodellas, V., Daniel, J. W., and Heilbrun, C. (2015). Intertidal percolation through beach sands as a source of ^{224,223}Ra to Long Island Sound, New York, and Connecticut, United States. *J. Mar. Res.* 73, 123–140. doi: 10.1357/002224015816665570

Brandes, J. A., and Devol, A. H. (1997). Isotopic fractionation of oxygen and nitrogen in coastal marine sediments. *Geochim. Cosmochim. Acta* 61, 1793–1801. doi: 10.1016/s0016-7037(97)00041-0

Briand, C., Plagnes, V., Sebilo, M., Louvat, P., Chesnot, T., Schneider, M., et al. (2013). Combination of nitrate (N, O) and boron isotopic ratios with microbiological indicators for the determination of nitrate sources in karstic groundwater. *Environ. Chem.* 10, 365–369.

Briand, C., Sebilo, M., Louvat, P., Chesnot, T., Vaury, V., Schneider, M., et al. (2017). Legacy of contaminant N sourves to the NO3-signature in rivers: a combined isotope delta N- 150NO3-, delta O-18- NO3-, delta B-11) and microbiological investigation. *Sci. Rep.* 7:41703.

Bronders, J., Tirez, K., Desmet, N., Widory, D., Petelet-Giraud, E., Bregnot, A., et al. (2012). Use of Compound-Specific Nitrogen ($\delta^{15}N$), Oxygen ($\delta^{18}O$), and Bulk Boron ($\delta^{11}B$) isotope ratios to identify sources of nitrate-contaminated waters: a guideline to identify polluters. *Environ. Forens.* 13, 32–38. doi: 10.1080/15275922.2011.643338

Brown, C. (2018). *Using Boron to Trace Anthropogenic Sources of Nitrogen in Long Island Sound*. Ph.D. Thesis, Stony Brook University, New Tork, NY.

Burnett, W. C., Bokuniewicz, H., Huettel, M., Moore, W. S., and Taniguchi, M. (2003). Groundwater and pore water inputs to the coastal zone. *Biogeochemistry* 66, 3–33. doi: 10.1023/b:biog.0000006066.21240.53

Buxton, H., and Modica, E. (1992). Patterns and rates of groundwater flow on Long Island. New York. *Ground Water* 30, 857–866. doi: 10.1111/j.1745-6584.1992.tb01568.x

Charbonnier, C., Anschutz, P., Poirier, D., Bujan, S., and Lecroart, P. (2013). Aerobic respiration in a high-energy sandy beach. *Mar. Chem.* 155, 10–21. doi: 10.1016/j.marchem.2013.05.003

Chetelat, B., Gaillardet, J., Freydier, R., and Négreic, Ph. (2005). Boron isotopes in precipitation: experimental constraints and field evidence from French Guiana. *Earth Plan. Sci. Lett.* 235, 16–30. doi: 10.1016/j.epsl.2005.02.014

De La Fuente, G. S. M. M., and Camacho, E. M. (2009). Boron removal by means of adsorption processes with magnesium oxide — Modelization and mechanism. *Desalination* 249, 626–634. doi: 10.1016/j.desal.2008.11.016

Demetriou, A., and Pashalidis, I. (2012). Adsorption of boron on iron-oxide in aqueous solutions. *Desalin. Water Treat.* 37/38, 315–320. doi: 10.1080/19443994.2012.661288

Doane, T. A., and Howarth, W. R. (2003). Spectrophotometric determination of nitrate with a single reagent. *Analy. Lett.* 36, 2713–2722. doi: 10.1081/al-120024647

Durand, J. (2014). *Characterization of the Spatial and Temporal Variations of Submarine Groundwater Discharge Using Electrical Resistivity and Seepage Measurements*. Ph.D. Thesis, Stony Brook University, New York, NY.

Eppich, G. R., Singleton, M. J., Wimpenny, J. B., Yin, Q.-Z., and Esser, B. K. (2013). *California GAMA Special Study: Stable Isotopic Composition of Boron in Groundwater – San Diego County Domestic Well Data. LLNL-TR-533174*. Livermore, CA: Lawrence Livermore National Lab.(LLNL), 22.

Erler, D. I, Santos, Y., Zhang, D., Tait, K., Befus, A., Hidden, L., et al. (2014). Nitrogen transformations within a tropical subterranean estuary. *Mar. Chem.* 164, 38–47. doi: 10.1016/j.marchem.2014.05.008

Garcia-Orellana, J. J.K, Bokuniewicz, C. H., Daniel, J. W. R., Rodellas, V., and Heilbrun, C. (2014). *Geochim. Cosmochim. Acta* 141, 314–330.

Glavee, G. N., Klabunde, K. J., Sorensen, C. M., and Hadjipanayis, G. C. (1995). Chemistry of borohydride reduction of iron(II) and iron(III) Ions in aqueous and nonaqueous media. formation of nanoscale Fe, FeB, and Fe_2B powders. *Inorga. Chem.* 34, 28–35. doi: 10.1021/ic00105a009

Gobler, C., and Sanudo-Wilhelm, S. (2001). Temporal variability of groundwater seepage and brown tide blooms in a Long Island embayment. *Mar. Ecol. Prog. Ser.* 217, 299–309. doi: 10.3354/meps217299

Goldberg, S., and Glaubig, R. (1985). Boron adsorption on aluminum and iron oxide minerals. *Soil Sci. Soc. Am. J.* 49, 1374–1379. doi: 10.2136/sssaj1985.03615995004900060009x

Granger, J., and Sigman, D. M. (2009). Removal of nitrite with sulfamic acid for nitrate N and O isotope analysis with the denitrifier method. *Rapid Commun. Mass Spectrom.* 23, 3753–3762. doi: 10.1002/rcm.4307

Guinoiseau, D., Louvat, P., Paris, G., Chen, J. B., Cheelat, B., Rocher, V., et al. (2018). Are boron isotopes a reliable tracer of anthropogenic inputs to rivers over time? *Sci. Total Environ.* 626, 1057–1068. doi: 10.1016/j.scitotenv.2018.01.159

Heiss, J. W., Michael, H. A., and Koneshloo, M. (2020). Denitrification hotspots in intertidal mixing zones linked to geologic heterogeneity. *Environ. Res. Lett*. (in press). doi: 10.1088/1748-9326/ab90a6

Howarth, R. W., and Marino, R. (2006). Nitrogen as the limiting nutrient for eutrophication in coastal marine ecosystems: evolving views over three decades. *Limnol. Oceanogr.* 51, 364–376. doi: 10.4319/lo.2006.51.1_part_2.0364

Kendall, C. (1998). *Tracing Nitrogen Sources and Cycling in Catchments*. Amsterdam: Elsevier.

Kendall, C., Elliott, E. M., and Wankel, S. D. (2008). "Tracing anthropogenic inputs of nitrogen to ecosystems," in *Stable Isotopes in Ecology and Environmental Science*, ed. R. H. M. A. K. Lajtha (Hoboken,NY: Blackwell Publishing), 375–449. doi: 10.1002/9780470691854.ch12

Komor, S. C. (1997). boron contents and isotopic compositions of hog manure, selected fertilizers, and water in minnestoa. *J. Environ. Qual.* 26, 1212–1222. doi: 10.2134/jeq1997.00472425002600050004x

Kroeger, K. D., and Charette, M. A. (2008). Nitrogen biogeochemistry of submarine groundwater discharge. *Limnol. Oceanogr.* 53, 1025–1039. doi: 10.4319/lo.2008.53.3.1025

Kruk, M. K., Mayer, B., Nightingale, M., and Laceby, J. P. (2020). Tracing nitrate sources with a combined isotope approach (d15NNO3, d18ONO3 and d11B) in a large mixed-use watershed in southern Alberta. Canada. *Sci. Total Environ.* 703:135043. doi: 10.1016/j.scitotenv.2019.135043

Lemarchand, D., Gaillardet, J., and Göpel, C., and Manhès, G. (2002). An optimized procedure for boron separation and mass spectrometry analysis for river samples. *Chem. Geol.* 182, 323–334. doi: 10.1016/S0009-2541(01)00329-1

Lemarchand, E., Schott, C., and Gaillardet, J. (2007). How surface complexes impact boron isotope fractionation: Evidence from Fe and Mn oxides sorption experiments. *Earth Planet. Sci. Lett.* 260, 277–296. doi: 10.1016/j.epsl.2007.05.039

Lindenbaum, J. (2012). *Identification of Sources of Ammonium in Groundwater Using Stable Nitrogen and Boron Isotopes in Nam Du*. Hanoi: Lund University.

McClymonds, N. E., and Franke, O. L. (1972). Water-transmitting properties of aquifers on Long Island, New York. *Geolo. Survey Profess. Paper* 627:24.

McPhail, M., Page, A., and Bingham, F. (1972). Adsorption interactions of monosilicic and boric acid on hydrous oxides of iron and aluminum. *Soil Sci. Soc. Am. J.* 36, 510–514. doi: 10.2136/sssaj1972.03615995003600030039x

Miranda, K. M., Espey, M. G., and Wink, D. A. (2001). A rapid, simple spectrophotometric method for simultaneous detection of nitrate and nitrite. *Nitric Oxide* 5, 62–71. doi: 10.1006/niox.2000.0319

Moore, W. S. (1999). The subterranean estuary: a reaction zone of ground water and sea water. *Mar. Chem.* 65, 111–125. doi: 10.1016/s0304-4203(99)00014-6

Paerl, H. W. (1995). Coastal eutrophication in relation to atmospheric nitrogen deposition: current perspectives. *Ophelia* 41, 237–259. doi: 10.1080/00785236.1995.10422046

Palmer, M. R., Spivack, A. J., and Edmond, J. M. (1987). Temperature and pH controls over isotopic fractionation during adsorption of boron on marine clay. *Geochim. Cosmochim. Acta* 51, 2319–2323. doi: 10.1016/0016-7037(87)90285-7

Presley, B., and Claypool, G. (1971). Techniques for analyzing interstitial water samples. *Part* 1, 1749–1755.

Ransom, K. M., Grote, M. N., Deinhart, A., Eppich, G., Kendall, C., Sanborn, M. E., et al. (2016). Bayesian nitrate source apportionment to individual groundwater wells in the Central Valley by use of elemental and isotopic tracers. *Water Resour. Res.* 52, 5577–5597. doi: 10.1002/2015WR018523

Rodellas, V., Garcia-Orellana, J., Masqué, P., Feldman, M., and Weinstein, Y. (2015). Submarine groundwater discharge as a major source of nutrients to the Mediterranean Sea. *Proc. Natl. Acad. Sci. U.S.A.* 112, 3926–3930. doi: 10.1073/pnas.1419049112

Saccon, P., Leis, A., Marca, A., Kaiser, J., Campisi, L., Bottcher, M. E., et al. (2013). Multi-isotope approach for the identification and characterization of nitrate pollution sources in the Marano lagoon (Italy) and parts of its catchment area. *Appl. Geochem.* 34, 75–89. doi: 10.1016/j.apgeochem.2013.02.007

Seiler, R. L. (2005). Combined use of 15N and 18O of nitrate and 11B to evaluate nitrate contamination in groundwater. *Appl. Geochem.* 20, 1626–1636. doi: 10.1016/j.apgeochem.2005.04.007

Shireen, F., Nawaz, M., Chen, C., Zhang, Q., and Zheng, Z. (2018). Boron: functions and approaches to enhance its availability in plants for sustainable agriculture. *Int. J. Mol. Sci.* 19:1856. doi: 10.3390/ijms19071856

Slomp, C. P., and Van Cappellen, P. (2004). Nutrient inputs to the coastal ocean through submarine groundwater discharge: controls and potential impact. *J. Hydrol.* 295, 64–86. doi: 10.1016/j.jhydrol.2004.02.018

Suffolk County Government (2019). Available online at: https://www.suffolkcountyny.gov/Departments/Economic-Development-and-Planning/Planning-and-Environment/ReclaimOurWaterInitiativeUpdate (accessed June 19, 2019).

Tamborski, J. J., Cochran, J. K., and Bokuniewicz, H. J. (2017a). Submarine groundwater discharge driven nitrogen fluxes to Long Island Sound, NY: Terrestrial vs. marine sources. *Geochim. Cosmochim. Acta* 218, 40–57. doi: 10.1016/j.gca.2017.09.003

Tamborski, J. J., Cochran, J. K., and Bokuniewicz, H. J. (2017b). Application of ^{224}Ra and ^{222}Rn for evaluating seawater residence times in a tidal subterranean estuary. *Mar. Chem.* 189, 32–45. doi: 10.1016/j.marchem.2016.12.006

Tamborski, J. J., Rogers, A. D., Bokuniewicz, H. J., Cochran, J. K., and Young, C. R. (2015). Identification and quantification of diffuse fresh submarine groundwater discharge via airborne thermal infrared remote sensing. *Remote Sens. Environ.* 171, 202–217. doi: 10.1016/j.rse.2015.10.010

Taniguchi, M., Dulai, H., Burnett, K. M. I, Santos, R., Sugimoto, R., Stieglitz, T., et al. (2019). Submarine groundwater discharge: updates on its measurement techniques, geophysical drivers, magnitudes, and effects. *Front. Environ. Sci.* 7:141. doi: 10.3389/fenvs.2019.00141

Tirez, K., Brusten, W., Widory, D., Petelet, E., Bregnot, A., Xue, D., et al. (2010). Boron isotope ratio (δ^{11}B) measurements in Water Framework Directive monitoring programs: comparison between double focusing sector field ICP and thermal ionization mass spectrometry. *J. Anal. Atom. Spectrom.* 25, 964–974.

Vengosh, A. (1998). The isotopic composition of anthropogenic boron and its potential impact on the environment. *Biolo. Trace Elem. Res.* 66, 145–151. doi: 10.1007/bf02783134

Vengosh, A., Barth, S., Heumann, K. G., and Eisenhut, S. (1999). Boron isotopic composition of freshwater lakes from central europe and possible contamination sources. *Acta Hydrochim. Hydrobiol.* 27, 416–421. doi: 10.1002/(sici)1521-401x(199912)27:6<416::aid-aheh416>3.0.co;2-2

Vengosh, A., Heumann, K. G., Juraske, S., and Kasher, R. (1994). Boron isotope application for tracing sources of contamination in groundwater. *Environ. Sci. Technol.* 28, 1968–1974. doi: 10.1021/es00060a030

Widory, D., Kloppmann, W., Chery, L., Bonnin, J., Rochdi, H., and Guinamant, J. L. (2004). Nitrate in groundwater: an isotopic multi-tracer approach. *J. Contam. Hydrol.* 72, 165–188. doi: 10.1016/j.jconhyd.2003.10.010

Widory, D., Petelet-Giraud, E., Brenot, A., Bronders, J., Tirez, K., and Boeckx, P. (2013). Improving the management of nitrate pollution in water by the use of isotope monitoring: the δ15N, δ18O and δ11B triptych. *Isotopes Environ. Health Stud.* 49, 29–47. doi: 10.1080/10256016.2012.666540

Widory, D., Petelet-Giraud, E., Négrel, P., and Ladouche, B. (2005). Tracking the sources of nitrate in groundwater using coupled nitrogen and boron isotopes: a synthesis. *Environ. Sci. Technol.* 39, 539–548. doi: 10.1021/es0493897

Young, C., Tamborski, J., and Bokuniewicz, H. (2015). Embayment scale assessment of submarine groundwater discharge nutrient loading and associated land use. *Estuar. Coast. Shelf Sci.* 158, 20–30. doi: 10.1016/j.ecss.2015.02.006

Conflict of Interest: The authors declare that the research was conducted in the absence of any commercial or financial relationships that could be construed as a potential conflict of interest.

Advantages of publishing in Frontiers

OPEN ACCESS
Articles are free to read for greatest visibility and readership

FAST PUBLICATION
Around 90 days from submission to decision

HIGH QUALITY PEER-REVIEW
Rigorous, collaborative, and constructive peer-review

TRANSPARENT PEER-REVIEW
Editors and reviewers acknowledged by name on published articles

Frontiers
Avenue du Tribunal-Fédéral 34
1005 Lausanne | Switzerland

Visit us: www.frontiersin.org
Contact us: frontiersin.org/about/contact

REPRODUCIBILITY OF RESEARCH
Support open data and methods to enhance research reproducibility

DIGITAL PUBLISHING
Articles designed for optimal readership across devices

FOLLOW US
@frontiersin

IMPACT METRICS
Advanced article metrics track visibility across digital media

EXTENSIVE PROMOTION
Marketing and promotion of impactful research

LOOP RESEARCH NETWORK
Our network increases your article's readership